

# **Parametric Evaluation of Seismic Behavior of Freestanding Spent Fuel Dry Cask Storage Systems**

**Sandia National Laboratories**

**U.S. Nuclear Regulatory Commission  
Office of Nuclear Regulatory Research  
Washington, DC 20555-0001**



## AVAILABILITY OF REFERENCE MATERIALS IN NRC PUBLICATIONS

### NRC Reference Material

As of November 1999, you may electronically access NUREG-series publications and other NRC records at NRC's Public Electronic Reading Room at <http://www.nrc.gov/reading-rm.html>. Publicly released records include, to name a few, NUREG-series publications; *Federal Register* notices; applicant, licensee, and vendor documents and correspondence; NRC correspondence and internal memoranda; bulletins and information notices; inspection and investigative reports; licensee event reports; and Commission papers and their attachments.

NRC publications in the NUREG series, NRC regulations, and *Title 10, Energy*, in the Code of *Federal Regulations* may also be purchased from one of these two sources.

1. The Superintendent of Documents  
U.S. Government Printing Office  
Mail Stop SSOP  
Washington, DC 20402-0001  
Internet: [bookstore.gpo.gov](http://bookstore.gpo.gov)  
Telephone: 202-512-1800  
Fax: 202-512-2250
2. The National Technical Information Service  
Springfield, VA 22161-0002  
[www.ntis.gov](http://www.ntis.gov)  
1-800-553-6847 or, locally, 703-605-6000

A single copy of each NRC draft report for comment is available free, to the extent of supply, upon written request as follows:

Address: Office of the Chief Information Officer,  
Reproduction and Distribution  
Services Section  
U.S. Nuclear Regulatory Commission  
Washington, DC 20555-0001  
E-mail: [DISTRIBUTION@nrc.gov](mailto:DISTRIBUTION@nrc.gov)  
Facsimile: 301-415-2289

Some publications in the NUREG series that are posted at NRC's Web site address <http://www.nrc.gov/reading-rm/doc-collections/nuregs> are updated periodically and may differ from the last printed version. Although references to material found on a Web site bear the date the material was accessed, the material available on the date cited may subsequently be removed from the site.

### Non-NRC Reference Material

Documents available from public and special technical libraries include all open literature items, such as books, journal articles, and transactions, *Federal Register* notices, Federal and State legislation, and congressional reports. Such documents as theses, dissertations, foreign reports and translations, and non-NRC conference proceedings may be purchased from their sponsoring organization.

Copies of industry codes and standards used in a substantive manner in the NRC regulatory process are maintained at—

The NRC Technical Library  
Two White Flint North  
11545 Rockville Pike  
Rockville, MD 20852-2738

These standards are available in the library for reference use by the public. Codes and standards are usually copyrighted and may be purchased from the originating organization or, if they are American National Standards, from—

American National Standards Institute  
11 West 42<sup>nd</sup> Street  
New York, NY 10036-8002  
[www.ansi.org](http://www.ansi.org)  
212-642-4900

Legally binding regulatory requirements are stated only in laws; NRC regulations; licenses, including technical specifications; or orders, not in NUREG-series publications. The views expressed in contractor-prepared publications in this series are not necessarily those of the NRC.

The NUREG series comprises (1) technical and administrative reports and books prepared by the staff (NUREG-XXXX) or agency contractors (NUREG/CR-XXXX), (2) proceedings of conferences (NUREG/CP-XXXX), (3) reports resulting from international agreements (NUREG/IA-XXXX), (4) brochures (NUREG/BR-XXXX), and (5) compilations of legal decisions and orders of the Commission and Atomic and Safety Licensing Boards and of Directors' decisions under Section 2.206 of NRC's regulations (NUREG-0750).

**DISCLAIMER:** This report was prepared as an account of work sponsored by an agency of the U.S. Government. Neither the U.S. Government nor any agency thereof, nor any employee, makes any warranty, expressed or implied, or assumes any legal liability or responsibility for any third party's use, or the results of such use, of any information, apparatus, product, or process disclosed in this publication, or represents that its use by such third party would not infringe privately owned rights.

---

---

# Parametric Evaluation of Seismic Behavior of Freestanding Spent Fuel Dry Cask Storage Systems

---

---

Manuscript Completed: December 2004  
Date Published: February 2005

Prepared by  
V.K. Luk<sup>1</sup>, B.W. Spencer<sup>1</sup>, I.P. Lam<sup>2</sup>  
R.A. Dameron<sup>3</sup>

<sup>1</sup>Sandia National Laboratories  
Operated by Sandia Corporation for the  
U.S. Department of Energy  
Albuquerque, NM 87185-0744

<sup>2</sup>Earth Mechanics, Inc  
Fountain Valley, CA 92706

<sup>3</sup>David Evans and Associates, Inc.  
San Diego, CA 92123

S.K. Shaukat, NRC Project Manager

**Prepared for**  
**Division of Engineering Technology**  
**Office of Nuclear Regulatory Research**  
**U.S. Nuclear Regulatory Commission**  
**Washington, DC 20555-0001**  
**NRC Job Code W6829**





## Abstract

One of the high priority issues for the continuous operation of nuclear power plants is how to manage and store spent fuel. In recent years, dry storage of spent fuel above ground has become a de facto fuel “repository” solution worldwide. Arrays of dry cask storage systems have been installed at Independent Spent Fuel Storage Installations (ISFSI) at many nuclear power plant sites. Most of these storage systems are freestanding, leading to stability concerns in terms of potential excessive sliding displacements and tipping over in an earthquake event. Sandia National Laboratories has been contracted by the Office of Nuclear Regulatory Research of the U.S. Nuclear Regulatory Commission (NRC) to conduct a research project to develop a comprehensive methodology for evaluating the nonlinear seismic behavior of these storage systems. The main objective of this effort is to perform parametric analyses to characterize the sensitivity of the cask response to a number of important input parameters, which provides a guideline to the range of applicability of analysis results. The results from these parametric analyses have been compiled in nomograms to facilitate the safety review of licensing applications by the staff at the Office of the Nuclear Material Safety and Safeguards (NMSS). This report documents the details of analysis models and all parametric analysis findings.

In this research effort, the cask response is investigated using the finite element method with explicit time integration. The ABAQUS/Explicit code is used to analyze three-dimensional coupled models consisting of a freestanding cask, a concrete pad, and a soil/rock foundation interacting with frictional contact at interfaces. This modeling approach allows a realistic simulation of soil-structure interaction effects and the nonlinear cask behavior after the onset of cask rocking or rolling motion due to applied ground motions. The earthquake ground motions applied to the model are derived from actual recorded ground motions, fitted to conform to selected spectral shapes, and adjusted using a deconvolution procedure that enables the ground motion to be applied at the base of the foundation model.

Prior to performing parametric analyses, the coupled finite element models were developed for three site-specific analyses including three-module rectangular Transnuclear West module/cask, and HI-STORM 100 casks at Hatch Nuclear Power Station and at Private Fuel Storage Facility. The lessons learned from the site-specific analyses help guide performing the much broader based parametric analyses.

The parametric analyses involve two cask system designs: the horizontal rectangular module with an aspect ratio of 0.58 defined as  $\frac{1}{2}$  the shorter width divided by the height of the center of gravity from the base and the vertical cylindrical cask with an aspect ratio of 0.56 defined as  $\frac{1}{2}$  the base diameter divided by the height of the center of gravity from the base. The seismic behavior of these cask designs was investigated with three different foundation types (soft soil, stiff soil, and rock) and three coefficients of friction (0.20, 0.55, and 0.80) at the cask/pad interface. Three spectral shapes (Regulatory Guide 1.60, NUREG/CR-0098, and NUREG/CR-6728) were selected, and for each of these spectral shapes, five different earthquake ground motion records were chosen. These ground motion records were linearly scaled to result in surface peak ground accelerations (PGA) ranging from 0.25 to 1.25 g. A total of 1165 analysis cases were performed in this investigation.

Nomograms of median cask responses +/- one standard deviation of maximum cask top sliding displacements and angular rotations versus peak ground accelerations are plotted at a 5% damped 1 Hertz frequency (1 second period) of pseudo spectral acceleration (PSA) after compiling from the pool of parametric analysis results. These nomograms may provide a meaningful and practical tool to cask designers and reviewers in interpreting the seismic behavior of dry cask storage systems.

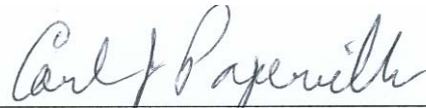


## Foreword

The U.S. Nuclear Regulatory Commission (NRC) regulates the operation of the Nation's 104 nuclear power plants by establishing regulatory requirements and issuing permits and licenses for plant design, construction, and operation. Many of the Nation's existing plants have operated for a few decades, and the spent nuclear fuel generated by these plants must be stored in a manner that adequately protects the health and safety of the public and the environment. Dry storage of spent fuel above ground is an accepted "repository" alternative through independent spent fuel storage installations (ISFSI), which the NRC licenses under Title 10, Part 72, of the *Code of Federal Regulations* (10 CFR Part 72).

The Engineering Research Applications Branch in the NRC's Office of Nuclear Regulatory Research contracted with Sandia National Laboratories (SNL) to investigate the seismic behavior of freestanding dry cask storage systems containing spent nuclear fuel. The primary objective of this research is to characterize the sensitivity of cask response to an earthquake. Toward that end, SNL developed analytical methods that focus on the important parameters that would affect the seismic behavior of dry cask storage systems. These parameters include seismic ground motion, soil properties, cask design, and coefficients of friction between the cask and the concrete pad on which the cask is freely standing. SNL conducted extensive analyses to determine the behavior of casks under a variety of conditions such as earthquakes of various intensities, and different soil foundations (e.g., soft soil, stiff soil, hard rock).

This report provides insight into important design parameters that could affect cask stability, relative stability of cask geometry (shape and dimension), and the expected behavior of casks in terms of potential tipping and sliding under seismic conditions. In addition, this report provides tools for the NRC staff to use in safety reviews of future licensing applications for dry cask storage systems.



---

Carl J. Paperiello, Director  
Office of Nuclear Regulatory Research  
U.S. Nuclear Regulatory Commission



# Table of Contents

<b>Abstract.....</b>	<b>iii</b>
<b>Foreword.....</b>	<b>v</b>
<b>Table of Contents .....</b>	<b>vii</b>
<b>Figures.....</b>	<b>ix</b>
<b>Tables .....</b>	<b>xi</b>
<b>Executive Summary .....</b>	<b>xiii</b>
<b>Acknowledgements .....</b>	<b>xvii</b>
<b>Acronyms .....</b>	<b>xviii</b>
<b>1. Introduction .....</b>	<b>1</b>
1.1 Project Objectives .....	1
1.2 Background.....	1
1.3 Report Organization.....	3
<b>2. Approaches to Evaluate Nonlinear Seismic Behavior of Casks .....</b>	<b>5</b>
2.1 Problem Description .....	5
2.2 Survey of Analysis Methods.....	5
<b>3. Coupled Finite Element Models.....</b>	<b>9</b>
3.1 Description of Analysis Approach.....	9
3.1.1 Coupled Modeling Methodology .....	9
3.1.2 Nonlinear Frictional Contact at Interfaces .....	13
3.1.3 Representation of Damping.....	16
3.1.4 Treatment of Seismic Ground Motions.....	17
3.1.5 Deconvolution Procedure.....	18
3.2 Details of Coupled Models .....	20
3.2.1 Vertical Cylindrical Cask .....	20
3.2.2 Rectangular Module .....	24
3.2.3 Foundation Submodel .....	27
3.2.4 Properties of Interfaces Between Submodels .....	30
<b>4. Scope of Parametric Analyses .....</b>	<b>31</b>
4.1 Seismic Loading – Time Histories of Accelerations .....	31
4.1.1 NUREG/CR-0098 Spectral Shape .....	40
4.1.2 Regulatory Guide 1.60 Spectral Shape .....	40
4.1.3 NUREG/CR-6728 Spectral Shape .....	40
4.1.4 Time Histories for the Three Spectral Shapes.....	41

4.2	<i>Frictional Contact at Cask/Pad Interface</i> .....	47
<b>5.</b>	<b>Analysis Results</b> .....	<b>49</b>
5.1	<i>Physics of Cask Behavior and Soil-Structure Interaction Effects</i> .....	49
5.1.1	Cask Behavior Before Onset of Relative Movement .....	49
5.1.2	Cask Behavior After Onset of Relative Movement.....	53
5.1.3	Demonstration of Soil Column Response and Soil-Structure Interaction.....	53
5.2	<i>Representative Analysis Results</i> .....	57
5.2.1	Representative Analysis Results for Cylindrical Cask.....	59
5.2.2	Representative Analysis Results for Rectangular Module .....	62
5.3	<i>Presentation of Analysis Results</i> .....	66
5.4	<i>Discussion of Analysis Results</i> .....	67
5.5	<i>Compilation of Analysis Results in Nomograms</i> .....	69
5.5.1	Nomograms for Specific Spectral Shapes .....	69
5.5.2	Combination of Spectral Shape Nomograms .....	75
5.5.3	Discussion and Limitations of Nomograms .....	81
<b>6.</b>	<b>Summary</b> .....	<b>85</b>
<b>7.</b>	<b>Conclusions</b> .....	<b>87</b>
<b>8.</b>	<b>References</b> .....	<b>89</b>
<b>Appendix I: Details in Background Information on Soil Profile and Properties Issues</b> .....		<b>93</b>
<b>Appendix II: Verification of Time-Domain Wave Propagation and Various Wave-Propagation Sensitivity Studies</b> .....		<b>101</b>
II.1	<i>One-Dimensional Site Response</i> .....	101
II.2	<i>Effects of Vertical Side Boundaries</i> .....	102
II.3	<i>Two Component Motions</i> .....	105
<b>Appendix III: Plots of Generated Time Histories of Ground Motions Conforming to the Three Spectral Shapes</b> .....		<b>125</b>
<b>Appendix IV: Plots of Analytical Soil Column Response</b> .....		<b>309</b>
<b>Appendix V: Complete Parametric Cask Analysis Results</b> .....		<b>327</b>
V.1	<i>Tabular Presentation of Results</i> .....	327
V.2	<i>Graphical Presentation of Results</i> .....	340
<b>Appendix VI: Nomograms of Cask Responses</b> .....		<b>361</b>
VI.1	<i>Nomograms for Individual Spectral Shapes with Combined Soil Types</i> .....	361
VI.2	<i>Nomograms for Combined Spectral Shapes in Terms of 1 Hz PSA</i> .....	380
<b>Appendix VII: Tabulation of Curve Fitting Parameters and Example Calculations</b> .....		<b>395</b>

VII.1	Tabulation of Curve Fitting Parameters .....	395
VII.2	Example Calculations.....	396

## Figures

Figure 1.1:	Operating Spent Fuel ISFSI Sites.....	2
Figure 1.2:	Potential New Applications for ISFSI Sites .....	2
Figure 2.1:	Design of a Vertical Cylindrical Cask with Multi-Purpose Canister Partially Inserted .....	6
Figure 2.2:	Design of a Horizontal Rectangular Module.....	6
Figure 2.3:	Typical HI-STORM 100 Cask Array on an ISFSI Pad at Hatch Nuclear Power Station.....	7
Figure 2.4:	Typical ISFSI Layout of Horizontal Rectangular Modules.....	8
Figure 3.1:	Typical Finite Element Model of Cask, Pad, and Foundation.....	10
Figure 3.2:	Multi-Point Constraints in Soil Foundation Layers.....	12
Figure 3.3:	Master/Slave Contact Concepts.....	14
Figure 3.4:	Idealized Mesh with Master/Slave Surface Assignments.....	14
Figure 3.5:	Soil Profiles Used in Parametric Deconvolution Site Response Analyses.....	17
Figure 3.6:	Finite Element Model of Cylindrical Cask, Pad, and Foundation.....	21
Figure 3.7:	Top View of Cylindrical Cask Mesh.....	22
Figure 3.8:	Detailed View of Pad for Cylindrical Cask .....	24
Figure 3.9:	Finite Element Model of Rectangular Module, Pad, and Foundation .....	25
Figure 3.10:	Representative Soil Foundation Submodel for Cylindrical Cask Analyses .....	27
Figure 3.11:	Representative Rock Foundation Submodel for Cylindrical Cask Analyses .....	28
Figure 4.1:	Boundary between Western US (WUS) and Central and Eastern US (CEUS) .....	32
Figure 4.2:	Plots of Horizontal and Vertical Spectral Shapes In Terms of Frequency (Logarithmic Scales) .....	37
Figure 4.3:	Plots of Horizontal Spectral Shapes In Terms of Period (Linear Scales).....	38
Figure 4.4:	Plots of Vertical Spectral Shapes In Terms of Period (Linear Scales) .....	39
Figure 4.5:	Histogram of Steel/Concrete Coefficient of Friction Test Results .....	47
Figure 5.1:	Diagram of a Cask.....	49
Figure 5.2:	Deformed Shape of Cylindrical Cask/Pad Pullback Test (Magnified 100x).....	51
Figure 5.3:	Spectral Shapes and Cask Periods with Various Soil Types .....	52
Figure 5.4:	Comparison of Original Surface Motion and Motion at Top of Soil Column Model, NUREG/CR-0098 Spectral Shape, Case 1 Earthquake, First Horizontal Component.....	54
Figure 5.5:	Spectral Response at Points on Surface of Soil Column Model, Soft Soil, NUREG/CR-0098 Spectral Shape, Case 1 Earthquake, 1 g PGA, 1 <sup>st</sup> Horizontal Component.....	55
Figure 5.6:	Spectral Response at Points on Surface of Soil Column Model, Stiff Soil, NUREG/CR-0098 Spectral Shape, Case 1 Earthquake, 1 g PGA, 1 <sup>st</sup> Horizontal Component.....	55
Figure 5.7:	Spectral Response at Points on Surface of Soil Column Model, Rock, NUREG/CR-0098 Spectral Shape, Case 1 Earthquake, 1 g PGA, 1 <sup>st</sup> Horizontal Component.....	56
Figure 5.8:	Explanation of Key Response Quantities .....	58
Figure 5.9:	Lateral Displacement Trajectories for Cylindrical Cask Top and Bottom, Iran Tabas Earthquake, NUREG/CR-0098 Spectral Shape, PGA=1.0 g, Stiff Soil Profile, Cask/Pad $\mu=0.55$ ...	59
Figure 5.10:	Time Histories of Cask Displacement Relative to Pad for Cylindrical Cask, Stiff Soil Profile, Cask/Pad $\mu=0.2$ , All 5 Earthquakes, NUREG/CR-0098 Spectral Shape, PGA=1.0 g .....	60
Figure 5.11:	Time Histories of Cask Displacement Relative to Pad for Cylindrical Cask, Stiff Soil Profile, Cask/Pad $\mu=0.55$ , All 5 Earthquakes, NUREG/CR-0098 Spectral Shape, PGA=1.0 g .....	61
Figure 5.12:	Time Histories of Cask Displacement Relative to Pad for Cylindrical Cask, Stiff Soil Profile, Cask/Pad $\mu=0.8$ , All 5 Earthquakes, NUREG/CR-0098 Spectral Shape, PGA=1.0 g .....	62

Figure 5.13: Lateral Displacement Trajectories for Rectangular Module Top and Base, Iran Tabas Earthquake, PGA=1.0 g, Stiff Soil Profile, $\mu=0.55$ .....	63
Figure 5.14: Time Histories of Cask Displacement Relative to Pad for Rectangular Module, Stiff Soil Profile, Cask/Pad $\mu=0.2$ , All 5 Earthquakes, NUREG/CR-0098 Spectral Shape, PGA=1.0 g .....	64
Figure 5.15: Time Histories of Cask Displacement Relative to Pad for Rectangular Module, Stiff Soil Profile, Cask/Pad $\mu=0.55$ , All 5 Earthquakes, NUREG/CR-0098 Spectral Shape, PGA=1.0 g .....	65
Figure 5.16: Time Histories of Cask Displacement Relative to Pad for Rectangular Module, Stiff Soil Profile, Cask/Pad $\mu=0.8$ , All 5 Earthquakes, NUREG/CR-0098 Spectral Shape, PGA=1.0 g .....	66
Figure 5.17: Peak Top Displacement Regression Fit, Linear Scale, Cylindrical Cask, NUREG/CR-0098 Earthquakes, Cask/Pad $\mu=0.55$ , Soft Soil Profile.....	71
Figure 5.18: Peak Top Displacement Regression Fit, Logarithmic Scale, Cylindrical Cask, NUREG/CR-0098 Earthquakes, Cask/Pad $\mu=0.55$ , Soft Soil Profile.....	71
Figure 5.19: Peak Top Displacement Regression Fit, Logarithmic Scale, Cylindrical Cask, NUREG/CR-0098 Earthquakes, Cask/Pad $\mu=0.55$ , Stiff Soil Profile .....	72
Figure 5.20: Peak Top Displacement Regression Fit, Logarithmic Scale, Cylindrical Cask, NUREG/CR-0098 Earthquakes, Cask/Pad $\mu=0.55$ , Rock Profile .....	73
Figure 5.21: Peak Top Displacement Regression Fit, Logarithmic Scale, Cylindrical Cask, NUREG/CR-0098 Earthquakes, Cask/Pad $\mu=0.55$ , All Soil Profiles.....	74
Figure 5.22: Peak Top Displacement Regression Fit in Terms of Peak Ground Velocity, Linear Scale, Cylindrical Cask, All Earthquakes, Cask/Pad $\mu=0.55$ , All Soil Profiles.....	77
Figure 5.23: Peak Top Displacement Regression Fit in Terms of Peak Ground Velocity, Linear Scale, Rectangular Module, All Earthquakes, Cask/Pad $\mu=0.55$ , All Soil Profiles .....	77
Figure 5.24: Peak Rotation Regression Fit in Terms of Peak Ground Velocity, Linear Scale, Cylindrical Cask, All Earthquakes, Cask/Pad $\mu=0.55$ , All Soil Profiles.....	78
Figure 5.25: Peak Rotation Regression Fit in Terms of Peak Ground Velocity, Linear Scale, Rectangular Module, All Earthquakes, Cask/Pad $\mu=0.55$ , All Soil Profiles .....	78
Figure 5.26: Peak Top Displacement Regression Fit in Terms of 1 Hz PSA, Linear Scale, Cylindrical Cask, All Earthquakes, Cask/Pad $\mu=0.55$ , All Soil Profiles.....	79
Figure 5.27: Peak Top Displacement Regression Fit in Terms of 1 Hz PSA, Linear Scale, Rectangular Module, All Earthquakes, Cask/Pad $\mu=0.55$ , All Soil Profiles .....	80
Figure 5.28: Peak Rotation Regression Fit in Terms of 1 Hz PSA, Linear Scale, Cylindrical Cask, All Earthquakes, Cask/Pad $\mu=0.55$ , All Soil Profiles.....	80
Figure 5.29: Peak Rotation Regression Fit in Terms of 1 Hz PSA, Linear Scale, Rectangular Module, All Earthquakes, Cask/Pad $\mu=0.55$ , All Soil Profiles.....	81

## Tables

Table 3.1: Cylindrical Cask Finite Element Model Material Properties by Layer .....	23
Table 3.2: Summary of Cylindrical Cask Finite Element Model Properties .....	23
Table 3.3: Rectangular Module Finite Element Model Material Properties by Layer.....	26
Table 3.4: Summary of Critical Rectangular Module Finite Element Model Properties.....	26
Table 3.5: Soft Soil Foundation Material Properties .....	29
Table 3.6: Stiff Soil Foundation Material Properties .....	29
Table 3.7: Rock Foundation Material Properties .....	30
Table 4.1: Scope of Parametric Analyses .....	31
Table 4.2: Tabulation of Spectral Shapes .....	34
Table 4.3-A: Startup Motions for NUREG/CR-0098 Spectral Shape .....	44
Table 4.3-B: Startup Motions for Regulatory Guide 1.60 Spectral Shape.....	45
Table 4.3-C: Startup Motions for NUREG/CR-6728 Spectral Shape.....	46
Table 5.1: Frequency of Cask Rocking Mode .....	52
Table 5.2: Comparison of Peak Cask Top Displacements (m) for Rigid Model and Models with Soil, Cylindrical Cask.....	57
Table 5.3: Peak Ground Acceleration, Velocity, and Displacement for Surface Ground Motion Records Conforming to NUREG/CR-00098 Spectral Shape .....	76
Table 5.4: Peak Ground Acceleration, Velocity, and Displacement for Surface Ground Motion Records Conforming to Regulatory Guide 1.60 Spectral Shape .....	76
Table 5.5: Peak Ground Acceleration, Velocity, and Displacement for Surface Ground Motion Records Conforming to NUREG/CR-6728 Spectral Shape .....	76
Table 5.6: Ratio of 5% Damped 1 Hz PSA to PGA for Spectral Shapes Used in Current Study .....	79
Table 5.7: NRC-Approved DCSS – General Use .....	83



## Executive Summary

The Spent Fuel Project Office (SFPO) in the Office of the Nuclear Material Safety and Safeguards (NMSS) at the Nuclear Regulatory Commission (NRC) is involved in investigating technical issues concerning the dry storage and transportation of spent nuclear fuel. Sandia National Laboratories (SNL) was contracted by the Engineering Research Applications Branch, Office of Nuclear Regulatory Research (RES) at the NRC for investigating the seismic behavior of dry cask storage systems (DCSS) to provide technical support in revising review guidelines. The results of this research are expected to aid the NMSS staff in performing the safety review of licensing applications of DCSSs.

Arrays of DCSSs have been installed at Independent Spent Fuel Storage Installations (ISFSI), licensed under 10 CFR Part 72, at many nuclear power plant sites. Most of these storage casks are freestanding on a concrete pad, leading to concerns of possible tipping over and collision with neighboring casks in an earthquake event. Therefore, in the safety review process of these cask systems, it is important to assess their dynamic response in terms of sliding displacements, rotations, and the integrity of cask internals under seismic loads.

The main objective of the research effort is to perform parametric analyses to characterize the sensitivity of the cask response to a number of important input parameters including cask designs, earthquake ground motions, soil conditions, and coefficients of friction at the cask/pad interface. A well-defined set of parametric analyses has been performed to provide results in nomograms to facilitate the safety review of licensing applications by the NMSS staff. This report documents the analysis methodology, the details of input parameters, and all parametric analysis findings.

In this project, the dynamic response of a freestanding cask system is investigated using the finite element method with explicit time integration. The ABAQUS/Explicit code is used to analyze three-dimensional coupled models consisting of a freestanding cask, a concrete pad, and a soil/rock foundation interacting with nonlinear friction contacts at interfaces. This coupled modeling approach provides a realistic simulation for soil-structure interaction effects and nonlinear cask responses after the cask starts to rock or precess due to applied ground motions. The earthquake ground motions applied to the model are derived from actual recorded ground motions, fitted to conform to selected spectral shapes, and adjusted using a deconvolution procedure that enables the ground motion to be applied at the base of the foundation model.

Three site-specific analyses were performed using the coupled models prior to conducting the parametric analyses. These site-specific analyses include the three-module rectangular Transnuclear West module/cask, and HI-STORM 100 casks at Hatch Nuclear Power Station and at Private Fuel Storage Facility. The lessons learned from the site-specific analyses help guide performing the much broader based parametric analyses. For the parametric analyses, a horizontal rectangular module and a vertical cylindrical cask are the two cask designs selected for investigation. The cask designs are characterized by the aspect ratio that is defined as  $\frac{1}{2}$  the base diameter (for a cylindrical cask) or  $\frac{1}{2}$  the shorter width (for a rectangular module) divided by the height of the center of gravity from the base. In the parametric study, an aspect ratio of 0.56 was used for the cylindrical cask and 0.58 for the rectangular module.

The selected ground motions are governed by three spectral shapes in NUREG/CR-0098, Regulatory Guide 1.60, and NUREG/CR-6728, and five different earthquake ground motion records were chosen for each of these spectral shapes. The five selected earthquake records for the WUS (western United States) sites appropriate for the NUREG/CR-0098 and the Regulatory Guide 1.60 spectral shapes are:

- 1) 1978 Iran Tabas
- 2) 1999 Taiwan Chi-Chi
- 3) 1992 Landers
- 4) 1994 Northridge
- 5) 1979 Imperial Valley

Likewise, five different earthquake records for the CEUS (central and eastern United States) sites appropriate for the NUREG/CR-6728 spectral shape were also selected:

- A) 1985 Nahanni
- B) 1988 Saguenay
- C) 1979 Imperial Valley
- D) 1989 Loma Prieta
- E) 1994 Northridge

These ground motion records were linearly scaled to result in surface peak ground accelerations (PGA) ranging from 0.25 to 1.25 g. Furthermore, the parametric analyses involve three different foundation types (soft soil, stiff soil, and rock) and three coefficients of friction (0.20, 0.55, and 0.80) at the cask/pad interface. In total, 1165 analysis cases were performed in the parametric evaluation.

The parametric analysis results documented the maximum sliding displacements at the cask top and the maximum angle of cask rotation with respect to the vertical axis. In all cases for the two cask designs under investigation, the DCSS is more susceptible to rolling/rocking motions with cases of high coefficients of friction at the cask/pad interface, and it experiences higher sliding displacements with low interfacial coefficients of friction. The horizontal rectangular module is more seismically stable than the vertical cylindrical cask because the geometry of the rectangular module allows only rocking and sliding, while the cylindrical cask can exhibit rolling about the base edge in addition to rocking and sliding. The cask response can be significantly higher in this rolling mode than in the rocking and sliding mode only.

The parametric analysis results are affected by the dynamic coupling between the DCSS and the foundation due to the soil-structure interaction. It has been demonstrated that directly beneath the pad, the ground motion at the soil surface is significantly affected by the interaction of the soil with the cask and pad. At points on the surface far away from the pad, the ground motions almost duplicate the prescribed input ground motions. These findings indicate that a reasonable modeling procedure has been developed for simulating a semi-infinite foundation using a finite model with appropriate boundary conditions and for performing deconvolution analyses of surface-defined ground motions by preserving their dynamic characteristics of amplitudes and frequency contents.

A large amount of scatter was observed in the analytical responses of the freestanding casks. This scatter is attributed to the fact that the cask is not anchored to the pad. The cask response is highly sensitive to the phasing of the cask motion with respect to the ground motion. Because of this scatter, it is not advisable to base design decisions on isolated analysis results. Instead, these decisions should be based on the statistics from a large number of analyses conducted under a variety of conditions. Regression analysis was employed to condense the analysis results obtained in this study into a usable form. Nomograms in the form of equations that describe the median response, as well as equations for 84% and 16% (median plus and minus one standard deviation, respectively) confidence bands have been developed from the analysis results. These nomograms have been developed for the peak lateral cask displacement magnitude relative to the pad and angular rotation of the cask for the three spectral shapes and the three cask/pad interfacial coefficients of friction.

The peak ground acceleration (PGA), or zero period spectral acceleration, is used extensively in this work as a parameter to describe the ground motion intensity, but this parameter is only useful when associated with a spectral shape. The cask response is more sensitive to the spectral content at lower frequencies than to the PGA. If the design ground motion at a specific site conforms to one of the three spectral shapes used in this study, the nomograms developed for that spectral shape can be used directly for evaluation of that design. However, it is also desirable to develop a procedure to apply these results to other spectral shapes. The results from the three spectral shapes were plotted together, and regression analysis was performed using a number of different parameters to describe the ground motion intensity. These parameters included the pseudo-spectral acceleration (PSA) at a number of frequencies and the peak ground velocity (PGV).

It was found that the PSA at 5% damped 1 Hertz (Hz) and the PGV are both reasonable parameters to describe the cask response, regardless of the spectral shape. The PGV, which is not a direct function of the spectral shape, is influenced by the spectral accelerations across the middle of the spectrum in the period range likely to be important to the cask response. The fitting of the results was slightly better with the 1 Hz PSA as the ground motion parameter than with the PGV. Because of this observation and the fact that the 1 Hz PSA can be directly tied to the design spectrum, it is recommended that the 1 Hz PSA be used as a ground motion parameter if it is desired to apply these results to other spectral shapes. In conclusion, nomograms in terms of 1 Hz PSA have been provided in this report in addition to those for specific spectral shapes.



## Acknowledgements

The project on seismic behavior of spent fuel dry cask storage systems took more than five years of hard work and concerted effort from many people to bring it to a successful completion. The Project Team deeply appreciates their support and cooperation.

The project team acknowledges the continuous guidance, support, and encouragement from S. Khalid Shaukat, Engineering Research Applications Branch, Division of Engineering Technology, Nuclear Regulatory Commission. The Project Team is also indebted to the Review Panel members for their invaluable technical advices. Seven Review Panel meetings were held in the course of this project. Participants included:

Representing NRC interests:

- S. Khalid Shaukat, Goutam Bagchi, Mahendra Shah, and Bhasker Tripathi (NRC)
- Yusef R. Rashid (ANATECH Corporation)

Representing industry interests:

- Robert Kassawara (EPRI), Robert Kennedy (RPK Structural Mechanics), Donald Moore (Southern Company), and Torrey Yee (Southern California Edison)

Special thanks are extended to Ignatius Po Lam (Earth Mechanics, Inc.) and Robert Dameron (David Evans and Associates) for their dedicated support and contribution to the success of this project. The project team would also like to thank colleagues, Jeffrey A. Smith and David A. Aube, for their valuable contributions in the early development of the coupled cask response models.

## Acronyms

CEUS	central and eastern United States
CG	center of gravity
DCSS	dry cask storage system
Hz	Hertz
ISFSI	Independent Spent Fuel Storage Installation
MPC	multipoint constraint
NMSS	Nuclear Materials Safety and Safeguards
NRC	Nuclear Regulatory Commission
PGA	peak ground acceleration
PGD	peak ground displacement
PGV	peak ground velocity
PSA	pseudo-spectral acceleration
SASSI	System for Analysis of Soil-Structure Interactions
SFPO	Spent Fuel Project Office
V/H	vertical/horizontal
WUS	western United States

# 1. Introduction

## 1.1 Project Objectives

Sandia National Laboratories conducted a research project, funded by the Engineering Research Applications Branch, Office of Nuclear Regulatory Research at the Nuclear Regulatory Commission (NRC), to pursue the following objectives:

1. To investigate the dynamic responses of freestanding dry cask storage systems subjected to a prescribed seismic excitation. Three site-specific analyses and a comprehensive set of parametric analyses were performed using the following procedure:
  - a) Develop a coupled finite element model of a freestanding cask/module, a concrete pad, and a foundation.
  - b) Apply appropriate sets of prescribed seismic time histories to the model.
  - c) Apply appropriately selected material properties to the submodels and coefficients of friction at their interfaces.
2. To provide support to the NRC in revising the regulatory guidelines and facilitate the safety review of licensing applications by the Nuclear Material Safety and Safeguards staff for the dry cask storage systems. The parametric analysis results were compiled in nomograms to assist this process.

## 1.2 Background

The Spent Fuel Project Office (SFPO) in the Office of the Nuclear Material Safety and Safeguards (NMSS) at the NRC has been involved in investigating technical issues concerning the dry storage and transportation of spent nuclear fuel. Sandia National Laboratories was contracted by the Engineering Research Applications Branch, Office of Nuclear Regulatory Research (RES) at the NRC for investigating the seismic behavior of dry cask storage systems (DCSS) containing spent fuel. The results of this research effort are expected to aid the NMSS staff in performing the safety review of licensing applications of DCSSs by assessing their dynamic response in terms of sliding, tipping, collision of neighboring casks, and the integrity of cask internals under seismic loads.

Dry storage of spent fuel above ground has become an accepted “repository” alternative by installing DCSSs at an Independent Spent Fuel Storage Installation (ISFSI) (which is licensed under 10 CFR Part 72 [1]), consisting of arrays of freestanding storage casks on a concrete pad. Many ISFSIs have been licensed and installed inside operating nuclear power plants, and a few sites are in the licensing application process, as shown in Figures 1.1, and 1.2, respectively.

Most of the casks/modules are freestanding on a concrete pad, rather than anchored like typical civil structures. This results in a rather complicated nonlinear contact problem at the cask/pad interface after the onset of cask rocking, rolling, or sliding motion. Consequently, there are safety concerns about the possibility of a cask tipping over and collision in an earthquake event. Three-dimensional coupled finite element models with explicit time integration were developed to investigate the highly nonlinear dynamic seismic responses of casks. The ABAQUS [2] finite element analysis program, Version 6.4, was used to analyze these coupled models consisting of three submodels: a cylindrical cask or a rectangular module, a flexible concrete pad, and an underlying foundation. Contact constraints were employed at the interfaces between the cask and pad and the pad and the foundation.. The seismic event was described by one vertical and two horizontal components of statistically independent seismic acceleration time histories. A deconvolution procedure was used to adjust the amplitudes and frequency contents of these three-component reference surface motions before applying them simultaneously at the foundation base.

# Operating ISFSI Locations

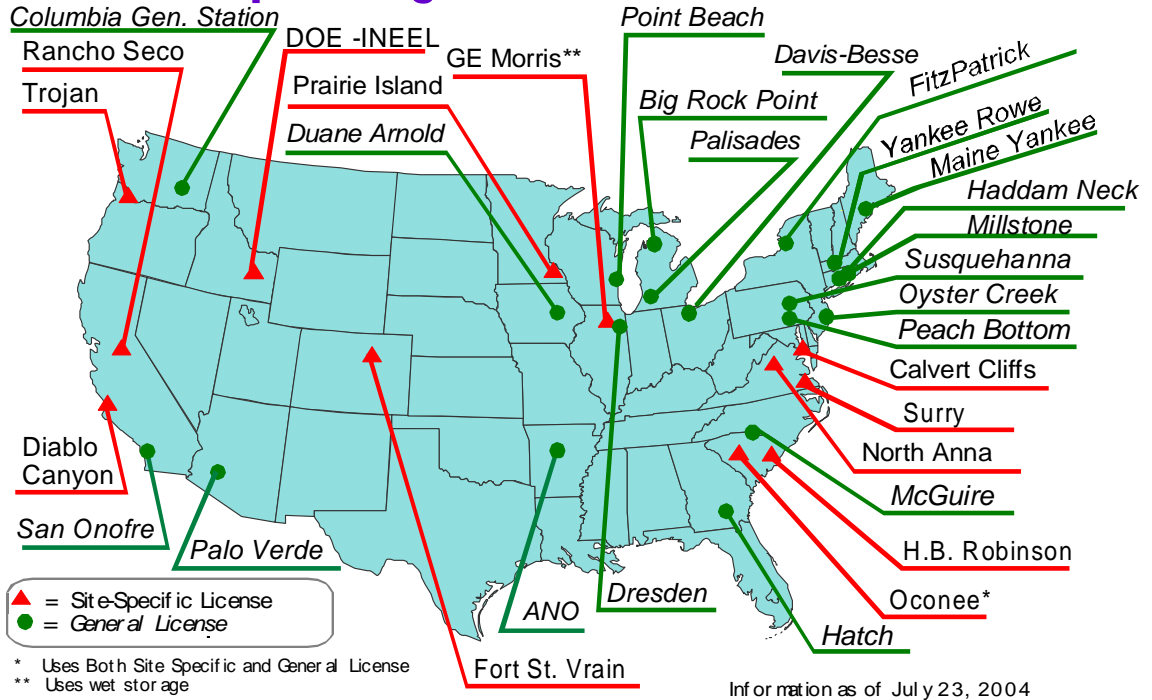


Figure 1.1: Operating Spent Fuel ISFSI Sites

# Potential Near-Term, New ISFSI Sites

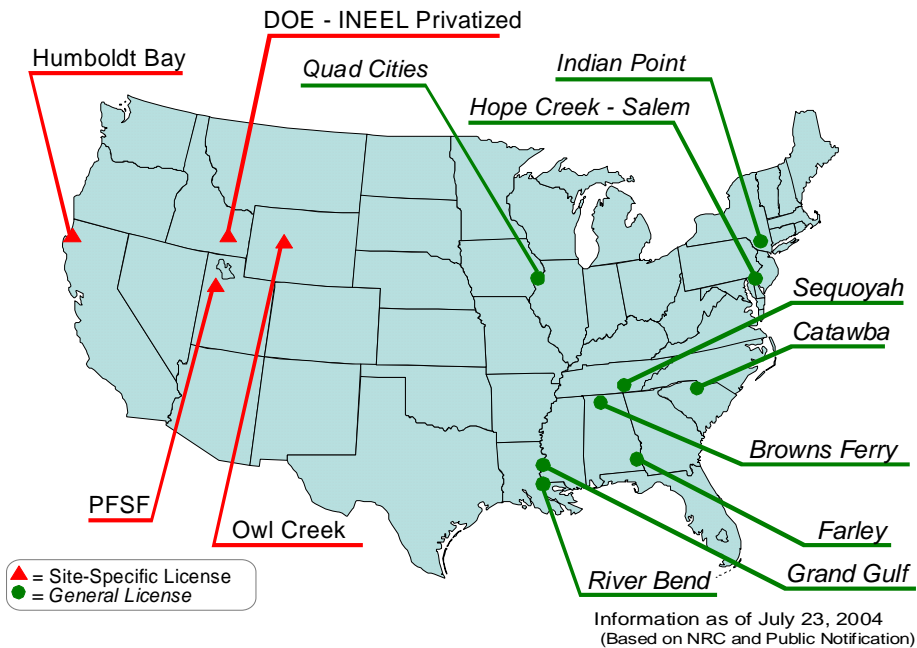


Figure 1.2: Potential New Applications for ISFSI Sites

Coupled models very similar to those used in the parametric study summarized in this report have already been used to perform three site-specific analyses for the three-module rectangular Transnuclear West module/cask [3] and HI-STORM 100 casks at Hatch Nuclear Power Station [4] and at Private Fuel Storage Facility [5]. Most of those analysis results indicated that the cask or module usually experiences higher sliding displacements with a lower coefficient of friction at the cask/pad interface and higher angular rotations with respect to the vertical axis for a higher coefficient of friction. The lessons learned from the site-specific analyses helped guide the much broader parametric analyses summarized in this report. This report documents the details of the coupled models as well as all analysis results from the parametric analyses.

### **1.3 Report Organization**

A variety of modeling approaches have been used to evaluate the nonlinear seismic behavior of casks/modules. Some modeling details and technical merits of these approaches will be discussed in Chapter 2. Chapter 3 is devoted to covering details of the coupled models including the coupled analysis philosophy and methodology as well as model details of vertical cylindrical casks and horizontal rectangular modules. The coupled modeling approach provides a realistic simulation for soil-structure interaction effects and the nonlinear cask behavior associated with the cask rocking or rolling motion. Applying simultaneously a vertical and two horizontal components of surface defined seismic acceleration time histories at the foundation base requires a mathematically based deconvolution procedure that preserves the dynamic characteristics of seismic ground motions. The modeling issues are further complicated by providing justification of simulating a semi-infinite foundation by a finite body with properly prescribed boundary conditions.

The scope of parametric analyses of two selected cask designs, vertical cylindrical casks and horizontal rectangular modules, are discussed in Chapter 4. The characteristics of the seismic input motions are governed by the selection of three spectral curve shapes (NUREG/CR-0098 [6], Regulatory Guide 1.60 [7], and NUREG/CR-6728 [8]), five selected earthquake records for each spectral shape, and five surface peak ground accelerations (PGA) ranging from 0.25 to 1.25 g. Three different foundation types are chosen for analyses including soft soil, stiff soil, and weathered rock foundations. The nonlinear contact at the cask/pad interface is simulated by three coefficients of friction covering the lower bound (0.20), the median (0.55), and the upper bound (0.80).

All parametric analysis results from the coupled models are presented and discussed in Chapter 5. Analysis results are plotted for graphical representation and compiled in nomograms. The parametric analysis findings are summarized in Chapter 6, conclusions are given in Chapter 7, and all relevant references are listed in Chapter 8.



## 2. Approaches to Evaluate Nonlinear Seismic Behavior of Casks

The research effort in this project focused on investigating the nonlinear dynamic behavior of freestanding dry cask systems in a seismic event. The cask and the pad experience translational and rotational motions relative to each other and to the foundation when subjected to seismic ground motions. The combination of frictional contact at the cask/pad interface and soil-structure interaction results in a highly nonlinear cask response. This chapter is devoted to describing the physical problem under investigation, various modeling approaches to analyze this problem, and the philosophy leading to the development of the coupled models used in this project.

### 2.1 Problem Description

In most Independent Spent Fuel Storage Installations (ISFSI), dry cask systems have been installed as freestanding structures on a concrete pad. Physically disconnecting the cask and the pad has financial benefits in terms of reduced installation and future decommissioning costs. In addition, it has enabled the U.S. Nuclear Regulatory Commission (NRC) to enunciate a clear regulatory position on storage casks, permitting the holder of a Part 50 license to deploy an NRC-certified storage cask on a concrete pad without further licensing reviews.

Relatively thin concrete pads have been used in most ISFSIs, nominally 0.61 m (2 feet) for the vertical cylindrical casks and 0.91 m (3 feet) for the horizontal rectangular modules. The design limitations of the casks for impact loads due to drop and tip over have dictated the use of thin concrete pads. As pointed out by Moore et al. [9], a flexible pad should be modeled to account for the out-of-plane flexibility of the ISFSI pad.

The parametric analyses performed in this project investigated the nonlinear responses of the vertical cylindrical casks and the horizontal rectangular modules. Figures 2.1 [10] and 2.2 [11] show typical designs of these two storage systems. Since there is a storage space limitation at most ISFSIs, a design goal is to install as many casks as permitted on a concrete pad, resulting in a fairly small separation distance (within allowable design limits) between neighboring casks, as depicted in Figures 2.3 [10] and 2.4 [11]. Consequently, the possible collision of neighboring casks is a concern in the safety review of the stability of casks in a prescribed earthquake event.

### 2.2 Survey of Analysis Methods

Moore et al. [9] performed a seismic evaluation of the cylindrical HI-STORM 100 casks in support of the ISFSI design at the Hatch Nuclear Power Plant. They analyzed the problem by investigating the soil-structure interaction to demonstrate the importance of including the out-of-plane flexibility of the pad in the models and its effects on the seismic response of casks. Their seismic model of the cask/pad assembly, developed with the SASSI (System for Analysis of Soil-Structure Interaction) code [12], consists of using plate elements to represent the pad, beam elements for the casks, and beam elements with springs to simulate the contact between the cask and the pad. The strain compatible soil profiles used in the models were generated using the program SHAKE91 [13].

Singh et al. [14] also performed dynamic analyses to predict the structural response of the HI-STAR 100 casks under seismic events. They used the computer code DYNAMO [15] to assemble the dynamic model for the cask system, which includes various internal components of the cask. The mechanical interaction between the cask base and the soil foundation was simulated using vertical compression-only gap elements and horizontal piecewise linear friction elements.

In this project, the research effort focused on providing a realistic assessment of the dynamic stability of storage cask systems under seismic events through truly coupled cask/pad/foundation models. The key features of these coupled models included investigating the highly nonlinear friction contact algorithms at the cask/pad interface and the dynamic soil-structure interaction effect by applying the three components of seismic excitation at the foundation base. The details of the coupled models and the analysis results are discussed in the following chapters.

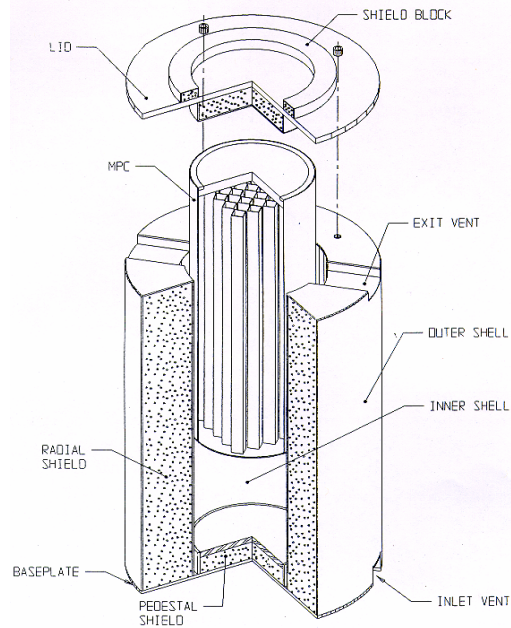


Figure 2.1: Design of a Vertical Cylindrical Cask with Multi-Purpose Canister Partially Inserted

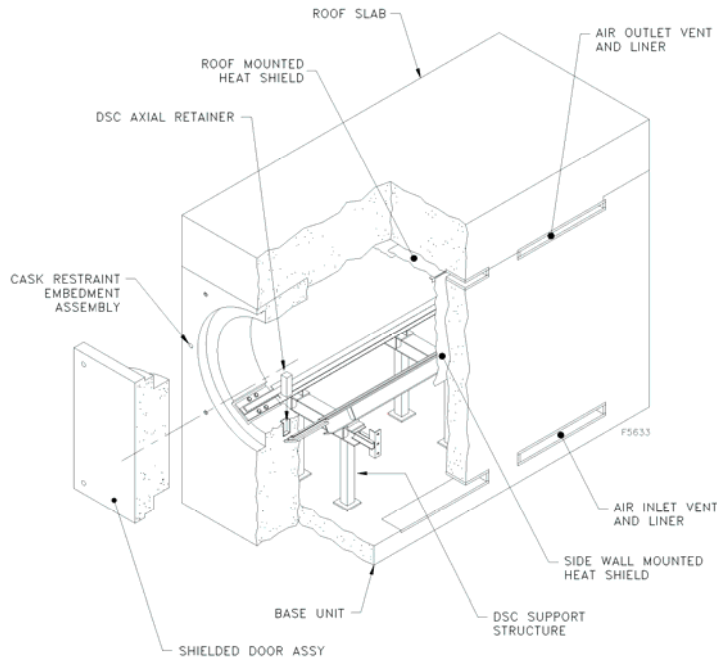


Figure 2.2: Design of a Horizontal Rectangular Module

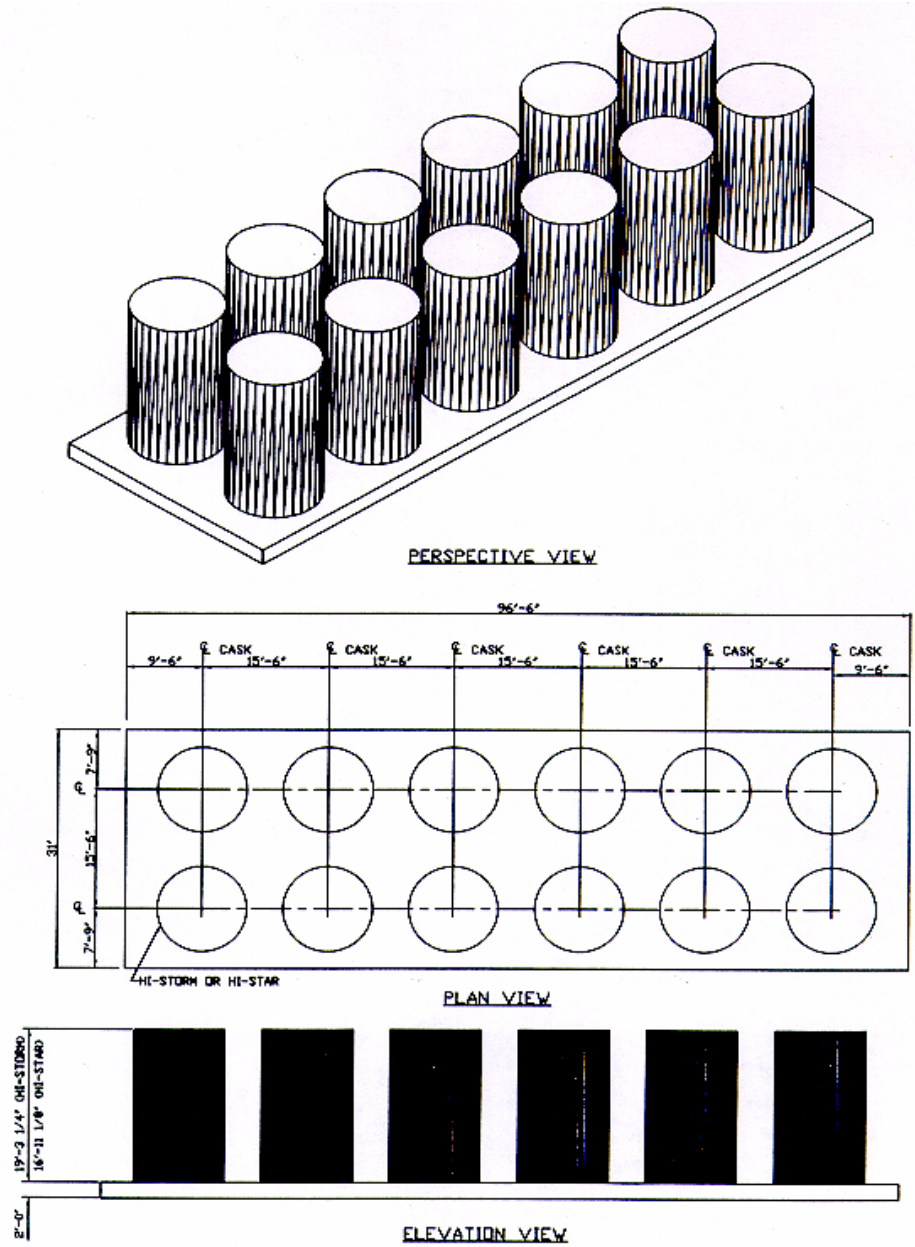


Figure 2.3: Typical HI-STORM 100 Cask Array on an ISFSI Pad at Hatch Nuclear Power Station  
 Note: 1ft = 30.48 cm

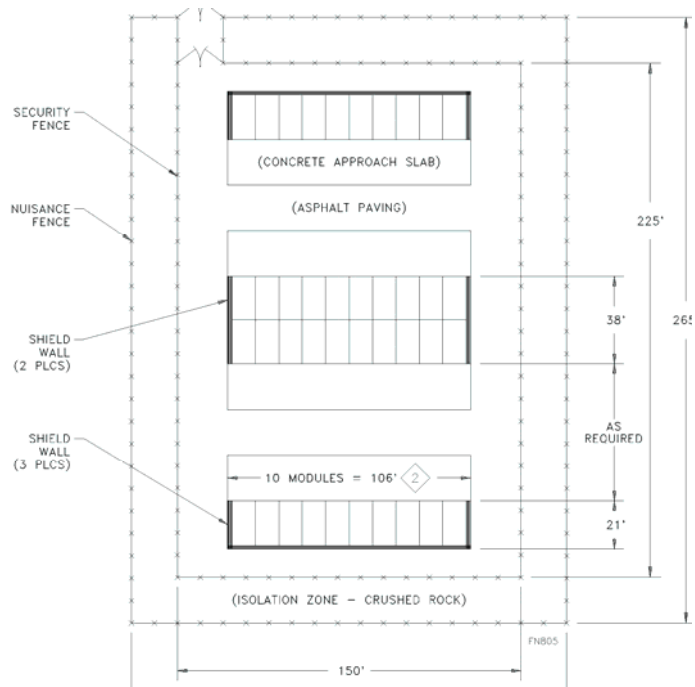


Figure 2.4: Typical ISFSI Layout of Horizontal Rectangular Modules

### 3. Coupled Finite Element Models

Because of the highly nonlinear nature of the cask response after the onset of sliding or uplift from the pad, it is difficult to apply appropriate methods to characterize the cask response. Realistically modeling the cask response is essential to determine the point at which the cask becomes unstable or collides with a neighboring cask. In the present work, nonlinear finite element analysis has been employed to characterize the full range of cask response. The details of the modeling approach used in this study will be described in this chapter.

#### 3.1 Description of Analysis Approach

##### 3.1.1 Coupled Modeling Methodology

The philosophy of the analysis effort has been to model the full nonlinear behavior of the freestanding cask system as realistically as possible. To that end, the freestanding cask, pad, and foundation are modeled as independent bodies, each capable of experiencing large independent movements relative to one another. Contact constraints are used to model realistically the interactions between these bodies.

The ABAQUS [2] finite element analysis program, Version 6.4, was used to perform these analyses. There are two major components of the ABAQUS program: ABAQUS/Standard, which uses an implicit solver, and ABAQUS/Explicit, which uses an explicit time integration approach. In this work, ABAQUS/Standard was used to apply the gravity load quasi-statically. Once the gravity load was applied, the analysis was re-started using the final state of the gravity load analysis, and ABAQUS/Explicit was used to analyze the effects of the seismic ground motion while retaining the gravity load. The explicit time domain analysis approach was employed in this work to handle the high degree of nonlinearity present in this problem. Explicit time stepping algorithms are typically used for modeling highly dynamic events of short duration. Very small time steps are used, and the accelerations at the previous time step are used to advance the solution to the current time step.

A solution for the contact constraints, which are an integral part of the problem at hand, can be extremely difficult using implicit methods. The explicit time stepping method was selected for this work because there was no need for an iterative solution of nonlinear equations, as is the case in the implicit methods typically used for analysis of structures under seismic events. Initial attempts were made to use an implicit procedure to perform the nonlinear analysis of the cask response due to earthquake loading, but obtaining a converged solution for this problem became extremely difficult once the cask began to move relative to the pad.

In the explicit method, the size of the time step is controlled by a stability limit, which is a function of the shortest amount of time required for a wave to traverse any of the elements in the model. This means that the time step is typically governed by the size of the smallest element in the model. As the size of the smallest element decreases, the critical time step also decreases, and the time required for the computation increases. For this reason, great care was taken to keep the smallest element as large as possible while still retaining accuracy of the model.

Figure 3.1 shows a finite element model representative of the physical configuration under investigation in this work. In this model, a cask rests on a concrete pad at the top center of a large foundation. Details of the models differ for the cylindrical casks and the rectangular modules selected for parametric analyses, but these models have much in common as discussed in the following subsections.

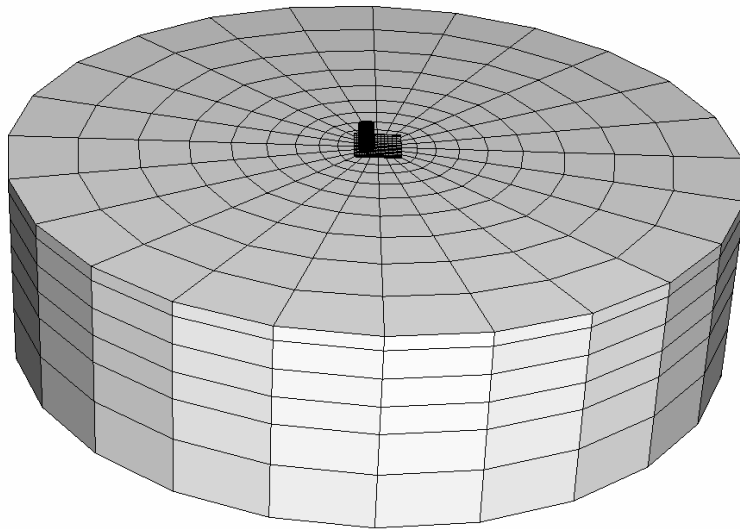


Figure 3.1: Typical Finite Element Model of Cask, Pad, and Foundation

### 3.1.1.1 Cask Submodel

In the case of the rectangular module model, the module was modeled using standard eight-noded reduced integration solid elements. However, the cylindrical cask was modeled as a rigid body. The rationale for these modeling approaches will be elaborated in the following sections.

### 3.1.1.2 Pad Submodel

Both types of cask designs rest on rectangular concrete pads. Although the dimensions of the pads used in the analysis models differ, a similar approach was used to model the pad in both cases. In explicit dynamic finite element analysis programs, the element library typically consists primarily of reduced integration elements. This is due to the fact that most of the computation time is spent in the element subroutines because there is no iterative solver. By using reduced integration elements with an hourglass control algorithm, the analysis time can be reduced significantly compared to the time required for fully integrated elements. Consequently, a minimum of approximately 4 or 5 layers of elements is required through the thickness of a body to avoid hourglassing problems in the computation.

The concrete pad is a relatively slender structure, with lateral dimensions much larger than the thickness dimension, which is 0.6–0.9 m (2–3 ft). If four layers of solid elements were to be used to model the pad, the dimension of the elements in the thickness of the pad would be sufficiently small to control the critical time step and increase the analysis time. In addition, a large number of elements would be required in the lateral dimension of the pad to maintain reasonable element aspect ratios to ensure the quality of analysis results. To circumvent these problems, the concrete pads are modeled using continuum shell elements. These special-purpose elements, available for the first time in ABAQUS Version 6.4, behave like shell elements in bending modes but have eight nodes with the appearance of conventional brick elements. Since the through-thickness dimension is modeled, these elements can capture the deformation through the shell thickness, unlike conventional shell elements. In the pad models, a single layer of continuum shell elements was used to model the pad, allowing the model to reasonably capture the physics of the problem with a minimum of computation time.

### 3.1.1.3 Foundation Submodel

The foundation was modeled as a cylinder comprised of horizontal layers of elements. Different sets of material properties were assigned to the foundation models for soft soil, stiff soil, and rock. Each of these three foundation types has material properties that vary with depth. The material properties of the elements in a given layer are uniform, and each layer in all of these models has material properties that reflect the properties of the soil at that depth. The seismic ground motion was applied at the foundation base.

In this study the top of the soil foundation was modeled as a flat surface with a concrete pad resting on its top surface. In many cask system designs, the concrete pad is embedded in soil, so that the top of the pad is level with the top of the surrounding soil. This embedment provides confinement, restricting lateral movement of the slab relative to the soil. This embedment was not explicitly modeled in the current work, but its lateral movement-resisting effect was approximated by increasing the coefficient of friction between the pad and the soil surface.

One of the challenging aspects of modeling the foundation is applying appropriate boundary conditions. In an idealized, infinitely wide stratified soil mass subjected to earthquake motions applied at the base, the displacements at any two points having the same vertical coordinate but differing horizontal coordinates should be equal at every time step. Because of this, the behavior of such a semi-infinite soil mass can be idealized as a one-dimensional soil column. If a structure is placed at the surface of this semi-infinite soil mass, there will be disturbances in the uniform displacement field in the region of the soil column near the structure due to the interaction between the soil mass and the structure. The effects of these local disturbances decrease as the distance from the structure increases because the waves radiating from the structure are damped out.

Ideally, the boundary conditions chosen for the finite element foundation model should allow for the foundation to behave globally as a one-dimensional soil column but allow for local soil-structure interaction effects in the region of the cask and the pad. As mentioned above, the ground motion is applied at the foundation base to allow for soil-structure interaction. A ground motion time history is initially specified for the surface. A deconvolution procedure, explained in detail in Section 3.1.5, is used to compute a time history of ground motion that, when applied to the foundation base, results in motion at the surface that approximates the initial specified surface ground motion. A fundamental assumption in the deconvolution procedure is that the foundation behaves as a semi-infinite layered medium and thus can be approximated as a one-dimensional soil column.

To approximate a semi-infinite soil mass while still accommodating local disturbances in the displacement field due to soil-structure interaction, the foundation was modeled as a large, layered cylinder. Multi-point constraints (MPC) were applied to tie together all of the nodes around the outside edge of a layer, as shown in Figure 3.2. One node on each layer was designated as a master node, and all of the other nodes on the outside boundary of the foundation on that layer were designated as slaves and constrained to have the same displacement as the master node.

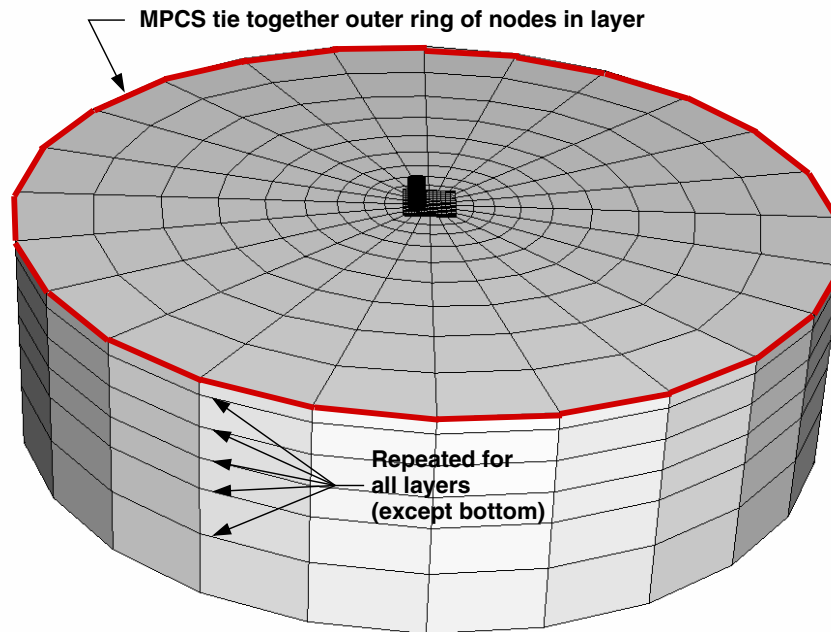


Figure 3.2: Multi-Point Constraints in Soil Foundation Layers

This approach allows for local disturbances in the region surrounding the cask and pad but forces the foundation to behave globally as a soil column. Shear deformations of the layers are allowed, but the MPCs prevent the column from deforming in a bending mode or expanding or contracting laterally. If the structure is removed and the foundation submodel is analyzed under an earthquake loading, all of the nodes in each layer have the same displacement at every point in time.

One issue often encountered in modeling semi-infinite media such as foundations is that waves can reflect from the boundary and cause undesirable effects in the region of interest. Infinite medium finite elements, which can be inserted at the boundary of the finite portion of the modeled medium, have been developed expressly for this purpose and are available in many general-purpose finite element analysis codes such as ABAQUS. These elements are designed to create “quiet” boundaries and not reflect waves back into the medium.

As part of this work, attempts were made to use such infinite elements at the boundaries, but it was found that when such boundaries were used, the ground motion computed at the surface had significantly different spectral characteristics from the specified surface ground motion. This is due to the fact that the infinite elements do not enforce the soil column constraints, so the column is able to deform in bending modes and expand and contract laterally.

To enforce soil column constraints while minimizing the effects of reflected waves, the approach taken in this work was to make the horizontal dimension of the soil column much larger than the dimensions of the structure to allow for waves radiating from the structure to be significantly damped out before they reflect back from the boundaries and reach the structure. A series of analyses were performed using varying dimensions of the soil column to determine the sensitivity of the response to those dimensions. These analyses indicated that the selected dimensions of the soil column are sufficiently large to not unduly affect the analysis results. The cylindrical shape was chosen for the foundation so that the

horizontal distance from the pad would be approximately the same in any direction. This shape also eliminates any effects that could be potentially caused by corners if a rectangular shape had been used.

It is important to remember that in addition to being reflected from the vertical edges that bound the foundation submodel in the horizontal direction, waves can be reflected from the base of the model, where the input motion is being applied. Since the horizontal dimensions of the foundation model are larger than the vertical dimension, the reflected waves are likely to come from the base rather than from the sides. Because of this, little benefit would be realized by increasing the lateral dimensions without also increasing the vertical dimension of the foundation submodel.

### **3.1.2 Nonlinear Frictional Contact at Interfaces**

Surface-based contact algorithms were used to prevent interpenetration between the cask and the concrete pad, and the concrete pad and the foundation. One of the most critical aspects of this analysis was correctly modeling these contact constraints. Using contact constraints allowed for a high degree of realism in modeling the cask motion. After the gravity load was applied, the cask and the pad, and the pad and the foundation are in full contact with each other. Until the point when the seismic ground motion is sufficiently high to cause uplift or sliding of these bodies relative to each other, they essentially behave as if they were bonded due to the presence of the gravity load and the friction at the contact interfaces.

Once uplift or sliding occurs, the cask, pad, and foundation move independently. The contact constraints govern the coupling between these bodies as they move relative to each other. The cask is free to lift up, rotate, and slide relative to the pad. Due to the fact that the gravity load is generally greater than the vertical acceleration caused by the ground motion, at least one point on the edge of cask base is typically in contact with the pad at any given time in the analysis. The contact constraints allow for the cask to move naturally, as governed by the motion applied at the base, and prevent penetration of the cask into the pad.

General-purpose finite element analysis codes such as ABAQUS typically offer the user a wide array of options in defining contact interactions. In ABAQUS/Explicit, for modeling surface-based contact, the user can choose between “general contact” and “contact pair” algorithms. General contact is a fairly new feature and allows for simple definition of contact interactions on a large number of surfaces with a minimum of user input. While the general contact algorithm permits some types of modeling that were not previously possible with the contact pair algorithm, there are still some options available in the contact pair algorithm that are not yet available with general contact. Because the cask model involves only two contact surfaces and maximum flexibility was desired with respect to contact options, the contact pair algorithm was used in this work.

ABAQUS employs a master/slave concept for contact interactions. In its simplest form, one of the two surfaces comprising a contact pair is designated as a master surface, and the other is designated as a slave surface. The contact algorithm checks for interpenetration of these two surfaces and adjusts nodal displacements to ensure that interpenetration does not occur. Figure 3.3 demonstrates the behavior of the master and slave surfaces. The surface designated as the master surface is comprised of element edges in two-dimensional analyses, or element faces in three-dimensional analyses. The slave surface is comprised of the nodes connected to the element faces that make up the surface. The slave nodes are constrained not to penetrate the master edges or faces. As shown in Figure 3.3, the nodes on the master surface are able to penetrate the edges or faces that make up the slave surface.

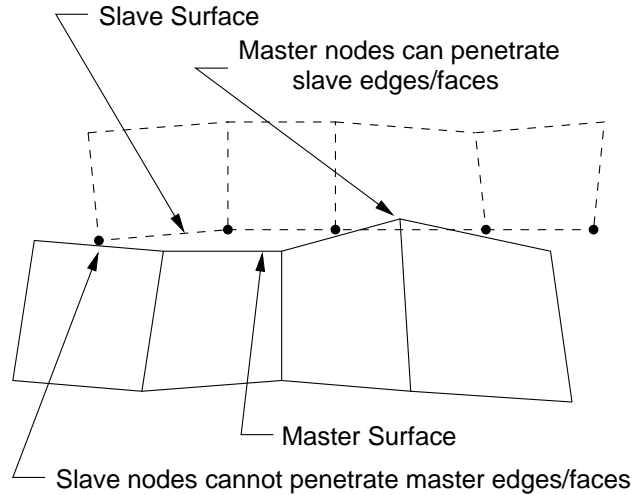


Figure 3.3: Master/Slave Contact Concepts

By default, ABAQUS/Explicit uses a balanced master/slave approach. This approach takes the average of the solutions obtained by setting one surface as a master and the other as a slave, and then reversing them. In this work, it is advantageous to use pure master/slave contact for both the cask/pad and the pad/foundation interface. Figure 3.4 shows an idealized diagram of the finite element meshes of the various submodels and the master/slave assignments used in this work.

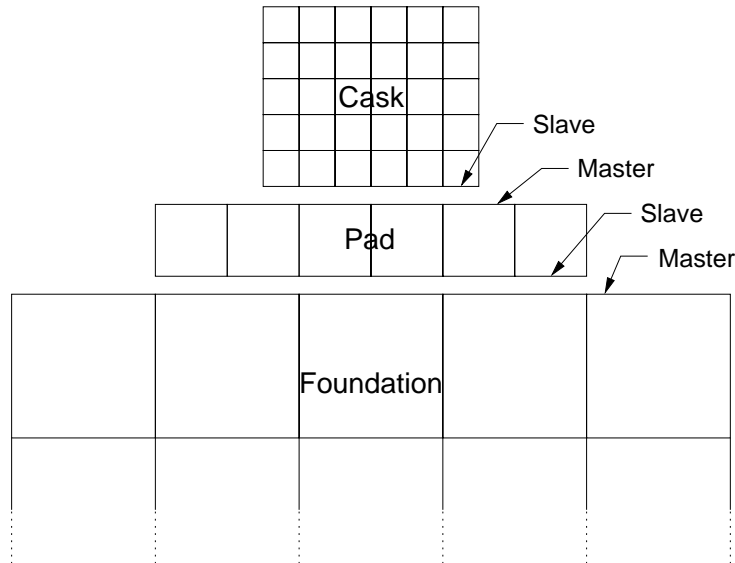


Figure 3.4: Idealized Mesh with Master/Slave Surface Assignments

There are three primary reasons for choosing this master/slave option. The first is that it is important for the corner of the cask not to penetrate the pad, and for the corner of the pad not to penetrate the foundation. Since the nodes on slave surfaces cannot penetrate master surfaces, the nodes at the corners of the cask and pad cannot penetrate the element faces on the top surfaces of the pad and foundation, respectively. The second reason is that if the elements adjacent to a slave surface have significantly more mass than the elements adjacent to its master counterpart, contact chatter can result. This high frequency noise can potentially resonate within the bodies and eventually result in an unrealistic response. In the models used in this work, the elements in the foundation are larger than those in the pad, and the elements

in the pad are larger than those in the cask. Pure master/slave contact in the chosen configuration results in minimal contact chatter. Finally, in the case of the cylindrical cask, the cask is modeled as a rigid body. In ABAQUS/Explicit, surfaces attached to rigid bodies must be designated as slave surfaces.

There are three types of sliding formulations in the ABAQUS/Explicit code: finite, small, and infinitesimal. The finite sliding formulation is the most general and allows for large changes in the position of the contacting surfaces in relation to each other during the computation. This allows for pairs of element faces and nodes that come into contact to change as the analysis proceeds. In the small and infinitesimal sliding formulations, assumptions are made that the nodes and element faces that are initially paired up will remain that way throughout the computation. This saves the computational cost of performing the search for paired nodes and element faces at every step if the relative movement of the surfaces is known to be small prior to the analysis. Since the freestanding cask can clearly experience large motions relative to the pad, the finite sliding formulation is used for the cask/pad interface. The pad experiences small motions relative to the top surface of the foundation in the cases studied here. The small sliding formulation provides an adequate approximation at that interface, but the savings in computational cost obtained by using that formulation have been shown to be very minimal in this case. Therefore, the finite sliding formulation was also used for the pad/foundation interface in the models used in this study.

In addition to the options mentioned above, the ABAQUS/Explicit user must choose between the kinematic and penalty method of contact constraint enforcement. The kinematic constraint algorithm uses a predictor/corrector approach to enforce contact constraints. The deformed configuration is initially computed without regard to contact constraints. If any of the contact constraints are violated, resisting forces are computed to oppose the penetration so that if they were applied during the increment, the contact constraint would be exactly satisfied. These forces are then distributed to the nodes connected to the faces comprising the master surface, and adjusted accelerations are computed so that the contact constraint is satisfied at that loading increment.

The penalty method of satisfying contact constraints applies equal and opposite forces to the two contacting surfaces that are linear functions of the penetration distance. This is conceptually similar to introducing stiff springs between the two surfaces. This method allows for the solution of a wider variety of problem types than can be solved using kinematic contact. To minimize errors due to penetration, it is important that the penalty stiffness be set as high as possible. Setting this stiffness high comes at a cost, however, because in the explicit time integration method, the critical time step is controlled by the stiffest element. The contact constraint essentially behaves as an element, so it can potentially control the time step. In ABAQUS/Explicit, the penalty stiffness is automatically computed to be as stiff as possible while having a minimal effect on the critical time step. The user has the option of specifying a multiplier that is applied to this automatically computed stiffness.

While the kinematic contact formulation allows for shorter execution times, it was found that the models are more prone to experience high frequency chatter at the interfaces with this option. This can result in an unreasonably large cask response to a seismic event. For this reason, the penalty contact formulation was used in the present work. A multiplier of 3 was applied to the automatically-computed penalty stiffness to decrease the potential negative effects of contact penetration while still minimally affecting the critical time step.

Finally, the constitutive behavior of the interacting surfaces must be defined. A simple Coulomb friction model is used in this work. If the shear stress on the interface is less than the product of the normal compressive stress and the friction coefficient, the surfaces are not allowed to slide relative to each other. Once the shear stress exceeds this limit, the surfaces can slide. A single coefficient of friction was used for both static and kinetic friction.

### 3.1.3 Representation of Damping

The method used to represent structural damping is an important consideration in the seismic modeling of the cask system. Since the foundation is assumed to behave as a linearly elastic material, there are no inherent energy dissipation mechanisms. Rayleigh damping is imposed on the foundation material to approximate the natural energy dissipation mechanisms. In Rayleigh damping, the damping matrix,  $\mathbf{C}$ , is formed by summation of the mass matrix,  $\mathbf{M}$ , and the stiffness matrix,  $\mathbf{K}$ :

$$\mathbf{C} = \alpha \mathbf{M} + \beta \mathbf{K} \quad (3.1)$$

The factors  $\alpha$  and  $\beta$  are used to control the amounts of mass-proportional and stiffness-proportional contributions to the damping matrix. The mass-proportional damping has a greater effect on the lower frequency modes of a structure, while the stiffness-proportional damping has its greatest influence on higher frequency modes. Typically, the values of  $\alpha$  and  $\beta$  are calibrated so that the desired level of damping is achieved for high and low frequency modes chosen by the analyst.

The application of an explicit time integration method presents some special challenges regarding damping. Contrary to intuition, introducing damping decreases the critical time step, making the analysis take longer to complete. In the presence of damping, the critical time step,  $\Delta t_{crit}$ , is computed as:

$$\Delta t_{crit} = \frac{2}{\omega_{max}} \left( \sqrt{1 + \xi_{max}^2} - \xi_{max} \right) \quad (3.2)$$

where  $\omega_{max}$  is the frequency of the highest frequency mode of the structure and  $\xi_{max}$  is the fraction of critical damping acting on that mode. It can be seen that an increase in the damping on the highest frequency mode can dramatically decrease the stable time step. Since mass-proportional damping has its greatest effect on low frequency modes, introducing this type of damping has little effect on the critical time step, but introducing even a small amount of stiffness-proportional damping can significantly decrease the critical time step. It should be noted that the ABAQUS/Explicit automatically introduces a small amount of bulk viscosity to provide damping against high-frequency vibrations.

Only mass-proportional damping was used in the parametric analyses because of the issues discussed above. The mass-proportional damping was applied to the foundation but not to the cask or the pad. Some analysis cases were executed using the stiffness-proportional damping, and analysis results indicate that the cask response was affected very little by the stiffness-proportional damping, while the analysis time increased significantly. The mass-proportional damping has an effect analogous to that of air friction. If such damping were applied to the cask or pad, which are independent bodies, it would limit their absolute motion. If high enough values of mass-proportional damping were applied to these bodies, they would remain essentially stationary as the foundation moves beneath them.

The target percentages of critical damping for the various layers of the foundation were computed to generate values compatible with the strains that occur with an earthquake conforming to the NUREG/CR-0098 spectral curve shape with a peak ground acceleration of 0.25 g, as described in Appendix I. These damping ratios are shown graphically for the soil profiles used in Figure 3.5. For each of the three foundation types, the fundamental frequency of an idealized one-dimensional soil column is computed, and the mass-proportional damping coefficient,  $\alpha$ , is computed for each of the layers to result in the target percentage of critical damping for that layer.

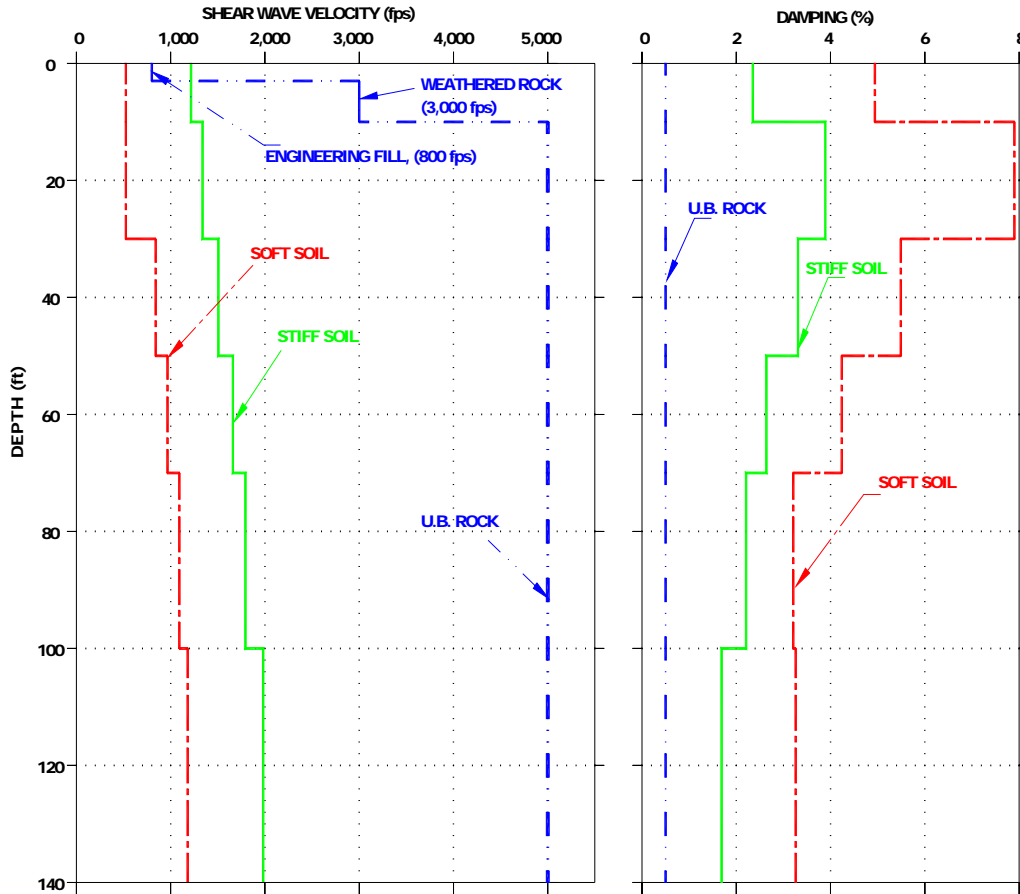


Figure 3.5: Soil Profiles Used in Parametric Deconvolution Site Response Analyses

### 3.1.4 Treatment of Seismic Ground Motions

The strategy for developing input ground motions for the coupled model has been geared toward supporting the NRC staff in the safety review of cask design licensing applications, which may cover a wide range in geographical regions, including the seismically active Western United States (WUS) and the less active Central and Eastern United States (CEUS).

In addition to varying levels of Peak Ground Acceleration (PGA) shaking levels, the ground motion characteristics from cask design licensing applications may contribute to a wide range of response spectral shapes to cover different seismological conditions between the WUS and the CEUS. Recent seismological studies conducted for the CEUS suggest a much lower shaking level for long period ground motions as compared to strong ground motion observed in historical data recorded in the WUS.

Differences in soil conditions, including soil versus rock site conditions, would also contribute to variations in ground motion characteristics and would especially account for differences in terms of spectral shapes. As a result of the wide range of variations, there is a need to conduct dynamic response analyses for a large number of cases of input motion conditions including varying PGA levels scaling to different response spectral shapes.

This project emphasized documenting in the project library a sufficiently wide range of cask response results, which would in turn allow cask design licensing applicants to compare the ground shaking

intensity to the range of input motion characteristics based on their response spectra. The resultant response solutions from the appropriate input motion can then be used for determining the response level of the specific design of a dry cask system.

In deciding the scope of the parametric study, three spectral shapes were selected: (1) NUREG/CR-0098 spectral shape [6], (2) Regulatory Guide 1.60 spectral shape [7] and (3) CEUS generic site spectral shape [8]. For each selected spectral shape, five sets of spectrum-compatible acceleration time histories were developed for supporting the parametric study. Further discussions on background information on the choice of the three spectral shapes and the number of sets of input ground motions for various PGA levels and spectral shapes are discussed in Section 4.1.

As previously discussed, the ground motions were input at the foundation base of the coupled model. However, cross-comparison of input motions between the project library with submittals from specific applications would be made in terms of free-field ground-surface (outcrop) motions, which would be different from the expected shaking intensity at the base of a foundation column. To address this issue, the first step was to develop the required time histories of ground motion for the conventional ground-surface outcrop condition to facilitate cross comparison to design ground motion criteria for site specific applications. The second step was to perform deconvolution analyses to generate input ground motions that would be appropriate as prescribed input ground motions to the foundation base of the coupled model. Additional discussions on the deconvolution procedures are presented in the following section.

### **3.1.5 Deconvolution Procedure**

Coupled response models consisting of the cask, pad, and foundation were developed in this study in order to incorporate soil-structure interaction effects. The presence of a foundation in the coupled response model requires the application of seismic motions, which are traditionally recorded and defined at the ground surface, at the foundation base. A deconvolution procedure was thus developed to generate input seismic motions based on the target surface ground motions in such a way that when the seismic motions are applied at the base of the foundation, the resulting motion at the top of the foundation is approximately the same as the original desired surface motions. The ground motions at the surface are different from the target motions in the immediate vicinity of the structure due to the soil-structure interaction effects, but the surface motions (measured at a point in the model on the surface of the foundation sufficiently far from the structure, or at the surface of a model of the foundation without the structure present) will be approximately equivalent to the original prescribed surface motions. Idriss and Seed [16] and Schnabel et al. [17] provide detailed discussions on the deconvolution procedure.

Concepts in the deconvolution analysis were originally developed as an extension of the classical site response analysis. The underlying principle in site response has been based on the vertically propagating body wave, where horizontal and vertical component ground motions are governed by vertically propagating shear and compression waves, respectively. Typically, the objective in conventional site response analyses was to account for how localized soil properties would modify ground-motion shaking levels as the earthquake propagates from a deep seismogenic zone (typically at tens of kilometers) up to the ground surface where most structures are located. Site response analysis results are generally used in conjunction with other seismological information (e.g., earthquake event magnitude and distance from seismic source to project site) for defining the appropriate ground-shaking level for design purposes.

Site response analyses are commonly conducted by using a widely distributed computer program, SHAKE91 [13], which models a soil column by way of a low-strain soil modulus profile in conjunction with a set of strain-dependent stiffness modification and damping-ratio functions to develop a set of strain-compatible soil properties (i.e., soil modulus and damping ratio profiles). After developing the appropriate equivalent linear soil stiffness and damping, transfer functions are calculated and then applied

to the expected bedrock motion at a depth to derive the ground-surface outcrop motion for design analysis of near surface structures. The concept of deconvolution is essentially making an inverse of the transfer functions and then applying them to a set of ground-surface outcrop motions to develop any ‘within’ motion representing the ground motion characteristics at a given depth. In this parametric study, the deconvolution analyses were performed using the SHAKE91 program.

In the context of this project, the deconvolution site response analysis was conducted so that the inherent site response solution implied by the dry cask model would reproduce the intended target benchmark free-field outcrop ground-shaking level. To achieve this objective, it is very important that the soil properties used in the deconvolution analysis be consistent with those used in the coupled-cask analysis model. In support of the parametric analyses, deconvolution solutions for three sets of soil properties have been obtained, including a so-called benchmark stiff as well as a soft-soil profile and an upper-bound rock profile as summarized in Figure 3.5. The top 0.9 m (3 ft) of the rock profile reflects the general practice of placing a thin layer of engineering fill followed by 2.1 m (7 ft) of a softer weathered rock, a condition that is expected to be prevalent at most rock sites. Additional details and background information leading to the selection of the adopted soil properties are included in Appendix I.

The equivalence of the original target surface motion and the motion obtained at the surface of a finite element model of the soil column was initially verified using a two-dimensional finite element model of the soil column using the DYNFLOW [18] finite element analysis program. Once the full three-dimensional model of the cask, pad, and soil had been developed, the cask and pad were removed from the soil column model, and the response at the surface of that finite element model was calculated, as described in Section 5.1.3.

In summary, deconvolution analyses have been performed using the referenced ground-surface spectrum-compatible motions as input for deducing the appropriate input motion at the foundation base of the coupled models. The same set of soil parameters (i.e., soil modulus and damping) are used in both the deconvolution analyses and the coupled cask responses analyses to maintain the compatibility in soil properties between the deconvolution and the coupled-model response solutions. Deconvolution analyses have been conducted for three sets of soil stiffness properties that can then be used to match soil properties in future licensing applications.

The soil models utilized in the coupled response model for this study are implicitly based on equivalent linear elasto-dynamic modeling approaches. It is not the intention of this study to address permanent nonlinear near-field soil yielding and deformation shear failure or liquefaction effects. The profiles presented in Figure 3.5 were strain compatible to shaking corresponding to spectrum-compatible time histories with a PGA of 0.25 g scaling to the NUREG/CR-0098 target spectral shape. The same profiles were used for input motions conforming to other spectral shapes and to other PGA values at 0.6 g, 1.0 g and 1.25 g. The decision was to minimize confusion for comparing dry cask response at different inertial input levels. Furthermore, the implication of the strain-compatible soil profile properties is relatively minor because of our approach to calibrate and to compare shaking at the ground surface. Also, some of the cask response solutions at the higher level of ground shaking (e.g., at 1.0 g and 1.25 g) are merely intended to approximate potential cask responses qualitatively at extreme levels of ground shaking. These high ground-motion levels would be very unlikely be encountered in future licensing situations.

One of the major contributions in this project relates to the advancement of the state-of-the-art soil-structure interaction analysis procedure to beyond the traditional frequency domain elasto-dynamic approaches due to the importance of the base contact separation issues on the cask response. The subject of site response and wave scattering has traditionally been treated by frequency domain computer codes such as SHAKE [17] or SASSI [12]. For past 20 years, these programs have been used in the nuclear power plant industry for seismic designs of containment systems, which are typically founded on

competent soil conditions. In earlier days, such approaches, which often permit substructuring to economize computer resources, were necessary. Because of the advancement of computer technologies, time-domain structural engineers prefer modeling the total soil-foundation-superstructure system. It is highly desirable that the wave propagation and scattering analyses be conducted in time domain, or in a numerical platform that is commonly used for global structural response analyses. This will allow both groups of specialists (geotechnical professionals who are familiar with wave propagation analyses and structural engineers performing the global structural model) to work simultaneously on the same computer platform to contribute both their expertise to the total problem. In many major seismic response projects (e.g., in highway bridges) such a time-domain total-system approach is preferred because it allows the structural engineers to capture various nonlinear response phenomena. Another major benefit is that it minimizes the amount of work for data transfer and the potential for error arising from solutions from separate numerical platforms.

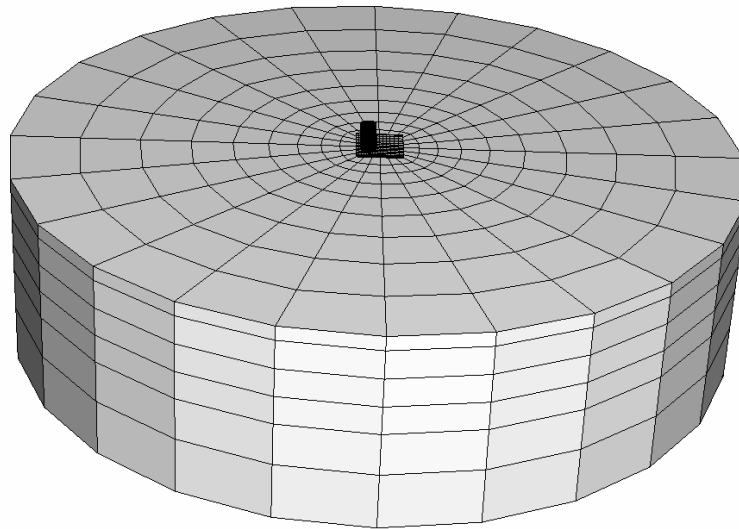
In order to advance the time-domain approach for solving wave propagation and wave scattering problems, these new approaches need to be verified to the classical proven approaches (e.g., solutions from SHAKE and SASSI). Appendix II presents some of these verifications and various sensitivity analyses for developing the appropriate input motions to a finite-domain finite-element model, and for minimizing wave reflection and refraction at the model's side boundaries. Numerical integration schemes and implementation of Rayleigh damping parameters are discussed. Careful examination of a wave traveling through the bottom boundary would allow proper modeling of the half-space below the region of interest.

## **3.2 Details of Coupled Models**

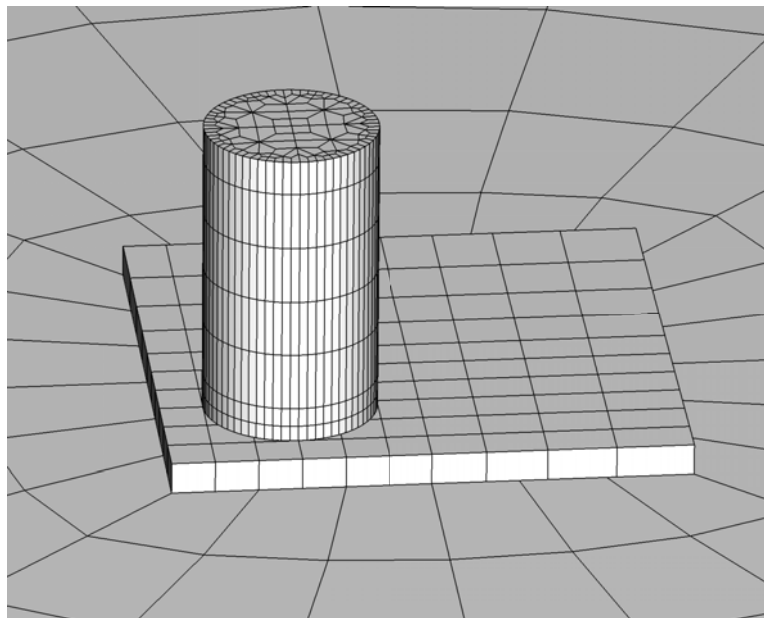
### **3.2.1 Vertical Cylindrical Cask**

In typical vertical cylindrical cask applications, an array of casks rests on a single concrete pad. The casks are typically arranged in two rows, as illustrated in Figure 2.3. For the parametric analyses performed in this study, the analysis model involves a single cask resting on one quadrant of a pad that can accommodate a 2x2 array of casks. Figure 3.6 shows views of the entire finite element model of the cylindrical cask, pad, and foundation.

Modeling a single cask instead of the whole array of casks simplifies the analysis procedure considerably and reduces the time required to run the analyses. To assess the validity of this simplified approach, a model very similar to that shown here was developed with four freestanding casks on a pad. In the cases that were studied with the four-cask model, the four casks exhibited responses that were very similar to those of the single cask under the same conditions. In those cases, the single cask had a higher response. Based on those analyses, it was determined that the single cask model provides a reasonable approximation of the response of a cask in a larger array.



(a) Overall Model



(b) Detailed View of Region of Model with Cask and Pad

Figure 3.6: Finite Element Model of Cylindrical Cask, Pad, and Foundation

### 3.2.1.1 Cask Submodel

Modeling the cylindrical cask in the framework of the finite element method with explicit time integration presents some challenges because of the cask geometry. In an upright cylindrical cask, the edge of the cask base contacting the pad is curved. When the cask begins to roll along the edge of its base, the discretization of this edge into a series of nodes connected by straight lines can potentially cause errors. As the number of elements around the edge of the base is increased, these errors decrease. An undesirable side effect of this modeling scheme is that to obtain a reasonable level of refinement along this curve, the edge lengths of the elements along the curve become the shortest of all elements in the model, and these elements control the size of the critical time step, and hence, the analysis time.

Figure 3.7 shows a top view of the finite element mesh for the cylindrical cask. A surface mesh was initially generated on the cask base. This surface mesh was then swept up through the cask to generate a solid mesh comprised of seven layers of three-dimensional, eight-noded hexahedral elements. The cross section of the cylinder is assumed constant through its height, so slices of the mesh taken perpendicular to the vertical axis of the cask at different heights are always the same. In the picture of the cask top, it can be seen that there are 64 elements around the edge of the cask. The mesh is more refined around the edge than in the middle to allow for fewer elements to be used where a high degree of refinement is not needed.

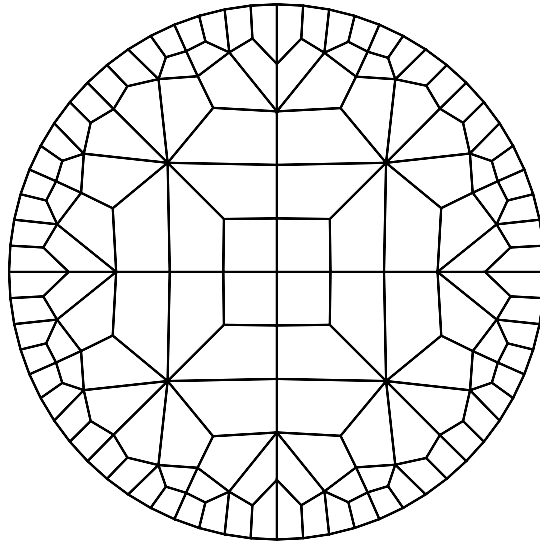


Figure 3.7: Top View of Cylindrical Cask Mesh

#### **3.2.1.1.1 Structural Features**

The cylindrical cask system usually consists of a multi-purpose canister and an overpack. The same overpack can be used with a number of different canisters, which have different designs to accommodate various types of spent fuel. The overall properties of the loaded overpack vary depending on the type of multi-purpose canister. For this study, it was assumed that the cylindrical cask contains a fully loaded multi-purpose canister, which is used for the storage of spent fuel from a Boiling Water Reactor (BWR). This cask design was chosen because the overall cask system is slightly heavier and has a slightly higher center of gravity than other alternatives. Therefore, the chosen cask design should result in the highest response of the available designs, but the results should be applicable to all designs because the differences are minor.

#### **3.2.1.1.2 Material Properties**

As mentioned above, the cask mesh is composed of seven layers of solid elements. Material properties were assigned to these layers to approximate the overall mass properties of the loaded cylindrical cask. The internals of the cask are complex but have little effect on the seismic response of the cask. The mass and stiffness properties of the cask internals were approximated and averaged out in the horizontal layers. The densities of the layers were iteratively adjusted to obtain a reasonable approximation of the overall mass, center of gravity height, and rotational moments of inertia of the cask. Table 3.1 shows the material properties for this cask design. The top and bottom element layers were assigned unique material properties, while the middle five layers were all assigned the same properties.

Table 3.1: Cylindrical Cask Finite Element Model Material Properties by Layer

Layer	Layer Thickness	Elastic Modulus	Poisson's Ratio	Density
1	0.203 m (8.0 in)	27.8 GPa (4031 ksi)	0.2	3379 kg/m <sup>3</sup> (211 lb/ft <sup>3</sup> )
2-6	4.994 m (196.6 in)	27.8 GPa (4031 ksi)	0.2	2984 kg/m <sup>3</sup> (186 lb/ft <sup>3</sup> )
7	0.676 m (26.6 in)	27.8 GPa (4031 ksi)	0.2	3850 kg/m <sup>3</sup> (240 lb/ft <sup>3</sup> )

Table 3.2 shows a summary of the mass properties of the cask submodel using the finite element mesh with the material properties listed in Table 3.1. For the purposes of the moment of inertia calculations, the  $x$  and  $y$  axes are oriented in the horizontal plane, and the  $z$  axis points in the vertical direction.

Table 3.2: Summary of Cylindrical Cask Finite Element Model Properties

Height of Center of Gravity	3.002 m (118.2 in)
Base Radius	1.683 m (66.25 in)
Overall Height	5.874 m (231.25 in)
Weight	161948 kg (357033 lb)
Moment of Inertia $I_{xx}$ , $I_{yy}$	$6.36 \times 10^5$ kg-m <sup>2</sup> ( $2.17 \times 10^9$ lb-in <sup>2</sup> )
Moment of Inertia $I_{zz}$	$2.36 \times 10^5$ kg-m <sup>2</sup> ( $8.08 \times 10^8$ lb-in <sup>2</sup> )

### 3.2.1.1.3 Rigid Cask Model

As mentioned in Section 3.2.1.1, modeling an upright cylindrical cask presents challenges because the elements around the cask boundary control the critical time step, resulting in long run times for the analysis. With the original cask model used in this study, the long run times dictated by these elements prohibited completing the large number of parametric analyses in a practically reasonable schedule. To overcome this problem, the cask was treated as an element-based rigid body. The ABAQUS code allows groups of elements to be treated as rigid bodies rather than elastic bodies with a very minor change to the input file. In this setting, the mass properties of the elastic material are used, but the material is no longer able to deform. Since the rigid body behavior of the cask is much more important than its deformation, this provides a reasonable approximation of the cask response.

When the cylindrical cask is treated as a rigid body, the cask elements no longer govern the critical time step. The thickness of the concrete pad becomes the controlling factor for the critical time step. The analysis time is reduced by approximately a factor of four by simulating the cask as a rigid body.

It is important to mention that initial analysis runs performed using the rigid cask model sometimes produced a higher than expected cask response, especially when a very stiff soil profile was used. The cause of this problem was that the default critical time step chosen by the ABAQUS code was too large for this particular model. The user has the ability either to control the analysis time step directly or to specify a multiplier to scale the automatically chosen value. It was found that using a multiplier to force the program to use a time step 50% the size of the automatically chosen value results in a stable solution. A convergence study indicated that further reducing the time step did not significantly change the results.

### 3.2.1.2 Concrete Pad Submodel

As mentioned above, the square reinforced concrete pad beneath the cylindrical cask is large enough to accommodate a 2x2 array of casks. The pad is 0.610 m (2.0 ft) thick and 10.06 m (33 ft) wide. The cask is positioned at the center of one quadrant of the pad. Figure 3.8 shows a detailed view of the mesh for the pad with the highlighted quadrant where the cask is positioned. In this figure, the element edges of the cask base are shown with light lines to differentiate them from the pad elements, the edges of which

are shown with dark lines. With these pad dimensions and positioning of the cask on the pad, the closest distance from the edge of the cask in its initial position to an edge of the pad is 0.8319 m (32.75 in). In earlier revisions of the model, the dimensions of the pad were smaller, but cases were encountered where the cask partially slid off the pad during the course of the analysis. The larger dimensions were chosen to ensure that the cask would remain on the pad except for the cases when it tips over. The dimensions of a pad in an actual application would be governed by the expected amount of sliding.

In Figure 3.8, the pad is modeled with a single layer of continuum shell elements. In the quadrant where the cask is located, these elements have lateral dimensions of 0.838 m (33 in). The mesh is coarsened slightly in the other three quadrants of the pad to reduce the model size. The reinforced concrete pad material is assumed to be linearly elastic, with an elastic modulus of 24.9 GPa (3605 ksi), and Poisson's ratio equal to 0.2. The density of the pad material is 2792 kg/m<sup>3</sup> (174 lb/ft<sup>3</sup>).

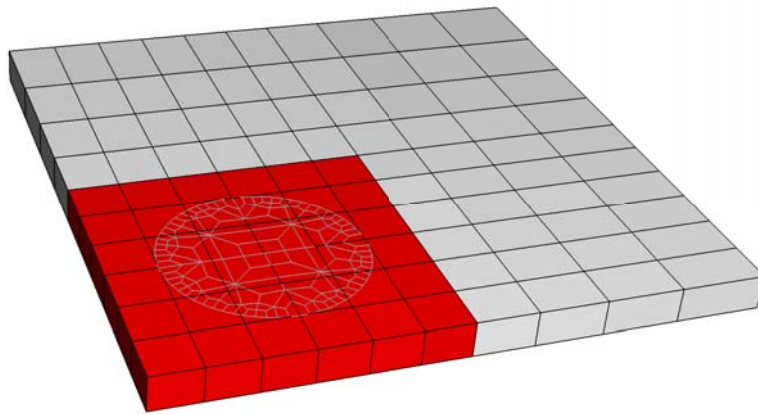


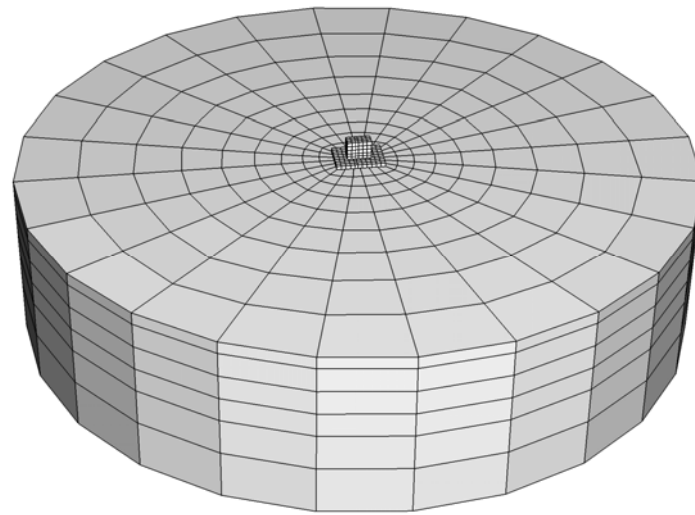
Figure 3.8: Detailed View of Pad for Cylindrical Cask

### 3.2.2 Rectangular Module

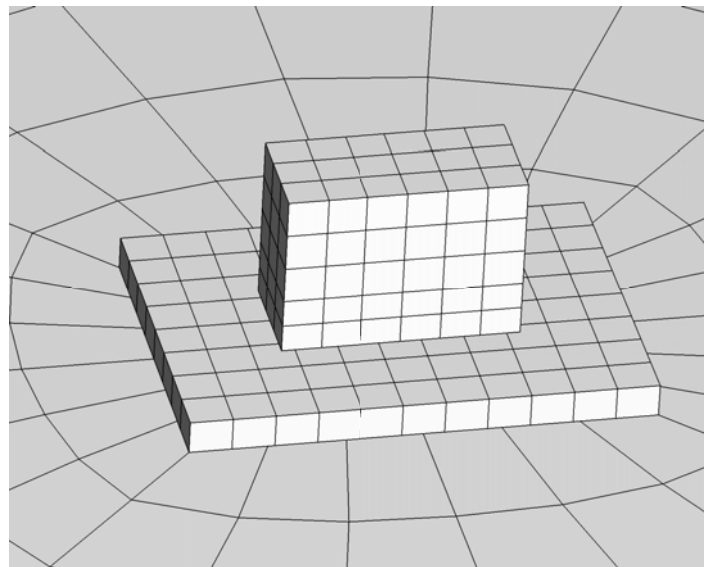
As illustrated in Figure 2.4, the rectangular modules are arranged in either a single row or pairs of rows. The side and rear walls of the rectangular modules are not thick enough to offer adequate shielding by themselves. There is not an issue if modules are placed side-by-side or back-to-back, but additional shielding walls must be placed at the ends of rows or along the backs of the modules if a single row configuration is used. There are 0.152-m (6-in) gaps between the sides of adjacent casks in rows and between the first or last cask in a row and the shield wall.

Because of these shielding considerations, a single rectangular module would never stand in isolation. For performing the parametric analyses, however, a relatively simple, bounding configuration was needed. A single module is more likely to tip over than a row of module, and would behave in approximately the same way as a row of modules in sliding. Therefore, for the parametric analyses, a single module was modeled with an attachment of the shield wall section.

Figure 3.9(a) shows a view of the overall model of the rectangular module with the pad and the foundation. A detailed view of the region around the module and pad is shown in Figure 3.9(b).



(a) Overall Model



(b) Detailed View of Region of Model with Module and Pad

Figure 3.9: Finite Element Model of Rectangular Module, Pad, and Foundation

### 3.2.2.1 Module Submodel

#### 3.2.2.1.1 Structural Features

Similar to the cylindrical cask system, the rectangular module system is comprised of a sealed canister containing spent fuel rods. The canister is inserted into a shielding overpack. As can be seen in the cut-away view of the module shown in Figure 2.2, the cylindrical cask is slid horizontally into a rectangular overpack. The rectangular module system can also accommodate a number of different types of canisters, which are used for different purposes. There are two different lengths of the rectangular modules. One type of module is 0.254 m (10 in) deeper than the other to accommodate longer canisters. For the analysis here, the shorter type of module is considered because it is more likely to be susceptible to tipping. The length difference has a negligible influence on the results because the cask is far more susceptible to tipping with the shorter dimension. The analysis results indicate only negligible rotations in the long dimension.

For the parametric analyses, the module is assumed to be loaded with the canister that contains spent fuel from Pressurized Water Reactor (PWR) plants. This is the heaviest of the canisters that can fit in the shorter module used in these analyses.

### 3.2.2.1.2 Material Properties

Similar to the cylindrical cask system, the rectangular module system is modeled with horizontal layers of solid elements whose densities are iteratively adjusted to achieve a reasonable approximation of the overall mass properties of the module. Since the overall shape of the module is a right rectangular prism, the mesh is much simpler than that for the cylindrical cask. The model used in the parametric analyses is fairly coarse. A more refined model of the module and pad was investigated, but a comparison of the results with this coarse model showed that the two models produced nearly identical displacement histories. The shortest edge length of the module elements is roughly equivalent to the pad thickness, so the module elements do not cause a decrease in the critical time step, as was the case for the elastic cylindrical cask. Thus, there was no need to use a rigid approximation of the rectangular module to save analysis time.

The rectangular module system is modeled with five layers of hexahedral continuum elements. Table 3.3 shows the properties assigned to these layers of elements. In the rectangular module design, the lower part of the module is essentially hollow and contains a steel support frame for the canister. The module is approximated as a solid block in the model. The elastic modulus and density of the lower layers are reduced to account for this hollow area at the module base.

Table 3.3: Rectangular Module Finite Element Model Material Properties by Layer

Layer	Layer Thickness	Elastic Modulus	Poisson's Ratio	Density
1	0.762 m (30 in)	18.1 GPa (2620 ksi)	0.2	1412 kg/m <sup>3</sup> (88.1 lb/ft <sup>3</sup> )
2	0.762 m (30 in)	11.4 GPa (1653 ksi)	0.2	749 kg/m <sup>3</sup> (46.7 lb/ft <sup>3</sup> )
3-4	2.032 m (80 in)	27.8 GPa (4031 ksi)	0.2	2620 kg/m <sup>3</sup> (164 lb/ft <sup>3</sup> )
5	1.016 m (40 in)	27.8 GPa (4031 ksi)	0.2	2016 kg/m <sup>3</sup> (126 lb/ft <sup>3</sup> )

Table 3.4 shows a summary of the mass properties of the finite element model of the rectangular module. As was done with the cylindrical cask, the densities of the material layers in the module were adjusted iteratively to obtain reasonable approximations of the overall mass, center of gravity height, and rotational moments of inertia. For the reported moments of inertia, the  $x$  axis points in the horizontal direction normal to the long side of the module, the  $y$  axis points in the horizontal direction normal to the short side of the module, and the  $z$  axis points in the vertical direction.

Table 3.4: Summary of Critical Rectangular Module Finite Element Model Properties

Height of Center of Gravity	2.54 m (100 in)
Width	2.95 m (116 in)
Depth (with Shield Wall)	6.40 m (252 in)
Overall Height	4.57 m (180 in)
Weight	170,098 kg (375001 lb)
Moment of Inertia $I_{xx}$	$8.85 \times 10^5$ kg-m <sup>2</sup> ( $3.02 \times 10^9$ lb-in <sup>2</sup> )
Moment of Inertia $I_{yy}$	$4.22 \times 10^5$ kg-m <sup>2</sup> ( $1.44 \times 10^9$ lb-in <sup>2</sup> )
Moment of Inertia $I_{zz}$	$7.63 \times 10^5$ kg-m <sup>2</sup> ( $2.61 \times 10^9$ lb-in <sup>2</sup> )

### 3.2.2.2 Concrete Pad Submodel

The concrete pad beneath the rectangular module is modeled in a manner similar to the pad for the cylindrical cask. The pad is 0.914 m (3 ft) thick and has lateral dimensions of 9.04 m (29.7 ft) x 12.5 m (41 ft). The module is placed at the center of the pad, and there is 3.048 m (10 ft) between the module and the edge of the pad in both lateral directions. The pad is modeled with a single layer of continuum shell elements. These elements are 0.914 m (36 in) thick and have lateral dimensions of 1.13 m (44.5 in) x 1.14 m (44.7 in). As with the pad beneath the cylindrical cask model, the material for this pad is assumed to be linearly elastic, with an elastic modulus of 24.9 GPa (3605 ksi), Poisson's ratio of 0.2, and density of 2792 kg/m<sup>3</sup> (174 lb/ft<sup>3</sup>).

### 3.2.3 Foundation Submodel

#### 3.2.3.1 Structural Features

Basic descriptions of the modeling technique for the foundation have been provided in previous sections. The foundation submodel meshes for the cylindrical cask and rectangular module models differ slightly because they are configured so that element edges are aligned with the edges of the pads, which have different dimensions. However, the outside dimensions and overall configurations of the meshes are the same. The outside diameter of all of the cylindrical foundation submodels is 167.5 m (549.6 ft), and they all have an overall depth of 42.7 m (140 ft). The largest diagonal dimension of the two types of concrete pads used in this project is 14.2 m (46.7 ft) for the cylindrical cask pad. The foundation is 11.8 times wider than this dimension. This configuration exceeds the recommendation of the US Army Corps of Engineers [19] that the foundation be at least 7 times wider than the dimension of the structure.

Figure 3.10 shows the foundation submodel used in the cylindrical cask analyses with the soft and stiff soil profiles. As can be seen in the figure, the mesh in the center of the top surface is rectangular and coincides with the shape of the pad. There are six elements across the region directly beneath the pad in both directions. For the cylindrical cask model, the pad is square, but for the rectangular module model, one dimension of the rectangular pad is greater than the other. Rings of elements encircle this rectangular zone. These rings become more circular in shape as the distance from the center increases. The surface mesh is swept through the depth of the foundation, so that horizontal cross sections of the mesh appear identical no matter where they are taken in the foundation depth.

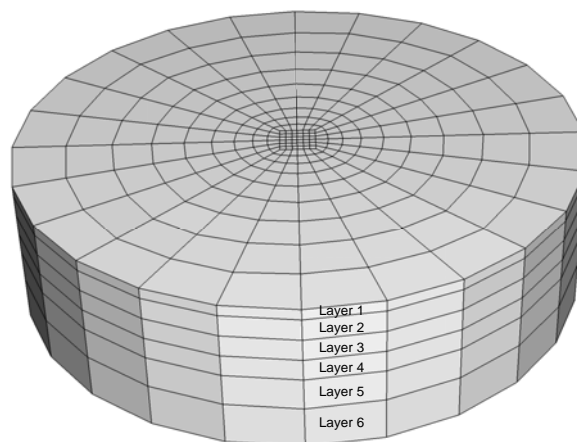


Figure 3.10: Representative Soil Foundation Submodel for Cylindrical Cask Analyses

The soil foundations with a depth of 42.7 m (140 ft) are comprised of six layers, each having unique material properties. The layers of elements in the soil foundation meshes coincide with these soil layers. The top layer is 3.05 m (10 ft) thick and the next three layers down are each 6.10 m (20 ft) thick. After that, the 5<sup>th</sup> layer is 9.14 m (30 ft) thick, and the bottom layer is 12.2 m (40 ft) thick. These six layers are labeled in Figure 3.10. The 42.7-m (240-ft) depth was chosen to reach a level below which the soil stiffness increases monotonically with depth. In addition, it was also based on satisfying the guidelines in American Society of Civil Engineers (ASCE) Standard [20].

As shown in Figure 3.11, the rock foundation submodels are essentially the same as those for the soil foundations. The overall dimensions of the foundations are the same, and the surface meshes that are swept through the layers of the foundation are the same as those that are used for the soil foundations. The only difference is that two different layers replace the top layer of the soil foundation. The uppermost of these layers is 0.914 m (3 ft) thick and is used to represent a thin layer of engineered fill material placed on top of the underlying rock material. Below this layer is a 2.13 m (7 ft) thick layer that represents weathered rock. Below this point, the mesh for the foundation is identical to that used in the soil foundation models. The layers below this point represent rock, and the material properties of the rock are constant through the rest of the depth.

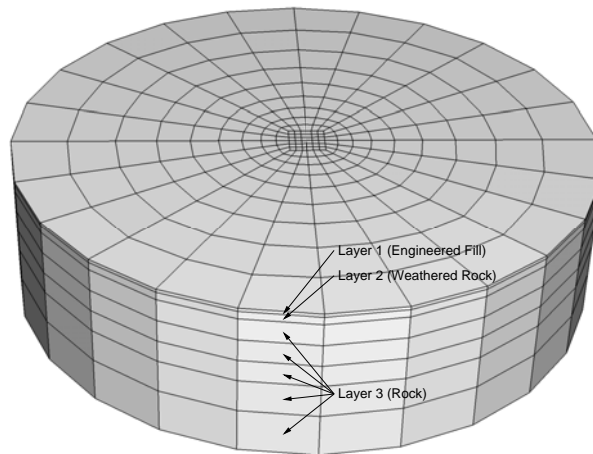


Figure 3.11: Representative Rock Foundation Submodel for Cylindrical Cask Analyses

### 3.2.3.2 Material Properties

The layered finite element meshes for the foundations have been described in the previous section. Three different foundation types have been used in this study. Soil profiles are very site-specific, and it is not possible to pick a generic soil profile that characterizes every site in the United States. The intent of this parametric study is to pick three soil profiles that bound the characteristics of a wide range of possible sites to investigate the sensitivity of the cask response to the selected soil profile. The three selected profiles represent a soft soil site, a stiff soil site, and a rock site.

It would be informative to calculate the equivalent shear velocity for the 42.7-m (140-ft) depth soil column model used in the cask response model to account for the variation of thickness and shear wave velocity of each of the six layers. Based on the ratio of the soil column height (i.e., 140 ft) to the time delay in a vertically propagating shear wave transmitting over the soil column for the soft soil, stiff soil and the rock profiles, the equivalent shear velocity for the 42.7-m (140-ft) depth soil column are 271, 500, and 1330 m/s (888, 1639 and 4364 ft/s), respectively.

### 3.2.3.2.1 Soft Soil Foundation

The material properties of the six layers in the soft soil profile are listed in Table 3.5. The elastic modulus, Poisson's ratio, density, and mass-proportional damping coefficient are material parameters, while the shear wave velocity is a function of the elastic properties and density.

Table 3.5: Soft Soil Foundation Material Properties

Layer	Layer Thickness	Elastic Modulus	Poisson's Ratio	Density	Shear Wave Velocity	Damping ( $\alpha$ )
1	3.05 m (10 ft)	133 MPa (19.3 ksi)	0.3	2002 kg/m <sup>3</sup> (125 lb/ft <sup>3</sup> )	160 m/s (524 ft/s)	1.19
2	6.10 m (20 ft)	181 MPa (26.2 ksi)	0.3	2002 kg/m <sup>3</sup> (125 lb/ft <sup>3</sup> )	186 m/s (612 ft/s)	1.91
3	6.10 m (20 ft)	341 MPa (49.5 ksi)	0.3	2002 kg/m <sup>3</sup> (125 lb/ft <sup>3</sup> )	256 m/s (840 ft/s)	1.33
4	6.10 m (20 ft)	451 MPa (65.4 ksi)	0.3	2002 kg/m <sup>3</sup> (125 lb/ft <sup>3</sup> )	294 m/s (966 ft/s)	1.02
5	9.14 m (30 ft)	577 MPa (83.6 ksi)	0.3	2002 kg/m <sup>3</sup> (125 lb/ft <sup>3</sup> )	333 m/s (1092 ft/s)	0.78
6	12.2 m (40 ft)	673 MPa (97.7 ksi)	0.3	2002 kg/m <sup>3</sup> (125 lb/ft <sup>3</sup> )	360 m/s (1180 ft/s)	0.79

### 3.2.3.2.2 Stiff Soil Foundation

The properties of the six layers of the stiff profile are outlined in Table 3.6. As mentioned previously, the finite element models used for the soft and stiff soil profiles are the same except for the foundation material properties.

Table 3.6: Stiff Soil Foundation Material Properties

Layer	Layer Thickness	Elastic Modulus	Poisson's Ratio	Density	Shear Wave Velocity	Damping ( $\alpha$ )
1	3.05 m (10 ft)	715 MPa (104 ksi)	0.3	2002 kg/m <sup>3</sup> (125 lb/ft <sup>3</sup> )	371 m/s (1216 ft/s)	0.95
2	6.10 m (20 ft)	865 MPa (125 ksi)	0.3	2002 kg/m <sup>3</sup> (125 lb/ft <sup>3</sup> )	408 m/s (1338 ft/s)	1.58
3	6.10 m (20 ft)	1096 MPa (159 ksi)	0.3	2002 kg/m <sup>3</sup> (125 lb/ft <sup>3</sup> )	458 m/s (1506 ft/s)	1.34
4	6.10 m (20 ft)	1331 MPa (193 ksi)	0.3	2002 kg/m <sup>3</sup> (125 lb/ft <sup>3</sup> )	506 m/s (1660 ft/s)	1.07
5	9.14 m (30 ft)	1552 MPa (225 ksi)	0.3	2002 kg/m <sup>3</sup> (125 lb/ft <sup>3</sup> )	546 m/s (1792 ft/s)	0.90
6	12.2 m (40 ft)	1896 MPa (275 ksi)	0.3	2002 kg/m <sup>3</sup> (125 lb/ft <sup>3</sup> )	604 m/s (1981 ft/s)	0.69

### 3.2.3.2.3 Rock Foundation

Table 3.7 lists the material properties of the rock foundation. Unlike the soil foundation models, the layers of finite elements do not necessarily have different material properties. The top two layers have unique material properties, but the properties are the same for all finite element layers below that point. The layer numbers in this table refer to layers of material rather than layers of finite elements.

Table 3.7: Rock Foundation Material Properties

Layer	Layer Thickness	Elastic Modulus	Poisson's Ratio	Density	Shear Wave Velocity	Damping ( $\alpha$ )
1	0.91 m (3 ft)	309 MPa (44.8 ksi)	0.3	2002 kg/m <sup>3</sup> (125 lb/ft <sup>3</sup> )	244 m/s (800 ft/s)	0.57
2	2.13 m (7 ft)	4349 MPa (630 ksi)	0.3	2002 kg/m <sup>3</sup> (125 lb/ft <sup>3</sup> )	914 m/s (3000 ft/s)	0.57
3	39.6 m (130 ft)	12082 MPa (1752 ksi)	0.3	2002 kg/m <sup>3</sup> (125 lb/ft <sup>3</sup> )	1523 m/s (5000 ft/s)	0.57

### 3.2.4 Properties of Interfaces Between Submodels

Contact interactions are defined at the interfaces between the cask and pad submodels, and between the pad and foundation submodels. A detailed overview of the various options available for modeling contact has been given in Section 3.1.2. When sufficiently high ground motions are applied to the base of the cask model, the cask can potentially experience very large motions relative to the pad. In contrast, the relative movements between the pad and foundation are generally quite small.

As mentioned previously, a single coefficient of friction is used for both static and kinetic friction. The intent in modeling the interfacial friction between the cask and pad is to use a reasonable estimate of the friction coefficient to simulate the cask behavior as accurately as possible for a variety of situations. In the parametric analyses, this friction coefficient is varied to represent a best estimate case, as well as lower and upper bound cases. The actual values used in the parametric analyses for the cask/pad friction coefficient, as well as the basis for the selection of these values are outlined in the next chapter.

During the analysis frictional contact surfaces were included between the pad and soil foundation primarily to allow for the pad to lift up slightly from the soil foundation. If the pad were directly bonded to the soil, the resulting system would be overly stiff. In many installations, the pad is embedded in the soil, so the soil on the sides of the pad provides a restraining effect against sliding. It would be possible to model explicitly this effect with additional contact surfaces around the sides of the pad, but the benefits of doing this would not justify the additional complexity required in the model.

To approximate this restraining effect while allowing for pad uplift, a relatively high coefficient of friction, 1.0, is used between the pad and the soil. The lateral displacements of the pad relative to the foundation observed in the analyses with this coefficient of friction are very small, and the desired ability for the pad to lift up from the foundation is maintained. It is important to realize that the relative sliding between the pad and foundation is likely to decrease the response of the pad because sliding would result in decreased seismic input being transferred to the pad. Therefore, using a higher coefficient of friction at this interface results in more conservative results than would be obtained with a lower coefficient of friction. In summary, the adopted modeling approach provides conservative results that are for pads that are embedded in the surrounding foundation material, as well as those that rest on top of the foundation.

## 4. Scope of Parametric Analyses

This research effort involved investigating the seismic response of dry cask storage systems using coupled three-dimensional finite element models of cask/pad/foundation. The objective of performing seismic analyses with these coupled models is to capture the nonlinear dynamic behavior of these storage systems including the nonlinear frictional contact algorithm at the cask/pad interface and the soil-structure interaction effects. A comprehensive series of parametric analyses was conducted to investigate the sensitivity of cask responses to a selected set of input parameters. The scope of parametric analyses, as shown in Table 4.1, is by no means exhaustive, but it does cover a broad and practical range of important parameters, with the intention of demonstrating the relative influence on the trend of variation of cask responses. These input parameters will be described in detail in this chapter.

Table 4.1: Scope of Parametric Analyses

Input Parameter	Description	Details
Coupled finite element models	2 Cask designs	Vertical cylindrical cask and horizontal rectangular module
	3 Foundation types	Soft soil, stiff soil, and rock
	3 Coefficients of friction at cask/pad interface	0.20, 0.55, and 0.80
Seismic ground motions	3 Spectral shapes	NUREG/CR-0098 Regulatory Guide 1.60 NUREG/CR-6728
	5 Selected earthquake records	NUREG/CR-0098 and Regulatory Guide 1.60: 1) 1978 Iran Tabas 2) 1999 Taiwan Chi-Chi 3) 1992 Landers 4) 1994 Northridge 5) 1979 Imperial Valley
		NUREG/CR-6728: A) 1985 Nahanni B) 1988 Saguenay C) 1979 Imperial Valley D) 1989 Loma Prieta E) 1994 Northridge
4 PGA (Peak Ground Acceleration) levels	0.25, 0.60, 1.00, and 1.25 g	

### 4.1 Seismic Loading – Time Histories of Accelerations

Current trend in the seismic design analysis recognizes that the earthquake ground motion should be regarded as stochastic processes, and thus the seismic response of a dry cask using one time history might not always lead to a predictable response. It is increasingly obvious that a suite of earthquake inputs should be examined in order to obtain statistically stable mean and standard variation in the response to form the basis for design decision. This would require multiple runs using several earthquake records. Furthermore, as discussed in Section 3.1.1, a sufficiently wide range in parametric variations in ground shaking characteristics would be needed for covering a wide variation in seismological and soil conditions.

In the parametric analyses of dry casks, the investigation scope includes formulating the ground motion characteristics having the target design response spectra in accordance with three spectral shapes: the NUREG/CR-0098, the Regulatory Guide 1.60, and the NUREG/CR-6728. These three spectral shapes

were chosen because of their potential use by cask design applicants. Furthermore, the three postulated spectral shapes would provide for a sufficiently wide range of coverage with respect to the variations in the seismological conditions including WUS (western United States) and CEUS (central and eastern United States) as well as the variation in ground motion characteristics due to different soil conditions.

Historically, due to the absence of strong motion data from actual recordings from the CEUS sites, seismic design practice in CEUS ground motion criteria has generally been developed by using smaller Peak Ground Acceleration (PGA) values applied to empirical WUS spectral shapes (e.g., the earlier discussed NUREG-0098 and the Regulatory Guide 1.60 methods) for developing the target design spectrum for CEUS conditions. Recent seismological studies confirmed by limited available CEUS strong motion recordings led to the current thinking that the historical practice on the use of WUS spectral shapes would still lead to unrealistic target shaking characteristics for the CEUS sites. Studies such as the NUREG/CR-6728 conclude that the differences in CEUS seismological conditions would not only result in lower shaking levels (i.e., lower PGA), but would also result in much lower long-period contents for the CEUS sites. The NUREG/CR-6728 studies have been adopted by the NRC for implementing more current seismological studies for CEUS design conditions that would be fundamentally different from historical WUS practice. Figure 4.1 presents the WUS and CEUS geographical boundary following the USGS seismic-hazard mapping program. The boundary basically follows the US Rocky Mountains passing through Montana, Wyoming, Utah, Arizona, then bending east through Southern Colorado, New Mexico and western Texas.

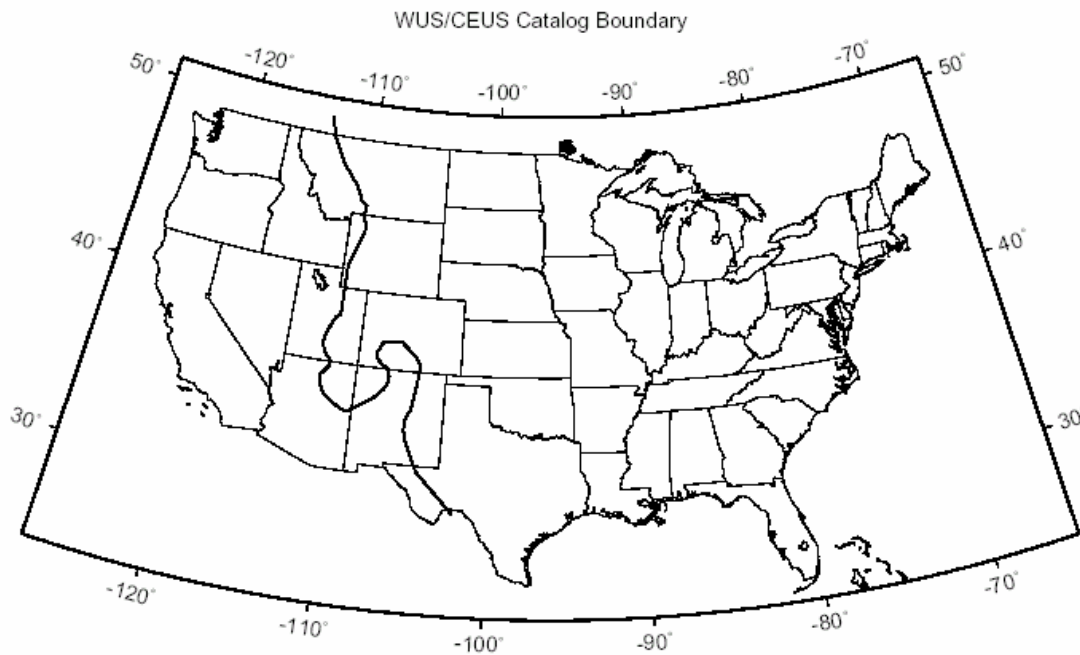


Figure 4.1: Boundary between Western US (WUS) and Central and Eastern US (CEUS)

Table 4.2 shows the tabulation of the spectral acceleration curve shapes, after normalizing by the horizontal motion for PGA Values. The NUREG/CR-6728 procedure has been used initially for developing the CEUS rock site spectral shapes. However, the report did not present a procedure suitable for developing generic soil site spectral shapes. The report assumed that site specific response analyses would be conducted for soil sites, which cannot be used for the current generic site study. Some generic randomized site response analyses were performed in order to rationalize a generic soil site spectral shape for the CEUS sites. Because of the relatively competent site soil conditions expected for typical nuclear power plant sites along with the relatively low level of shaking expected for typical CEUS conditions, differences of ground shaking between rock and soil sites in CEUS is not anticipated to be a very big factor. Ultimately, the generic CEUS soil site spectrum based on the randomized site response analyses was adopted to complement the procedure for the two WUS (i.e., NUREG/CR-0098 and the Regulatory Guide 1.60 spectral shapes) spectral shapes in the parametric response study. The NUREG/CR-6728 CEUS spectral shape would provide reasonable representations for both soil and rock sites for CEUS ground motion conditions.

Figure 4.2 presents a plot to compare the three spectral acceleration curve shapes for (a) the horizontal and (b) the vertical motions in terms of log-log plots of normalized spectral acceleration versus frequency. Corresponding comparisons of horizontal and vertical shaking, in terms of linear plots of normalized spectral displacement and acceleration versus period, are showed in Figures 4.3 and 4.4, respectively.

From these presented figures, it can be observed that the shaking demand for the three spectral shapes, especially at increasingly longer periods, decreases progressively and systematically from the Regulatory Guide 1.60 to the NUREG/CR-0098 and then to the lowest shaking NUREG/CR-6728 CEUS spectral shape. It should be noted that even though the three cited procedures were used for formulating the spectral shapes in developing the period-dependent demand of target ground motion, they are not intended to establish the demand level for project specific designs. There should be a wider degree of latitude in utilizing the response solutions from the project library so long as the cross comparison of reference ground surface design response spectra between project specific cases are made to the parametric library. For example, the reference surface spectra using the NUREG/CR-6728 CEUS spectral shape might be found to compare favorably to the ground motion shaking characteristics established for WUS rock sites in some site-specific projects. In such cases, even though the reference surface spectra are developed in accordance with the NUREG/CR-6728 CEUS spectral procedure for CEUS seismological conditions, they can also be used for WUS rock sites.

It should be observed that for a specific PGA, the variation in spectral demands among the three spectral shapes at longer periods ranges from about 3 times at about 1-second period, to as much as 10 folds at periods longer than 4 seconds. This sufficiently wide range may be adequate to cover the potential ranges in ground motion demanded from various cask design applicants, including variations in seismological and soil conditions. It should also be recognized that the three adopted spectral shapes are nicely separated to allow a reasonable interpolation of response solutions for different cask design applicants. The following sections provide background details regarding each of the three adopted spectral shape procedures.

Table 4.2: Tabulation of Spectral Shapes

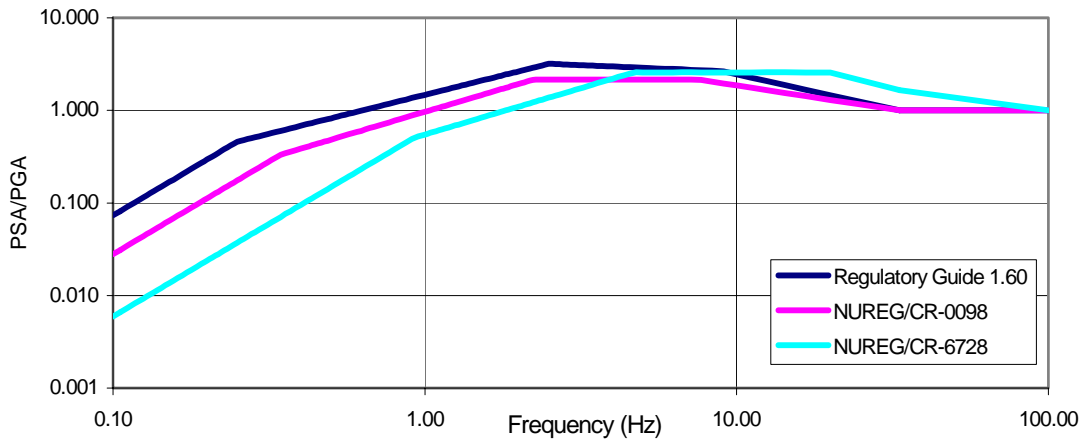
PERIOD (SECOND)	Frequency (Hz)	SA/PGA							
		REG. GUIDE 1.60, HOR.	REG. GUIDE 1.60, VERT.	NUREG/CR- 0098, HOR.	NUREG/CR- 0098, VERT.	CEUS, HOR. ROCK	CEUS, VERT. ROCK	CEUS, HOR. SOIL	CEUS, VERT. SOIL
0.01	100.00	1.0000	1.0000	1.0000	0.6500	1.0000	1.0000	1.0000	1.0000
0.03	33.33	0.9998	0.9998	1.0000	0.6500	2.2391	2.1719	1.6532	2.3565
0.04	25.00	1.2321	1.2321	1.1554	0.7510	2.2375	1.9690	2.1180	2.1363
0.05	20.00	1.4572	1.4572	1.2976	0.8434	2.1911	1.8076	2.5692	1.9613
0.06	16.67	1.6714	1.6714	1.4267	0.9273	2.1285	1.7050	2.5719	1.8500
0.07	14.29	1.8769	1.8769	1.5458	1.0047	2.0593	1.6233	2.5785	1.7613
0.08	12.50	2.0752	2.0752	1.6569	1.0770	1.9883	1.5420	2.5814	1.6731
0.09	11.11	2.2674	2.2674	1.7616	1.1450	1.9184	1.4633	2.5656	1.5877
0.10	10.00	2.4544	2.4544	1.8608	1.2095	1.8509	1.3882	2.5692	1.5062
0.11	9.09	2.6368	2.6368	1.9554	1.2710	1.7866	1.3400	2.5722	1.4539
0.12	8.33	2.6861	2.6776	2.0459	1.3298	1.7257	1.2943	2.5746	1.4043
0.13	7.69	2.7172	2.6996	2.1329	1.3864	1.6683	1.2512	2.5767	1.3576
0.14	7.14	2.7462	2.7201	2.1622	1.4054	1.6141	1.2106	2.5785	1.3135
0.15	6.67	2.7735	2.7393	2.1623	1.4055	1.5630	1.1723	2.5801	1.2719
0.16	6.25	2.7993	2.7574	2.1623	1.4055	1.5147	1.1361	2.5713	1.2326
0.17	5.88	2.8237	2.7746	2.1624	1.4056	1.4691	1.1018	2.5730	1.1955
0.18	5.56	2.8470	2.7908	2.1624	1.4056	1.4258	1.0694	2.5746	1.1603
0.19	5.26	2.8691	2.8063	2.1625	1.4056	1.3847	1.0385	2.5761	1.1268
0.20	5.00	2.8903	2.8210	2.1625	1.4057	1.3456	1.0092	2.5774	1.0950
0.21	4.76	2.9106	2.8351	2.1626	1.4057	1.3083	0.9812	2.5785	1.0647
0.22	4.55	2.9301	2.8486	2.1626	1.4057	1.2727	0.9546	2.4983	1.0357
0.23	4.35	2.9488	2.8616	2.1627	1.4057	1.2387	0.9290	2.3896	1.0080
0.24	4.17	2.9669	2.8740	2.1627	1.4058	1.2061	0.9046	2.2901	0.9815
0.25	4.00	2.9843	2.8860	2.1628	1.4058	1.1749	0.8812	2.1985	0.9561
0.26	3.85	3.0011	2.8976	2.1628	1.4058	1.1449	0.8587	2.1139	0.9317
0.27	3.70	3.0174	2.9088	2.1628	1.4058	1.1161	0.8371	2.0356	0.9082
0.28	3.57	3.0332	2.9196	2.1629	1.4059	1.0884	0.8163	1.9629	0.8857
0.29	3.45	3.0485	2.9301	2.1629	1.4059	1.0617	0.7963	1.8952	0.8640
0.30	3.33	3.0634	2.9403	2.1629	1.4059	1.0360	0.7770	1.8321	0.8430
0.31	3.23	3.0778	2.9501	2.1630	1.4059	1.0112	0.7584	1.7730	0.8229
0.32	3.13	3.0918	2.9597	2.1630	1.4059	0.9873	0.7405	1.7176	0.8034
0.33	3.03	3.1055	2.9690	2.1630	1.4060	0.9642	0.7231	1.6655	0.7846
0.34	2.94	3.1188	2.9781	2.1630	1.4060	0.9419	0.7064	1.6165	0.7664
0.35	2.86	3.1318	2.9869	2.1631	1.4060	0.9203	0.6902	1.5703	0.7489
0.36	2.78	3.1445	2.9955	2.1631	1.4060	0.8994	0.6745	1.5267	0.7319
0.37	2.70	3.1569	3.0039	2.1631	1.4060	0.8792	0.6594	1.4855	0.7154
0.38	2.63	3.1690	3.0121	2.1631	1.4060	0.8596	0.6447	1.4464	0.6995
0.39	2.56	3.1808	3.0201	2.1632	1.4061	0.8406	0.6305	1.4093	0.6841
0.40	2.50	3.1924	3.0279	2.1632	1.4061	0.8222	0.6167	1.3740	0.6691
0.41	2.44	3.1267	2.9547	2.1632	1.4061	0.8044	0.6033	1.3405	0.6546
0.42	2.38	3.0638	2.8849	2.1632	1.4061	0.7871	0.5903	1.3086	0.6405
0.43	2.33	3.0037	2.8183	2.1633	1.4061	0.7703	0.5778	1.2782	0.6269
0.44	2.27	2.9461	2.7547	2.1633	1.4061	0.7541	0.5655	1.2491	0.6136
0.45	2.22	2.8909	2.6940	2.1465	1.3952	0.7382	0.5537	1.2214	0.6007
0.46	2.17	2.8378	2.6359	2.0998	1.3649	0.7229	0.5421	1.1948	0.5882
0.47	2.13	2.7869	2.5802	2.0551	1.3358	0.7079	0.5310	1.1694	0.5761
0.48	2.08	2.7379	2.5269	2.0123	1.3080	0.6934	0.5201	1.1450	0.5643
0.49	2.04	2.6907	2.4757	1.9712	1.2813	0.6793	0.5095	1.1217	0.5528
0.50	2.00	2.6453	2.4266	1.9318	1.2557	0.6656	0.4992	1.0992	0.5417
0.51	1.96	2.6016	2.3794	1.8939	1.2311	0.6523	0.4892	1.0777	0.5308
0.52	1.92	2.5594	2.3340	1.8575	1.2074	0.6393	0.4795	1.0570	0.5203
0.53	1.89	2.5186	2.2903	1.8225	1.1846	0.6267	0.4700	1.0370	0.5100
0.54	1.85	2.4793	2.2482	1.7887	1.1627	0.6144	0.4608	1.0178	0.5000
0.55	1.82	2.4413	2.2077	1.7562	1.1415	0.6025	0.4519	0.9993	0.4903
0.56	1.79	2.4045	2.1686	1.7248	1.1211	0.5909	0.4431	0.9815	0.4808
0.57	1.75	2.3689	2.1308	1.6946	1.1015	0.5795	0.4347	0.9642	0.4716
0.58	1.72	2.3345	2.0944	1.6654	1.0825	0.5685	0.4264	0.9476	0.4626
0.60	1.67	2.2687	2.0251	1.6098	1.0464	0.5474	0.4105	0.9160	0.4454
0.62	1.61	2.2069	1.9603	1.5579	1.0126	0.5273	0.3955	0.8865	0.4291
0.64	1.56	2.1487	1.8995	1.5092	0.9810	0.5082	0.3812	0.8588	0.4136
0.66	1.52	2.0937	1.8424	1.4635	0.9513	0.4901	0.3676	0.8328	0.3989
0.68	1.47	2.0417	1.7886	1.4204	0.9233	0.4730	0.3547	0.8083	0.3849
0.70	1.43	1.9925	1.7379	1.3799	0.8969	0.4566	0.3425	0.7852	0.3716
0.72	1.39	1.9458	1.6900	1.3415	0.8720	0.4411	0.3308	0.7634	0.3590
0.74	1.35	1.9014	1.6447	1.3053	0.8484	0.4264	0.3198	0.7427	0.3470
0.76	1.32	1.8591	1.6017	1.2709	0.8261	0.4123	0.3092	0.7232	0.3355
0.78	1.28	1.8189	1.5610	1.2383	0.8049	0.3989	0.2992	0.7046	0.3246
0.80	1.25	1.7805	1.5223	1.2074	0.7848	0.3862	0.2897	0.6870	0.3143

Table 4.2. Tabulation of Spectral Shapes (cont'd)

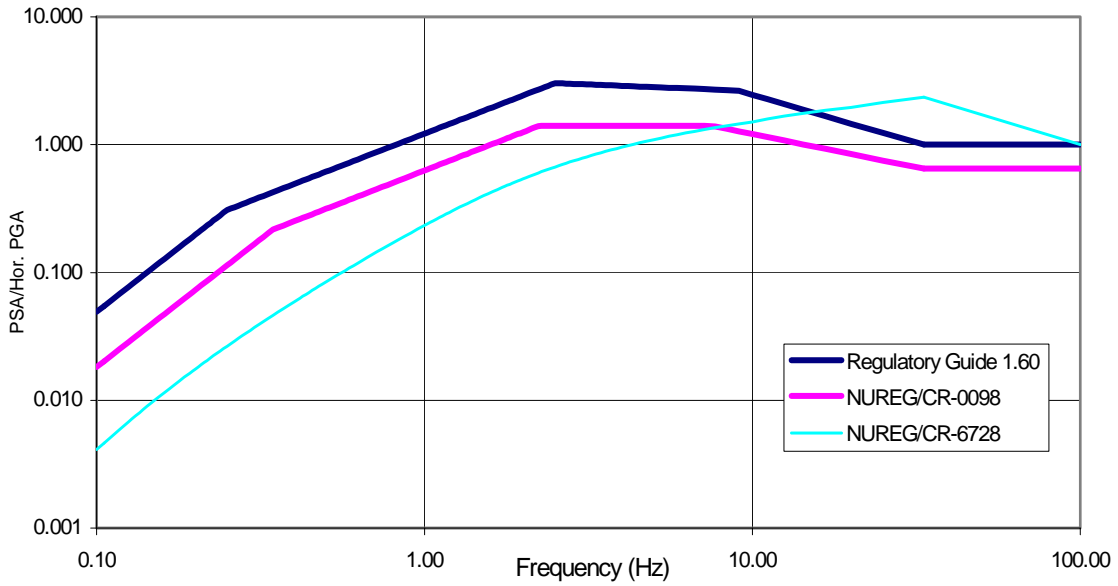
PERIOD (SECOND)	Frequency (Hz)	SAP/GA							
		REG. GUIDE 1.60, HOR.	REG. GUIDE 1.60, VERT.	NUREG/CR- 0098, HOR.	NUREG/CR- 0098, VERT.	CEUS, HOR. ROCK	CEUS, VERT. ROCK	CEUS, HOR. SOIL	CEUS, VERT. SOIL
0.82	1.22	1.7439	1.4854	1.1779	0.7657	0.3741	0.2805	0.6703	0.3044
0.84	1.19	1.7088	1.4503	1.1499	0.7474	0.3625	0.2719	0.6543	0.2950
0.86	1.16	1.6753	1.4169	1.1231	0.7300	0.3514	0.2636	0.6391	0.2860
0.88	1.14	1.6432	1.3849	1.0976	0.7135	0.3409	0.2557	0.6246	0.2774
0.90	1.11	1.6123	1.3544	1.0732	0.6976	0.3308	0.2481	0.6107	0.2692
0.92	1.09	1.5828	1.3252	1.0499	0.6824	0.3212	0.2409	0.5974	0.2614
0.94	1.06	1.5543	1.2972	1.0276	0.6679	0.3120	0.2340	0.5847	0.2539
0.96	1.04	1.5270	1.2704	1.0061	0.6540	0.3032	0.2274	0.5725	0.2467
0.98	1.02	1.5007	1.2447	0.9856	0.6407	0.2948	0.2211	0.5608	0.2399
1.00	1.00	1.4754	1.2200	0.9659	0.6278	0.2867	0.2150	0.5496	0.2333
1.05	0.95	1.4160	1.1623	0.9199	0.5979	0.2679	0.2010	0.5235	0.2180
1.10	0.91	1.3616	1.1099	0.8781	0.5708	0.2510	0.1883	0.4908	0.2043
1.15	0.87	1.3116	1.0620	0.8399	0.5459	0.2357	0.1768	0.4497	0.1918
1.20	0.83	1.2654	1.0181	0.8049	0.5232	0.2218	0.1664	0.4133	0.1805
1.25	0.80	1.2226	0.9777	0.7727	0.5023	0.2092	0.1569	0.3812	0.1702
1.30	0.77	1.1829	0.9404	0.7430	0.4830	0.1976	0.1482	0.3515	0.1608
1.35	0.74	1.1458	0.9058	0.7155	0.4651	0.1871	0.1403	0.3264	0.1522
1.40	0.71	1.1113	0.8737	0.6899	0.4485	0.1773	0.1330	0.3032	0.1443
1.45	0.69	1.0789	0.8438	0.6661	0.4330	0.1684	0.1263	0.2826	0.1370
1.50	0.67	1.0485	0.8159	0.6439	0.4186	0.1601	0.1201	0.2645	0.1303
1.55	0.65	1.0200	0.7898	0.6232	0.4051	0.1525	0.1143	0.2476	0.1241
1.60	0.63	0.9931	0.7653	0.6037	0.3924	0.1454	0.1090	0.2327	0.1183
1.65	0.61	0.9676	0.7423	0.5854	0.3805	0.1388	0.1041	0.2188	0.1129
1.70	0.59	0.9436	0.7206	0.5682	0.3693	0.1326	0.0995	0.2057	0.1079
1.75	0.57	0.9209	0.7002	0.5519	0.3588	0.1269	0.0952	0.1942	0.1033
1.80	0.56	0.8993	0.6809	0.5366	0.3488	0.1216	0.0912	0.1834	0.0989
1.85	0.54	0.8787	0.6627	0.5221	0.3394	0.1166	0.0874	0.1740	0.0948
1.90	0.53	0.8592	0.6453	0.5084	0.3304	0.1119	0.0839	0.1643	0.0910
1.95	0.51	0.8406	0.6289	0.4953	0.3220	0.1074	0.0806	0.1568	0.0874
2.00	0.50	0.8229	0.6133	0.4830	0.3139	0.1033	0.0775	0.1488	0.0841
2.05	0.49	0.8060	0.5985	0.4712	0.3063	0.0994	0.0745	0.1412	0.0809
2.10	0.48	0.7898	0.5843	0.4600	0.2990	0.0957	0.0718	0.1347	0.0779
2.15	0.47	0.7743	0.5709	0.4493	0.2920	0.0922	0.0692	0.1286	0.0750
2.20	0.45	0.7594	0.5580	0.4390	0.2854	0.0889	0.0667	0.1227	0.0724
2.25	0.44	0.7452	0.5457	0.4293	0.2790	0.0858	0.0643	0.1178	0.0698
2.30	0.43	0.7315	0.5339	0.4200	0.2730	0.0828	0.0621	0.1124	0.0674
2.35	0.43	0.7184	0.5226	0.4110	0.2672	0.0800	0.0600	0.1079	0.0651
2.40	0.42	0.7057	0.5118	0.4025	0.2616	0.0774	0.0580	0.1030	0.0630
2.50	0.40	0.6819	0.4915	0.3864	0.2511	0.0724	0.0543	0.0950	0.0589
2.60	0.38	0.6597	0.4728	0.3715	0.2415	0.0680	0.0510	0.0882	0.0553
2.70	0.37	0.6391	0.4554	0.3577	0.2325	0.0639	0.0479	0.0813	0.0520
2.80	0.36	0.6198	0.4393	0.3450	0.2242	0.0602	0.0451	0.0761	0.0489
2.90	0.34	0.6018	0.4242	0.3331	0.2165	0.0567	0.0426	0.0707	0.0462
3.00	0.33	0.5848	0.4102	0.3113	0.2024	0.0536	0.0402	0.0661	0.0436
3.10	0.32	0.5689	0.3971	0.2916	0.1895	0.0507	0.0380	0.0619	0.0413
3.20	0.31	0.5539	0.3848	0.2736	0.1779	0.0481	0.0360	0.0579	0.0391
3.30	0.30	0.5397	0.3732	0.2573	0.1672	0.0456	0.0342	0.0547	0.0371
3.40	0.29	0.5263	0.3623	0.2424	0.1576	0.0433	0.0325	0.0517	0.0352
3.50	0.29	0.5136	0.3520	0.2287	0.1487	0.0412	0.0309	0.0483	0.0335
3.60	0.28	0.5016	0.3423	0.2162	0.1405	0.0392	0.0294	0.0461	0.0319
3.70	0.27	0.4901	0.3331	0.2047	0.1330	0.0374	0.0280	0.0434	0.0304
3.80	0.26	0.4792	0.3244	0.1940	0.1261	0.0357	0.0267	0.0412	0.0290
3.90	0.26	0.4689	0.3162	0.1842	0.1197	0.0340	0.0255	0.0391	0.0277
4.00	0.25	0.4590	0.3083	0.1751	0.1138	0.0325	0.0244	0.0372	0.0265
4.10	0.24	0.4368	0.2935	0.1667	0.1083	0.0311	0.0233	0.0354	0.0253
4.20	0.24	0.4163	0.2796	0.1588	0.1032	0.0298	0.0224	0.0337	0.0243
4.30	0.23	0.3972	0.2667	0.1515	0.0985	0.0286	0.0214	0.0321	0.0232
4.40	0.23	0.3793	0.2547	0.1447	0.0941	0.0274	0.0205	0.0307	0.0223
4.50	0.22	0.3626	0.2435	0.1384	0.0899	0.0263	0.0197	0.0294	0.0214
4.60	0.22	0.3470	0.2330	0.1324	0.0861	0.0252	0.0189	0.0281	0.0205
4.70	0.21	0.3324	0.2232	0.1268	0.0824	0.0242	0.0182	0.0269	0.0197
4.80	0.21	0.3187	0.2140	0.1216	0.0790	0.0233	0.0175	0.0258	0.0190
4.90	0.20	0.3058	0.2053	0.1167	0.0759	0.0224	0.0168	0.0248	0.0182
5.00	0.20	0.2937	0.1972	0.1121	0.0729	0.0216	0.0162	0.0238	0.0176

Table 4.2. Tabulation of Spectral Shapes (cont'd)

PERIOD (SECOND)	Frequency (Hz)	SA/PGA							
		REG. GUIDE 1.60, HOR.	REG. GUIDE 1.60, VERT.	NUREG/CR- 0098, HOR.	NUREG/CR- 0098, VERT.	CEUS, HOR. ROCK	CEUS, VERT. ROCK	CEUS, HOR. SOIL	CEUS, VERT. SOIL
5.10	0.20	0.2823	0.1895	0.1077	0.0700	0.0208	0.0156	0.0229	0.0169
5.20	0.19	0.2716	0.1823	0.1036	0.0674	0.0200	0.0150	0.0220	0.0163
5.40	0.19	0.2518	0.1690	0.0961	0.0625	0.0186	0.0140	0.0204	0.0151
5.60	0.18	0.2342	0.1571	0.0893	0.0581	0.0173	0.0130	0.0190	0.0141
5.80	0.17	0.2183	0.1464	0.0833	0.0541	0.0162	0.0121	0.0177	0.0132
6.00	0.17	0.2040	0.1368	0.0778	0.0506	0.0151	0.0114	0.0165	0.0123
6.20	0.16	0.1910	0.1281	0.0729	0.0474	0.0142	0.0106	0.0155	0.0115
6.40	0.16	0.1793	0.1202	0.0684	0.0445	0.0133	0.0100	0.0145	0.0108
6.60	0.15	0.1686	0.1130	0.0643	0.0418	0.0125	0.0094	0.0137	0.0102
6.80	0.15	0.1588	0.1065	0.0606	0.0394	0.0117	0.0088	0.0129	0.0096
7.00	0.14	0.1499	0.1005	0.0572	0.0372	0.0111	0.0083	0.0121	0.0090
7.20	0.14	0.1417	0.0949	0.0540	0.0351	0.0104	0.0078	0.0115	0.0085
7.40	0.14	0.1341	0.0899	0.0512	0.0333	0.0098	0.0074	0.0109	0.0080
7.60	0.13	0.1271	0.0852	0.0485	0.0315	0.0093	0.0070	0.0103	0.0076
7.80	0.13	0.1207	0.0809	0.0461	0.0299	0.0088	0.0066	0.0098	0.0072
8.00	0.13	0.1147	0.0769	0.0438	0.0285	0.0083	0.0062	0.0093	0.0068
8.50	0.12	0.1016	0.0681	0.0388	0.0252	0.0073	0.0055	0.0082	0.0059
9.00	0.11	0.0907	0.0607	0.0346	0.0225	0.0064	0.0048	0.0073	0.0052
9.50	0.11	0.0814	0.0545	0.0310	0.0202	0.0057	0.0043	0.0066	0.0046
10.00	0.10	0.0734	0.0491	0.0280	0.0182	0.0050	0.0038	0.0060	0.0041

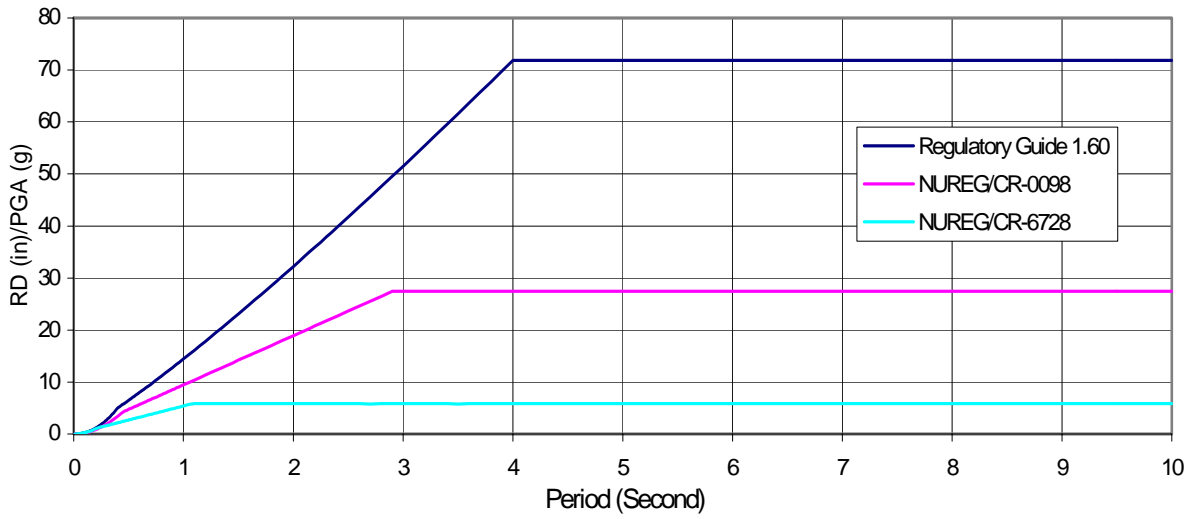


(a) Spectral Shapes for Horizontal Motion

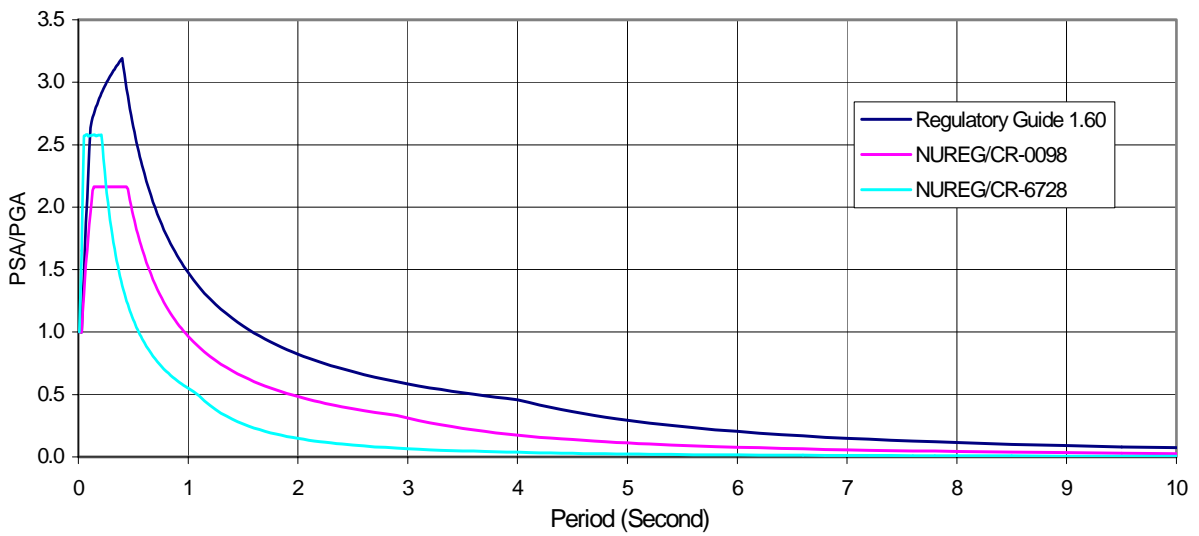


(b) Spectral Shapes for Vertical Motion

Figure 4.2: Plots of Horizontal and Vertical Spectral Shapes In Terms of Frequency (Logarithmic Scales)

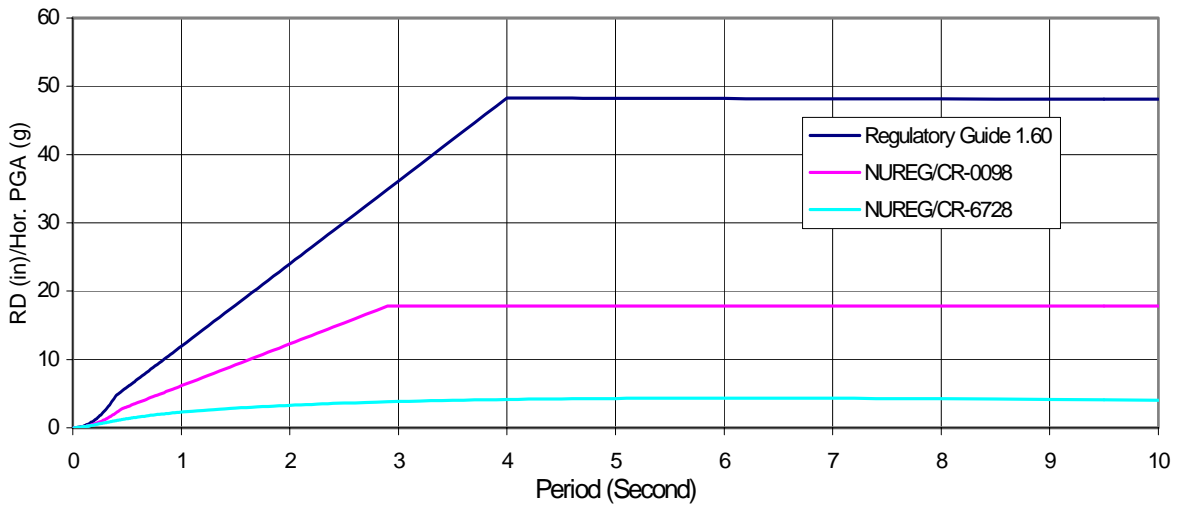


(a) Spectral displacement vs. period

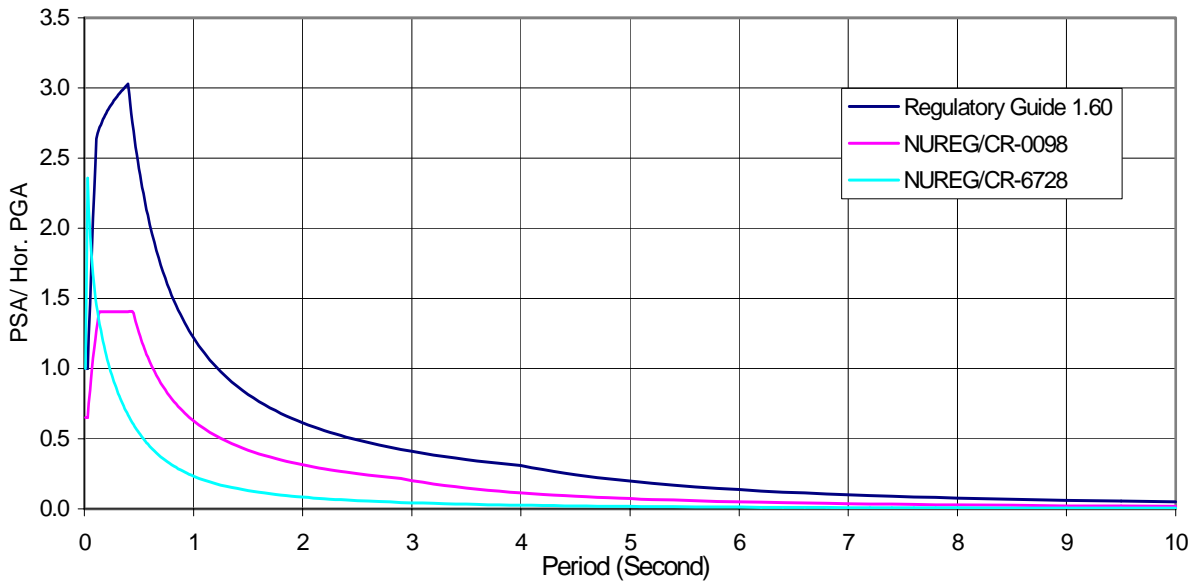


(b) Spectral acceleration vs. period

Figure 4.3: Plots of Horizontal Spectral Shapes In Terms of Period (Linear Scales)



(a) Spectral displacement vs. period



(b) Spectral acceleration vs. period

Figure 4.4: Plots of Vertical Spectral Shapes In Terms of Period (Linear Scales)

#### **4.1.1 NUREG/CR-0098 Spectral Shape**

The NUREG/CR-0098 spectral procedure, which was originally developed by Newmark based on actual strong-motions recorded in western US earthquakes, was followed to develop the horizontal spectral shape. The procedure has been widely used in the industry in other sectors besides the nuclear industry and probably considered as the best-estimated ground-motion characteristics for WUS, reflecting the empirical strong motion database. Hidden conservatism, inherent in most design procedures, has been deliberately avoided for this adopted spectral shape. The median spectral amplification factors, which represent the 50<sup>th</sup> percentile, were used rather than the 84% spectral amplification factors.

According to NUREG/CR-0098, a Peak Ground Velocity to PGA (PGV/PGA) of 36 in/s per g should be used to develop the PGV parameter to anchor the PGV period range. A  $PGD \cdot A / (PGV^2)$  coefficient of 6 should be used to develop the peak ground displacement (PGD) parameter for anchoring constant displacement range, where consistent units should be used for PGD (in L), A (in  $LT^{-2}$ ) and PGV (in  $LT^{-1}$ ). These listed velocity and displacement parameters were selected so that the spectral shapes would be compatible to a median earthquake (e.g., Magnitude 6.5) range that was considered to be the typical condition for designs of many plant sites, especially outside California, which likely require more special site-specific studies.

##### **4.1.1.1 NUREG/CR-0098 Vertical Motion Spectral Shape**

The NUREG/CR-0098 recommends that the vertical response spectrum be equal to 2/3 of the horizontal response spectrum uniformly at all periods.

#### **4.1.2 Regulatory Guide 1.60 Spectral Shape**

The Regulatory Guide 1.60 spectral procedure was selected in the parametric analyses because it has been widely used for designing many of the existing nuclear power plants. However, the Regulatory Guide 1.60 spectral procedure has been found to be unrealistically conservative when compared with the empirical strong motion data from several recent studies sponsored by the NRC (see discussions in NUREG/CR-6728). This procedure might become obsolete for future nuclear power projects, as more updated procedures are implemented with more up-to-date studies by geoscientists. Nevertheless, it is believed that this approach can serve as an upper bound evaluation case along with its merits in terms of past applications.

##### **4.1.2.1 Regulatory Guide 1.60 Vertical Motion Spectral Shape**

The Regulatory Guide 1.60 spectral procedure was followed in developing the vertical motion spectral shape. It should be noted that at the zero period, the Regulatory Guide 1.60 assumes the same PGA for both horizontal and vertical component motions, but the V/H ratios are period dependent.

#### **4.1.3 NUREG/CR-6728 Spectral Shape**

For the parametric analyses in this project, it was decided to follow the recommendations in the NUREG/CR-6728 spectral procedure to reflect the state-of-the-art practice toward ground motion hazards in the CEUS sites. Randomized site response analyses were performed in searching and evaluating potential candidate generic CEUS spectral shapes for both rock and soil sites. Eventually, a M-6.5 generic CEUS soil site spectral shape was selected. The rationale of selecting the CEUS spectral shape is that this CEUS spectral shape, along with the two WUS spectral shapes represented by the NUREG/CR-0098 and the Regulatory Guide 1.60 spectral shape procedures, provides for a reasonable range of variation in long period shaking intensities. In addition, the collection of cask response results arising from the response analyses would provide a comprehensive set of parametric response results for cross comparison to applicant submittals.

The comparison of the CEUS spectral shapes between generic rock and generic soil sites showed relatively small differences. Therefore, the CEUS generic soil site spectral shapes can provide reasonable representations for the CEUS generic rock site conditions in regards to the expected ground-surface shaking demand. As discussed earlier, the relatively low long-period contents in the adopted CEUS spectral shape could also provide coverage of generic rock site response conditions for both CEUS and WUS sites.

#### **4.1.3.1 CEUS Generic Vertical Motion Spectral Shape**

The NUREG/CR-6728 spectral procedure was followed in developing the vertical motion spectral shapes. The report presented three sets of period dependent V/H ratios as a function of the PGA levels. A PGA at 0.25 g would represent typical design conditions of most of the non-western US sites, and the vertical motion spectral shape for the V/H ratios for PGA at 0.2–0.5 g from the report was chosen to develop the spectral shape for the generic CEUS spectral shape.

#### **4.1.4 Time Histories for the Three Spectral Shapes**

Time histories of seismic accelerations were input to the coupled cask/pad/foundation model. After developing the three target spectral shapes, the next step involved generating a suite of input ground motions that would have shaking characteristics matching the target spectral shapes. These ground motions were then scaled to yield earthquakes with varying values of PGA to apply to the analysis models.

There are various ways for generating input time histories for dynamic response analyses. One includes scaling historical earthquake records by a constant scaling factor (i.e., uniform factor for all periods). Another modifies recorded motions by period-dependent scaling factors so that the resulting records would match the intended smooth spectral shape throughout the entire period range. There are relative merits in either approach. Whereas the first approach might result in theoretically more correct solutions (because of its ability to preserve inherent variations in strong ground motion data), this method requires a prohibitively large number of sets of input motions (probably over 20) to obtain a statistically stable set of response solutions. In recognition of the fact that this approach is impractical, the second approach of spectrum-compatible motions was chosen for the parametric analyses.

As discussed earlier, the stochastic nature of earthquake response of structures needs to be respected, and a design decision should not be based on a single analysis. The parametric analyses were expected to develop a meaningful set of statistical parameters describing the expected cask response, which could then be used to develop guidelines for reviewing cask design submittals. Logically, a larger number of time history inputs might be more appropriate to develop statistically stable response measures. However, in practice, it is very rare that adequate resources are available to support a sufficiently large number of input motion characteristics to meet the theoretical objective. The number of input motions for establishing statistically stable response measures depends on the complexity of the structural model and the degree of nonlinearity in the structural response. Common design practice involves inherent conservatism in the design criteria to compensate for the insufficient number of input motions. For example, in designing major bridges, enveloping the calculated demands for all the motion sets is rather common for applying up to three sets of input motion. Developing statistical parameters to design for a specified confidence level would generally require a minimum of seven to ten sets of input motions. For this project, it was decided as a compromise to conduct analyses for five sets of three component motions for each of the three adopted spectral shapes. Furthermore, the spectral compatible motion approach was adopted to maximize the chance that the resultant solutions be statistically stable (i.e., that the mean and standard deviation be meaningful) for the limited five sets of input motions.

This project used startup motion records contained in the strong motion database recommended by the NUREG/CR-6728. Five earthquake records for the WUS sites appropriate for the NUREG/CR-0098 and the Regulatory Guide 1.60 spectral shapes were selected:

- 1) 1978 Iran Tabas
- 2) 1999 Taiwan Chi-Chi
- 3) 1992 Landers
- 4) 1994 Northridge
- 5) 1979 Imperial Valley

Likewise, five different earthquake records for the CEUS sites appropriate for the NUREG/CR-6728 spectral shape were also selected:

- A) 1985 Nahanni
- B) 1988 Saguenay
- C) 1979 Imperial Valley
- D) 1989 Loma Prieta
- E) 1994 Northridge

Table 4.3 tabulates the startup motion records selected for developing the needed spectrum-compatible motions for the cask response parametric study. The steps in modifying the selected strong motion records for spectrum compatibility are listed below:

- (1) Find principal major and minor horizontal shaking directions.
- (2) Rotate startup motion to the principal directions.
- (3) Transform each component motion to frequency domain.
- (4) Based on the response spectra of startup motion and the target spectrum, adjust the Fourier amplitudes for each frequency but keep the phase angle unchanged. Repeat this process iteratively (typically no more than 5 iterations) for convergence to target spectrum.
- (5) Conduct baseline corrections of spectrum-compatible motion.
- (6) Recheck for spectrum compatibility and repeat (3) through (5) if necessary.
- (7) Check the cross correlation of the two orthogonal horizontal component motions and repeat (1) through (6) if necessary.

The three right columns in Table 4.3 tabulate the peak accelerations, velocity and displacement values of each component motion after modifications for spectrum compatibility. The peak values presented in Table 4.3 have been normalized for a horizontal PGA of 1 g. The appropriate horizontal PGA can be used as a uniform scaling factor applied to each of the component motion records to develop a three component input motion for design analyses. For the dry cask parametric studies, the ground motions shown in Table 4.3 were scaled to a variety of horizontal PGA values at ranging from 0.25 g to 1.25 g to calculate the cask response at various shaking levels.

As discussed earlier, for each of the ground surface spectrum-compatible motion records, deconvolution analyses were conducted using three profiles (as presented in Figure 3.5) to provide startup motion records at the foundation base in the coupled response model. These analyses allowed for variations of potential coefficient of restitution implied by different soil conditions. Appendix III has been included to document each set of the generated input motions. In the course of the project, some questions have been raised regarding how soil properties (e.g., strain-compatible properties) affect the selected ground motions. Appendix I is provided to offer some information on these issues. The following paragraphs provide a brief summary of the procedure.

As discussed earlier, it was intended that the three spectral shapes be scaled to various PGA levels. The resulting spectra could then be compared against the ground surface design spectrum documented by dry cask applicants to determine the appropriate dry cask response cases in terms of the relevant level of input motion intensity. While the PGA was used as a parameter to scale the ground motion records, it is important to remember that this parameter only characterizes the response of a zero period structure. The cask response is more sensitive to the spectral acceleration at other frequencies than it is to the PGA.

After selecting the input motion records, the next step was to choose soil profiles that represent a wide range of site conditions likely to be found throughout the United States. In the process of selecting ground motion records, the ground motion at the surface is assumed to be independent of the soil profile. The ground motions applied at the base of the foundation differ for the various soil types, but in theory, the resulting surface motions for the same earthquake with different soil types should be the same if no errors were introduced in the deconvolution process or in the foundation model. Thus, the sensitivity of the response with respect to the soil profile is primarily due to soil-structure interaction effects that are most pronounced in the upper layers of the foundation in the vicinity of the cask. Thus, if these analyses are to be applied to a site-specific investigation, the soil properties near the surface at the site should be compared with the properties of the generic soil profiles near the surface to determine which analysis results are most applicable to that site.

Table 4.3-A: Startup Motions for NUREG/CR-0098 Spectral Shape

No.	Earthquake Event	Year	Magnitude	Faulting Mechanism	Station	Distance (Km)	Site Code	Startup Motion Component, File Name	PGA (g)	PGV (cm/s)	PGD (cm)	Modified Motion Component, File Name	PGA (g)	PGV (cm/s)	PGD (cm)
1	Tabas, Iran	1978	7.4	Reverse	Tabas	3.0	Deep narrow Soil Profile	TABASITAB-UP TABASITAB-LN TABASITAB-TR	0.688 0.836 0.852	45.6 97.8 121.4	17.04 36.92 94.58	SET-1-H1 SET-1-H2 SET-1-UP	-1.000 -1.000 0.670	-90.0 -78.5 -46.7	44.6 -39.7 -21.4
2	Taiwan, Chi-Chi	1999	7.4	Reverse	W/GK	11.1	Deep soil Vs = 180-360 m/s at Upper 30m	W/GK-V W/GK-E W/GK-N	0.180 0.334 0.484	25.0 69.0 74.4	16.28 35.70 66.92	SET-2-H1 SET-2-H2 SET-2-UP	-1.000 -1.000 0.667	-84.8 67.6 44.9	40.1 -34.4 26.7
3	Landers	1992	7.3	Strike/Slip	Joshua Tree #	11.6	Shallow stiff soil	LANDERSUOS-UP LANDERSUOS000 LANDERSUOS090	0.181 0.274 0.284	15.0 27.5 43.2	9.39 9.82 14.51	SET-3 H1 SET-3 H2 SET-3 UP	1.000 -1.000 -0.667	-96.2 -89.0 -53.2	-27.8 33.3 25.4
4	Northridge	1994	6.7	Reverse	Jensen Filter Plant	6.2	Deep soil Vs = 180-360 m/s at Upper 30m	NORTHRUEN-UP NORTHRUEN022 NORTHRUEN292	0.300 0.080 0.200	34.1 106.2 99.3	8.89 43.06 24.00	SET-4 H1 SET-4 H2 SET-4 UP	1.000 -1.000 -0.667	-104.2 -75.1 -52.0	-53.4 37.7 21.7
5	Imperial Valley	1979	5.2	Strike/Slip	Calxico Fire Station	15.0	Deep soil Vs = 180-360 m/s at Upper 30m	IMPVALLIA-CXO-UP IMPVALLIA-CXO225 IMPVALLIA-CXO315	0.900 0.450 0.400	0.9 8.0 5.2	0.05 0.87 0.51	SET-5 H1 SET-5 H2 SET-5 UP	1.000 1.000 0.667	-91.9 -84.9 -51.2	32.8 -42.3 23.2

Table 4.3-B: Startup Motions for Regulatory Guide 1.60 Spectral Shape

No.	Earthquake Event	Year	Magnitude	Faulting Mechanism	Station	Distance (km)	Site Code	Startup Motion Component, File Name	PGA (g)	PGV (cm/s)	PGD (cm)	Modified Motion Component, File Name	PGA (g)	PGV (cm/s)	PGD (cm)
1	Tabas, Iran	1978	7.4	Reverse	Tabas	3.0	Deep narrow Soil Profile	TABASTAB-UP TABASTAB-LN TABASTAB-TR	0.688 0.836 0.852	45.6 97.8 121.4	17.04 36.92 94.58	SET-1-H1 SET-1-H2 SET-1-UP	-1.000 -1.000 0.670	-166.9 160.3 -99.3	124.9 102.7 -63.2
2	Taiwan, Chi-Chi	1999	7.4	Reverse	WGK	11.1	Deep soil Vs = 180-360 m/s at Upper 30m	WGK-V WGK-E WGK-N	0.180 0.334 0.484	25.0 69.0 74.4	16.28 35.70 66.92	SET-2-H1 SET-2-H2 SET-2-UP	-1.000 -1.000 0.667	-167.8 130.9 93.5	101.8 -85.5 67.1
3	Landers	1992	7.3	Strike/Slip	Joshua Tree #	11.6	Shallow stiff soil	LANDERSJOS-UP LANDERSJOS000 LANDERSJOS090	0.181 0.274 0.284	15.0 27.5 43.2	9.39 9.82 14.51	SET-3 H1 SET-3 H2 SET-3 UP	1.000 -1.000 -0.667	-156.4 -153.8 -110.8	71.2 -94.7 64.7
4	Northridge	1994	6.7	Reverse	Jensen Filter Plant	6.2	Deep soil Vs = 180-360 m/s at Upper 30m	NORTHRJEN-UP NORTHRJEN022 NORTHRJEN292	0.300 0.090 0.200	34.1 106.2 99.3	8.89 43.06 24.00	SET-4 H1 SET-4 H2 SET-4 UP	1.000 -1.000 -0.667	189.2 -132.1 -109.8	-136.4 93.7 87.1
5	Imperial Valley	1979	5.2	Strike/Slip	Calexico Fire Station	15.0	Deep soil Vs = 180-360 m/s at Upper 30m	IMPVALLA-CXO-UP IMPVALLA-CXO225 IMPVALLA-CXO315	0.900 0.450 0.400	0.9 8.0 5.2	0.05 0.87 0.51	SET-5 H1 SET-5 H2 SET-5 UP	1.000 1.000 0.667	146.8 -161.7 -117.4	80.7 -106.5 63.5

Table 4.3-C: Startup Motions for NUREG/CR-6728 Spectral Shape

No.	Earthquake Event	Year	Magnitude	Faulting Mechanism	Station	Distance (km)	Site Code	Startup Motion Component, File Name	PGA (g)	PGV (cm/s)	PGD (cm)	Modified Motion Component, File Name	PGA (g)	PGV (cm/s)	PGD (cm)
1	Nahanni	1985	6.8	Reverse/ Oblique	NW Terr, Canada: Mackenzie, St 1	6.0	IZA	S1-Up S1-010 S1-280	2.066 0.978 1.096	40.5 46.0 46.1	12.12 9.67 14.58	SET-1-H1 SET-1-H2 SET-1-UP	-1.000 -1.000 0.670	46.5 41.7 20.1	8.3 9.0 8.1
2	Sequenay	1988	5.9 ??		GSC Site-Baie-St. Pau	95.6	CBC	1125S07-V 1125S07-L 1125S07-V	0.122 0.122 0.173	2.6 4.7 5.7	0.28 0.51 0.66	SET-2-H1 SET-2-H2 SET-2-UP	-1.000 -1.000 0.667	42.9 45.7 21.8	8.9 5.5 4.5
3	Imperial Valley	1979	6.5	Strike/Slip	El Centro Array #1	15.5	AQD	H-E01-Up H-E01-140 H-E01230	0.164 0.280 0.277	5.1 19.0 11.3	2.39 6.41 5.44	SET-3 H1 SET-3 H2 SET-3 UP	1.000 -1.000 -0.667	40.6 40.6 19.2	7.5 8.2 4.6
4	Loma Prieta	1989	6.9	Reverse/ Oblique	Corralitos	6.1	B	CLS-Up CLS-000 CLS-090	1.300 1.328 1.060	28.8 57.4 49.4	9.34 7.22 7.43	SET-4 H1 SET-4 H2 SET-4 UP	1.000 -1.000 -0.667	42.6 35.7 20.3	7.8 6.4 6.5
5	Northridge	1994	6.7	Reverse	Pacoima Dam, Kagel Canyon	8.2	B	PKC-Up PKC-000 PKC-090	0.559 0.752 0.978	23.7 34.3 48.5	9.84 11.48 8.38	SET-5 H1 SET-5 H2 SET-5 UP	1.000 1.000 0.667	36.4 51.2 19.3	8.2 10.7 -5.5

## 4.2 Frictional Contact at Cask/Pad Interface

A literature search was performed to gather the results of experimental studies investigating the coefficient of friction between steel and concrete. The reports of several relevant studies were identified. There were a variety of goals in the studies. Two studies [21, 22] investigated the bond strength between steel plates and concrete that had been cast against the steel plates, and also measured the coefficient of friction after the bond was broken. Another study [23] investigated the coefficient of friction between wire brush and steel plate skids and concrete at low and high speeds for aircraft landing gear applications. While the wire brush skid data is not directly applicable to this work, the flat plate data proved useful. The study documented in Idun and Darwin [24] was conducted to investigate the effect of an epoxy coating on the coefficient of friction for applications to the bond between reinforcing bars and concrete. The data given for uncoated reinforcing bars is applicable to this work. Bonding of reinforcing bars also motivated the work of Baltay and Gjelsvik [25], where the coefficient of friction was measured over a wide range of normal pressures to investigate the effect of the normal pressure. Finally, an investigation of the coefficient of friction between steel and concrete at low sliding speeds is documented in Olofsson and Holmgren [26]. This investigation was motivated by a design of a natural gas storage room in which a steel plate slides slowly against a concrete surface.

A variety of conditions could potentially exist at the interface between the cask and the pad. It is possible for moisture to accumulate in that region, decreasing the coefficient of friction. It is also possible that the two surfaces could develop a bond over time, effectively increasing the coefficient of friction. The experimental studies referenced here indicate that the coefficient of friction can be influenced by the presence of mill scale on the steel surface, as well as by the normal pressure applied to the interface. The data from the experimental results on a steel/concrete interface has been compiled to obtain an estimate of the statistical variation in the coefficient of friction. All of the relevant data in the referenced experimental results of a coefficient of friction at the steel/concrete interface has been compiled and plotted in the form of a histogram in Figure 4.5. Also shown in this plot is a normal probability distribution fitted to this data.

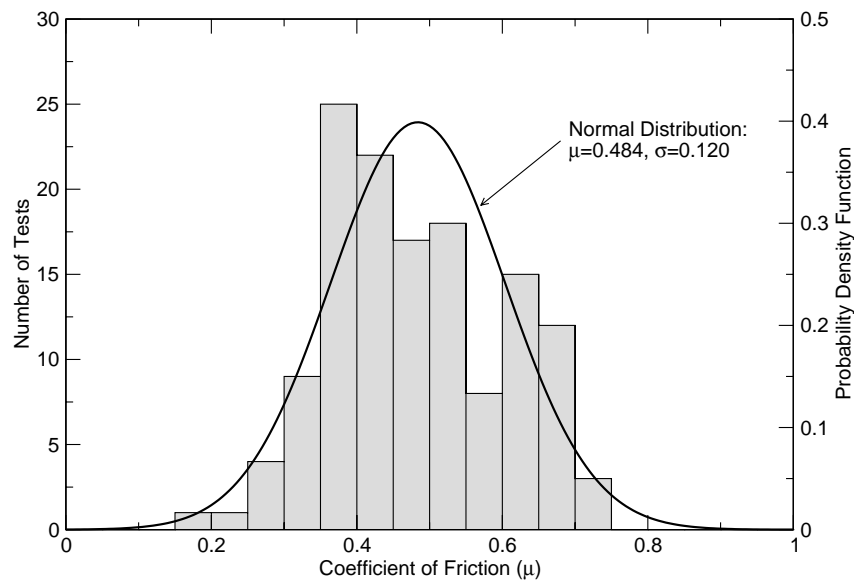


Figure 4.5: Histogram of Steel/Concrete Coefficient of Friction Test Results

The data included in this plot comes from all of the sources referenced above. In some cases, data was excluded because it was not relevant. The epoxy-coated bar data in Idun and Darwin [24] was not

included, and the wire brush skid data in Dreher [23] was also not included. Idun and Darwin [24] provide a table showing the averages of 10 experiments of a given type. These averages were each counted as a single data point, but they could arguably be weighted by a factor of 10. The overall statistics are not affected significantly by changing the weighting of these data points. Also, in Baltay and Gjelsvik [25], some low values were obtained for cases with low normal pressure and with mill slag on the plates. The lowest pressures in these experiments were around 6.9 kPa (1 psi). The nominal contact pressure between the cask and pad ranged between 88 kPa (13 psi) and 180 kPa (26 psi). There may be a case for excluding those data points because such conditions would not be observed, but they were included in the plot to represent a wide range of conditions. The cases where the concrete was initially bonded to the steel resulted in higher values for the coefficient of friction, but they were included to give a representation of cases where the cask might develop a bond with the concrete over time.

As noted on the plot, a normal distribution fitted to the data has a mean of 0.484 and a standard deviation of 0.120. The lowest recorded value was 0.2 for a case with mill slag on the steel and a very low normal pressure. The highest recorded value was 0.72. This was from an experiment where the concrete was initially bonded to the steel, and that bond was broken before the coefficient of friction was measured. For the parametric study, the goal was to select an extreme lower bound, an extreme upper bound, and a best estimate value for the coefficient of friction between the cask and pad. Values of 0.2, 0.8, and 0.55 were selected for these cases, respectively. Based on the normal distribution fitted to the experimental data, the lower bound value of 0.2 is about 2.4 standard deviations below the mean, and the upper bound value of 0.8 is about 2.6 standard deviations above the mean. About 99% of all samples fall within these bounds.

The surveyed data is for the coefficient of friction at steel/concrete interfaces. Dry cask storage systems can have either steel or concrete at the base, where contact is made with the concrete pad. The coefficient of friction between concrete and concrete is likely to be somewhat higher than that between steel and concrete, but the upper and lower bounds of 0.2 and 0.8 used for cask with steel bases are judged to still provide useful bounding estimates of the behavior of casks with concrete bases.

## 5. Analysis Results

Some basic understanding of the mechanics of freestanding dry cask storage systems (DCSS) in response to seismic ground motion is instrumental for interpreting the analysis results of the parametric study. The dynamic response of DCSSs interacting with the underlying soil/rock foundation is of particular interest. Three main response parameters were used to describe the behavior of the analytical cask models: (1) the lateral displacement at the cask base relative to the pad (as a measure of cask sliding), (2) the angular rotation of the cask with respect to the vertical coordinate axis (as a measure of cask tipping angle), and (3) the lateral displacement at the cask top relative to the pad (as a measure of overall lateral movement of the cask). There is considerable scatter in the cask response results. Consequently, linear regression analyses were performed on these results to generate nomograms, which can be used as a practical tool for cask system reviewers and designers to assess the seismic behavior of casks.

### 5.1 Physics of Cask Behavior and Soil-Structure Interaction Effects

It is instructive to examine the basic physics of the freestanding cask problem before proceeding with the presentation of analysis procedures and results. In this discussion, the behavior of the cask is examined both before and after the onset of cask motion relative to the pad.

#### 5.1.1 Cask Behavior Before Onset of Relative Movement

##### 5.1.1.1 Static Equilibrium Calculations

Figure 5.1 shows a diagram of the cross section of a cask with some essential dimensions. The distance from the base of the cask to the center of gravity is denoted as  $h_{cg}$ , and the shortest horizontal distance from the center of gravity to the edge of the cask is denoted as  $r$ . In the case of a rectangular module,  $r$  is half the shortest base dimension. For an upright cylindrical cask,  $r$  is the radius of the cask base.

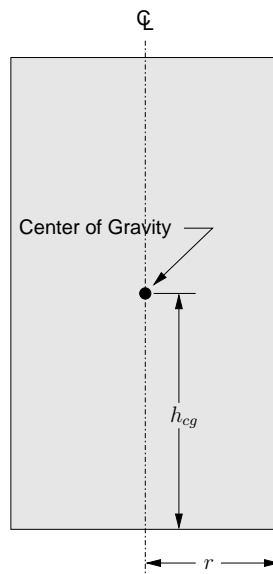


Figure 5.1: Diagram of a Cask

A freestanding cask subjected to a seismic ground motion will not experience any motion relative to the slab upon which it rests if the ground motion is below certain threshold values. It is assumed that the cask/pad interface follows Coulomb's law of friction, where slippage occurs between two surfaces only

when the lateral force acting to cause sliding exceeds the product of the friction coefficient,  $\mu$ , and the compressive normal force on these surfaces.

Principles of statics can be applied to determine the point at which the cask could experience sliding or tipping relative to the pad. Prior to cask tipping or sliding, the cask moves together with the pad as if they were bonded together. If  $a_h$  is the magnitude of the horizontal ground acceleration vector during a seismic event and  $a_v$  is the vertical ground acceleration at that same time (downward acceleration is positive), one can show that by applying Coulomb's friction law the following condition must be met for sliding to occur:

$$\mu < \frac{a_h}{(g - a_v)} \quad (5.1)$$

where  $g$  is the acceleration of gravity.

Equation 5.1 can be adapted to solve for the horizontal acceleration that will cause sliding to initiate. To aid in this, it is useful to introduce a variable,  $v$ , which is the ratio of  $a_v$  to  $a_h$ , at any given time step.

$$v = \frac{a_v}{a_h} \quad (5.2)$$

Substituting Equation 5.2 into Equation 5.1 and solving for  $a_h$  results in the following condition for sliding:

$$\frac{a_h}{g} > \frac{1}{(1/\mu) + v} \quad (5.3)$$

In a similar manner, by solving for moment equilibrium, a criterion can also be defined for the initiation of tipping, assuming that the cask has not already begun to slide:

$$\frac{r}{h_{cg}} < \frac{a_h}{(g - a_v)} \quad (5.4)$$

Substituting Equation 5.2 into this and solving for  $a_h$  results in a condition for tipping:

$$\frac{a_h}{g} > \frac{1}{(h_{cg}/r) + v} \quad (5.5)$$

By comparing Equations 5.1 and 5.4, it can be seen that if  $\mu > \frac{r}{h_{cg}}$ , tipping will occur before sliding,

whereas if  $\mu < \frac{r}{h_{cg}}$ , sliding will occur first. For both sliding and tipping, the most critical situation is

when there is a large downward vertical acceleration at the same time as a large horizontal acceleration. This situation results in a combination of a high force inducing sliding or tipping, and a low resisting force. In the sign convention employed here, this happens whenever  $v$  has a high positive value. Because  $v$  is a ratio of two constantly changing quantities,  $v$  changes constantly during the seismic event. For simple capacity calculations using the equations presented above, it is reasonable to use a critical value of  $v$ , equal to the absolute value of the ratio of the maximum vertical acceleration to the maximum horizontal acceleration. For the earthquake ground motions in this study, the critical  $v$ , computed as described above, ranges from 0.67 to 1.0. The above equations are useful for understanding whether the cask is likely to move at all, and if so, whether tipping or sliding is likely to be the dominant type of motion.

For the cylindrical cask in the study,  $r$  is 1.68 m (66.25 in), and  $h_{cg}$  is 3.00 m (118.2 in). The ratio  $r/h_{cg} = 0.56$  for this design, meaning that if  $\mu$  is less than 0.56, the cask is dominated by sliding behavior rather than by tipping behavior. In the case of the rectangular module,  $r$  is 1.47 m (58.0 in) and  $h_{cg}$  is 2.54 m (100.0 in), resulting in a ratio  $r/h_{cg}$  of 0.58.

### 5.1.1.2 Soil-Structure Interaction Effects

If the ground motion is not sufficiently high to cause the cask to lift off the pad or slide relative to the pad, the cask behaves essentially as if it were bonded to the pad. The interaction between the cask and the soil takes place in a manner very similar to typical soil-structure interaction problems involving fixed structures. The deformability of the soil to which the structure is attached reduces the stiffness of the overall system.

The cask itself is a quite rigid structure. The finite element model of the cylindrical cask was modified to determine the effect of the foundation on the fundamental frequency of the cask before uplift or sliding occurs. The contact interactions between the cask and pad, and the pad and soil were changed to bonded surfaces. The nodes at the base and sides of the soil column were constrained against displacement. A horizontal force was applied to the nodes on the top of the cask, and this load was abruptly released. The frequency of the fundamental rocking mode of the cask can be determined from the time history of the cask response after the load is released.

A second model was created in which the elements comprising the soil foundation were removed, leaving only the cask and pad. This is used to determine the fundamental rocking frequency of the cask/pad system without the effect of the soil to determine the effect that the soil foundation has on the fundamental frequency of the system. As before, the cask/pad interface is bonded. The nodes at the bottom of the pad are restrained against displacement. Figure 5.2 shows the deformed shape of this model just before the load is released.

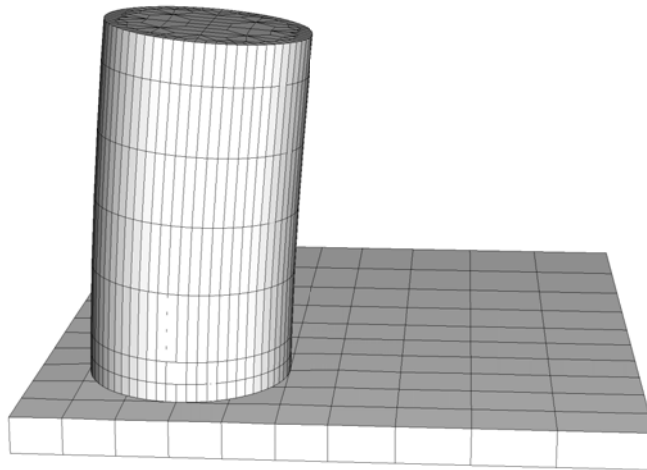


Figure 5.2: Deformed Shape of Cylindrical Cask/Pad Pullback Test (Magnified 100x)

Table 5.1 shows the frequencies of this rocking mode obtained from the various analysis cases in the study. In the soil column investigation, both the elastic cask and the rigid cask models were used to determine the effect of the rigid cask modeling approach on this soil-structure interaction effect. It can be seen that the frequencies of the rigid cask models are slightly lower than those for the elastic cask model, but the difference is relatively minor. The rigid cask was not analyzed for the model with only the cask

and pad because the main source of flexibility in that case is the cask, and the results with the rigid cask would not be meaningful.

Table 5.1: Frequency of Cask Rocking Mode

	Elastic Cask	Rigid Cask
Soft Soil	7.7 Hz	7.5 Hz
Stiff Soil	13.6 Hz	12.4 Hz
Rock	14.2 Hz	13.0 Hz
Cask and Pad Only	28.3 Hz	N/A

From this table, it can be seen that the shift in the frequency of the rocking mode due to the presence of the foundation is quite significant, especially for the softer foundations. The difference between the rock and stiff soil foundations is not particularly large due to the presence of the layers of engineered fill and weathered rock at the top of the rock foundation model.

Figure 5.3 shows the spectral shapes of the earthquakes used in this study. These spectral shapes are normalized to the peak ground acceleration (PGA), so the quantity plotted on the y axis is the ratio of the pseudo-spectral acceleration (PSA) to the PGA. The periods of the elastic cask model are also shown as vertical lines for the soft soil, stiff soil, and rock foundations, as well as for the fixed base model of the cask and pad only. It can be seen that for the NUREG/CR-0098 and the Regulatory Guide 1.60 earthquakes, the fixed base cask experiences accelerations that are only slightly higher than the PGAs. The decrease in the stiffness due to the foundation significantly increases the acceleration experienced by the cask before uplift or sliding occurs due to the soil-structure interaction effect. The NUREG/CR-6728 spectrum has more high-frequency content, and even the fixed base cask experiences accelerations greater than the PGA.

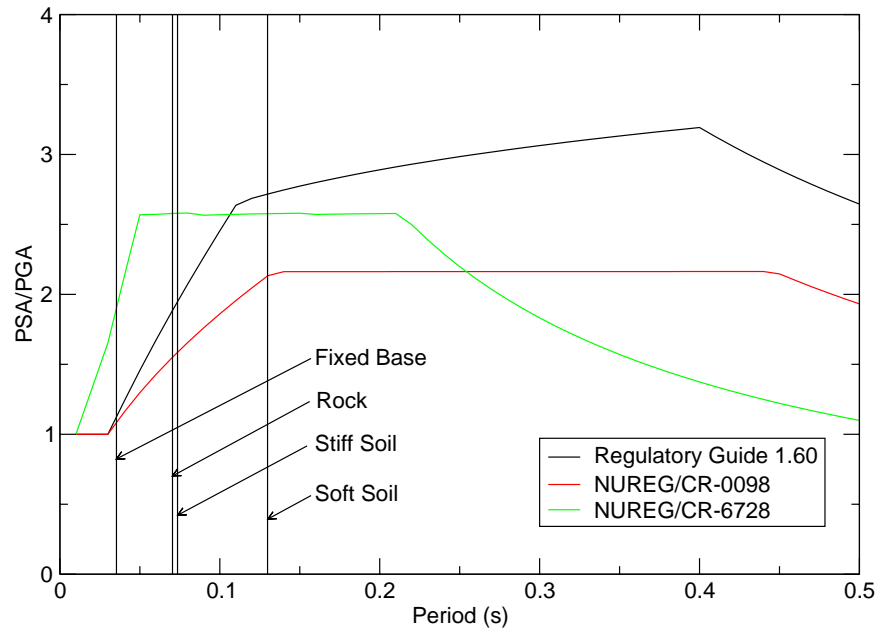


Figure 5.3: Spectral Shapes and Cask Periods with Various Soil Types

The statics-based equations presented in the previous section assumed that the cask system is rigid enough that the peak acceleration experienced by the cask is equal to the PGA. It can be clearly seen from Figure 5.3 that before uplift or sliding, the cask actually can experience accelerations much greater than the PGA. The accelerations used in the equations of the previous section should be multiplied by the

ratio of PSA to PGA to account for this. The accelerations that the cask experiences before uplift under a given seismic event can potentially be close to 3 times higher than the PGA if the soil foundation is sufficiently compliant. This highlights the importance of including the foundation in a model of the freestanding cask. If the foundation is not included in the model, the model may significantly under-predict the magnitude of the seismic event required to initiate tipping of the cask.

### **5.1.2 Cask Behavior After Onset of Relative Movement**

After the cask begins to tip, it is no longer valid to assume that the cask is bonded to the pad. Before uplift, the cask has a unique fundamental frequency. The frequency of the free vibration of the cask is independent of the vibration amplitude. Once an edge of the cask lifts up from the pad, the frequency of that rocking motion becomes a highly nonlinear function of the amplitude of that motion. A method to characterize the rocking frequency of the cask as a function of the tipping angle was proposed by Housner [27]. The function resulting from this method shows that the rocking period is zero at a tipping angle of zero, and that the period asymptotically approaches infinity as the tipping angle approaches the angle at which the center of gravity is directly above the corner of the cask.

As the cask rocks back and forth, energy is absorbed every time the cask impacts the pad. This can be a significant energy dissipation mechanism, and the type of soil underlying the pad can have a noticeable effect on the amount of energy dissipated. This mechanism is believed to be the most important soil-structure interaction effect after the cask begins to tip. It is important to note that the cylindrical cask can assume either a rocking motion or a rolling motion. Significant energy is dissipated if the cask is rocking back and forth, but very little energy is dissipated in the rolling motion.

### **5.1.3 Demonstration of Soil Column Response and Soil-Structure Interaction**

As described in Section 3.1.5, the target surface ground motions have been modified using a deconvolution procedure to produce acceleration histories to be applied to the base of the soil column. The deconvolution procedure is based on the assumption that the soil mass behaves as an idealized one-dimensional soil column. If the soil column used in the finite element models perfectly replicates those assumptions, the ground motion measured at the surface of the soil column without the presence of any structures should closely match the original surface motion.

To assess the performance of the model in this project to replicate the original surface ground motion, the cask and pad have been removed from the soil column models, and each of the three soil columns (soft soil, stiff soil, and rock) has been subjected to the five deconvolved base ground-motion records for each of the three spectral shapes in the parametric study. The boundary conditions on the soil column model ensure that the ground motion is nearly identical at any two nodes located on the same vertical layer of the column.

Figure 5.4 shows a representative comparison of the spectral shape of the original surface ground motion with spectral shapes of the surface motion obtained from the analytical models without the presence of the cask and pad. The plots in this figure show the first horizontal component of the ground motion with the Case 1 earthquake conforming to the NUREG/CR-0098 spectral shape. Spectral responses are shown with a 5% damping for the soft soil, stiff soil, and rock columns, as well as for the original surface motion. Plots of the soil column response spectra are provided for all three spectral shapes and all three soil profiles in the first horizontal and vertical directions in Appendix IV. The response of the soil column without the cask and pad matches the original surface motion quite closely at periods above about 0.3 s. At higher frequencies, there are occasionally high peaks in the soil column model response. Once the cask lifts up from the pad, it is believed to respond most to spectral content in the range of 0.5 Hertz (Hz) to 2 Hz, so these high frequency differences likely have a negligible effect on the cask response. If

they do have an effect, it would be to increase the response, so the results obtained in this study are believed to be conservative.

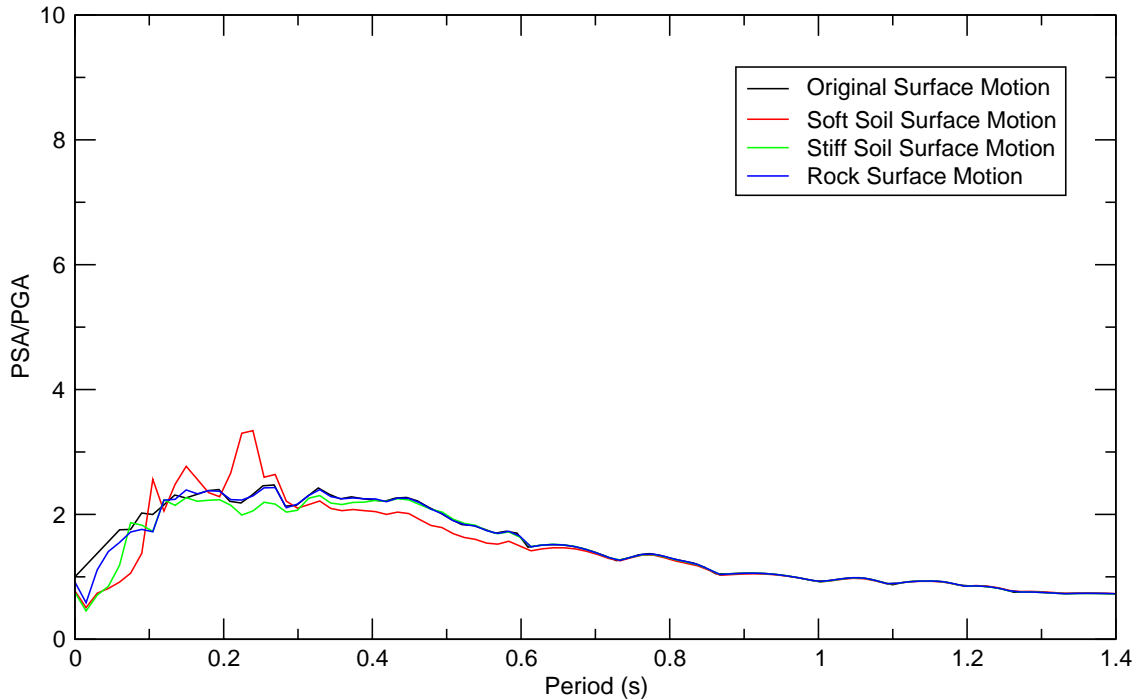


Figure 5.4: Comparison of Original Surface Motion and Motion at Top of Soil Column Model, NUREG/CR-0098 Spectral Shape, Case 1 Earthquake, First Horizontal Component

The spectral shapes in Appendix IV show the response of the soil column without the presence of cask and pad. Since there is no structure present on the surface of the ground and the layers are uniform, the response is not dependent on the horizontal location on the soil mass. When the cask and pad are present, the soil-structure interaction effects cause local disturbances in the soil response. The magnitude of these disturbances increases in regions near the cask and pad.

To demonstrate the local disturbances in the region of the cask and pad in the soil column, spectral shapes have been derived from the acceleration time histories taken at a number of locations in the full analysis model. These are shown for the first horizontal component of the ground motion with the Case 1 earthquake conforming to the NUREG/CR-0098 spectral shape, scaled to 1 g PGA, with the soft soil profile in Figure 5.5. Similar sets of plots are shown for the stiff soil in Figure 5.6, and for the rock profile in Figure 5.7. In all these cases, the cask experienced significant motion but did not tip over. The earthquake ground motions used in these plots are the same as those in Figure 5.4.

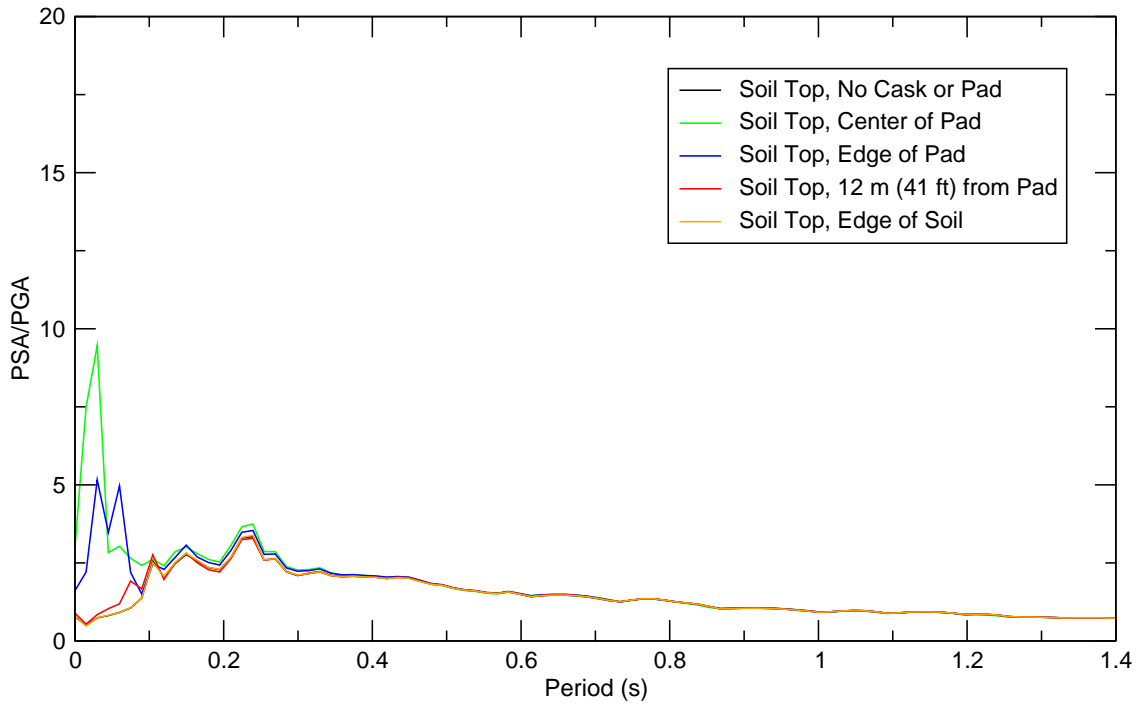


Figure 5.5: Spectral Response at Points on Surface of Soil Column Model, Soft Soil, NUREG/CR-0098 Spectral Shape, Case 1 Earthquake, 1 g PGA, 1<sup>st</sup> Horizontal Component

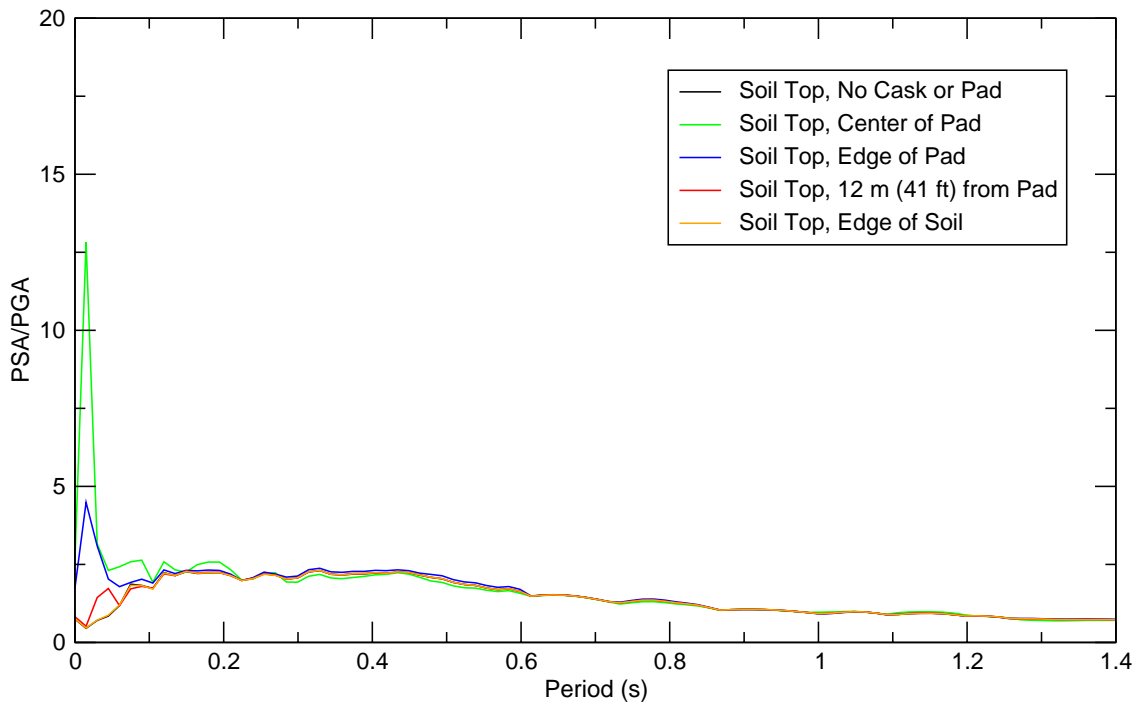


Figure 5.6: Spectral Response at Points on Surface of Soil Column Model, Stiff Soil, NUREG/CR-0098 Spectral Shape, Case 1 Earthquake, 1 g PGA, 1<sup>st</sup> Horizontal Component

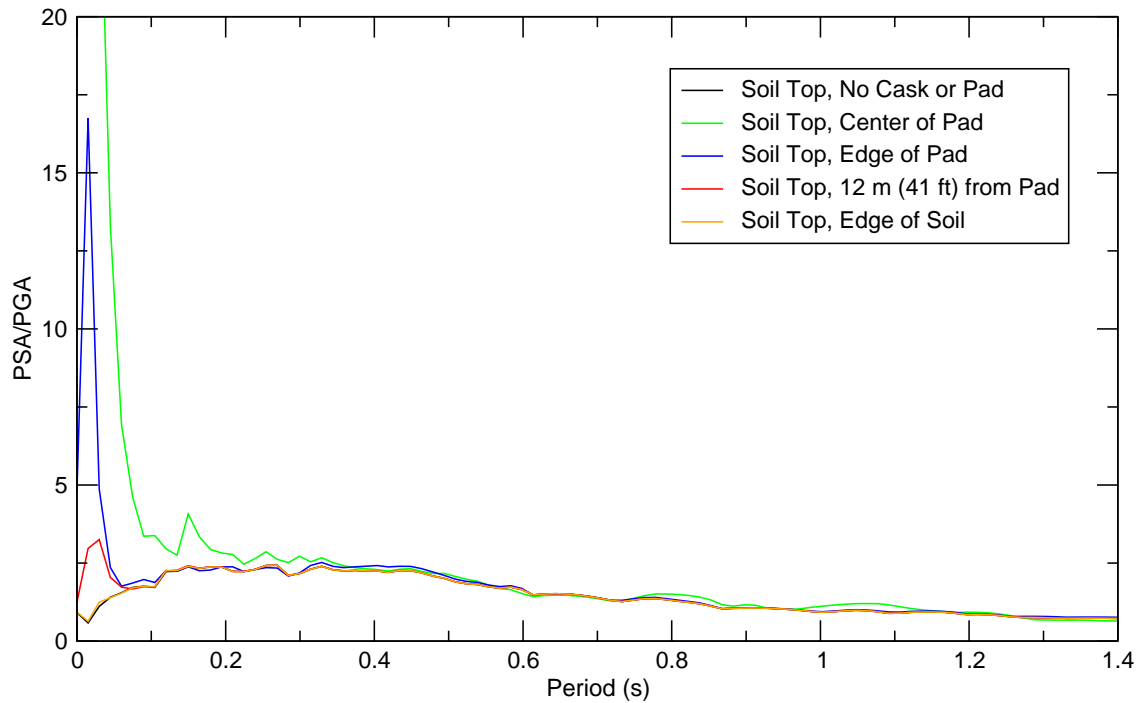


Figure 5.7: Spectral Response at Points on Surface of Soil Column Model, Rock, NUREG/CR-0098 Spectral Shape, Case 1 Earthquake, 1 g PGA, 1<sup>st</sup> Horizontal Component

The results for all three soil profiles have similar characteristics. Locations immediately below the pad experience extremely high frequency responses. As the recording location is moved away from the pad, the response approaches that of the bare soil column. For all three soil profiles, the response at the far edge of the soil column matches that of the bare soil column almost exactly, and the two lines are indistinguishable. It is interesting to note that the high frequency peaks in the response spectrum for the points directly below the pad increase in magnitude as the stiffness of the foundation increases. In the case of the rock profile, this effect may be caused by the presence of the soft layer of engineered fill.

The plots shown in this section and in Appendix IV demonstrate that the soil column model reasonably replicates the target surface ground motion and still allows for soil-structure interaction effects to occur. As mentioned previously, allowing for soil-structure interaction is important both before and after the cask begins to move relative to the pad. Before the cask begins to move relative to the pad, the reduction in effective frequency of the cask system can cause a significant increase in the accelerations of the pad. After the cask begins to lift off from the pad, the soil-structure interaction effects are primarily evident in the amount of rebound of the cask after impact with the pad.

To demonstrate the effect of soil-structure interaction, a modified version of the model of the cylindrical cask has been created without the soil column. The cask and pad models are exactly the same as in the full model, but the nodes at the base of the pad have an imposed acceleration. The ground motion record applied to the pad base has been adjusted to fit the target spectral shape but has not undergone the deconvolution procedure. Thus, the ground motion at the base of this “rigid” model is equivalent to the ground motion at the surface of the soil column model in the far field away from the cask. This model is useful to demonstrate the behavior of the cask without the soil-structure interaction effects. Comparing the results from the rigid model with those from the coupled models that include the soil or rock foundation can provide insights into the soil-structure interaction effects.

A small subset of the parametric analysis cases has been analyzed using this rigid cask model. The ground motion records applied to this model are the Case 1 records conforming to the Regulatory Guide 1.60 spectral shape. The cask/pad friction coefficient has been set to 0.55. Analyses were performed with the PGA at 0.25g, 0.4g, 0.5g, and 0.6g. The peak cask top lateral displacement magnitudes relative to the pad for analyses with the soft, stiff, and rock profiles, as well as for the rigid model, are reported in Table 5.2. The analyses that include the soil column will be discussed in more detail later in this report.

Table 5.2: Comparison of Peak Top Displacements (m) of a Cylindrical Cask for Rigid Model and Coupled Models with Soil or Rock Foundation (Note: 1 m = 3.28 ft)

PGA (g)	Soft	Stiff	Rock	Rigid
0.25	0.00711	0.00142	0.00309	0.0000289
0.4	0.351	0.206	0.456	0.124
0.5	1.134	1.362	0.856	0.364
0.6	2.46	1.90	2.10	Tips

In an analysis of this nature, it is expected that there should be a large amount of scatter. A larger sampling of analysis cases would be required to provide a rigorous demonstration of the soil-structure interaction effect. However, there are clear trends that can be seen even from this small set of analysis results.

The static threshold of horizontal motion at which tipping would begin to occur is computed using Equation 5.5. For the Regulatory Guide 1.60 ground motion records, the peak vertical acceleration is equal to the peak horizontal acceleration, so it is assumed that  $\nu=1.0$  for the purposes of this calculation. For the cylindrical cask, this threshold is 0.36 g. As mentioned previously, soil-structure interaction can actually cause the cask to begin tipping at accelerations below this level. Because the rigid model does not include soil-structure interaction, there should be very minimal tipping for horizontal ground motions below 0.36 g.

From Table 5.2, it can be seen that at 0.25 g, all models experience minimal response, but the response of the rigid model is orders of magnitude lower than that of the models with soil. At 0.4 g, which is slightly above the static tipping threshold, the response of the rigid model is roughly half that of the coupled models with soil or rock foundation. This is also true at 0.5 g. At 0.6 g, the cask response in all models is significant, and they are all on the verge of tipping. The rigid model actually tips over, while none of the other models tip.

The soil-structure interaction effects are particularly important if the PGA is below, or slightly above, the static tipping threshold. Soil-structure interaction can cause the cask to begin tipping much earlier than it would without this effect. Once the cask has begun to tip, the soil-structure interaction effects appear to have a reduced influence on the cask response. It is important to keep in mind, however, that accurately modeling the point at which tipping first occurs can have a significant effect on the response later on in an analysis, even in a case where the cask would tip without including soil-structure interaction effects in the model.

## 5.2 Representative Analysis Results

A large number of analyses were conducted using the parameters outlined in the previous chapter to examine the sensitivity of cask response to these parameters. Because of the large number of analyses, it is not practical to include all results for every analysis in this report. A few key results from each of the analyses are discussed in Section 5.3. Detailed analysis results of some selected cases are presented here to provide an understanding of the key phenomena.

Figure 5.8 provides an illustration of some meaningful measures of cask response that are used in the parametric study. Annotations are made on a deformed mesh plot from an analysis of the cylindrical cask, but the same measures are also used for the rectangular module. At the beginning of an analysis, the cask is upright, and the center of the cask base rests on the initial cask position denoted in the figure. During an earthquake event, the cask can experience very large movements, as illustrated in the figure. These movements potentially consist of a combination of sliding, rocking, and rolling.

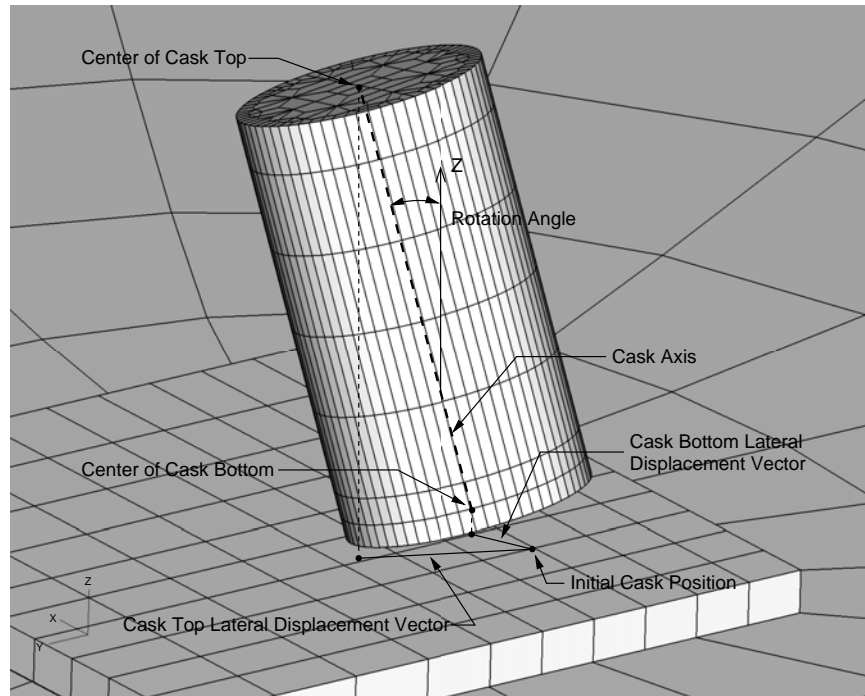


Figure 5.8: Explanation of Key Response Quantities

The three primary measures of cask response used in the parametric study and illustrated in Figure 5.8 are the lateral displacement of the cask base relative to the initial position on the pad, the lateral displacement of the cask top relative to the initial position on the pad, and the angle of rotation from the vertical axis. Magnitudes of the relative displacement vectors are more useful than the values of the components of these vectors in the two lateral directions because the cask could potentially move in any direction. The magnitude of the relative lateral displacement vector between the cask base and pad is a reflection of the amount of cask sliding. It is important to realize, however, that for a cylindrical cask, the cask can also roll along the edge of the base, and that rolling can contribute to the relative lateral base displacement. The rotation angle is the angle between the axis of the cask and the vertical coordinate axis. This is a direct way to assess the amount of rotation at a given time and could be used to determine a factor of safety against tipping. The magnitude of the relative lateral displacement vector between the cask top and the pad is a measure that combines the effects of sliding, rotation, and rolling. This physical quantity is a good overall measure of cask response and can be directly applied to determine whether collision would occur between adjacent casks in an array.

All quantities mentioned above vary significantly in the duration of an analysis. A post-processing program has been developed to extract time histories of these measures from the analysis output file. Time histories of these measures are presented in the next section for a selected set of analyses to provide

a basic understanding of the phenomena. The maximum values of these three measures over the duration of the earthquake are reported for the full set of parametric analysis cases.

### 5.2.1 Representative Analysis Results for Cylindrical Cask

The cylindrical cask has a strong tendency to undergo a rolling motion in preference to a rocking motion if the ground motion is sufficiently high to put the cask into motion and the coefficient of friction is sufficiently high to prevent sliding. Figure 5.9 shows a representative plot of the lateral displacement trajectories of both the cask top and bottom relative to the pad for the cylindrical cask subjected to a high ground motion. In this case, the stiff soil profile is used, the coefficient of friction between the cask and pad is 0.55, and the Iran Tabas earthquake (Case 1) is used, fitted to the NUREG/CR-0098 spectral shape and scaled for a PGA of 1.0 g.

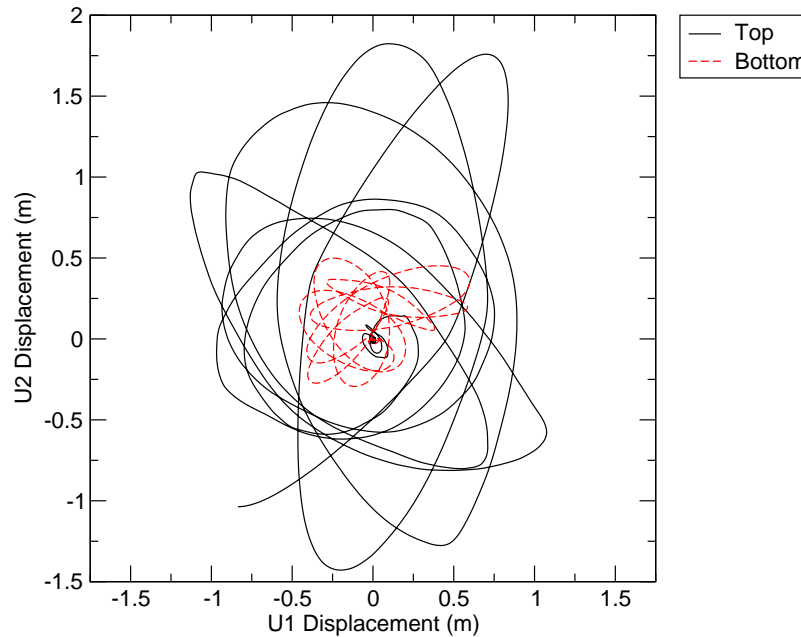


Figure 5.9: Lateral Displacement Trajectories for Cylindrical Cask Top and Bottom, Iran Tabas Earthquake, NUREG/CR-0098 Spectral Shape, PGA=1.0 g, Stiff Soil Profile, Cask/Pad  $\mu=0.55$

When the lower bound friction coefficient of 0.2 between the cask and pad is used, a sufficiently high lateral force to initiate rocking or rolling motion cannot be developed, and the cask slides on the pad. The displacement of the cask top is nearly identical to that of the cask base. Figure 5.10 shows plots of the time histories of the magnitudes of the top and bottom lateral displacements relative to the pad for the cylindrical cask with the stiff soil profile and the cask/pad  $\mu=0.2$ . Plots are shown for all five of the earthquakes conforming to the NUREG/CR-0098 spectral shape, and the earthquakes are all scaled so that the PGA is equal to 1.0 g. It can be seen that the plots of cask top and base displacement are nearly identical because the cask experiences only minor rotation. When the top and bottom displacements are almost the same, only the red line shows in the plots.

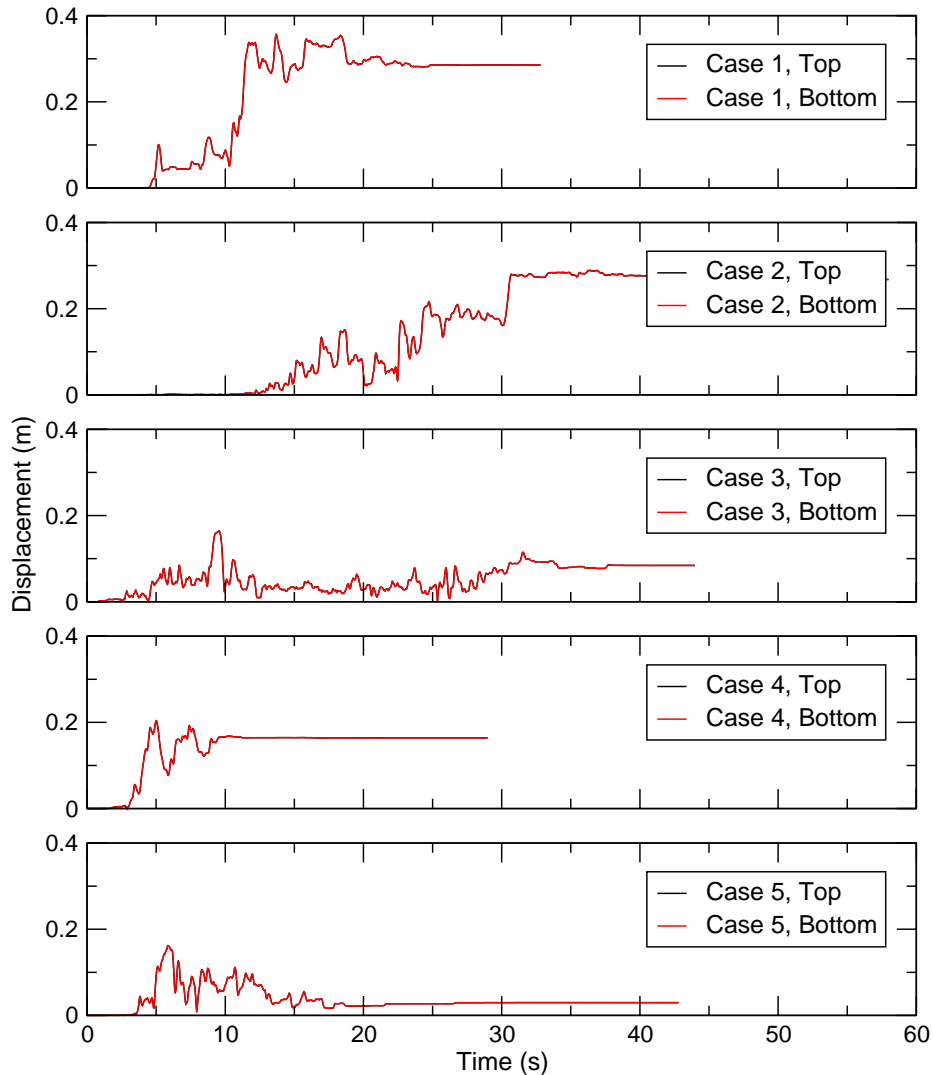


Figure 5.10: Time Histories of Cask Displacement Relative to Pad for Cylindrical Cask, Stiff Soil Profile, Cask/Pad  $\mu=0.2$ , All 5 Earthquakes, NUREG/CR-0098 Spectral Shape, PGA=1.0 g

Figure 5.11 shows a similar plot for all five earthquake records, but with a cask/pad coefficient of friction of 0.55. Here it can be seen that the cask base and top displacements significantly deviate from each other in some cases, indicating a relatively high rotational angle. In some cases, the cask undergoes a rolling motion, and the cask top experiences very high displacements relative to the pad. In other cases, the cask has more of a tendency to rock back and forth, and the cask top displacements are typically much smaller. Once the cask begins to move relative to the pad, the response becomes highly nonlinear and highly dependent on the phasing of the ground motion with respect to the phasing of the cask response.

As the ground motion increases, the cask response tends to increase. If an input ground motion record is scaled linearly, the cask response will not always increase monotonically as a function of the ground motion. Since the cask response is dependent on the state of the cask when subjected to a ground motion pulse, the ground motion could either increase or decrease the motion of the cask. It sometimes occurs that scaling up the ground motion causes the cask to move in such a way so that the pulses that may have previously excited the cask actually decrease the energy in the cask. If the peak responses of the cask

subjected to a number of ground motion records are averaged out, the average response will almost always increase monotonically as a function of the ground motion.

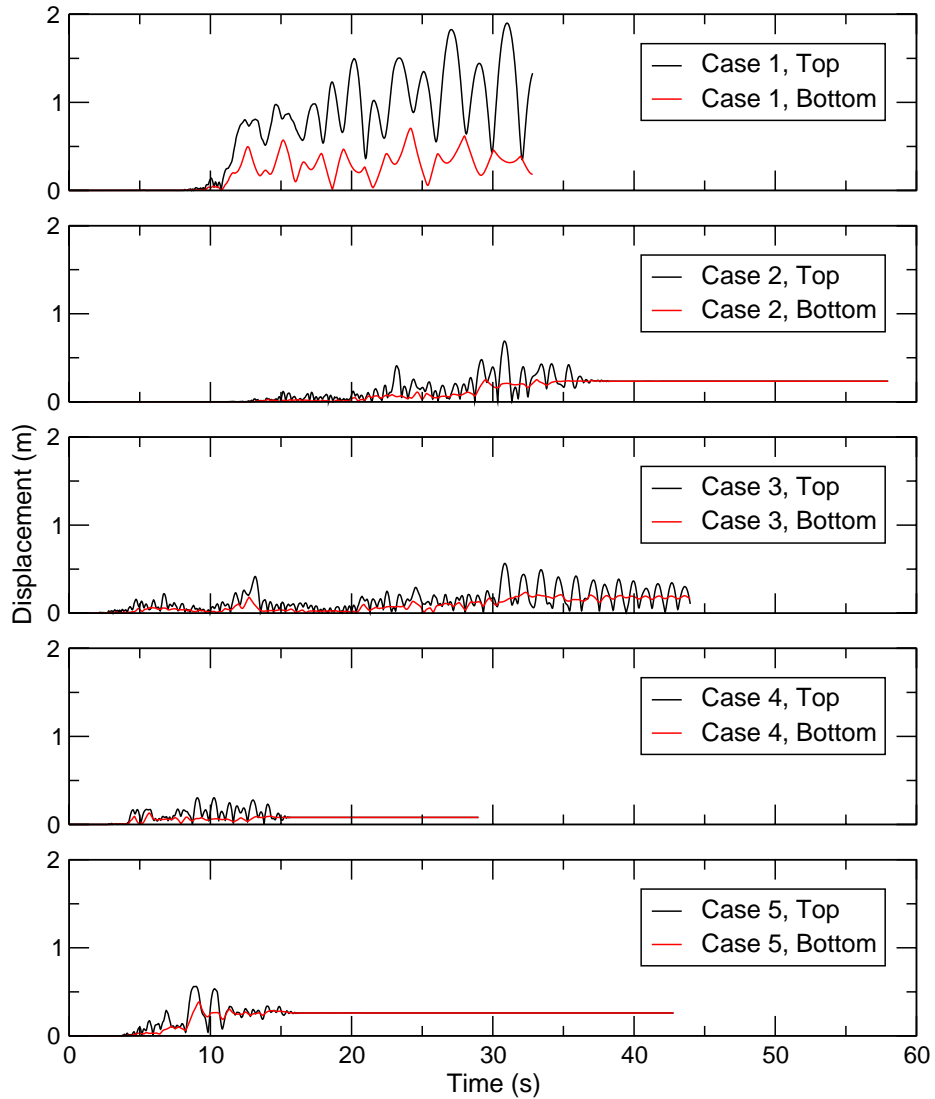


Figure 5.11: Time Histories of Cask Displacement Relative to Pad for Cylindrical Cask, Stiff Soil Profile, Cask/Pad  $\mu=0.55$ , All 5 Earthquakes, NUREG/CR-0098 Spectral Shape, PGA=1.0 g

Figure 5.12 shows a series of cask displacement histories similar to those shown in the previous two figures, but with a coefficient of friction of 0.8 between the cask and pad. The responses are in general quite similar to those with  $\mu=0.55$ , but they are slightly larger. It is interesting to note that in Case 2, the cask tips over.

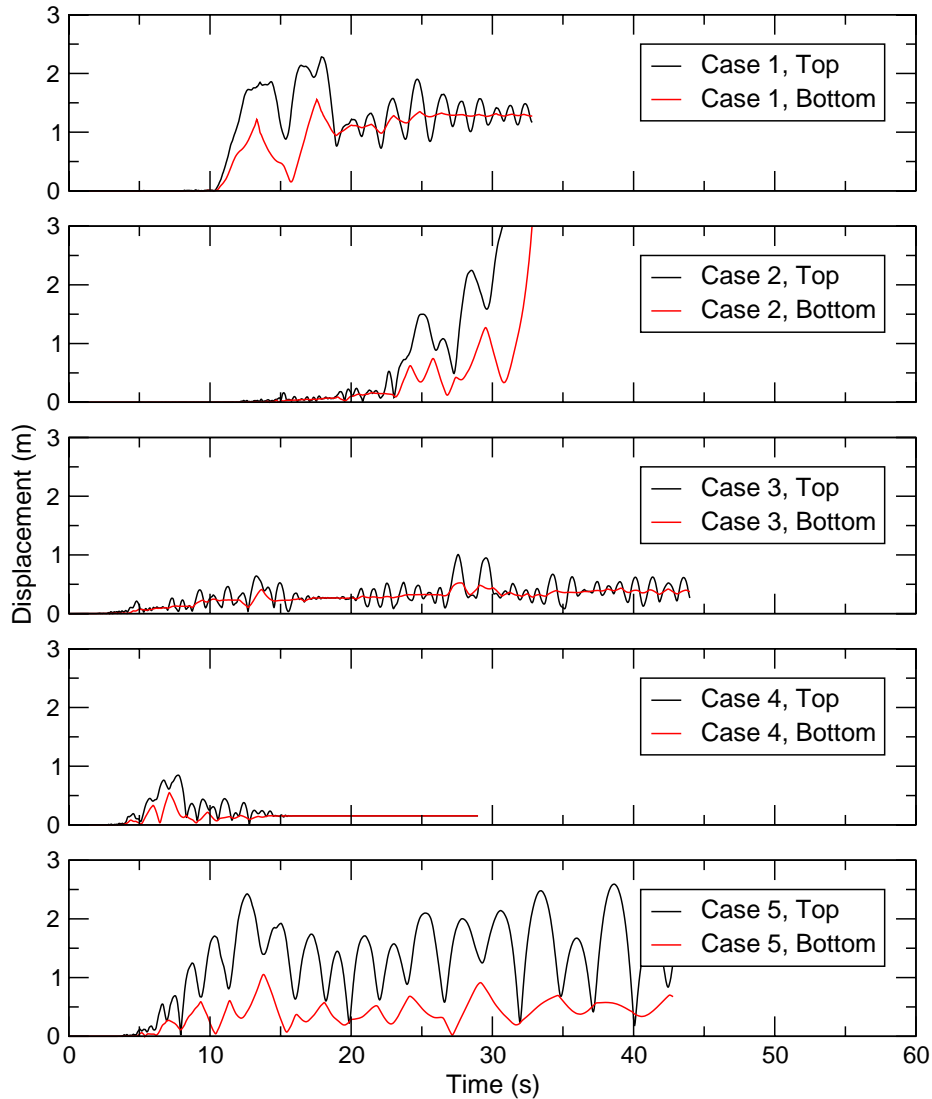


Figure 5.12: Time Histories of Cask Displacement Relative to Pad for Cylindrical Cask, Stiff Soil Profile, Cask/Pad  $\mu=0.8$ , All 5 Earthquakes, NUREG/CR-0098 Spectral Shape, PGA=1.0 g

### 5.2.2 Representative Analysis Results for Rectangular Module

Because of the rectangular shape of the module base, this type of module generally exhibits much lower response than that experienced by a cylindrical cask subjected to the same ground motion. The rectangular module base prevents it from assuming a rolling motion. The module is forced to either rock about one of the edges or slide. Since one of the edges is significantly longer than the other, it always tends to rock about the shorter edge. Figure 5.13 shows an example of the relative lateral displacement trajectories for the module top and base for a case in which the coefficient of friction is 0.55. The stiff soil profile was used, and the ground motion came from the Iran Tabas earthquake record fitted to the NUREG/CR-0098 spectra, scaled to PGA=1.0. These are the same conditions used to generate the plot in

Figure 5.9, but it can be seen that the response is much lower in this case. The motions of the top and base are nearly identical to each other, and the module experiences minimal sliding.

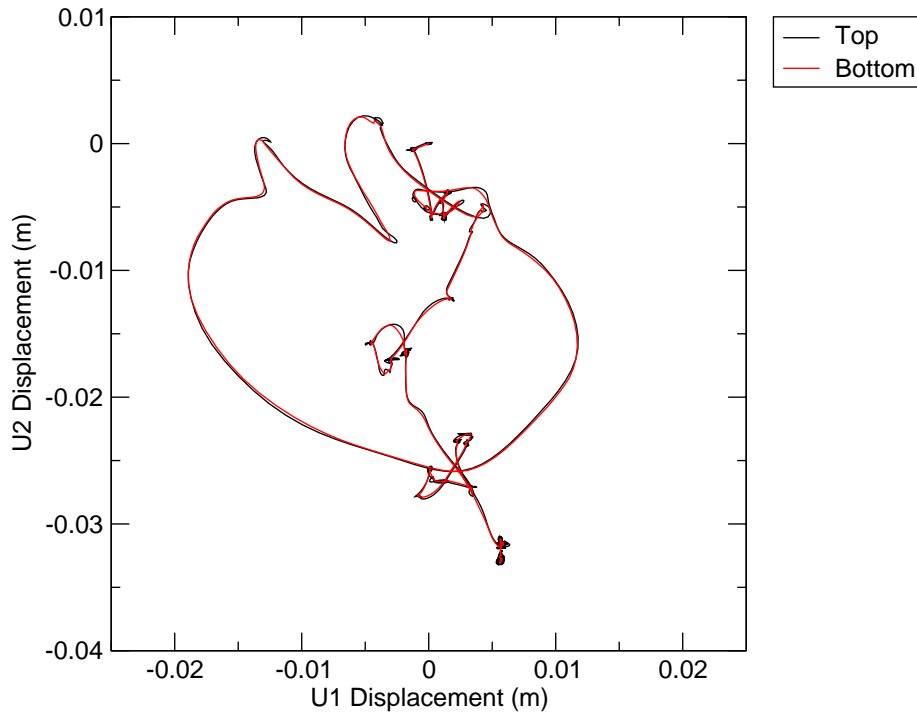


Figure 5.13: Lateral Displacement Trajectories for Rectangular Module Top and Base, Iran Tabas Earthquake, PGA=1.0 g, Stiff Soil Profile,  $\mu=0.55$

Plots similar to those provided in Figure 5.10, Figure 5.11, and Figure 5.12 are provided for the rectangular module. Figure 5.14 shows the response of the module subjected to 5 earthquake records with  $\mu=0.2$ . Figure 5.15 shows the same series of plots for  $\mu=0.55$ , and Figure 5.16 shows them for  $\mu=0.8$ . The plots for  $\mu=0.2$  are nearly identical to those for the cylindrical cask. This is to be expected because the response consists of nearly pure sliding, so geometric details of the cask do not affect the response. The response is lower when  $\mu=0.55$  because the sliding is limited. There is still sufficient sliding to limit rocking. When  $\mu=0.8$ , the sliding is further limited, and the cask exhibits some rocking motions. The overall response, however, is still quite small, even at the peak ground acceleration of 1.0 g used to generate these plots.

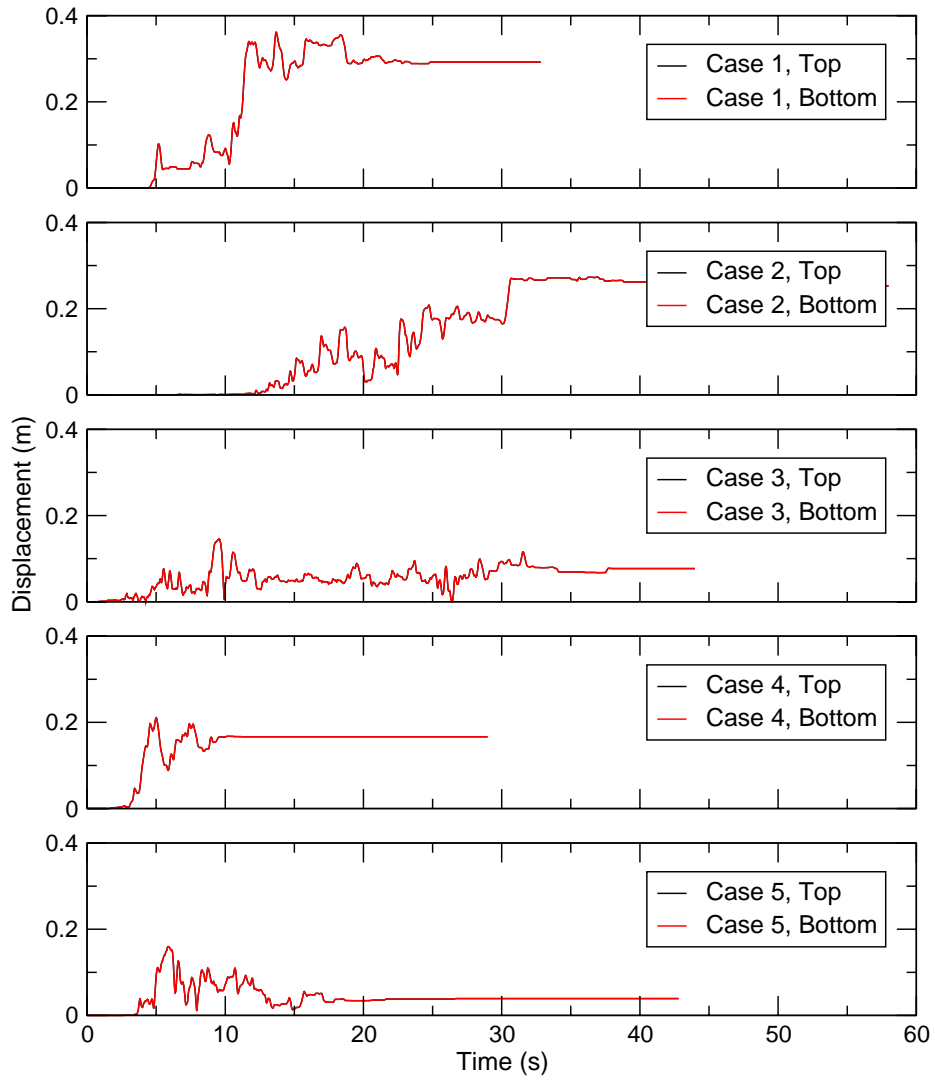


Figure 5.14: Time Histories of Cask Displacement Relative to Pad for Rectangular Module, Stiff Soil Profile, Cask/Pad  $\mu=0.2$ , All 5 Earthquakes, NUREG/CR-0098 Spectral Shape, PGA=1.0 g

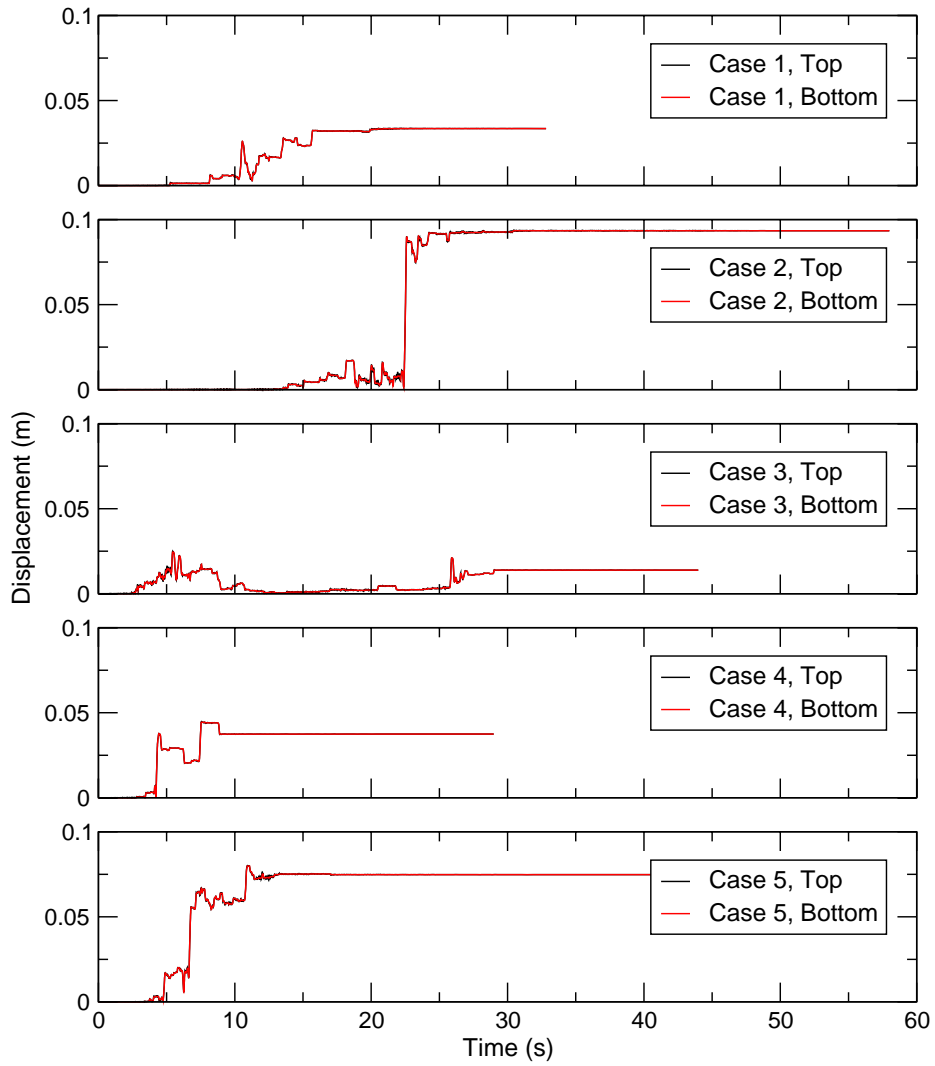


Figure 5.15: Time Histories of Cask Displacement Relative to Pad for Rectangular Module, Stiff Soil Profile, Cask/Pad  $\mu=0.55$ , All 5 Earthquakes, NUREG/CR-0098 Spectral Shape, PGA=1.0 g

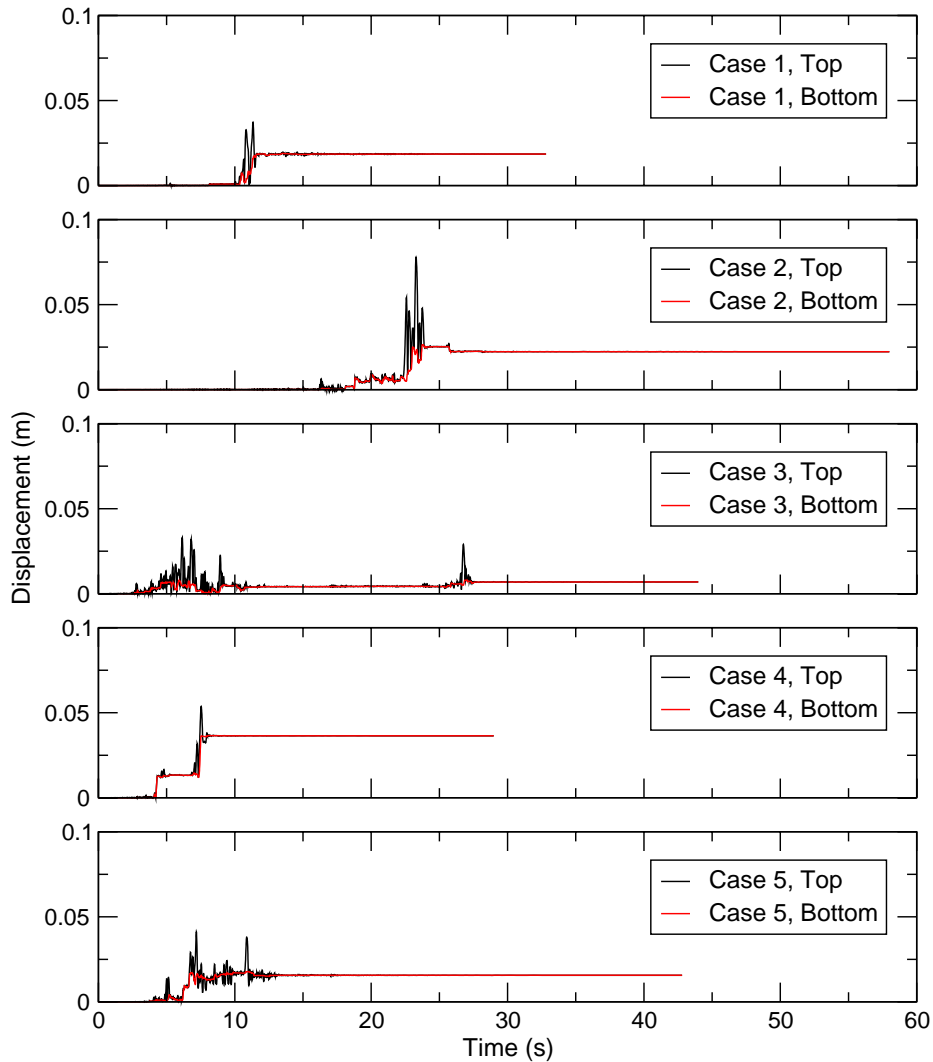


Figure 5.16: Time Histories of Cask Displacement Relative to Pad for Rectangular Module, Stiff Soil Profile, Cask/Pad  $\mu=0.8$ , All 5 Earthquakes, NUREG/CR-0098 Spectral Shape, PGA=1.0 g

### 5.3 Presentation of Analysis Results

A total of 1165 analyses were performed in completing the set of parametric analyses outlined in Table 4.1 for the cylindrical cask and the rectangular module. Due to the large number of analyses, the complete time histories of all of these analysis cases are not presented here. Instead, the three key quantities used to characterize the analysis results as outlined in Section 5.2 and illustrated in Figure 5.8 are reported for each case. These quantities are the peak magnitude of the lateral displacement vectors at the cask top and bottom relative to the pad and the peak cask rotation from the vertical. These results are tabulated for all analysis cases in Appendix V.

In the tables of analysis results in Appendix V, there are cases labeled as “Tips”, which designate cases when the cask system tips over. Since cask displacements and rotations carry very little meaning in these “Tips” cases, they are omitted in the tables. In parametric cases for the cylindrical casks subjected to earthquake ground motions conforming to the Regulatory Guide 1.60 spectral shape, the higher cask responses were observed at a given level of PGA. Almost all analyses with PGA=1.0 g resulted in the

cask tipping over, so the analyses were not run with PGA=1.25 g. To provide more data points for plotting results, these analyses were run with PGA=0.4 g and PGA=0.5 g.

Relatively coarse increments in ground motion intensity were used to provide a broad coverage of a wide range of potential events. The undesirable consequence of this is that if a cask tips over at a given level of ground motion, it is difficult to identify the level of ground motion at which the cask is on the threshold of tipping. For example, if a cask tips over at PGA=1.0 g, but it exhibits minimal response under the same conditions but with the ground motion of PGA=0.6 g, the threshold of tipping could be anywhere between 0.6 g and 1.0 g PGA. To decrease the uncertainty in the level of ground motion required to overturn the cask, additional analyses at more refined increments of PGA were performed in the cases when the cask tipped over. The results of these additional analyses are also included in the tables in Appendix V.

In addition to the tabular presentation of the cask response parameters for each of the analysis cases, graphical presentations of a subset of these same results are also provided in Section V.2 of Appendix V. For each combination of cask type, soil type, and spectral shape, plots of peak relative cask top displacement and peak rotation as functions of PGA are provided. These two measures of cask response are likely to be the most useful for assessing the safety of a cask design under given site and seismic conditions. Because the cask motion is often dominated by rocking, the peak displacement of the cask top is almost always greater than the peak displacement of the cask bottom, so this parameter is the most useful for safeguarding against collision of adjacent casks. In only 6 of the 1165 analysis cases, the displacement of the cask bottom was slightly greater than that of the cask top. In all of these cases, the cask response was dominated by sliding rather than tipping. The largest difference between the peak bottom and top displacement within these 6 cases was 7 mm (0.3 in). Because the peak top displacement is almost always greater than the peak bottom displacement, the peak bottom displacement is not included in the plots.

In each of the plots in Appendix V, 15 lines are used to connect the results with a given set of parameters at varying levels of ground motion. There is a separate line for each combination of ground motion record and coefficient of friction between the cask and pad. The ground motion records are denoted as Case 1-5 for the five startup ground motion records fitted to the NUREG/CR-0098 or Regulatory Guide 1.60 spectral shapes. A different set of startup ground motion records was used for the earthquake records that were fitted to the NUREG/CR-6728. To differentiate these, they are denoted as Case A-E. The actual names of the ground motion records corresponding to these identifiers are listed in Section 4.1.4. A total of 18 combinations of cask type, soil type, and spectral shape were studied. Thus, to provide separate plots of the three key cask response quantities, 54 plots are required. The first 18 plots show the relative cask top displacement results, the second 18 plots show the cask rotation results, and the final 18 plots show the relative cask bottom displacement results.

## **5.4 Discussion of Analysis Results**

The analysis results presented in Appendix V demonstrate the wide range of responses that the cask could potentially exhibit under a variety of conditions. It can be seen that in many cases, there is a large amount of scatter in the results when five different time histories are used for the seismic input with other parameters held constant. These are expected results because of the nonlinearities present in the analysis models.

As expected, the cask response tends to increase as the ground motion increases. In some cases, however, the cask response under a given set of input parameters is lower with a higher level of ground motion than with a lower level. The cask response is very sensitive to the timing of the ground motion pulses. The earthquake records are scaled linearly in this study, but the cask response is not expected to increase linearly as a function of the ground motion scaling. Because the cask response is nonlinear, changing the

scaling of the ground motion can dramatically change the timing of the cask motion. At a given level of ground motion, the cask may be in a position that maximizes its response to a critical ground motion pulse. At a higher level of ground motion, the cask may be positioned differently at the time of that same pulse, causing it to exhibit a very minimal response. Although some isolated cases indicate a non-monotonic increase in the response as a function of the ground motion, the mean response of the 15 cases with 5 different ground motion records and 3 cask/pad coefficients of friction always increased monotonically in this study. Due to the randomness in the cask response, it is clearly important to evaluate the cask response under a number of different earthquakes and compute statistics of those results. Basing decisions on an isolated analysis case could be incorrect because of the large scatter in the results.

The parametric analysis results indicate that the cask response is very sensitive to the value of the cask/pad friction coefficient,  $\mu$ . In most of the plots in Appendix V, the five sets of results using a given value of  $\mu$  are generally clustered together. As discussed previously, the upper and lower bound values of  $\mu$  used in this project are extreme values, about 2.5 standard deviations above and below the mean value. The selected range of  $\mu$  provides useful upper and lower bound measures of response that can be used for design review.

The cylindrical cask tended to result in a much higher response than the rectangular module under the same conditions. Once the vertical cylindrical cask begins to lift up from the pad, it can either begin to rock back and forth, or assume a rolling motion. Much less energy is absorbed in the rolling mode than in the rocking mode. In addition, ground motion pulses in any direction can cause rocking or rolling of cylindrical casks. This is in contrast to rectangular modules, which due to their geometry, tend to only rock about the short dimension. Because of these characteristics, cylindrical casks tend to assume a rolling motion. The cylindrical cask is only slightly more slender than the rectangular module. The ratios of center of gravity height-to-base dimension are nearly the same for these two designs.

At high levels of ground motion, rocking and rolling motions dominate the cylindrical cask response. There is not a marked difference between the responses obtained when  $\mu=0.55$  and when  $\mu=0.8$  because the lower of these two coefficients of friction is sufficiently high to cause the cask to favor tipping over sliding. Further increasing  $\mu$  above this level does little to change the response. The lower bound cases ( $\mu=0.2$ ) produced the highest response only in some cases when low levels of ground motion (PGA=0.25 g) were applied to the cask.

The opposite of the above statements about the effect of the cask/pad coefficient on the cask response can generally be stated for the rectangular module analyses. Due to the geometry of this module, it does not assume a rolling motion. The cask top displacement is generally higher when a lower bound coefficient of friction is used than with higher values. It should be noted that the lower bound coefficient of friction of 0.2 is sufficiently low that neither of the cask designs investigated here exhibit any significant tipping. As a result, when  $\mu=0.2$ , the response of the rectangular module is generally very close to that of the cylindrical cask under the same conditions.

The response of both cask designs is highly dependent on the spectral shape of the ground motion. The ground motion records conforming to the NUREG/CR-6728 spectral shape produced the lowest response. The NUREG/CR-0098 earthquakes produced a medium response, and the Regulatory Guide 1.60 earthquakes resulted in the highest response levels. The cylindrical cask never tipped over under the NUREG/CR-6728 ground motion, even with PGA=1.25 g. At that level of ground motion, the highest observed peak lateral displacement of the cask top relative to the pad is 0.83 m (33 in). Under the NUREG/CR-0098 ground motion records, the highest observed cask top displacement is 1.63 m (64 in) with PGA=0.6 g. When these records are scaled up so that the PGA=1.0 g, 2 of 45 cases result in the cask overturning. When the cylindrical cask is subjected to earthquakes conforming to the Regulatory

Guide 1.60 spectra with PGA=0.5 g, the peak observed cask top displacement is 2.42 m (95 in). Scaling up these records to PGA=0.6 g results in overturning for 2 of 45 cases.

Similar trends were observed for the rectangular module, although the response is lower and the cask never overturns. The highest observed peak top displacement with the NUREG/CR-6728 spectral shape earthquakes is 0.26 m (10 in) at PGA=1.25 g. Under the NUREG/CR-0098 earthquakes at the same PGA, this increases to 0.52 m (21 in). When subjected to the Regulatory Guide 1.60 earthquakes at PGA=1.25 g, the peak top displacement of a rectangular module is 1.7 m (67 in).

## 5.5 Compilation of Analysis Results in Nomograms

### 5.5.1 Nomograms for Specific Spectral Shapes

As mentioned previously, there is a large amount of scatter in the cask response results. The cask typically responds quite differently to the five different ground motion records fitted to the same spectral shape. This scatter is to be expected and is analogous to the scatter that would be observed in the response of identical casks subjected to various actual earthquakes. To facilitate evaluation of cask designs, it is useful to consolidate these results in a statistical manner. To this end, least squares regression curve fits have been performed on the cask analysis results, providing equations that describe the cask response as a function of the ground motion intensity.

The cask response as a function of ground motion intensity has been found to be fit reasonably by an exponential equation of the form:

$$y = A x^B \quad (5.6)$$

where  $y$  is a variable describing the cask response,  $A$  and  $B$  are parameters of the fitted curve, and  $x$  is a variable describing the ground motion intensity. Taking the natural logarithm of both sides of this equation yields the following:

$$\ln(y) = \ln(A) + B \ln(x) \quad (5.7)$$

It can be seen that an equation of this form appears as a linear function when  $x$  and  $y$  are both plotted on logarithmic scales. Thus, standard linear regression procedures can be used to compute the values of  $A$  and  $B$ . Pairs of data points,  $x_i$  and  $y_i$ , from each analysis case,  $i$ , are transformed by taking their natural logarithms, and linear regression is performed on the transformed values:  $\ln(x_i)$  and  $\ln(y_i)$ .

In linear regression, there is an implicit assumption that the distribution of  $y$  with  $x$  held constant ( $Y/x$ ) conforms to a normal probability distribution. The best-fit line thus represents the mean or expected value of the random variable. Because the linear regression is performed on data that have undergone a logarithmic transformation in this case, the distribution of  $y$  with  $x$  held constant is implicitly assumed to follow a lognormal distribution. The best-fit line thus represents the median value, and the mean is greater than the median.

Once the linear regression is performed, two parameters describing the scatter of the data and the quality of the fit are computed. These parameters are computed based on the transformed data and the transformed fitted function using the standard methods as described in Ang and Tang [28].  $S_{Y/x}$  is the conditional standard deviation and is a measure of the dispersion of the data points about the fitted function. In this case, it is the conditional standard deviation of the underlying normal distribution, and is computed using the following equation:

$$S^2_{y|x} = \frac{1}{n-2} \sum_{i=1}^n (\ln(y_i) - y'_i)^2 \quad (5.8)$$

where  $n$  is the number of data points and  $y'_i$  is the value of the transformed fitted function evaluated at  $x_i$ :

$$y'_i = \ln(A) + B \ln(x_i) \quad (5.9)$$

The parameter  $r^2$  provides a measure of the ability of the fitted curve to represent the data and can vary from 0 to 1. Higher values of this parameter indicate better fits. This parameter is also based on the transformed data, and is computed with the formula:

$$r^2 = 1 - \frac{S^2_{y|x}}{S_Y^2} \quad (5.10)$$

where  $S_Y^2$  is computed from the transformed data as:

$$S_Y^2 = \frac{1}{n-1} \sum_{i=1}^n \left( \ln(y_i) - \frac{1}{n} \sum_{i=1}^n \ln(y_i) \right)^2 \quad (5.11)$$

The conditional standard deviation can be used to produce functions representing envelopes of the data. For the exponential equation employed here, an equation for a confidence band at the median plus  $m$  standard deviations is expressed as:

$$y = A x^B \exp(m S_{y|x}) \quad (5.12)$$

All of the plots of the regression fits of the response data shown in this section show the equation for the median fitted curve, including the values of the  $A$  and  $B$  parameters. The values of  $S_{y|x}$  and  $r^2$  are reported in the legend of the plot next to the equation for the median response. In addition, the 84% and 16% confidence bands are shown in the regression plots along with the equations for these functions. These represent the median plus and minus one standard deviation, respectively, and were computed using Equation 5.12.

Figure 5.17 shows a representative plot of the function obtained to fit a series of analysis results using least squares to compute the values of  $A$  and  $B$  in a way that minimizes the residual error. The fitted curve provides functions describing the peak cask top displacement as a function of PGA for earthquakes conforming to the NUREG/CR-0098 spectral shape with a cask/pad friction coefficient of 0.55 and the soft soil profile. This plot is shown using linear scales, while Figure 5.18 shows the same data and fitted curves plotted on logarithmic scales. These plots show three fitted curves along with points that represent individual analysis results. The median curve is the function that minimizes the residual error. The equation for that function is shown in the legend of the plot.

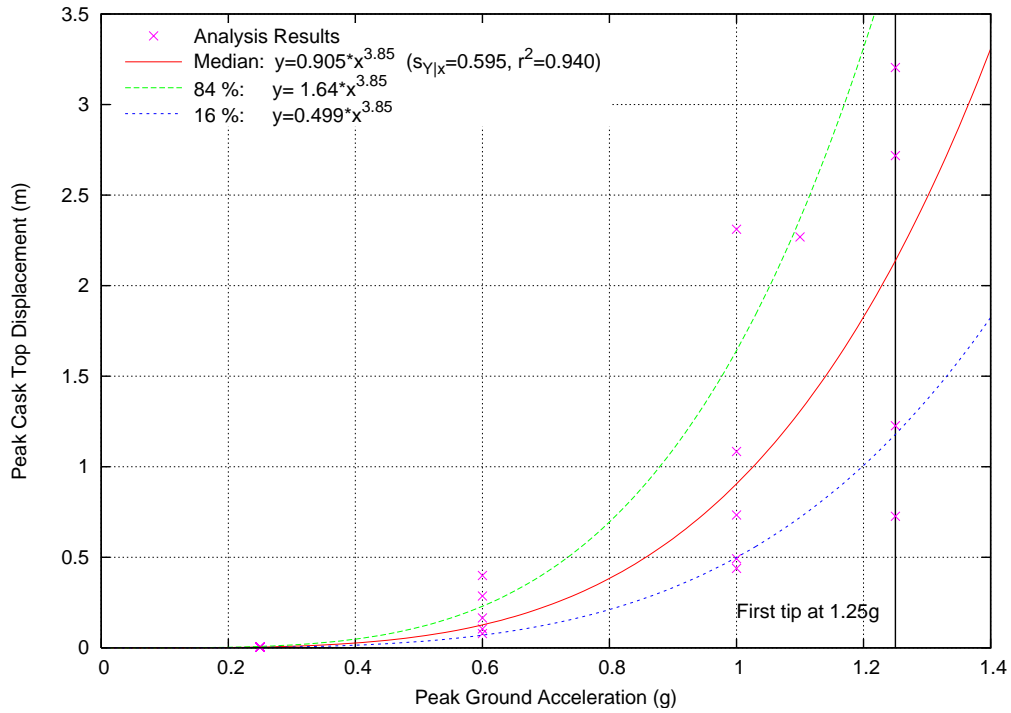


Figure 5.17: Peak Top Displacement Regression Fit, Linear Scale, Cylindrical Cask, NUREG/CR-0098 Earthquakes, Cask/Pad  $\mu=0.55$ , Soft Soil Profile

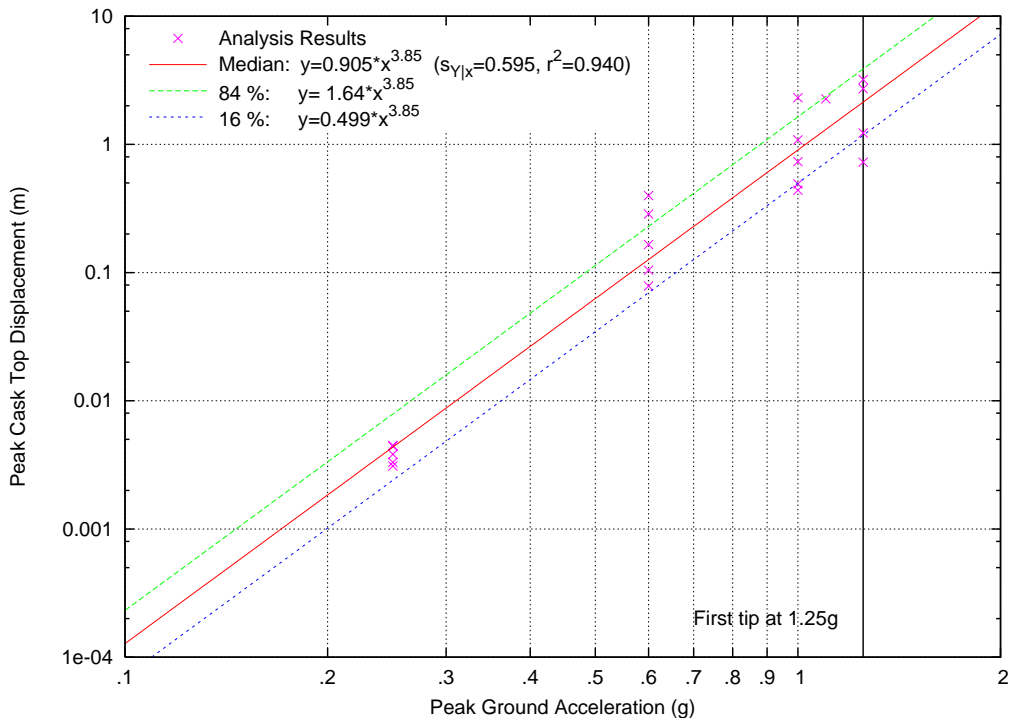


Figure 5.18: Peak Top Displacement Regression Fit, Logarithmic Scale, Cylindrical Cask, NUREG/CR-0098 Earthquakes, Cask/Pad  $\mu=0.55$ , Soft Soil Profile

A note should be made of the heavy vertical line that appears at 1.25 g PGA on these plots. In the regression plots developed in this study, a heavy vertical line is used to denote the lowest ground motion intensity at which a cask tipped over in that set of results. The results of the analyses in which the cask tipped over are not included in the plots. In some cases, analyses at higher ground motion levels indicated that a cask that tipped over at a lower level of ground motion does not tip over at a higher ground motion level. This is to be expected sometimes because of the nonlinear nature of the cask response. These results are not, however, included in the regression fits.

The plots provided in Figure 5.17 and Figure 5.18 show regression fits of the peak cask top displacement as a function of PGA for one cask design, one spectral shape, one coefficient of friction, and one soil profile. It is desirable to group together the results that are not particularly sensitive to input parameters. As mentioned before, the cask results are very sensitive to the cask design due to the fact that the behavior of the cylindrical cask is fundamentally different from that of the rectangular module. The cask response is also quite sensitive to the spectral shape and the coefficient of friction. In the analysis cases run here, the cask response does not appear to be particularly sensitive to the soil profile. There are certainly differences in the results obtained using the different soil profiles, but relative to the overall amount of scatter seen in the results, the differences due to the soil profile are quite small.

To demonstrate the similarities in the trends of the results with differing soil profiles, plots of the regression fits of the peak cask top displacement as a function of PGA are provided for the cylindrical cask subjected to the NUREG/CR-0098 earthquakes with the cask/pad  $\mu=0.55$  for the stiff soil and rock profiles in Figure 5.19 and Figure 5.20, respectively. These are provided on logarithmic scales and can be compared with Figure 5.18, in which everything else is the same as in these plots except that the soft soil profile is used.

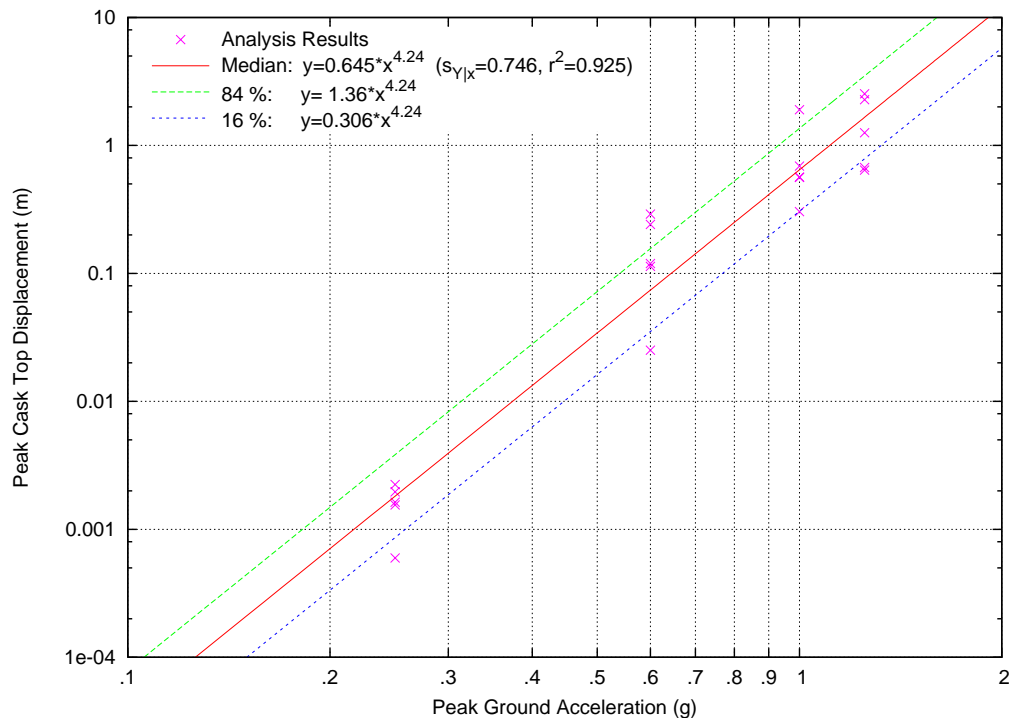


Figure 5.19: Peak Top Displacement Regression Fit, Logarithmic Scale, Cylindrical Cask, NUREG/CR-0098 Earthquakes, Cask/Pad  $\mu=0.55$ , Stiff Soil Profile

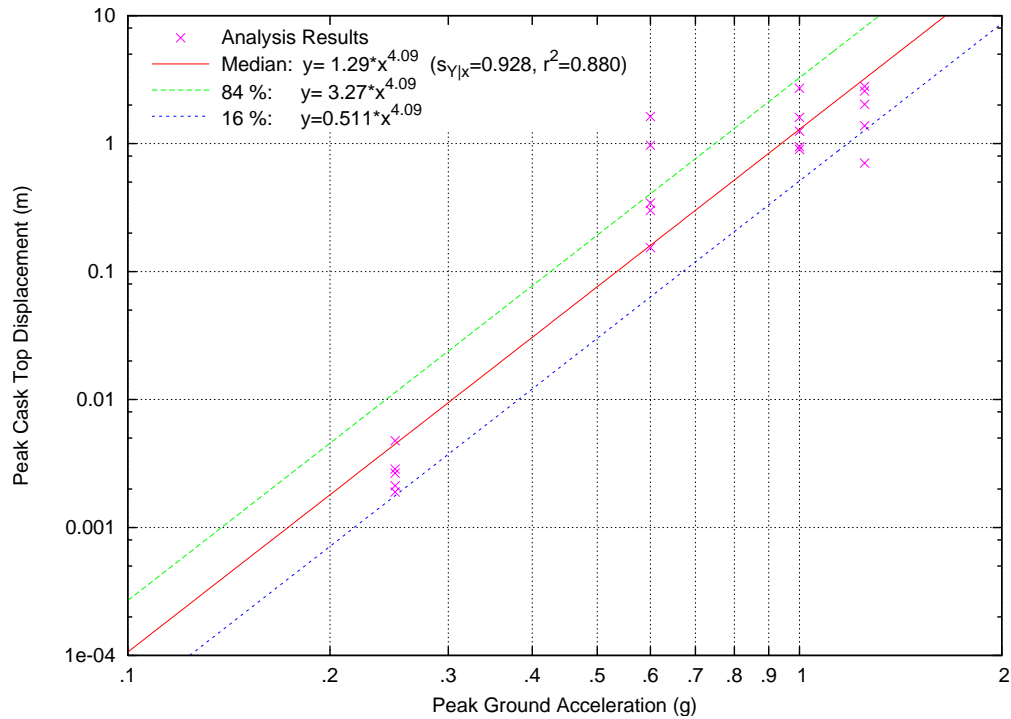


Figure 5.20: Peak Top Displacement Regression Fit, Logarithmic Scale, Cylindrical Cask, NUREG/CR-0098 Earthquakes, Cask/Pad  $\mu=0.55$ , Rock Profile

There are differences in the regression fits for these data sets, but in general, these differences are minor. Because the soil type does not have a significant effect on the response, the data points for all three soil profiles can be grouped together for regression fitting. Figure 5.21 shows a regression fit of the peak cask top displacements with the soft soil, stiff soil, and rock profile results grouped together for the cylindrical cask with the NUREG/CR-0098 spectral shape and  $\mu=0.55$ . Different types of symbols are used to denote the results from the three soil profiles. It can be seen that there is not a large difference in the response with the different soil types. Combining these results provides more data points for a fitted curve that can be applied to a broad range of soil types.

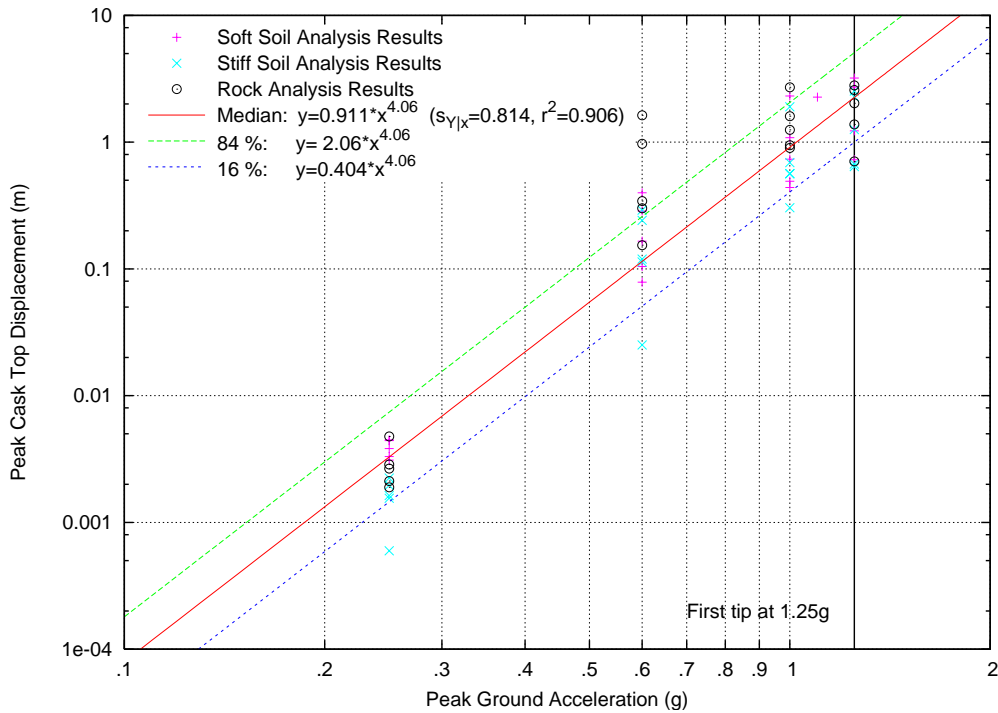


Figure 5.21: Peak Top Displacement Regression Fit, Logarithmic Scale, Cylindrical Cask, NUREG/CR-0098 Earthquakes, Cask/Pad  $\mu=0.55$ , All Soil Profiles

Plots similar to those shown in Figure 5.21 are provided in Appendix VI for both cask designs, all three spectral shapes, and all three values of the cask/pad friction coefficient used in this study. These plots are provided for both the peak cask top displacement as well as the peak cask rotation as functions of PGA. They can be used as nomograms for evaluating the response of these cask designs subjected to earthquakes conforming to the spectral shapes used here. The conditional standard deviation for a given fitted curve can be used in conjunction with the equation of the fitted curve to develop the probability distribution of the response of a given cask with a given friction coefficient subjected to an earthquake conforming to one of the three spectral shapes used in this study. Functions are provided for the median response and the 84% and 16% confidence bands, but the response at a different degree of confidence can be easily computed using Equation 5.8.

It is important to note that in general, the quality of the fitted curves, as indicated by the  $r^2$  value, is quite good, but there are some data sets that are not fit very well. In general, the regression fits of the peak cask rotations are not as good as those for the peak cask displacements. For the cases where the cask response is dominated by sliding, the rotation angles are quite low, and the regression fits are not very good because of the large amount of noise in this data. In these cases, the angles of rotation are low, so the poor fitting of the data is not likely to have serious consequences for cask design review. Even if the required level of confidence for design purposes were increased significantly in these cases to account for the poor fits, the cask rotations would still be quite low in general.

It is very important to point out that all parametric analyses were performed for specific designs of a cylindrical cask and a rectangular module, freestanding on selected foundation types subjected to earthquake excitations conforming to selected spectral shapes. The principal objective of the parametric analyses is to compile analysis results in nomograms to provide meaningful and practical interpretation of seismic behavior of dry cask systems to cask designers and reviewers. The users of these nomograms are reminded to compare the design details of their dry cask storage systems and site-specific seismicity to

those used in the parametric analyses. Any significant differences in these comparisons may limit the applicability of the nomograms of analysis results to specific cask design cases.

### **5.5.2 Combination of Spectral Shape Nomograms**

Up to this point, the parameter used to describe the magnitude of the ground motion has been the PGA. If the ground motion at a given site is expected to conform to one of the three spectral shapes used in this study, the spectrum-specific nomograms can be used to find the expected cask response at a given level of PGA. As is clearly evident by the large differences in the response as a function of PGA for the three spectral shapes studied here, the cask response is clearly not a direct function of PGA. Peak ground acceleration is simply a measure of the response of an infinitely stiff structure. The cask's fundamental period is a highly nonlinear function of the tipping angle, but it is more sensitive to the spectral content of the ground motion in the 0.5-s to 2-s period range than to the high frequency content.

For useful comparisons of results from different spectral shapes, it is necessary to use a parameter to describe the ground motion that is more indicative of the cask response than is the PGA. Two parameters that appear to have promise for this purpose are the peak ground velocity (PGV) and the pseudo-spectral acceleration (PSA) at 5% damped 1 Hz. The PGV, which is not a direct function of the spectral shape, is influenced by the spectral accelerations across the middle of the spectrum in the period range likely to be important to the cask response.

Table 5.3 shows the peak ground acceleration, velocity, and displacement for the surface motion records conforming to the NUREG/CR-0098 spectral shape used in the parametric study. These are all scaled so that the PGA is equal to 1.0 g. The peak ground accelerations reported are in the two orthogonal horizontal directions in which the earthquake ground motion is defined. The ground motions in both of these directions are scaled so that their peak accelerations are equal. The acceleration in the orthogonal direction is typically very low at the time of the peak acceleration in one direction, so that the peak magnitude of the horizontal acceleration vector is very close to that of the peak acceleration components in the two directions. Thus, the peak accelerations reported in the table are for the two directions. The reported peak ground velocity and displacement, on the other hand, are the peak magnitudes of the horizontal velocity and displacement vector, respectively. These are typically significantly higher than the peak velocity and displacements in the two directions in which the ground motion is defined. Similar data is shown for the Regulatory Guide 1.60 spectral shape earthquakes in Table 5.4, and Table 5.5 shows this information for the NUREG/CR-6728 earthquakes. The average of these quantities for the five records is also shown in these tables.

Table 5.3: Peak Ground Acceleration, Velocity, and Displacement for Surface Ground Motion Records Conforming to NUREG/CR-00098 Spectral Shape

Ground Motion Record	Peak Ground Acceleration (g)	Peak Ground Velocity (m/s)	Peak Ground Displacement (m)
1	1.0	1.08	0.478
2	1.0	1.03	0.411
3	1.0	1.02	0.346
4	1.0	1.06	0.538
5	1.0	0.919	0.424
Average	1.0	1.02	0.439

Table 5.4: Peak Ground Acceleration, Velocity, and Displacement for Surface Ground Motion Records Conforming to Regulatory Guide 1.60 Spectral Shape

Ground Motion Record	Peak Ground Acceleration (g)	Peak Ground Velocity (m/s)	Peak Ground Displacement (m)
1	1.0	1.88	1.36
2	1.0	1.70	1.05
3	1.0	1.62	0.947
4	1.0	1.94	1.37
5	1.0	1.69	1.08
Average	1.0	1.77	1.16

Table 5.5: Peak Ground Acceleration, Velocity, and Displacement for Surface Ground Motion Records Conforming to NUREG/CR-6728 Spectral Shape

Ground Motion Record	Peak Ground Acceleration (g)	Peak Ground Velocity (m/s)	Peak Ground Displacement (m)
A	1.0	0.465	0.0999
B	1.0	0.486	0.100
C	1.0	0.507	0.0879
D	1.0	0.429	0.0781
E	1.0	0.561	0.115
Average	1.0	0.490	0.0963

Least squares regression fits of the response in terms of the PGV have been developed for the combined data for all three spectral shapes and all soil types for a given cask design and friction coefficient. The PGA used for each analysis was multiplied by the average ratio of PGV to PGA as presented in Tables 5.1–5.3 for the appropriate spectral shape. These results are then combined into a single, larger data set for regression fitting. These plots have been developed for the peak cask top displacement and peak cask rotation. Regression fits of the peak cask top displacement and rotation for the cylindrical cask and rectangular module in terms of PGV for all spectral shapes with  $\mu=0.55$  are provided on linear plots in Figures 5.22 through 5.25.

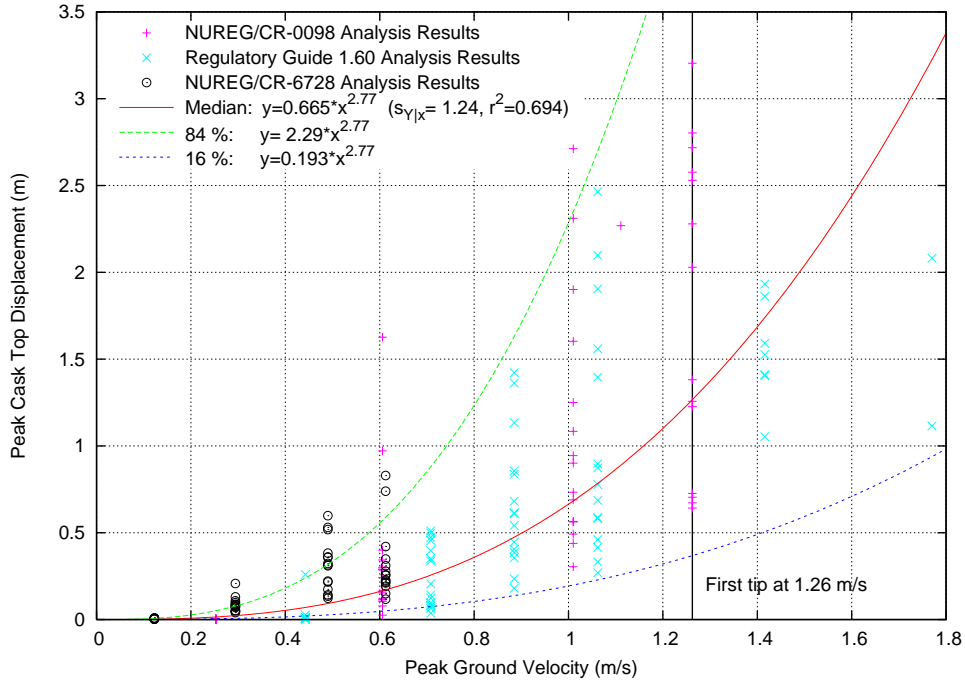


Figure 5.22: Peak Top Displacement Regression Fit in Terms of Peak Ground Velocity, Linear Scale, Cylindrical Cask, All Earthquakes, Cask/Pad  $\mu=0.55$ , All Soil Profiles

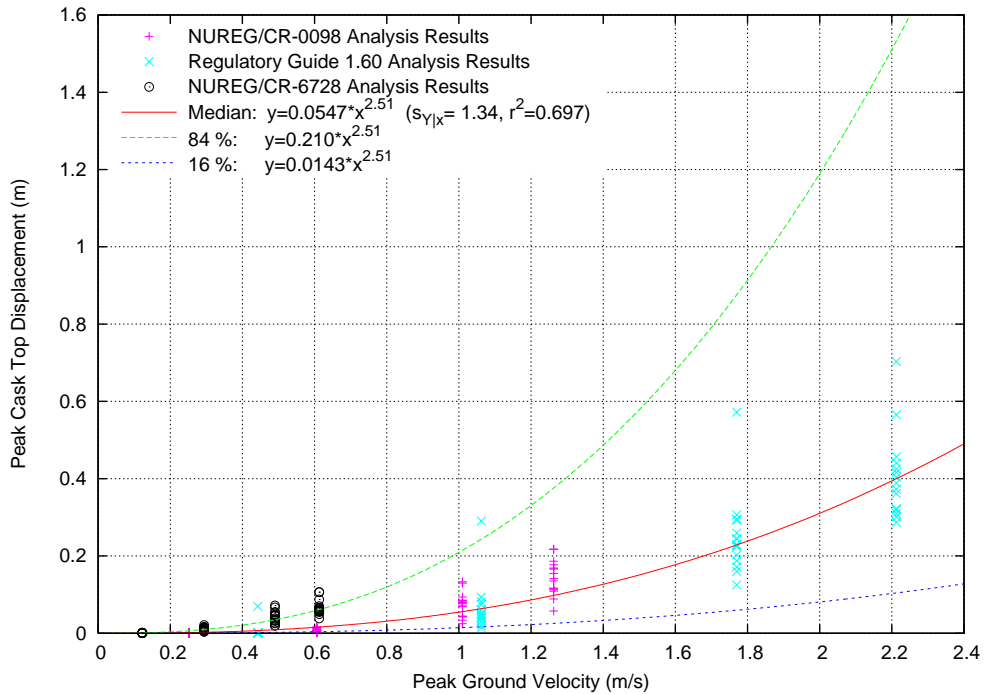


Figure 5.23: Peak Top Displacement Regression Fit in Terms of Peak Ground Velocity, Linear Scale, Rectangular Module, All Earthquakes, Cask/Pad  $\mu=0.55$ , All Soil Profiles

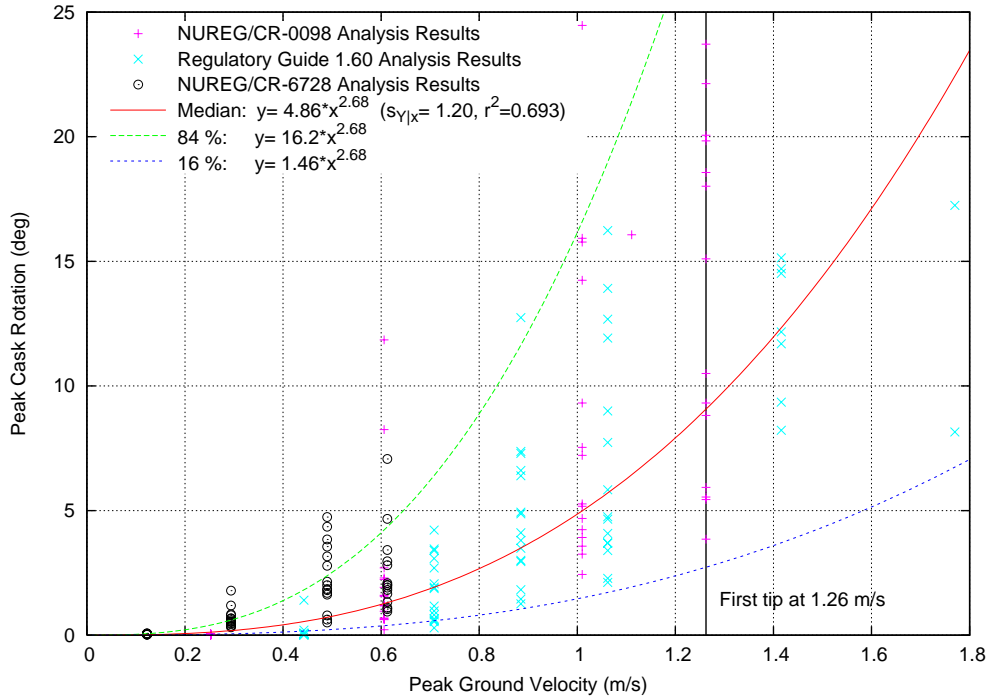


Figure 5.24: Peak Rotation Regression Fit in Terms of Peak Ground Velocity, Linear Scale, Cylindrical Cask, All Earthquakes, Cask/Pad  $\mu=0.55$ , All Soil Profiles

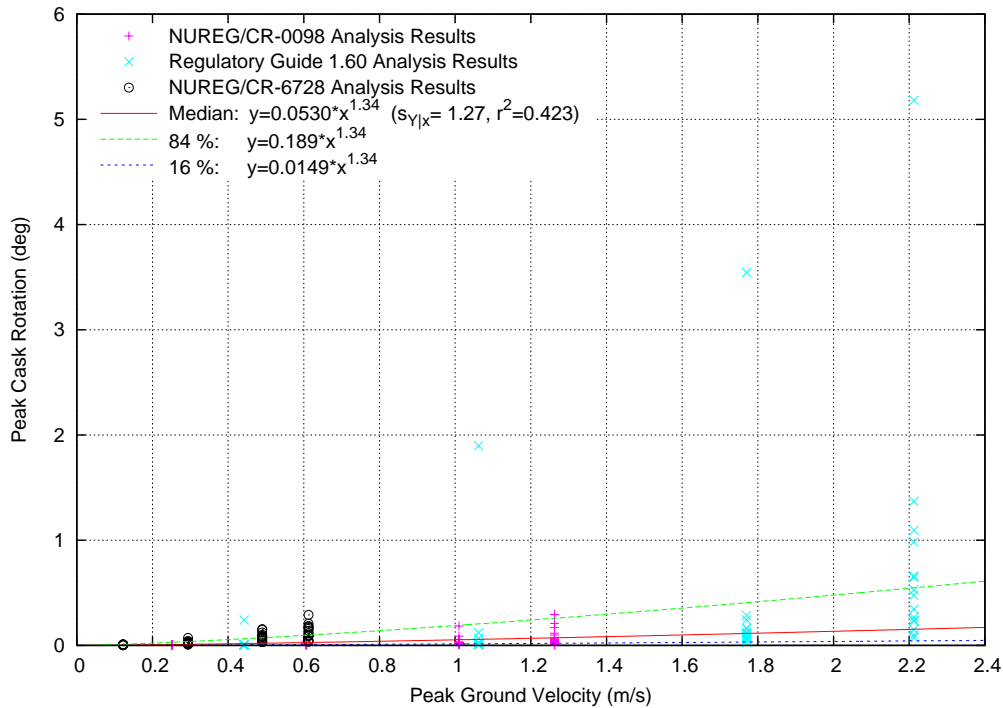


Figure 5.25: Peak Rotation Regression Fit in Terms of Peak Ground Velocity, Linear Scale, Rectangular Module, All Earthquakes, Cask/Pad  $\mu=0.55$ , All Soil Profiles

A methodology similar to that used to perform regression analysis on the cask response results using PGV as the ground motion parameter can also be applied to provide fitted curves for the cask response in terms of the PSA at 1 Hz. Table 5.6 shows the ratios of the 5% damped 1 Hz PSA to the PGA for the three spectral shapes used here. The value of PGA used for each analysis was multiplied by this factor for the appropriate spectral shape, and the analysis results for all three spectral shapes were plotted together as was done for the plots in terms of PGV. Plots of the data and regression fits on linear scales for the top displacement and rotation in terms of the 1 Hz PSA are provided in Figure 5.26 through Figure 5.29 for the analyses with  $\mu=0.55$ .

Table 5.6: Ratio of 5% Damped 1 Hz PSA to PGA for Spectral Shapes Used in Current Study

Spectral Shape	1Hz PSA/PGA
NUREG/CR-0098	1.475
Regulatory Guide 1.60	0.966
NUREG/CR-6728	0.550

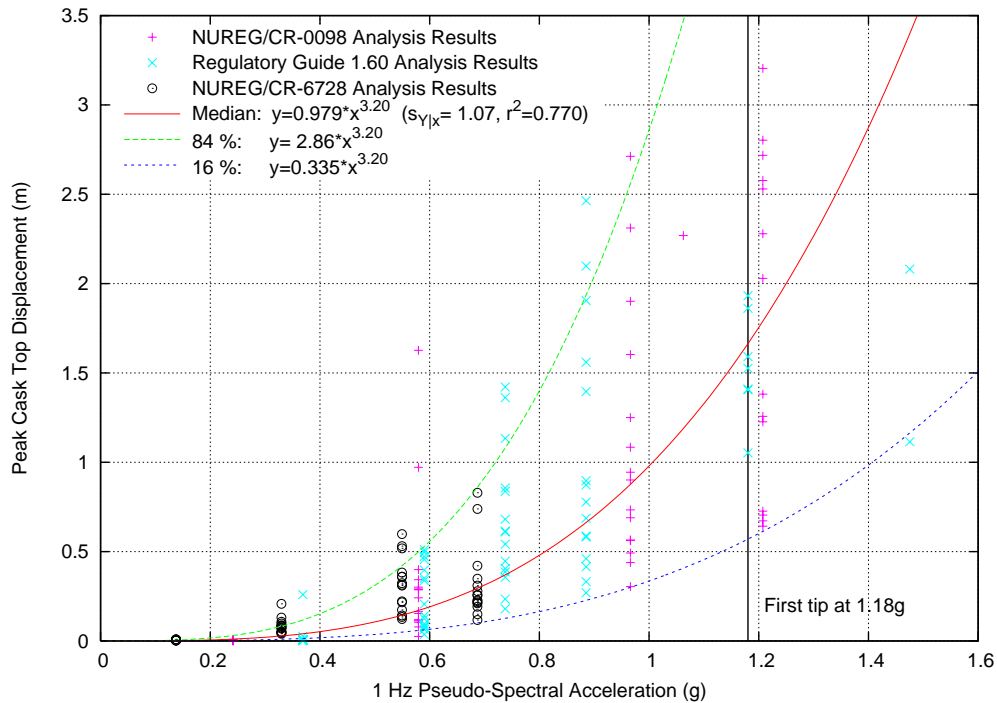


Figure 5.26: Peak Top Displacement Regression Fit in Terms of 1 Hz PSA, Linear Scale, Cylindrical Cask, All Earthquakes, Cask/Pad  $\mu=0.55$ , All Soil Profiles

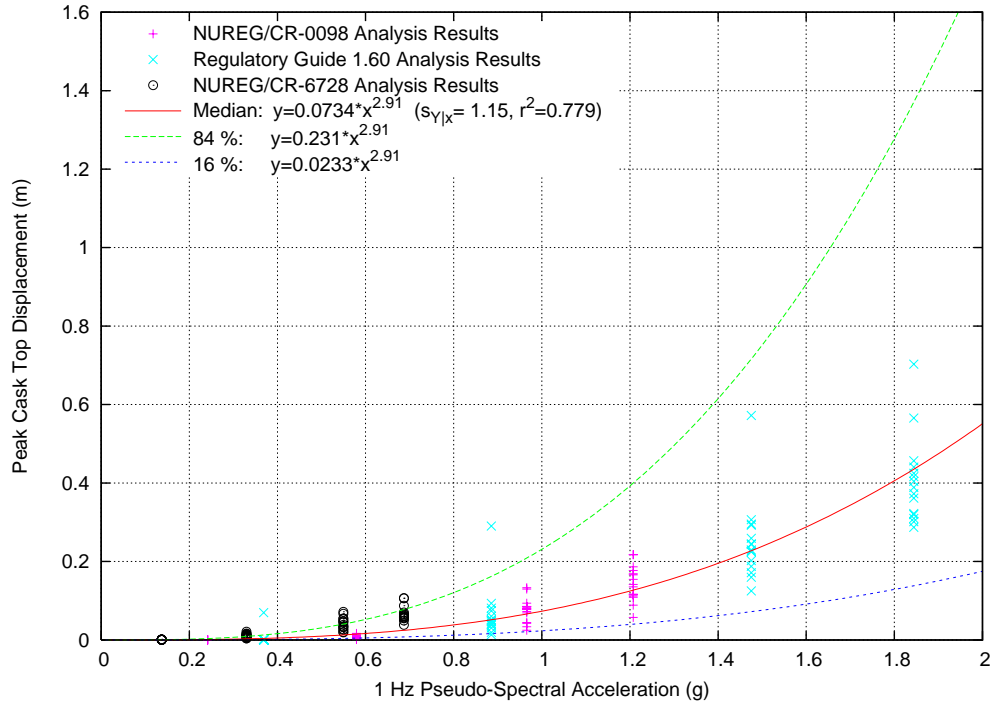


Figure 5.27: Peak Top Displacement Regression Fit in Terms of 1 Hz PSA, Linear Scale, Rectangular Module, All Earthquakes, Cask/Pad  $\mu=0.55$ , All Soil Profiles

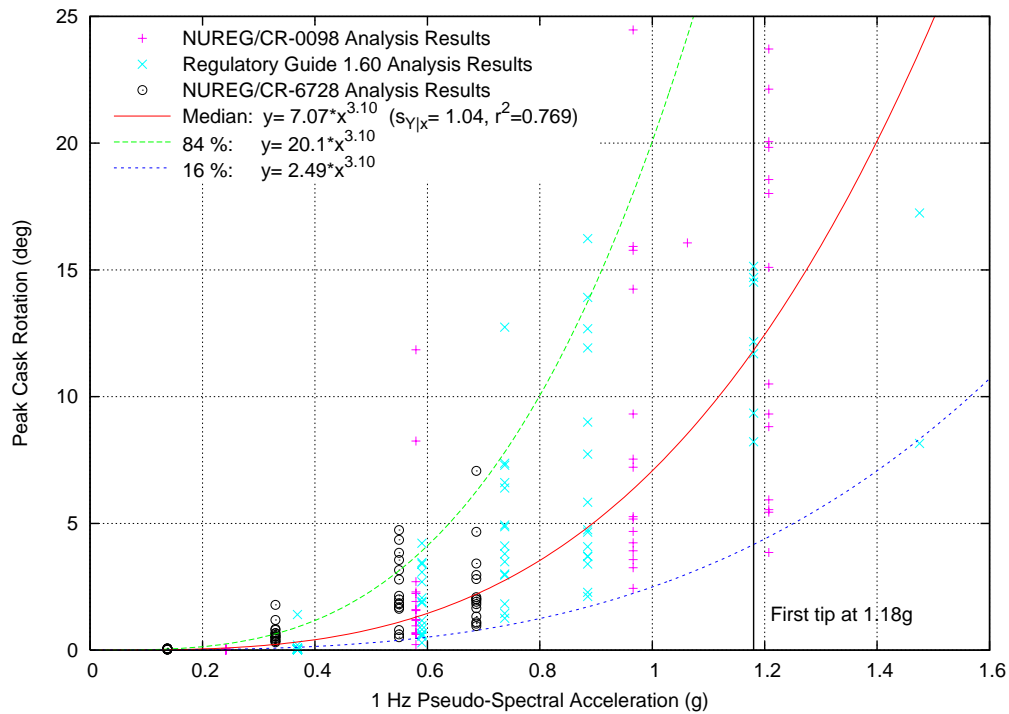


Figure 5.28: Peak Rotation Regression Fit in Terms of 1 Hz PSA, Linear Scale, Cylindrical Cask, All Earthquakes, Cask/Pad  $\mu=0.55$ , All Soil Profiles

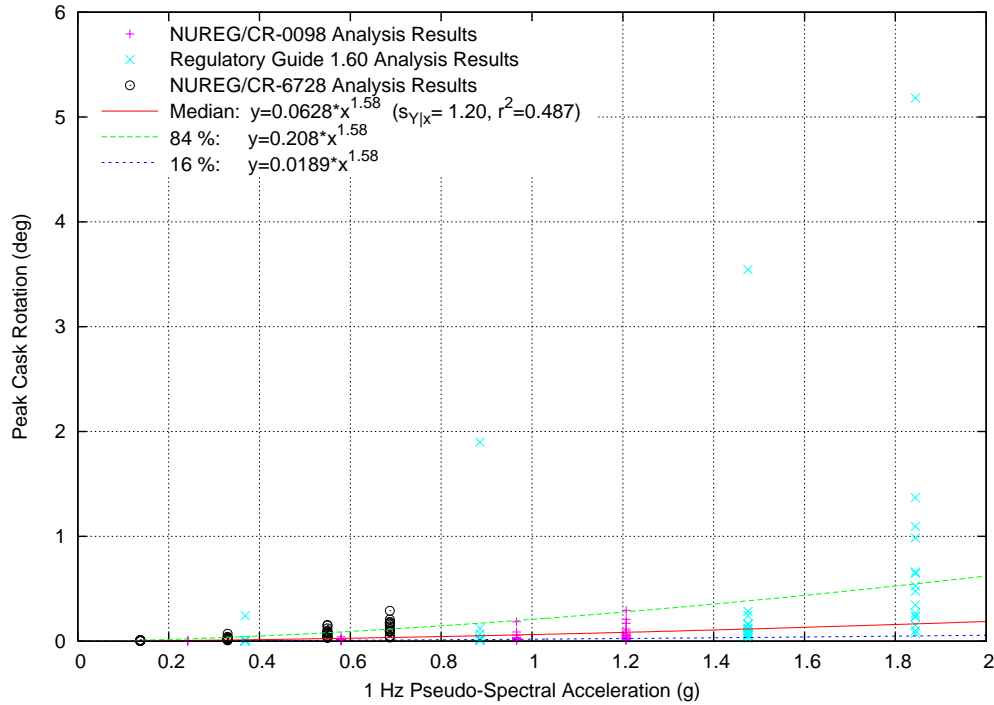


Figure 5.29: Peak Rotation Regression Fit in Terms of 1 Hz PSA, Linear Scale, Rectangular Module, All Earthquakes, Cask/Pad  $\mu=0.55$ , All Soil Profiles

The quality of the regression fits using the 5% damped 1 Hz PSA as the ground motion parameter is consistently higher than that of the fits where the PGV was used. The  $r^2$  parameter is consistently higher, and the confidence bands are consistently narrower for the fits produced using the 1 Hz PSA. Because of this, and the fact that using a pseudo-spectral acceleration at a given frequency provides a much more direct path from a design spectrum to determine the cask response, the 1 Hz PSA appears to be the most suitable parameter to characterize the ground motion for these general nomograms. A complete set of fitted curves for each of the cask designs and friction coefficients is provided in Appendix VI, plotted on both logarithmic and linear scales. These can be used as nomograms to evaluate the response of casks subjected to earthquakes that conform to response spectra that may differ from those used in this study. The curve fitting coefficients for these nomograms are tabulated in Appendix VII, and example problems are provided to illustrate the application of these nomograms to a site-specific application.

### 5.5.3 Discussion and Limitations of Nomograms

The fitted curves describing the cask response in terms of the PGV or 1 Hz PSA are based on the three selected spectral shapes. While these ground motion parameters are both far better indicators of the cask response under an arbitrary spectral shape than the PGA, they are still both simple measures of very complex phenomena. If it is desired to apply the results of this study to a different spectral shape with similar characteristics, one could determine the pseudo-spectral acceleration at 1 Hz and use the fitted curves presented in Appendix VI to apply the results of this study to that application.

The curve fits for the peak cask top displacements are of reasonable quality, although not as good as the separate fits for the individual spectral shapes. Since the quality of the fitted curves is lower when the three spectral shapes are combined, the fitted curves for the individual spectral shapes in terms of PGA should be used if the desired ground motion conforms to one of the spectral shapes.

It should be noted that there is more scatter in the peak cask rotation results, especially for the rectangular module. The curve fits are sometimes quite poor for the rotation results, especially in cases where the response is dominated by sliding rather than by tipping. The rotation response is generally quite low in these cases, but in many of these cases, there are several outlying analysis results that are significantly higher than the 84% confidence curve. While this is certainly a concern, it is important to keep in mind that the rotations are still generally quite low in these cases. Requiring a higher confidence level in the design would not likely be a significant penalty in these cases because the response would still be quite low.

The three spectral shapes used in this study are the NUREG/CR-0098, Regulatory Guide 1.60, and NUREG/CR-6728 spectral shapes. Plots of these spectral shapes were provided for the lateral motion in Figure 4.2 and Figure 4.3, and the spectral shape of the vertical component of the motion was provided in Figure 4.4. This strategic selection of spectral shapes provides a reasonable representation of their practical range of application. Based on the results from these spectra, the 5% damped 1 Hz PSA appears to be a reasonable parameter to characterize the effect that an earthquake would have on a cask system. Series of analyses using a much broader range of spectra would be required to validate this approach for spectral shapes that deviate significantly from those used in this study. Judgment is certainly required in applying these results to site-specific spectra that have different shapes than those used in this study. The degree of confidence required for a specific application should be increased as a function of the amount of deviation of the shape of the response spectrum from the shape of those used in this study.

The results represented by these regression fits are for two specific cask designs having the characteristics outlined in Section 3.2.1.1 for the vertical cylindrical cask and Section 3.2.2.1 for the rectangular module. These casks have characteristics fairly typical of those designs in common use. The aspect ratio, defined here as  $\frac{1}{2}$  of the shortest dimension of the base divided by the height of the center of gravity (CG) from the base, is one of the most important parameters affecting the stability of the cask. For cylindrical casks, the  $\frac{1}{2}$  base width dimension is simply the radius of the cask base. Table 5.7 provides a listing of the  $\frac{1}{2}$  base width, CG height, and aspect ratio for storage casks approved by the NRC as of September 2004. The properties are not listed for the Advanced NUHOMS 24PT1 because it is a special case. That system, which was designed for regions of high seismicity, employs multiple horizontal modules, which are attached together, significantly increasing the effective aspect ratio. As a result, sliding would be a greater concern than tipping for seismic evaluations of that system.

From Table 5.7, it can be seen that the aspect ratio of the NRC-approved storage cask designs ranges from 0.43 to 0.68. The cylindrical casks and rectangular modules used in this parametric study have aspect ratios of 0.56 and 0.58, respectively, so they are approximately midway between the extreme upper and lower bounds of the NRC-approved casks. Because stability increases as the aspect ratio increases, it would be conservative to apply the results of this study to casks with higher aspect ratios. Applying these results to casks with lower aspect ratios might be nonconservative and should be done only with extreme care.

Table 5.7: NRC-Approved DCSS (September 2004) – General Use

Vendor	Model Name	Certificate of Compliance Issue Date (Docket)	$\frac{1}{2}$ Base Width, $r$ m (in)	Height of CG, $h_{cg}$ m (in)	Aspect Ratio, $r/h_{cg}$
General Nuclear Systems, Inc.	CASTOR V/21	08/17/1990 (72-1000)	1.20 (47.25)	2.44 (96.2)	0.49
NAC International, Inc.	NAC S/T	08/17/1990 (72-1002)	1.19 (47.0)	2.26 (88.8)	0.53
NAC International, Inc.	NAC-C28 S/T	08/17/1990 (72-1003)	1.19 (47.0)	2.26 (88.8)	0.53
BNFL Fuel Solutions Corp.	VSC-24	05/07/1993 (72-1007)	1.68 (66.0)	2.79 (109.9)	0.60
Transnuclear Inc.	TN-24	11/04/1993 (72-1005)	1.20 (47.4)	2.23 (87.8)	0.54
Transnuclear, Inc.	NUHOMS-24P NUMOMS-52B NUHOMS-61BT NUHOMS-24PHB NUHOMS-32PT	01/23/1995 (72-1004)	1.47 (58.0)	2.54 (100.0)	0.58
Holtec International	HI-STAR 100	10/04/1999 (72-1008)	1.22 (48.0)	2.79 (109.9)	0.44
NAC International, Inc.	NAC-MPC	04/10/2000 (72-1025)	1.63 (64.0)	2.50 (98.5)	0.65
Transnuclear, Inc.	TN-32	04/19/2000 (72-1021)	1.24 (49.0)	2.41 (94.9)	0.52
Transnuclear, Inc.	TN-68	05/28/2000 (72-1027)	1.07 (42.25)	2.47 (97.2)	0.43
Holtec International	HI-STORM 100	06/01/2000 (72-1014)	1.68 (66.25)	3.00 (118.2)	0.56
NAC International, Inc.	NAC-UMS (Stg.)	11/20/2000 (72-1015)	1.73 (68.0)	2.94 (115.7)	0.59
BNFL Fuel Solutions Corp.	FuelSolutions WSNF-220	02/15/2001 (72-1026)	1.75 (69.0)	2.96 ~ 3.05 (116.4 ~ 120.1)	0.59 ~ 0.57
	WSNF-221		1.75 (69.0)	2.61 (102.9)	0.67
	WSNF-223		1.75 (69.0)	2.58 (101.6)	0.68
Transnuclear, Inc.	Advanced NUHOMS-24PT1	02/05/2003 (72-1029)	N/A	N/A	N/A



## 6. Summary

This research project investigated the seismic response of freestanding spent fuel dry cask storage systems in earthquake events. Since the dry cask system is freestanding on a concrete pad, a significant portion of the modeling effort has been focused on examining the nonlinear frictional contact algorithm at the cask/pad interface. Three-dimensional finite element coupled models of the cask/pad/foundation using the ABAQUS/Explicit code were developed to incorporate this nonlinear interfacial contact as well as the soil-structure interaction effect when evaluating the dynamic nonlinear responses of dry cask systems subjected to prescribed seismic ground motions.

The principal objective of the research project was to perform parametric analyses, using the coupled response models and a selected group of input parameters, to provide to cask design licensing reviewers and applicants a set of generic responses of dry cask systems. Prior to conducting the parametric study, the coupled response models were closely examined and evaluated through performing three site-specific analyses including the three-module rectangular Transnuclear West module/cask, and HI-STORM 100 casks at Hatch Nuclear Power Station and at Private Fuel Storage Facility. Since the relevancy and usefulness of the parametric analysis results depend very much on the input parameters, an elaborate procedure was adopted in identifying them and in selecting their appropriate ranges of variation.

Key input parameters include cask designs, foundation types, coefficients of friction at cask/pad interface, and earthquake ground motions at different PGA (peak ground acceleration) levels conforming to selected spectral shapes. There is a huge matrix of input variables for the pool of input parameters, and a finite subset of this matrix was chosen in the parametric study for practical reasons. The chosen parameters include:

- 2 cask designs: A cylindrical cask with an aspect ratio of 0.56 and a rectangular module with an aspect ratio of 0.58. (The aspect ratio is defined as  $\frac{1}{2}$  the base diameter (for a cylindrical cask) or  $\frac{1}{2}$  the shorter width (for a rectangular module) divided by the height of the center of gravity from the base.)
- 3 foundation types: Soft soil, stiff soil, and rock
- 3 coefficients of friction at cask/pad interface: 0.20, 0.55, and 0.80
- 3 spectral shapes: NUREG/CR-0098, Regulatory Guide 1.60, and NUREG/CR-6728
- 5 earthquake records: NUREG/CR-0098 and Regulatory Guide 1.60:
  - 1) 1978 Iran Tabas
  - 2) 1999 Taiwan Chi-Chi
  - 3) 1992 Landers
  - 4) 1994 Northridge
  - 5) 1979 Imperial ValleyNUREG/CR-6728:
  - A) 1985 Nahanni
  - B) 1988 Saguenay
  - C) 1979 Imperial Valley
  - D) 1989 Loma Prieta
  - E) 1994 Northridge
- 4 PGA levels: 0.25, 0.60, 1.00, and 1.25 g

Various individual studies were performed to examine the sensitivity of model results to different model details such as element types, mesh sizes, number of nodes at the edge of cask base, and friction models at the cask/pad interface. A very careful procedure was undertaken in selecting the lateral dimension and

the depth of the foundation submodel with properly assigned lateral boundary conditions to demonstrate the appropriateness of using a finite submodel to simulate a semi-infinite foundation. Both explicit and implicit time integration methods were investigated in analyzing the coupled response models, and the explicit time integration method was eventually chosen because it provides very small time increments to assure the solution convergence of the highly dynamic nonlinear cask responses.

The selection of five different earthquake records conforming to the three spectral shapes and three foundation types provides a reasonable variation range of dynamic characterization of seismic ground motions. It is very important for the cask design licensing reviewers and applicants to cross compare the dynamic characterization of site-specific ground motions to those used in the parametric study. In cases with favorable comparisons, the analysis results from the parametric study could be used to guide design and review activities. Otherwise, site-specific cask response analyses might be needed to obtain results in demonstrating the adequacy of cask designs.

The parametric analysis results were examined closely to demonstrate the existence of the dynamic coupling between the dry cask system and the foundation due to the soil-structure interaction, which is one of the primary rationales for the development of coupled response models. In addition, the analysis results in free-field surface motions almost duplicate the prescribed input ground motions. These findings indicate that a reasonably proper modeling procedure has been developed in simulating a semi-infinite foundation using a finite model with appropriately prescribed boundary conditions, and in performing deconvolution analyses of surface-defined ground motions by preserving their dynamic characteristics of amplitudes and frequency contents.

The analysis results from the parametric study are expressed in terms of the peak lateral displacements at cask top and base and the peak cask angular rotation. In general, the cylindrical casks exhibit a higher amount of movements than the rectangular modules when subjected to the same level of seismicity and coefficient of friction at the cask/pad interface. This is because the base of the cylindrical cask is prone to a highly nonlinear rolling motion in an earthquake event resulting in its rather randomized trace on the concrete pad. On the other hand, the rectangular module can undergo only a rocking motion, which is inherently more stable, because of its rectangular base. In conclusion, the analysis results indicate a wide scatter of cask responses, in particular with the cylindrical casks.

Least squares regression curve fits on the cask analysis results as a function of the ground motion intensity have been performed to consolidate the widely scattered cask response results. The curve fitting plots are provided for both the peak cask top displacement and the peak cask rotation for the two cask designs, all three spectral shapes, and all three values of the cask/pad friction coefficient used in this study. The regression curve fits are plotted in terms of median cask response as well as median cask response plus and minus one standard deviation, representing 84% and 16% confidence bands, respectively. These plots are used as nomograms for evaluating the response for selected designs of casks subjected to earthquakes conforming to the spectral shapes used in the study.

The peak ground velocity (PGV) and the pseudo-spectral acceleration (PSA) at 5% damped 1 Hz frequency are the two parameters used to plots nomograms. The PGV, which is not a direct function of the spectral shape, is influenced by the spectral accelerations across the middle of the spectrum in the period range relevant to the cask response. Since the quality of the regression fits using the PSA at 1 Hz frequency as the ground motion parameter is consistently higher than that of the fits with the PGV, the PSA at 5% damped 1 Hz frequency was chosen to characterize the ground motion for the nomograms.

## 7. Conclusions

After an in-depth evaluation of parametric analysis results and nomograms, the following conclusions are made:

1. The cylindrical cask is less seismically stable than the rectangular module. The cylindrical cask is vulnerable seismically after it starts to roll at its base while the rectangular module is limited to a rocking motion because of its rectangular base.
2. The seismic response of cask/module is very sensitive to the coefficient of friction at the cask/pad interface,  $\mu$ . In cases with low coefficients of friction such as  $\mu = 0.20$ , the seismic response of cask/module is governed by sliding displacement. The angular rotation of cask/module increases with  $\mu$ , and it becomes a dominating contributor to the seismic response of the cask/module when  $\mu = 0.80$ .
3. The aspect ratio of a cask, defined here as  $\frac{1}{2}$  of the shortest dimension of its base divided by the height of its center of gravity, is one of the most important parameters affecting the stability of the cask. The cylindrical casks and rectangular modules used in the parametric study have aspect ratios of 0.56 and 0.58, respectively. Since cask stability increases as the aspect ratio increases, it would be conservative to apply the results of this study to casks with higher aspect ratios. Applying these results to casks with lower aspect ratios might not be conservative and should be done only with extreme care.
4. The linear elastic model is used to simulate the foundation in the coupled finite element model. Therefore, these models are not intended to provide results to address soil failure, in particular, underneath the edges of concrete pad.
5. The cask/module is seismically stable at low levels of peak ground accelerations (PGA) such as 0.25 g, as evidenced from the parametric analysis results.
6. The seismic response of cask/module is quite sensitive to foundation types at low PGA levels such as 0.25 g. However, this sensitivity diminishes with increasing PGA, as evidenced from the parametric analysis results with PGA = 0.6 g.
7. Nomograms of parametric analysis results are compiled for median response of cask/module +/- one standard deviation at a 5% damped 1 Hertz frequency (1 second period) of pseudo-spectral acceleration (PSA) after performing linear regression analyses on the pool of analysis results generated from earthquake ground motions conforming to a given spectral shape and all three foundation types. These nomograms provide seismic responses of the cask/module in term of maximum cask top sliding displacements relative to concrete pad and maximum angular rotations within the ranges of 16 and 84 percentiles.



## 8. References

1. Code of Federal Regulations, *Title 10*. January 1, 2004.
2. ABAQUS, Inc. “ABAQUS User’s Manual, Version 6.4.” 2003.
3. Luk, V. K., J. A. Smith, D. A. Aube, and R. A. Dameron. “NRC Project on Seismic Behavior of Spent Fuel Storage Cask Systems - Final Report on Seismic Analysis of Three-Module Rectangular Transnuclear West Module/Cask.” December 21, 2001.
4. Luk, V. K., J. A. Smith, D. A. Aube, R. A. Dameron, and I. P. Lam. “NRC Project on Seismic Behavior of Spent Fuel Storage Cask Systems - Final Report on Seismic Analysis of HI-STORM 100 Casks at Hatch Nuclear Power Plant.” June 28, 2001.
5. Luk, V. K., J. A. Smith, D. A. Aube, R. A. Dameron, and I. P. Lam. “NRC Project on Seismic Behavior of Spent Fuel Storage Cask Systems – Seismic Analysis Report on HI-STORM 100 Casks at Private Fuel Storage Facility, Rev 1.” March 31, 2002.
6. Newmark, N. M. and W. J. Hall. NUREG/CR-0098, “Development of Criteria for Seismic Review of Selected Nuclear Power Plants.” U.S. Nuclear Regulatory Commission: Washington D.C. May 1978.
7. Regulatory Guide 1.60, “Design Response Spectra for Seismic Design of Nuclear Power Plants.” U.S. Atomic Energy Commission, Directorate of Regulatory Standards. 1973.
8. McGuire, R. K., W. J. Silva, and C. J. Costantino. NUREG/CR-6728, “Technical Basis for Revision of Regulatory Guidance on Design Ground Motions: Hazard- and Risk-considered Ground Motion Spectra Guidelines.” U.S. Nuclear Regulatory Commission: Washington D.C. October 2001.
9. Moore, D. P., G. S. Bjorkman, and R. P. Kennedy. “Seismic Analysis of Plant Hatch ISFSI Pad and Stability Assessment of Dry Casks.” Proceedings of ICONE 8, Paper # 8499. Baltimore, MD, USA. April 2-6, 2000.
10. Hsu, P., G. V. Jones, D. P. Moore, T. H. Springfield, and D. S. Walden. “Design of Plant Hatch Independent Spent Fuel Storage Installation Pads.” Proceedings of ICONE 8, Paper # 8498. Baltimore, MD, USA. April 2-6, 2000.
11. The Final Safety Analysis Report for the Standardized NUHOMS® Horizontal Modular Storage System for Irradiated Nuclear Fuel, Rev. 6. October 2001.
12. Stevenson & Associates, Inc. “SUPER SASSI/PC User’s Manual.” May 1996.
13. Idriss, I. M. and J. I. Sun. User's Manual for SHAKE91, “A Computer Program for Conducting Equivalent Linear Seismic Response Analysis of Horizontally Layered Soil Deposits.” Program modified based on the original SHAKE program published in December 1972 by Schnabel, Lysmer, and Seed. University of California, Davis: Davis, CA. November 1992.
14. Singh, K. P., A. I. Soler, and M. G. Smith. “Predicting the Structural Response of Free-Standing Spent Fuel Storage Casks under Seismic Events.” 16<sup>th</sup> Conference on Structural Mechanics in Reactor Technology (SMiRT 16). Washington, D.C. August 12-17, 2001.

15. Holtec Proprietary Computer code DYANMO, QA Validation Manual, HI-91700. 1991.
16. Idriss, I. M. and H. B. Seed. "Seismic Response of Horizontal Layers." *Journal of the Soil Mechanics and Foundation Division*. ASCE, Vol. 94, No. SM 4. July 1968.
17. Schnabel, P. B., J. Lysmer, and H. B. Seed. "SHAKE: A Computer Program for Earthquake Response Analysis of Horizontally Layered Sites." Report No. UCB/EERC-72/12. Earthquake Engineering Research Center, University of California: Berkeley, CA. December 1972.
18. Prevost, J. H. "DYNAFLOW: Finite Element Analysis for the Static and Transient Response of Linear and Nonlinear Two and Three Dimensional System." Princeton University: Princeton, NJ. 1996.
19. US Army Corps of Engineers. Engineer Technical Letter No. 1110-2-339. March 1993.
20. American Society of Civil Engineers (ASCE). "Seismic Analysis of Safety-Related Nuclear Structures and Commentary." ASCE: New York, NY. 1998.
21. Tennessee Valley Authority. "All Projects, Steel to Concrete Coefficient of Friction Preliminary Tests." Report No. CEB 77-46. December 5, 1977.
22. Rabbat, B. G. and H. G. Russell. "Friction Coefficient of Steel on Concrete or Grout." *Journal of Structural Engineering*. American Society of Civil Engineers, Vol. 111, No. 3, pp. 505-515: March 1985.
23. Dreher, R. C. "Friction and Wear Characteristics of Wire-Brush Skids." NASA Technical Paper 1495. National Aeronautics and Space Administration. 1979.
24. Idun, E. K. and D. Darwin. "Bond of Epoxy-Coated Reinforcement: Coefficient of Friction and Rib Face Angle." *ACI Structural Journal*, Vol. 96, No. 4, pp. 609-615: July-August 1999.
25. Baltay, P. and A. Gjelsvik. "Coefficient of Friction for Steel on Concrete at High Normal Stress." *Journal of Materials in Civil Engineering*. ASCE, Vol. 2, No. 1, pp. 46-49: February 1990.
26. Olofsson, U. and M. Holmgren. "Friction Measurement at Low Sliding Speed Using a Servohydraulic Tension-torsion Machine." *Experimental Mechanics*. Vol. 34, No. 3, pp. 202-207: September 1994
27. Housner, G. W. "The Behavior of Inverted Pendulum Structures During Earthquakes." *Bulletin of the Seismological Society of America*. Vol. 53, No. 2, pp. 403-417: February 1963.
28. Ang, A. H-S. and W. H. Tang. *Probability Concepts in Engineering Planning and Design, Volume I- Basic Principles*. John Wiley & Sons: New York. 1975.

## **Appendix I: Details in Background Information on Soil Profile and Properties Issues**



## **Appendix I: Details in Background Information on Soil Profile and Properties Issues**

A major technical issue in the parametric analyses relates to the difficulties in defining the appropriate input parameters, especially regarding ground motion hazard levels and site soil properties to obtain meaningful and relevant cask response for review of cask design applications. Ultimately, in order for the library of cask response solutions to be usable to the Nuclear Regulatory Commission staff in the safety review of cask design licensing applications, there needs to be a relatively simple and systematic way for cross comparison of ground shaking input as well as soil properties between the parametric study and the site-specific applications.

It would be logical to separate ground motion from soil properties issues. The implication of site soil properties toward ground motion site response in the context of the parametric study would be quite different from conventional design projects, where site response analysis is primarily part of the seismic study for defining the hazard level of ground motion to meet design requirements. Since the inherent process involves calibrating ground surface shaking, a different treatment would be required to implement site soil properties to the specifics of parametric analyses. The adopted procedure has a built-in safeguard for achieving the properly targeted ground surface shaking, so long as a consistency in soil parameters (including modulus and damping) is maintained between deconvolution solution of input motion and the resultant coupled cask response models. Lam et al. [1] documented the detailed procedure to achieve the intended ground shaking input to the coupled cask/pad/foundation model. Furthermore, it is important to match appropriate soil properties with issues related to the coefficient of restitution, which would be dominated by the localized surface soil condition. This discussion provides further background information on the soil profiles summarized in Figure 3.5 in the main text.

An extensive literature search was conducted in the parametric study to gather information on generic site soil properties, particularly those used in the nuclear power industry. Eventually, the selected soil profiles and properties adopted for the parametric study were based on two Electric Power Research Institute (EPRI) reports [2 and 3]. For example, Figure I-1, which shows shear wave velocity profiles for generic nuclear power plant sites, has been extracted from the 1989 EPRI report [2]. The benchmark soil profiles in the parametric study (referred to as stiff soil site conditions) are based on the Standard Profile in Figure I-1. Similarly, the Lower Range Profile in this figure was used to generate the soft soil profile. After discretization, the two referenced (referred to as Standard and Lower Range) shear wave velocity profiles led to the two low-strain shear wave velocity (referred to as stiff and soft soil) profiles in the site response models as shown in Figure I-2.

Deconvolution analyses were performed to provide soil column base motions at 140-ft depth for the two cited stiff and soft soil profiles as well as the upper bound rock profiles using the SHAKE91 program [4]. In these analyses, the parametric study adopted the 1993 EPRI procedure [3] on depth-dependent sand modulus and damping ratio versus shear strain curves as shown in Figure I-3. In performing deconvolution analyses, the ground surface shaking level was scaled to a peak ground acceleration (PGA) of 0.25 g that would likely be the most representative PGA for licensing applications of existing power plant sites on the east coast. The deconvolution analyses were performed for each of the two horizontal component motions for each of the five selected sets of motions fitted to the NUREG/CR-0098 [5] spectral shape (see Table 4.2). The iterated strain-compatible shear wave velocity and damping profiles for the 10 runs were then averaged to develop the generic iterated strain-compatible shear wave velocity and damping profiles. The deconvolution analyses were then repeated using the averaged profiles to develop column base motions. Parallel to the column base motions, the corresponding soil modulus and

damping properties for all the stiff and soft soil and the upper bound rock profiles were developed for compatibility in soil parameters between deconvolution and coupled cask response models.

As discussed in the report, it is very important to cross compare the soil condition (in terms of shear wave velocity) between the parametric study and cask design applications for surface soils to make sure that the inherent coefficient of restitution be comparable. It would be intuitive to assume that the coefficient of restitution is not sensitive to deeper soil stiffnesses. Based on typical dry cask dimensions, the analysis procedure is concentrated on the soil profile at the upper 10-ft range only.

It should be noted that there are subtle differences between low-strain shear wave velocity profiles (relevant for referencing) versus the iterated strain-compatible soil profiles (used in the parametric study), as shown in Figure I-2. Rigorously speaking, cross-referencing to site-specific project cases is based on the definition of low-strain shear wave velocity profiles (from geophysical sounding in the field). However, the soil modulus (and strain-compatible shear wave velocity) needs to be adjusted for various levels of shaking in numerical analyses. The analysis team feels that maintaining full rigor regarding strain-compatibility issues would bring in unnecessary complexity and thus is not warranted within the range of uncertainty on the overall problem. Furthermore, differences between the low-strain and the iterated shear wave velocity (modulus) profiles are rather small (less than 10 percent), as evidenced in Figure I-2. The rationale behind this observation is that the free stress boundary condition for the ground surface would inherently ensure relatively small shearing strains near the ground surface. To avoid any unnecessary confusion, the iterated shear wave velocity profile has been documented in Figure 3.5 and can be used for cross comparison in cask design applications.

It is important to point out that soil properties would have an insignificant role in defining ground motion shaking levels because of the inherent procedure for calibrating shaking at the ground surface reference point. For this reason, and also to minimize confusion, it has been elected to utilize the same soil profiles (iterated for 0.25 g ground shaking) for cask response analyses for different parametric PGA response cases, including PGA at 0.6 g, 1.0 g and 1.25 g, without repeating iterative solutions for other shaking levels. Cask response solutions at higher levels of ground shaking are merely intended to appreciate potential cask response qualitatively. These high ground motion levels would very unlikely be encountered in licensing situations. In addition, it is well known that the strain-compatible soil properties shown in Figure I-3 along with standard site response analysis procedures work well only to moderate levels of ground shaking. The conventional site response procedure starts to deteriorate at higher ground shaking levels and can result in unrealistic ground motions. In most projects in California, subjective judgmental modifications of the strain-compatible property procedures would be required on project specific basis, which would be difficult to implement for the parametric cask response study without defining the true site-specific soil conditions.

Besides the site soil profiles, there is a need to provide information for an upper bound soil stiffness case. It has been elected to use a stiffer soil stiffness (higher shear wave velocity) profile above the upper bound range recommended by the 1989 EPRI report [2], as shown in Figure I-1, so that the profile can cover even the rock site cases. Since the cask response solutions indicate higher cask responses for stiffer soil profiles, the adopted profile can provide a bounding case. Figure 3.5 in the report summarized the three parametric soil profiles adopted in the parametric response study. It can be observed from this figure that the chosen shear wave velocity value of 5,000 fps would be sufficiently high to cover the very stiff rock found at the eastern United States. However, softening of the rock at the ground surface would be very prevalent and likely be encountered at almost all rock sites. In addition, most cask design contractors appear to favor overlaying the rock surface by a thin layer of engineering fill. Therefore, the rock site profile at the upper 10-ft layer has been modified to reflect the expected conditions to ensure that the analysis model would capture the proper coefficient of restitution.

## References

1. Lam, Ignatius Po, H.Law, and C. T. Yang. "Modeling of Seismic Wave Scattering on Pile Group and Caissons." Report submitted to MCEER, February 25, 2004.
2. Electric Power Research Institute (EPRI). "Probabilistic Seismic Hazard Evaluations at Nuclear Plant Sites in the Central and Eastern United States: Resolution of the Charleston Earthquake Issue," Special Report, NP-6395-D, Research Project P101-53. EPRI: Palo Alto, CA. April 1989.
3. Electric Power Research Institute (EPRI). "Guidelines for Determining Design Basis Ground Motions," Final Report, EPRI TR-102293. EPRI: Palo Alto, CA. November 1993.
4. Idriss, I. M. and J. I. Sun. User's Manual for SHAKE91, "A Computer Program for Conducting Equivalent Linear Seismic Response Analysis of Horizontally Layered Soil Deposits." Program modified based on the original SHAKE program published in December 1972 by Schnabel, Lysmer, and Seed. University of California, Davis: Davis, CA. November 1992.
5. Newmark, N. M. and W. J. Hall. NUREG/CR-0098, "Development of Criteria for Seismic Review of Selected Nuclear Power Plants." U.S. Nuclear Regulatory Commission: Washington D.C. May 1978.

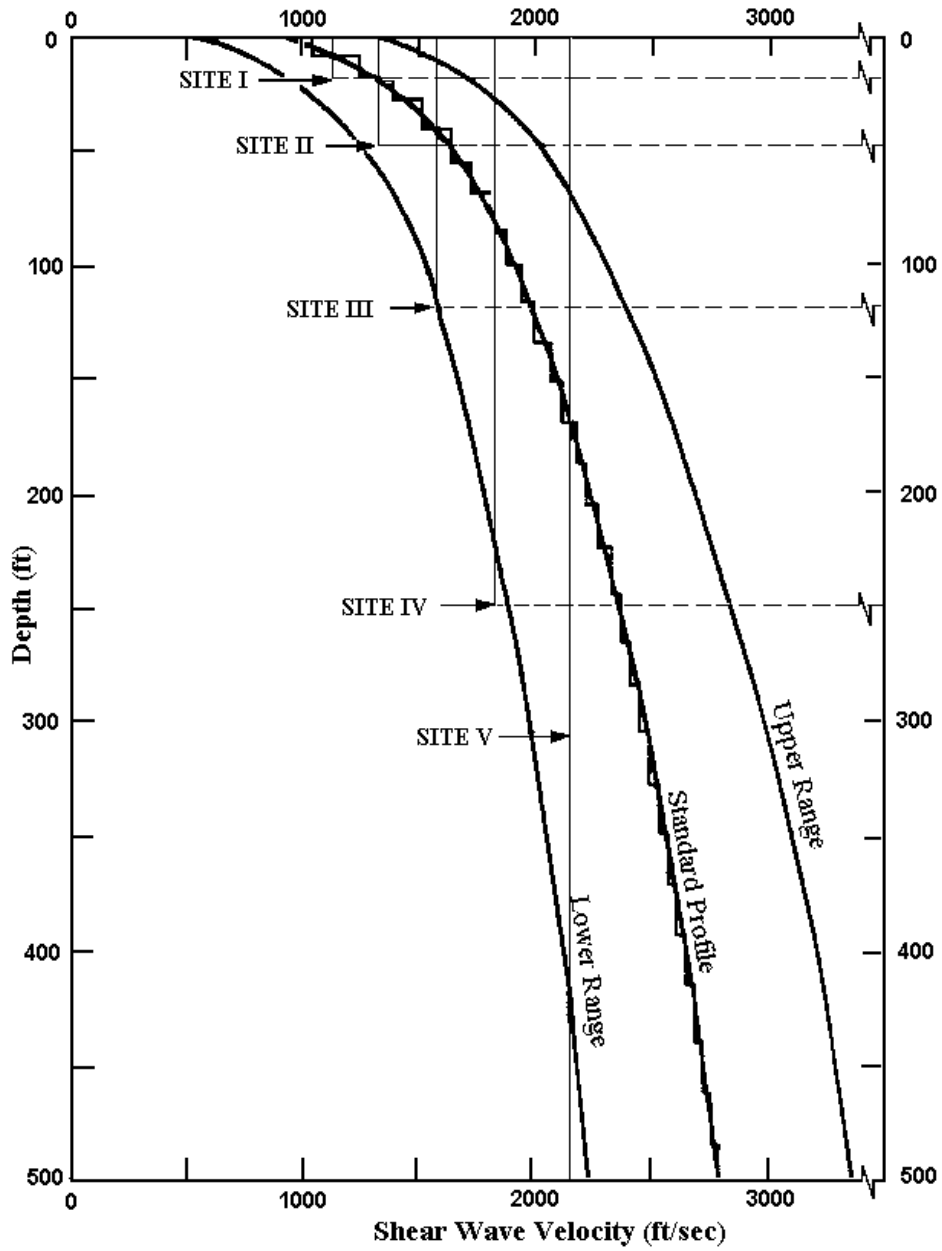


Figure I-1: Typical Shear Wave Velocity Profiles for Nuclear Power Plant Sites

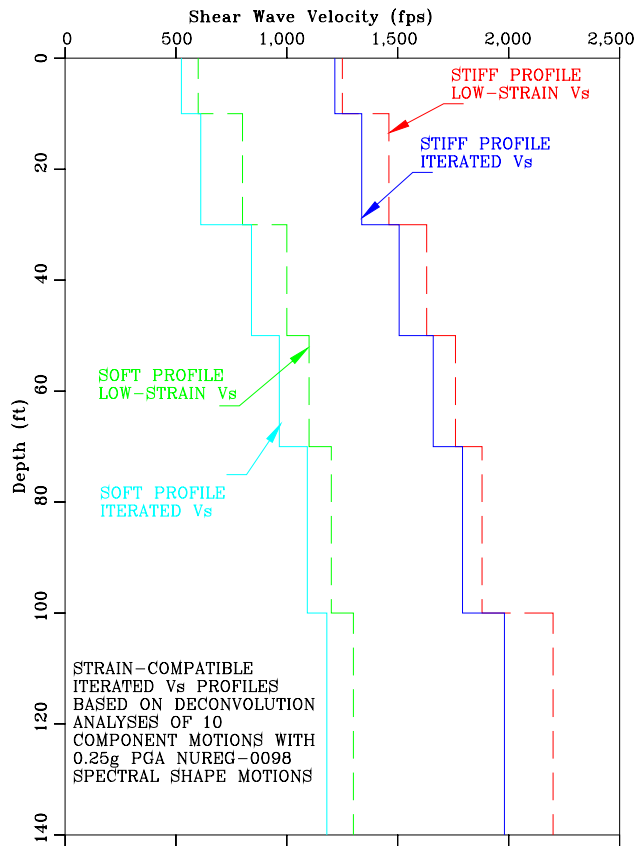


Figure I-2: Shear Wave Velocity Profiles for Soil Sites in Parametric Analyses

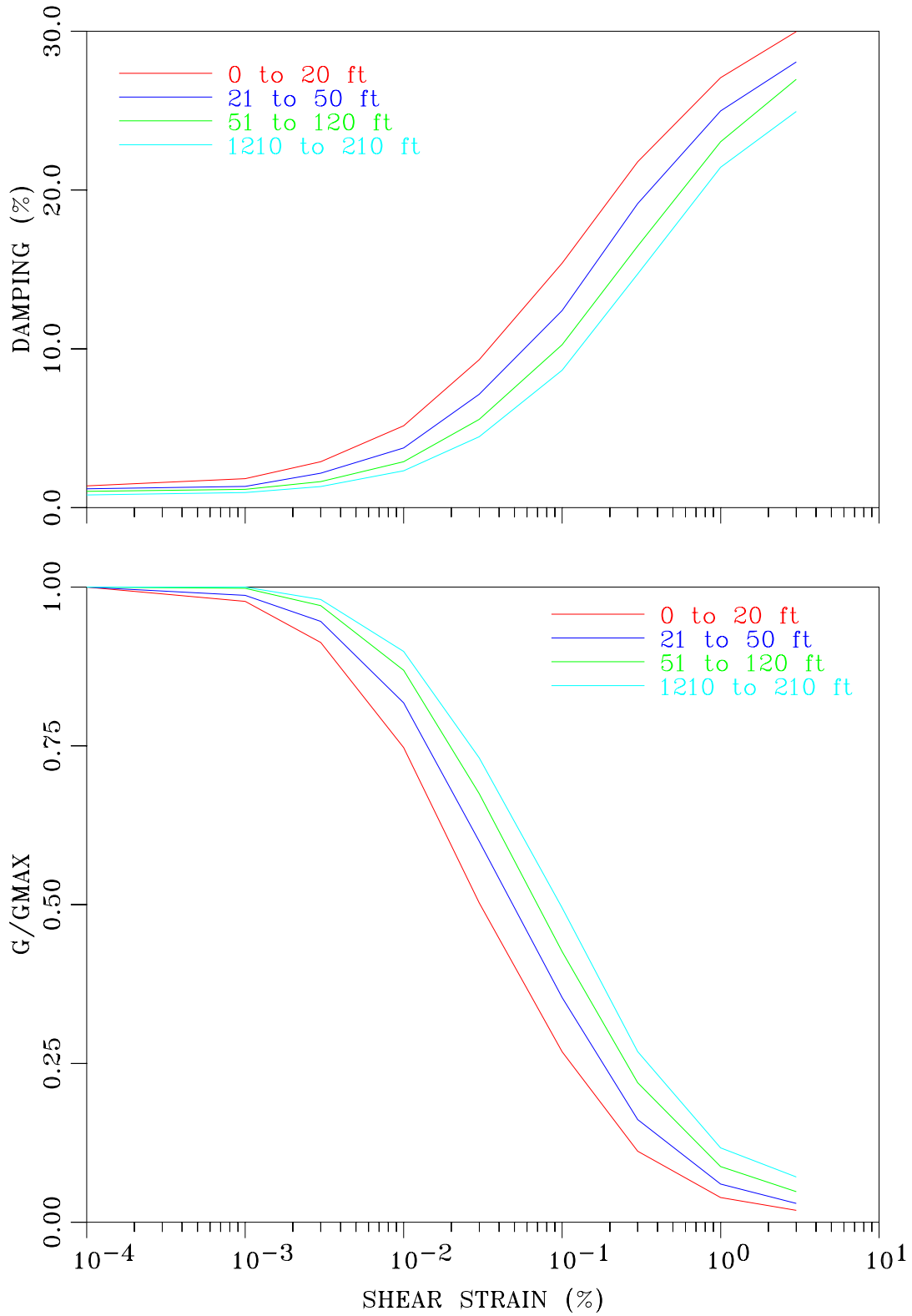


Figure I-3: Strain Compatible Soil Properties in Deconvolution Analyses

## **Appendix II: Verification of Time-Domain Wave Propagation and Various Wave-Propagation Sensitivity Studies**



## **Appendix II: Verification of Time-Domain Wave Propagation and Various Wave-Propagation Sensitivity Studies**

This appendix was extracted from Section 3 of a more complete report entitled *Modeling of Seismic Wave Scattering on Pile Group and Caisson* by Ignatius Po Lam, Hubert Law and Chien-Tai Yang, funded by the Multidisciplinary Center for Earthquake Engineering Research (MCEER) at the University of New York at Buffalo, through a grant from the FHWA (FHWA Contract Number DTFH61-92-C-00112). This report was submitted to MCEER on February 25, 2004 and is currently under review for publication.

Section 3 of the cited MCEER report addresses the issue of using a time-domain numerical method for conducting the classical one-dimensional site response analysis. This section is presented in this appendix to summarize some of the major background information relevant for the dry cask response problem. Other sections of the MCEER report, not included as part of this current report, includes comparing time-domain two-dimensional wave scattering of embedded foundation systems to SASSI [1] solutions.

### **II.1 One-Dimensional Site Response**

When a seismologist develops a reference rock motion, it usually represents an outcrop motion. The rock outcrop motion is employed in a one-dimensional site response program (e.g., SHAKE91 [2]) to compute free-field motions for subsequent studies required for foundation designs. Consistent with the definition of the outcrop motion, the input acceleration to SHAKE91 must be treated as ‘outcrop’ motion, not as ‘within’ motion. By treating as ‘outcrop’, the layer below the boundary where the outcrop motion is specified becomes infinite space, eliminating the potential for wave reflection/refraction at the boundary.

When the input motion to SHAKE91 is used as ‘within’ motion, the boundary is treated as a rigid base resulting in ‘prescribed motion’ at the base of the soil column. Consequently, if the input rock motion intended for ‘outcrop’ is used as ‘within’ motion in SHAKE91, overly conservative and sometimes erroneous solutions are obtained. This is a result of wave trapping within the soil deposit. Unfortunately, some practicing geotechnical engineers do not recognize these mechanics and continue to make these mistakes not only in SHAKE91 but also in other site response analysis programs.

There are cases where seismologists define a reference motion at the ground surface, especially where rock-like material cannot be located within a reasonable depth (e.g., within 200 feet). In this situation, they rely on soil attenuation relationships based on recorded surface motions to establish the reference motions at the ground surface. Depth-varying free-field motions can be computed from the reference surface motion by conducting a deconvolution analysis with the program SHAKE91. The deconvoluted motion at any depth may be requested as ‘outcrop’ or ‘within’ motion.

For the purpose of this research, we consider hypothetical soil strata, as illustrated in Figure II-1 showing the material properties assigned to each soil stratum. The reference motions chosen for this study are at the ground surface; Figures II-2 and II-3 present the characteristics of the reference motions in two directions, horizontal and vertical, defined at the ground surface. These motions have been spectrum-matched to certain design response spectra. Given the reference motions defined at the surface, deconvolution analyses were conducted to compute the free-field motions at every soil layer as ‘within’ motion, while the bottommost layer is requested as both ‘within’ and ‘outcrop’ motions. The free-field motions as computed from SHAKE91 are illustrated in Figures II-4 and II-5 for the horizontal and vertical directions, respectively.

Here attempts are made to reproduce the SHAKE91 solutions using the ADINA [3] program. The base input acceleration to ADINA model is the ‘within’ motion at the bottommost layer computed from the deconvolution analysis using SHAKE91. The prime reason of using the SHAKE91 ‘within’ motion to excite the ADINA finite element model is that rigid base excitation is implemented without employing transmitting boundary conditions. If the solutions are correct, the surface motion computed from ADINA should duplicate the reference surface motion.

Several parameters affect the ADINA solutions. To understand how they influence the numerical results, comparison between the ADINA solutions and the SHAKE91 solutions is made by performing a parametric study that addresses the following issues:

- Effects of vertical side boundaries
- Effects of time integration schemes
- Implementation of damping

## II.2 Effects of Vertical Side Boundaries

A two-dimensional finite element method is used to simulate the one-dimensional wave propagation in order to investigate the effectiveness of various side boundary conditions. The finite element domain representing the same layered soils used in SHAKE91 is shown in Figure II-6. Seismic response analyses of the soil strata were performed using the following boundary conditions:

- Free side boundary
- Fixed side boundary
- Edge column boundary
- Slaving of left and right boundaries
- Transmitting side boundary

Schematics of these side boundary conditions are shown in Figure II-7.

Figure II-7 (a) is a finite element model with free side boundaries indicating no constraint at the side boundary nodes. These side boundary nodes are free to move in any direction.

Figure II-7 (b) illustrates a finite element model with fixed side boundaries implying that no vertical and horizontal movement relative to the base is allowed at the two side boundaries.

Figure II-7 (c) represents a model with two edge columns at the side boundaries where two corresponding nodes of the soil column at same elevations are slaved together. The intent is to create shear beam columns near the boundaries.

Figure II-7 (d) is an illustration of how one-dimensional wave propagation is modeled by means of slaving the leftmost nodes to the rightmost nodes at the side boundaries. Slaving is done in the both directions, horizontal and vertical, such that the slaved nodes move together.

Figure II-7 (e) depicts treatment of the side boundaries using dashpots similar to those used at the base of some numerical models to represent a half space suggested by Lysmer and Kulemeyer [4].

In all the cases discussed above, rigid base excitation is the primary form of seismic loading to the ADINA finite element model. This is accomplished by assigning the ‘within’ motion computed from the SHAKE91 deconvolution analysis at the base of the soil column. Only horizontal site response behavior is assessed in this exercise (i.e., vertical motion is not included). The horizontal ground response is

computed at the surface (depth 0 ft) from each of the finite element model, and the result is compared with the reference ground motion in Figure II-8 in terms of acceleration response spectra.

It can be seen that the ground response of the fixed-side-boundary model is largely magnified by reflected waves as overly restraint conditions were imposed in the analysis. The free side boundaries also yield a superfluous response that is not satisfactory as compared to the reference surface motion. Although free or fixed boundary condition is typically available in general finite element codes, neither could provide accurate ground response simulating one-dimensional wave propagation.

The finite element with dashpot side boundary also yields unsatisfactory ground response. However Lysmer and Kulemeyer report the effectiveness of the dashpot concept when used at the base representing the half space to absorb seismic energy, and the efficiency of absorbing energy decreases largely with the increase of the incident angle. The efficiency is about 95% for a zero incident angle but reduces to around 10% for a 30-degree incident angle. However, no discussion is found for the dashpot concept being used at the side boundary. Based on the result obtained from this study, the dashpot concept applied at the side boundaries is not very effective in modeling the one-dimensional shear beam problem. Perhaps the side boundary where the dashpots are attached is too close to the center of the finite element. Of course, if the side boundaries are moved 'far' away from the centerline of the model, the solutions would converge to the one-dimensional situation regardless of the type of boundary.

The solution of the model with a two-edge column concept shows a reasonable degree of accuracy as compared to the benchmark surface motion. In this model, the width of edge column is 61 feet. It is anticipated that width of the edge columns might influence the solutions, and its effects will be discussed later.

The response for the finite element model, which slaves the leftmost nodes to the rightmost nodes converges very close to the benchmark surface motion, and the model appears to be the most suitable for simulating a simple shear beam theory. While this boundary condition can be used for simple models where the left side and right side of the finite element mesh have similar geometric configurations and properties, it would not be suitable if the two sides have different ground elevations, such as retaining walls or sloping ground conditions.

For these parametric studies, it appears that the edge column concept and the slaving left-and-right boundary concept show promising results that can be used for general application depending on situations. To further examine the results, the depth varying motions from these two models are compared with SHAKE91 depth-varying motions, as shown in Figures II-9 and II-10.

## **II.2.1 Effects of Edge Column Widths**

As discussed earlier, the technique of slaving the leftmost nodes to the rightmost nodes is not always suitable for all the geotechnical problems, such as situations where there is a retaining wall, wharf structure or sloping ground. In these cases, the edge column concept may be used. To use two edge columns for general application, it is necessary to understand the effects of edge column widths. For this report different edge column widths were considered while keeping the distance to the boundary from the centerline of the model unchanged.

In this sensitivity analysis, we elect to use the same hypothetical soil strata as shown in Figure II-1, which has a total thickness of 185 ft. The side boundaries are 246 ft away from the centerline of the model. Each of the side boundaries is attached to an edge column with varying widths, as shown in Figure II-11. The following edge column widths were considered:

- Edge Column Width =  $1/6 H$
- Edge Column Width =  $1/3 H$
- Edge Column Width =  $2/3 H$
- Edge Column Width =  $H$

where  $H$  is the thickness of the ground. The solutions with different column widths are provided in Figure II-12. When compared to the benchmark surface motion, closer agreements are obtained with the increase of edge column widths. One can imagine that a narrower edge column tends to behave more like a free side boundary, and that a wider edge column approaches to a shear beam model when only horizontal excitation is considered.

In theory, the solutions of the model with a sufficiently wide edge column should approach to the response of the free field motions derived from a shear beam model under horizontal excitation. However, it becomes a tradeoff between the finite element size (or the computing time) and the accuracy. For practical purposes in most bridge engineering applications, a minimum edge column width should be  $1/3 H$  or larger in order to obtain reasonable structural responses beyond 0.5-sec periods. It would be desirable to perform sensitivity analyses, like the one presented here, using site specific soil conditions prior to performing actual designs.

## II.2.2 Effects of Distances to the Boundary

In the preceding section, the effect of edge column width is evaluated while keeping the distance to the side boundary from the centerline of the model unchanged. In addition to the edge column width, the solutions would also depend on proximity to the side boundary. The sensitivity analyses were performed by varying the distance to the side boundary but maintaining the edge column width to  $1/3 H$ . The following side boundary distances were evaluated:

- Distance to Side Boundary =  $1.2 H$
- Distance to Side Boundary =  $1.5 H$
- Distance to Side Boundary =  $1.8 H$

where  $H$  is the thickness of the ground. We consider these distances to be within a practical range for most design applications. Figure II-13 shows comparison of surface motions from the three models with increasing distances to the side boundary. It appears that the solutions are not very sensitive to the distance to the boundary in this study. However, it is not advisable to have the side boundaries too close to the centerline.

## II.2.3 Effects of Time Integration Schemes

In the time domain schemes as employed by ADINA and other computer codes, the differential equations are solved using a numerical step-by-step integration procedure. Several integration schemes are available based on different interpolations between displacements, velocity and acceleration, as well as the time step of the equilibrium established [5]. The following integration schemes were investigated:

- Wilson's  $\theta$  Method
- Newmark Method ( $\delta = 0.5$  and  $\alpha = 0.25$ )
- Newmark Method ( $\delta = 0.65$  and  $\alpha = 0.331$ )

Figure II-14 shows results of three different integration schemes for the model with the edge column concept. The responses vary with the different time integration schemes; however the difference is obvious only in a high frequency range. For practicality, any of the time integration methods is considered acceptable.

## II.2.4 Treatment of Rayleigh Damping

Perhaps the greatest difference between SHAKE91 and ADINA is the treatment of damping in the respective numerical procedures. The frequency response function computed within SHAKE91 uses a damping ratio, which is frequency independent. This will result in constant energy dissipation across the spectrum. However, most finite element programs including ADINA employ a Rayleigh damping concept, which would lead to frequency dependent damping characteristics. When using Rayleigh damping for dynamic analyses, it is possible to adopt one of the following procedures:

- Mass proportional damping only ( $\alpha$ )
- Stiffness proportional damping only ( $\beta$ )
- Both mass and stiffness proportional damping ( $\alpha$  and  $\beta$ )

Because the damping values vary with frequency in the Rayleigh damping concept, it is necessary to anchor the desired damping ratio at a specific frequency, e.g., the vibration period of the system. For the mass proportional damping or stiffness proportional damping, only one anchoring point can be selected. When mass and stiffness proportional damping is used, two anchoring points must be chosen.

For a general case where both mass and stiffness related damping is used, the coefficients  $\alpha$  and  $\beta$  can be determined from

$$\alpha + \beta \omega_i^2 = 2 \omega_i \xi_i$$

where  $\xi_i$  is damping ratio at angular frequency  $\omega_i$ . The relationship requires two frequencies to solve both coefficients ( $\alpha$ ,  $\beta$ ). If mass proportional damping is used, then the coefficient  $\alpha$  is determined as

$$\alpha = 2 \omega_i \xi_i$$

When stiffness proportional damping is used, the coefficient becomes

$$\beta = 2 \xi_i / \omega_i$$

Sensitivity analyses were conducted using the three different Rayleigh damping methods; all were calibrated to the same damping ratio used in SHAKE91. Using mass and stiffness proportional damping could offer more flexible means of calibrating the damping ratio. Table II-1 tabulates Rayleigh damping parameters for each case, and Figure II-15 shows the results of the sensitivity analyses. Note that the finite element mesh with the left and right boundaries slaved together was employed. From comparison among the solutions resulting from different implementation of the damping parameters, it appears that all the methods offer reasonable solutions.

## II.3 Two Component Motions

So far, horizontal motion is the only base excitation accounted for in the finite element analyses, and thus the response can be checked against the behavior of vertically propagating shear waves that can be treated

with a classical shear beam theory. However, most seismic designs consider earthquake loading in two or three directions. To implement two component motions in the finite element model, the reference vertical motion defined at the ground surface requires deconvolution in order to obtain the input base motion; this was accomplished with SHAKE91. The ADINA finite element model is then excited with the vertical and horizontal motions simultaneously. The material properties used in ADINA are based on linearly elastic continua adhering to general Hooke's law where Young's modulus (E) and shear modulus (G) are related through Poisson's ratio ( $\nu$ ) such that

$$E = 2(1+\nu)G$$

In practice however when computing depth varying horizontal and vertical motions with SHAKE91, separate computer runs are made; one with S-wave velocity (Shear Modulus) profile, and one with P-wave (Constraint Modulus) profile. Often, a few iterations are performed within SHAKE91 to achieve strain compatible moduli, and it is carried out separately for the horizontal direction and vertical direction. The iteration process could result in incompatibility between S-wave and P-wave velocities. If the iterative solutions are adopted in SHAKE91, it is difficult to compromise the comparison between SHAKE91 and ADINA.

In order to reconcile results of two-component shaking from ADINA with those of SHAKE91, one must verify that the P-wave velocity and S-wave velocity employed by SHAKE91 are uniquely related, similar to the general Hooke's law.

The comparison between SHAKE91 and ADINA on the two-component motion is shown in Figure I-16 using the finite element model that slaves the left boundary to the right boundary. The comparison is very favorable although there are some discrepancies in the treatment of damping. For example, SHAKE91 uses the different damping ratios in the horizontal deconvolution from the vertical deconvolution, while ADINA allows only one set of Rayleigh damping parameters that are applied to the entire system, which is excited by horizontal and vertical motions simultaneously. The Rayleigh damping used in the finite element model has been calibrated to the damping ratios of the horizontal SHAKE91 profile. Based on this observation, it seems that minor discrepancy in soil damping does not contribute to significant differences in the seismic response of the ground.

A similar comparison is made between SHAKE91 and ADINA using the two-edge column concept; the results are shown in Figure II-17. The following summarizes the ADINA model:

Distance to the side boundary from the centerline = 246 ft  
Width of the edge column = 65 ft

The ADINA solutions using the two-edge columns are not as good as those results presented in Figure II-16. Attempts were made to improve the ADINA solutions by increasing the width of the edge column; however the degree of improvement is poor. The reason is attributed to the fact that the finite element model with two-edge columns is unable to maintain the constraint conditions required in one-dimensional wave propagation especially when vertical motion is introduced. Imagine a P-wave propagation in the finite element model with two edge columns. Due to the Poisson's ratio effects, the vertical strain in soil due to passage of P-wave would lead to horizontal displacement pushing the edge columns outward. This would have resulted in a violation of the constraint modulus assumption made in SHAKE91 for the vertical wave propagation problem.

To make this point, site response analysis was performed using the vertical input motion only, and snapshots of relative deformation profiles of the two edge boundaries are plotted in Figure II-18. Without horizontal excitation, the edge boundaries deform laterally as a result of the Poisson's effect. If a true

one-dimensional condition is maintained, the two side boundaries would have moved together, and the profiles of the two edge columns would have been identical. From inspection of the edge boundary profiles, it is obvious that the two-edge column model tends to deviate from one-dimensional behavior when the vertical motion is introduced. If the vertical motion is absent, the response of the edge column model seems to yield reasonable results.

## References

1. Stevenson & Associates, Inc. "SUPER SASSI/PC User's Manual." May 1996.
2. Idriss, I. M. and J. I. Sun. User's Manual for SHAKE91, "A Computer Program for Conducting Equivalent Linear Seismic Response Analysis of Horizontally Layered Soil Deposits." Program modified based on the original SHAKE program published in December 1972 by Schnabel, Lysmer, and Seed. University of California, Davis: Davis, CA. November 1992.
3. ADINA R&D Inc. User's Guide for ADINA: Automatic Dynamic Incremental Nonlinear Analysis. MA. June 2003.
4. Lysmer, J. and Kulemeyer, R.L. "Finite Dynamic Model for Infinite Media," *Journal of Engineering Mechanics Division*. ASCE, Vol. 95, No., EM4, pp. 859-877. August 1969.
5. Bath, K-J. *Finite Element Procedures in Engineering Analysis*. Prentice-Hall Inc. 1982.

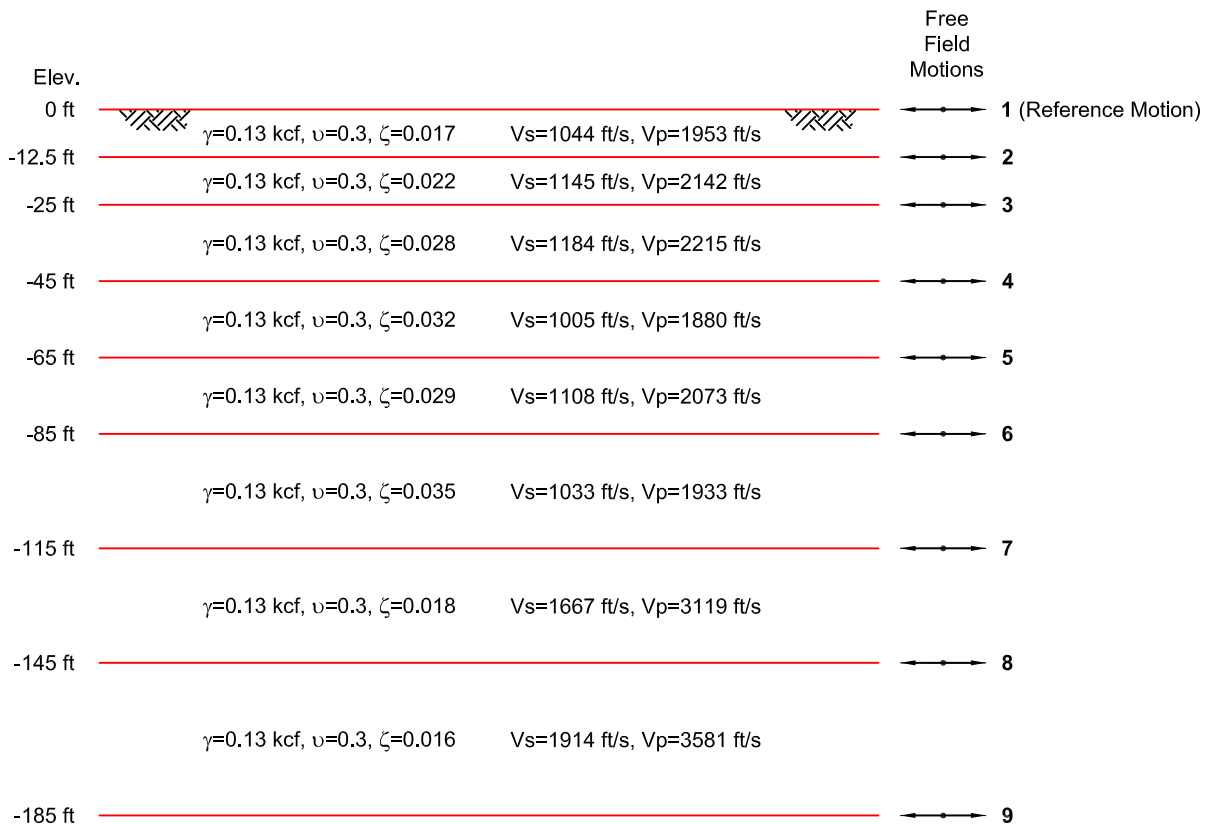


Figure II-1. Hypothetical Soil Strata

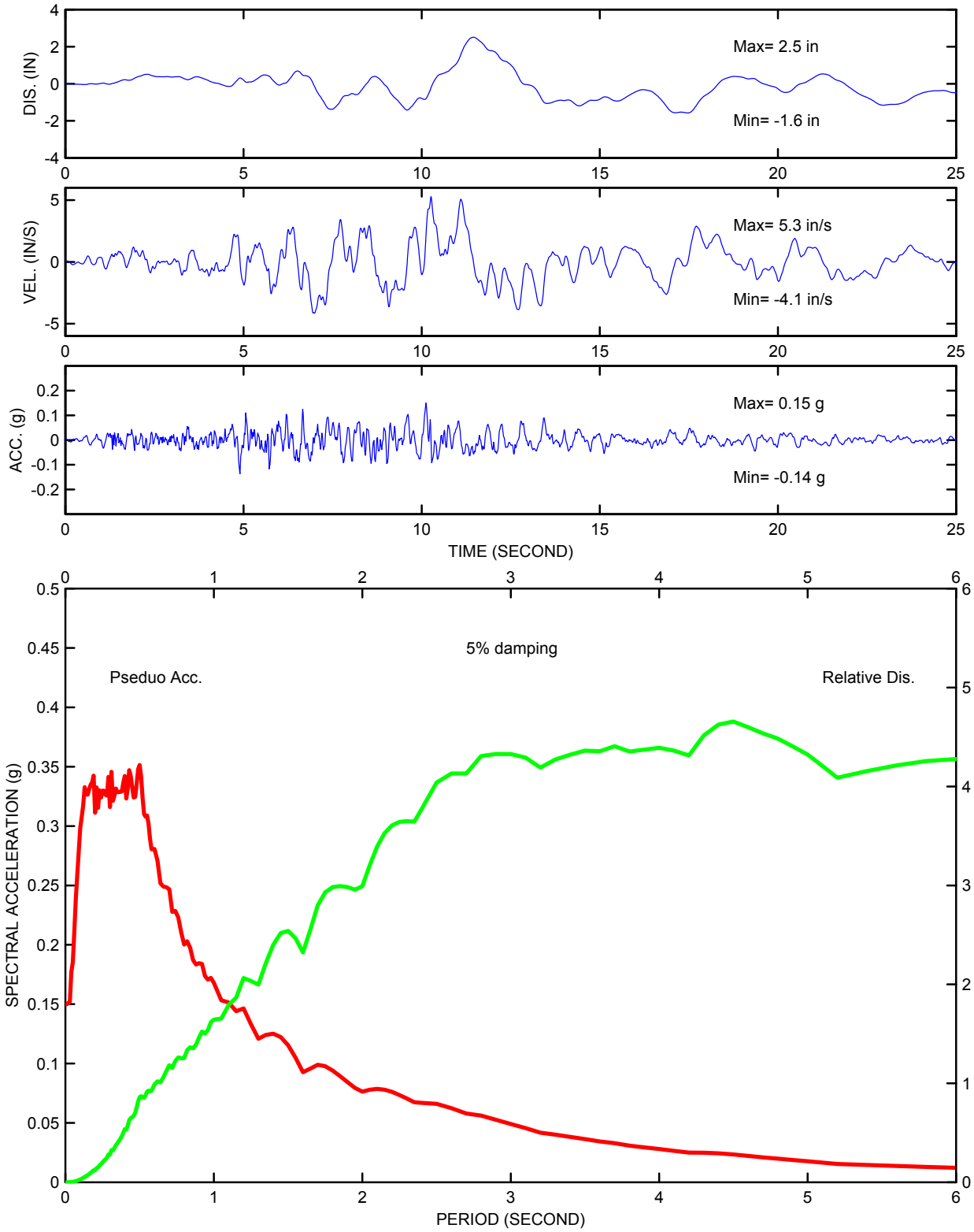


Figure II-2. Reference Horizontal Ground Motion at Surface

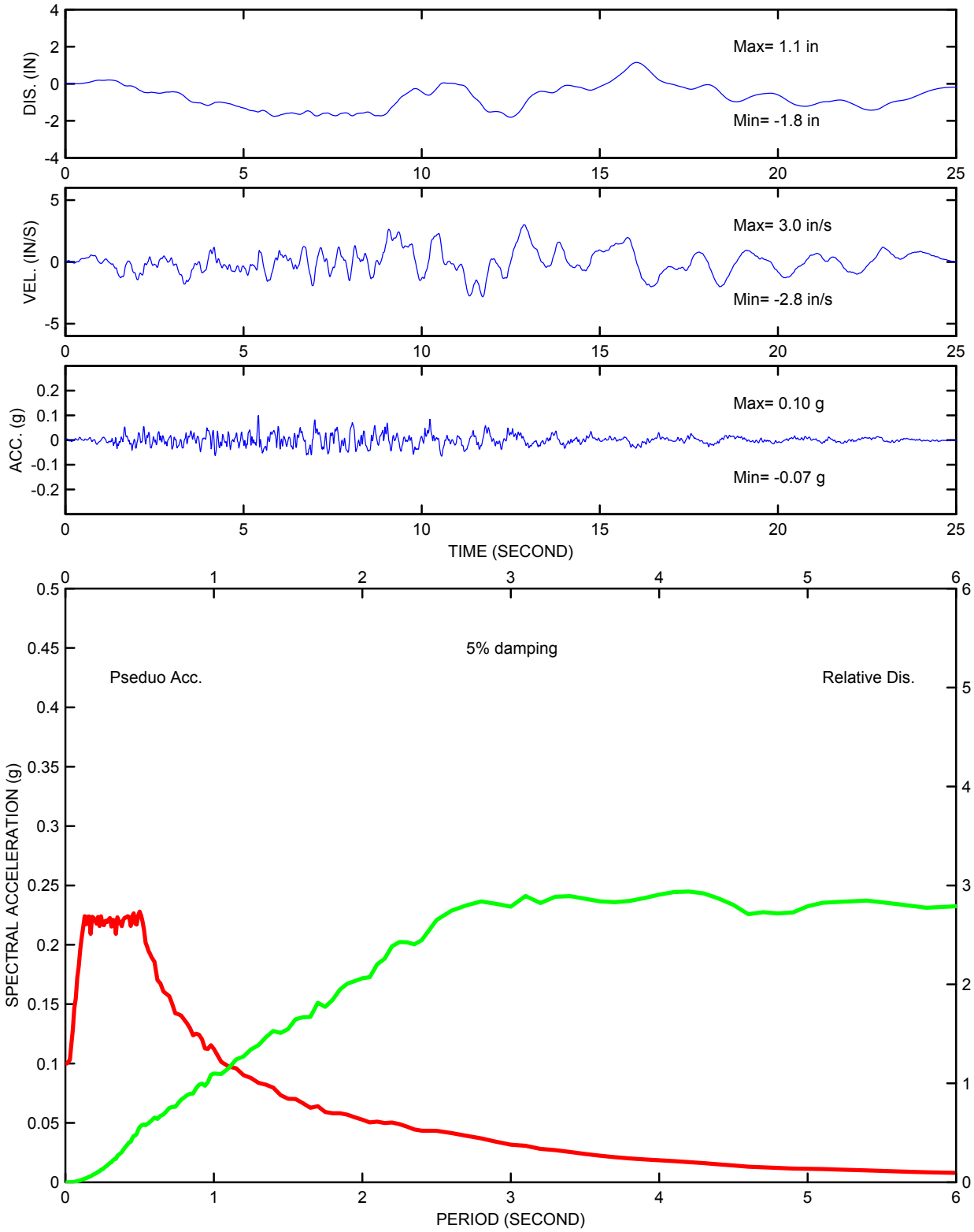


Figure II-3. Reference Vertical Ground Motion at Surface

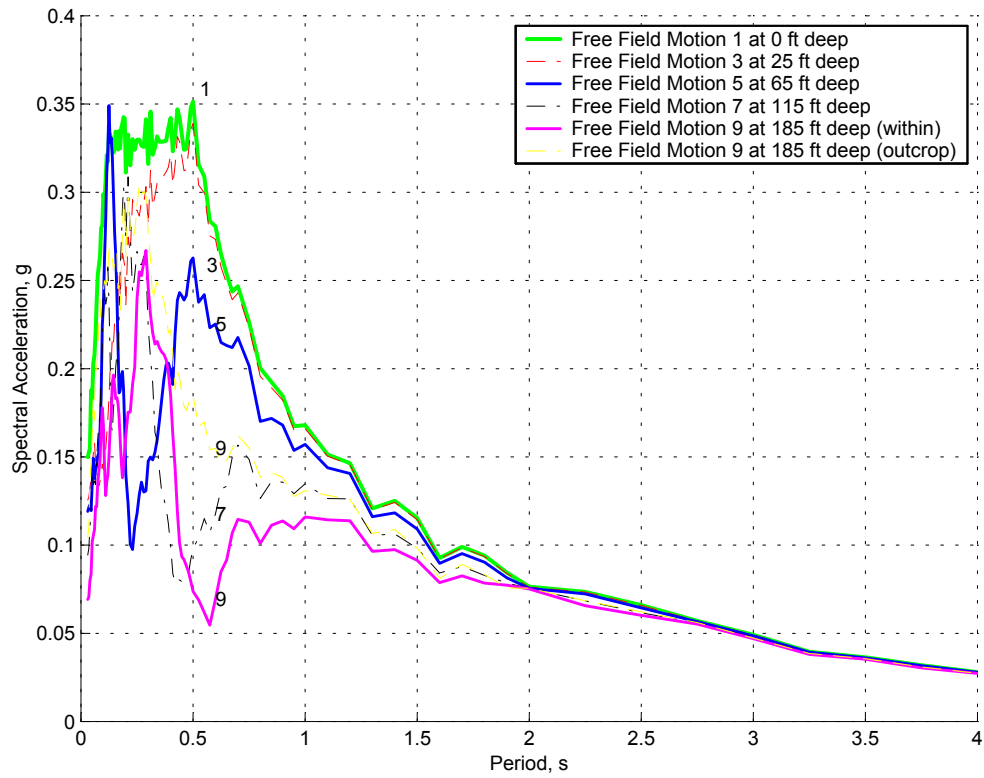


Figure II-4. Depth Varying Free Field Horizontal Motions

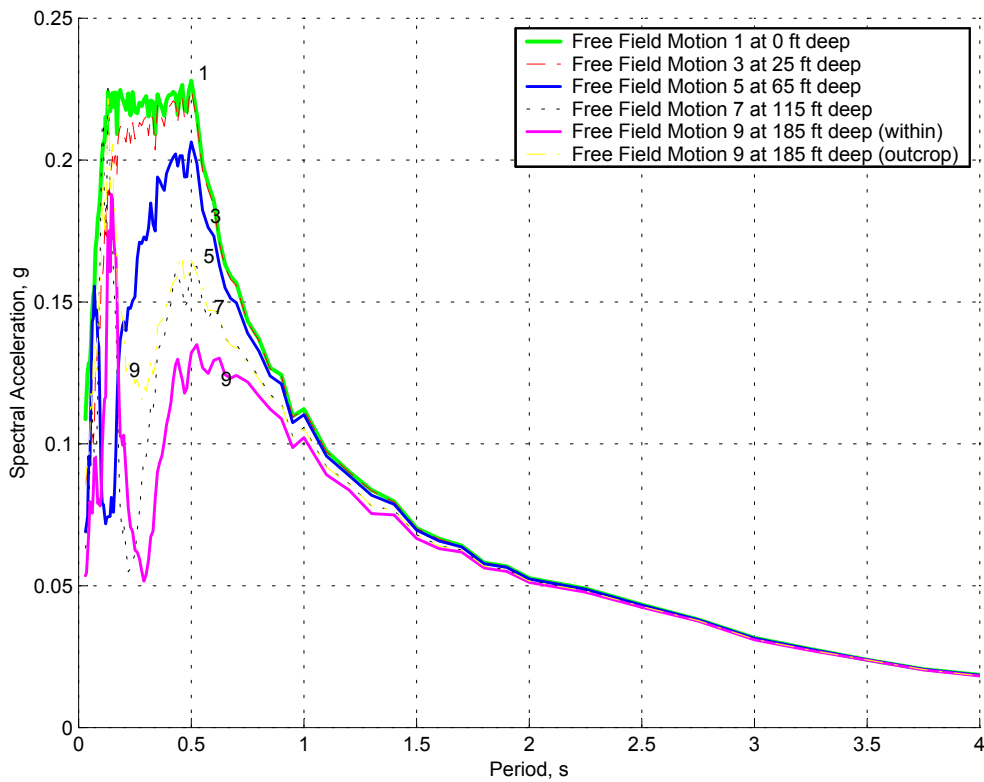


Figure II-5. Depth Varying Free Field Vertical Motions

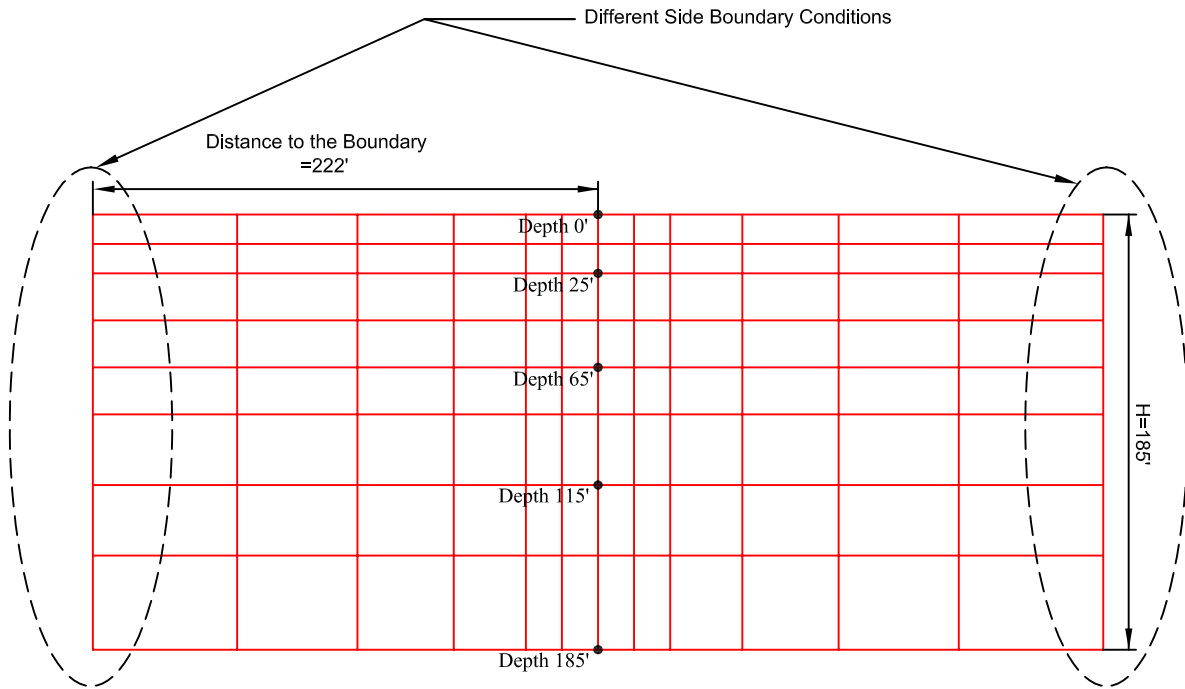
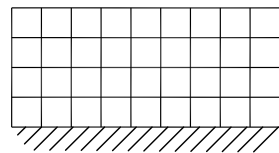
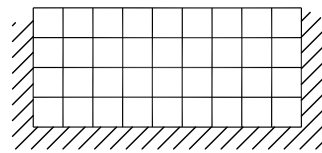


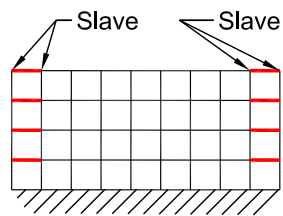
Figure II-6. Finite Element Model



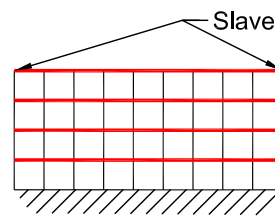
(a) Free Side Boundary



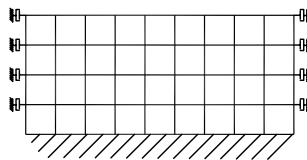
(b) Fixed Side Boundary



(c) Two Edge Columns



(d) Slave Left & Right Boundaries



(e) Transmitting Side Boundary

Figure II-7. Different Side Boundary Conditions

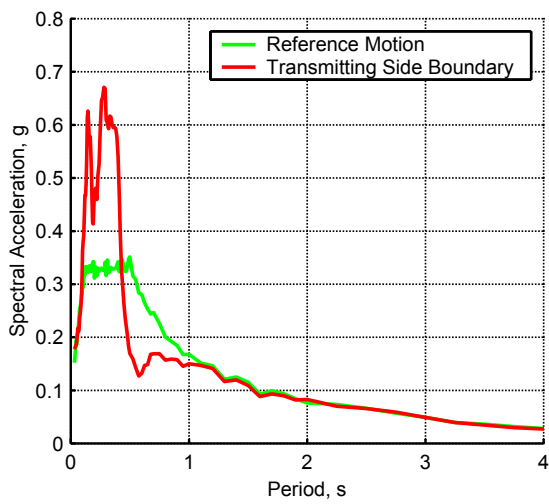
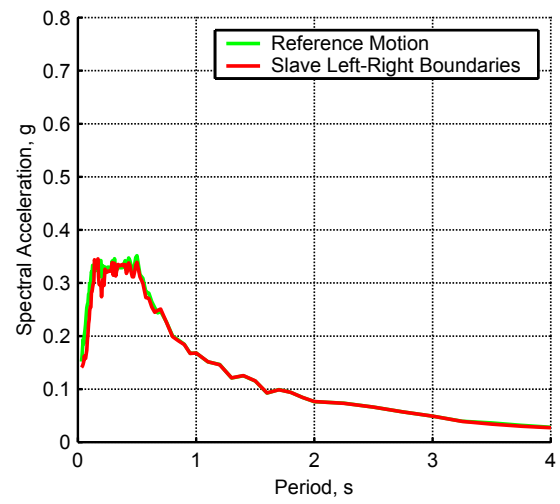
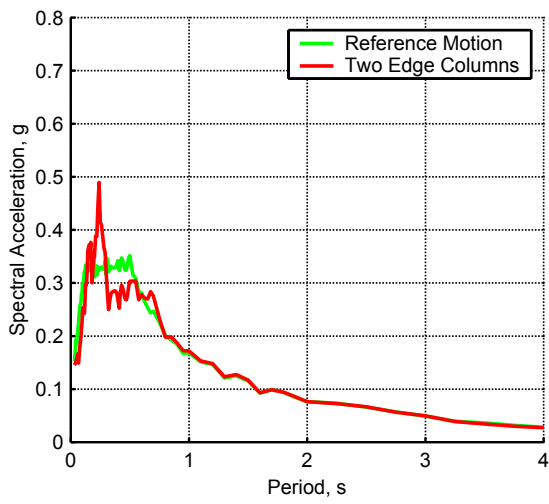
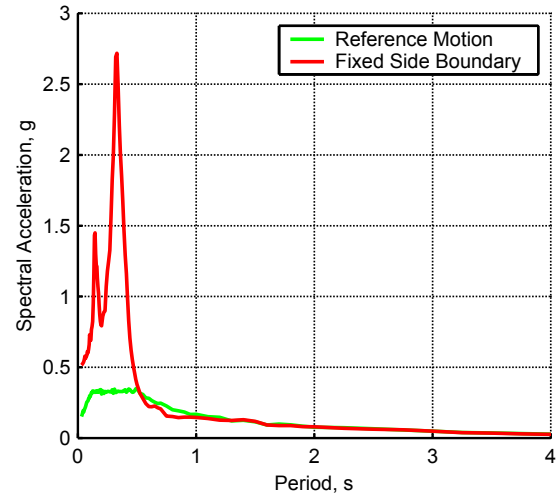
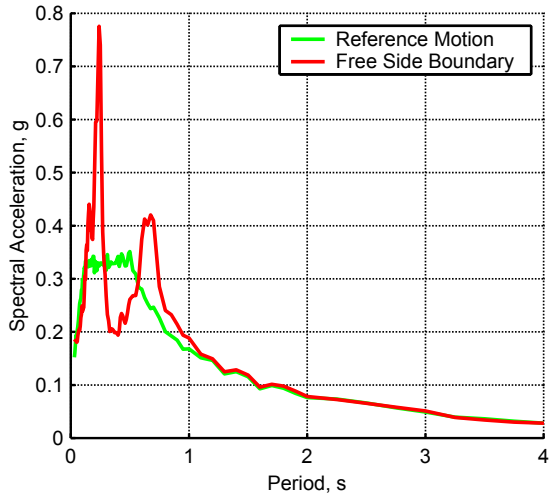


Figure II-8. Effects of Side Boundary Conditions

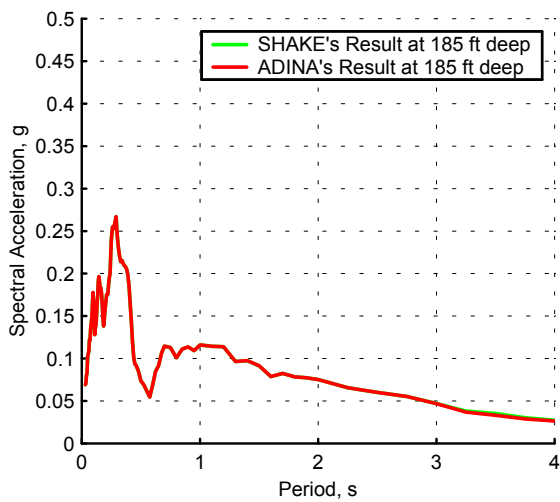
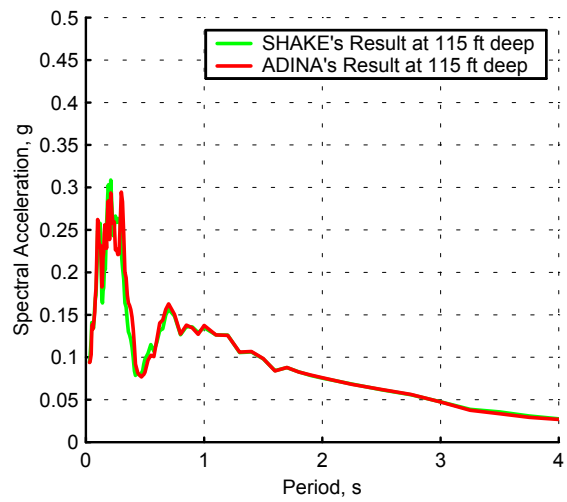
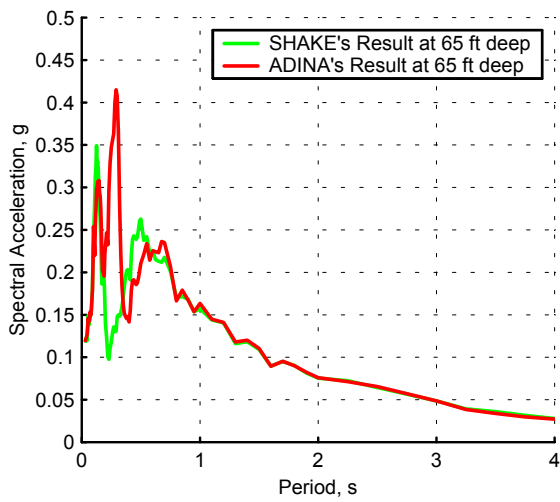
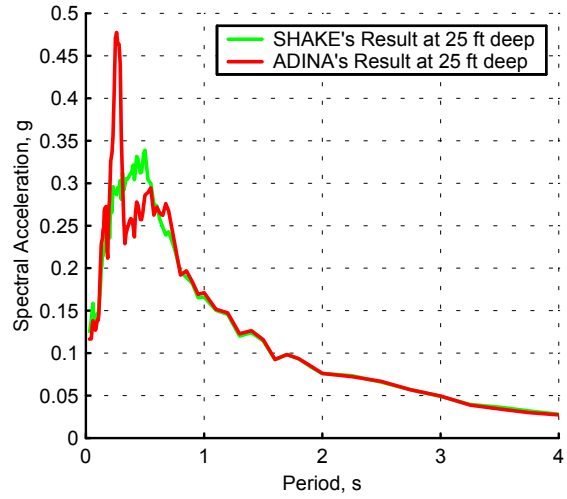
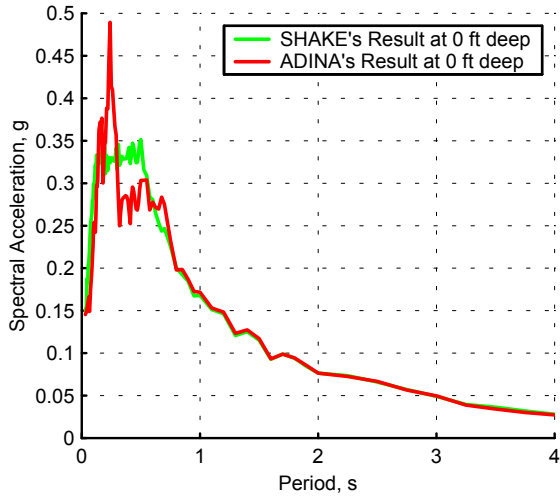


Figure II-9. Comparison of SHAKE Results and ADINA Results Of the Model with Two Edge Columns

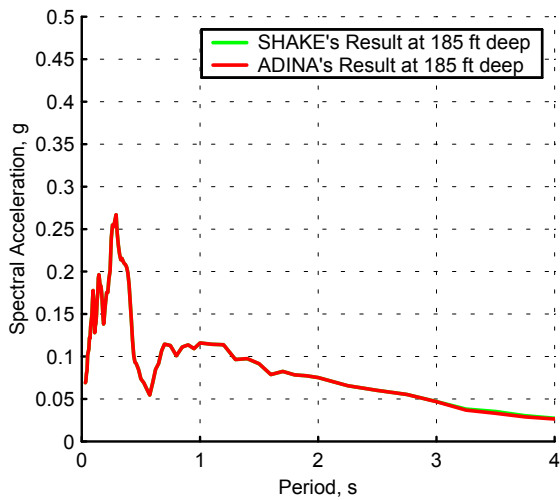
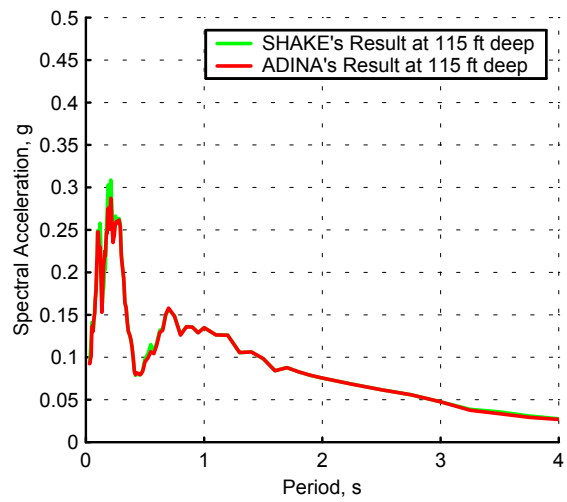
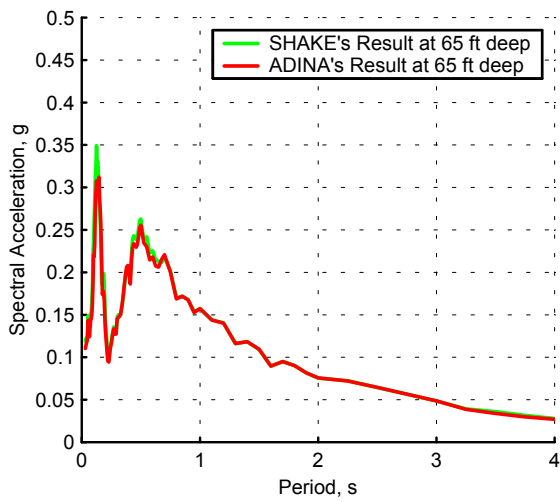
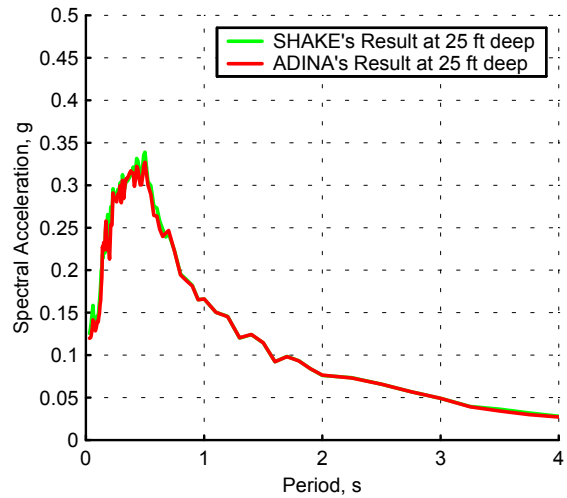
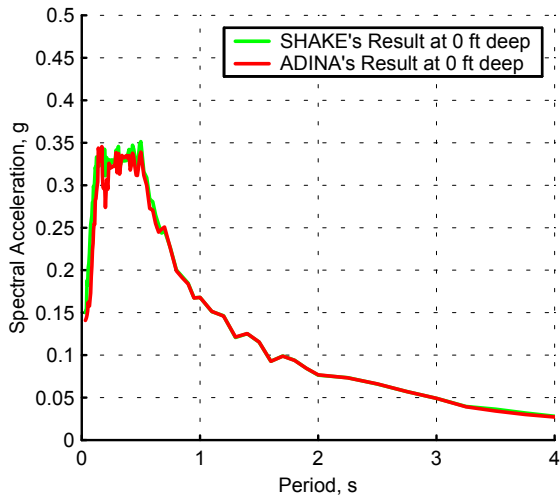


Figure II-10. Comparison of SHAKE Results and ADINA Results of the Model with Slaving Left and Right Boundaries

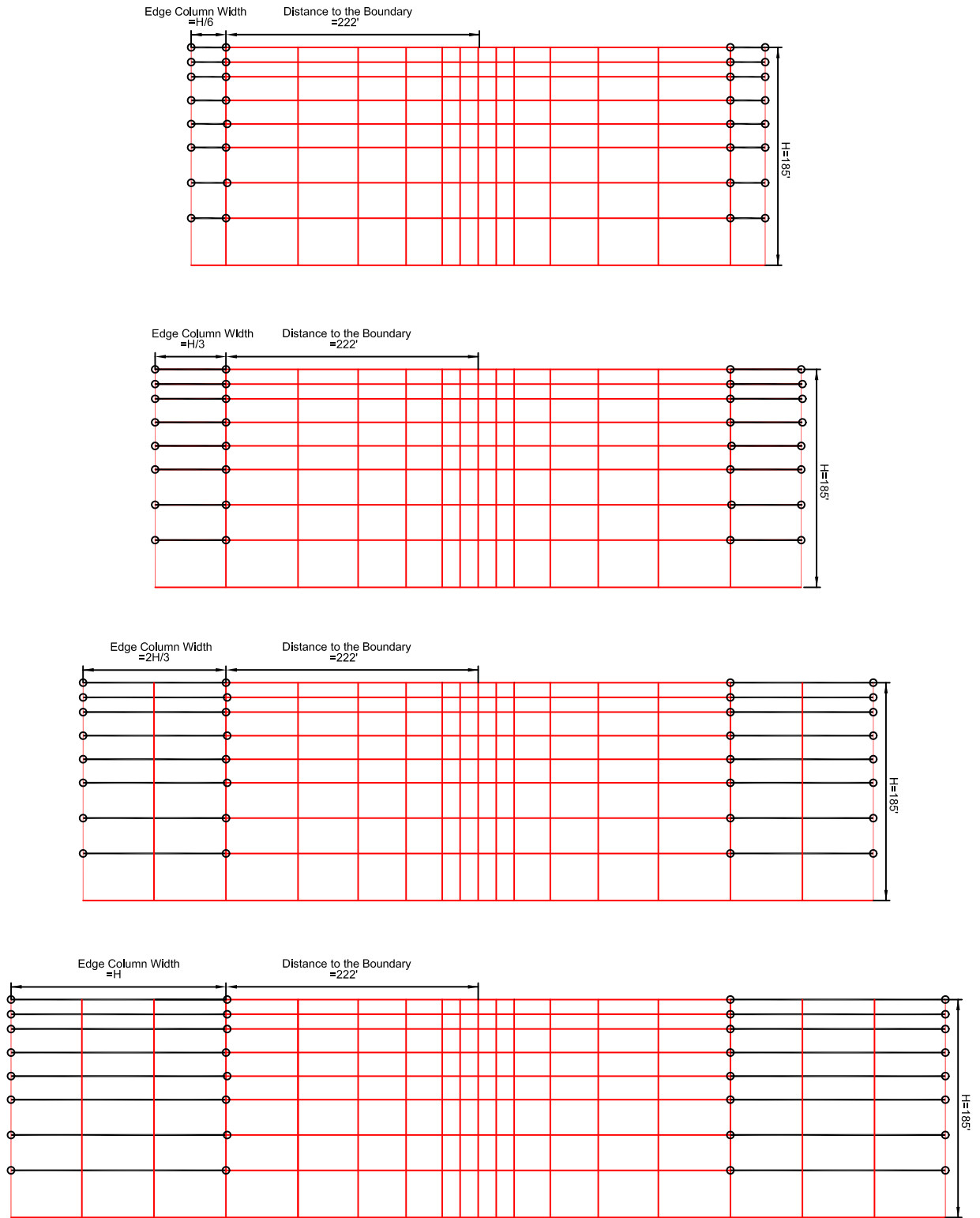


Figure II-11. FEM Model with Different Edge Column Widths

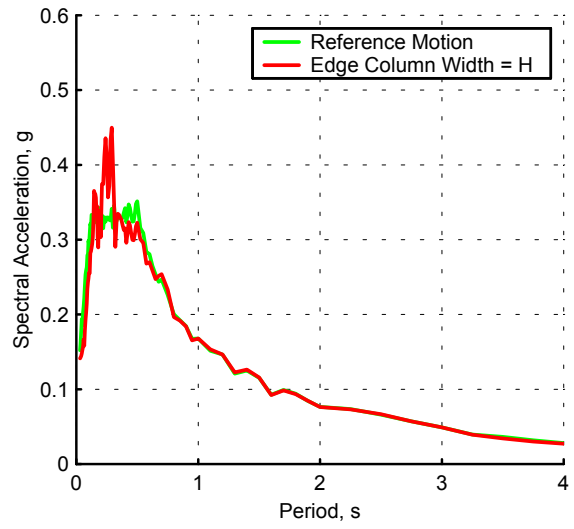
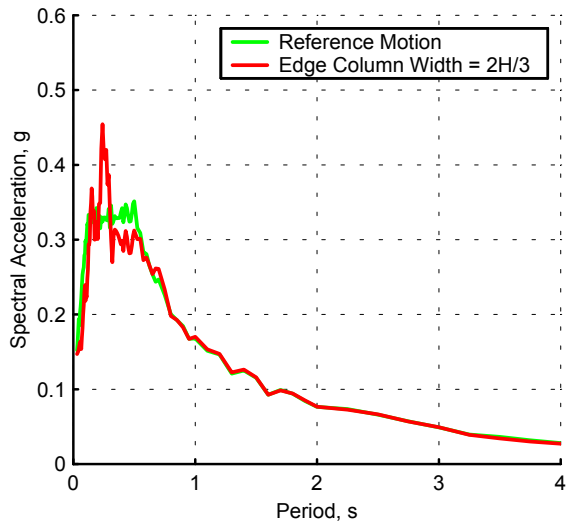
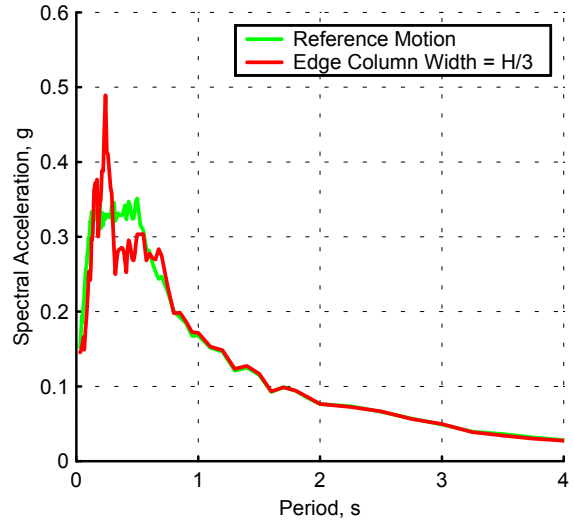
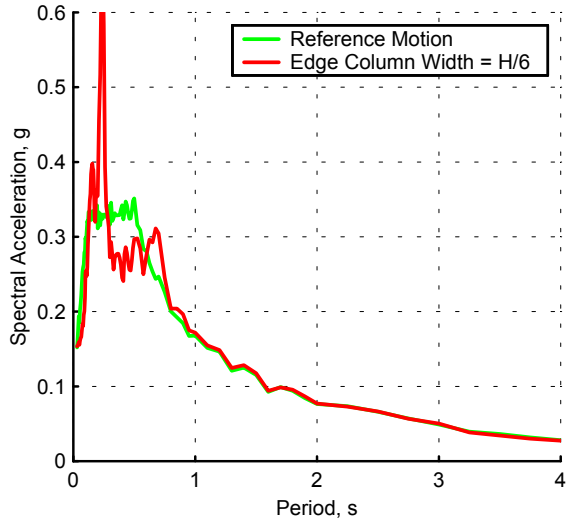


Figure II-12. Effects of Edge Column Widths

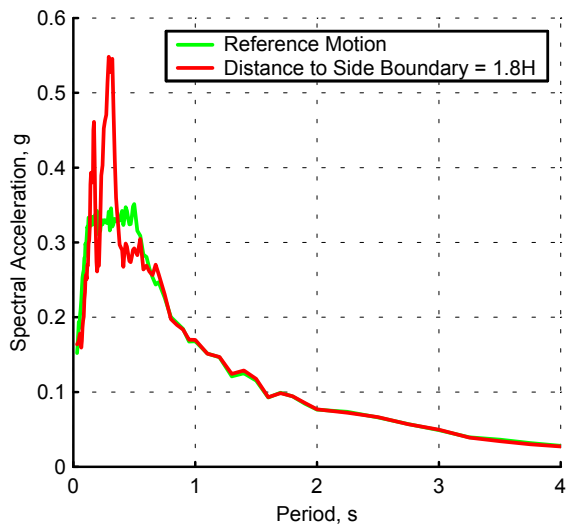
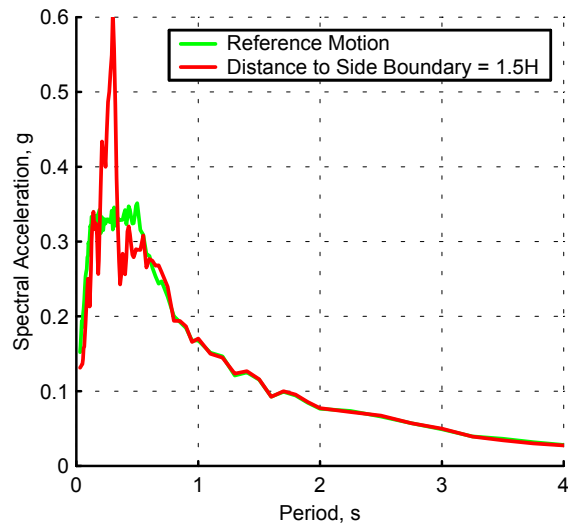
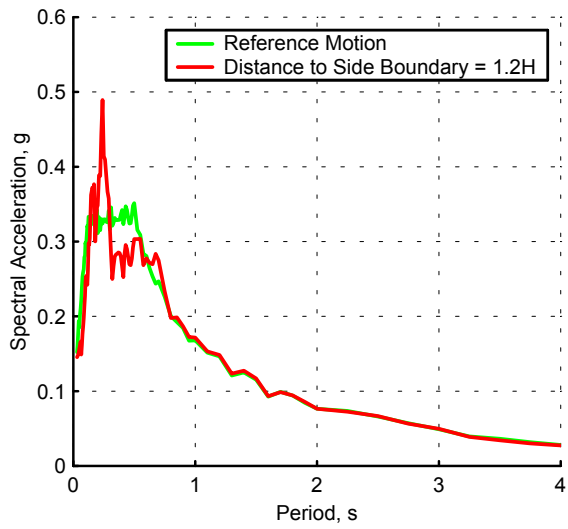


Figure II-13. Effect of Different Distance to Boundary

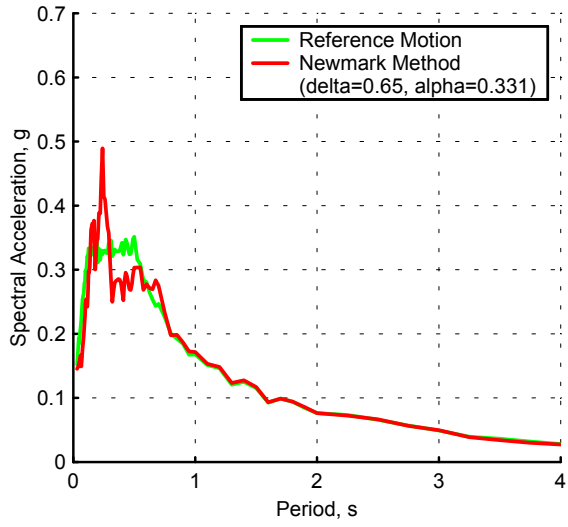
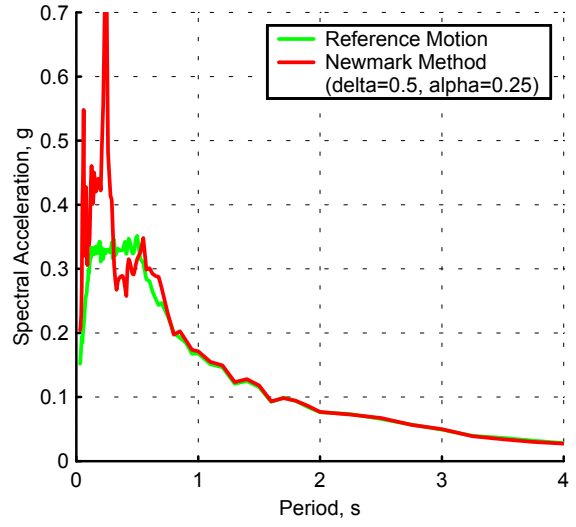
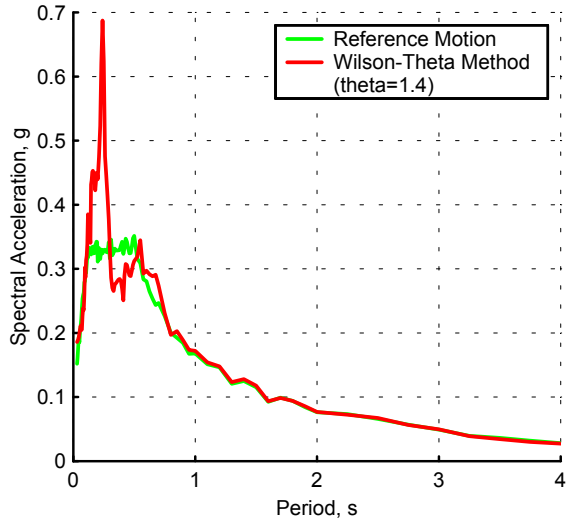


Figure II-14. Effect of Different Integration Scheme

Table II-1. Rayleigh Damping Parameters

Damping Ratio ( $\zeta$ )	Mass-Proportional Damping Only	Stiffness-Proportional Damping Only	Rayleigh Damping	
	$\alpha$	$\beta$	$\alpha$	$\beta$
0.017	0.403	0.00287	0.202	0.00143
0.022	0.522	0.00371	0.261	0.00186
0.028	0.664	0.00472	0.332	0.00236
0.032	0.759	0.00540	0.379	0.00270
0.029	0.688	0.00489	0.344	0.00245
0.035	0.830	0.00590	0.415	0.00295
0.018	0.427	0.00304	0.213	0.00152
0.016	0.379	0.00270	0.190	0.00135

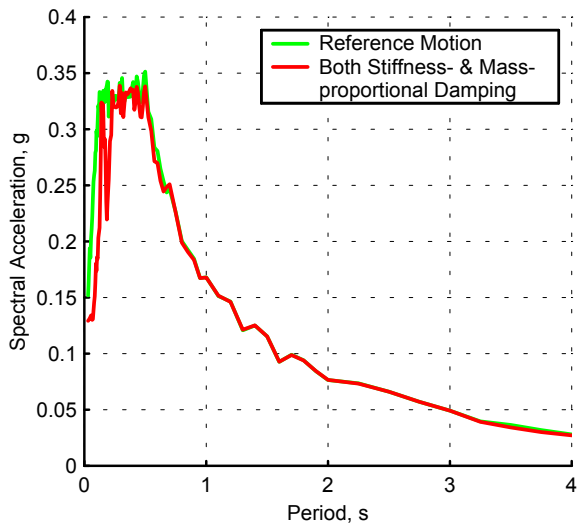
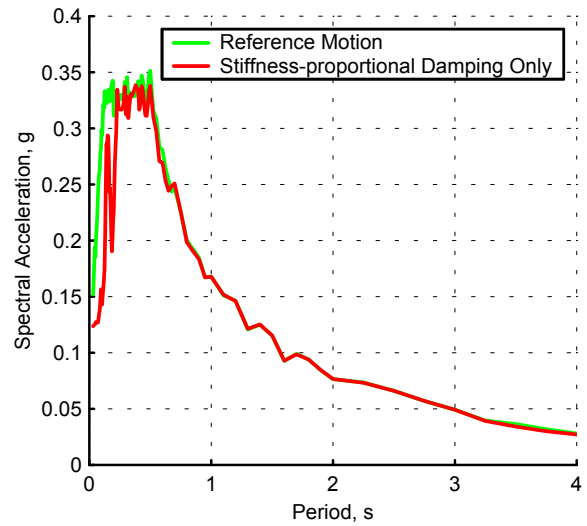
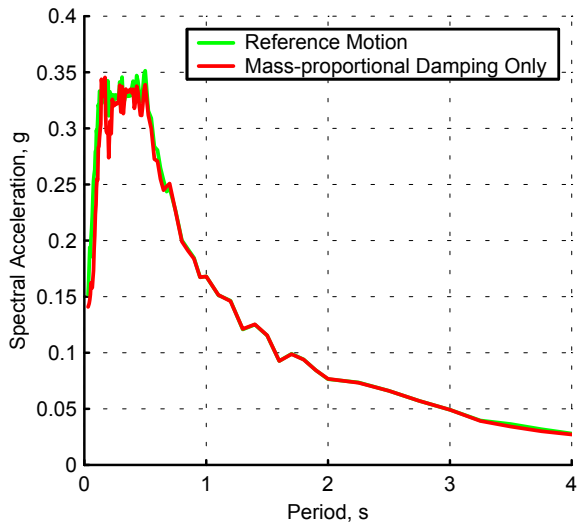


Figure II-15. Effect of Different Damping Assignments

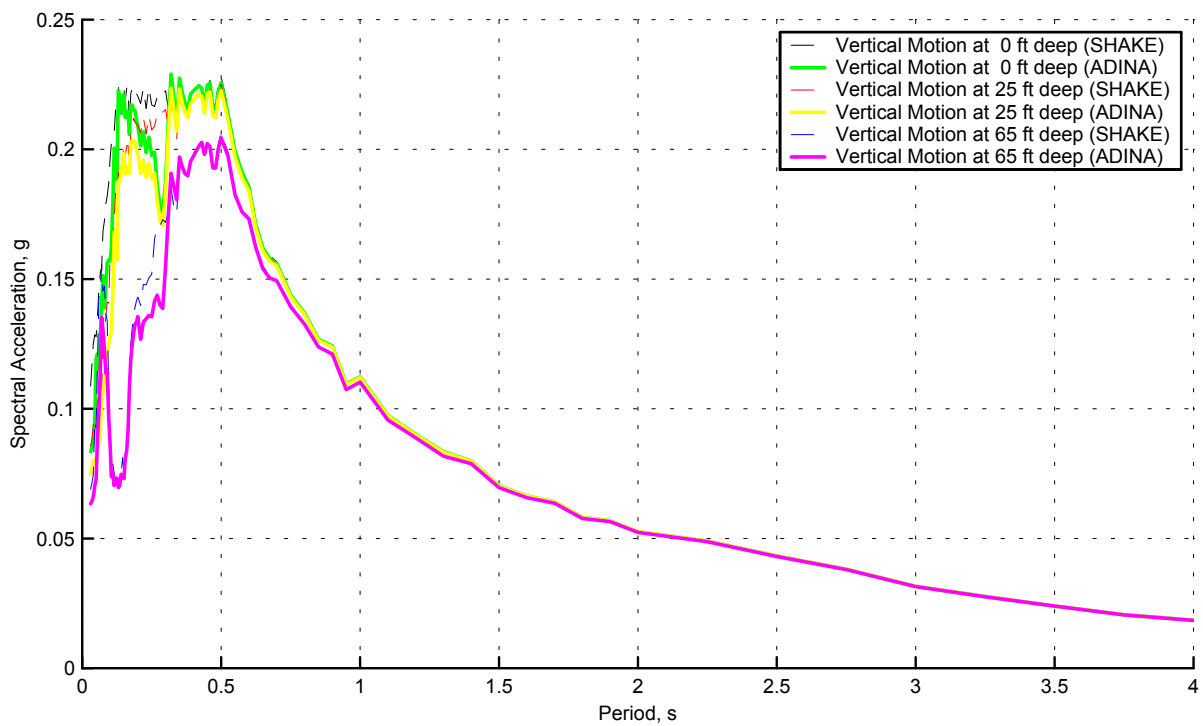
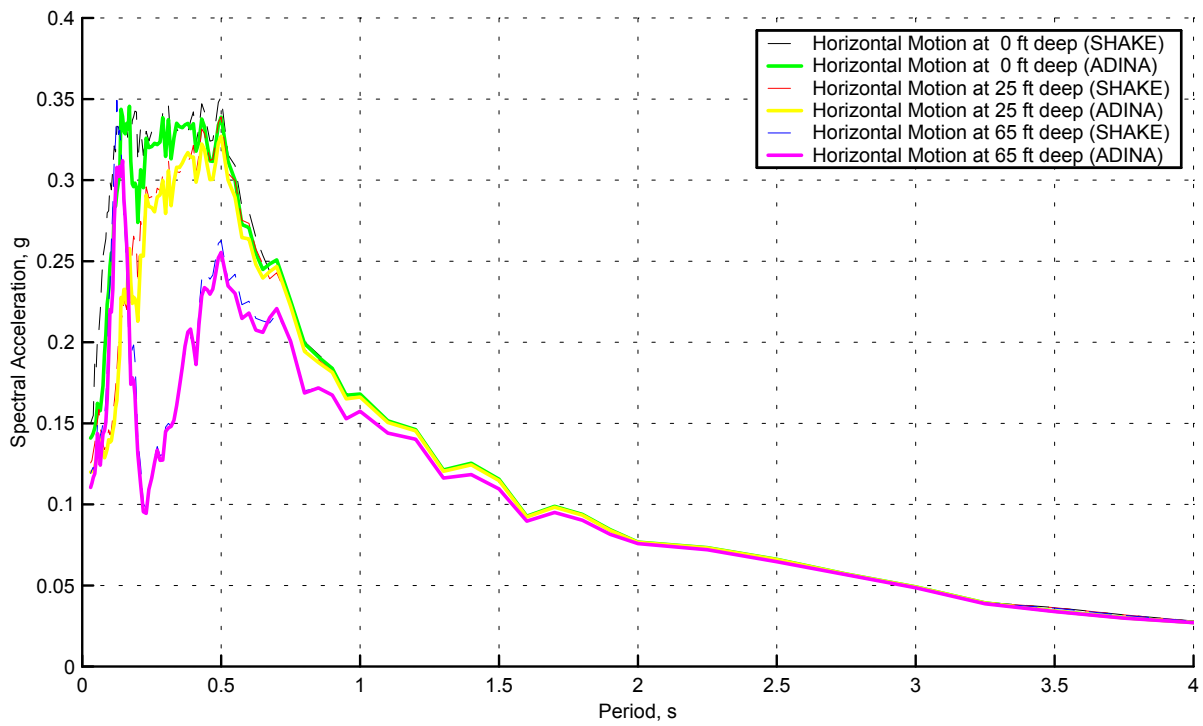


Figure II-16. Two Component Motions for ADINA Model with Slaving Left and Right Boundaries

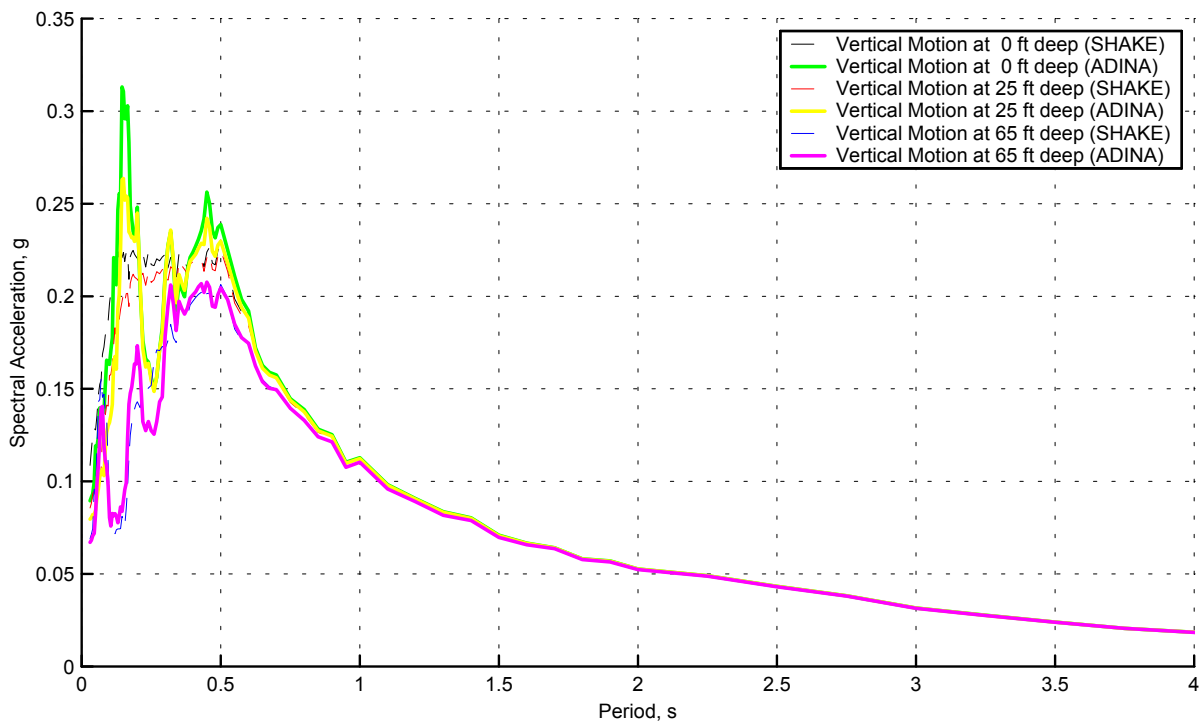
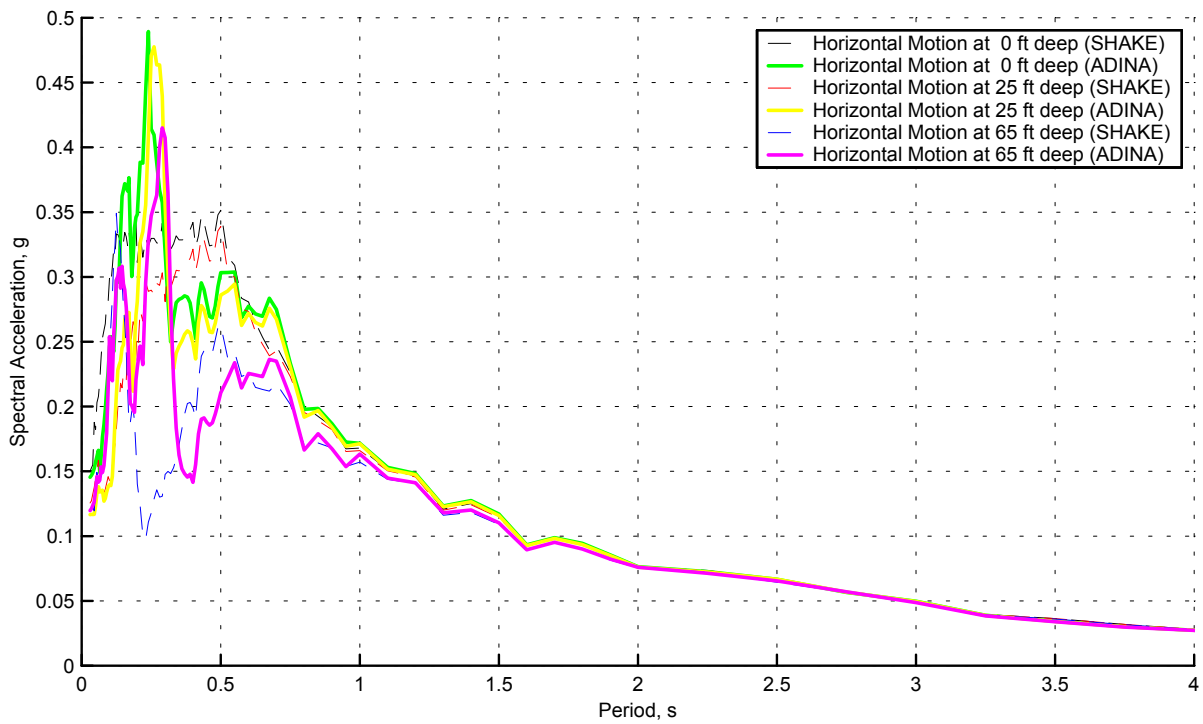


Figure II-17. Two Component Motions for ADINA Model with Two Edge Columns

Deformations are amplified 1000 times (Vertical Motion Only)

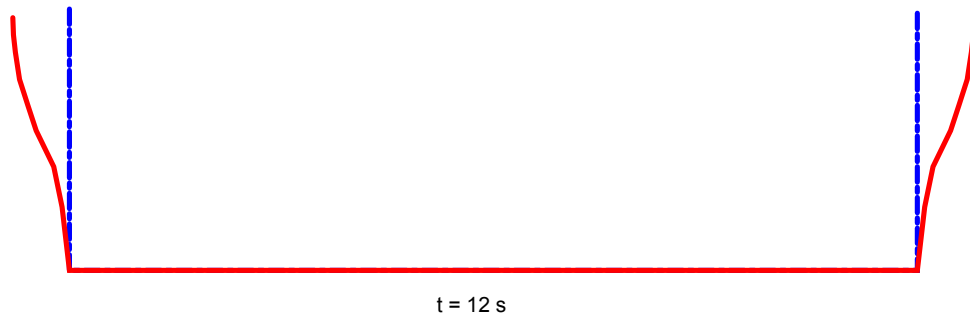
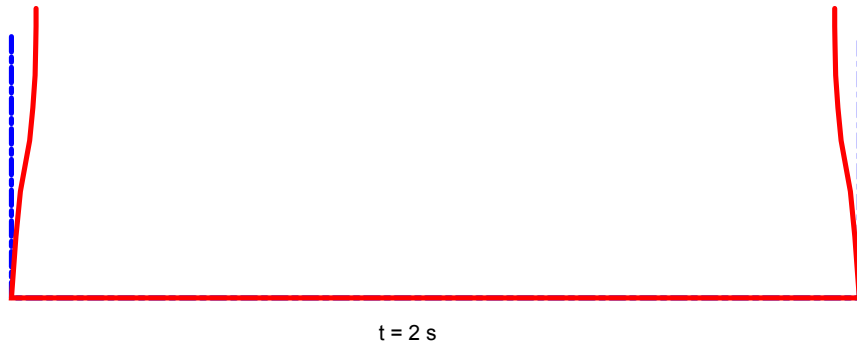


Figure II-18. Snapshots of Profile of Side Boundary

## **Appendix III: Plots of Generated Time Histories of Ground Motions Conforming to the Three Spectral Shapes**



## **Appendix III: Plots of Generated Time Histories of Ground Motions Conforming to the Three Spectral Shapes**

This appendix presents plots of the generated time histories of earthquake records for ground motions to be input in the coupled response models of dry cask systems. A total of 180 plots are included as an attachment to this appendix to document the three sets of motions generated with target shaking matched to the three spectral shape procedures, including the NUREG/CR-0098, the Regulatory Guide 1.60 and the NUREG/CR-6728 (central and eastern United States) spectra procedures. Each of the spectrum motion sets has been documented by sixty figures. Figures 1 through 60 provide plots for the NUREG/CR-0098 spectral shape motions. Figures 61 through 120 provide plots for the Regulatory Guide 1.60 spectral shape motions. Figures 121 through 180 provide plots for the NUREG/CR-6728 (central and eastern United States) spectral shape motions. In each figure, time histories of acceleration, velocity and displacement are shown on the upper part of the plot. The lower part of the plot presents its corresponding 5-percent damped pseudo acceleration response spectrum along with cross comparison to its target ground surface reference response spectrum.

For each of the three spectral shapes, fifteen figures are included for each component motion developed for each spectral shape for the original ground surface reference motions which would be spectrum-compatible to each of the three target spectrum. In each of these fifteen figures documenting the benchmark ground surface time histories, acceleration spectra at 5, 10 and 15% damping are also plotted and can be compared to the respective 5% damped smooth spectral shape. The additional forty-five figures were included for each component of deconvoluted motion for the three profiles: (i) stiff soil, (ii) soft soil and (iii) upper bound rock conditions. In each figure presenting the deconvoluted 'within' motions, the 'within' motion has been overlaid on top of the corresponding ground-surface reference spectrum-compatible motions for cross comparison to the 'within' motions.

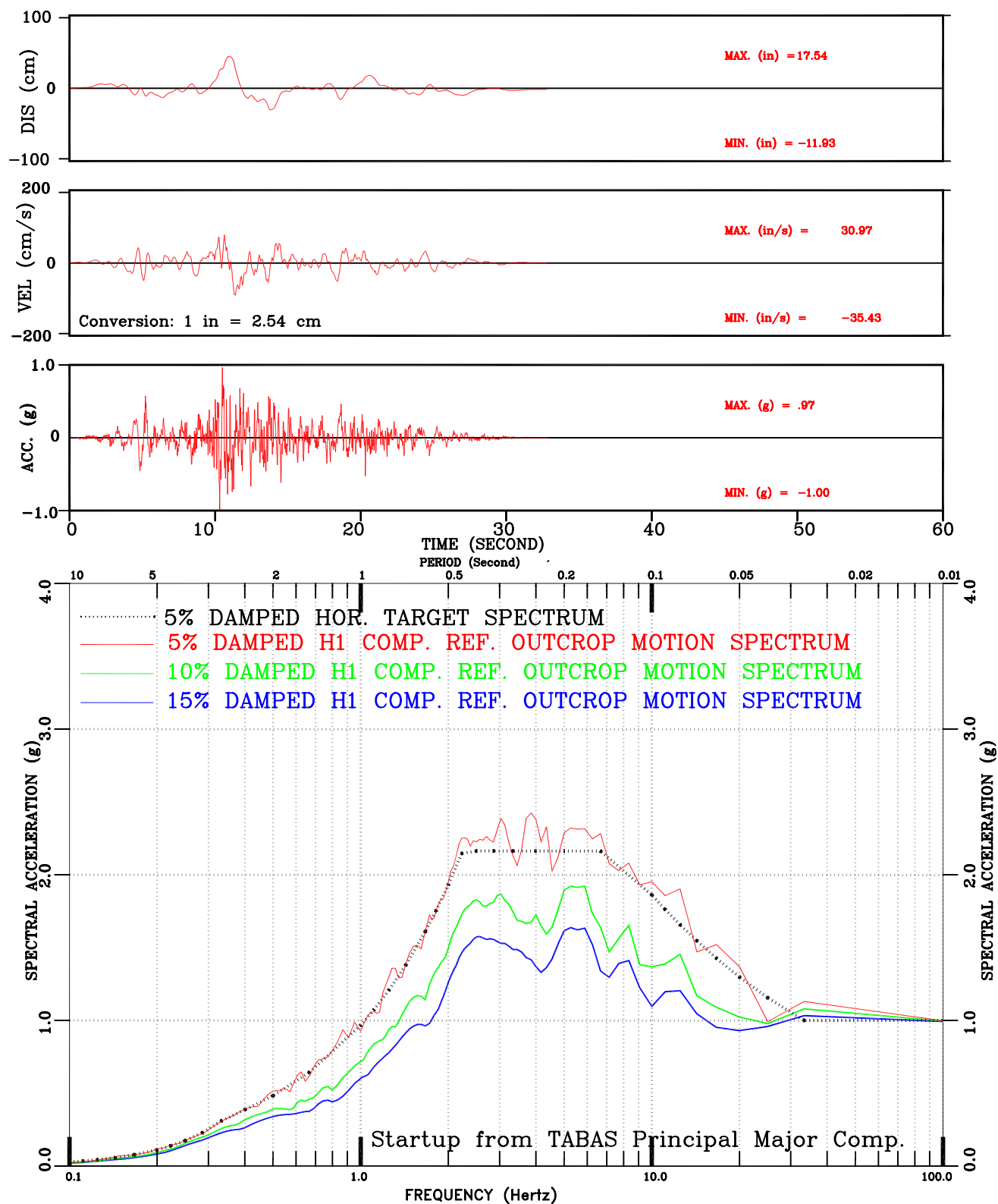


Figure III-1: Set-1 H1 Comp. Motion Conforming to NUREG/CR-0098 Spectral Shape

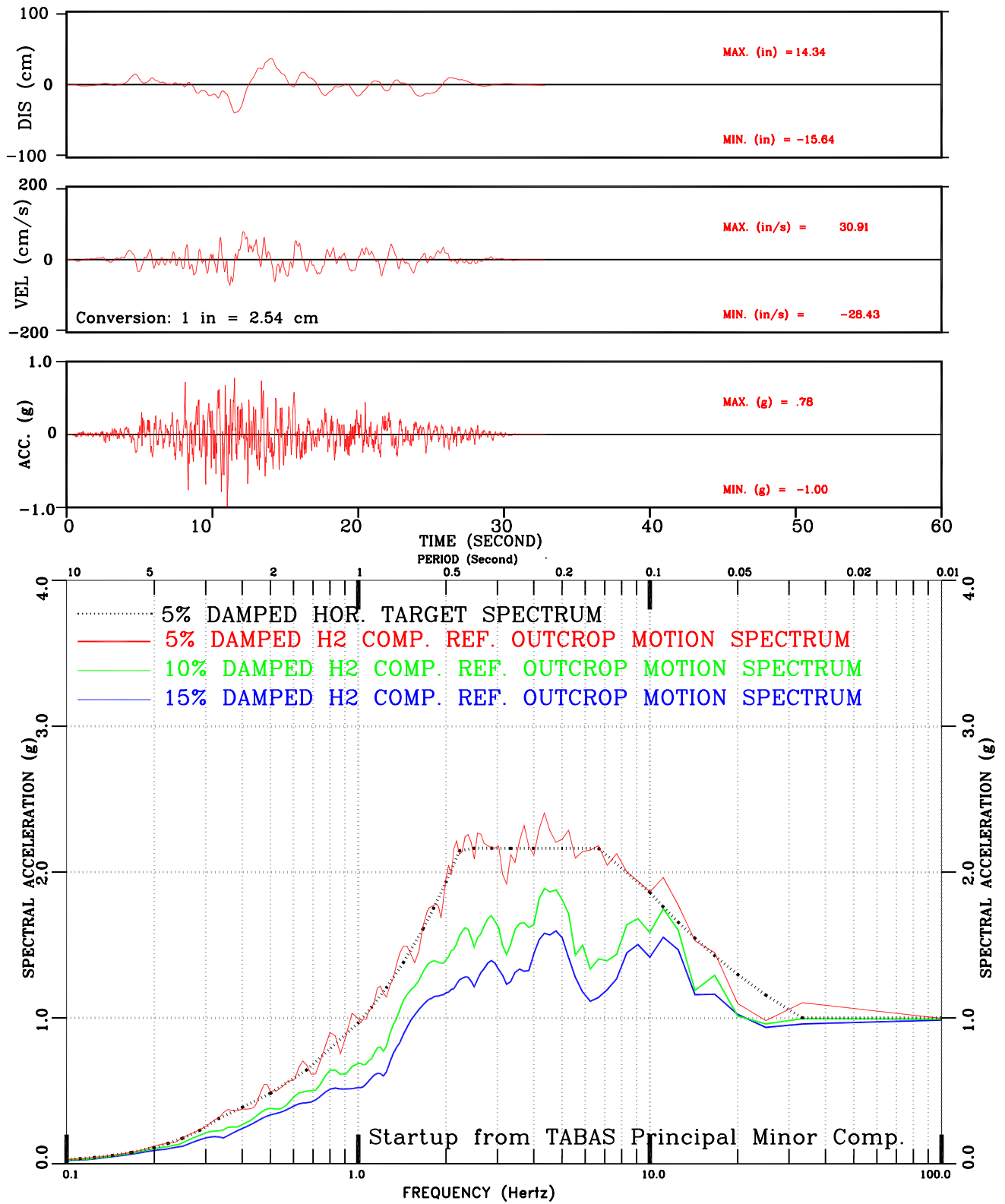


Figure III-2: Set-1 H2 Comp. Motion Conforming to NUREG/CR-0098 Spectral Shape

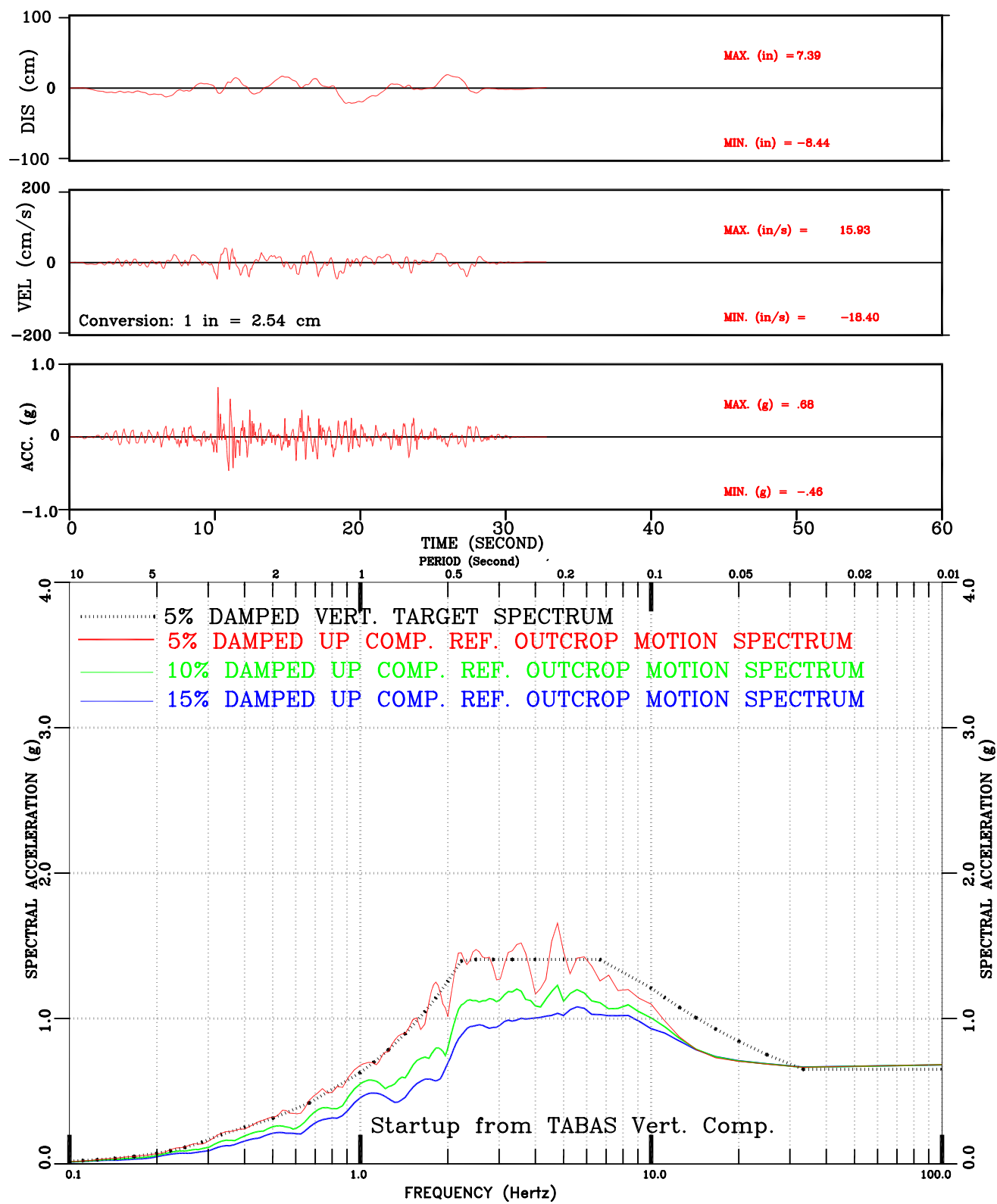


Figure III-3: Set-1 Vert. Comp. Motion Conforming to NUREG/CR-0098 Spectral Shape

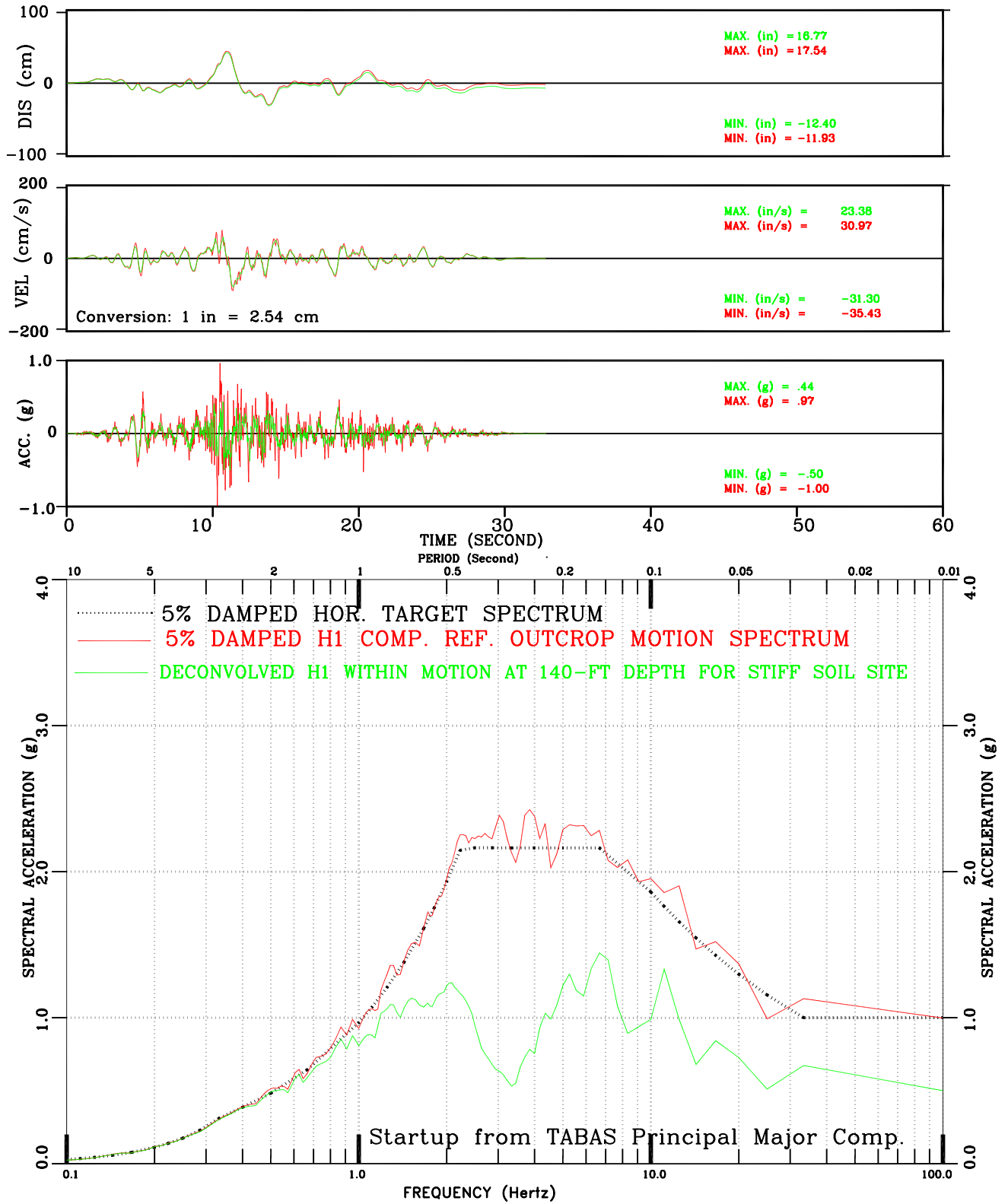


Figure III-4: Deconvolved Within vs. Surface Motion for Stiff Soil Set-1 H1 Comp. Motion Conforming to NUREG/CR-0098 Spectral Shape

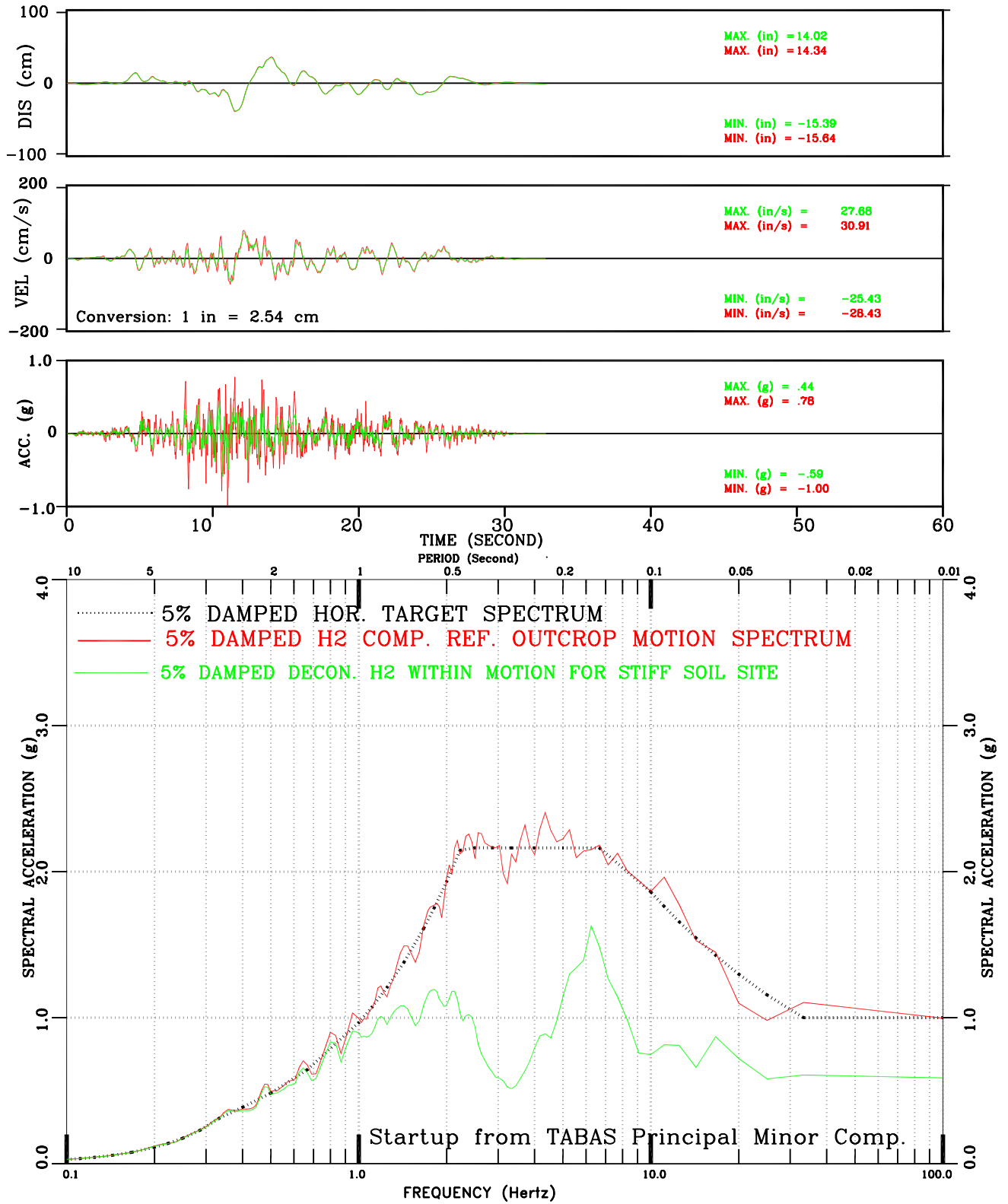


Figure III-5: Deconvolved Within vs. Surface Motion for Stiff Soil Set-1 H2 Comp. Motion Conforming to NUREG/CR-0098 Spectral Shape

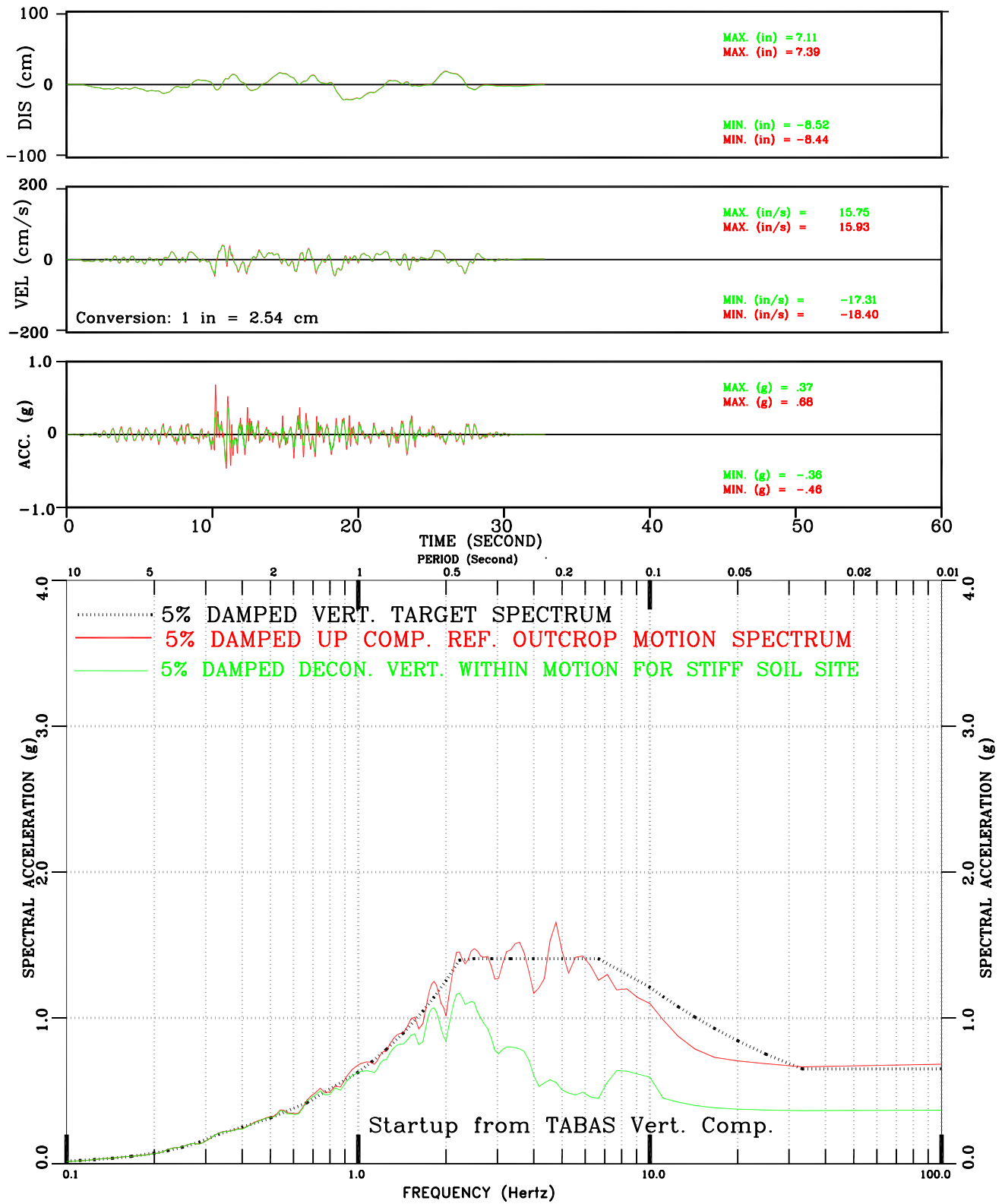


Figure III-6: Deconvolved Within vs. Surface Motion for Stiff Soil Set-1 Vert. Comp. Motion Conforming to NUREG/CR-0098 Spectral Shape

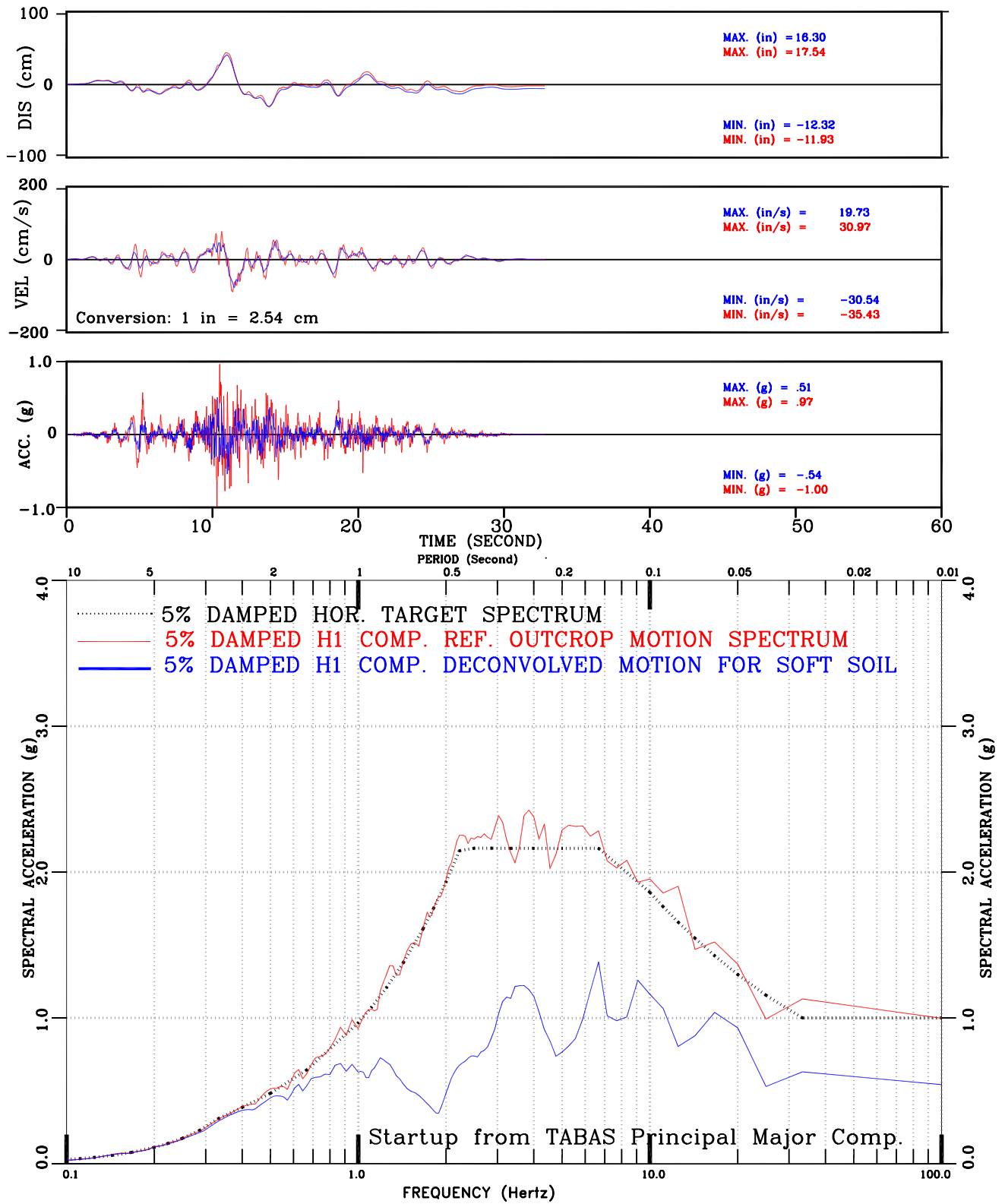


Figure III-7: Deconvolved Within vs. Surface Motion for Soft Soil Set-1 H1 Comp. Motion Conforming to NUREG/CR-0098 Spectral Shape

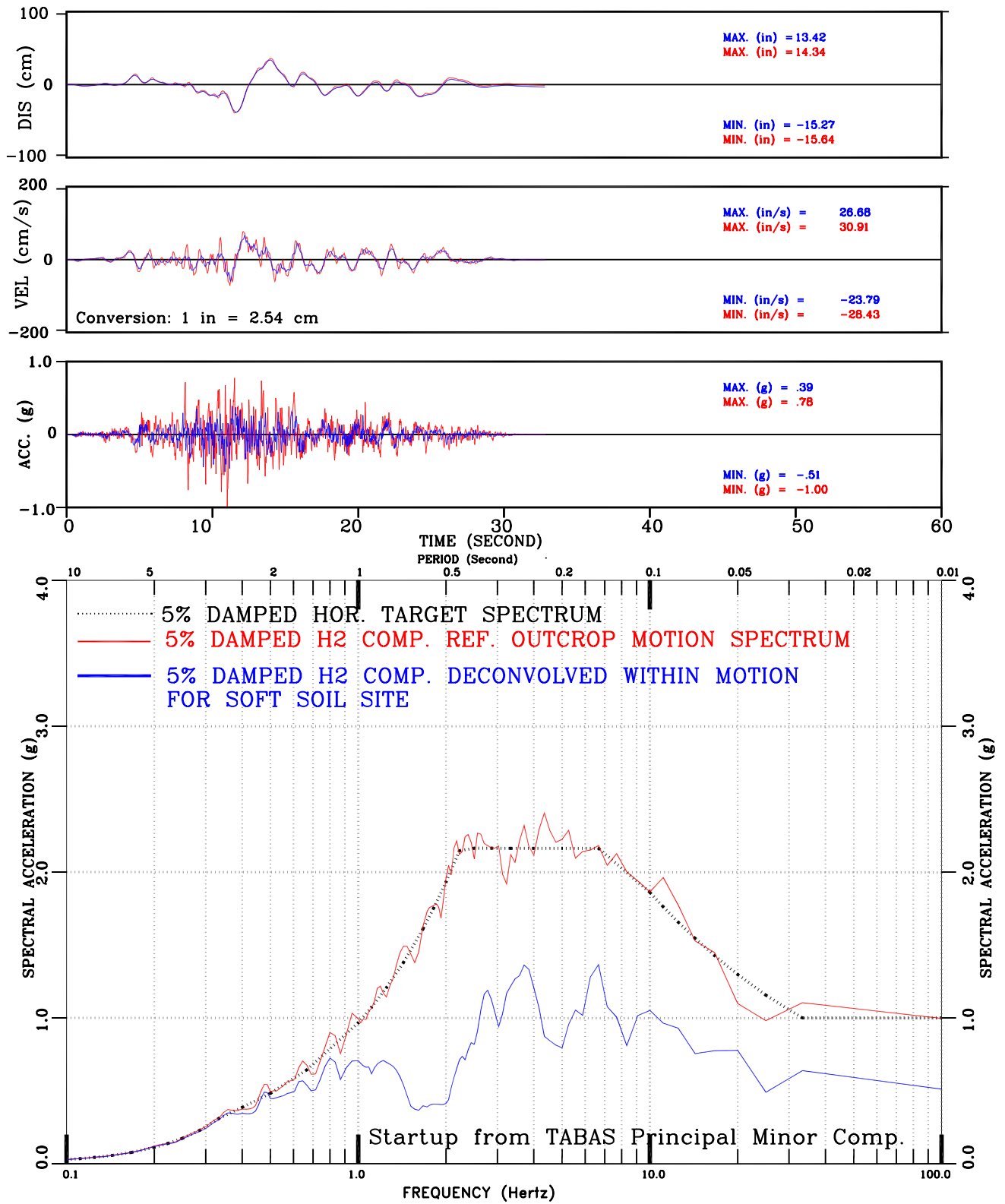


Figure III-8: Deconvolved Within vs. Surface Motion for Soft Soil Set-1 H2 Comp. Motion Conforming to NUREG/CR-0098 Spectral Shape

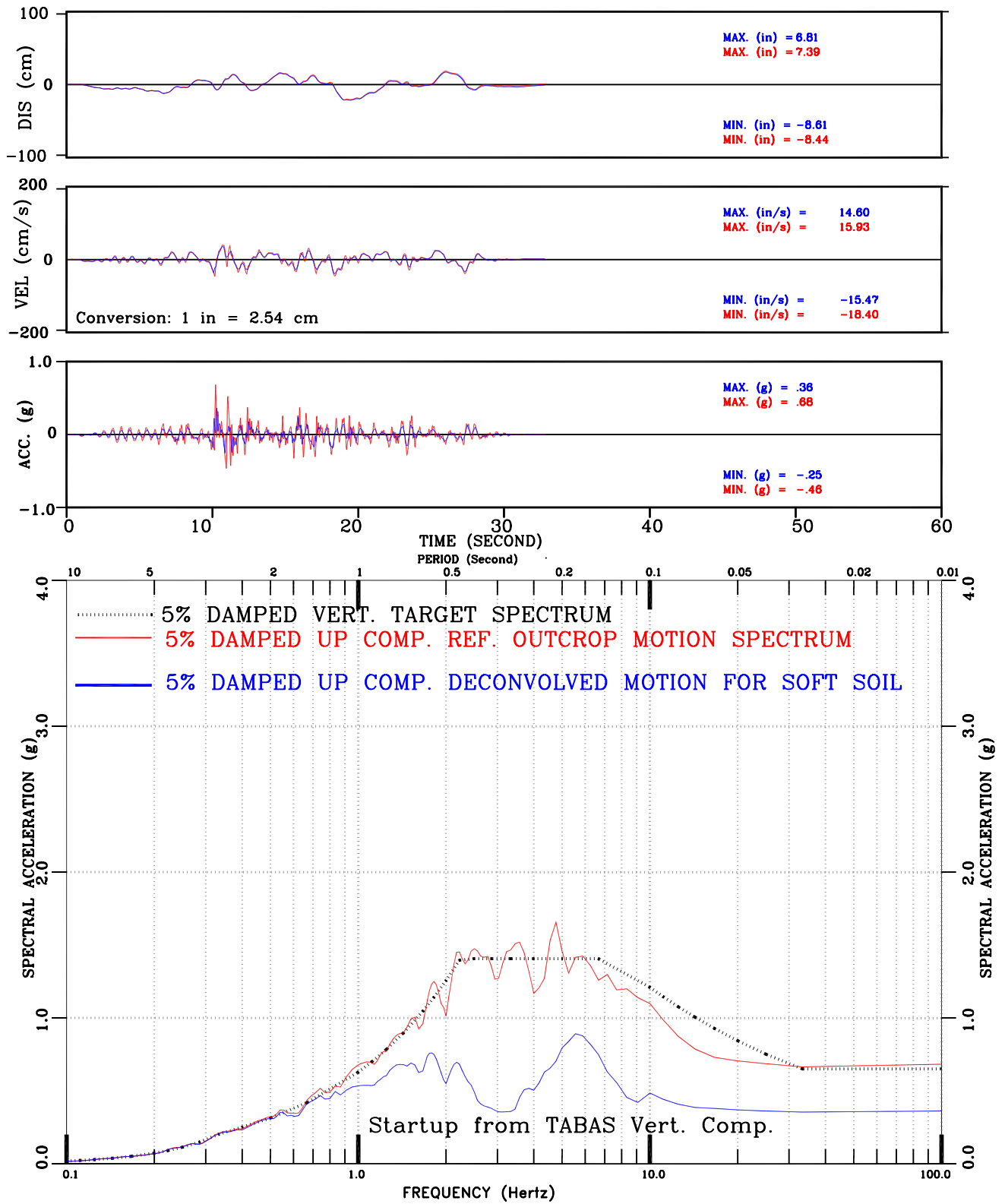


Figure III-9: Deconvolved Within vs. Surface Motion for Soft Soil Set-1 Vert. Comp. Motion Conforming to NUREG/CR-0098 Spectral Shape

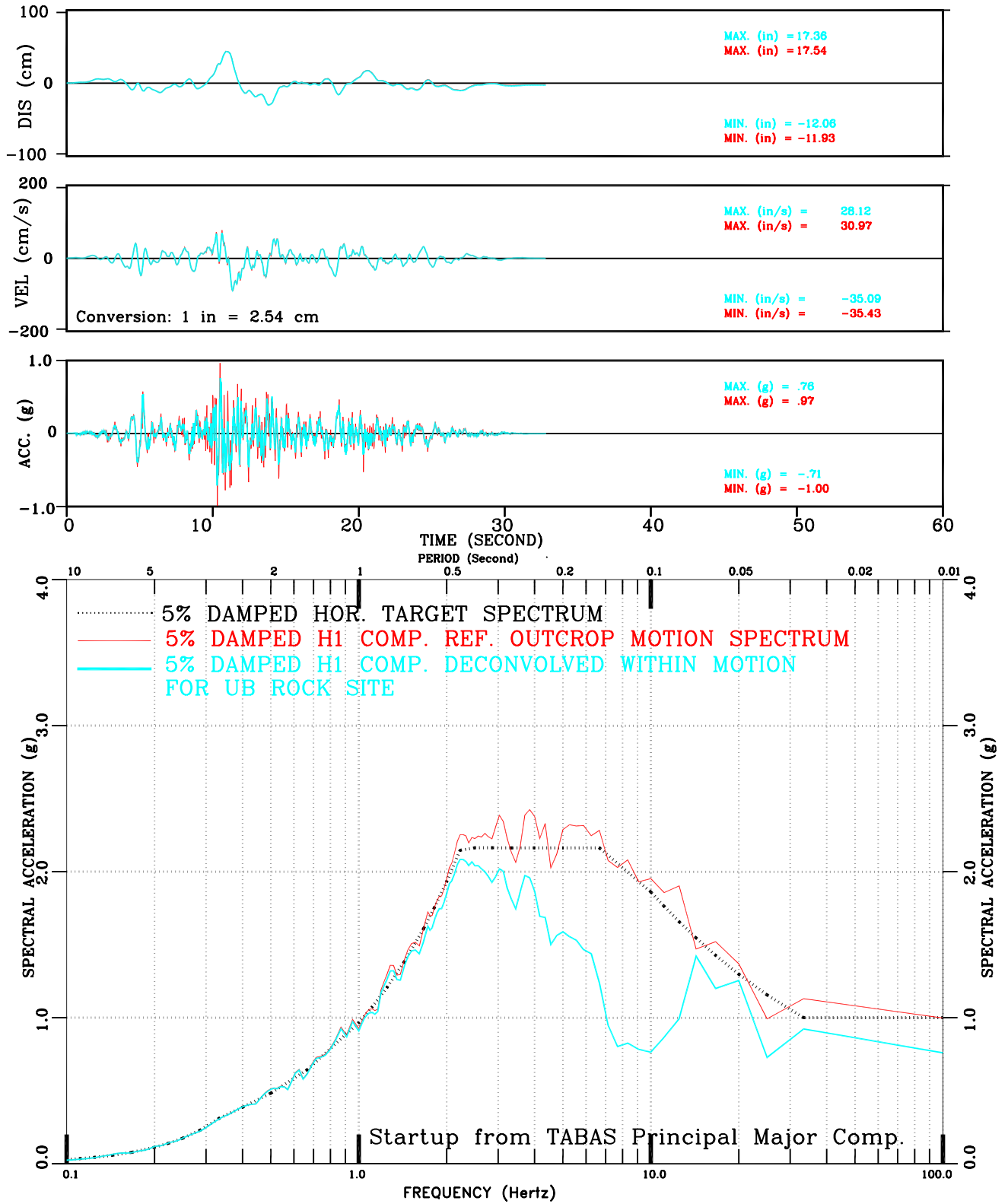


Figure III-10: Deconvolved Within vs. Surface Motion for UB Rock Set-1 H1 Comp. Motion Conforming to NUREG/CR-0098 Spectral Shape

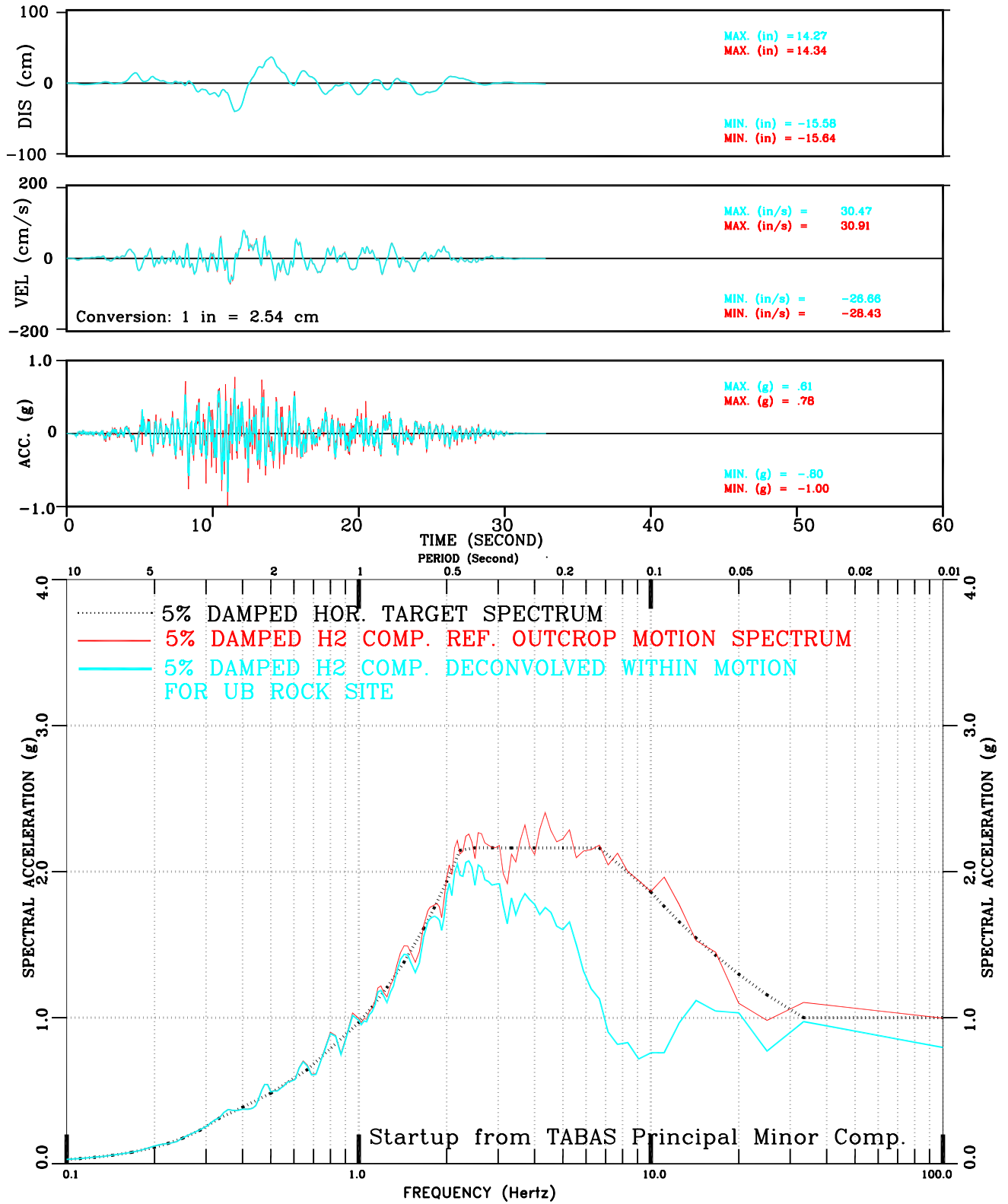


Figure III-11: Deconvolved Within vs. Surface Motion for UB Rock Set-1 H2 Comp. Motion Conforming to NUREG/CR-0098 Spectral Shape

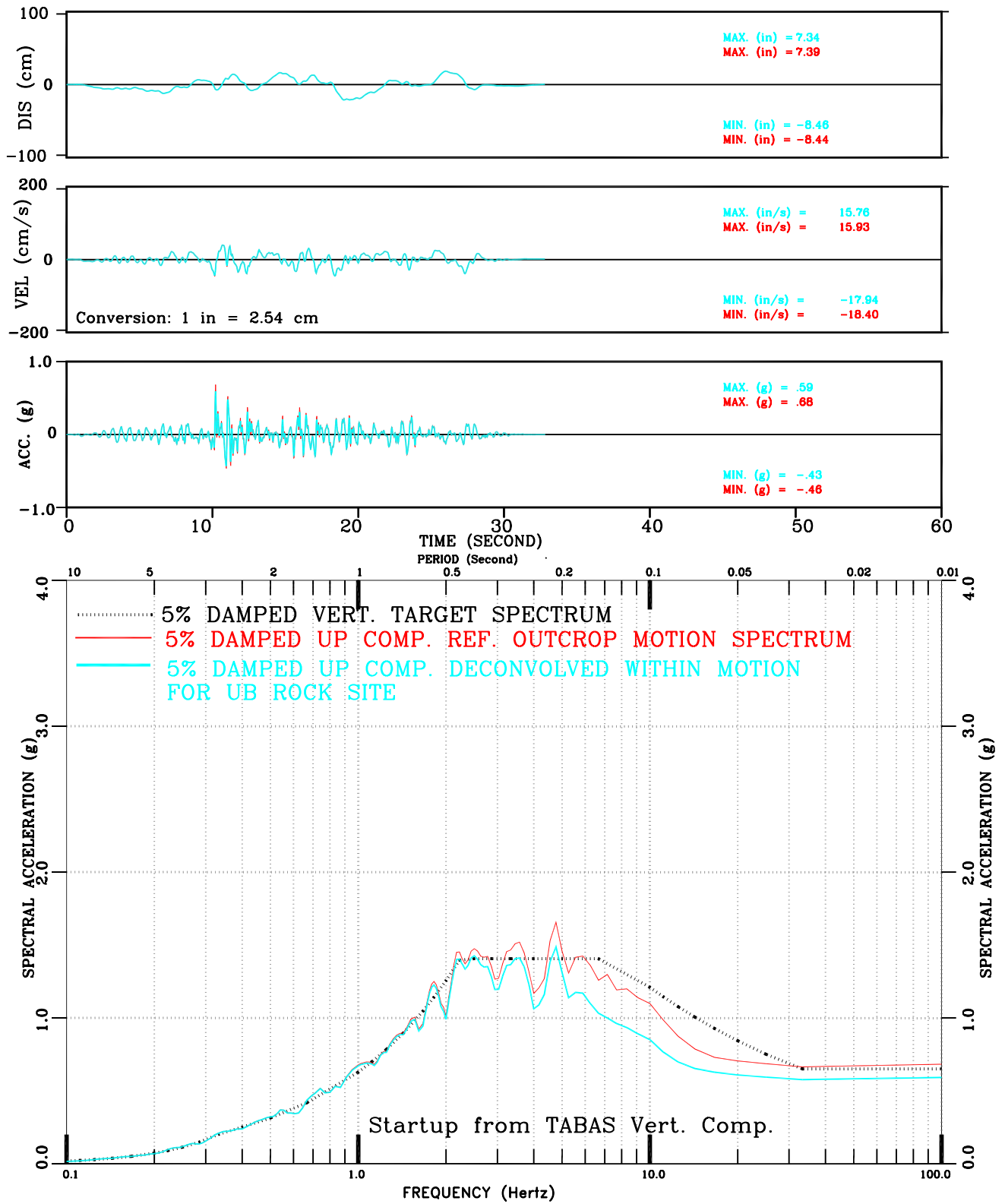


Figure III-12: Deconvolved Within vs. Surface Motion for UB Rock Set-1 Vert. Comp. Motion Conforming to NUREG/CR-0098 Spectral Shape

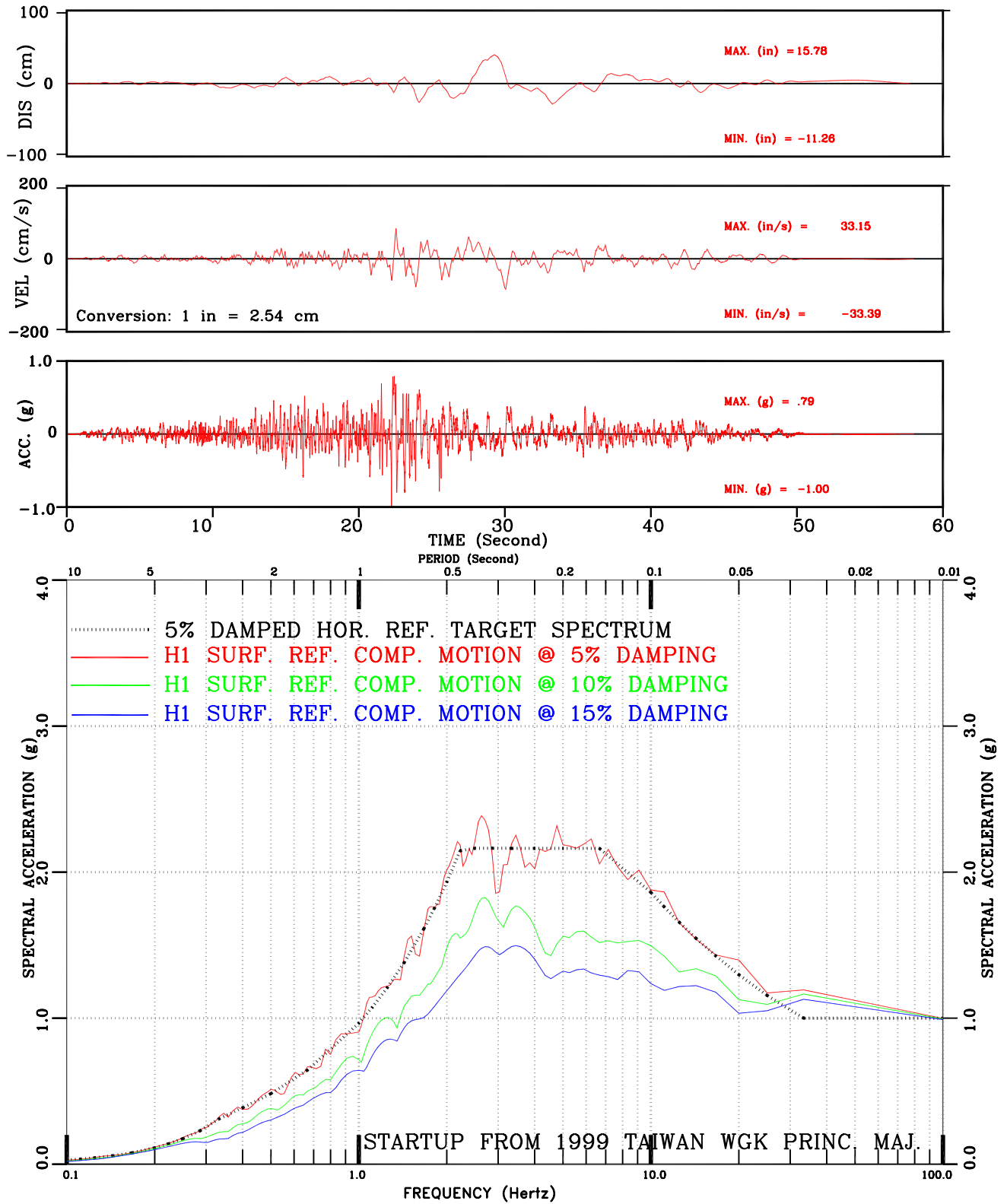


Figure III-13: Set-2 H1 Comp. Motion Conforming to NUREG/CR-0098 Spectral Shape

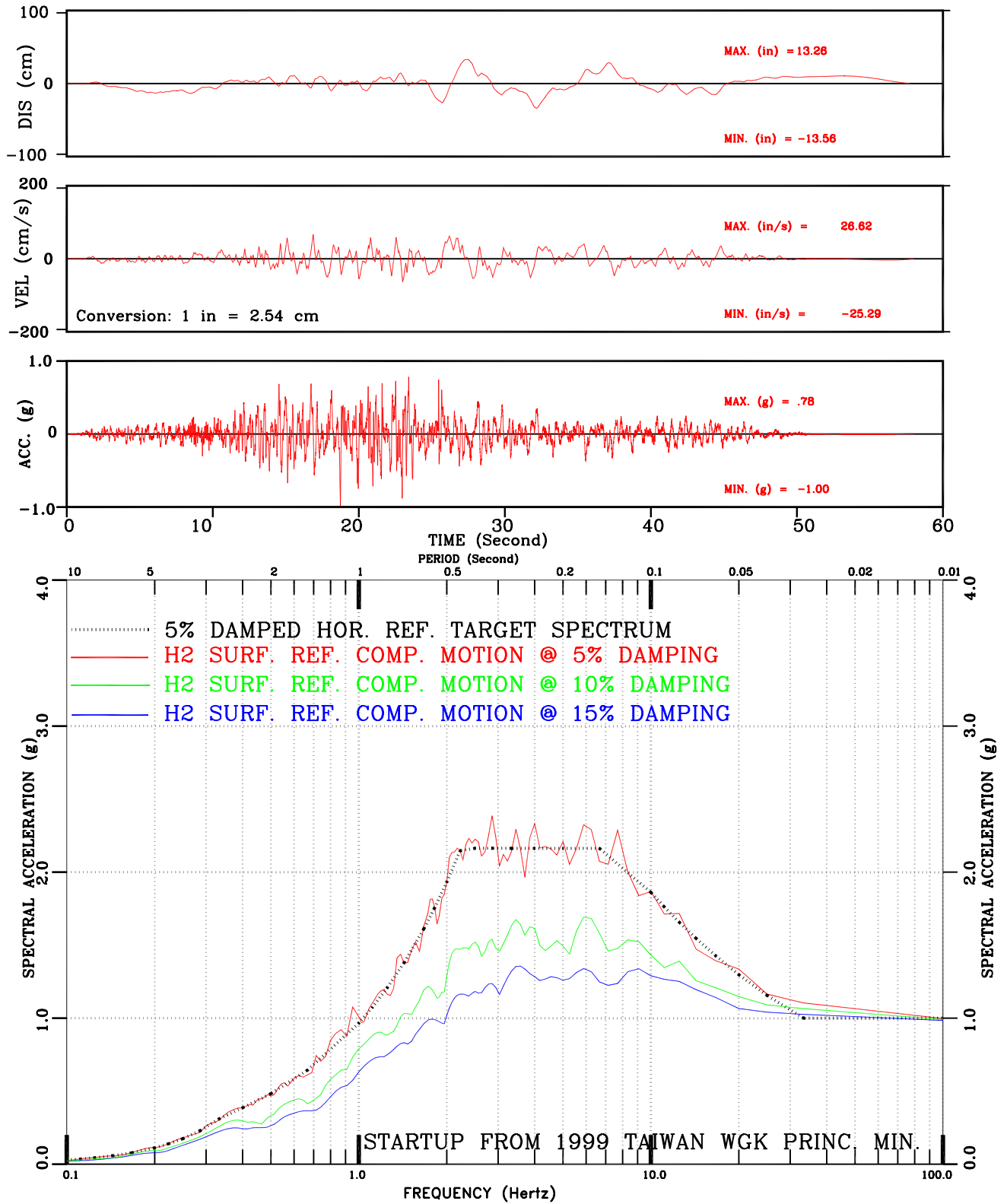


Figure III-14: Set-2 H2 Comp. Motion Conforming to NUREG/CR-0098 Spectral Shape

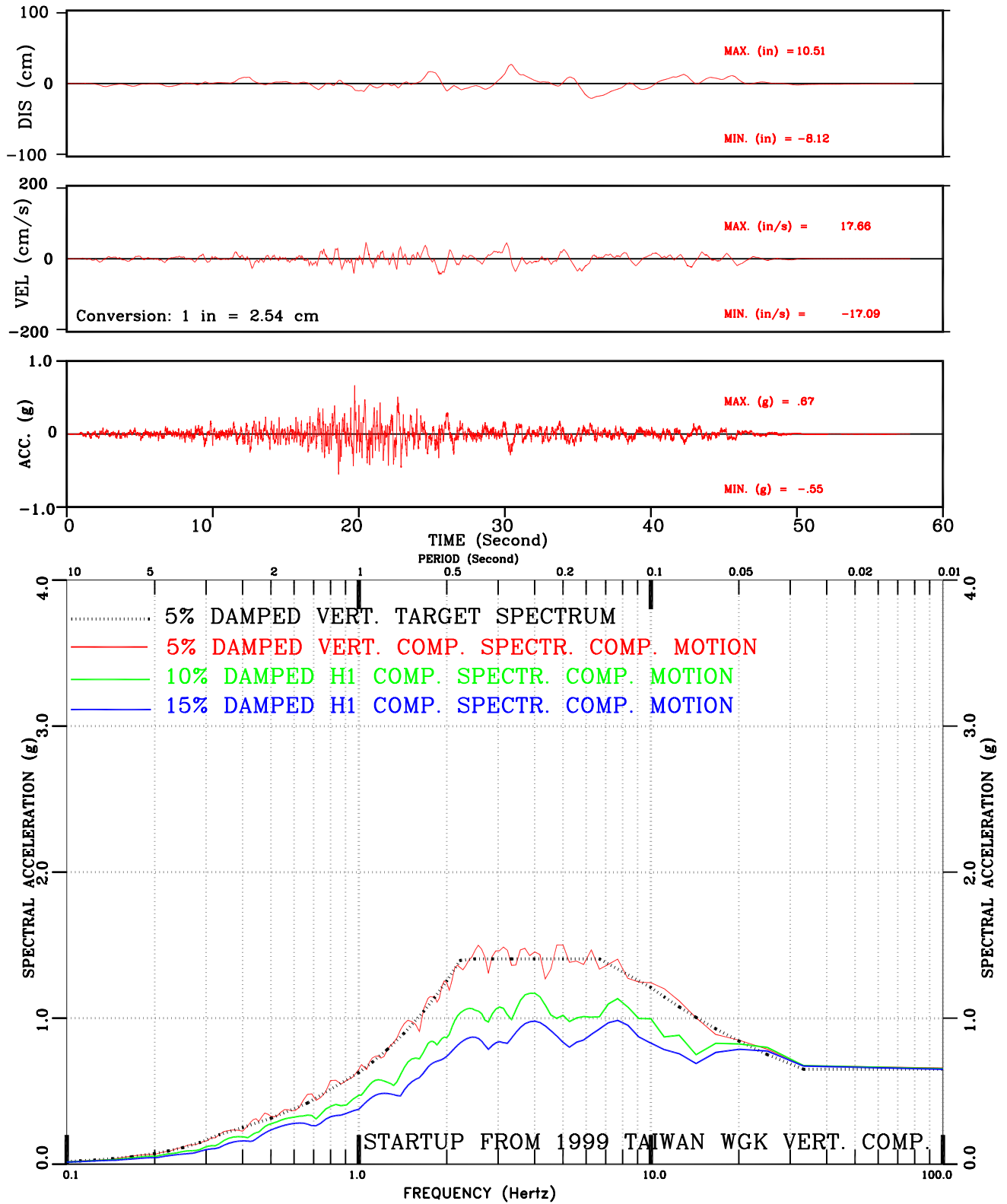


Figure III-15: Set-2 Up Comp. Motion Conforming to NUREG/CR-0098 Spectral Shape

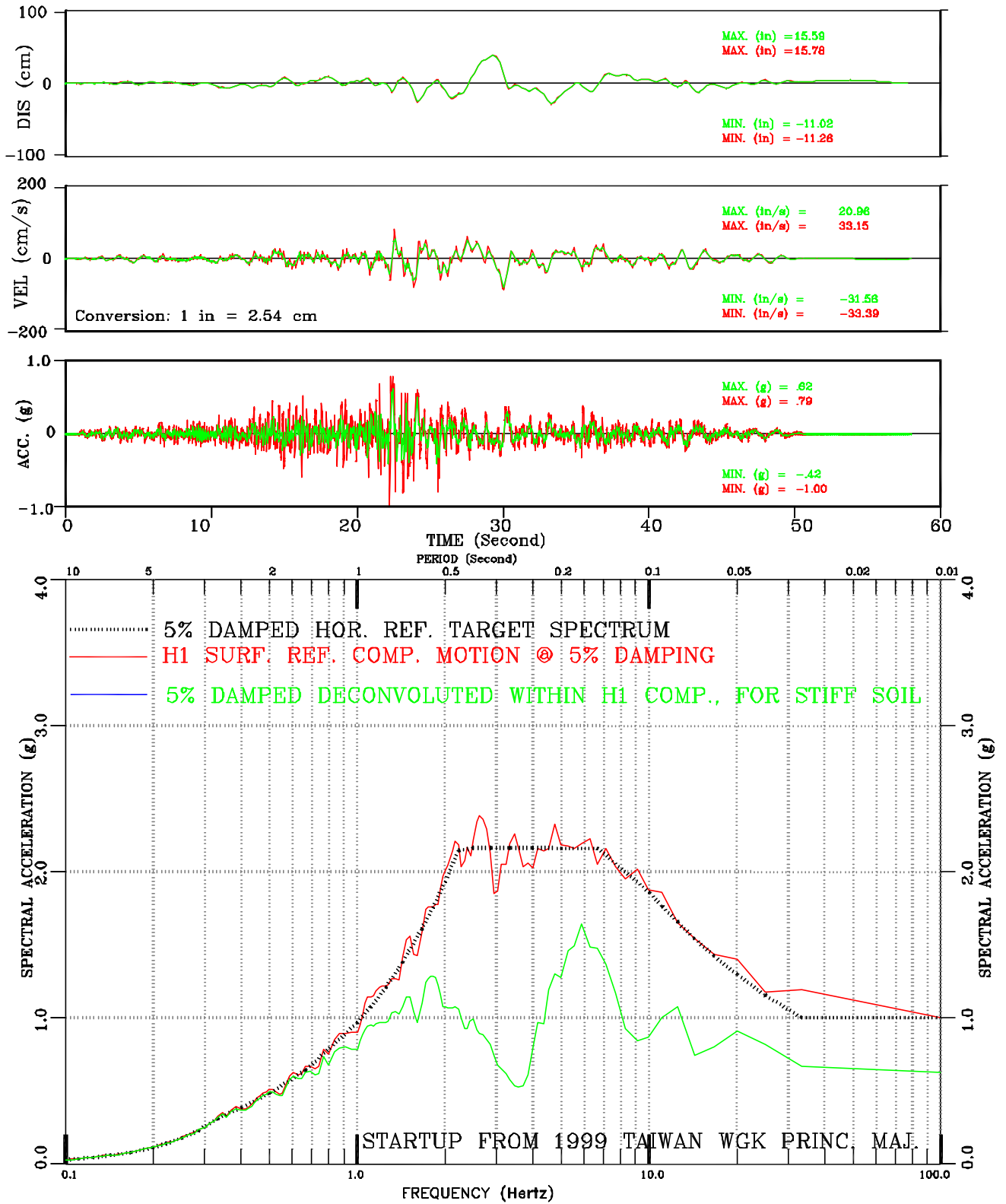


Figure III-16: Deconvoluted Within vs. Surface Motion for Stiff Soil Set-2 H1 Comp. Motion Conforming to NUREG/CR-0098 Spectral Shape

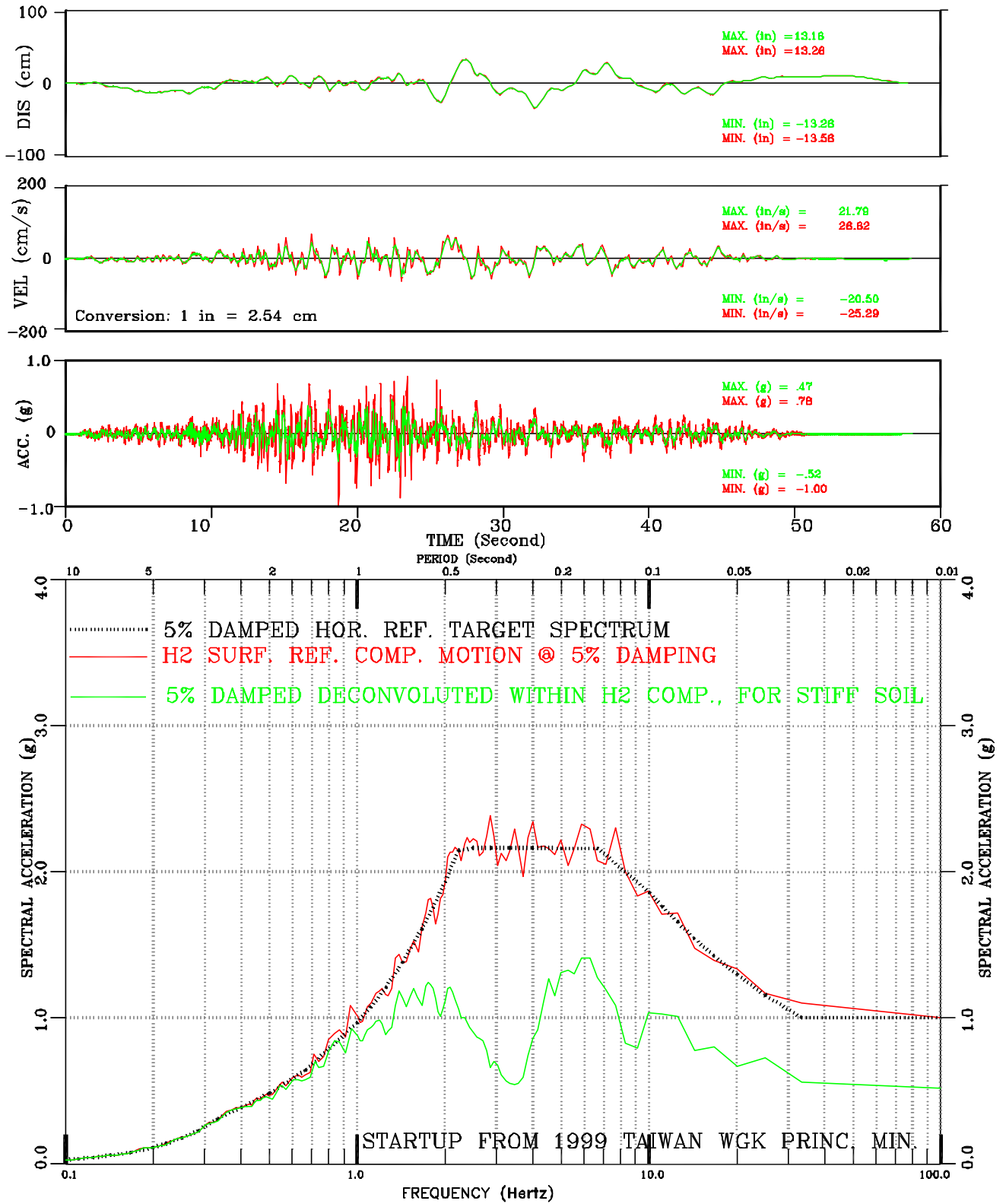


Figure III-17: Deconvoluted Within vs. Surface Motion for Stiff Soil Set-2 H2 Comp. Motion Conforming to NUREG/CR-0098 Spectral Shape

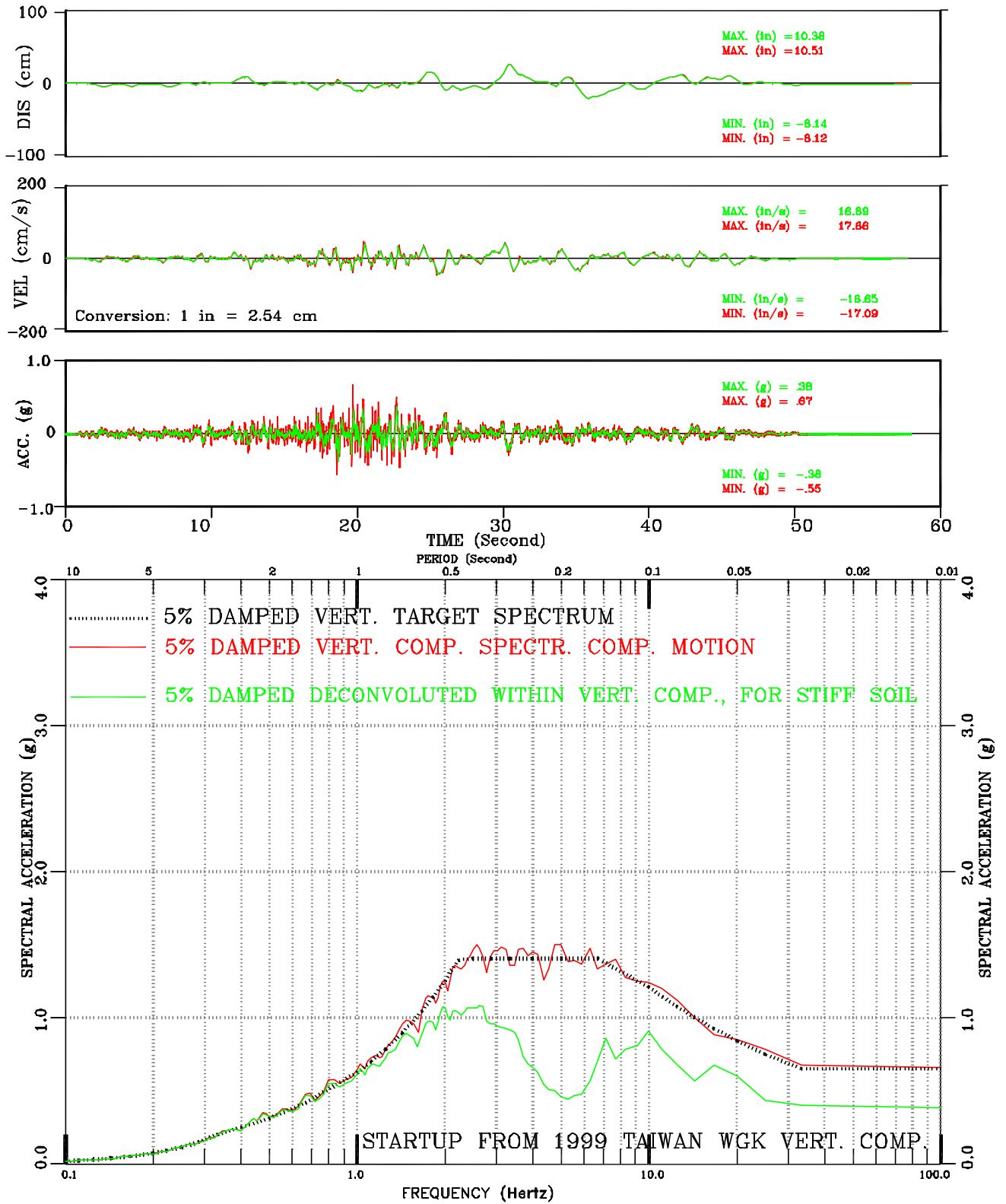


Figure III-18: Deconvoluted Within vs. Surface Motion for Stiff Soil Set-2 Vert. Comp. Motion Conforming to NUREG/CR-0098 Spectral Shape

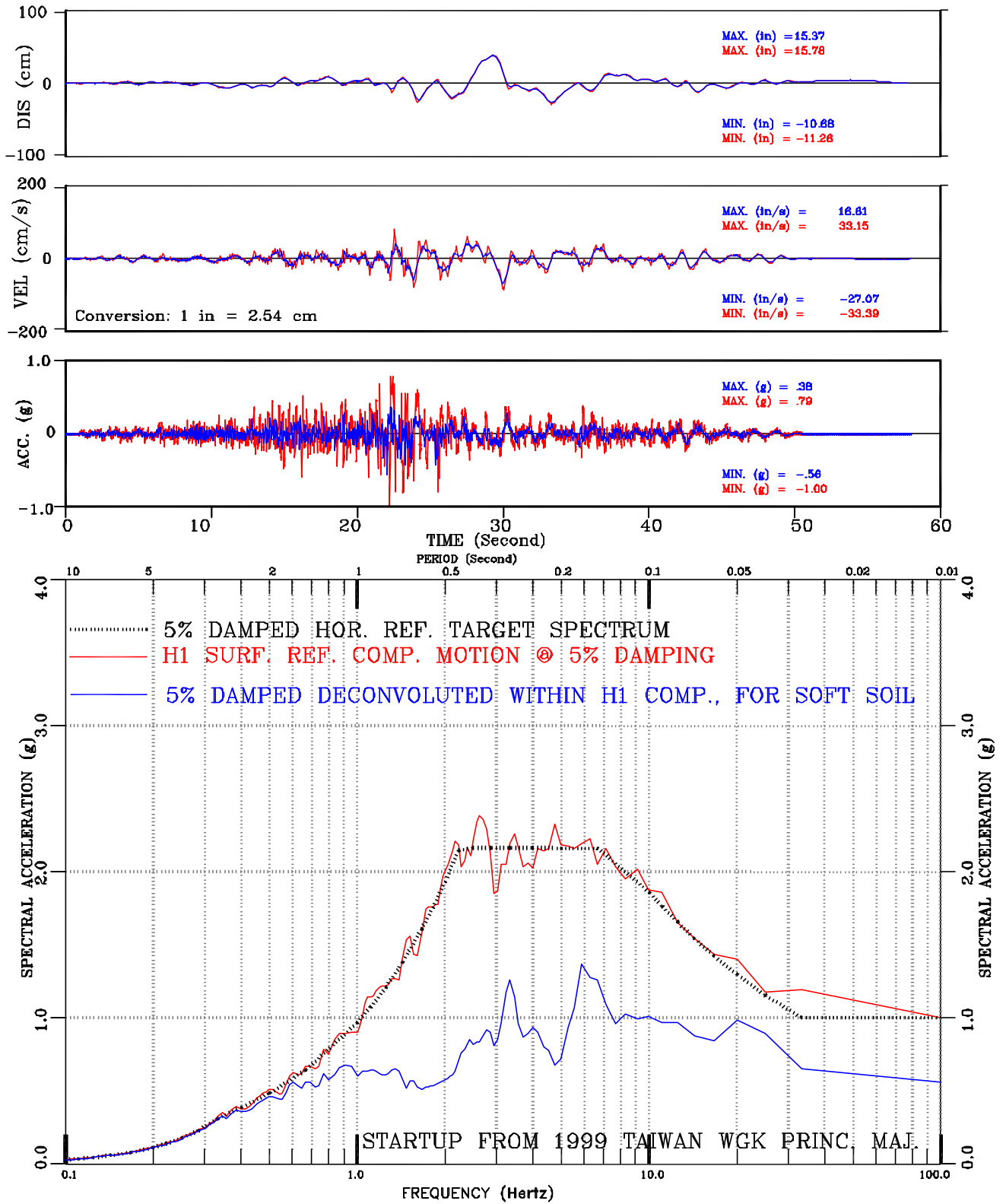


Figure III-19: Deconvoluted Within vs. Surface Motion for Soft Soil Set-2 H1 Comp. Motion Conforming to NUREG/CR-0098 Spectral Shape

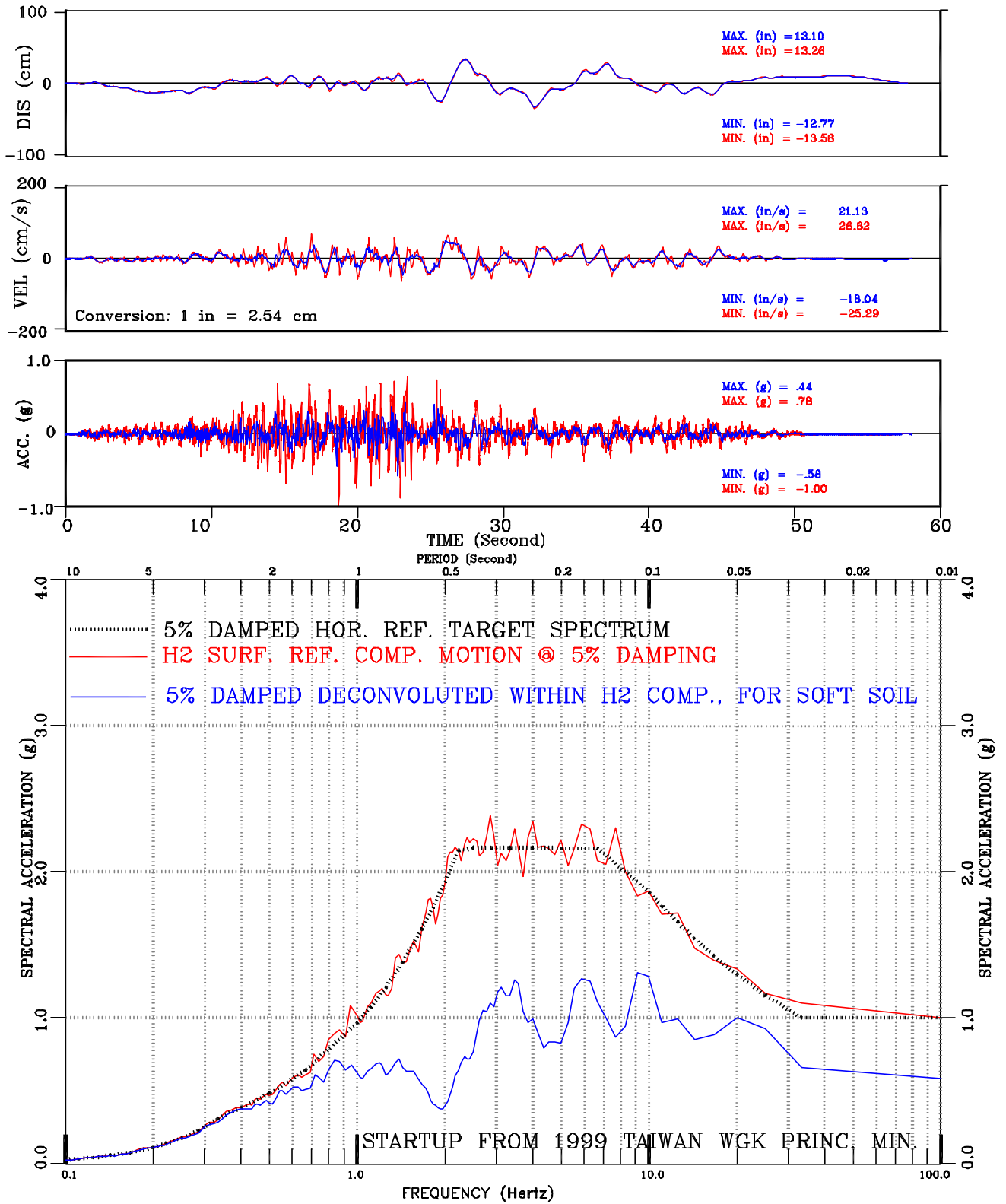


Figure III-20: Deconvoluted Within vs. Surface Motion for Soft Soil Set-2 H2 Comp. Motion Conforming to NUREG/CR-0098 Spectral Shape

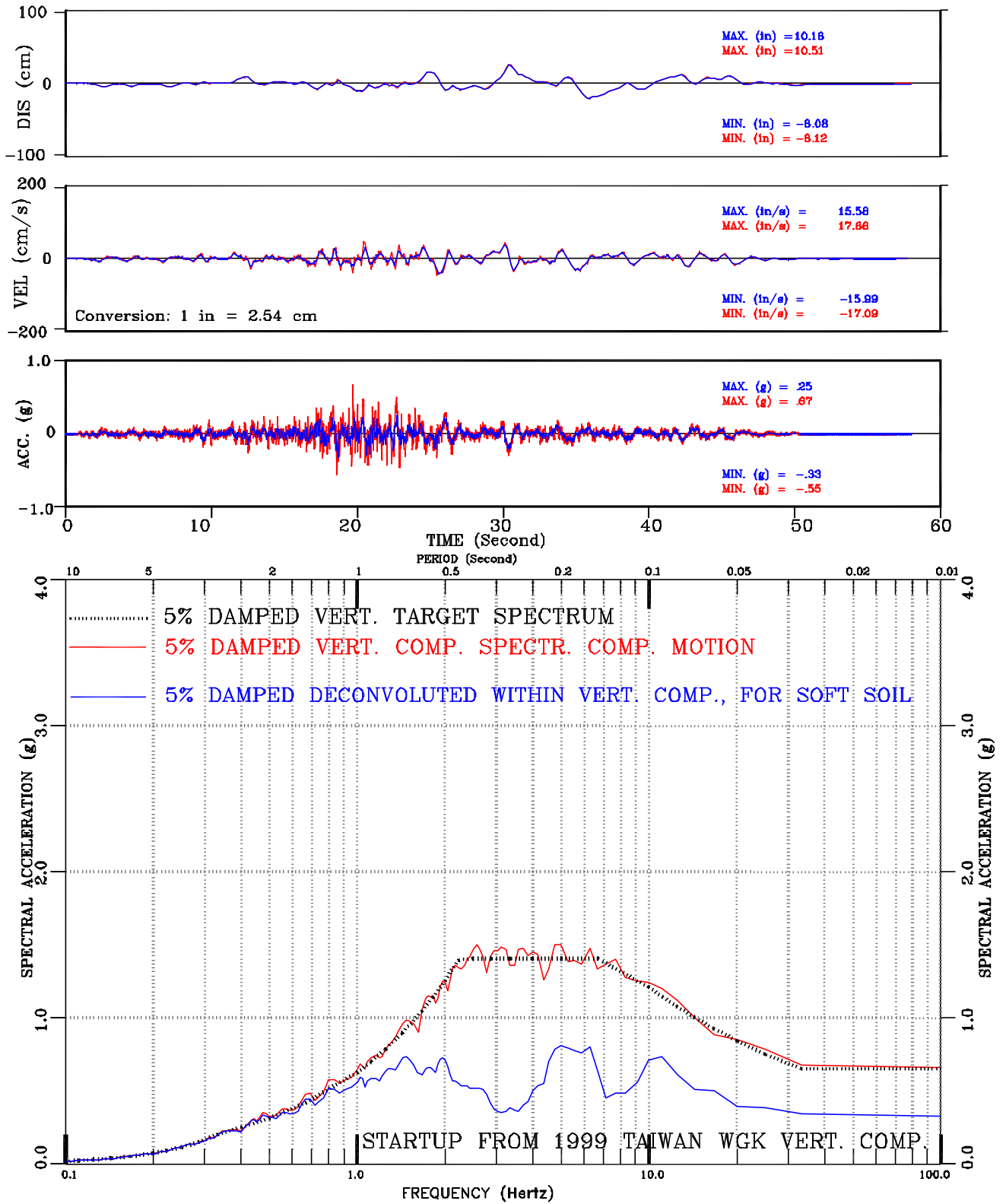


Figure III-21: Deconvoluted Within vs. Surface Motion for Soft Soil Set-2 Vert. Comp. Motion Conforming to NUREG/CR-0098 Spectral Shape

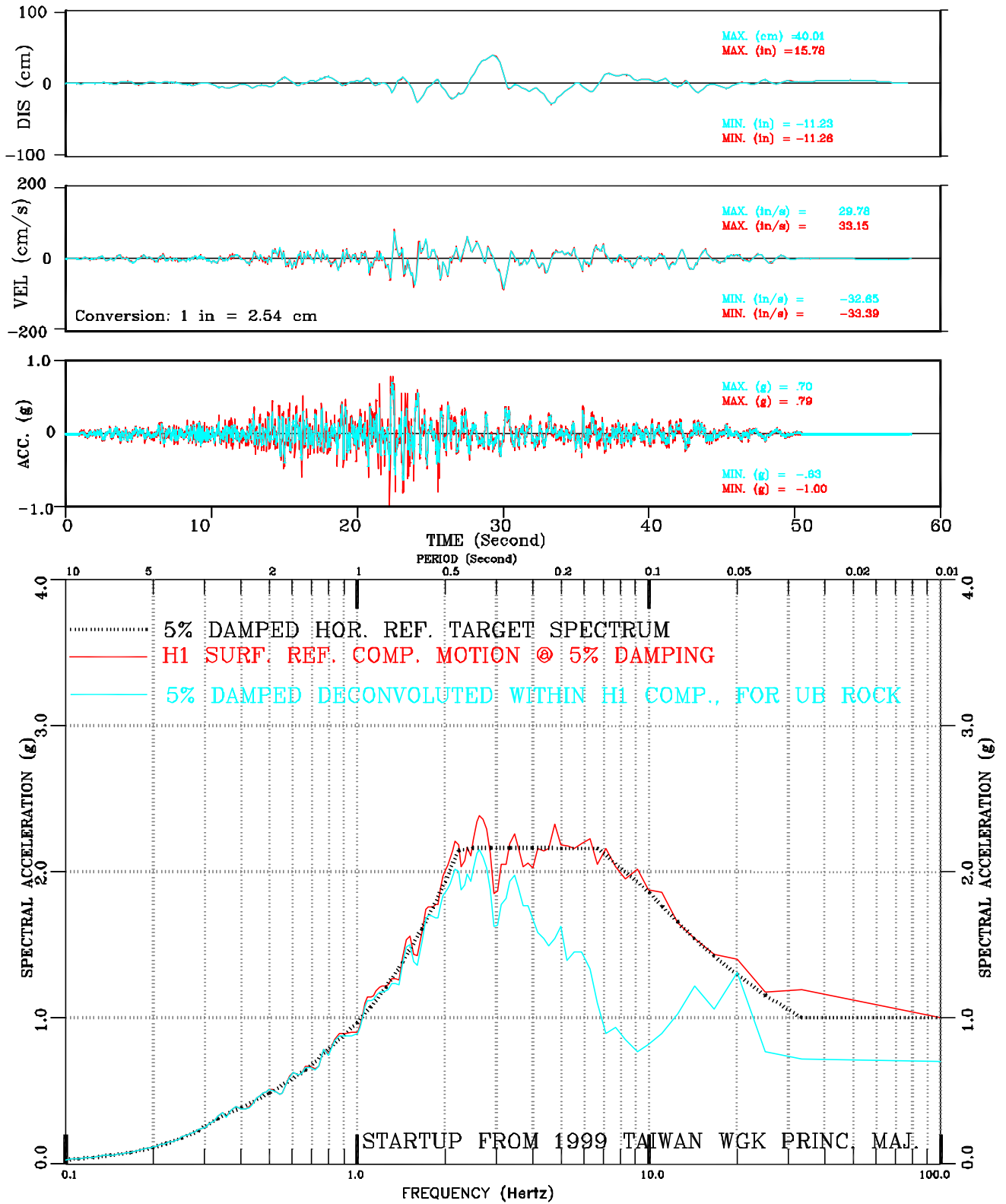


Figure III-22: Deconvoluted Within vs. Surface Motion for UB Rock Set-2 H1 Comp. Motion Conforming to NUREG/CR-0098 Spectral Shape

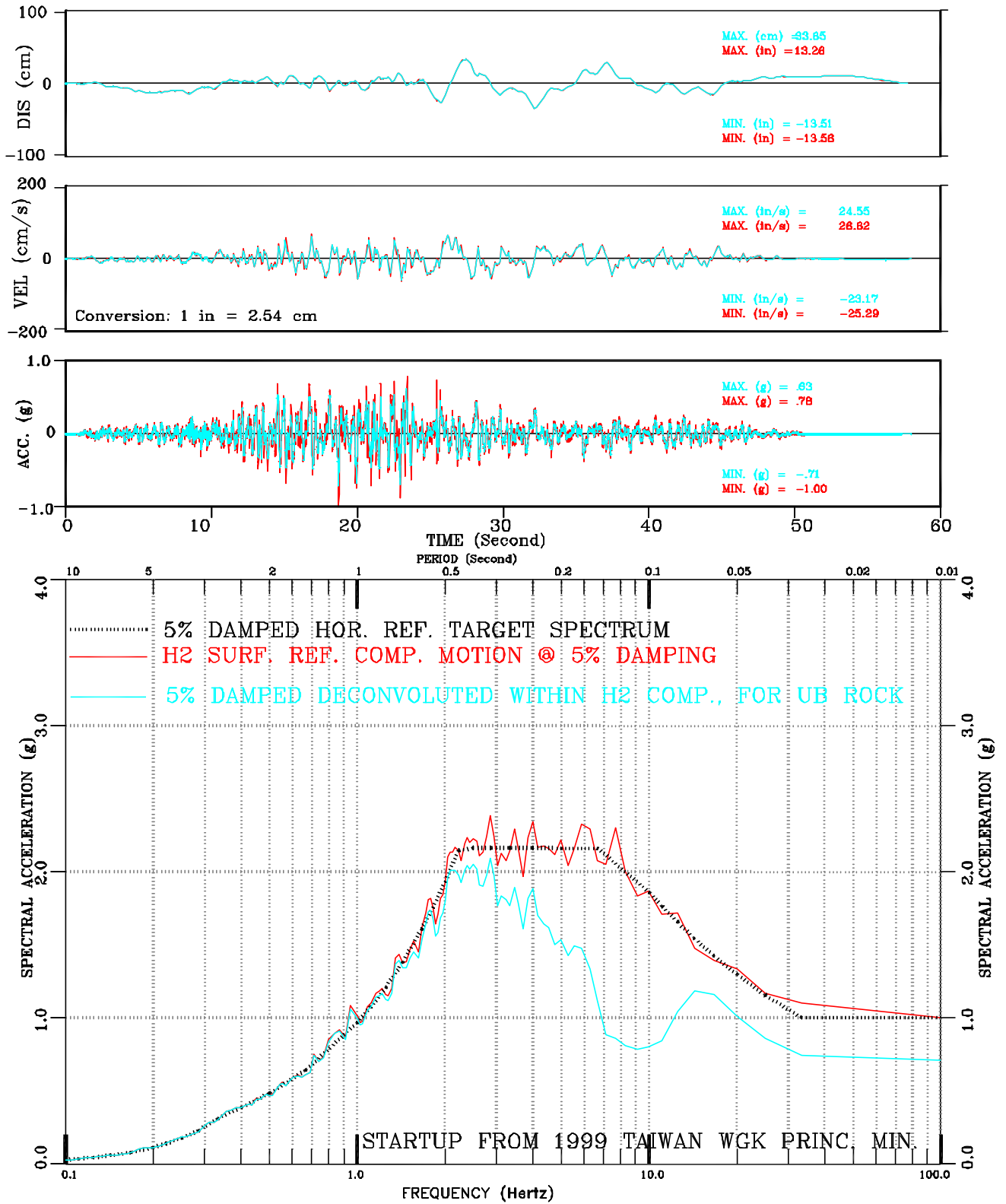


Figure III-23: Deconvoluted Within vs. Surface Motion for UB Rock Set-2 H2 Comp. Motion Conforming to NUREG/CR-0098 Spectral Shape

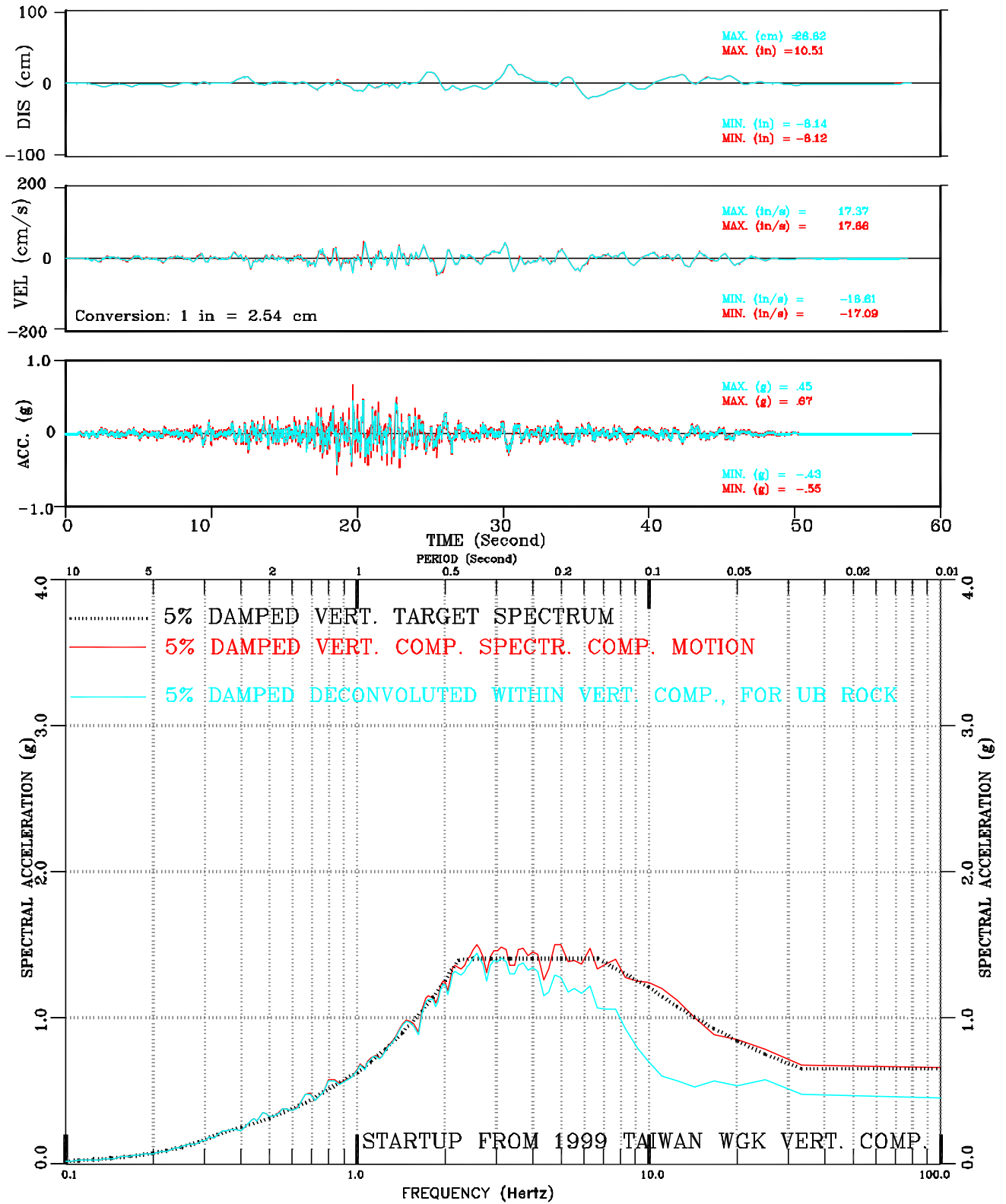


Figure III-24: Deconvoluted Within vs. Surface Motion for UB Rock Set-2 Vert. Comp. Motion Conforming to NUREG/CR-0098 Spectral Shape

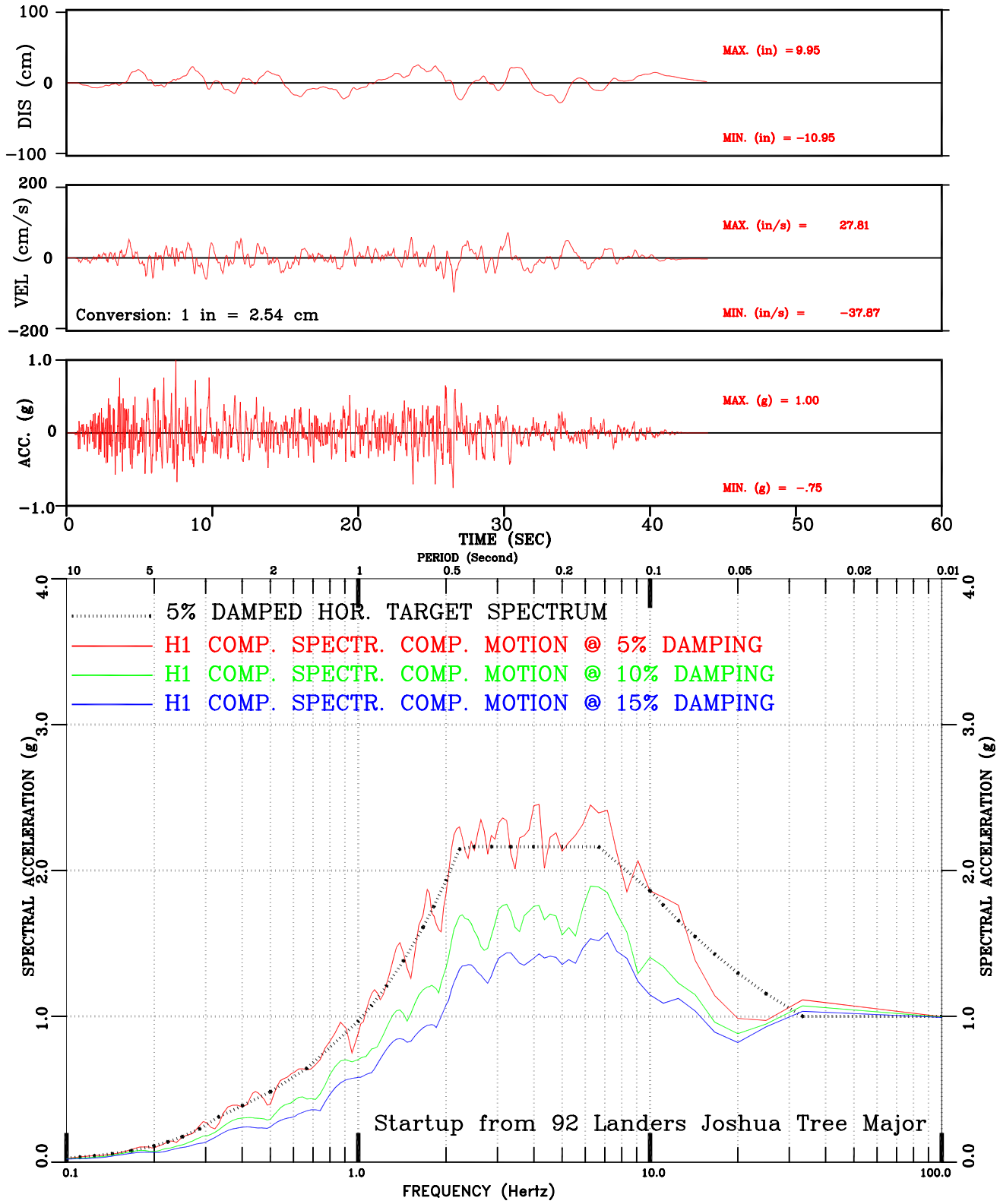


Figure III-25: Set-3 H1 Comp. Motion Conforming to NUREG/CR-0098 Spectral Shape

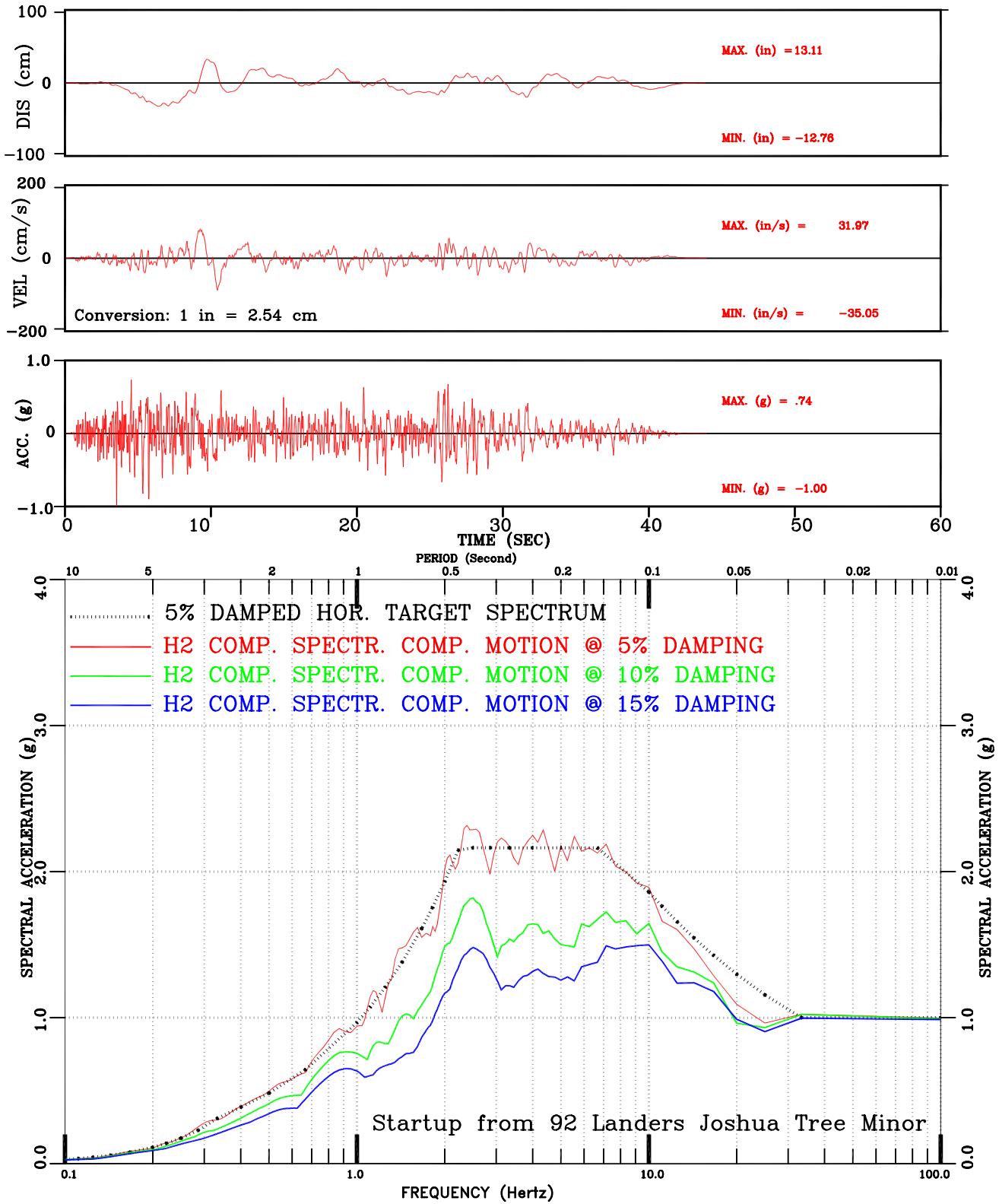


Figure III-26: Set-3 H2 Comp. Motion Conforming to NUREG/CR-0098 Spectral Shape

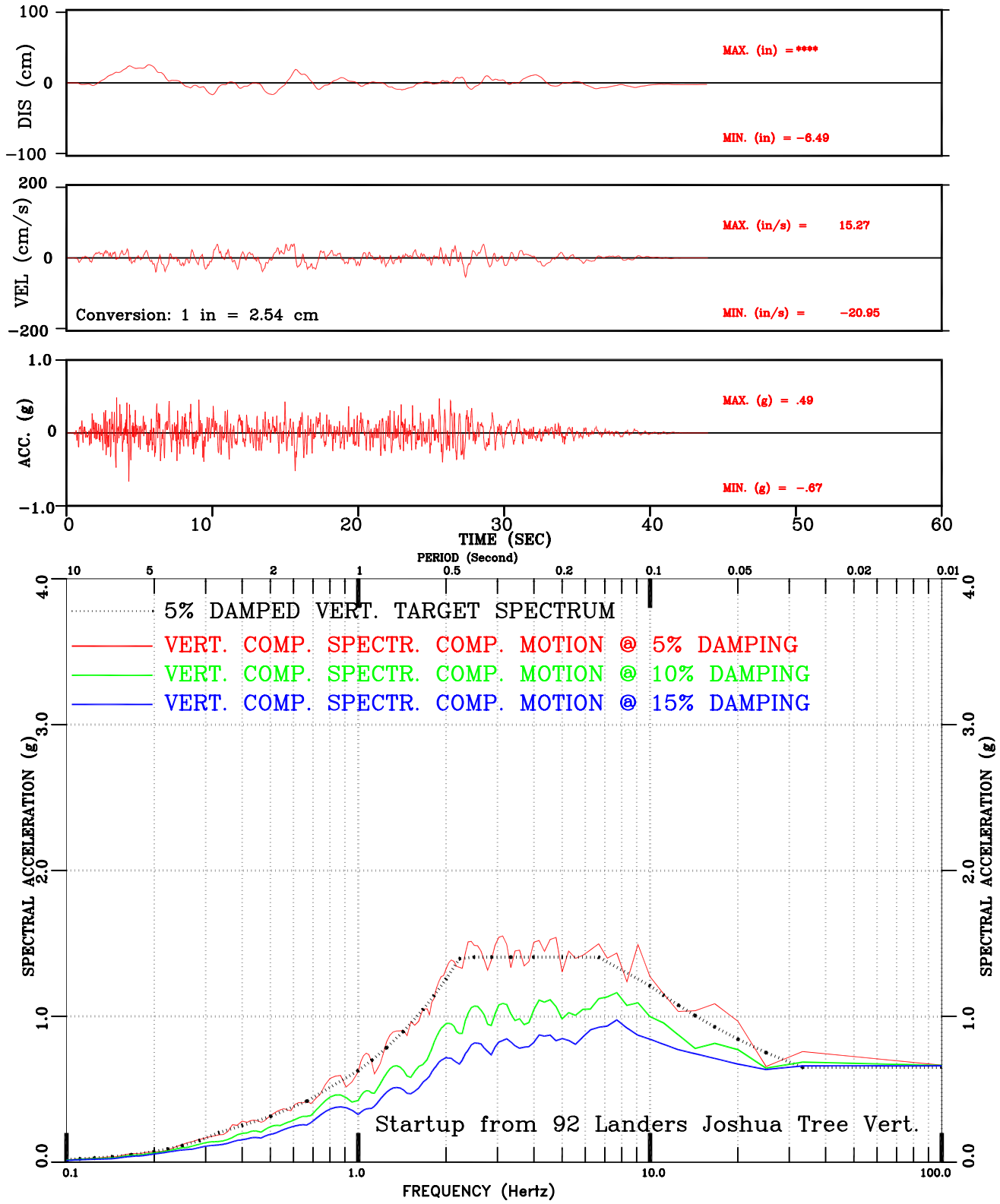


Figure III-27: Set-3 Vert. Comp. Motion Conforming to NUREG/CR-0098 Spectral Shape

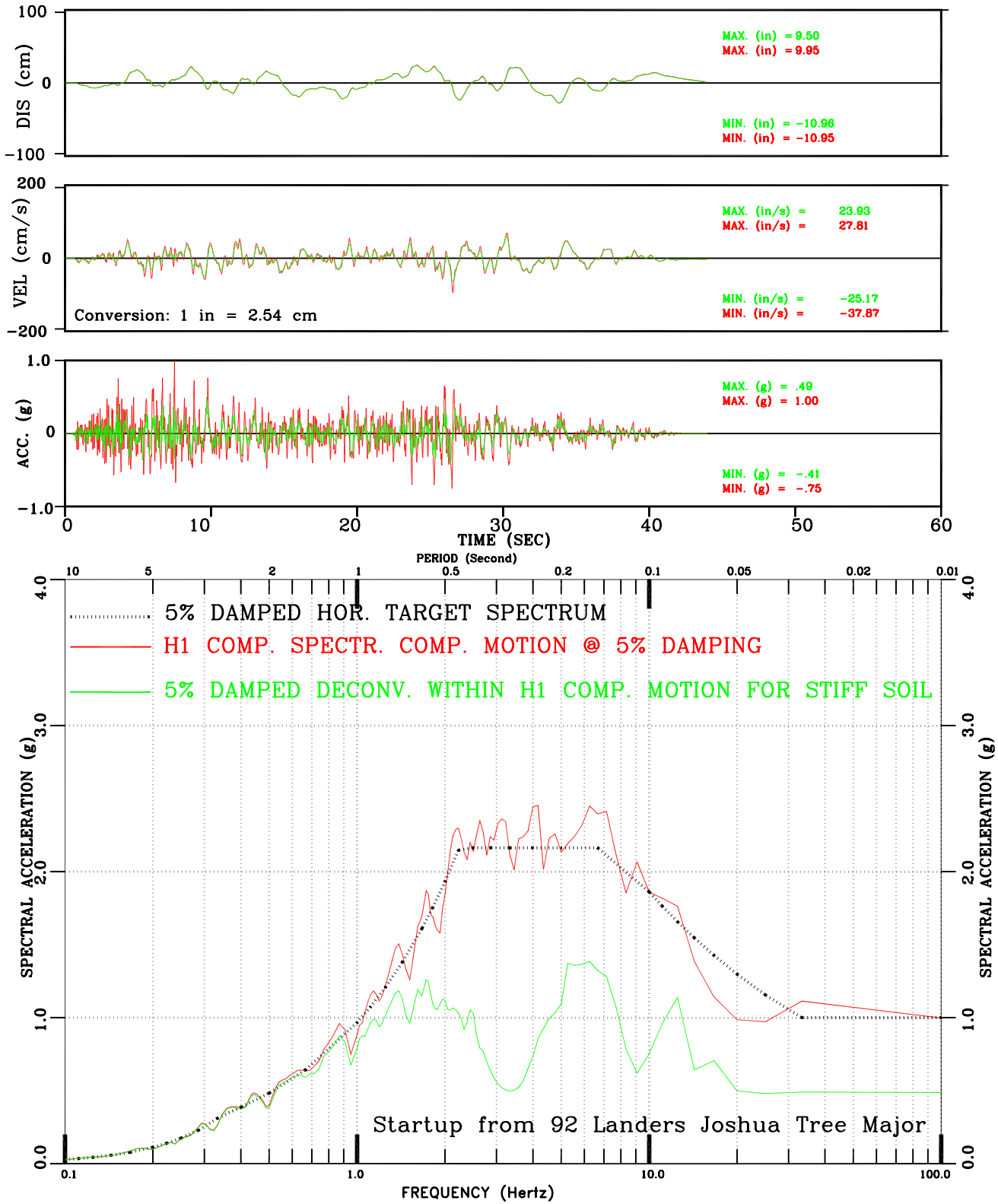


Figure III-28: Deconv. Within vs. Surface Motion for Stiff Soil  
Set-3 H1 Comp. Motion Conforming to NUREG/CR-0098 Spectral Shape

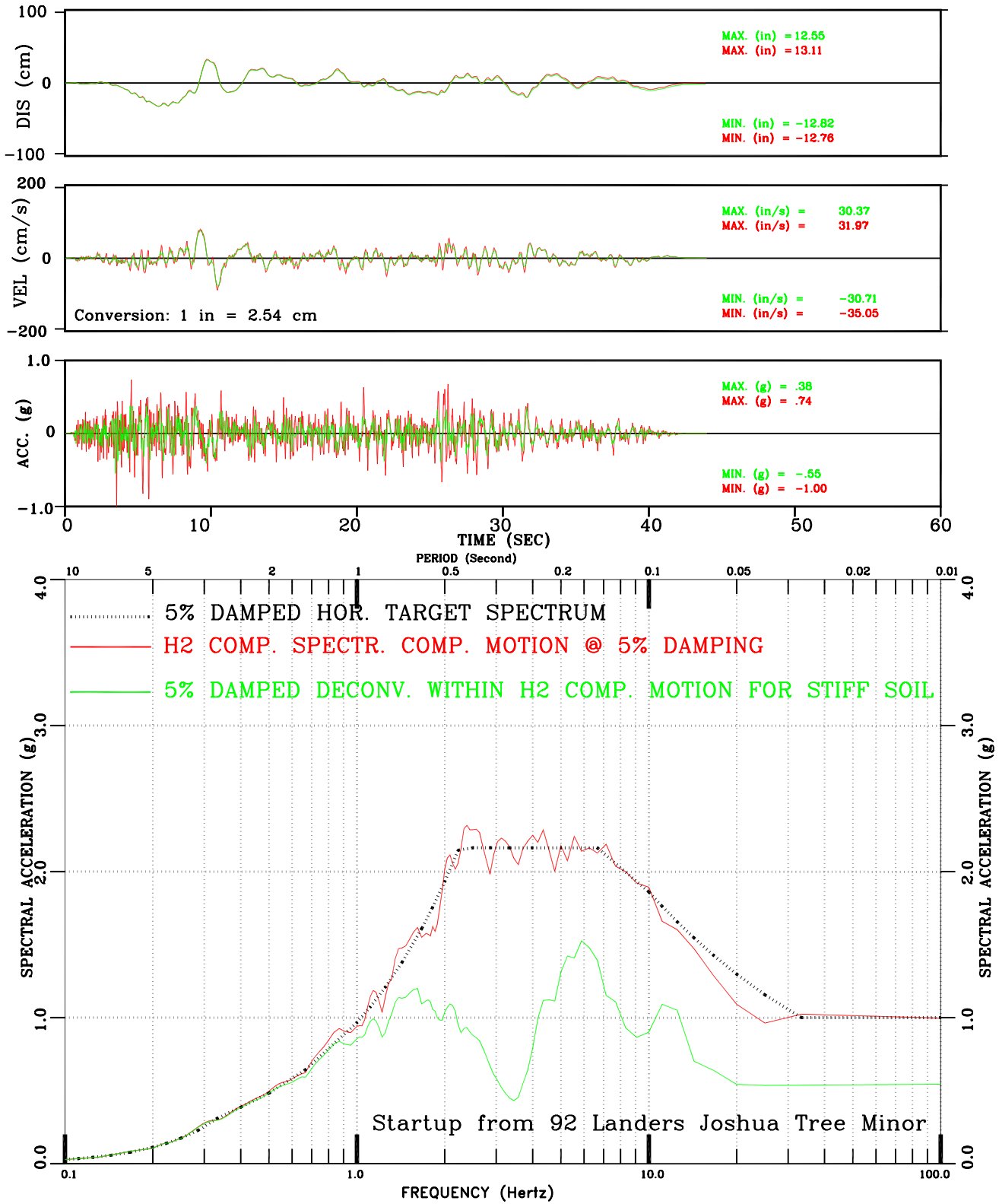


Figure III-29: Deconv. Within vs. Surface Motion for Stiff Soil Set-3 H2 Comp. Motion Conforming to NUREG/CR-0098 Spectral Shape

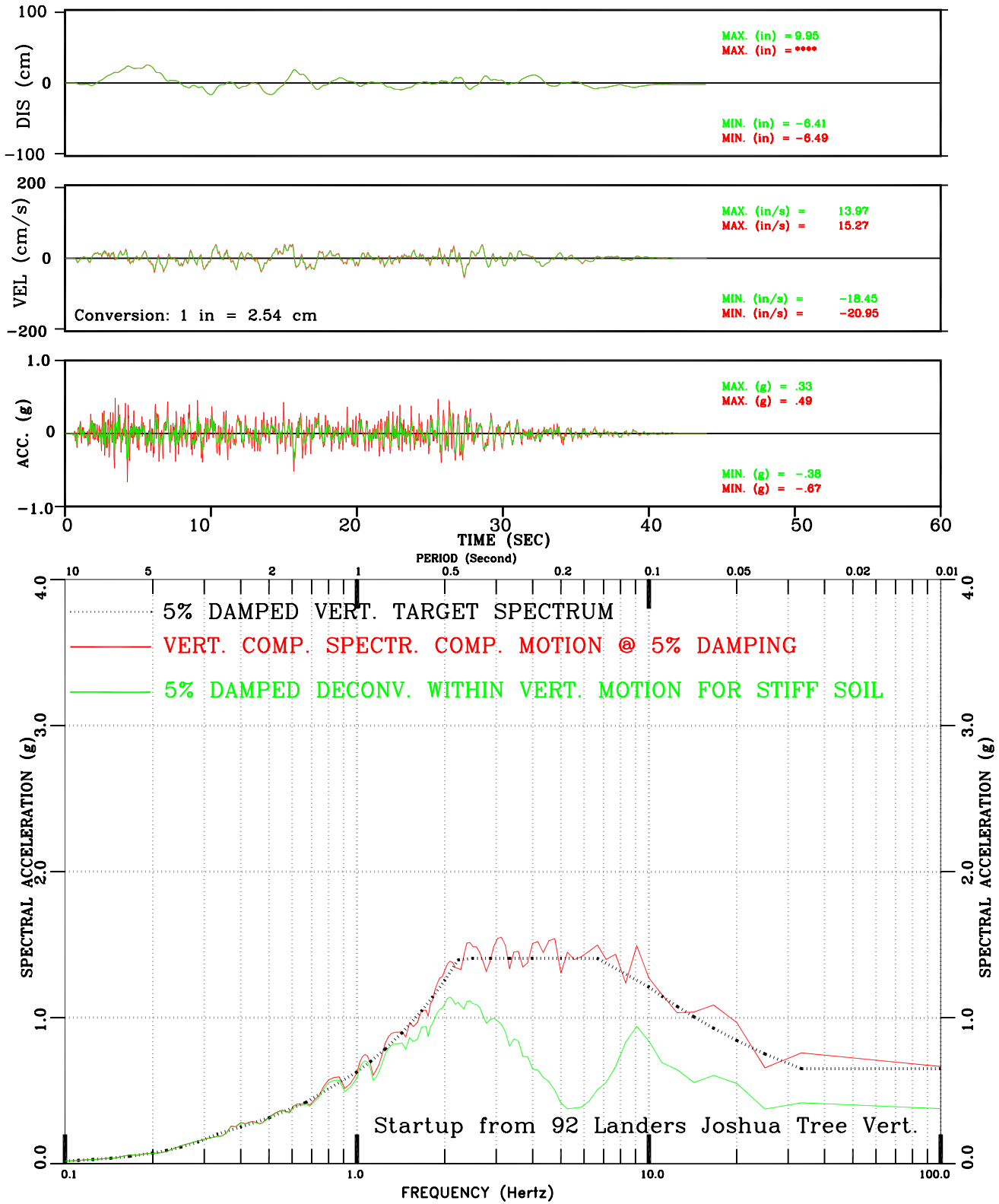


Figure III-30: Deconv. Within vs. Surface Motion for Stiff Soil Set-3 Vert Comp. Motion Conforming to NUREG/CR-0098 Spectral Shape

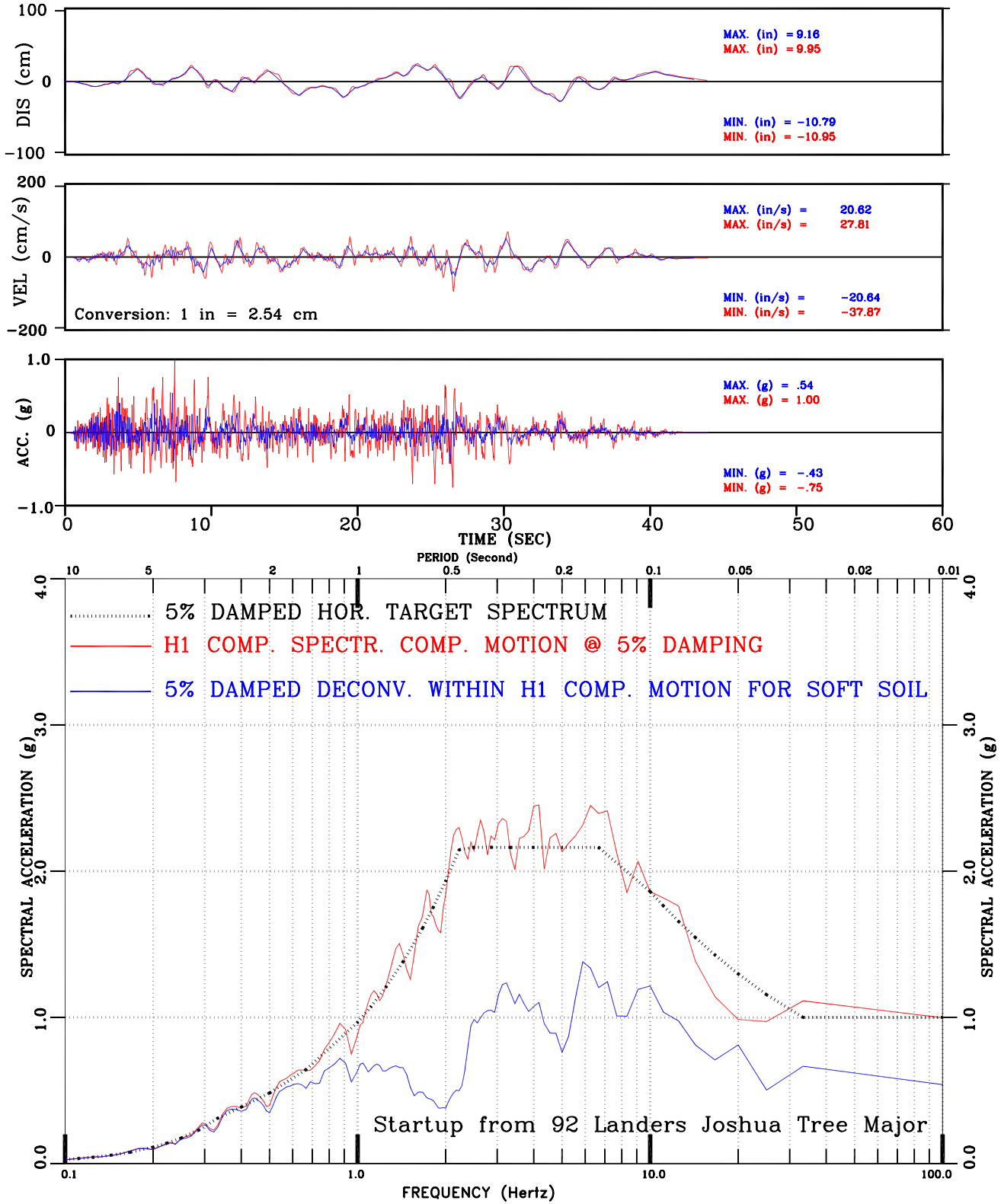


Figure III-31: Deconv. Within vs. Surface Motion for Soft Soil Set-3 H1 Comp. Motion Conforming to NUREG/CR-0098 Spectral Shape

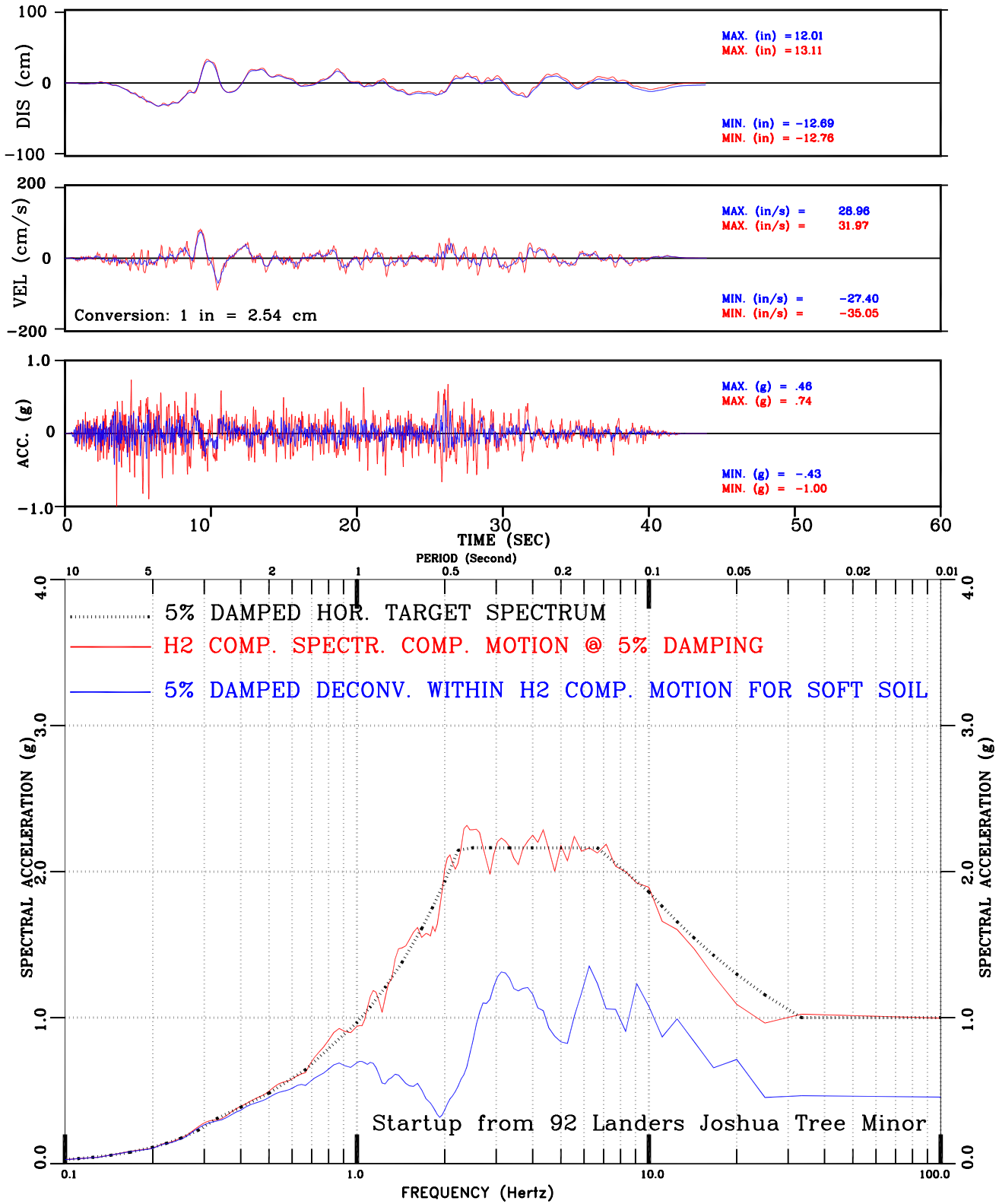


Figure III-32: Deconv. Within vs. Surface Motion for Soft Soil Set-3 H2 Comp. Motion Conforming to NUREG/CR-0098 Spectral Shape

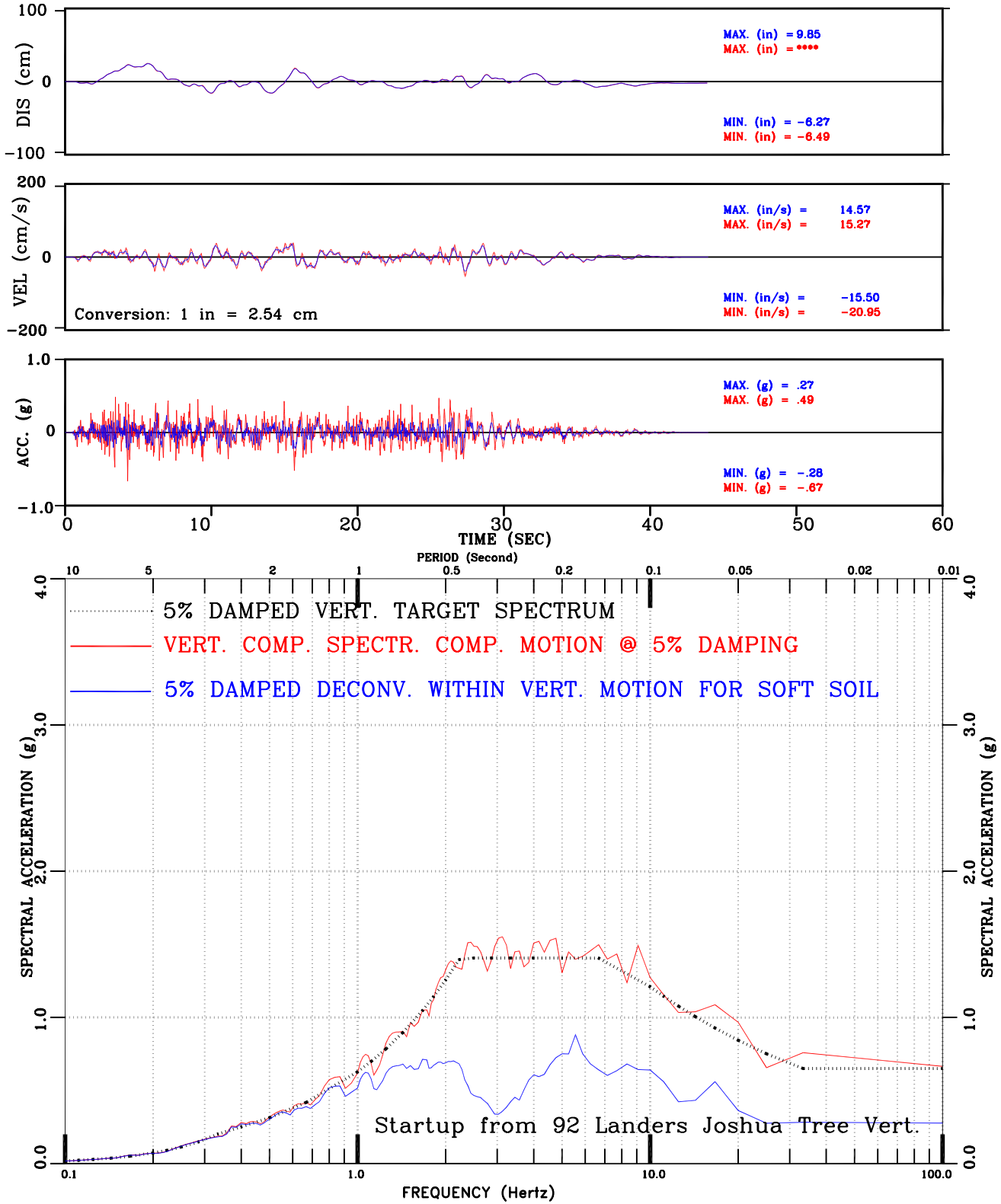


Figure III-33: Deconv. Within vs. Surface Motion for Soft Soil Set-3 Vert Comp. Motion Conforming to NUREG/CR-0098 Spectral Shape

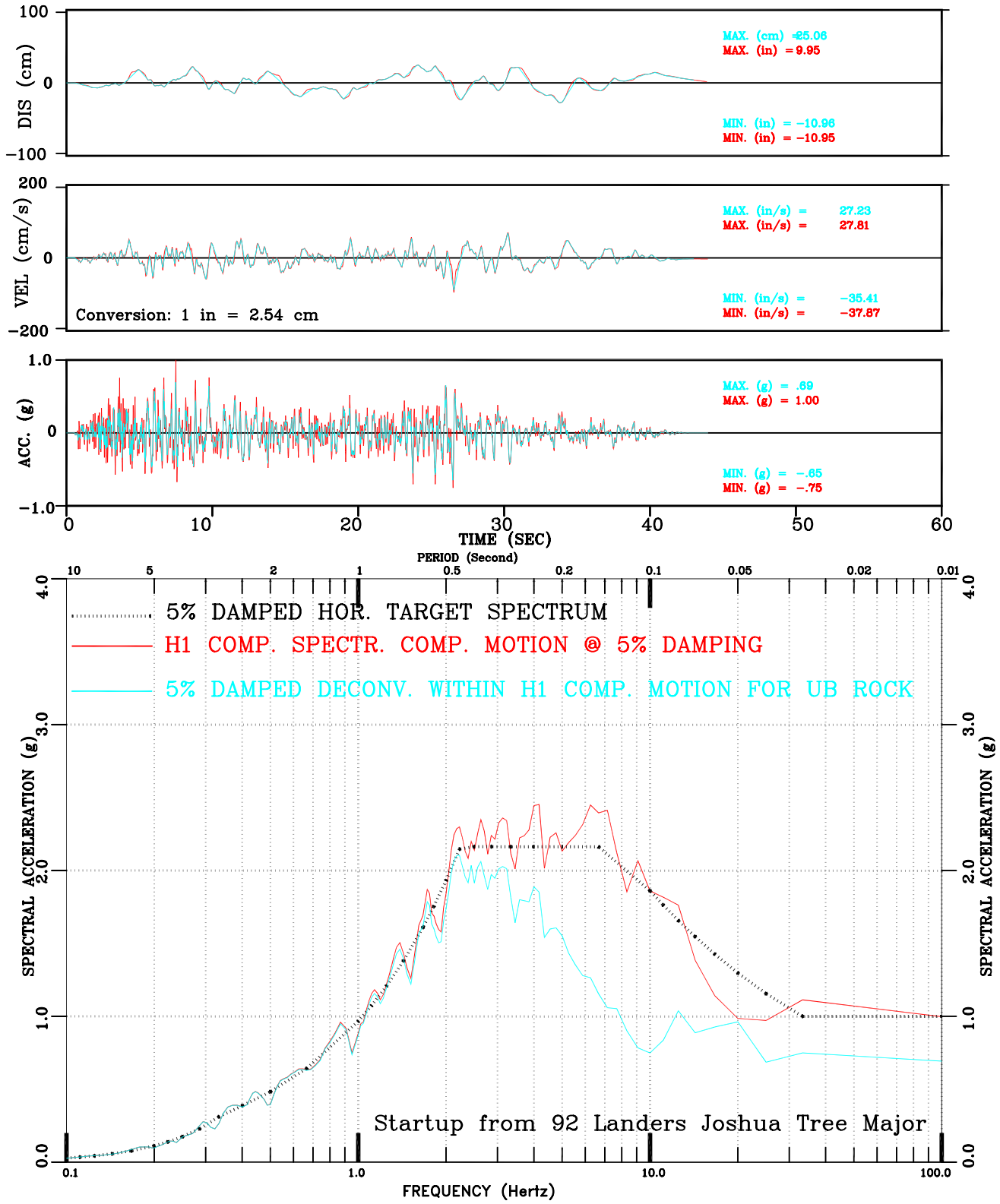


Figure III-34: Deconv. Within vs. Surface Motion for UB Rock Set-3 H1 Comp. Motion Conforming to NUREG/CR-0098 Spectral Shape

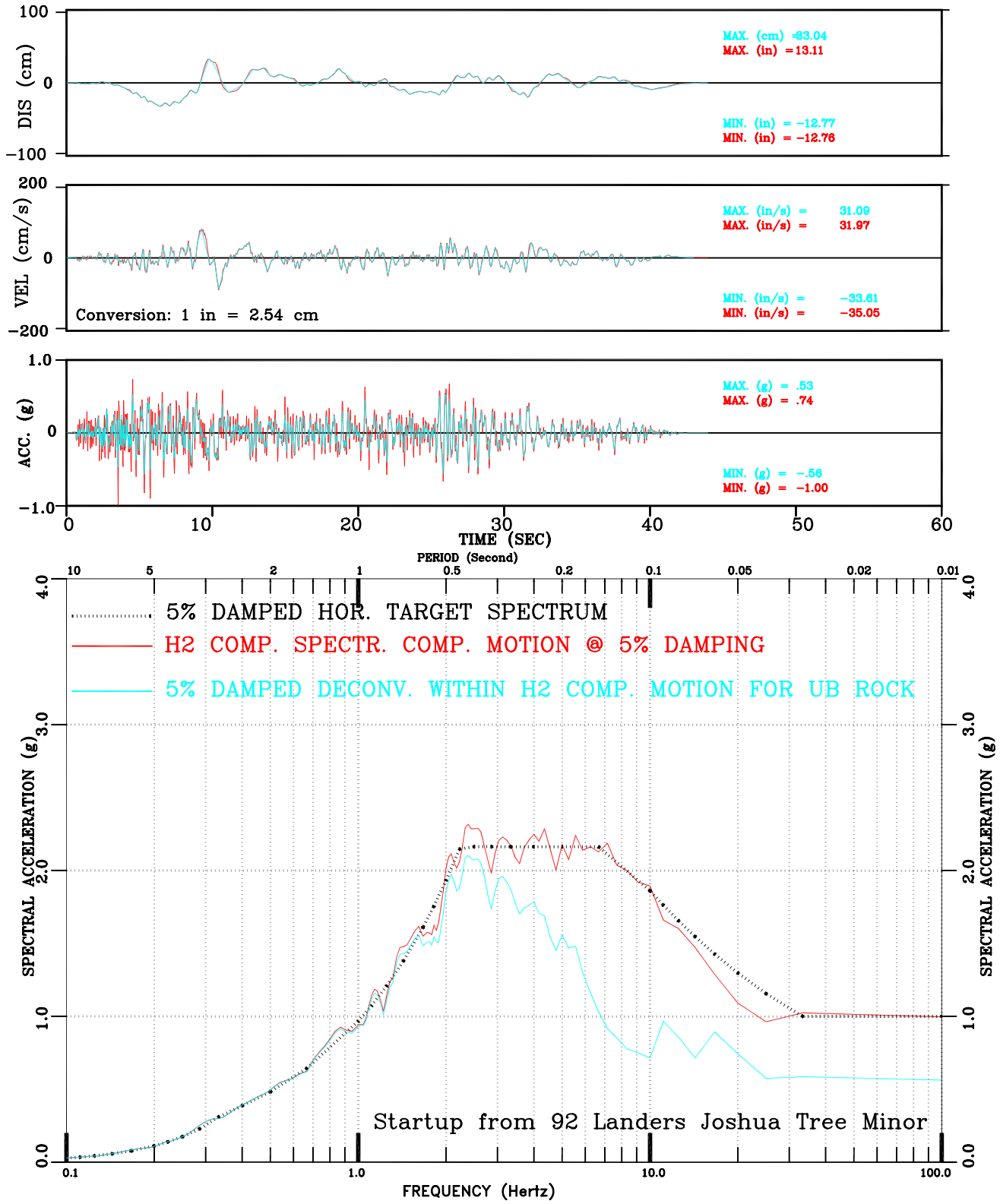


Figure III-35: Deconv. Within vs. Surface Motion for UB Rock Set-3 H2 Comp. Motion Conforming to NUREG/CR-0098 Spectral Shape

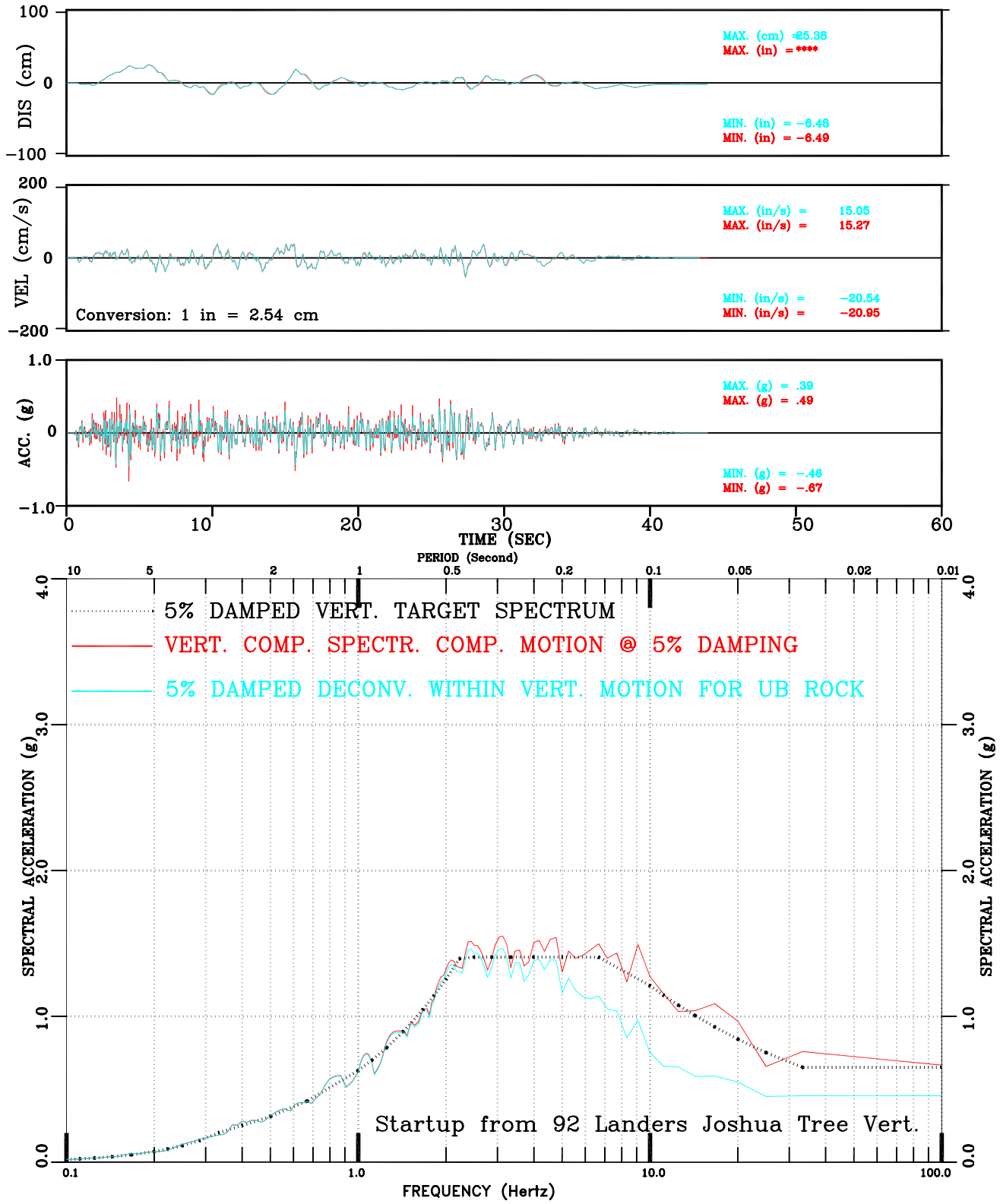


Figure III-36: Deconv. Within vs. Surface Motion for UB Rock Set-3 Vert Comp. Motion Conforming to NUREG/CR-0098 Spectral Shape

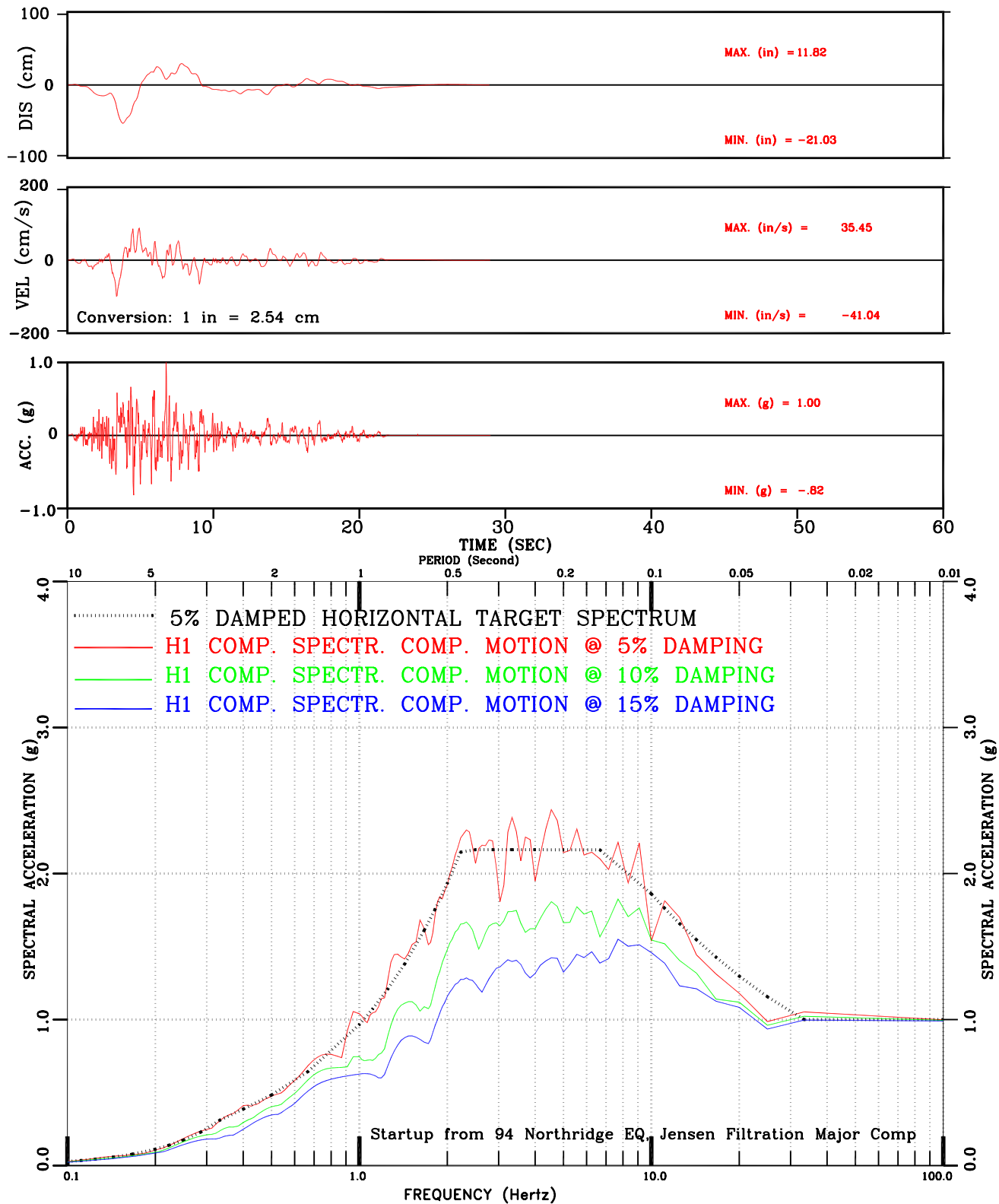


Figure III-37: Set-4 H1 Comp Motion Conforming to NUREG/CR-0098 Spectral Shape

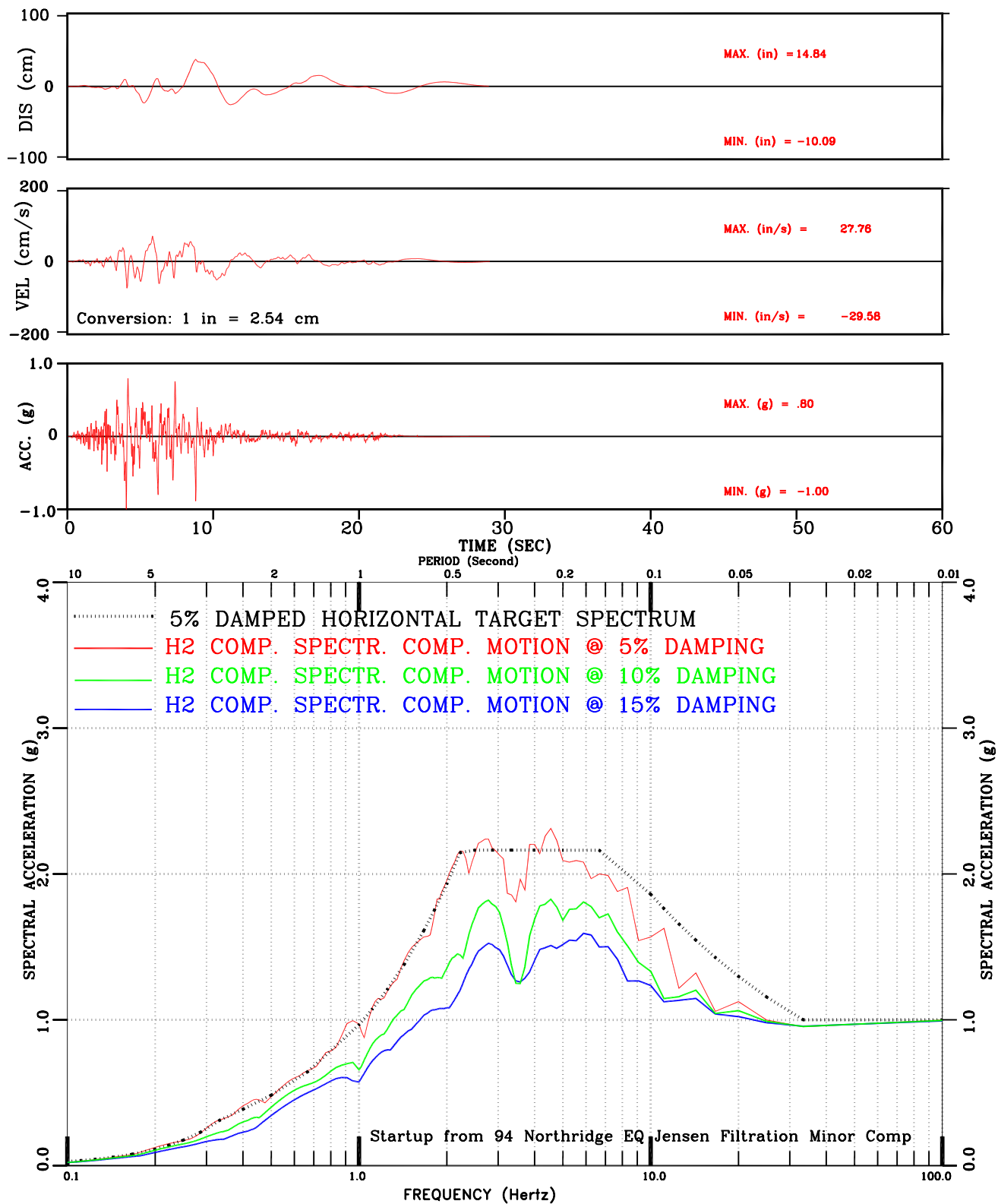


Figure III-38: Set-4 H2 Comp Motion Conforming to NUREG/CR-0098 Spectral Shape

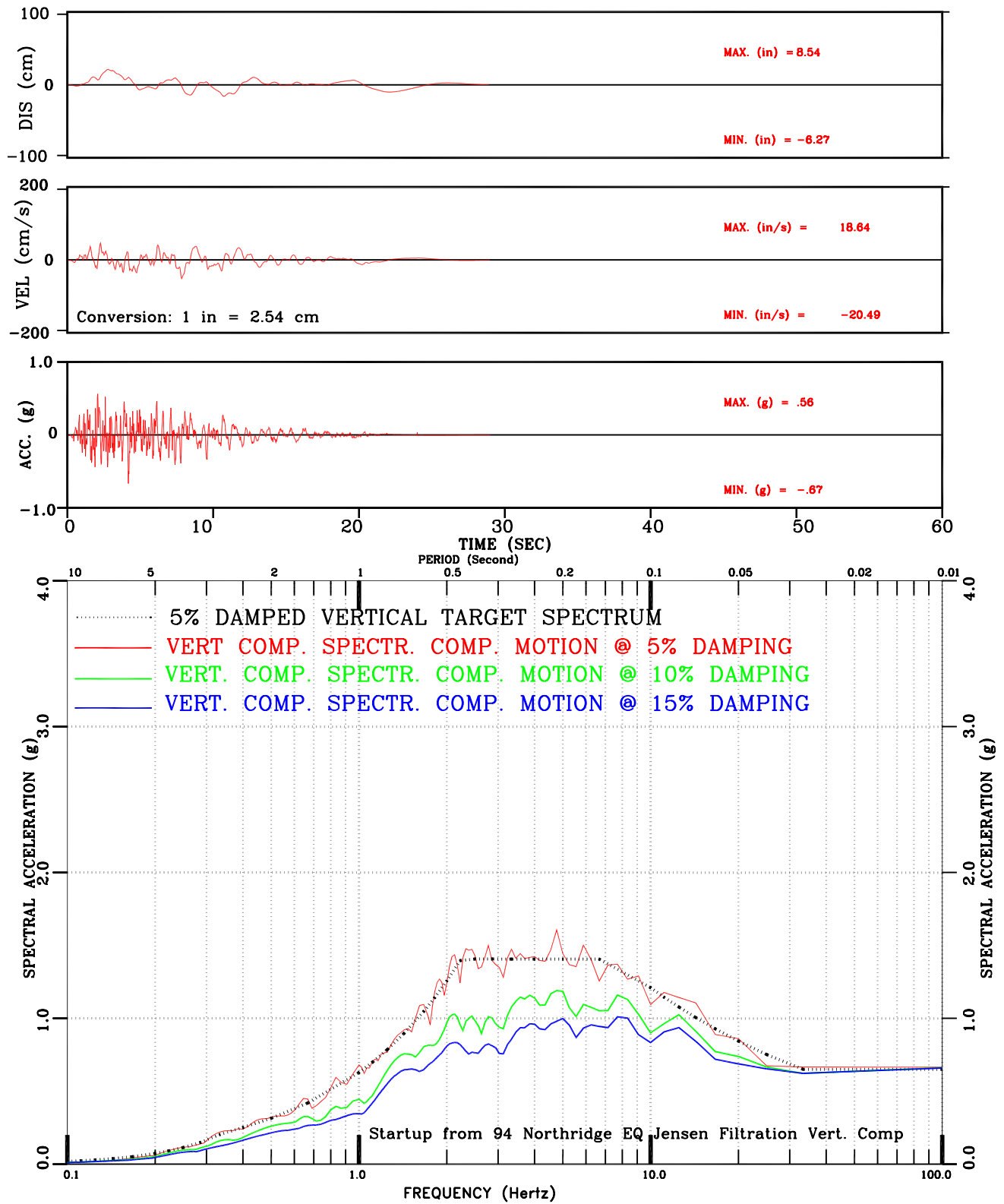


Figure III-39: Set-4 Vert Comp Motion Conforming to NUREG/CR-0098 Spectral Shape

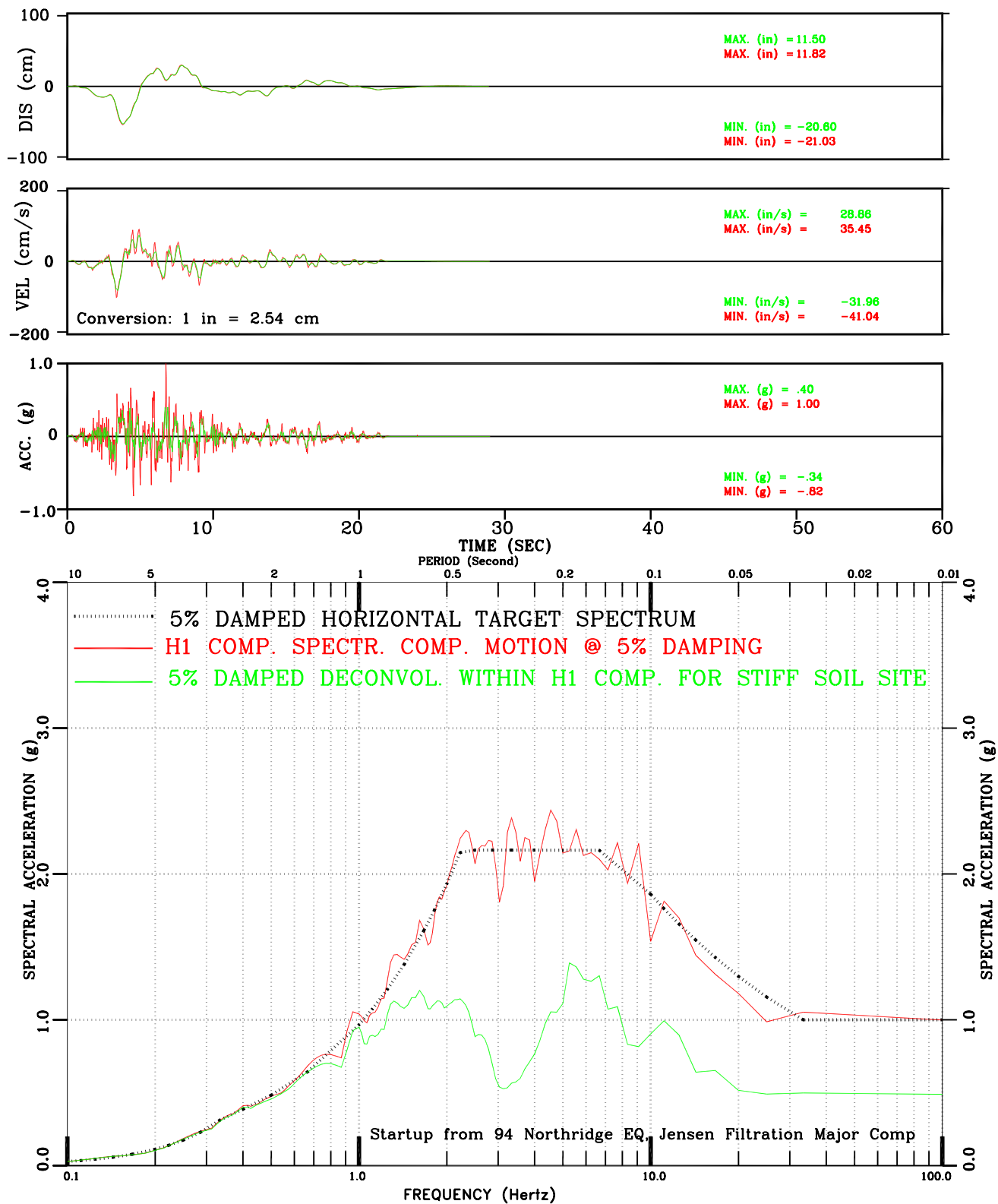


Figure III-40: Deconvolved Within vs. Surface Motion for Stiff Soil Set-4 H1 Comp. Motion Conforming to NUREG/CR-0098 Spectral Shape

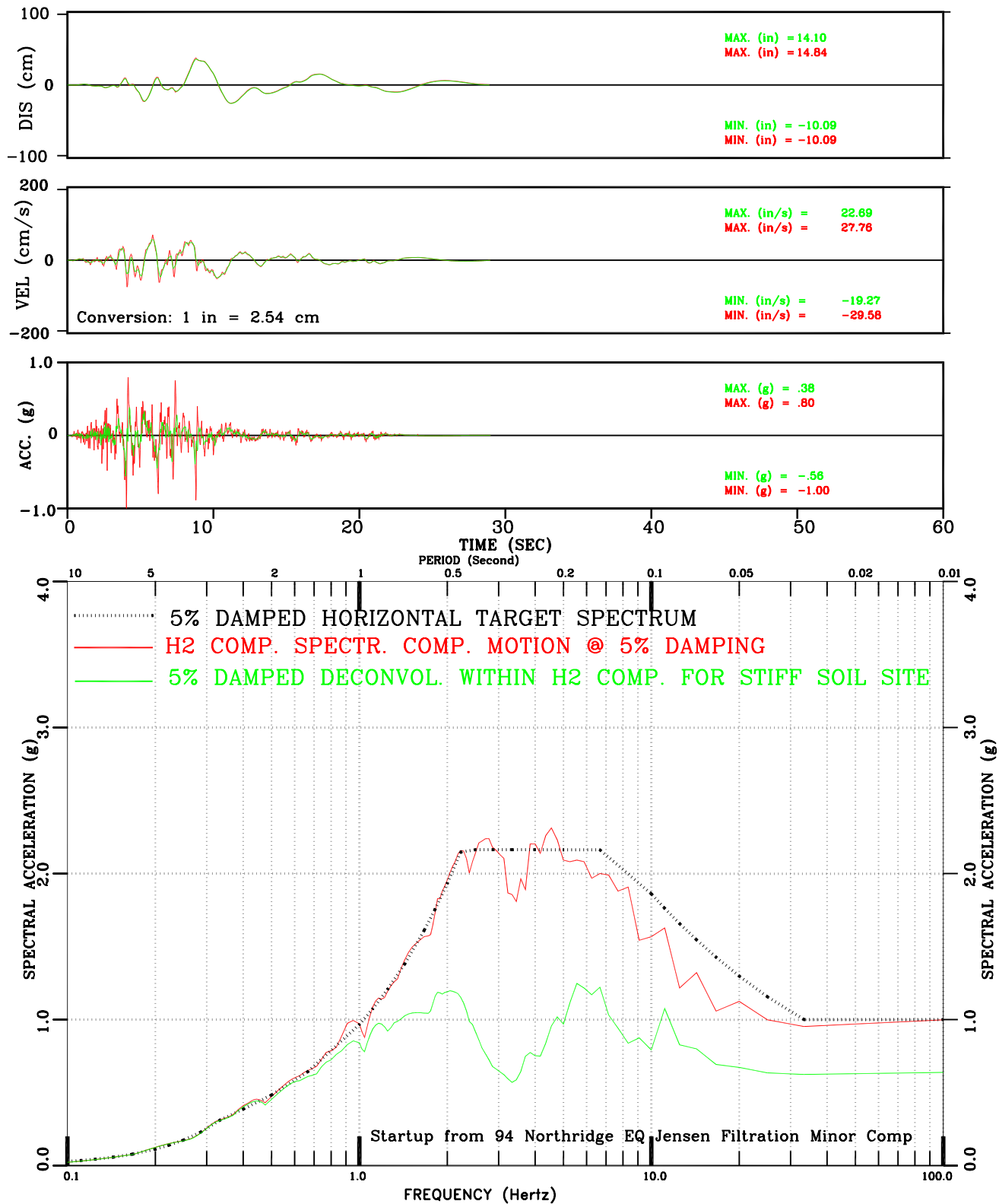


Figure III-41: Deconvolved Within vs. Surface Motion for Stiff Soil Set-4 H2 Comp. Motion Conforming to NUREG/CR-0098 Spectral Shape

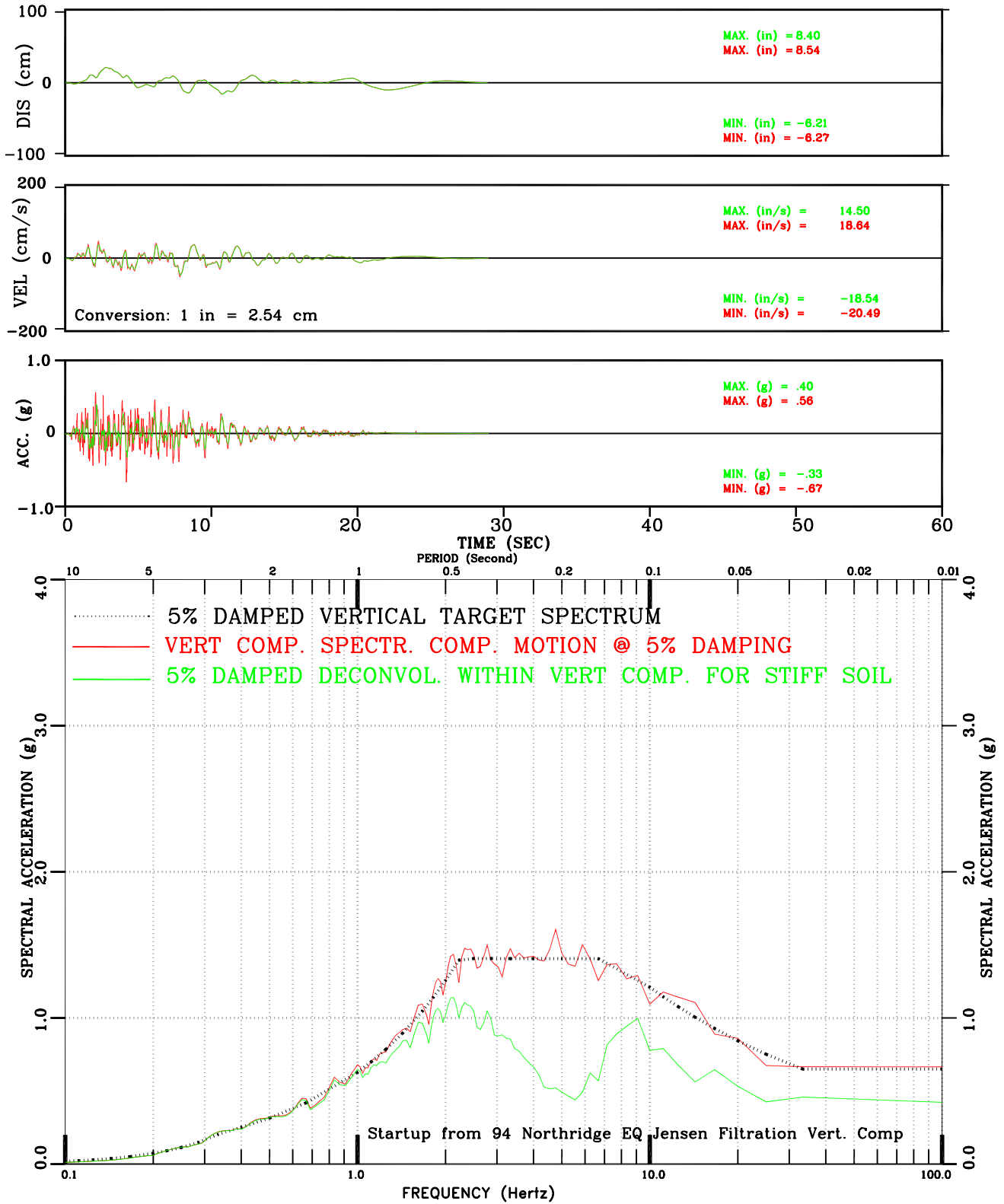


Figure III-42: Deconvolved Within vs. Surface Motion for Stiff Soil Set-4 Vert Comp. Motion Conforming to NUREG/CR-0098 Spectral Shape

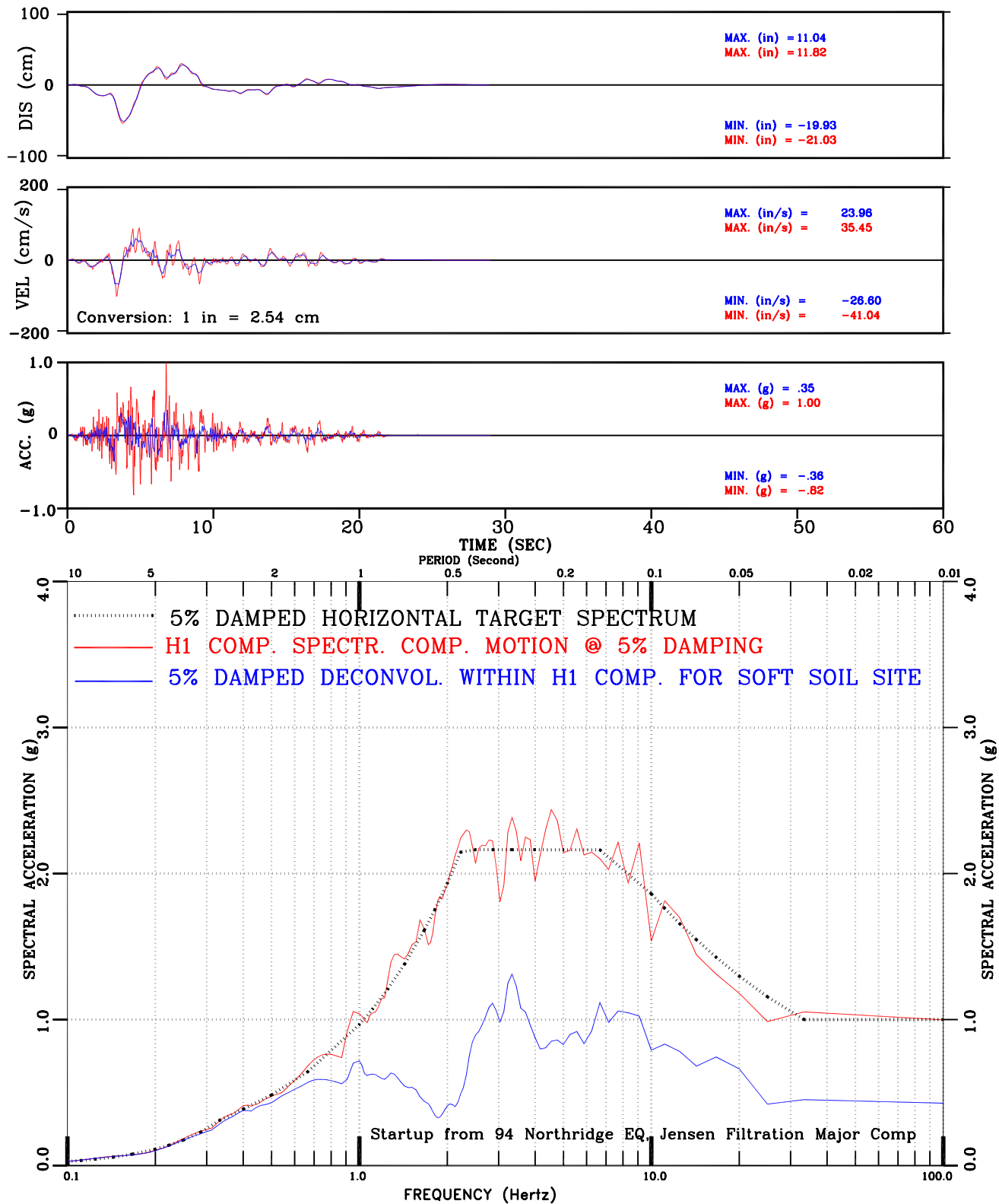


Figure III-43: Deconvolved Within vs. Surface Motion for Soft Soil Set-4 H1 Comp. Motion Conforming to NUREG/CR-0098 Spectral Shape

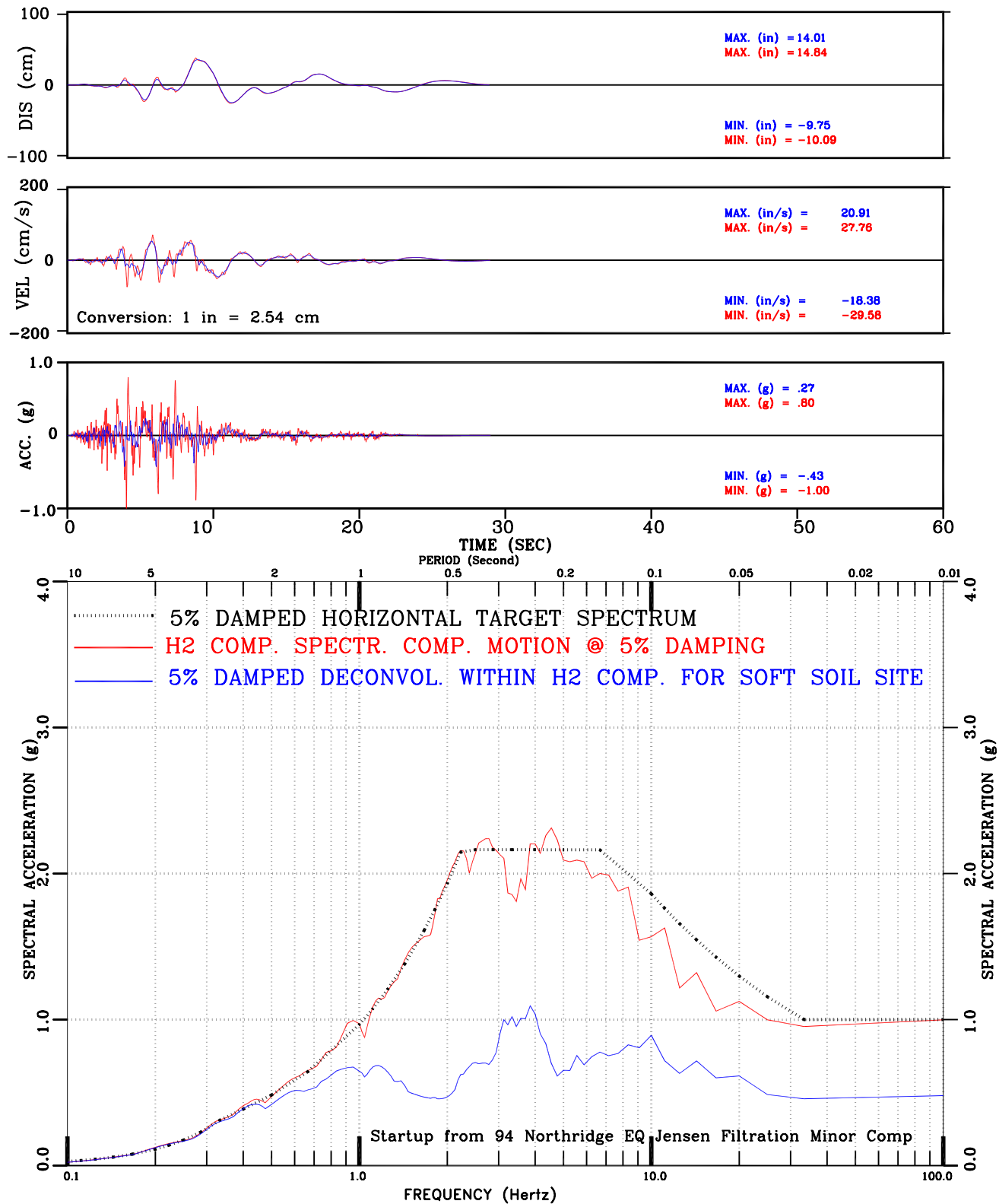


Figure III-44: Deconvolved Within vs. Surface Motion for Soft Soil Set-4 H2 Comp. Motion Conforming to NUREG/CR-0098 Spectral Shape

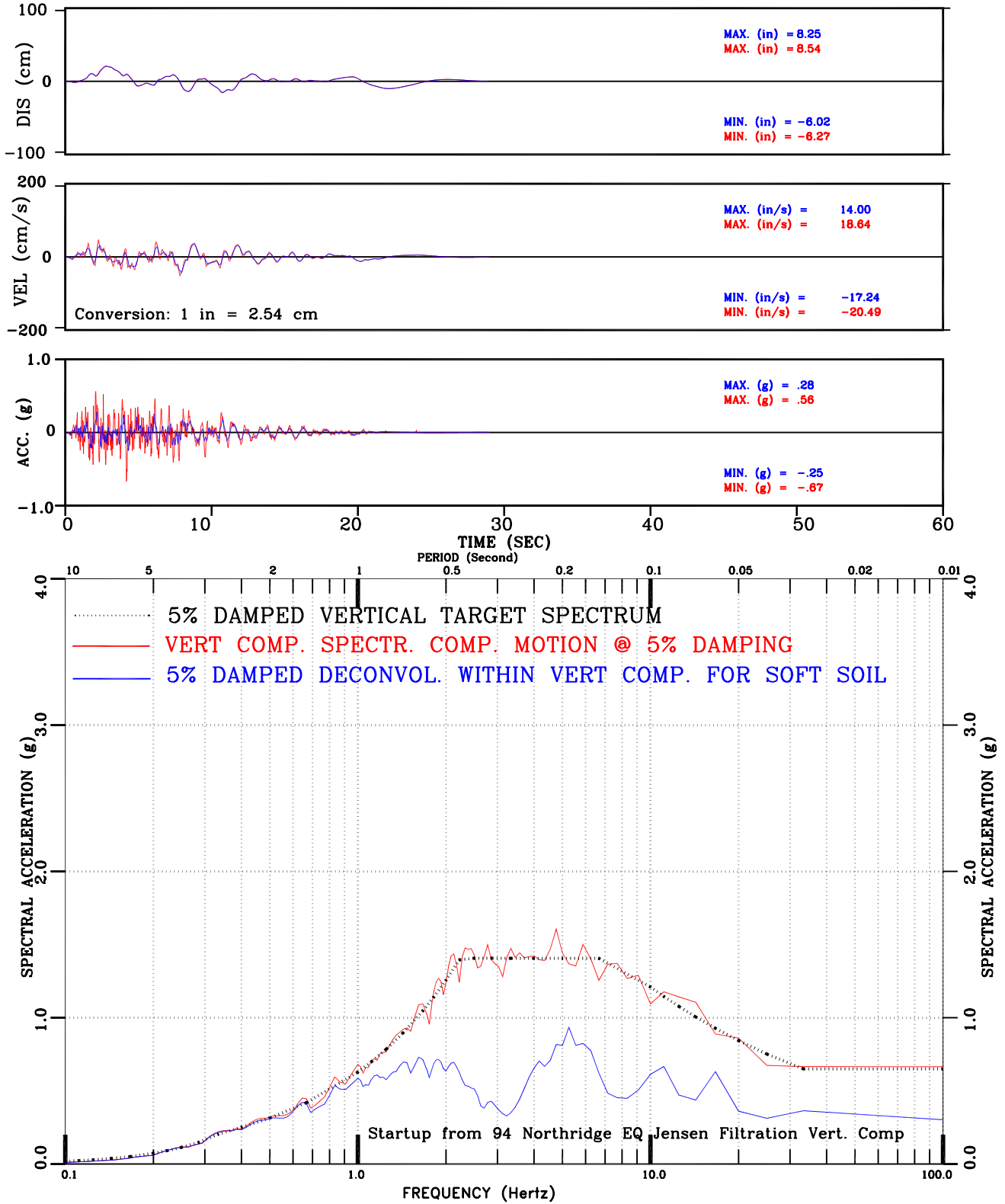


Figure III-45: Deconvolved Within vs. Surface Motion for Soft Soil Set-4 Vert Comp. Motion Conforming to NUREG/CR-0098 Spectral Shape

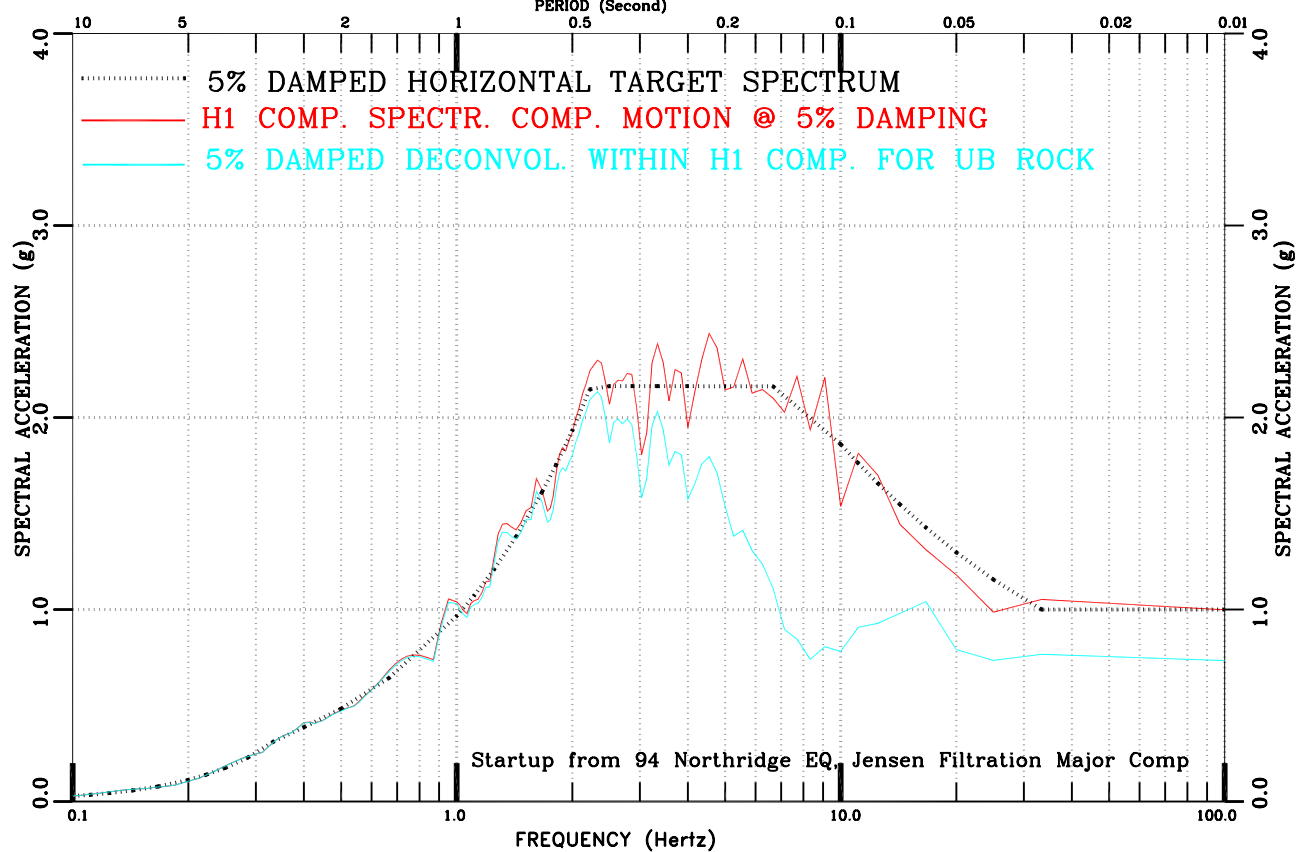
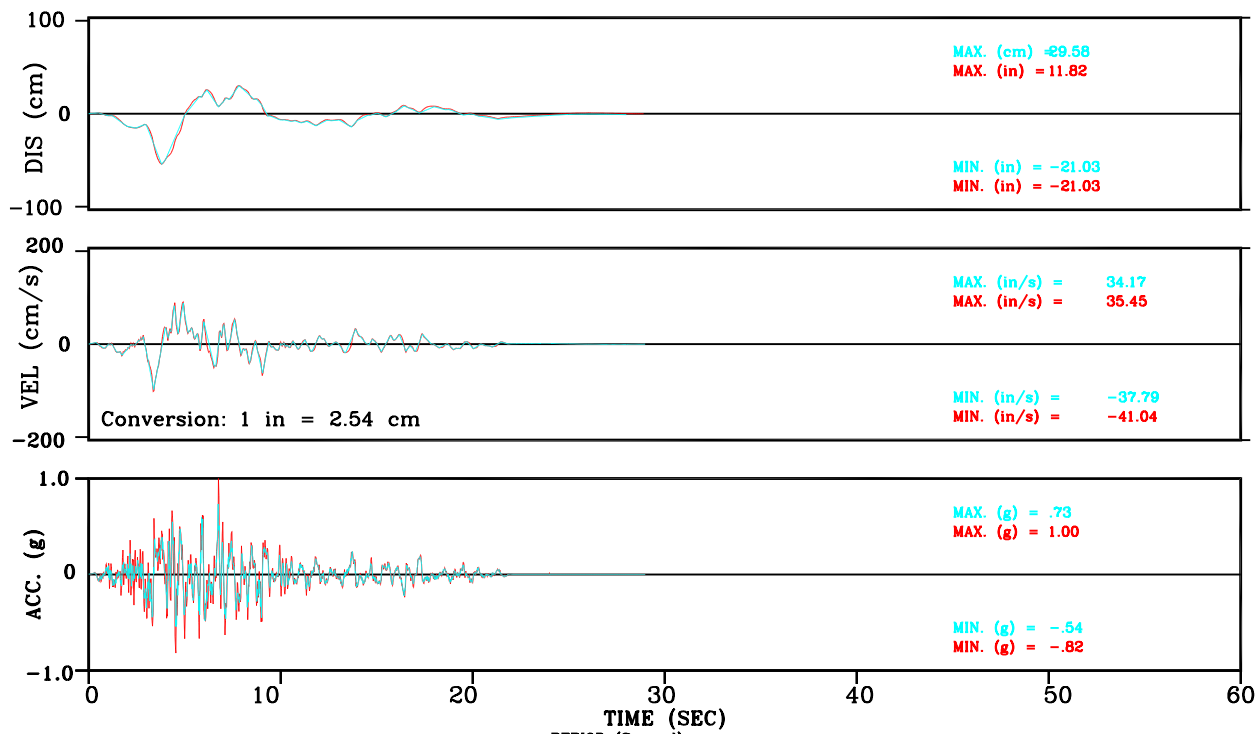


Figure III-46: Deconvolved Within vs. Surface Motion for UB Rock Set-4 H1 Comp. Motion Conforming to NUREG/CR-0098 Spectral Shape

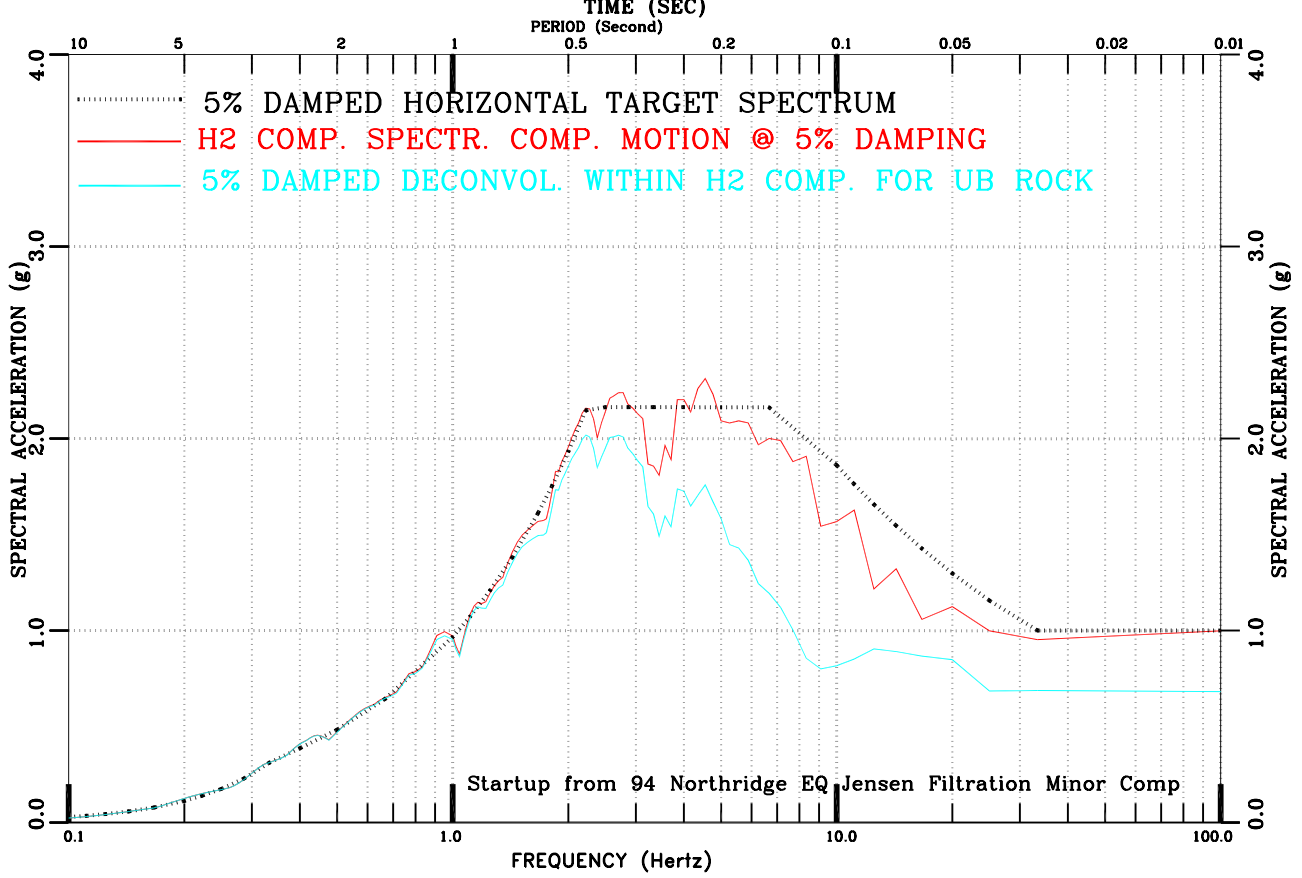
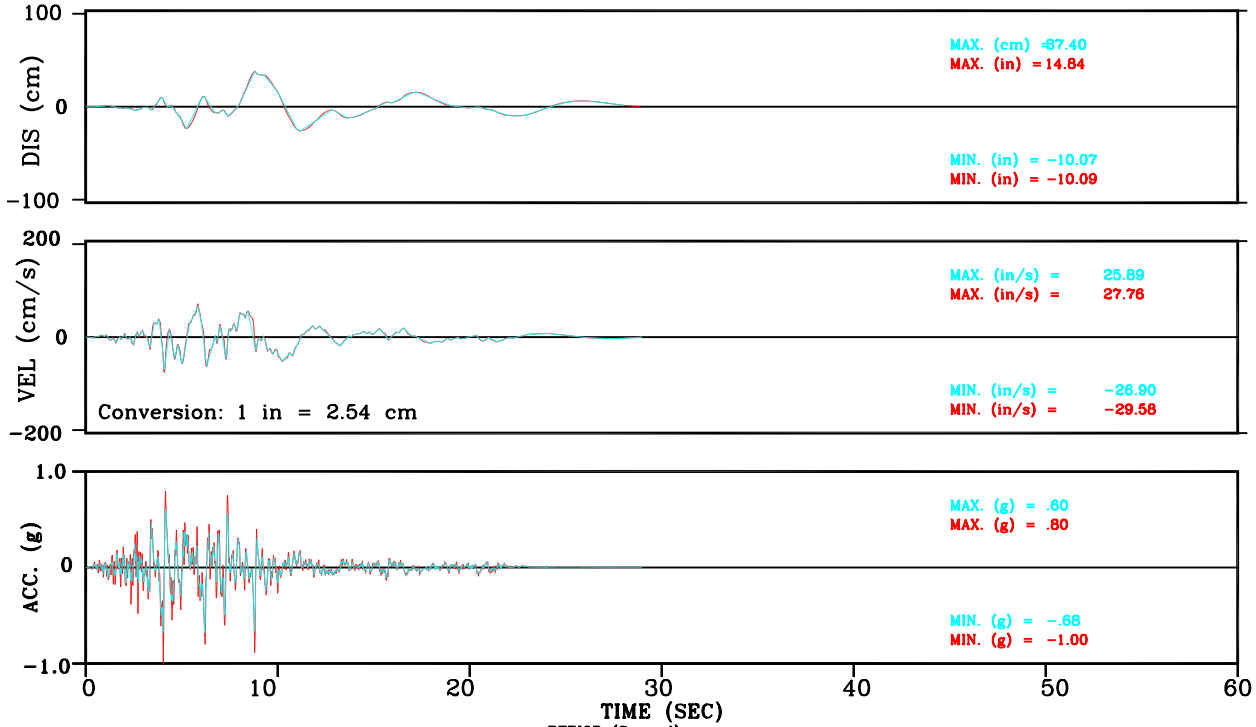


Figure III-47: Deconvolved Within vs. Surface Motion for UB Rock Set-4 H2 Comp. Motion Conforming to NUREG/CR-0098 Spectral Shape

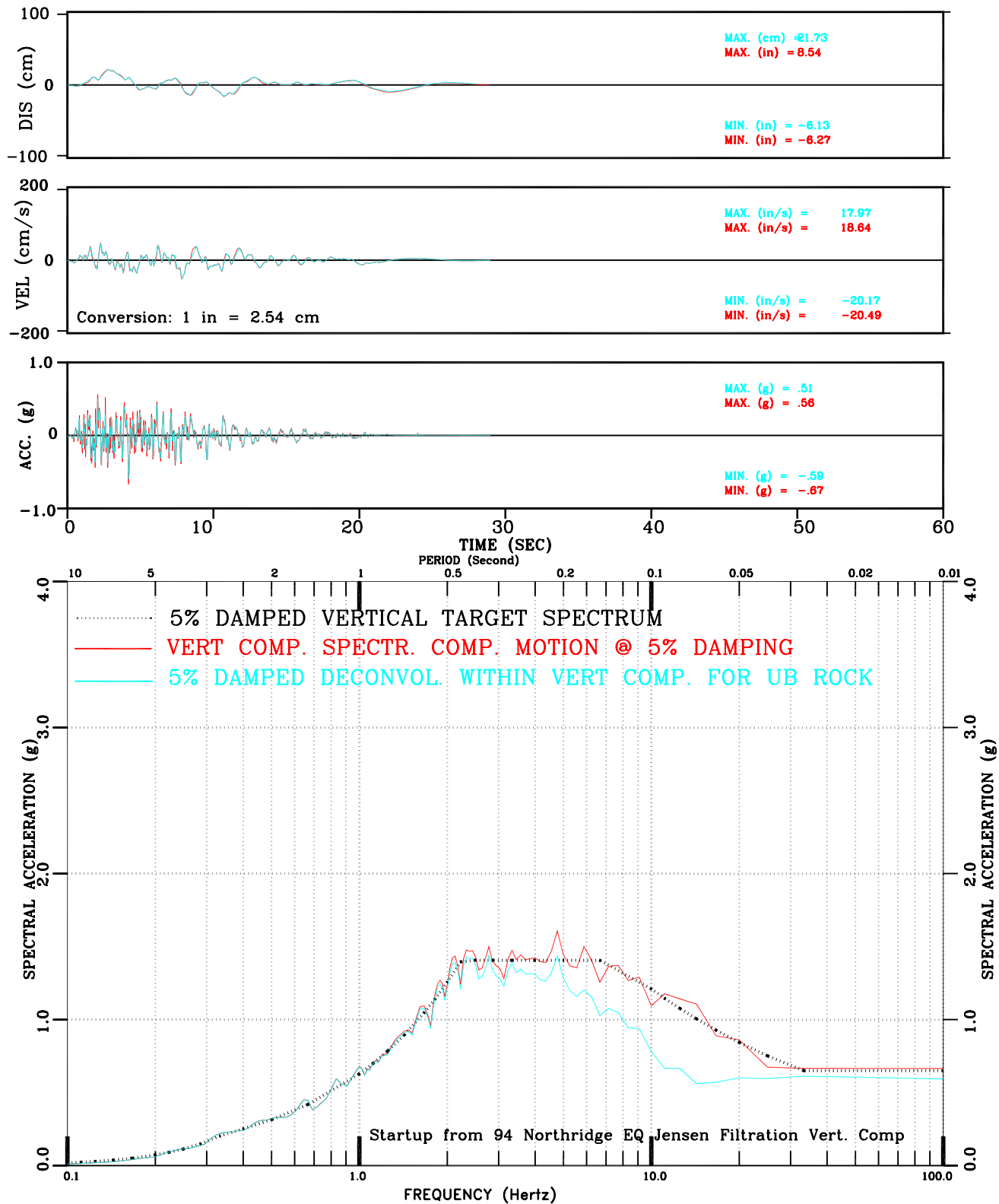


Figure III-48: Deconvolved Within vs. Surface Motion for UB Rock Set-4 Vert Comp. Motion Conforming to NUREG/CR-0098 Spectral Shape

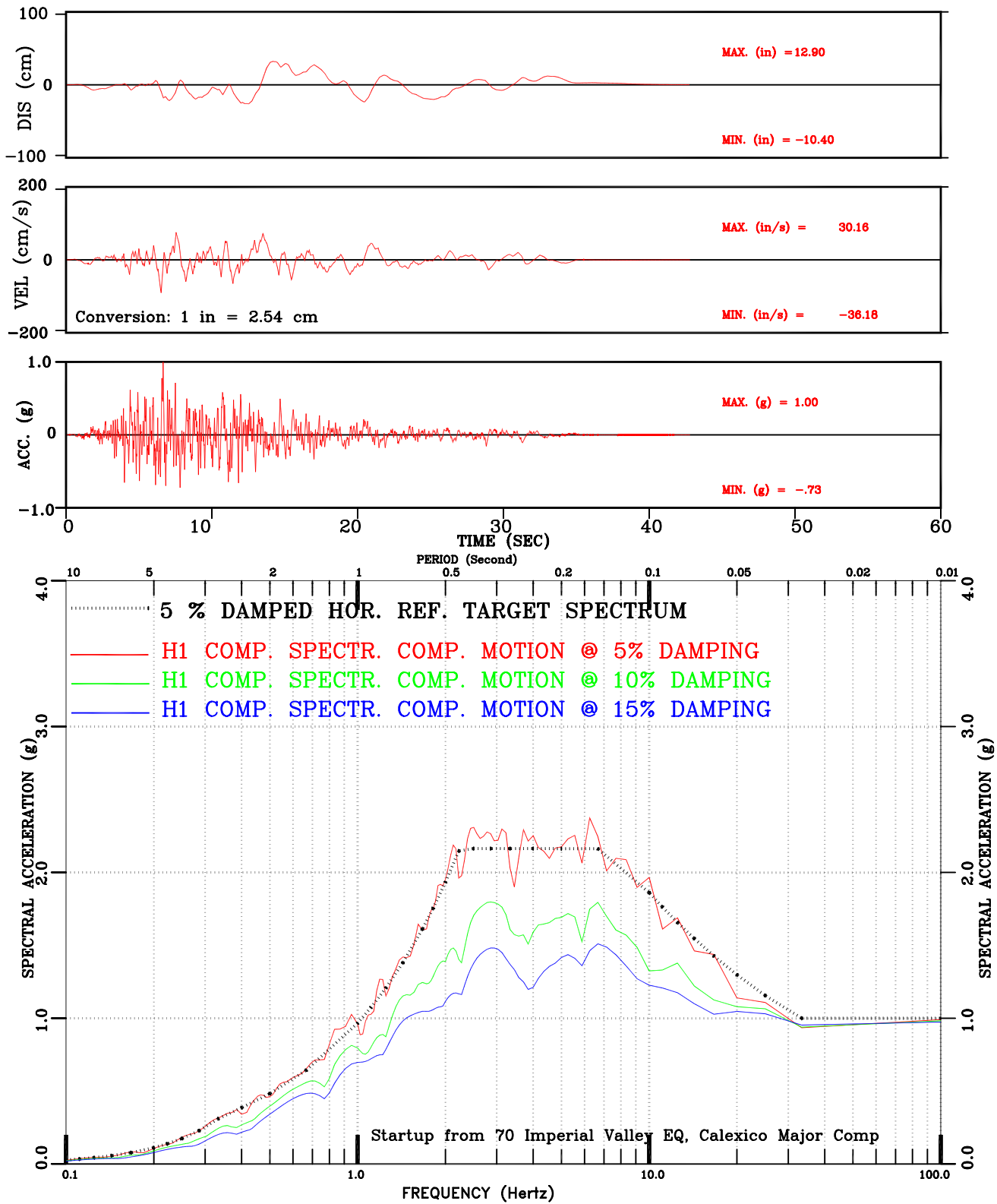


Figure III-49: Set-5 H1 Comp. Motion Conforming to NUREG/CR-0098 Spectral Shape

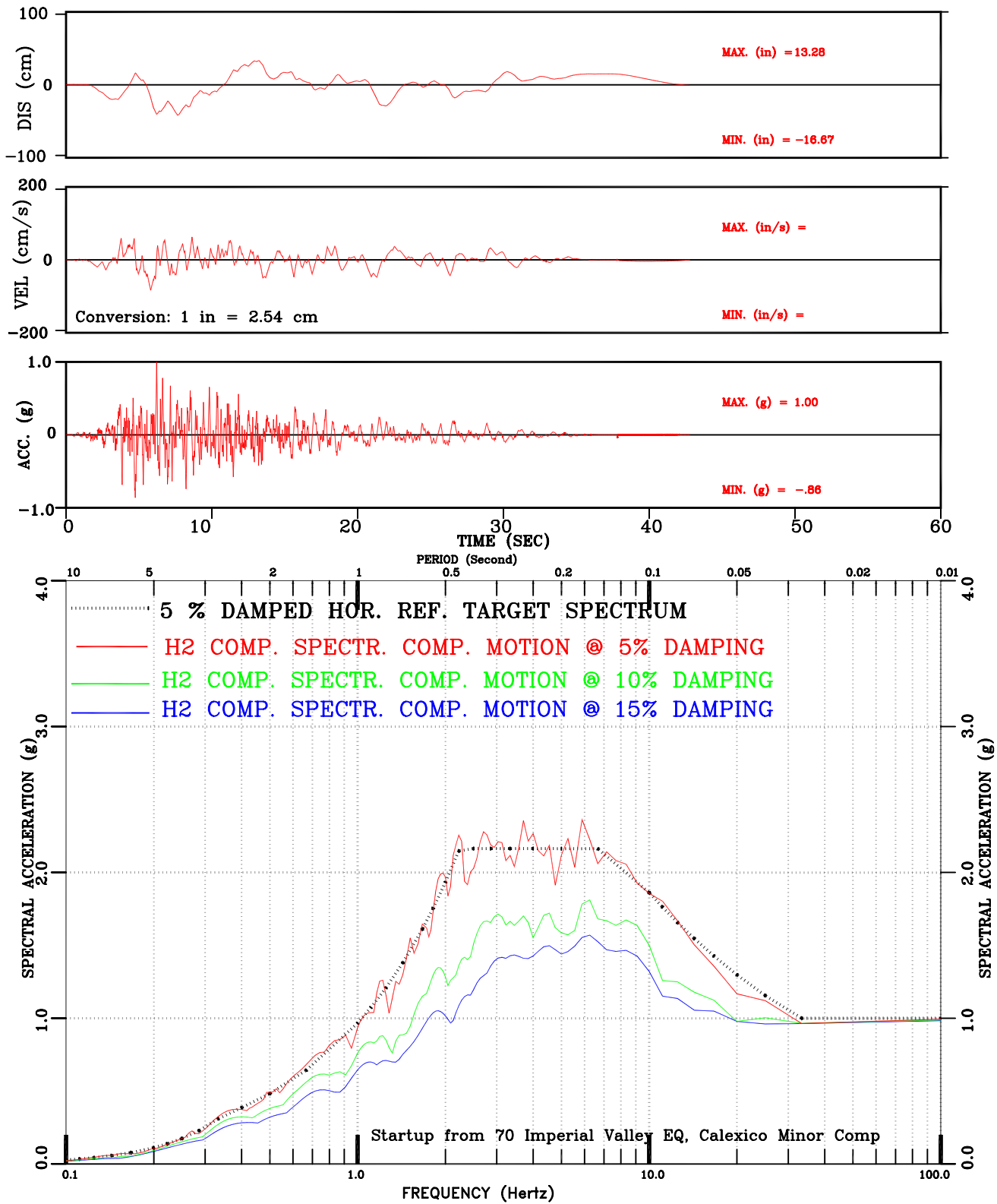


Figure III-50: Set-5 H2 Comp. Motion Conforming to NUREG/CR-0098 Spectral Shape

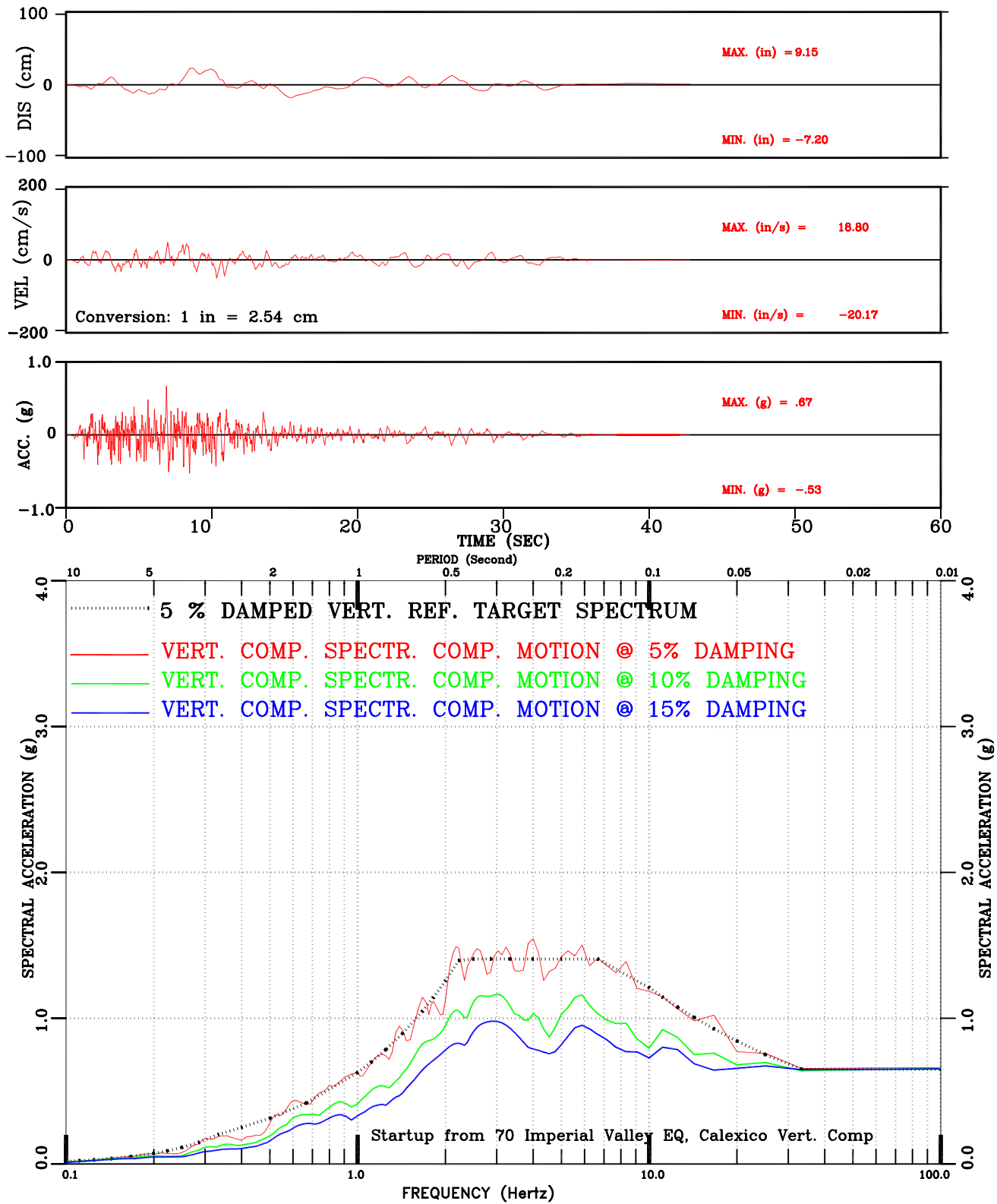


Figure III-51: Set-5 VERT Motion Conforming to NUREG/CR-0098 Spectral Shape

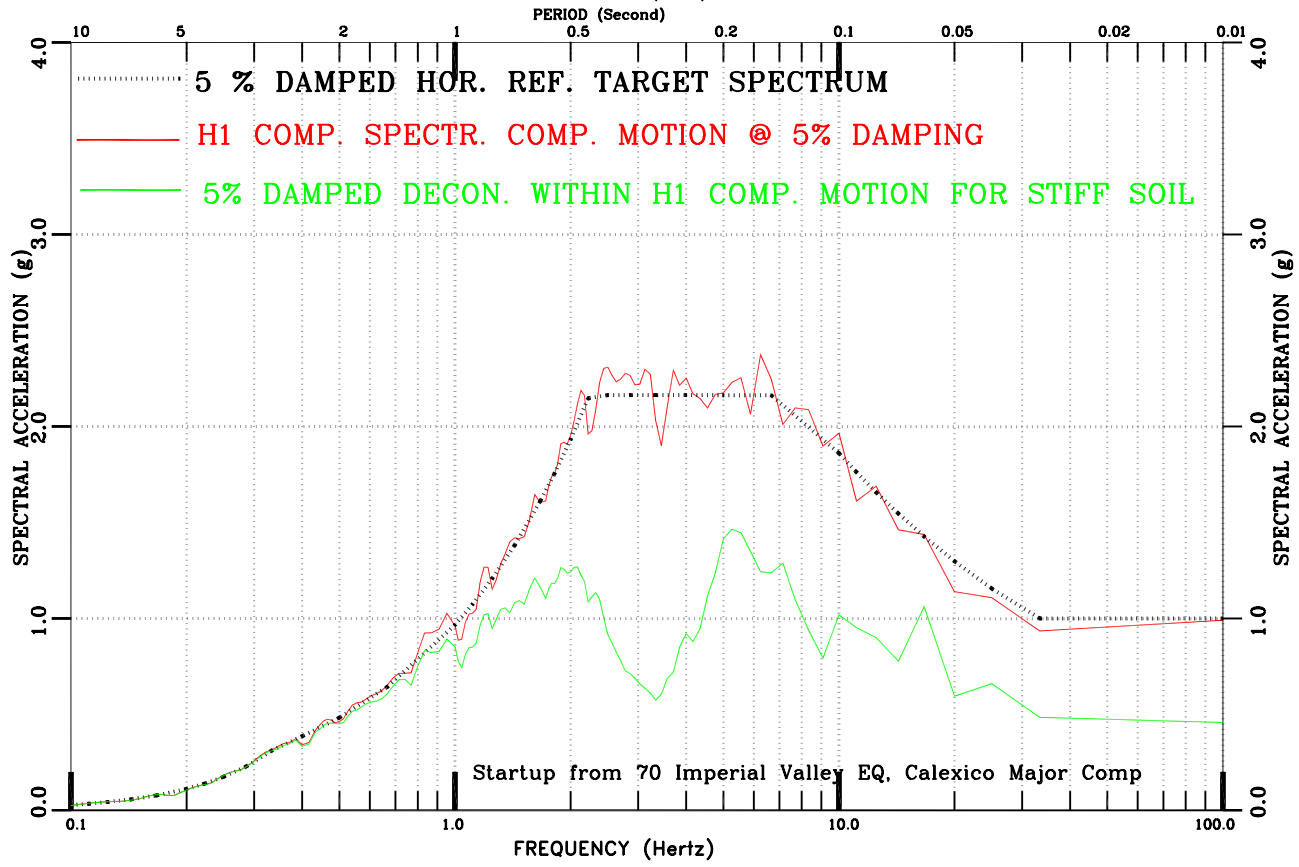
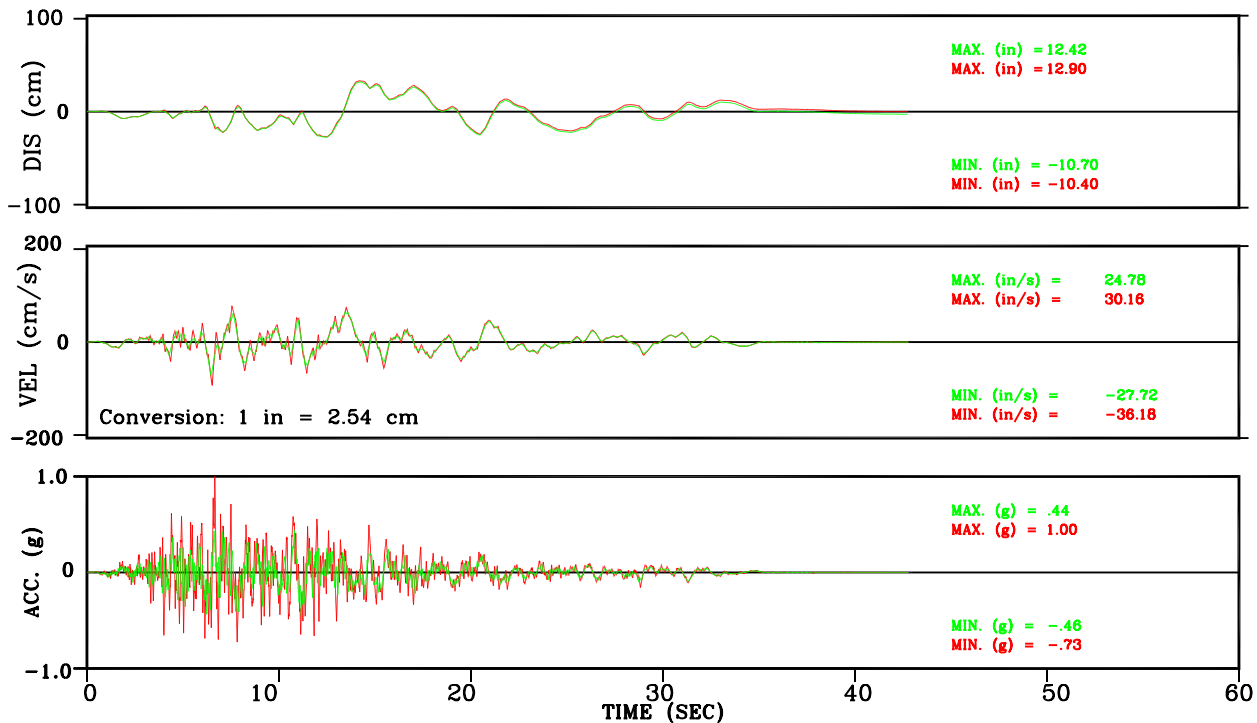


Figure III-52: Deconvolved Within vs. Surface Motion for Stiff Soil Set-5 H1 Comp. Motion Conforming to NUREG/CR-0098 Spectral Shape

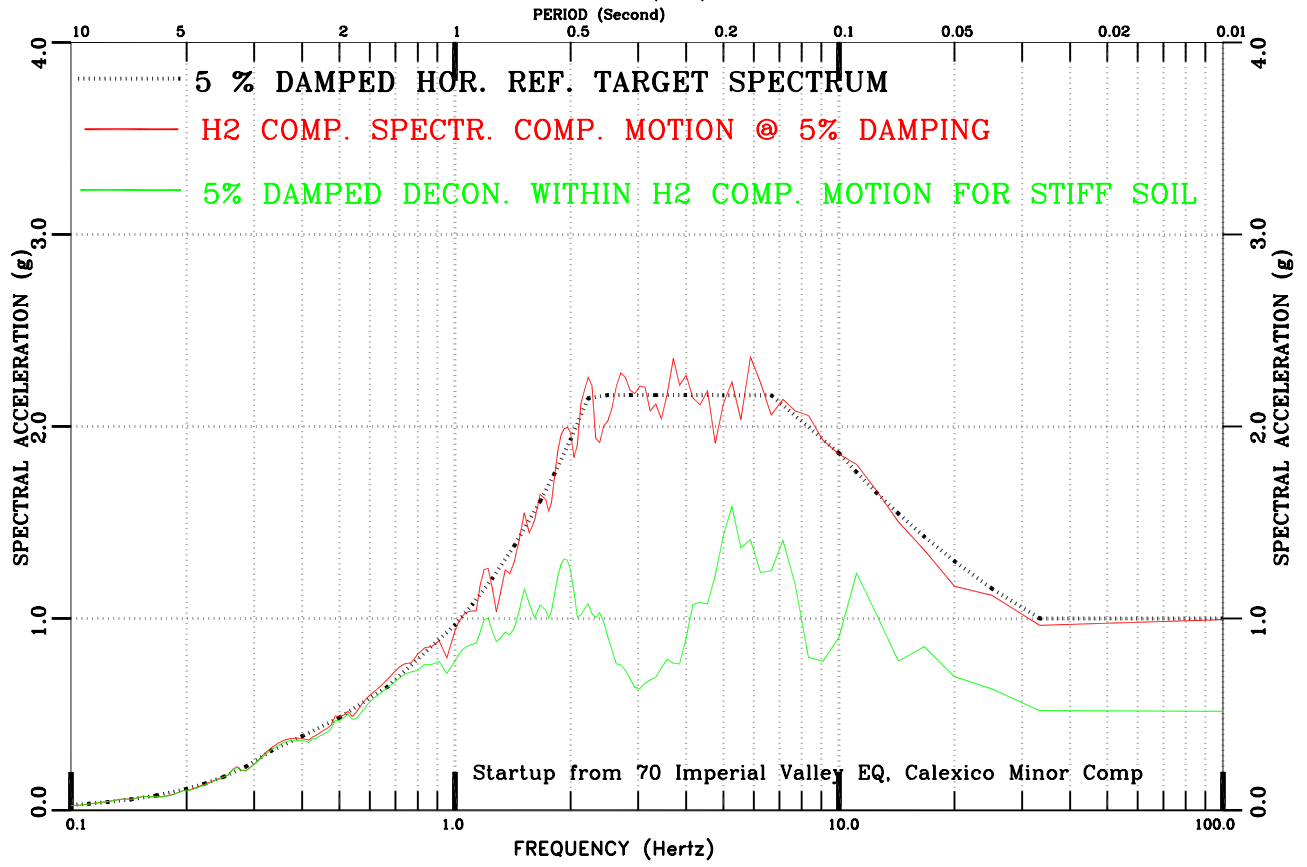
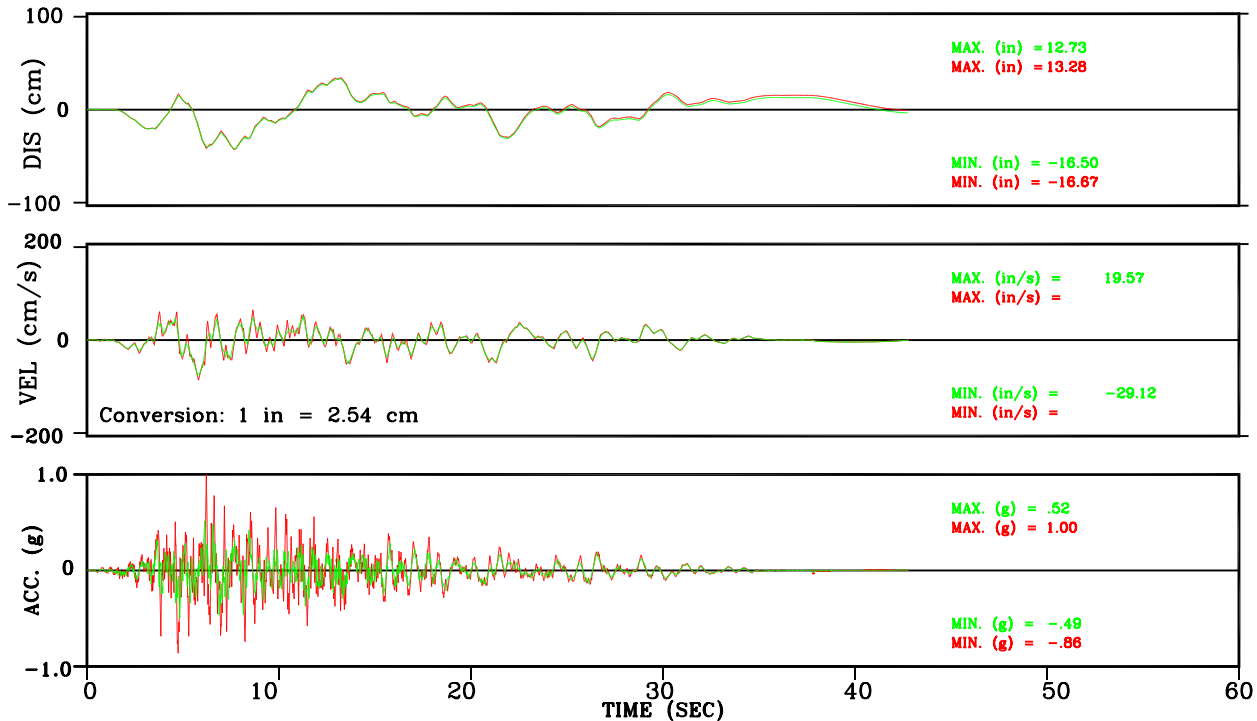


Figure III-53: Deconvolved Within vs. Surface Motion for Stiff Soil Set-5 H2 Comp. Motion Conforming to NUREG/CR-0098 Spectral Shape

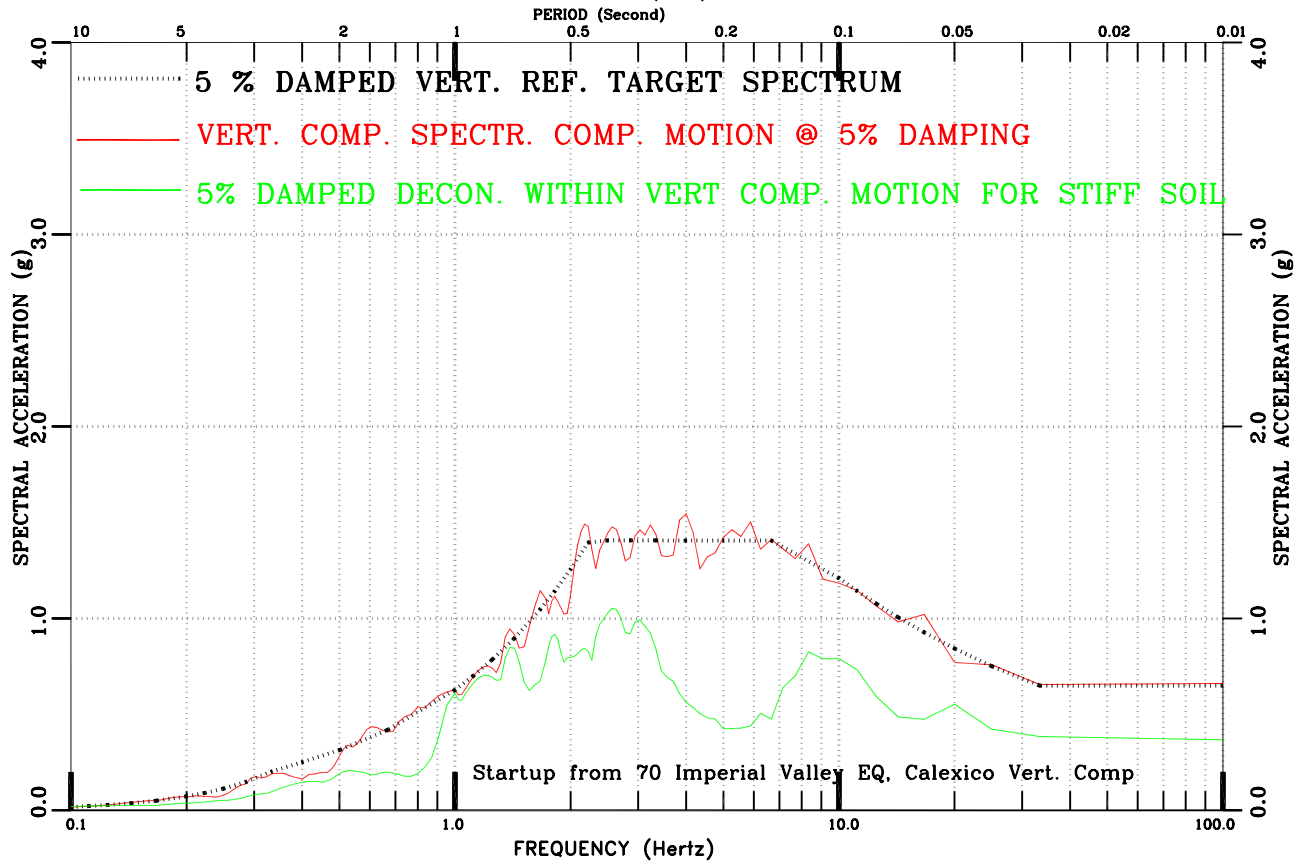
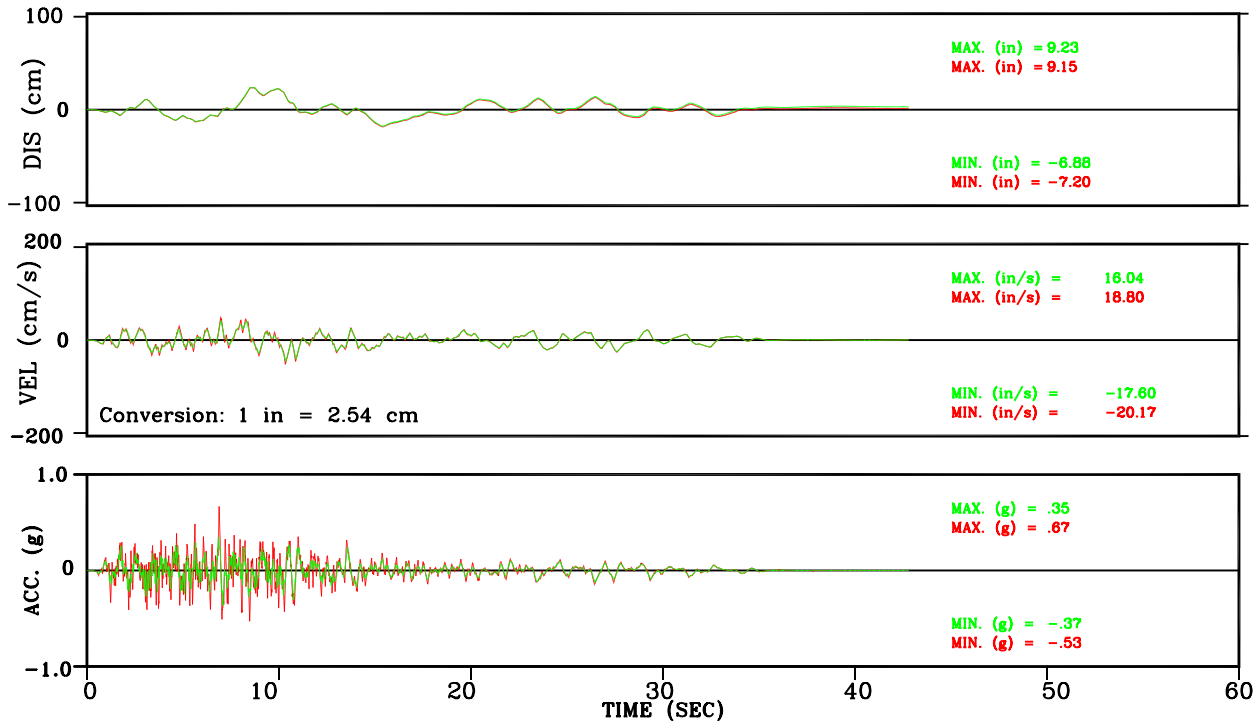


Figure III-54: Deconvolved Within vs. Surface Motion for Stiff Soil Set-5 VERT Comp. Motion Conforming to NUREG/CR-0098 Spectral Shape

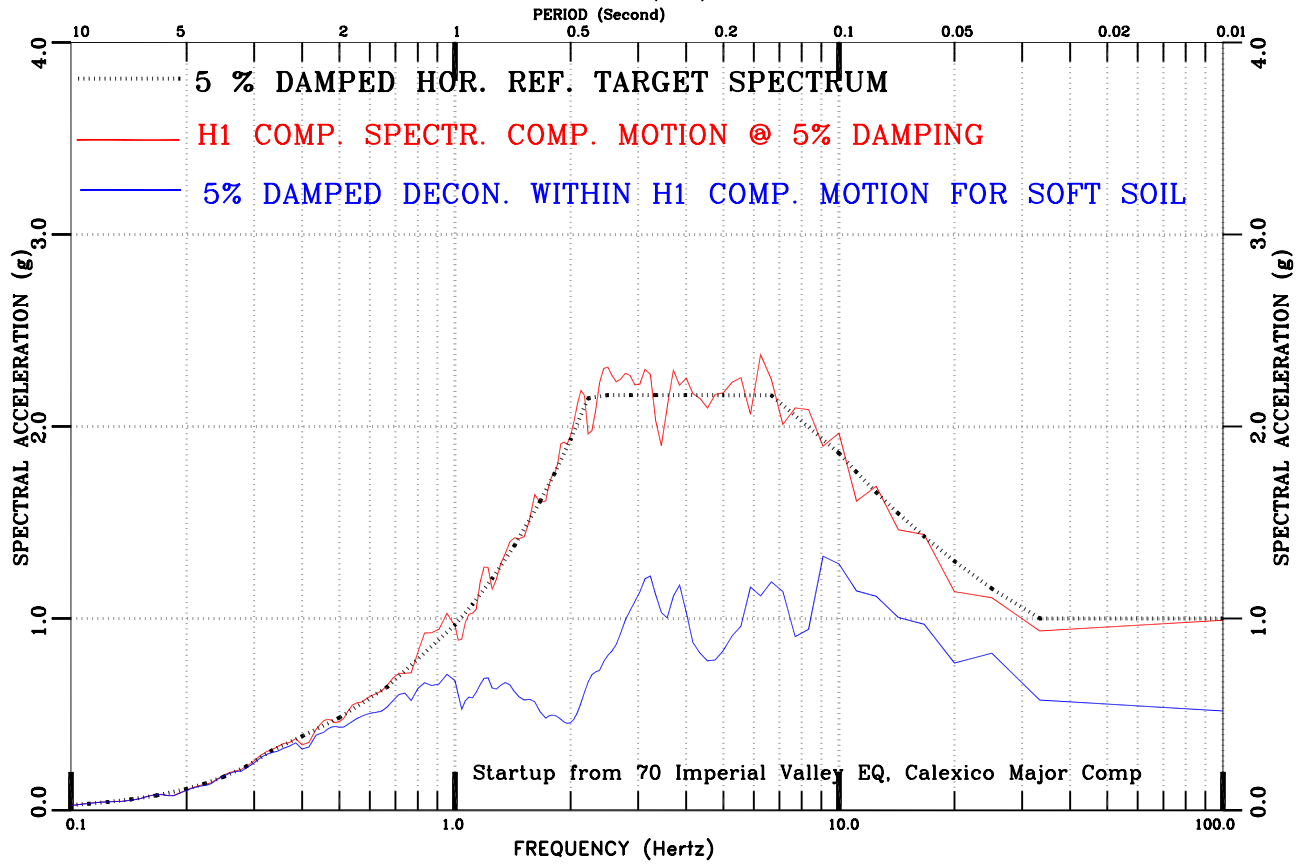
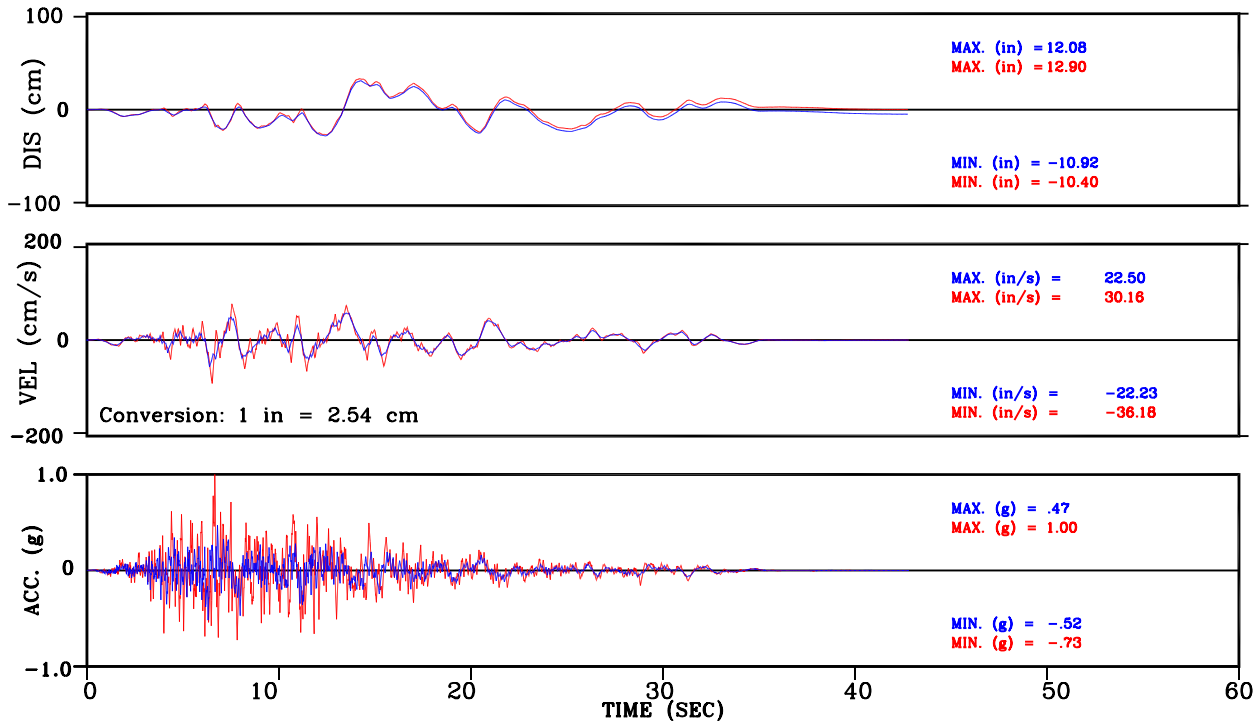


Figure III-55: Deconvolved Within vs. Surface Motion for Soft Soil Set-5 H1 Comp. Motion Conforming to NUREG/CR-0098 Spectral Shape

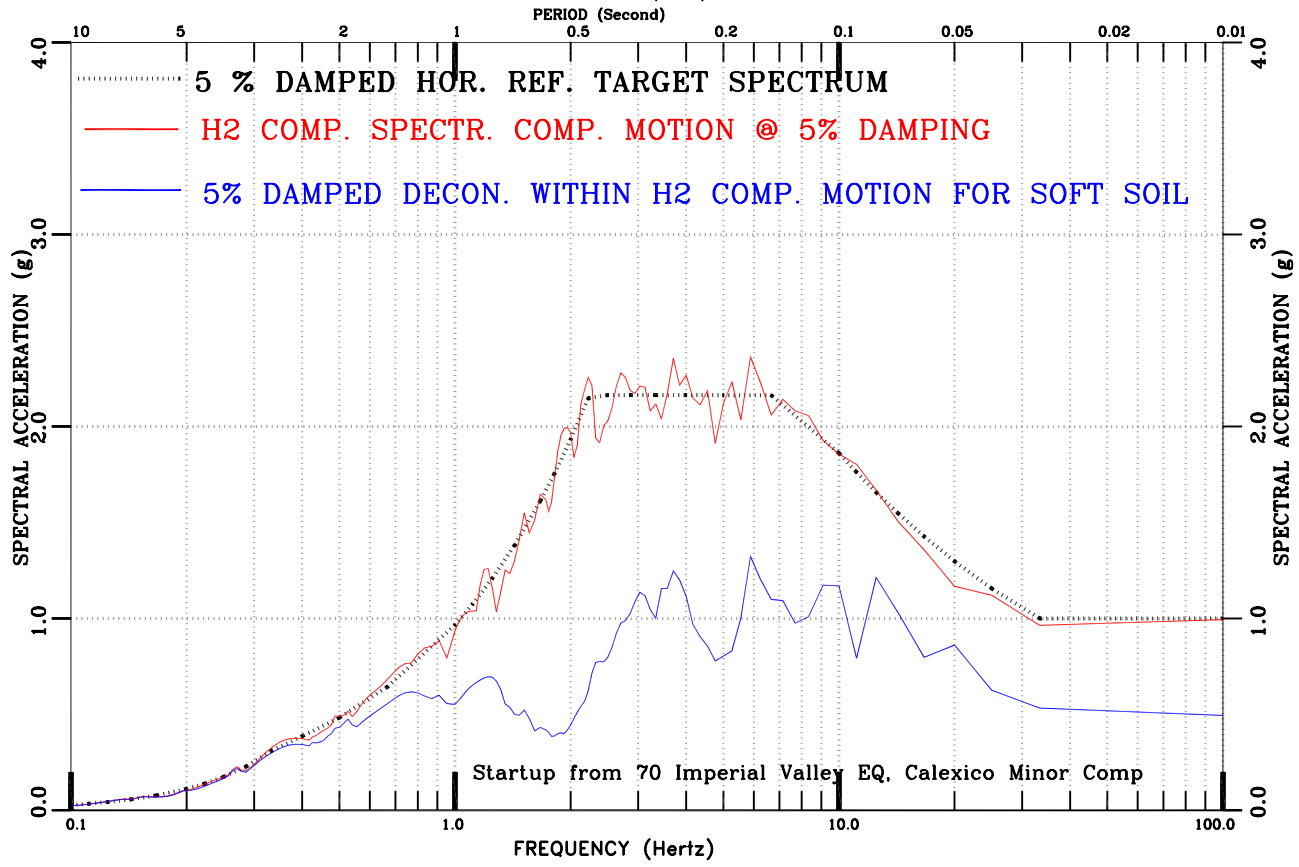
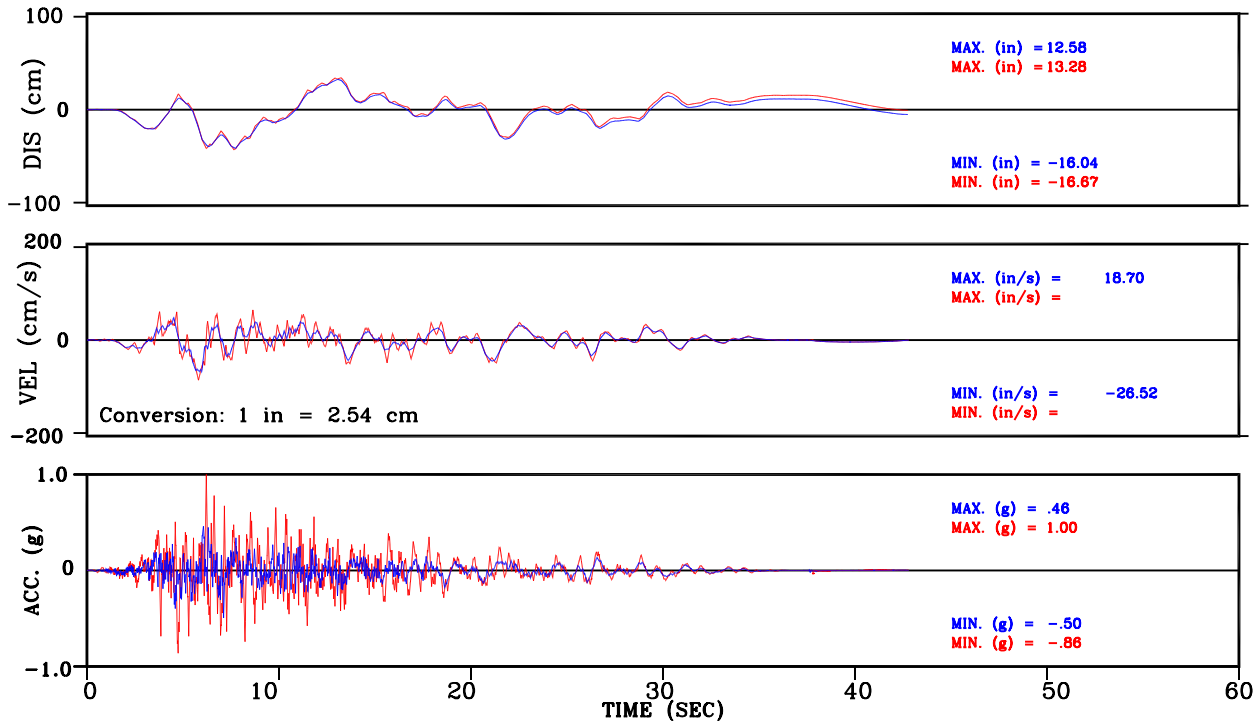


Figure III-56: Deconvolved Within vs. Surface Motion for Soft Soil Set-5 H2 Comp. Motion Conforming to NUREG/CR-0098 Spectral Shape

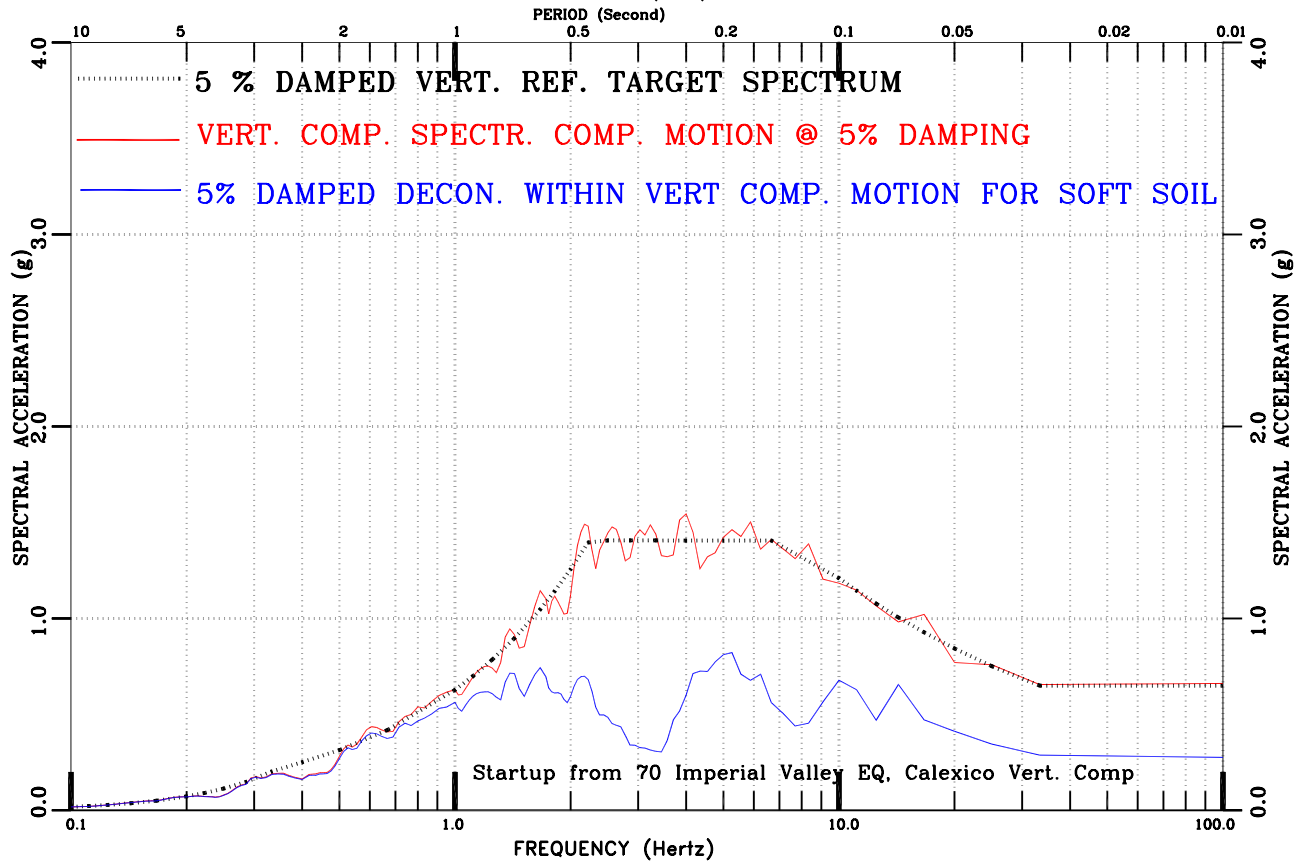
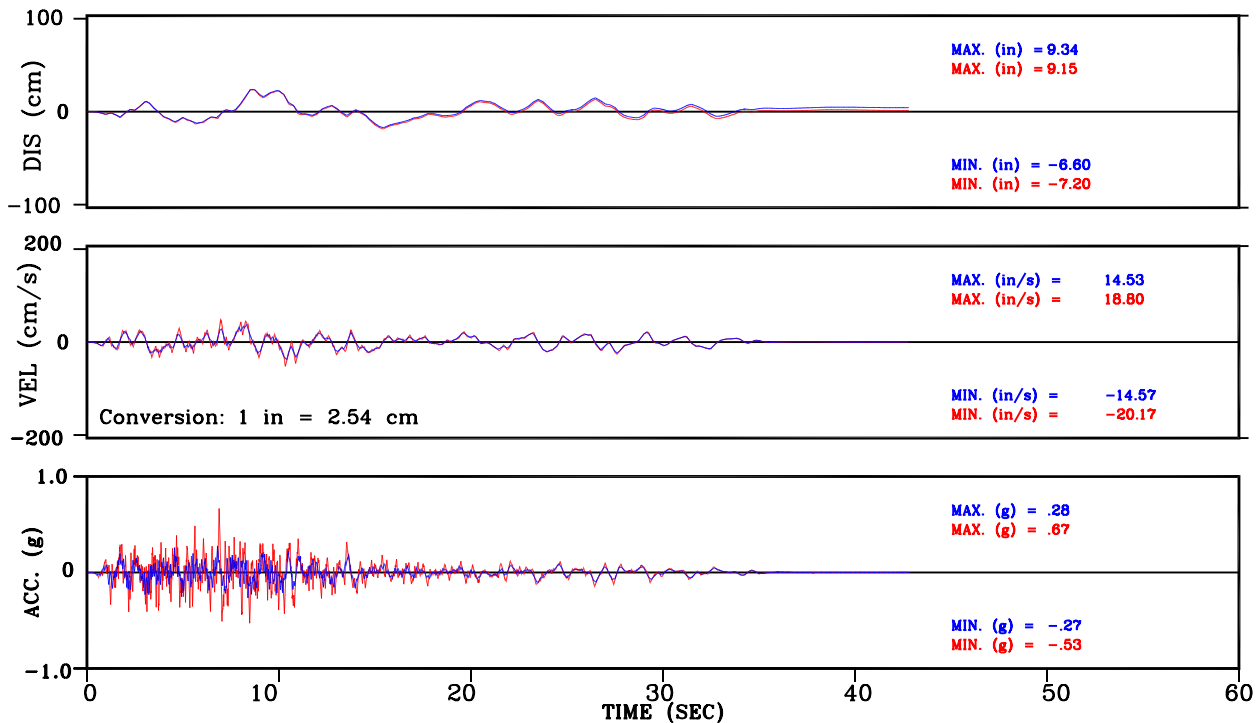


Figure III-57: Deconvolved Within vs. Surface Motion for Soft Soil Set-5 VERT Comp. Motion Conforming to NUREG/CR-0098 Spectral Shape

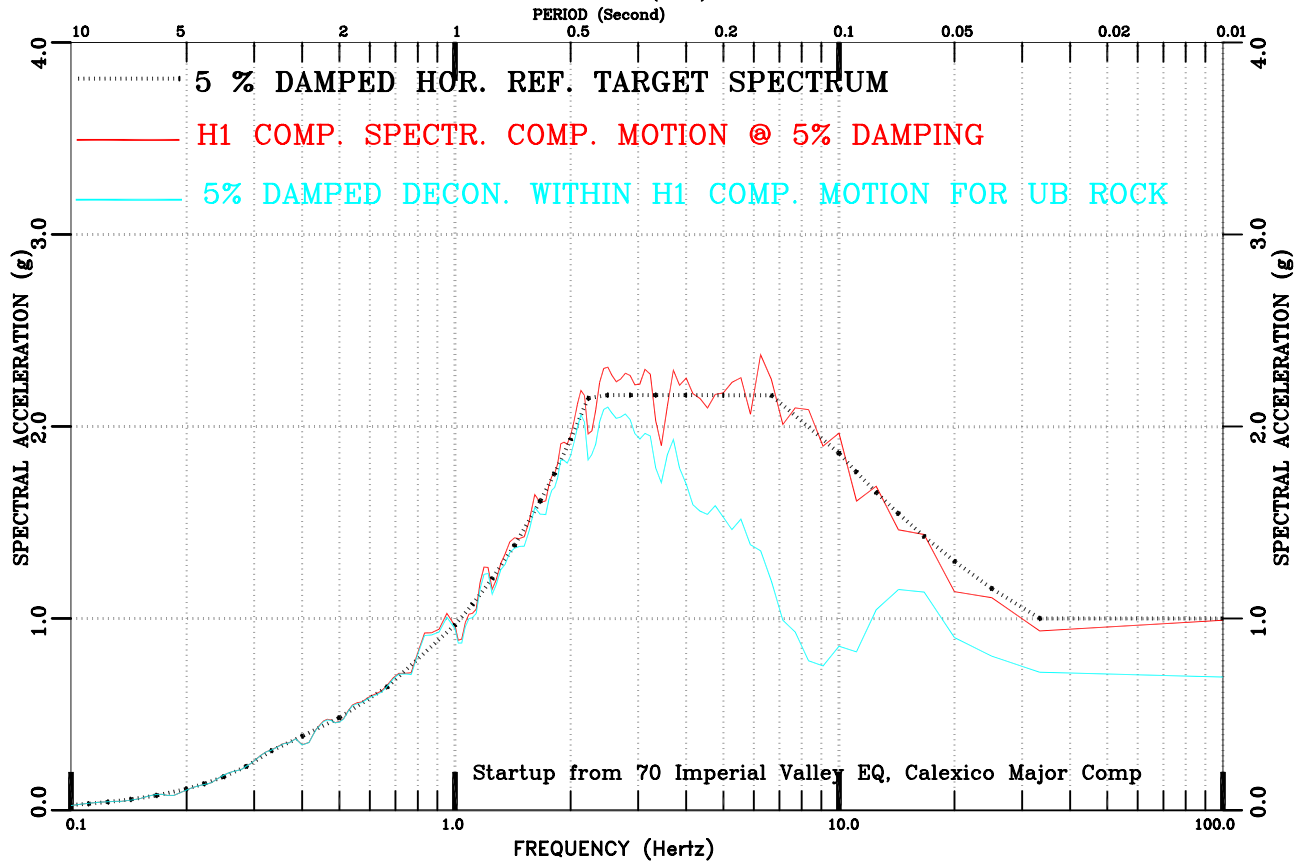
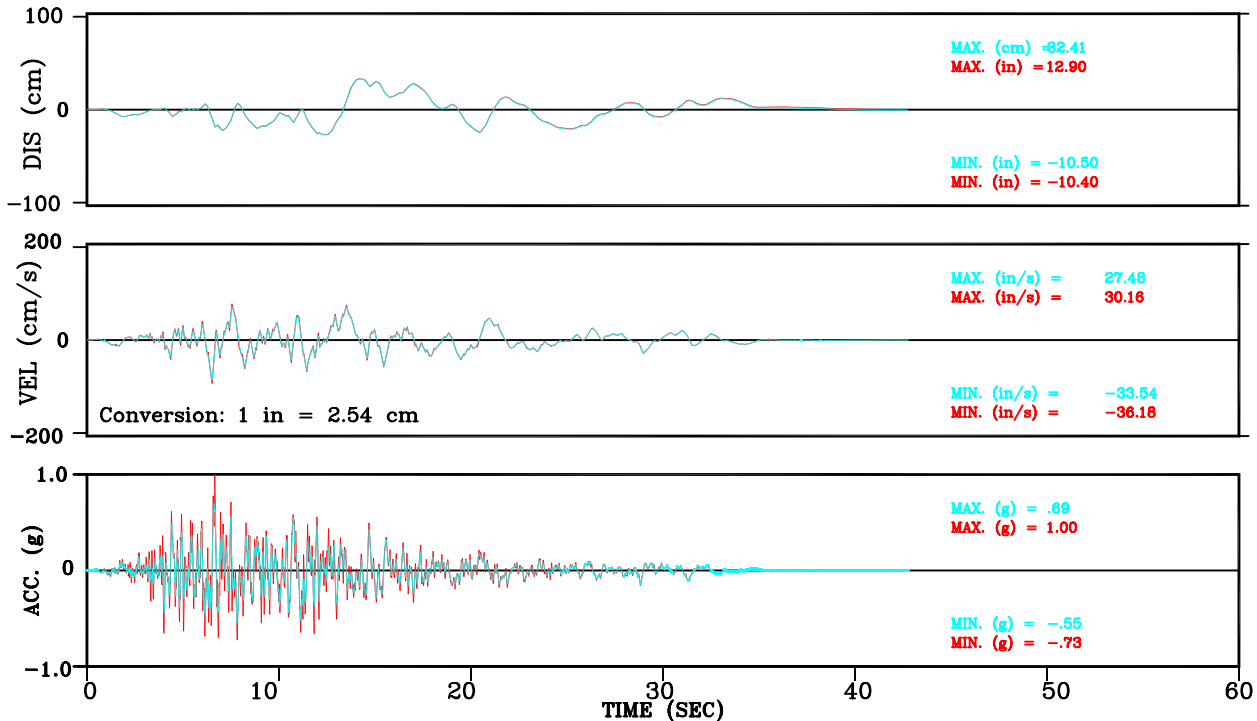


Figure III-58: Deconvolved Within vs. Surface Motion for UB Rock Set-5 H1 Comp. Motion Conforming to NUREG/CR-0098 Spectral Shape

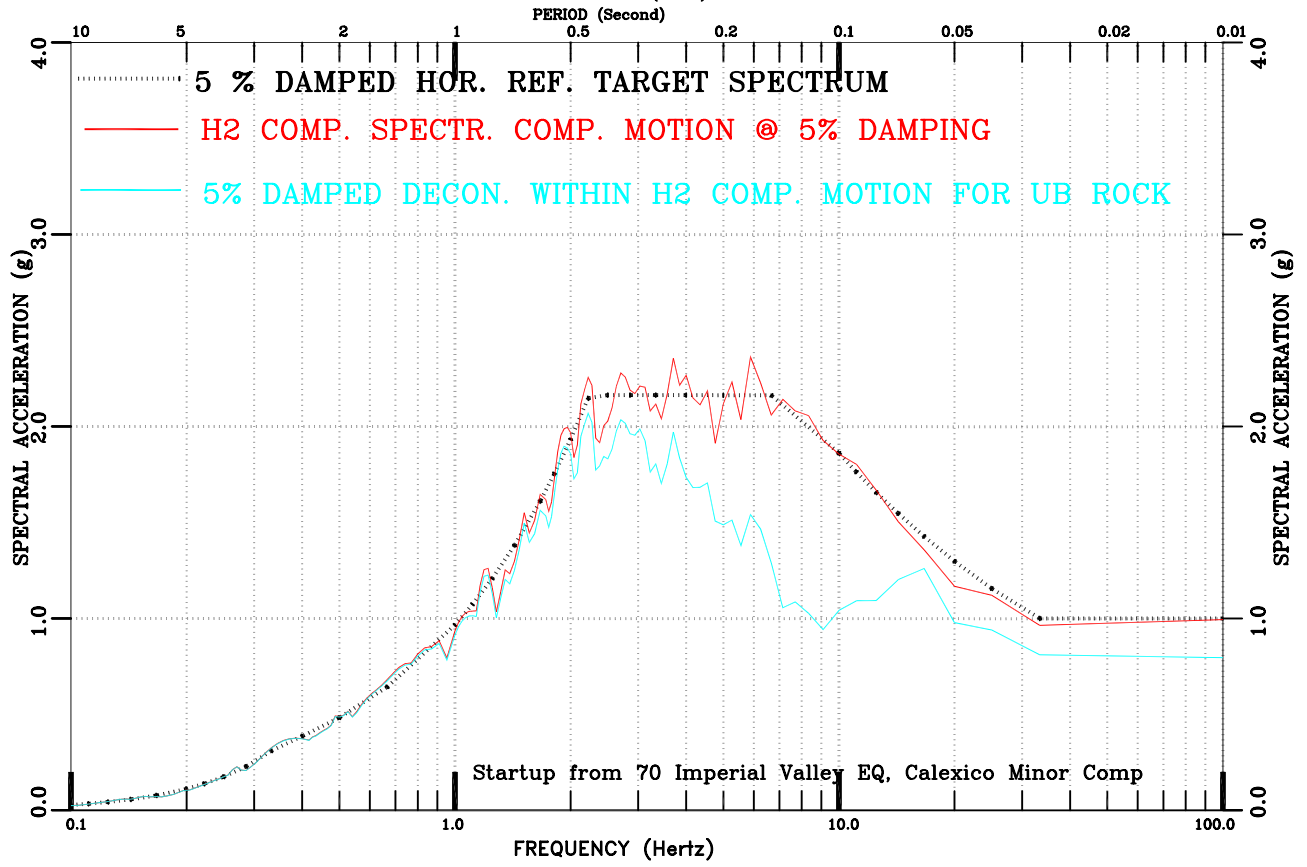
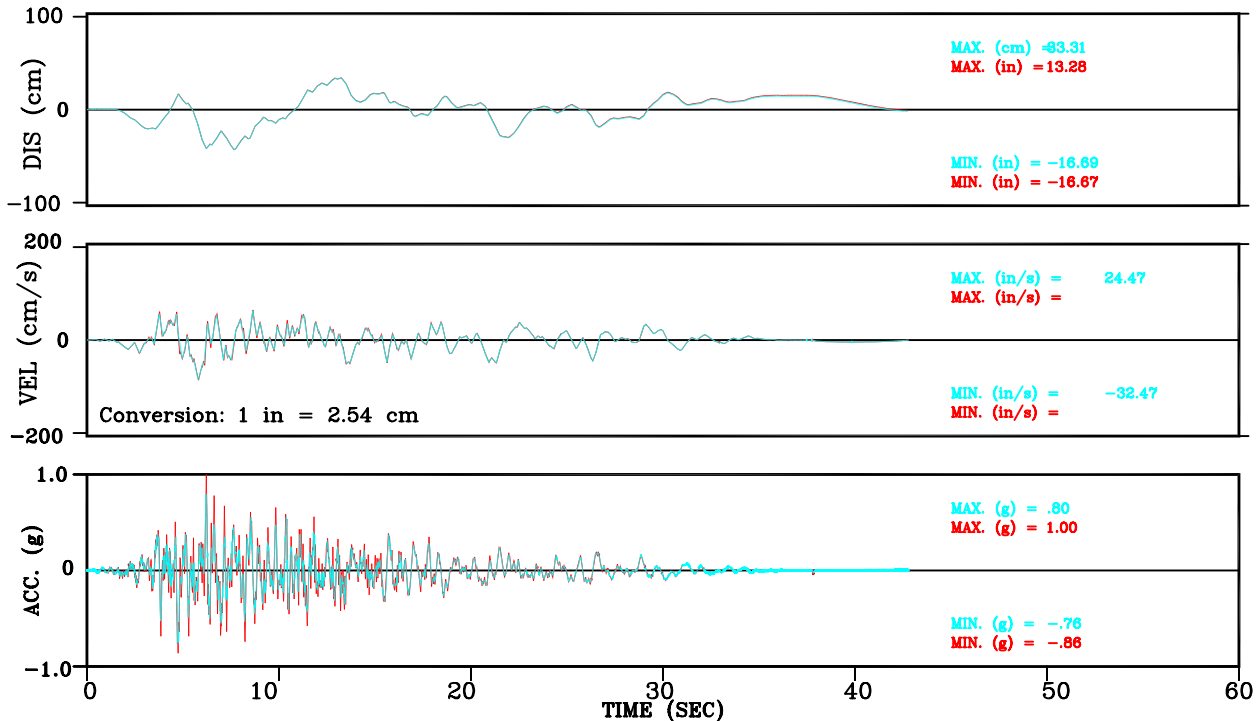


Figure III-59: Deconvolved Within vs. Surface Motion for UB Rock Set-5 H2 Comp. Motion Conforming to NUREG/CR-0098 Spectral Shape

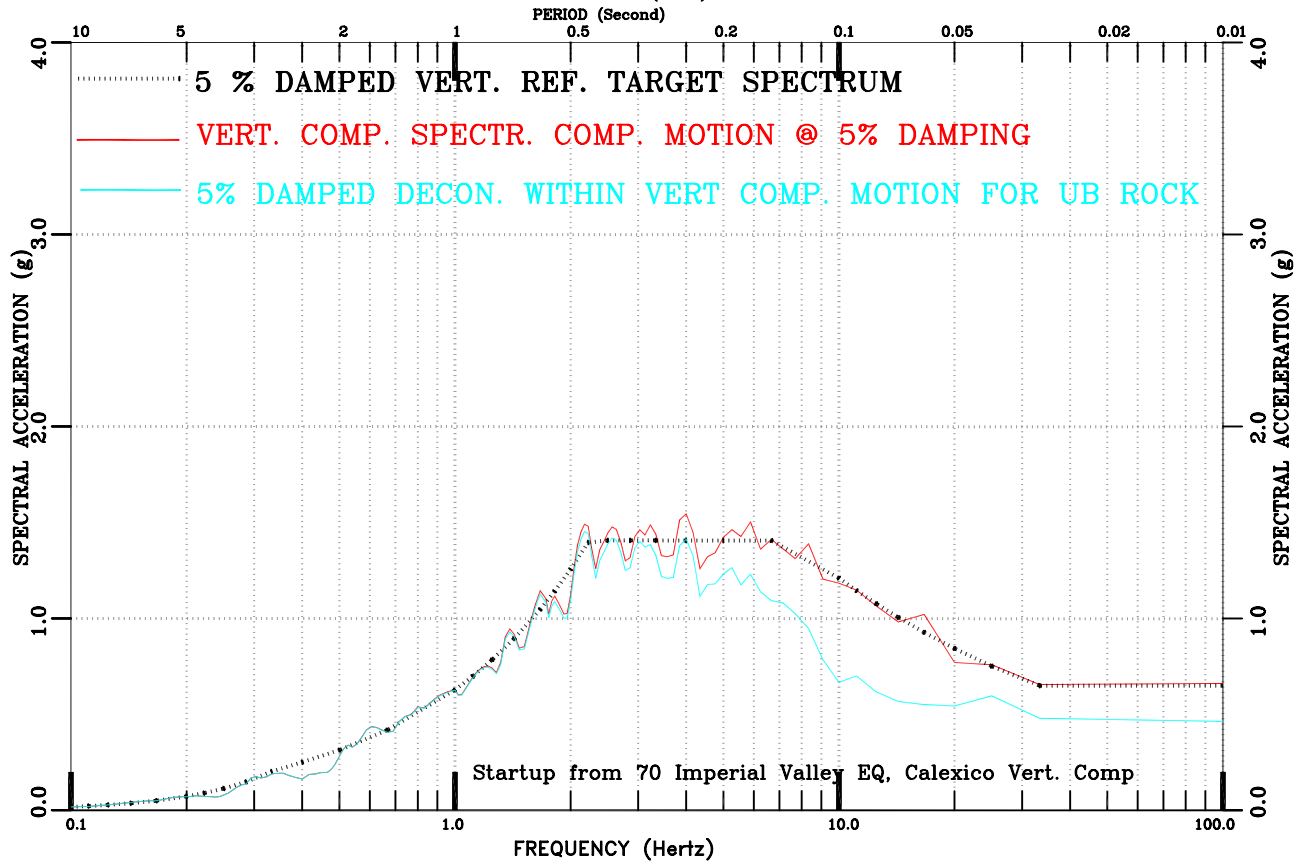
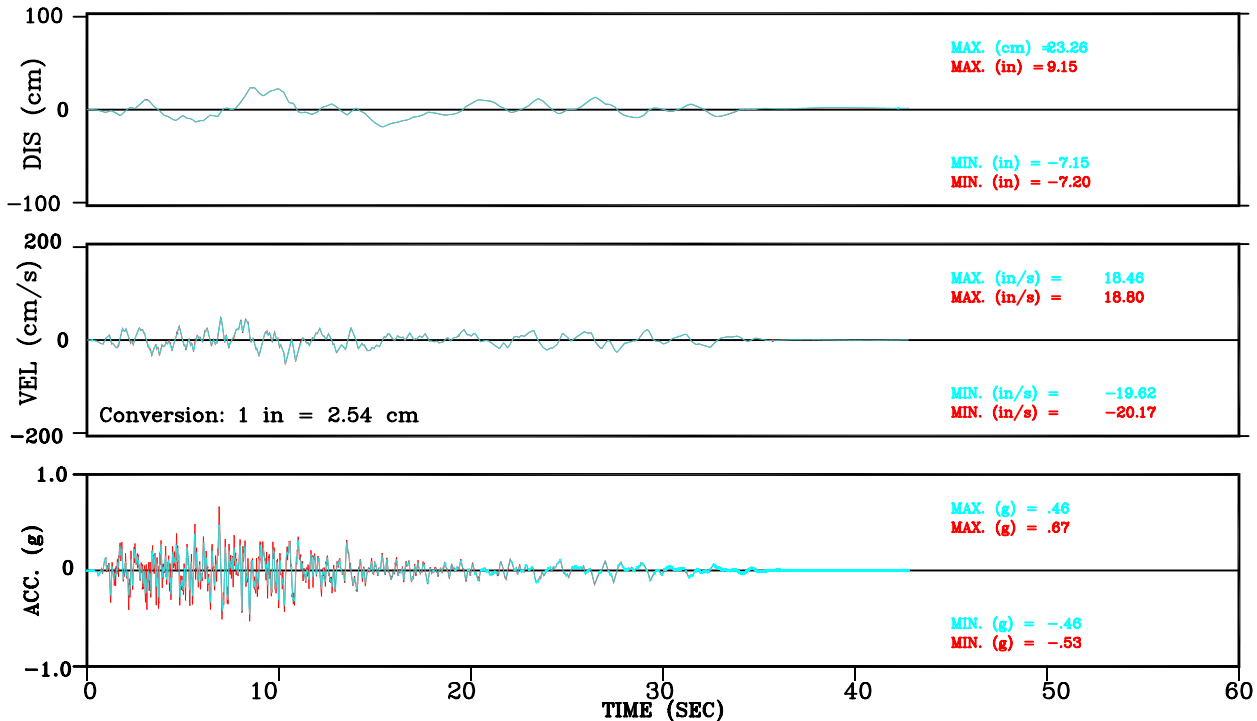


Figure III-60: Deconvolved Within vs. Surface Motion for UB Rock Set-5 VERT Comp. Motion Conforming to NUREG/CR-0098 Spectral Shape

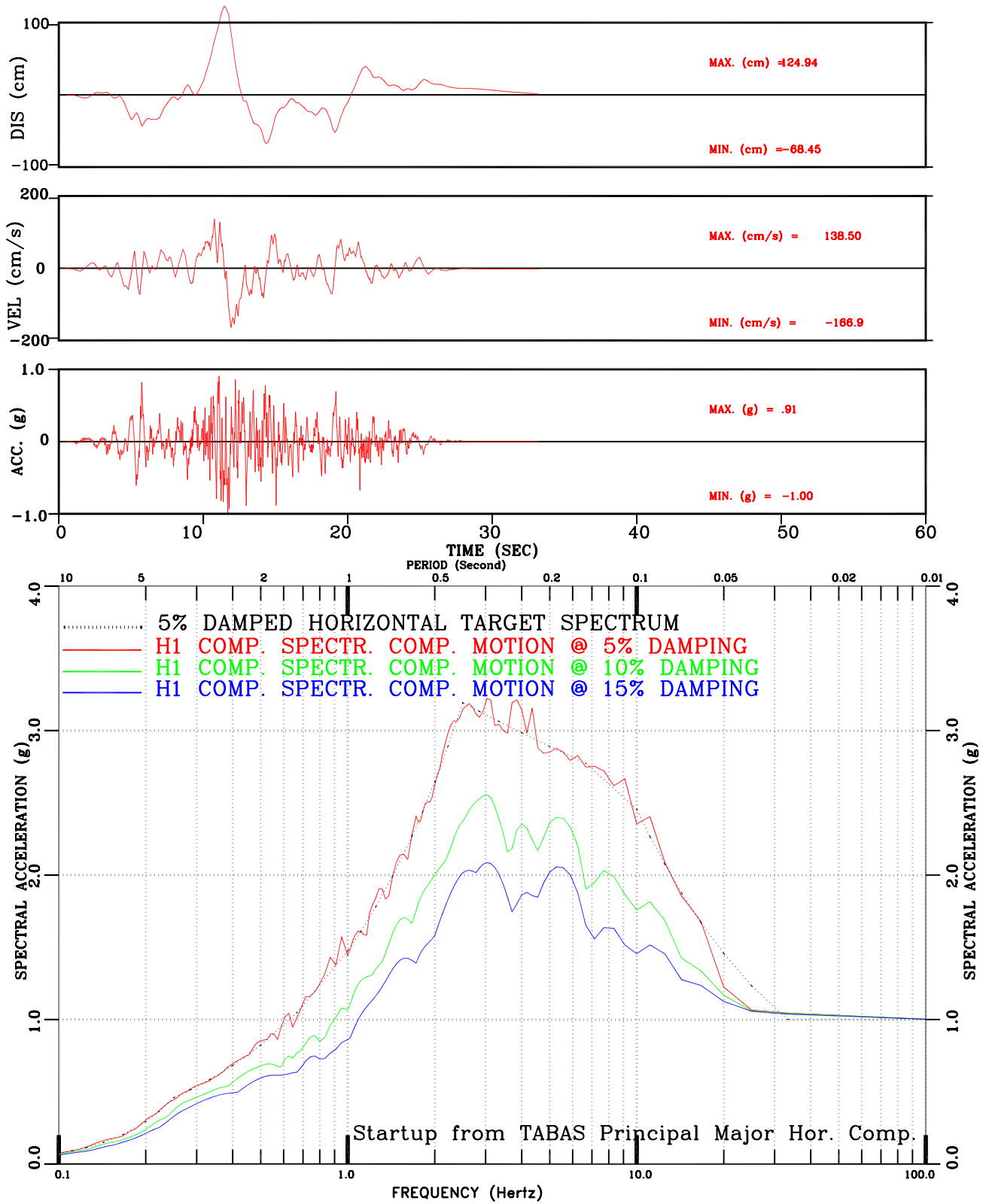


Figure III-61: Set-1 H1 Comp. Motion Conforming to Regulatory Guide 1.60 Spectral Shape

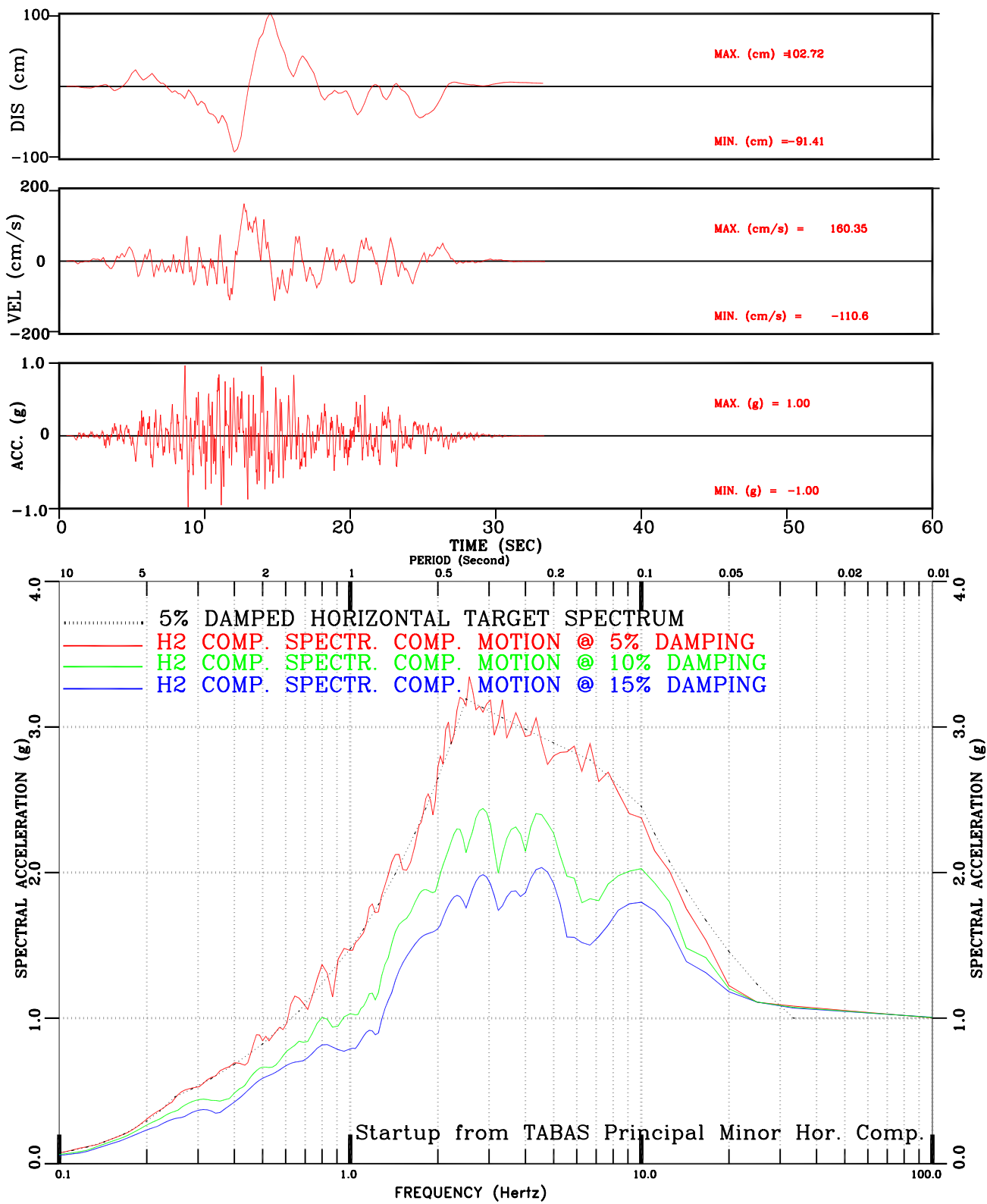


Figure III-62: Set-1 H2 Comp. Motion Conforming to Regulatory Guide 1.60 Spectral Shape

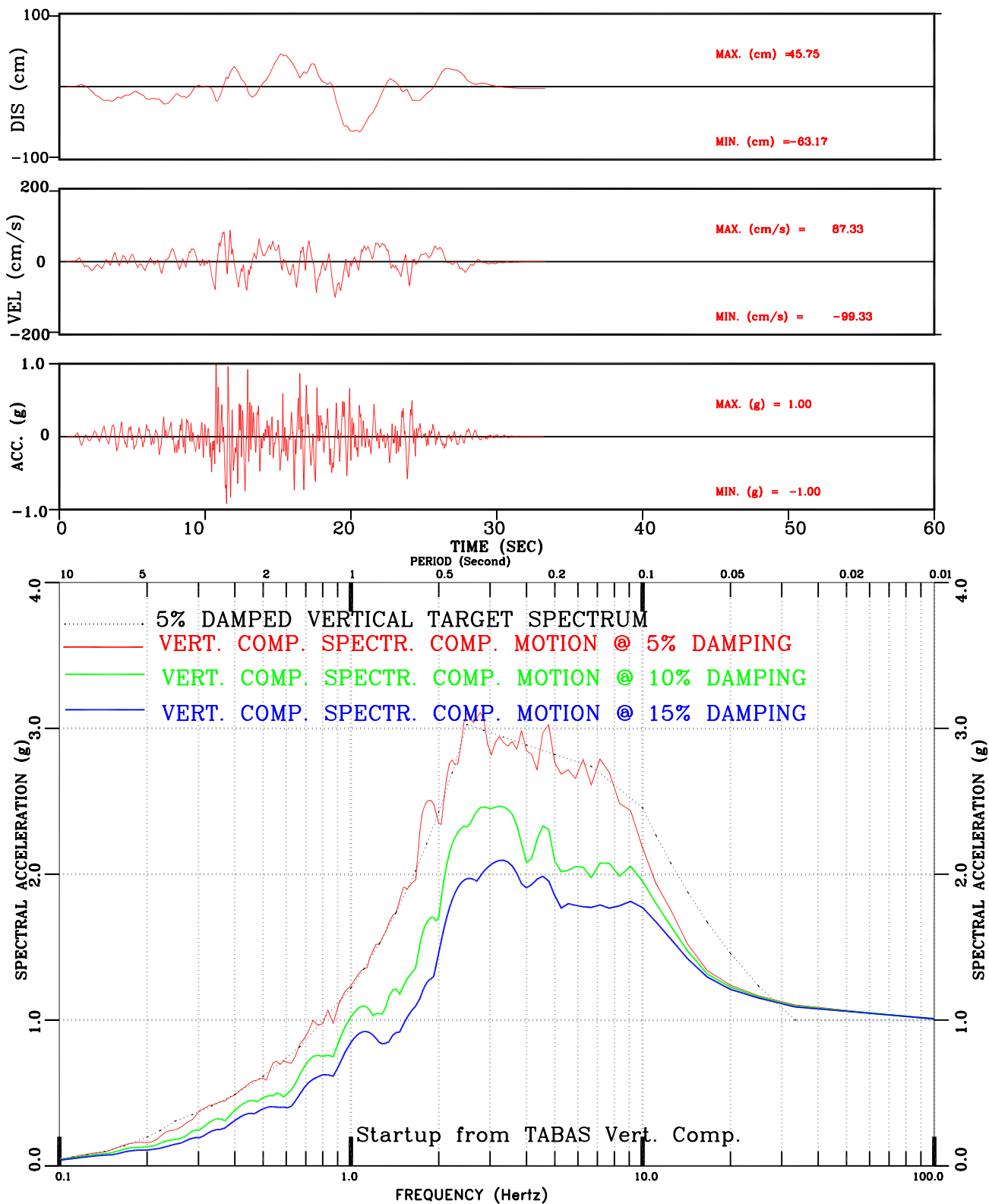


Figure III-63: Set-1 Vert Comp. Motion Conforming to Regulatory Guide 1.60 Spectral Shape

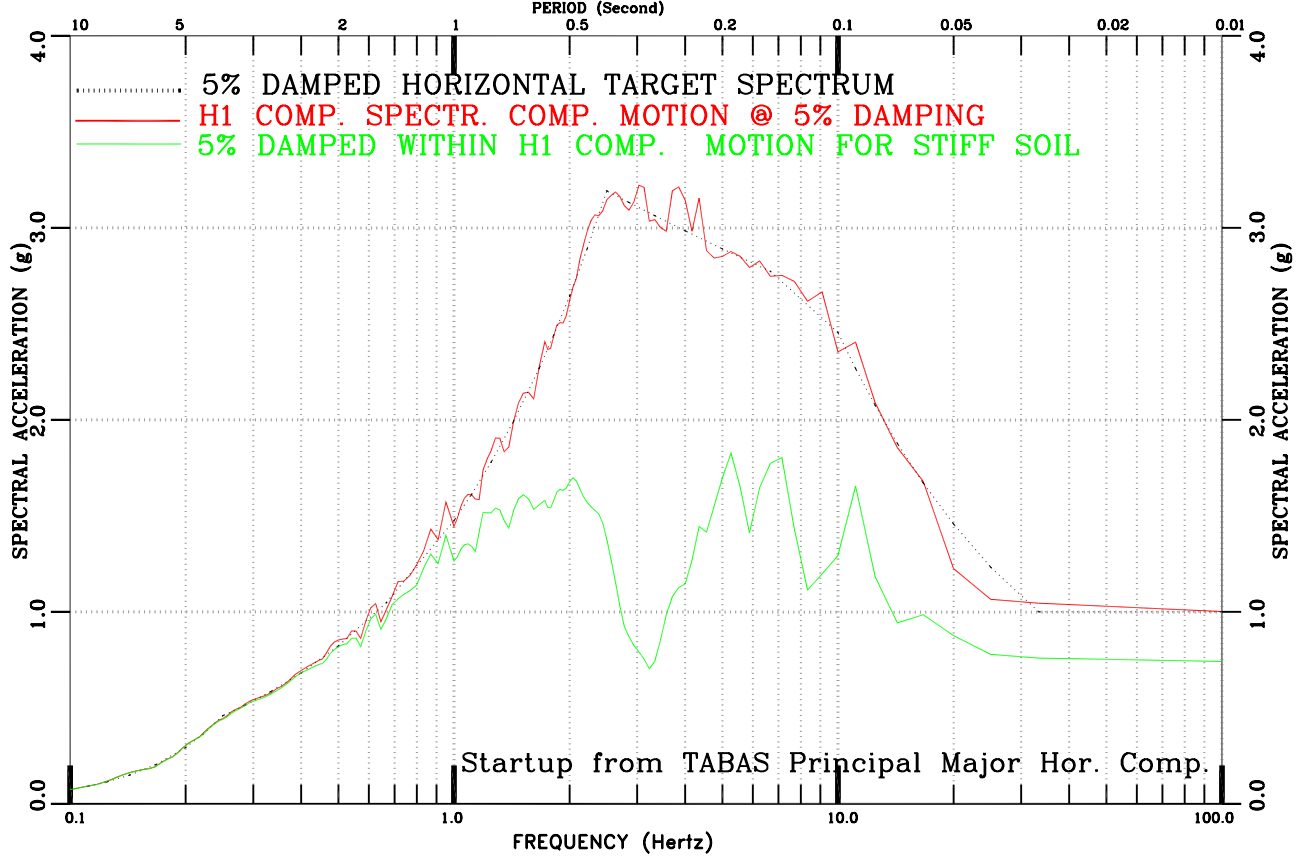
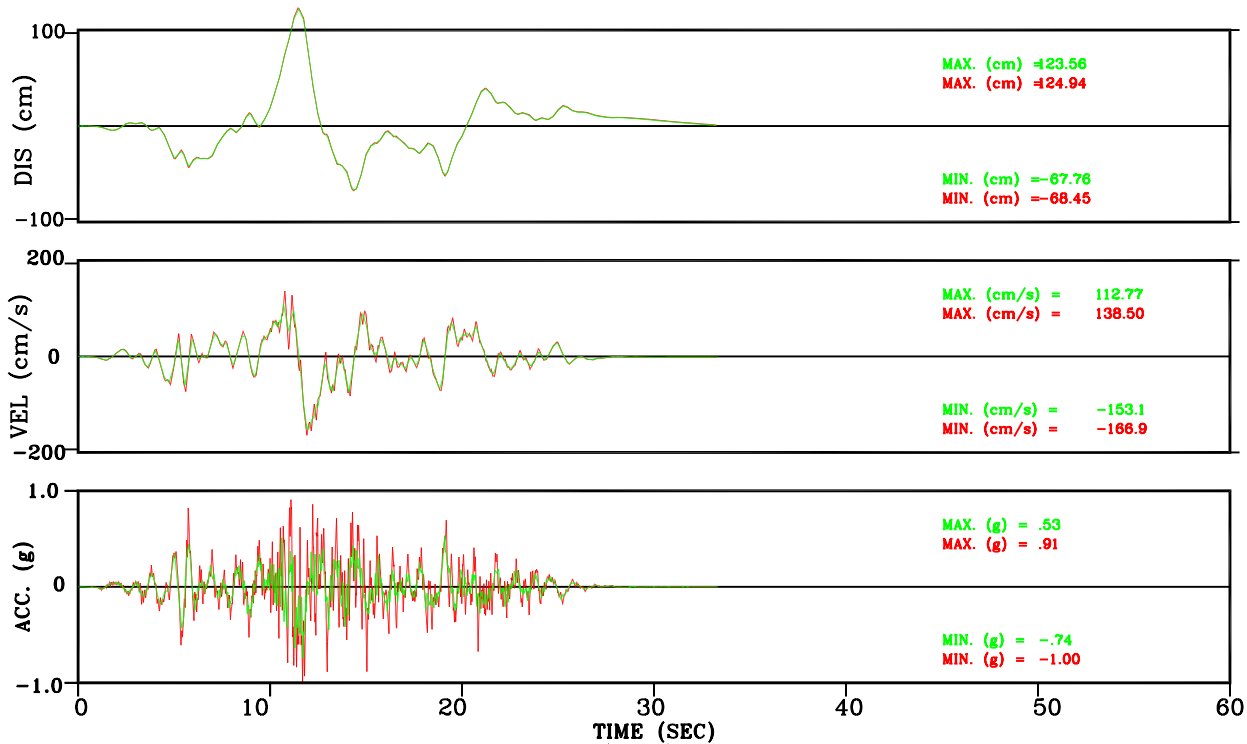


Figure III-64: Within vs. Surface Motion for Stiff Soil  
Set-1 H1 Comp. Motion Conforming to Regulatory Guide 1.60 Spectral Shape

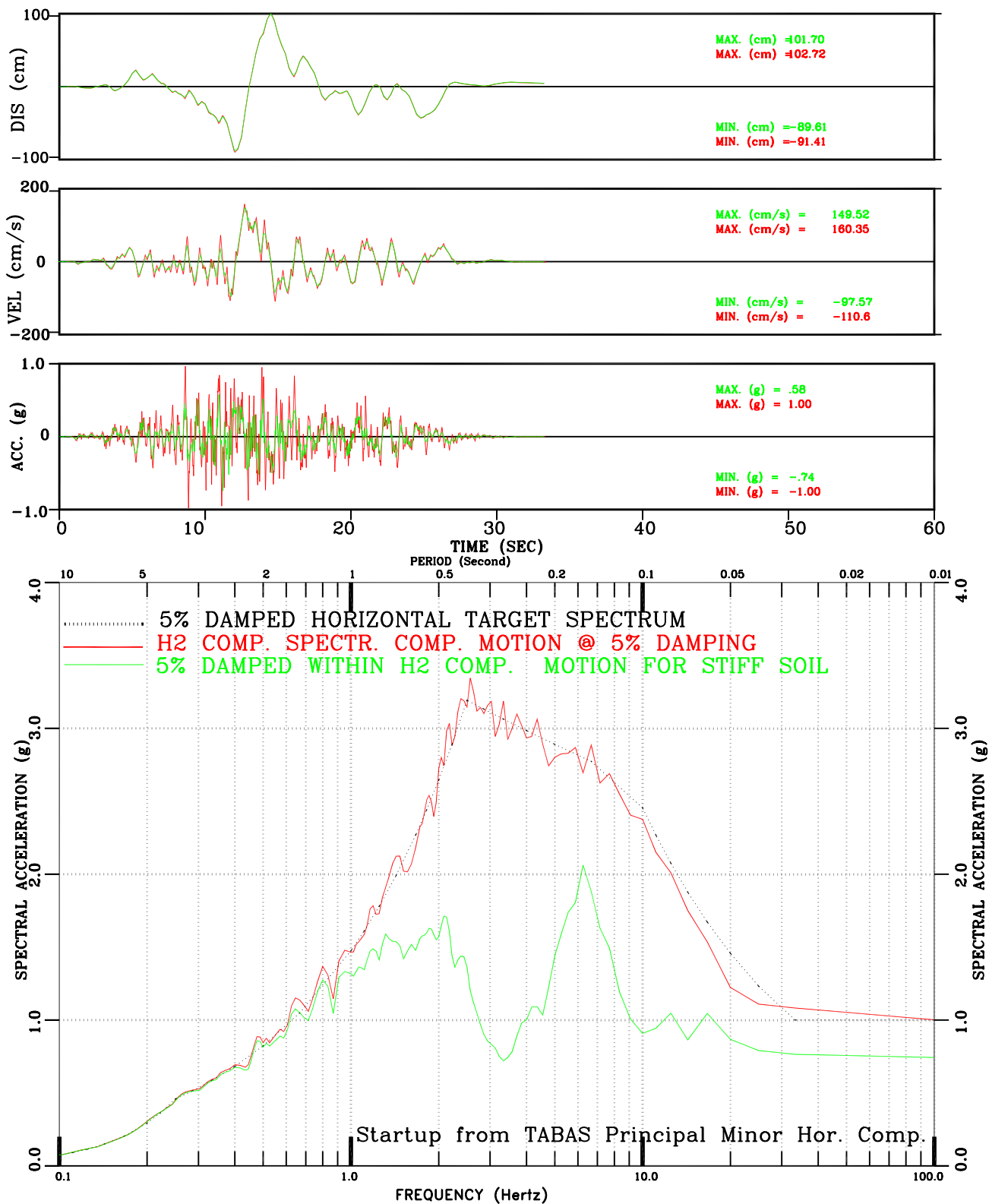


Figure III-65: Within vs. Surface Motion for Stiff Soil  
Set-1 H2 Comp. Motion Conforming to Regulatory Guide 1.60 Spectral Shape

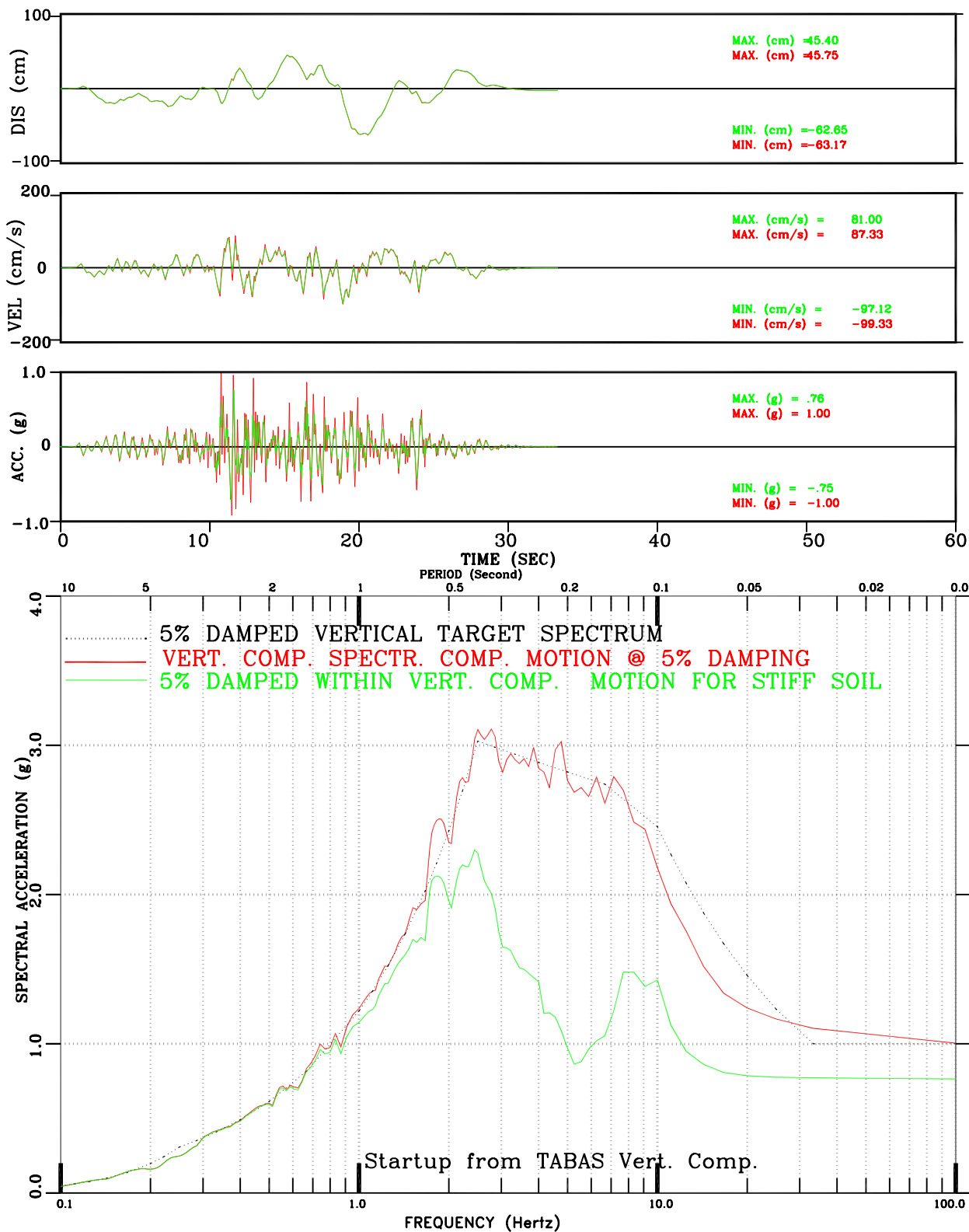


Figure III-66: Within vs. Surface Motion for Stiff Soil  
 Set-1 Vert. Comp. Motion Conforming to Regulatory Guide 1.60 Spectral Shape

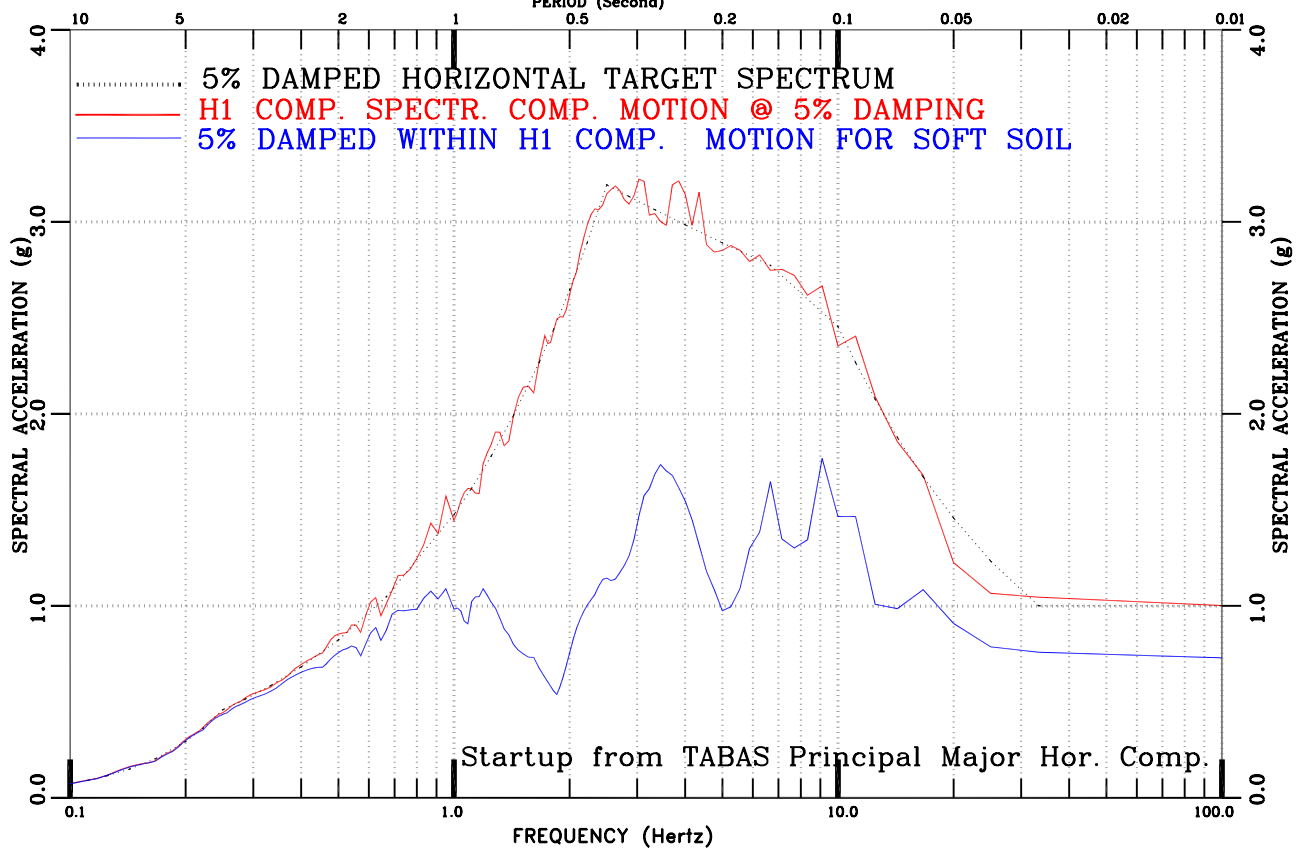
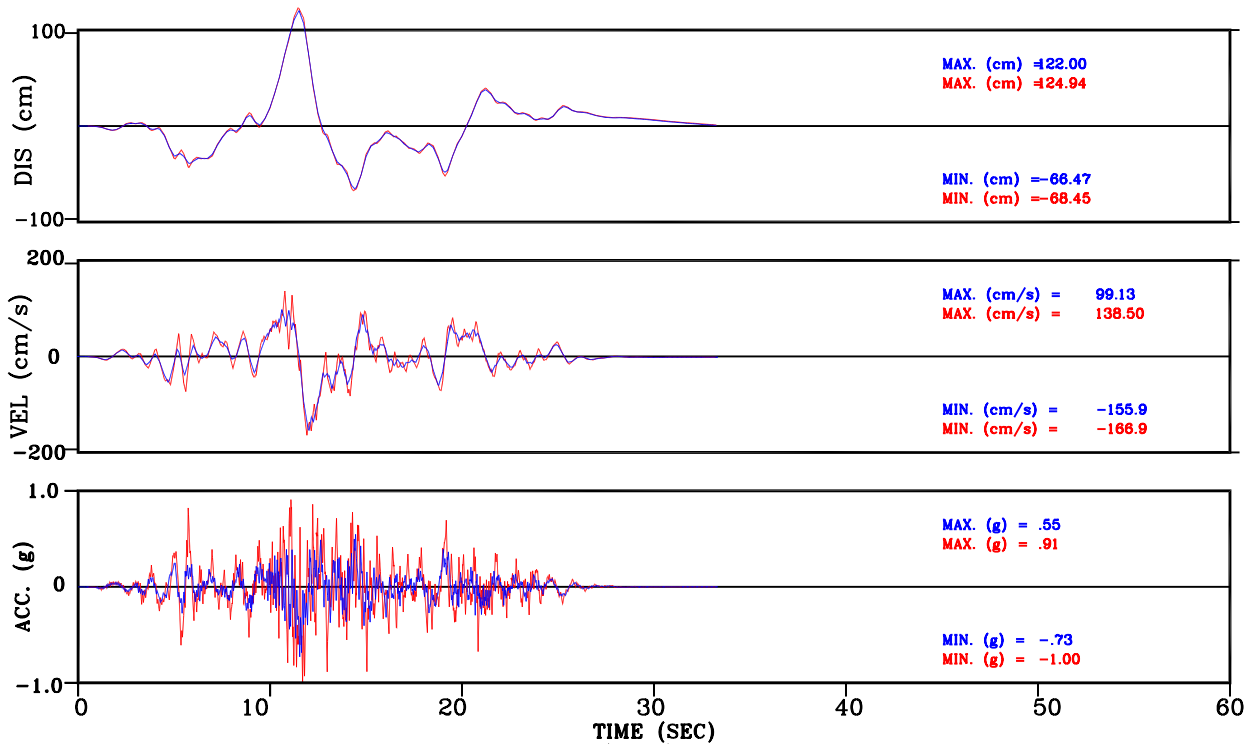


Figure III-67: Within vs. Surface Motion for Soft Soil Set-1 H1 Comp. Motion Conforming to Regulatory Guide 1.60 Spectral Shape

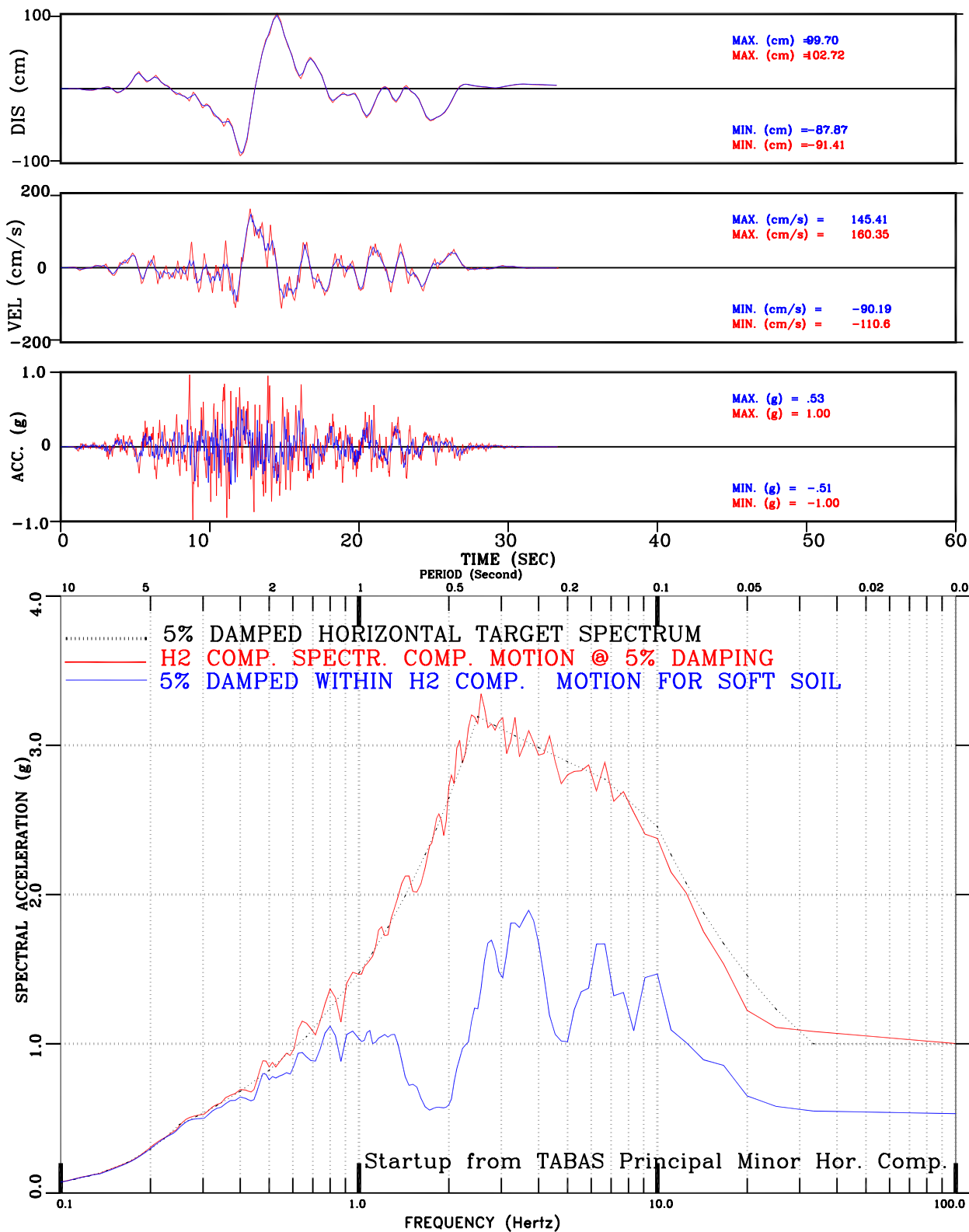


Figure III-68: Within vs. Surface Motion for Soft Soil  
Set-1 H2 Comp. Motion Conforming to Regulatory Guide 1.60 Spectral Shape

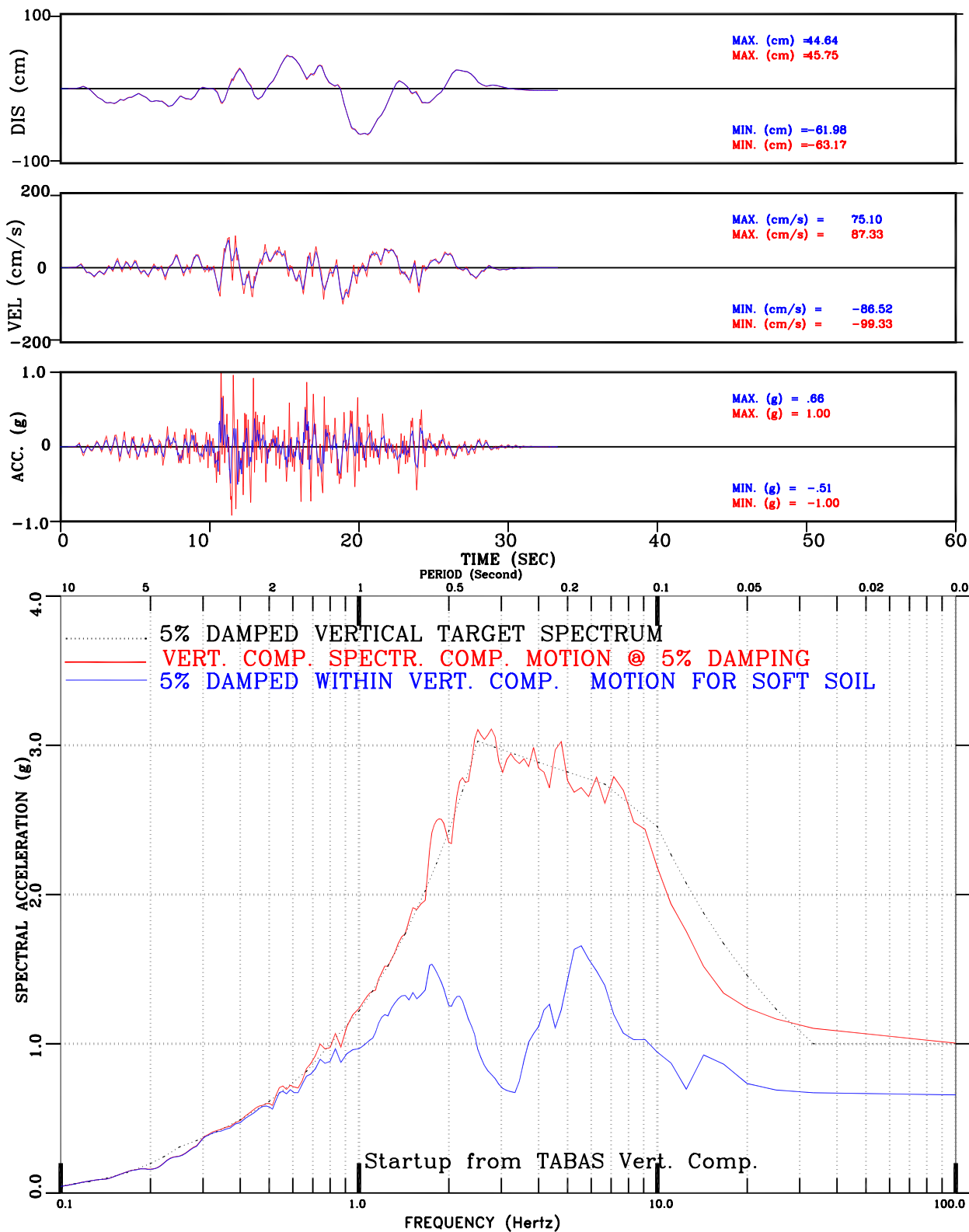


Figure III-69: Within vs. Surface Motion for Soft Soil  
 Set-1 Vert. Comp. Motion Conforming to Regulatory Guide 1.60 Spectral Shape

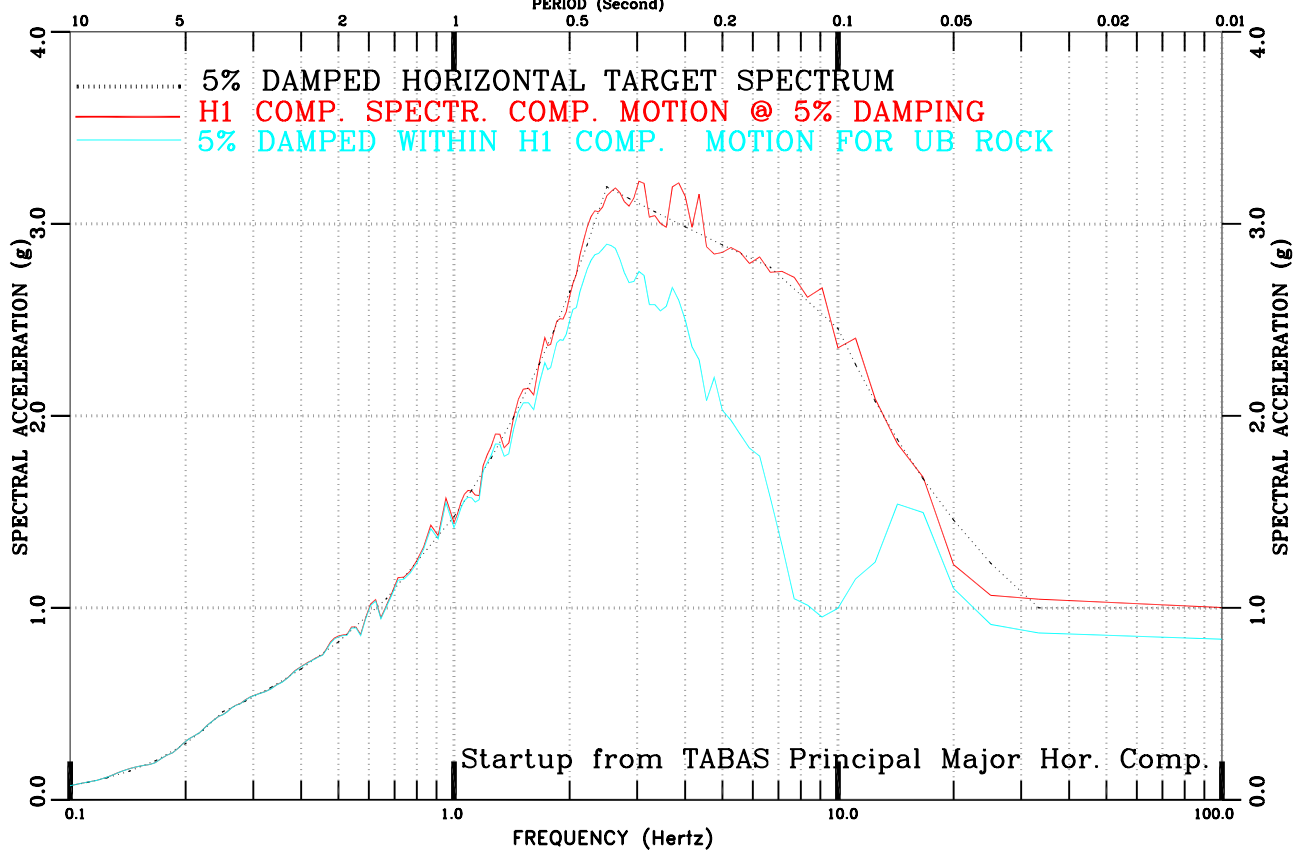
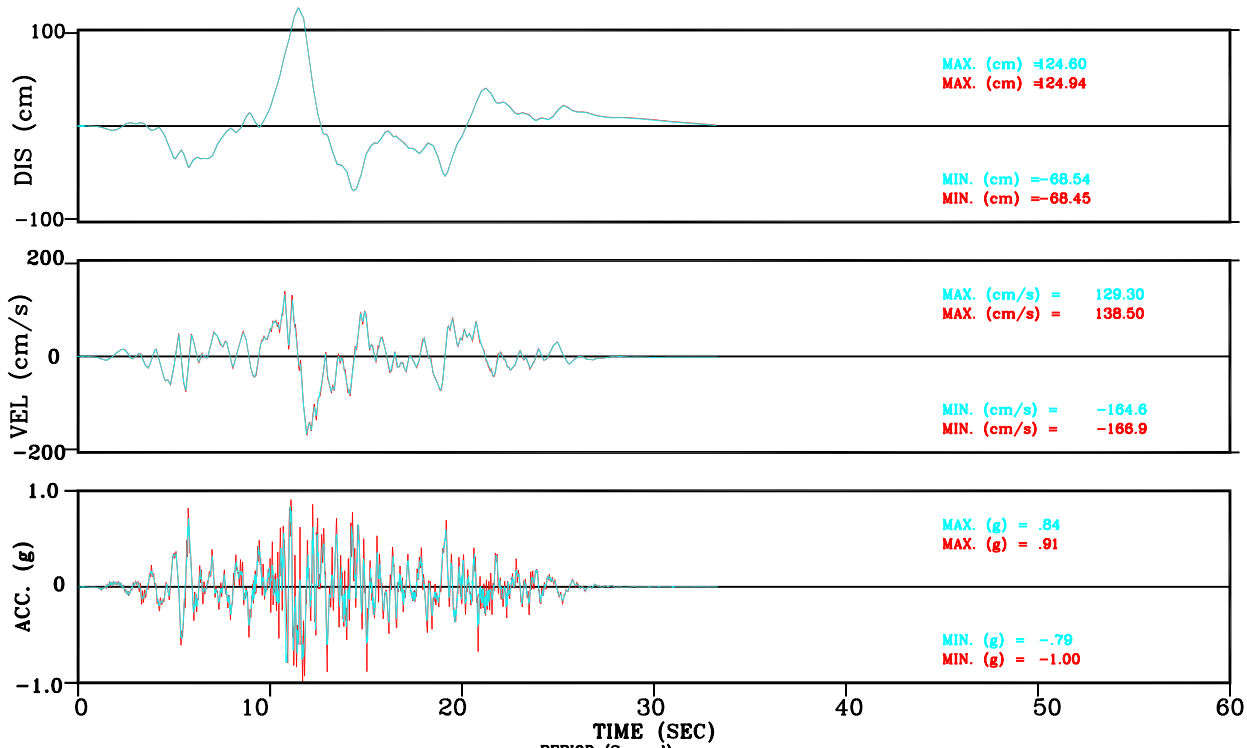


Figure III-70: Within vs. Surface Motion for UB Rock Set-1 H1 Comp. Motion Conforming to Regulatory Guide 1.60 Spectral Shape

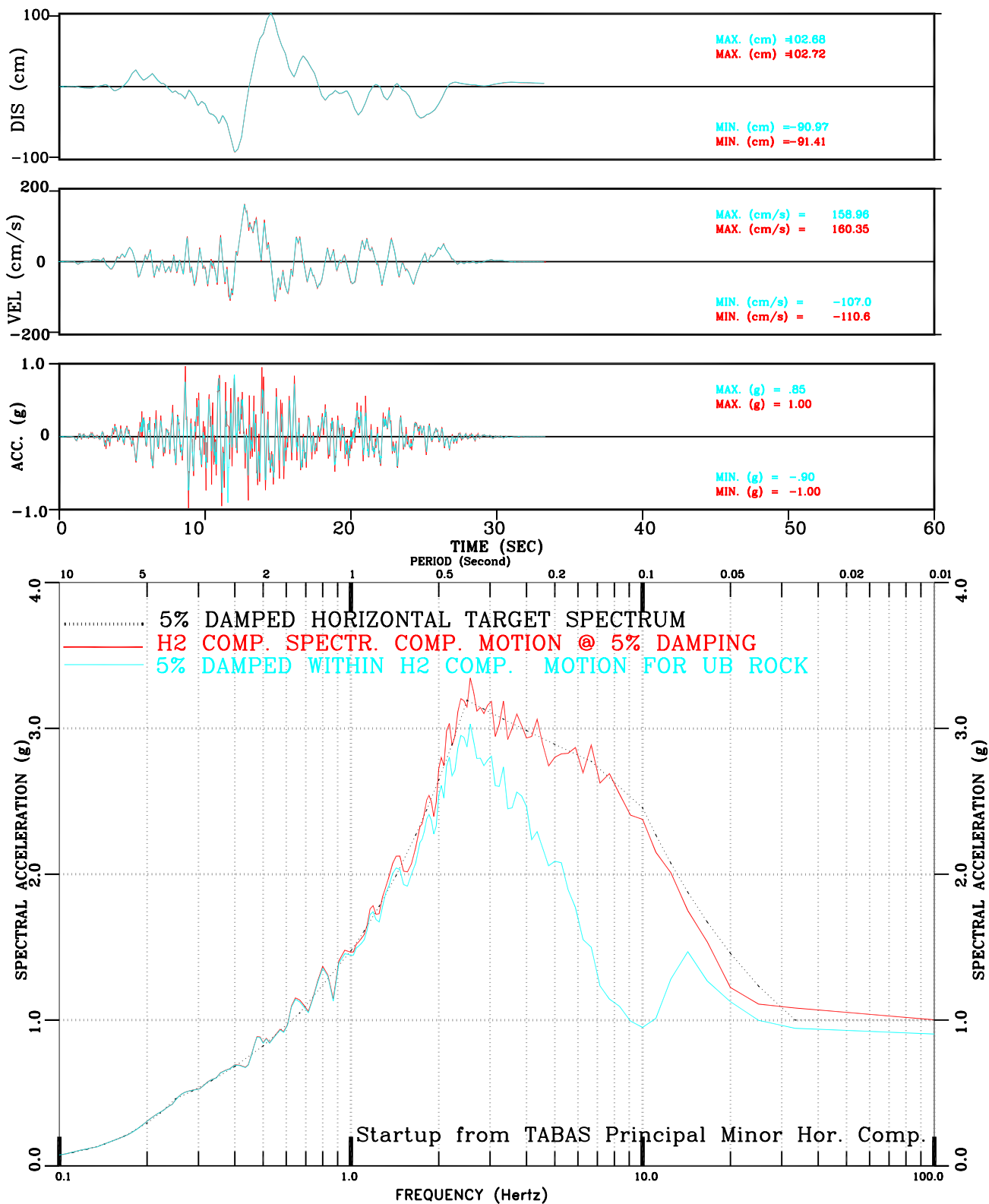


Figure III-71: Within vs. Surface Motion for UB Rock Set-1 H2 Comp. Motion Conforming to Regulatory Guide 1.60 Spectral Shape

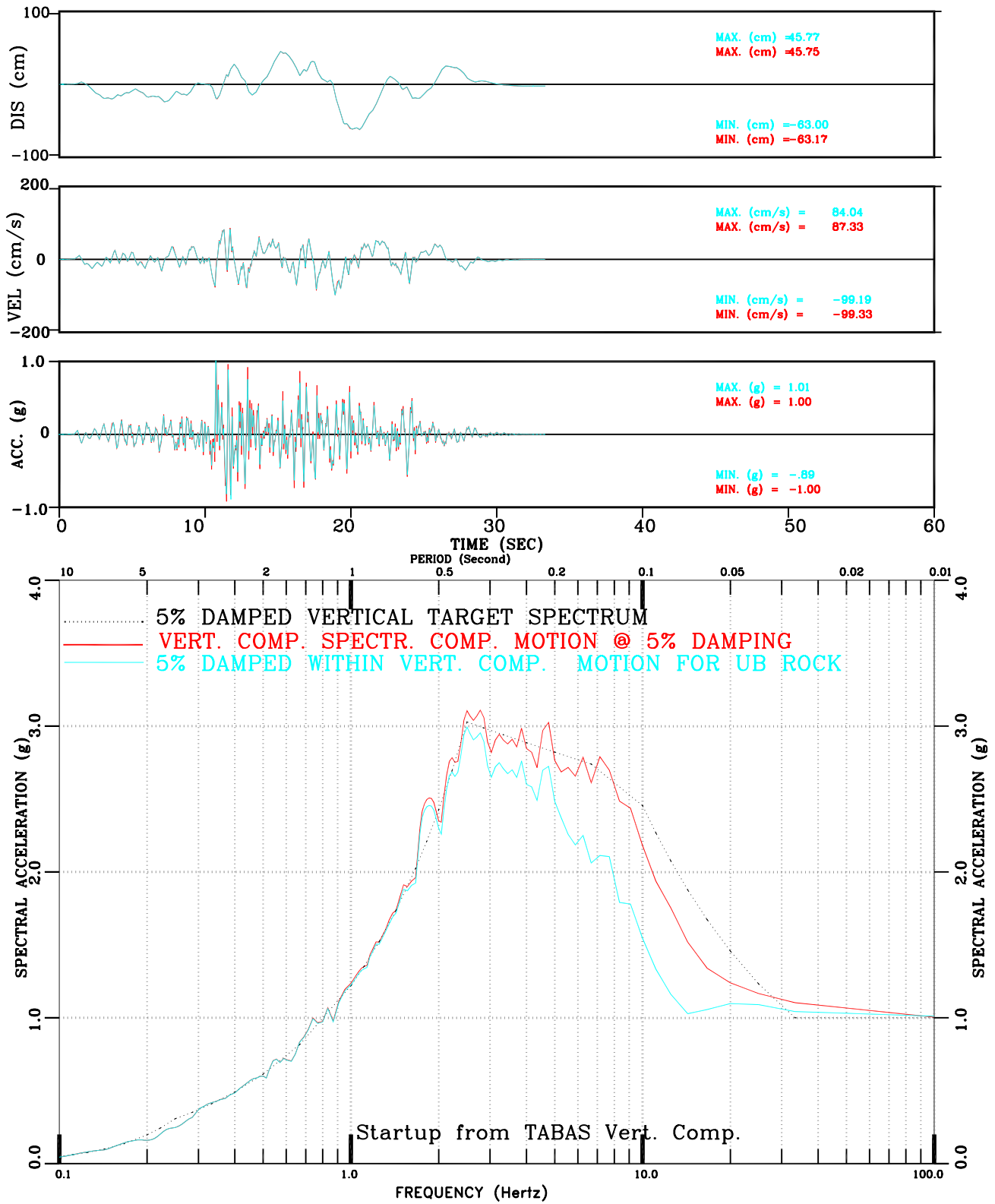


Figure III-72: Within vs. Surface Motion for UB Rock Set-1 Vert. Comp. Motion Conforming to Regulatory Guide 1.60 Spectral Shape

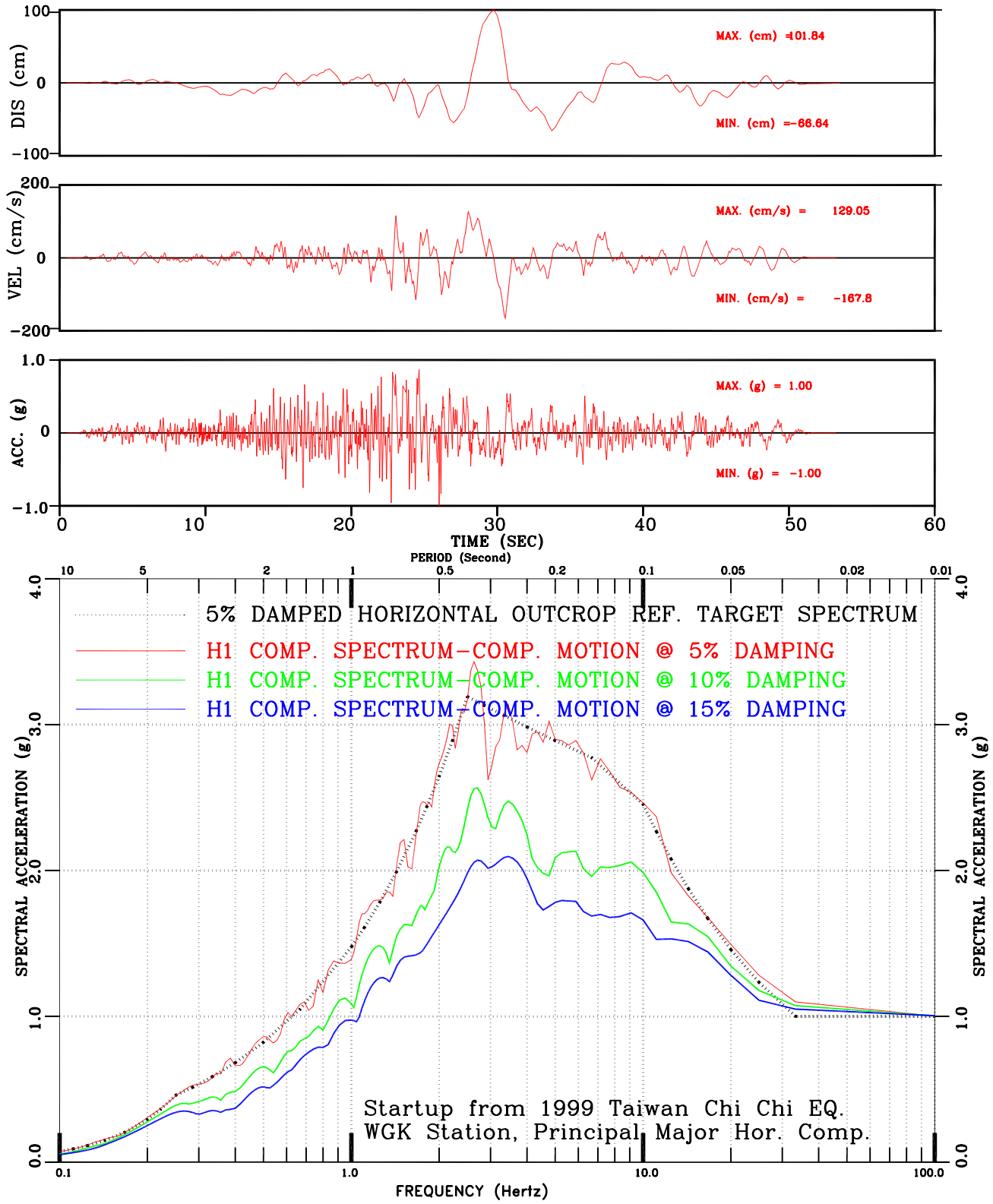


Figure III-73: Set-2 H1 Comp. Motion Conforming to Regulatory Guide 1.60 Spectral Shape

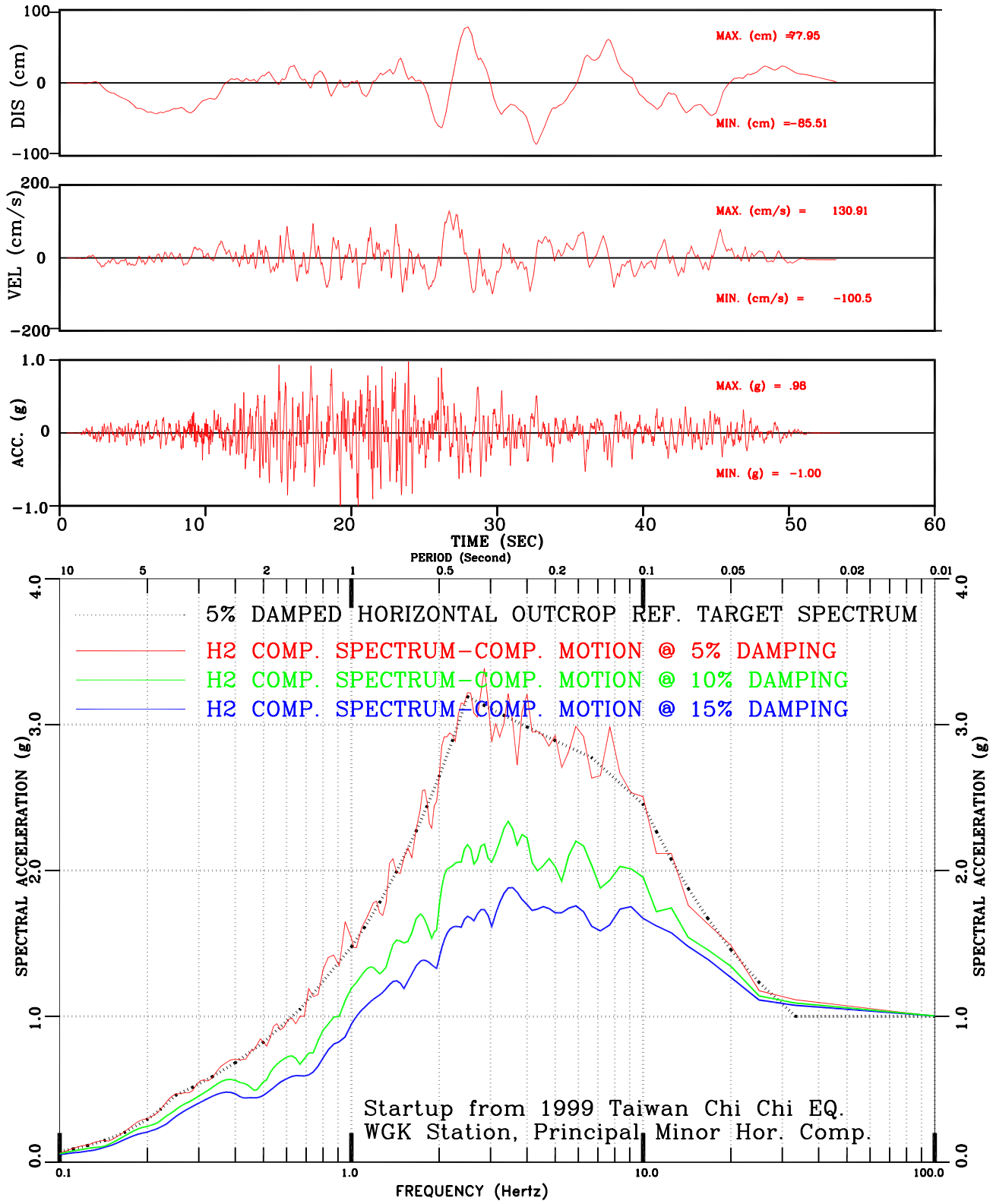


Figure III-74: Set-2 H2 Comp. Motion Conforming to Regulatory Guide 1.60 Spectral Shape

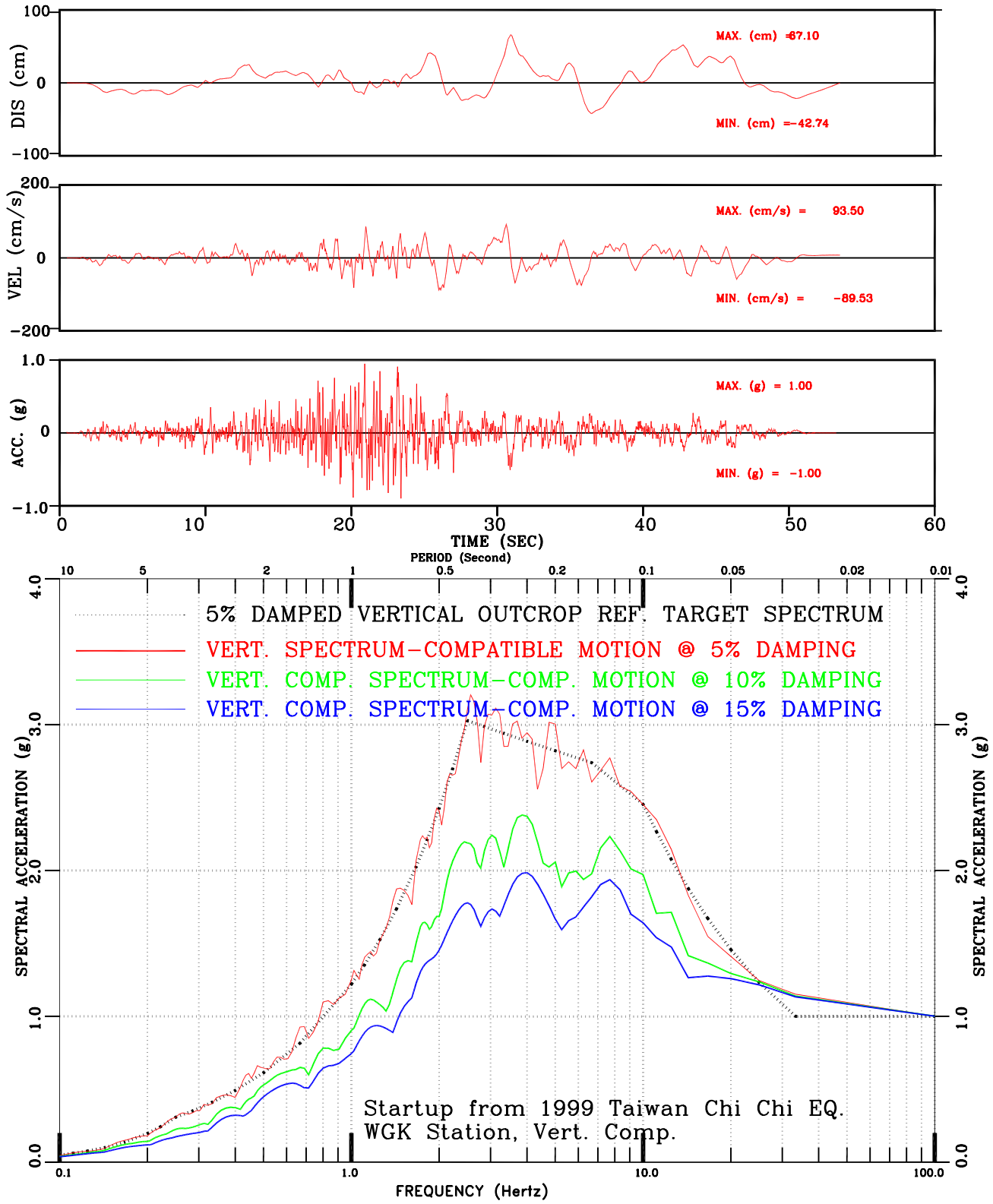


Figure III-75: Set-2 Vert Comp. Motion Conforming to Regulatory Guide 1.60 Spectral Shape

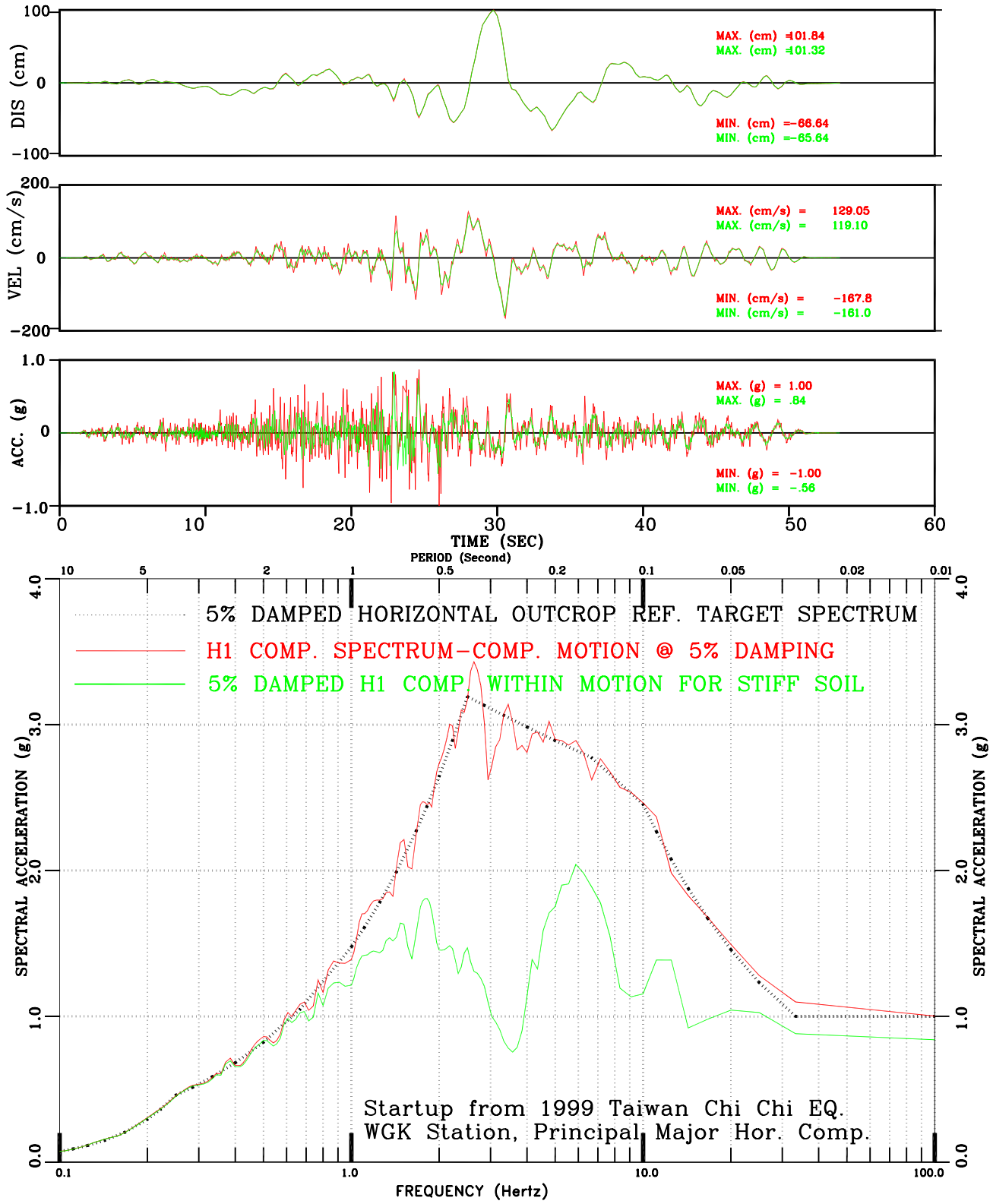


FIGURE III-76: Within vs. Surface Motion for Stiff Soil  
 Set-2 H1 Comp. Motion Conforming to Regulatory Guide 1.60 Spectral Shape

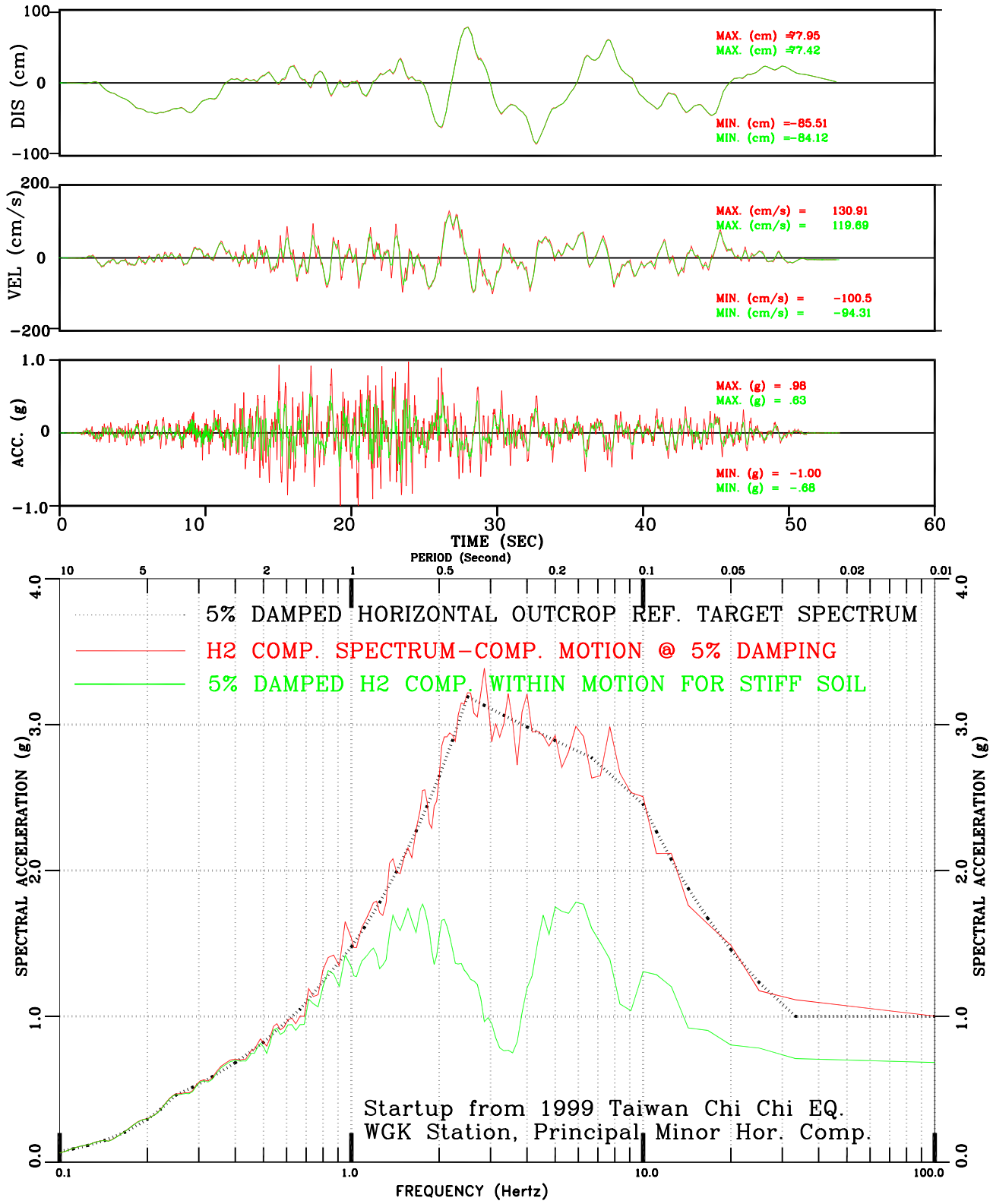


Figure III-77: Within vs. Surface Motion for Stiff Soil  
 Set-2 H2 Comp. Motion Conforming to Regulatory Guide 1.60 Spectral Shape

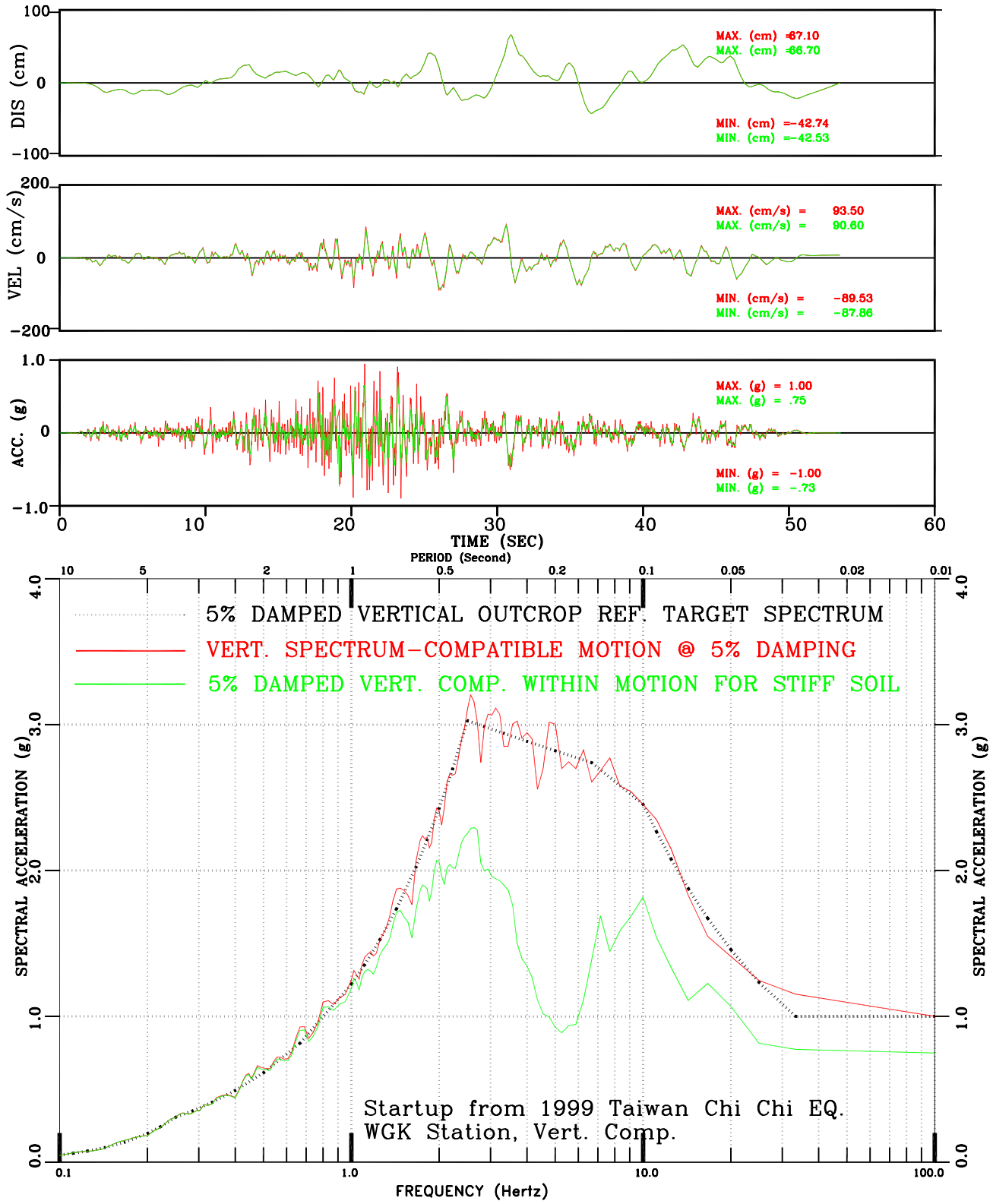


Figure III-78: Within vs. Surface Motion for Stiff Soil Set-2 Vert. Comp. Motion Conforming to Regulatory Guide 1.60 Spectral Shape

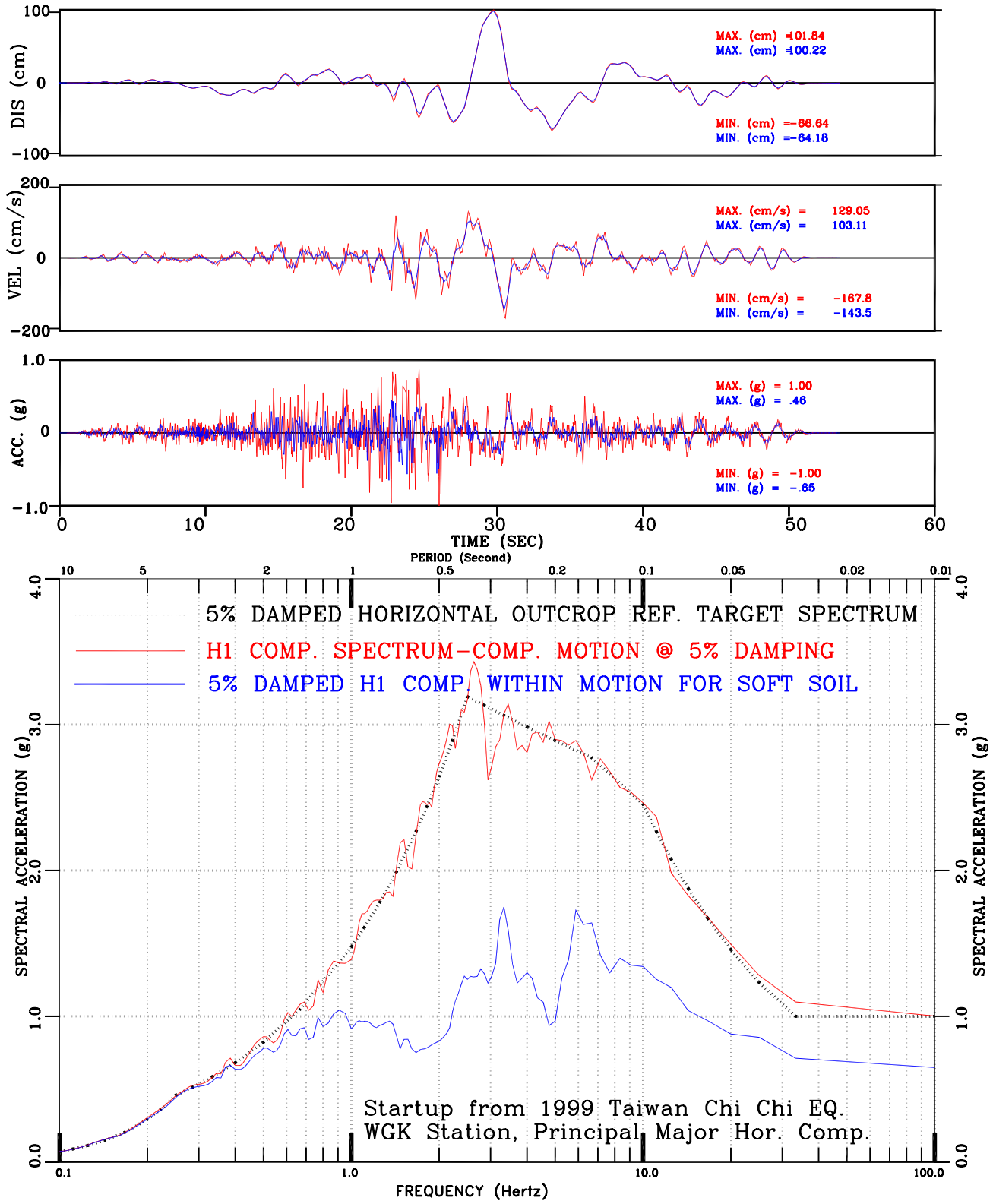


Figure III-79: Within vs. Surface Motion for Soft Soil  
Set-2 H1 Comp. Motion Conforming to Regulatory Guide 1.60 Spectral Shape

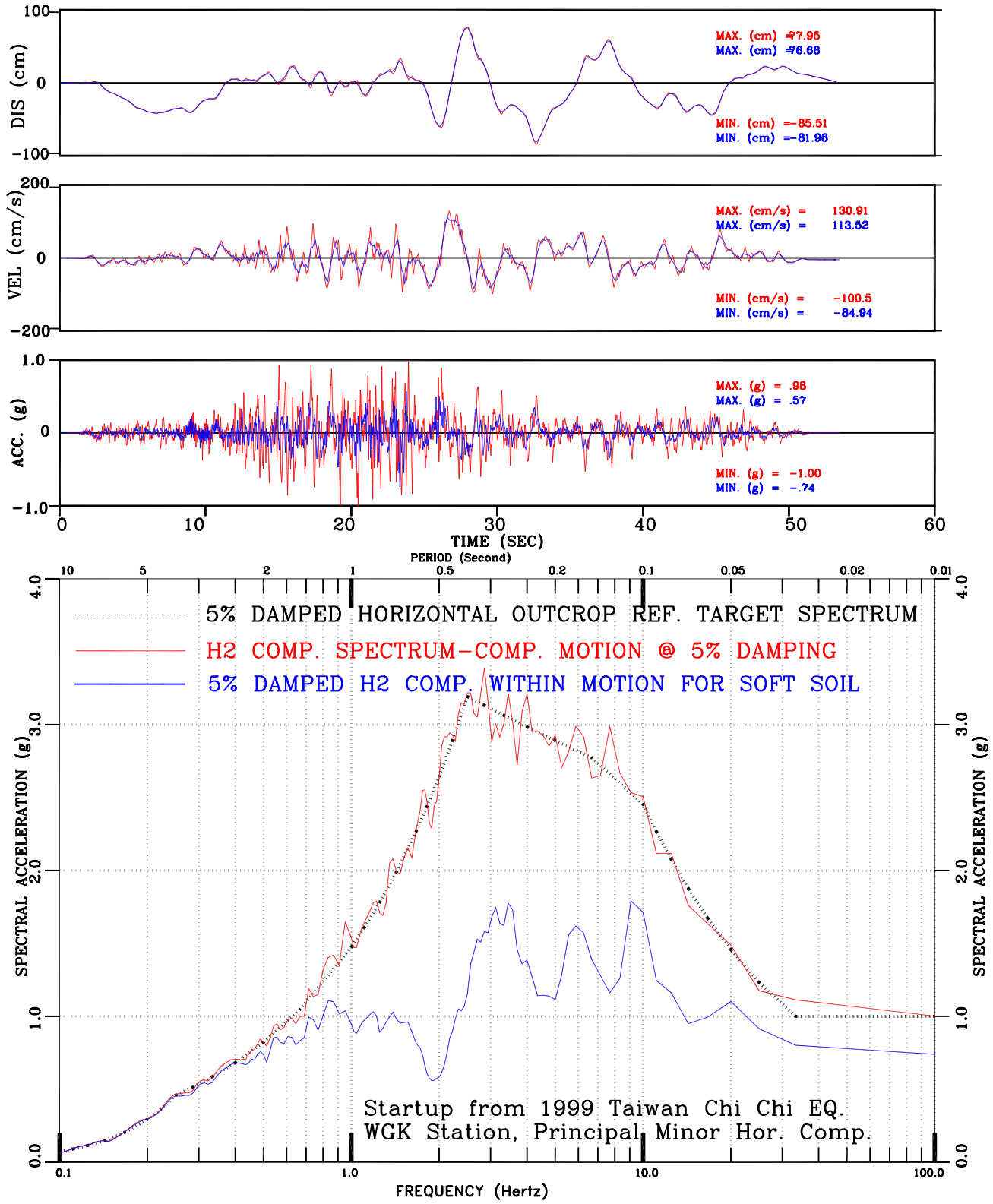


Figure III-80: Within vs. Surface Motion for Soft Soil  
 Set-2 H2 Comp. Motion Conforming to Regulatory Guide 1.60 Spectral Shape

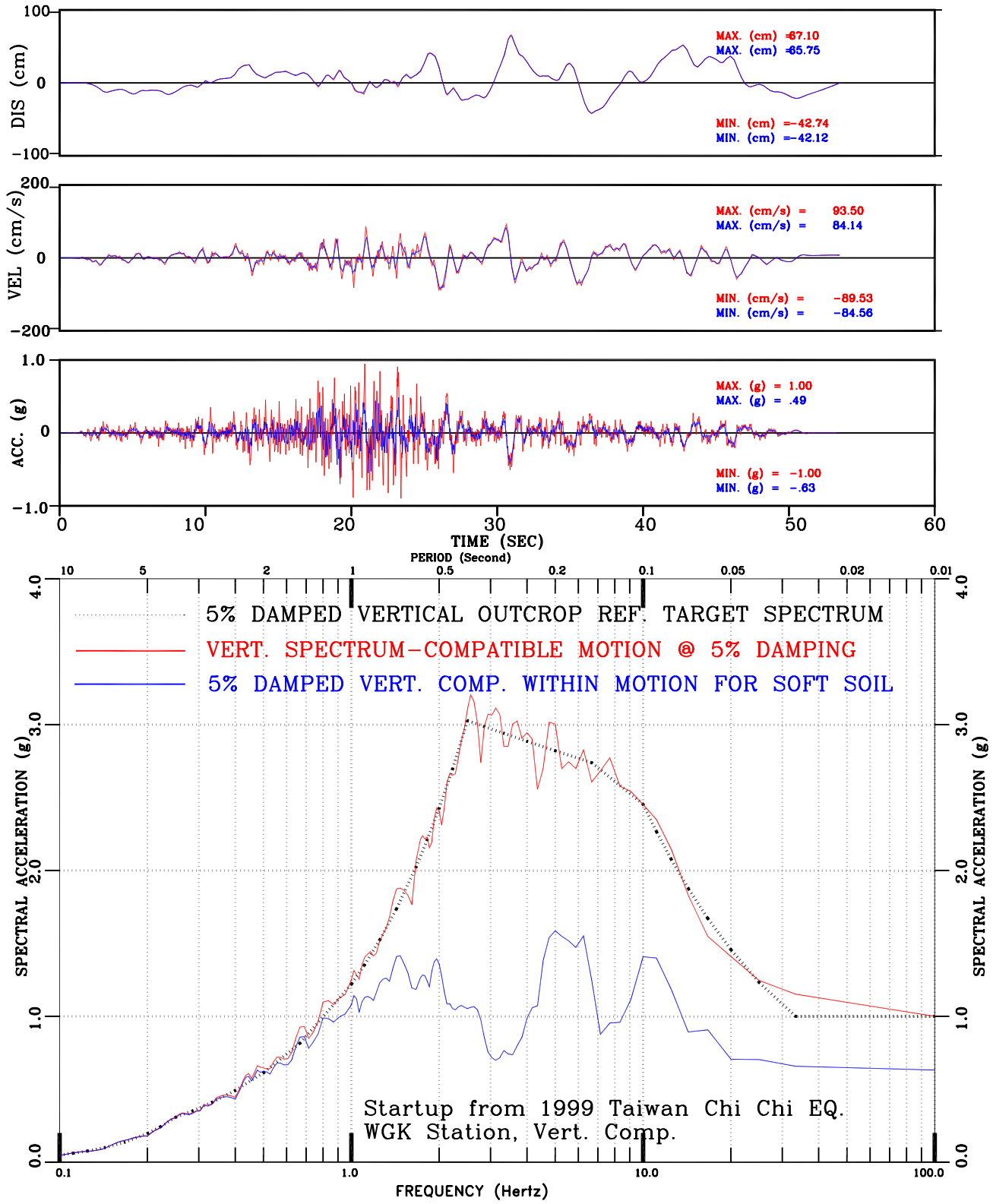


Figure III-81: Within vs. Surface Motion for Soft Soil Set-2 Vert. Comp. Motion Conforming to Regulatory Guide 1.60 Spectral Shape

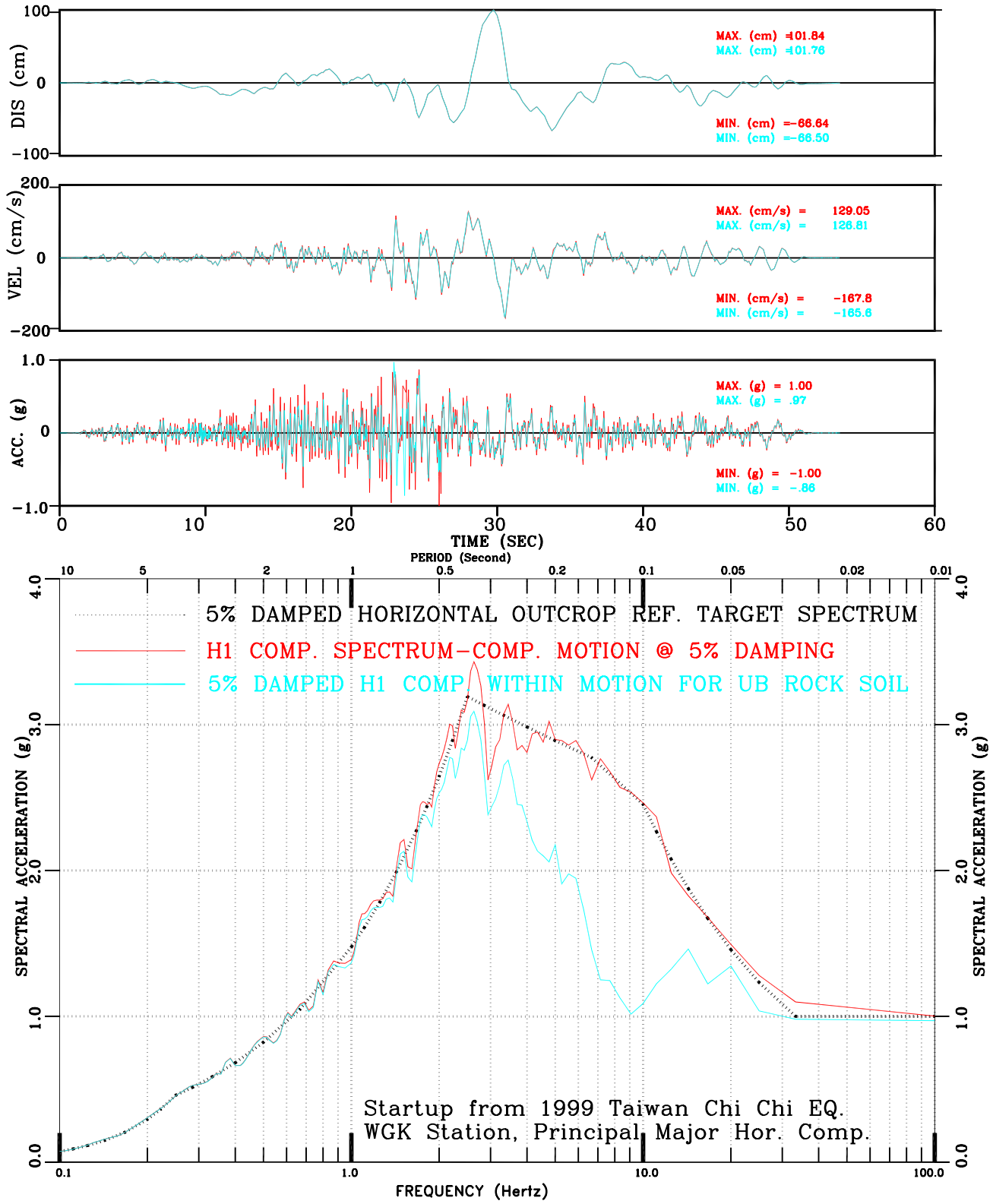


Figure III-82: Within vs. Surface Motion for UB Rock Set-2 H1 Comp. Motion Conforming to Regulatory Guide 1.60 Spectral Shape

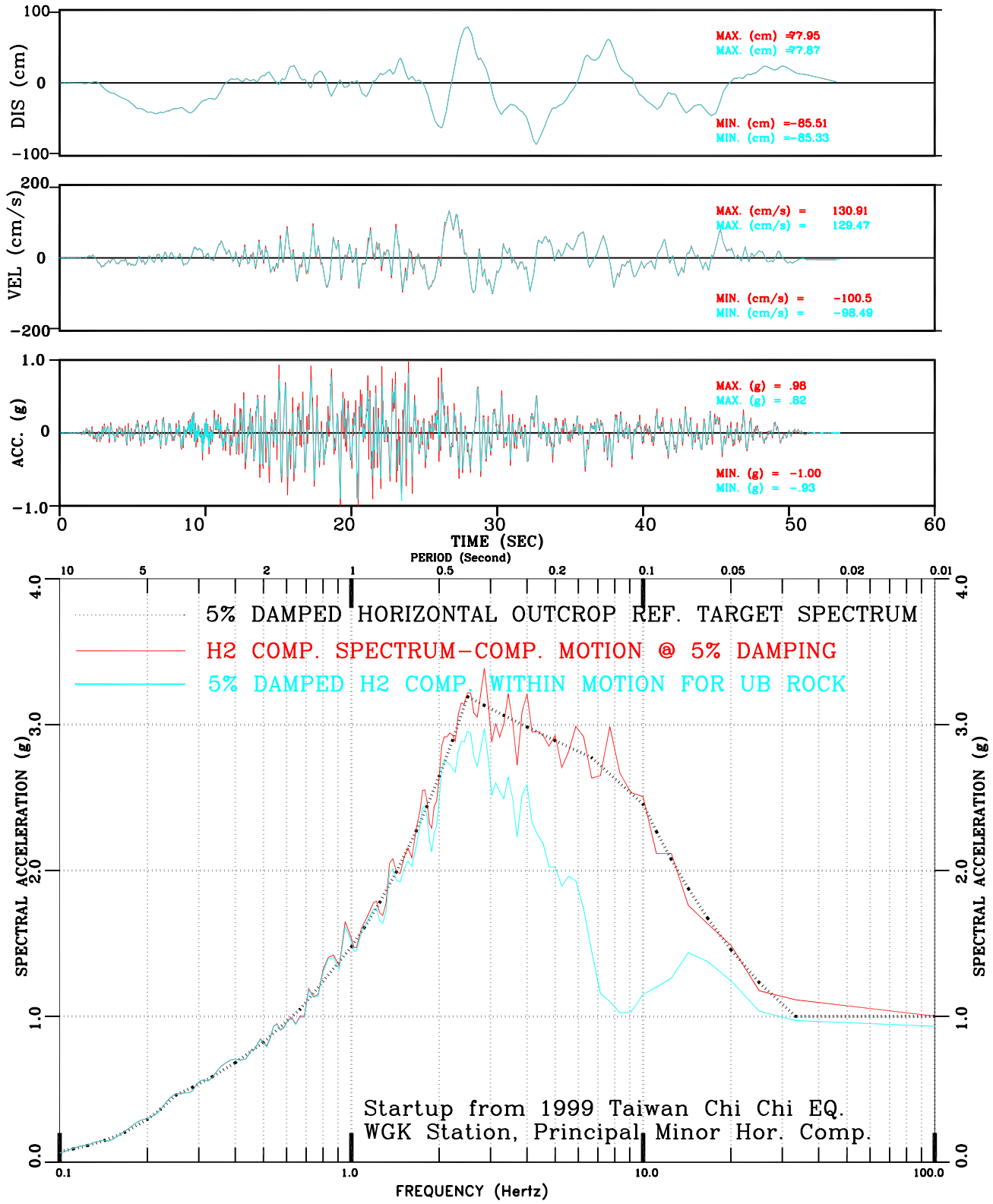


Figure III-83: Within vs. Surface Motion for UB Rock  
 Set-2 H2 Comp. Motion Conforming to Regulatory Guide 1.60 Spectral Shape

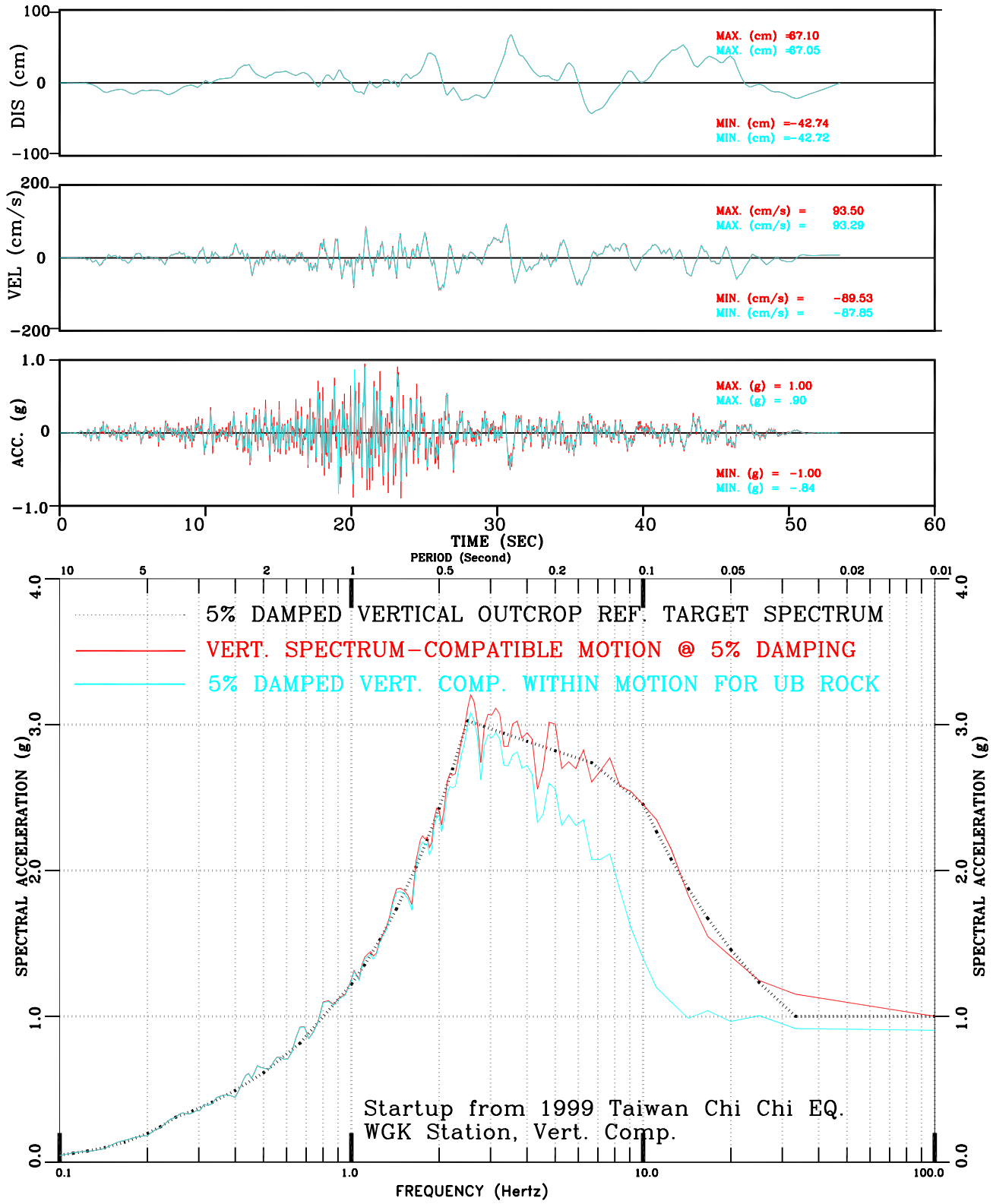


Figure III-84: Within vs. Surface Motion for UB Rock Set-2 Vert. Comp. Motion Conforming to Regulatory Guide 1.60 Spectral Shape

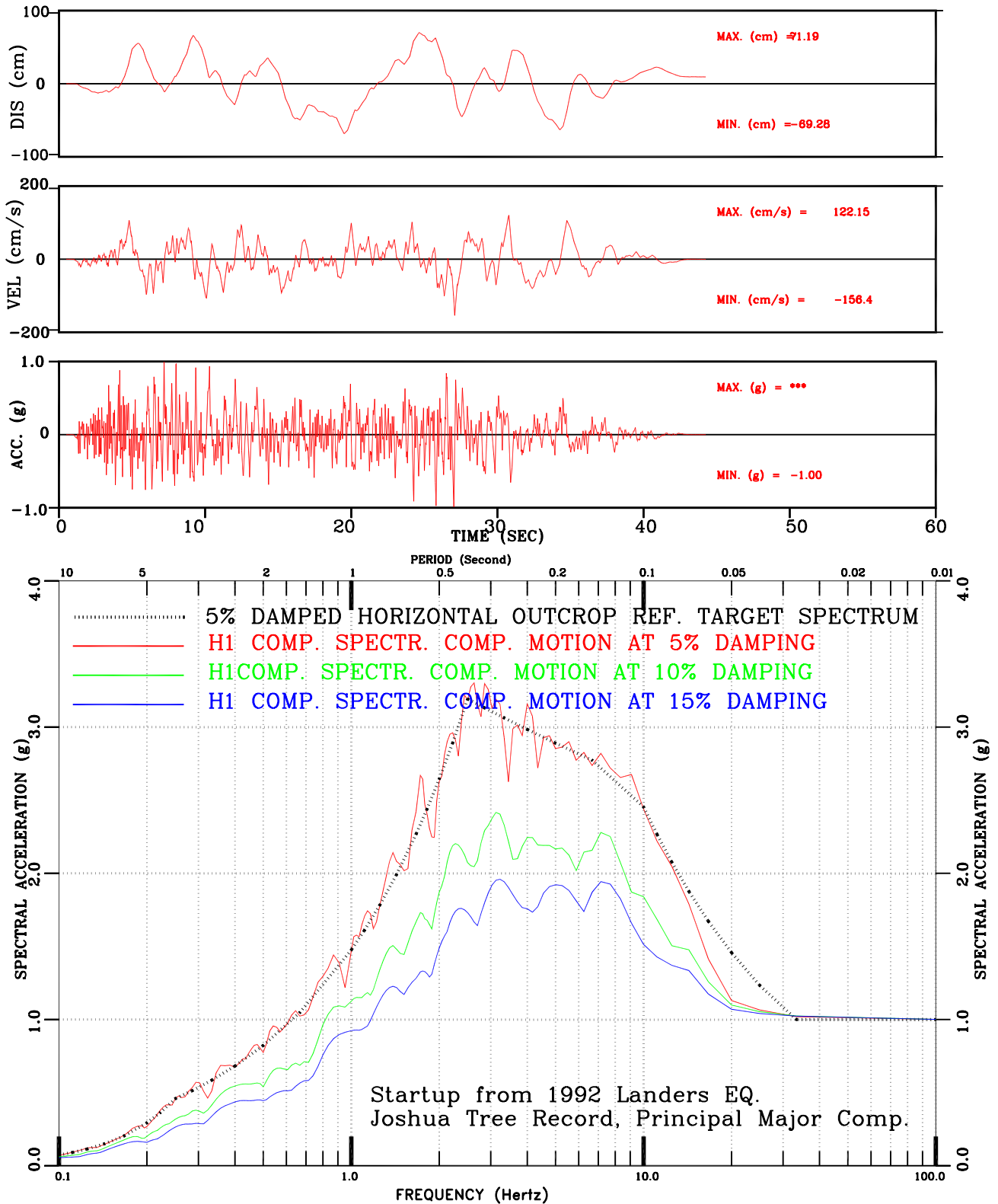


Figure III-85: Set-3 H1 Comp. Motion Conforming to Regulatory Guide 1.60 Spectral Shape

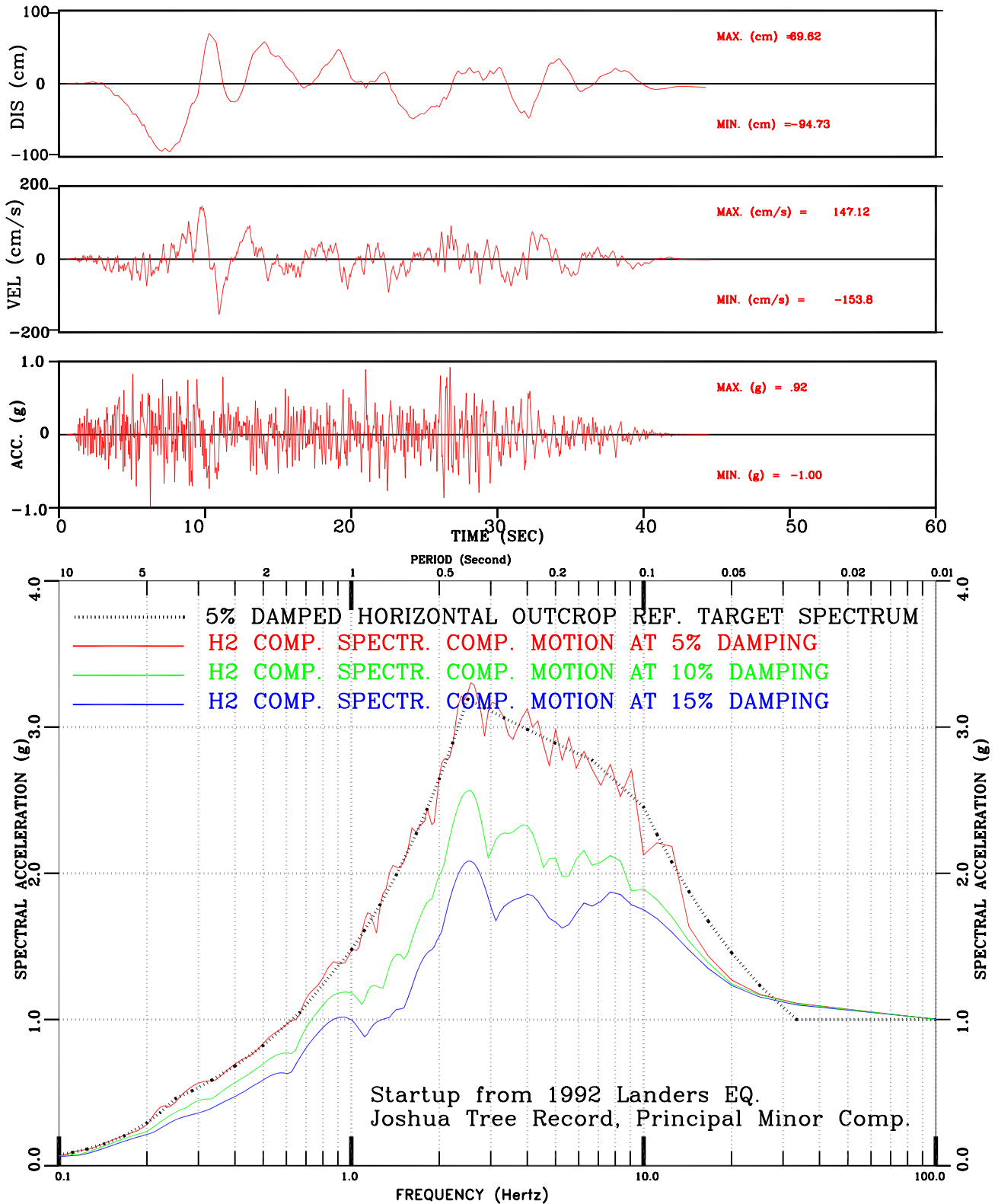


Figure III-86: Set-3 H2 Comp. Motion Conforming to Regulatory Guide 1.60 Spectral Shape

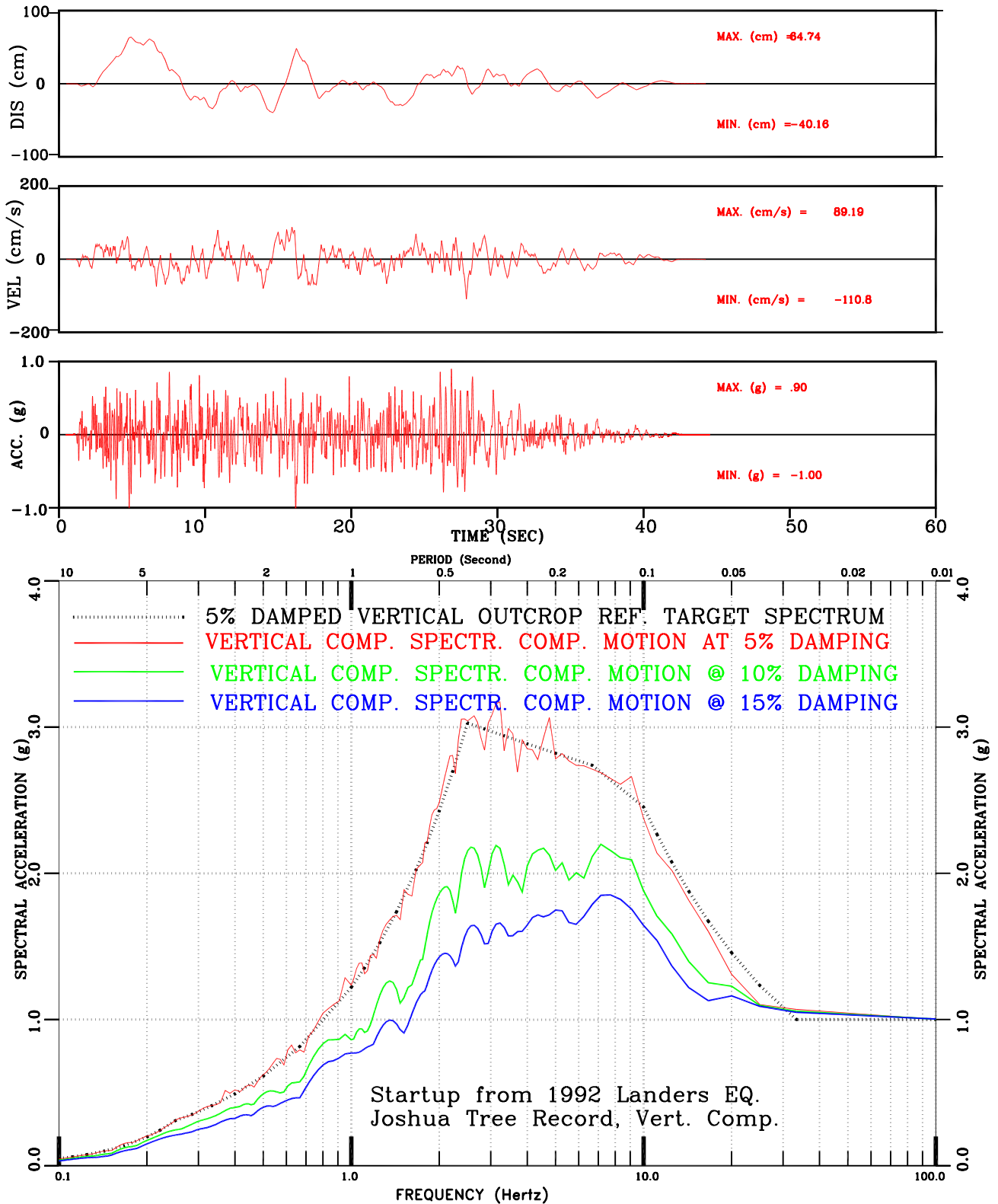


Figure III-87: Set-3 Vert. Comp. Motion Conforming to Regulatory Guide 1.60 Spectral Shape

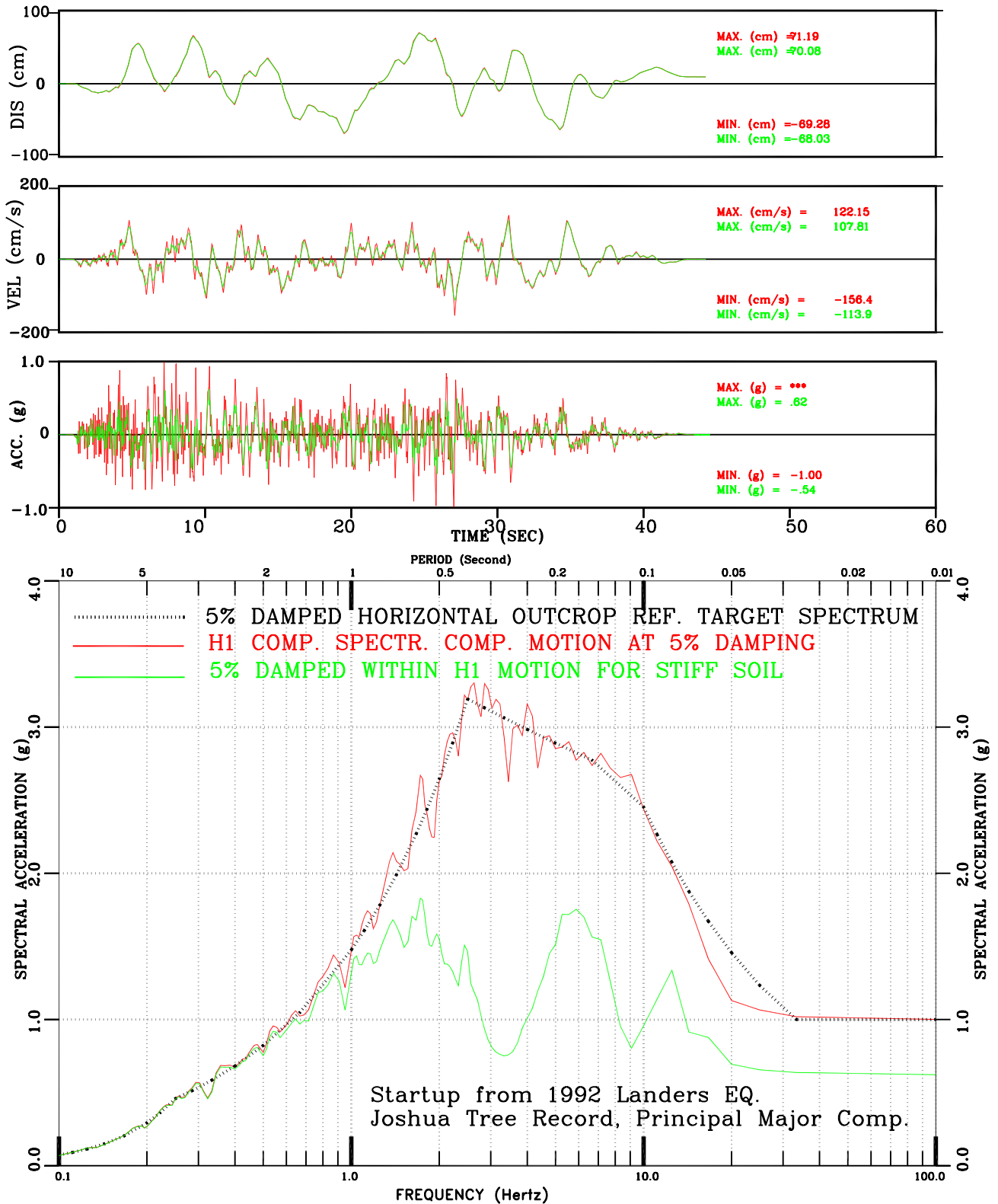


Figure III-88: Within vs. Surface Motion for Stiff Soil  
Set-3 H1 Comp. Motion Conforming to Regulatory Guide 1.60 Spectral Shape

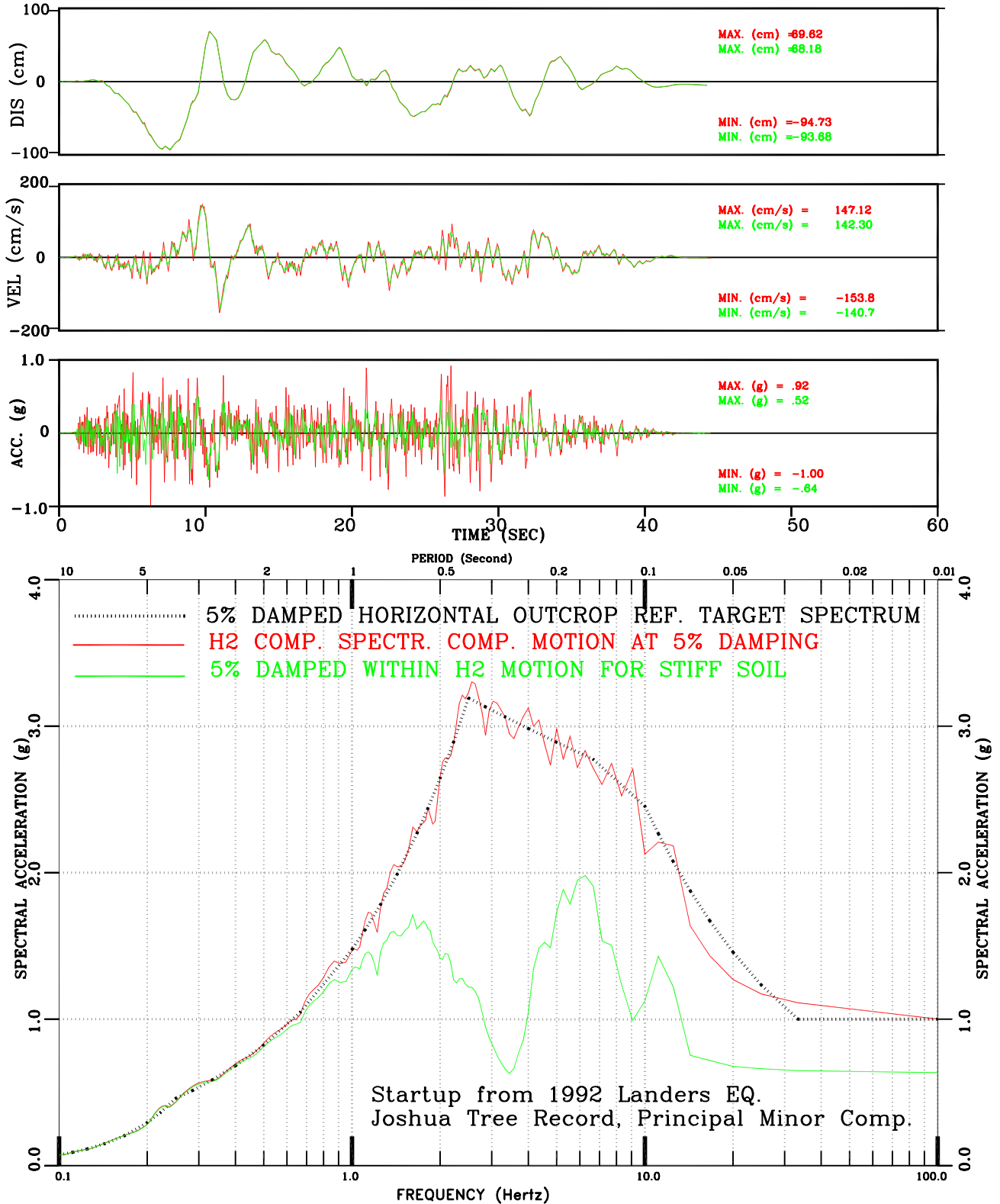


Figure III-89: Within vs. Surface Motion for Stiff Soil  
 Set-3 H2 Comp. Motion Conforming to Regulatory Guide 1.60 Spectral Shape

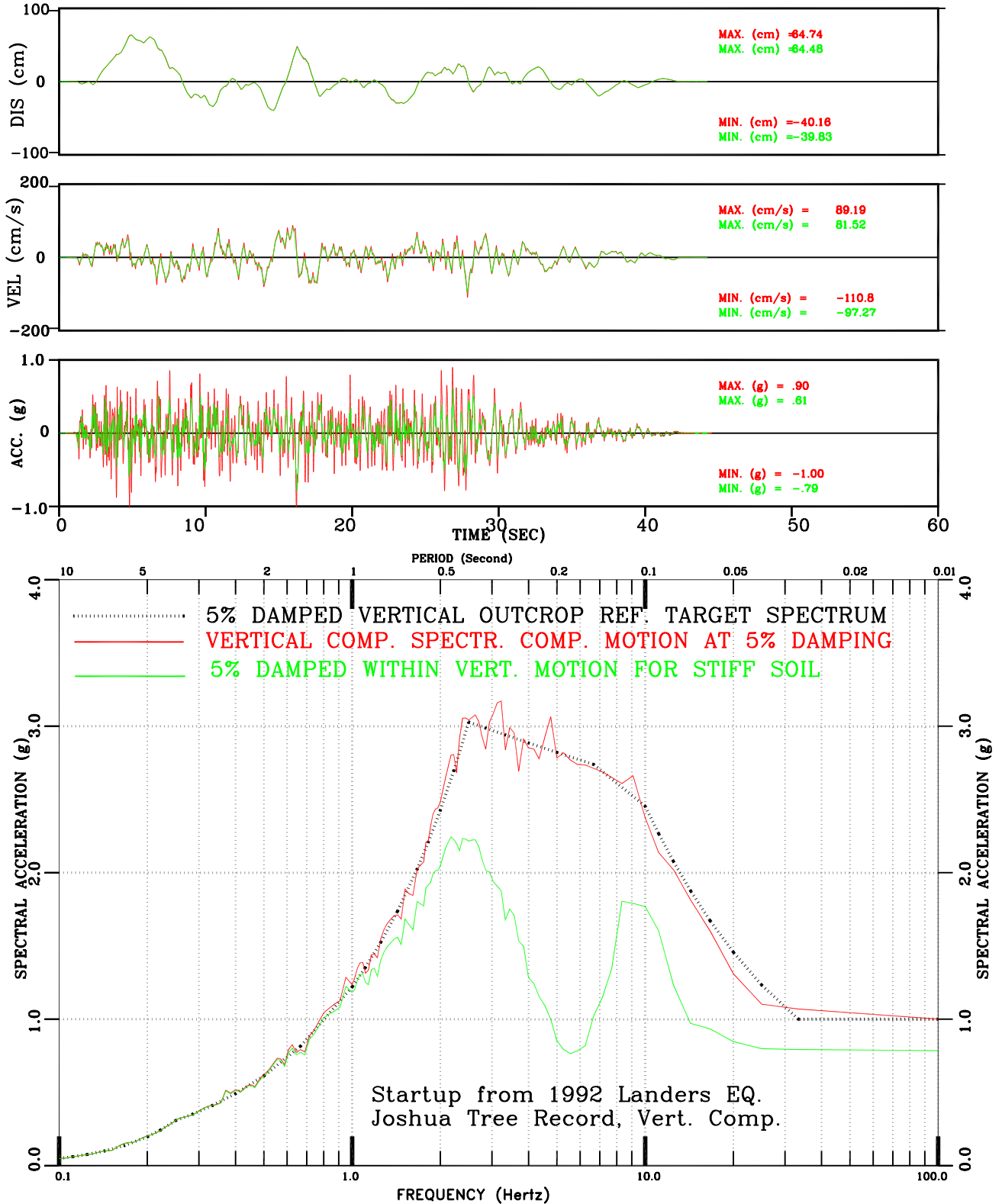


Figure III-90: Within vs. Surface Motion for Stiff Soil  
 Set-3 Vert. Comp. Motion Conforming to Regulatory Guide 1.60 Spectral Shape

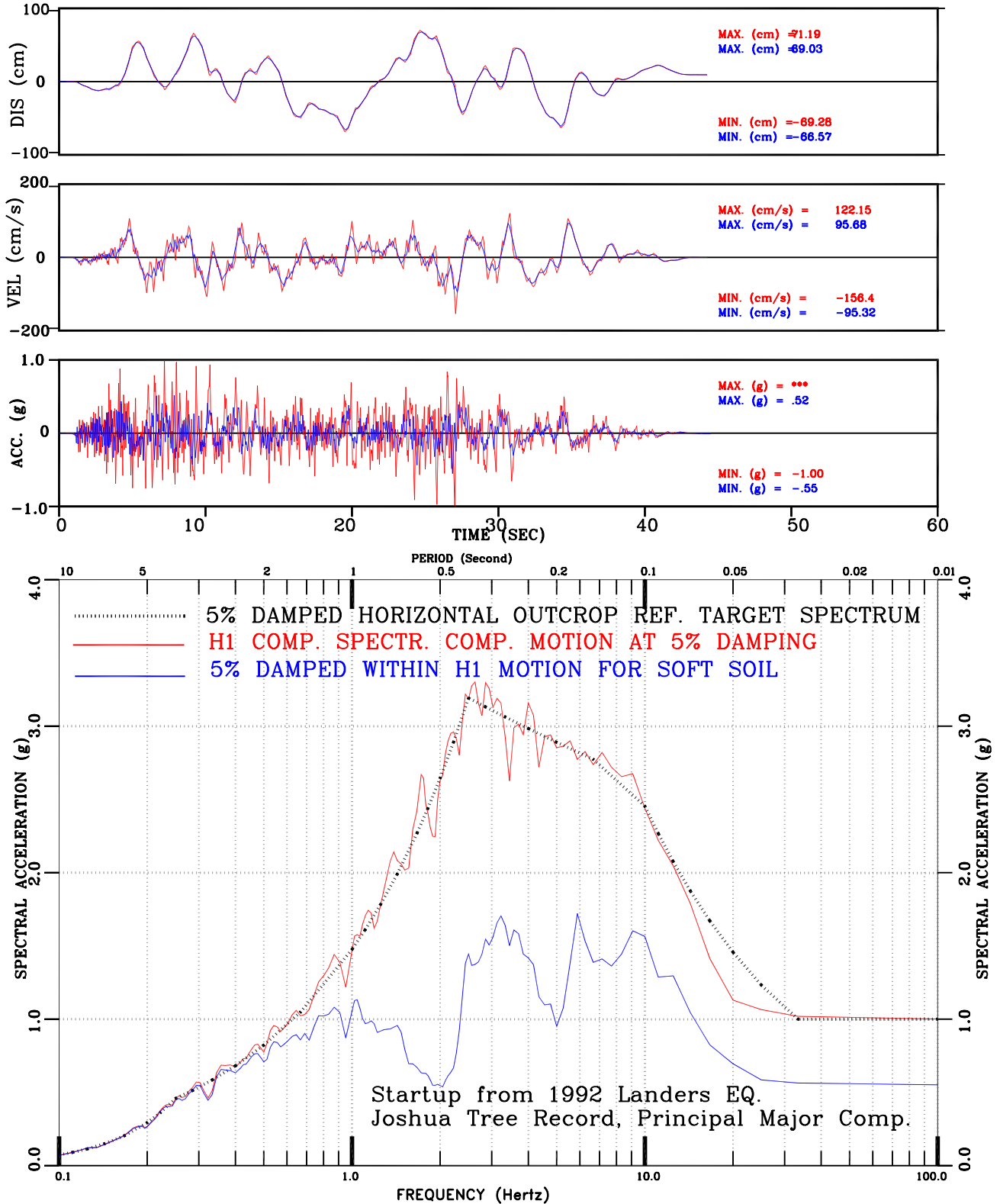


Figure III-91: Within vs. Surface Motion for Soft Soil  
Set-3 H1 Comp. Motion Conforming to Regulatory Guide 1.60 Spectral Shape

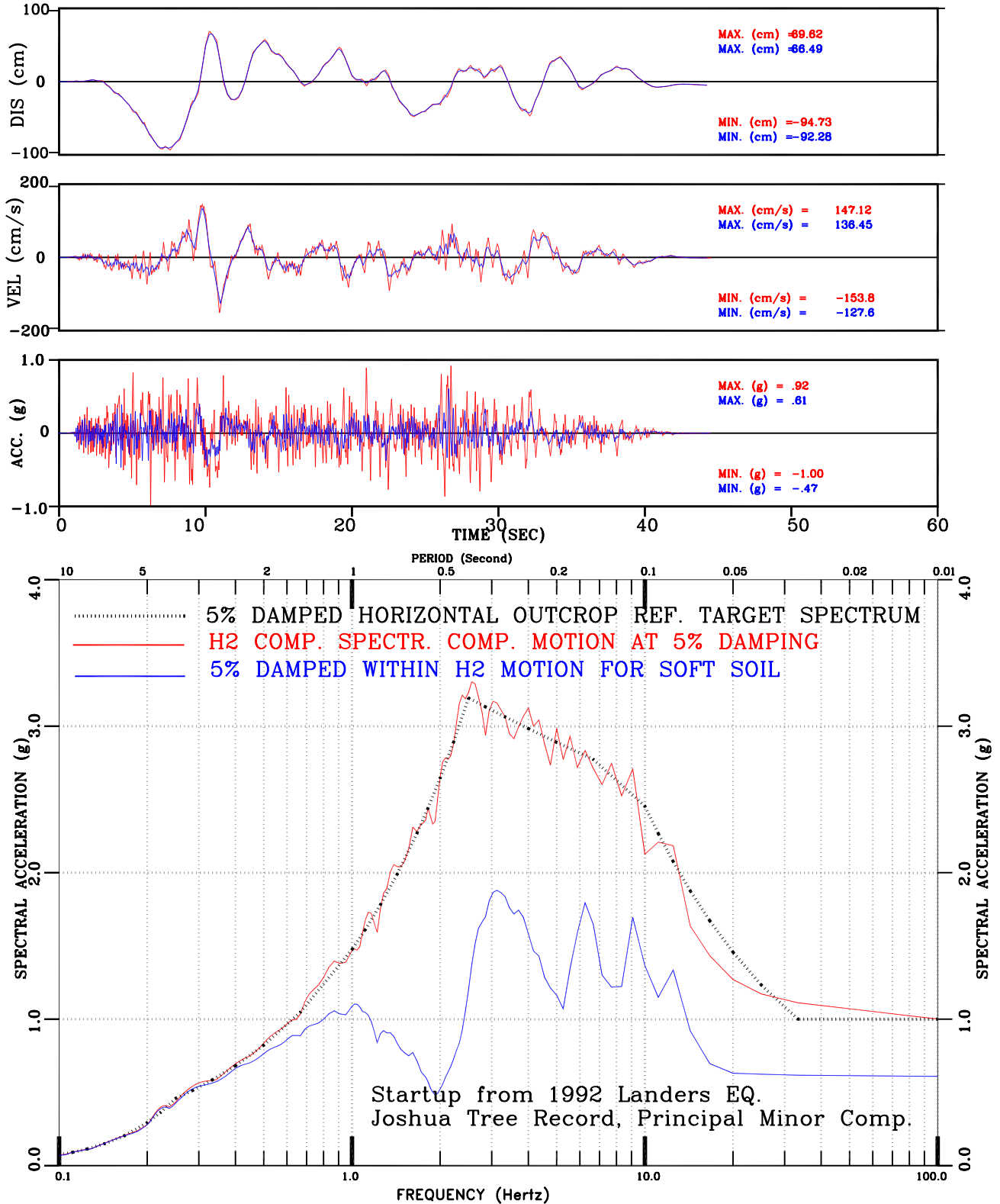


Figure III-92: Within vs. Surface Motion for Soft Soil  
Set-3 H2 Comp. Motion Conforming to Regulatory Guide 1.60 Spectral Shape

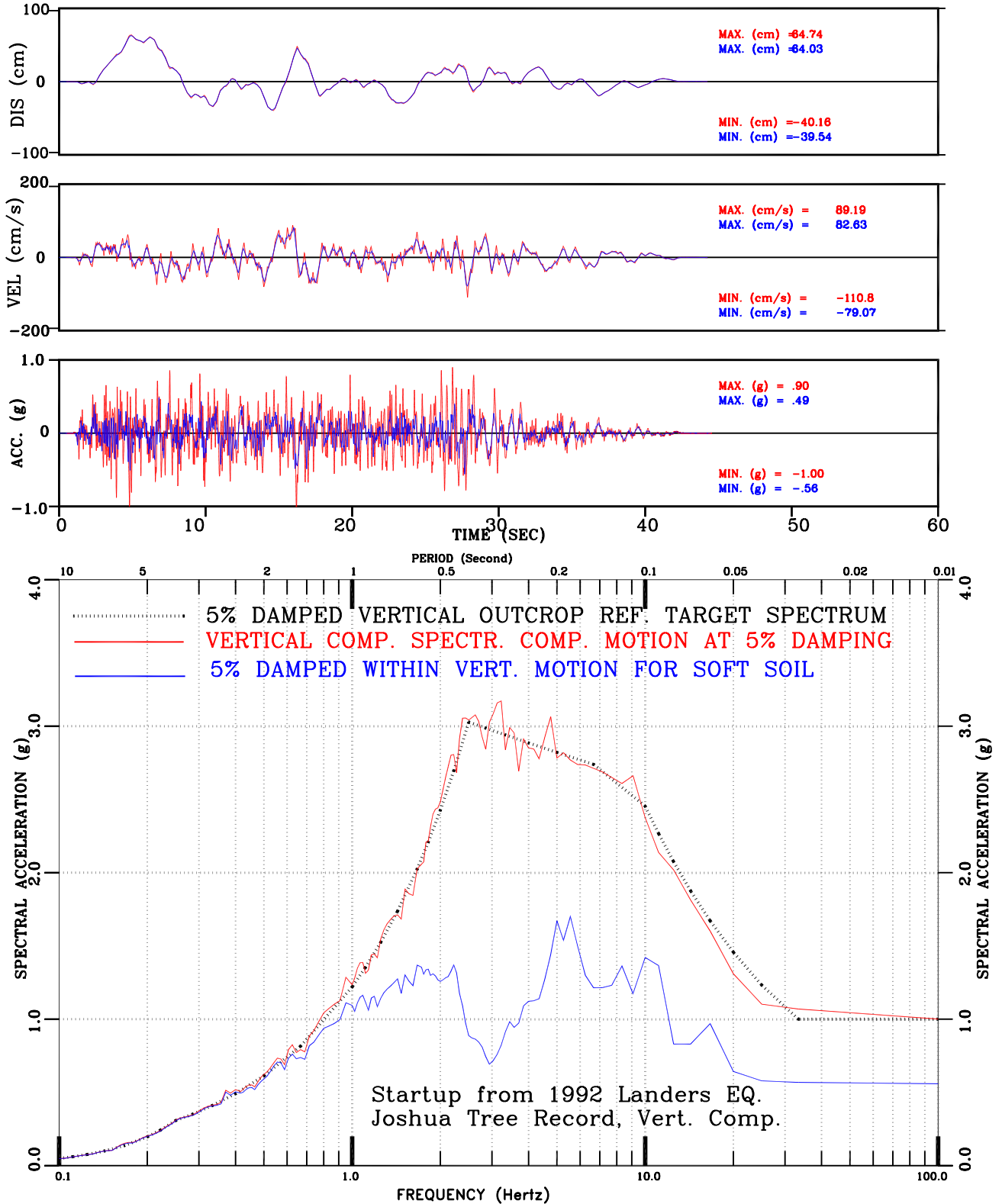


Figure III-93: Within vs. Surface Motion for Soft Soil  
Set-3 Vert. Comp. Motion Conforming to Regulatory Guide 1.60 Spectral Shape

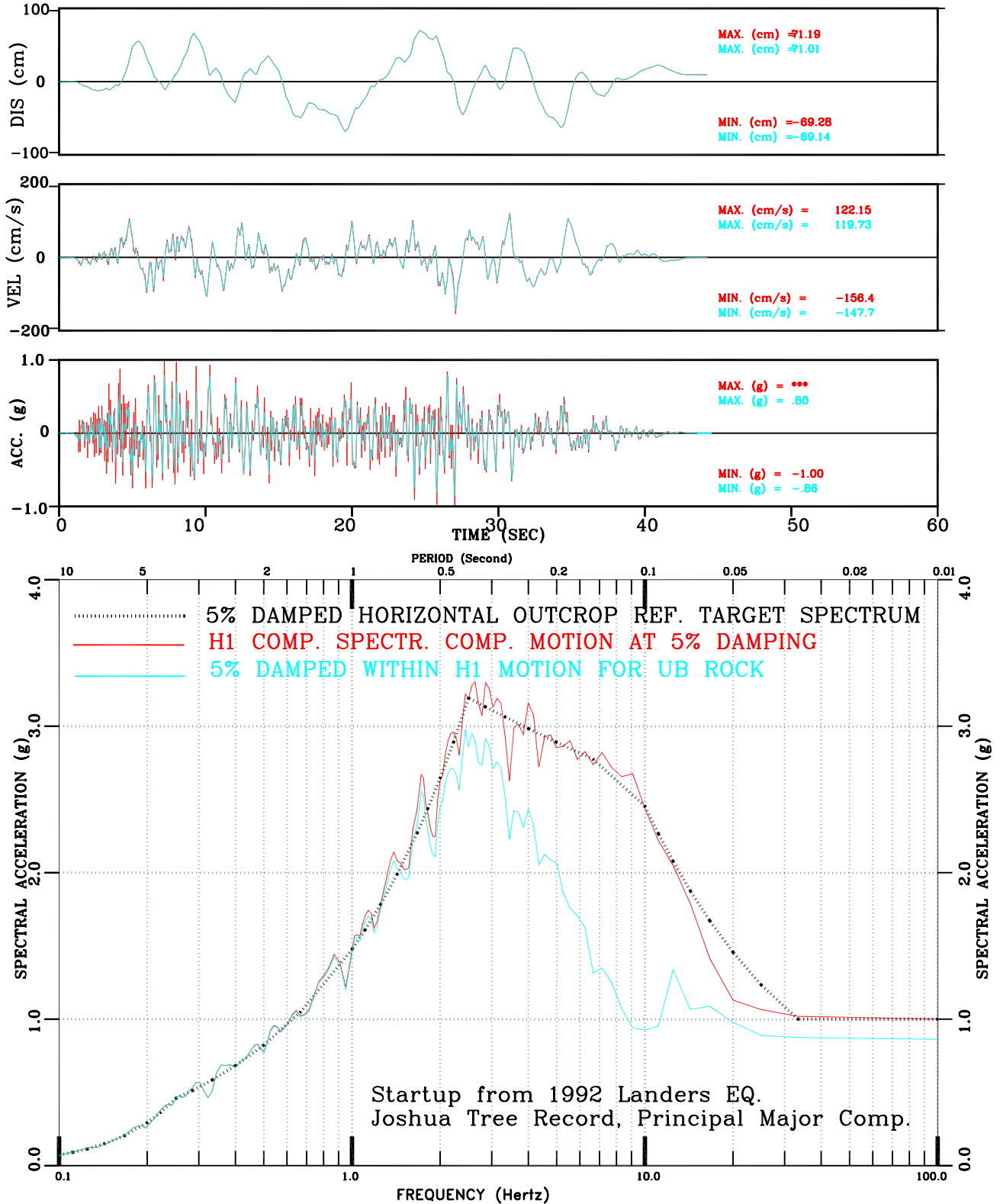


Figure III-94: Within vs. Surface Motion for UB Rock  
 Set-3 H1 Comp. Motion Conforming to Regulatory Guide 1.60 Spectral Shape

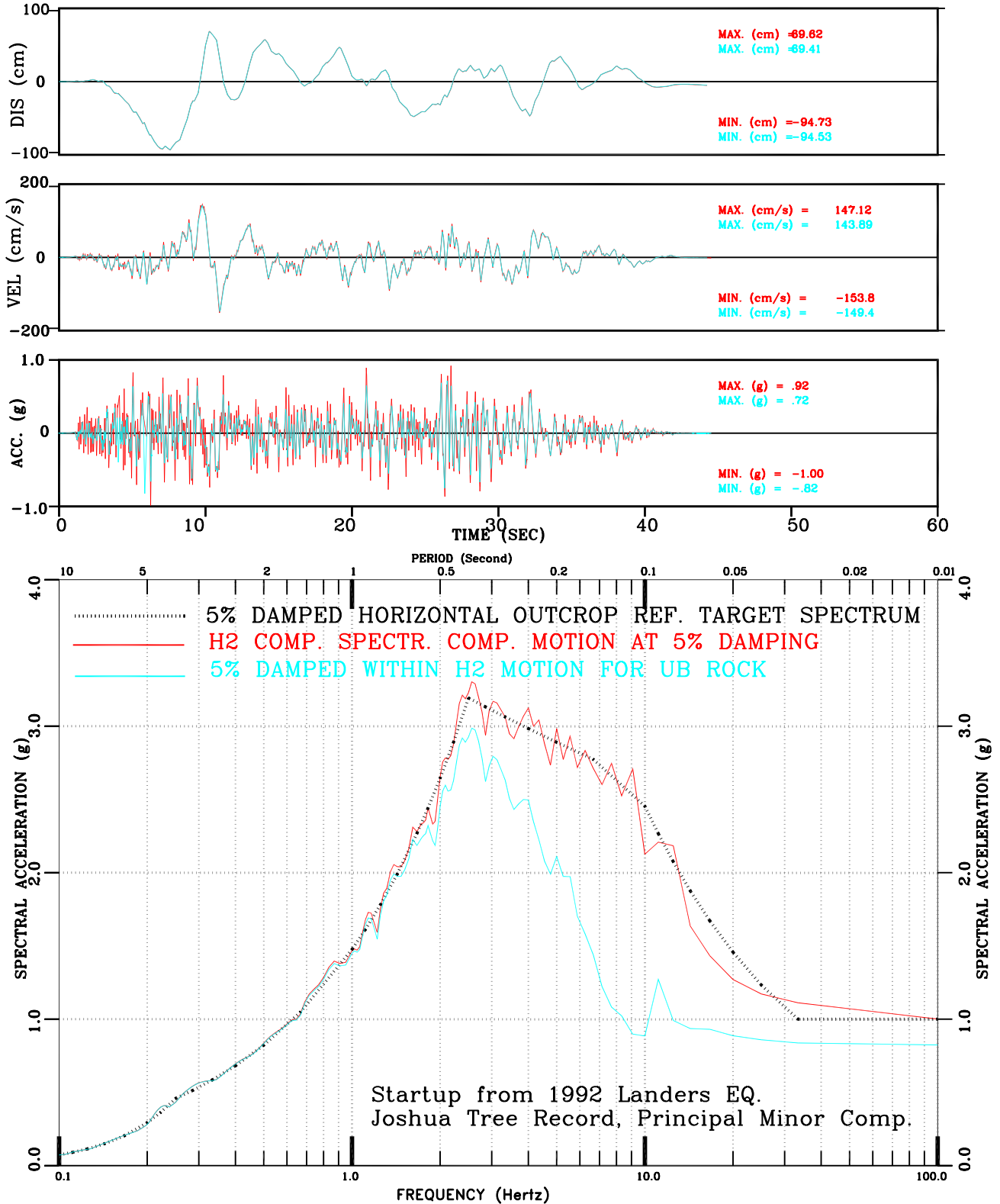


Figure III-95: Within vs. Surface Motion for UB Rock  
Set-3 H2 Comp. Motion Conforming to Regulatory Guide 1.60 Spectral Shape

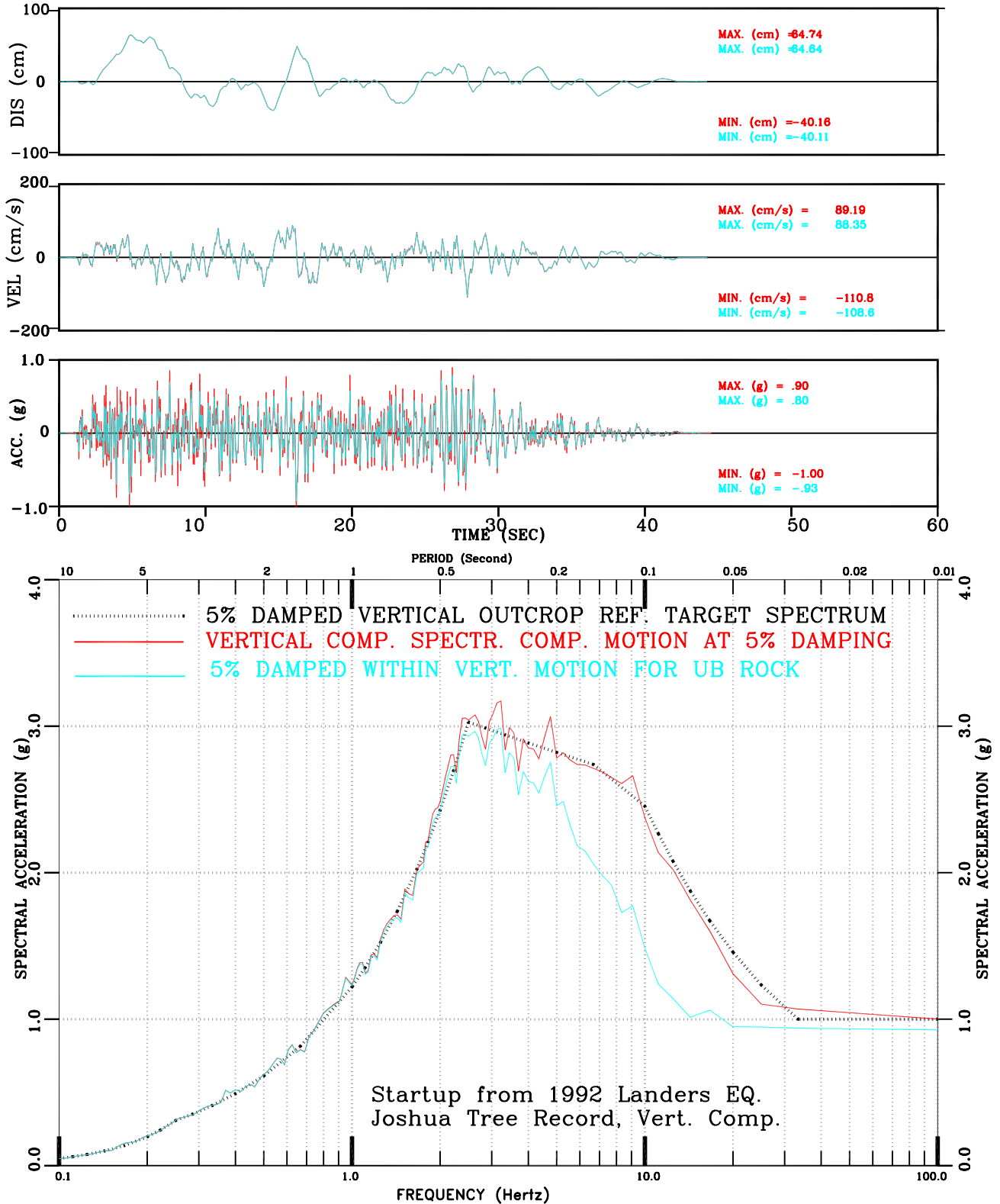


Figure III-96: Within vs. Surface Motion for UB Rock Set-3 Vert. Comp. Motion Conforming to Regulatory Guide 1.60 Spectral Shape

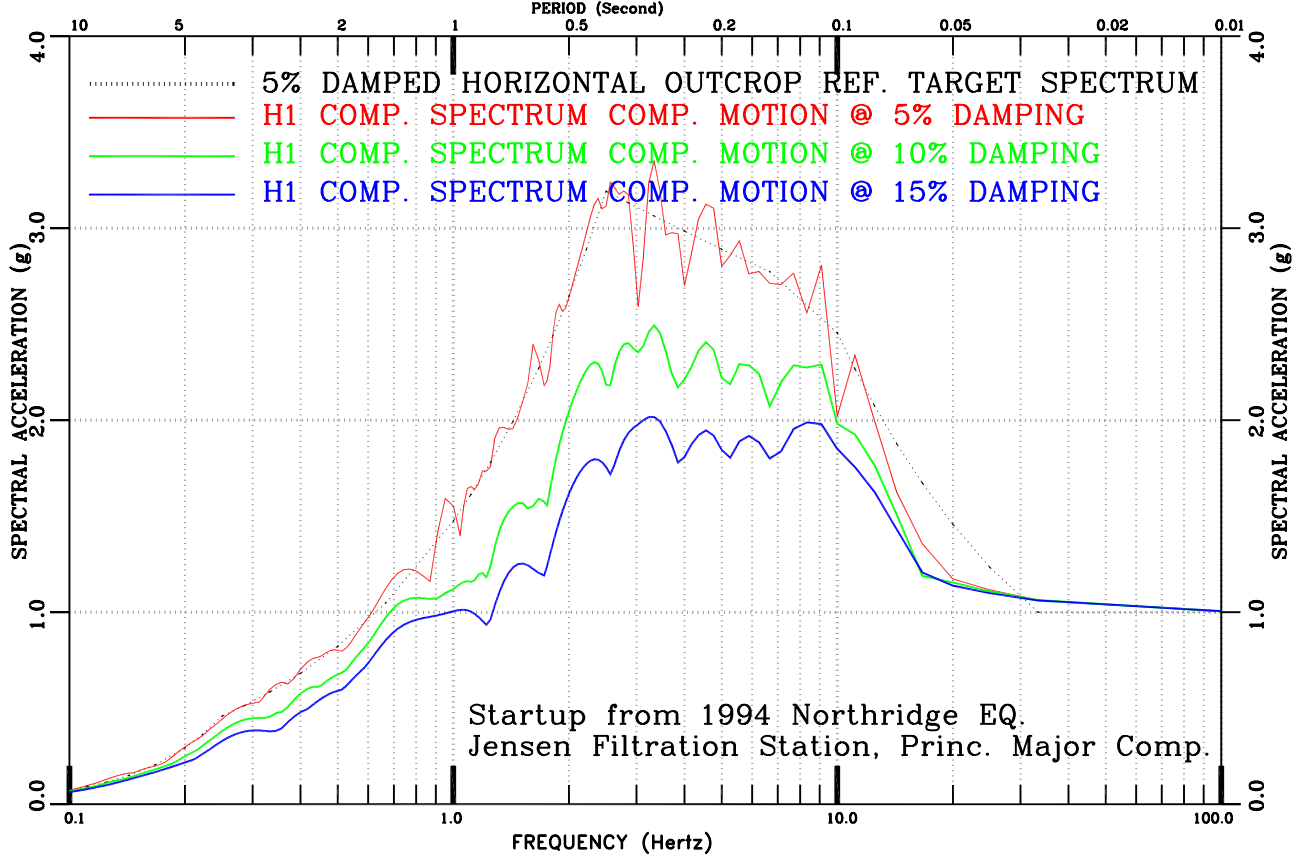
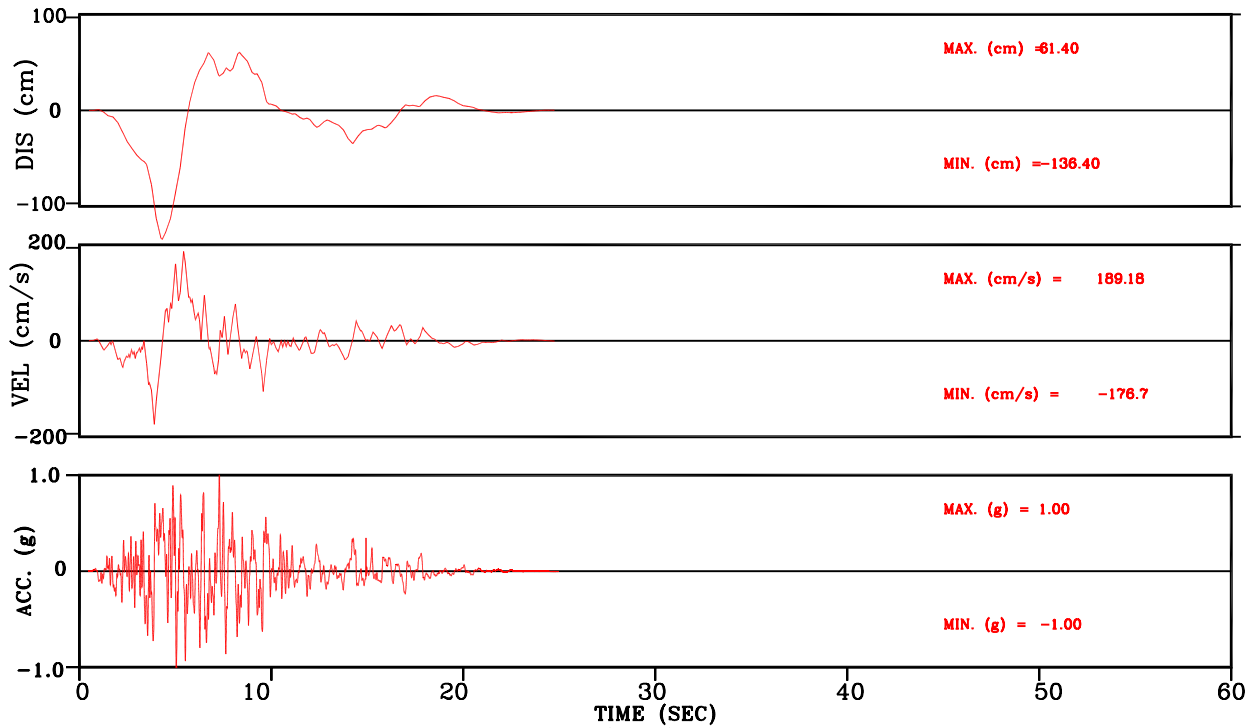


Figure III-97: Set-4 H1 Comp. Motion Conforming to Regulatory Guide 1.60 Spectral Shape

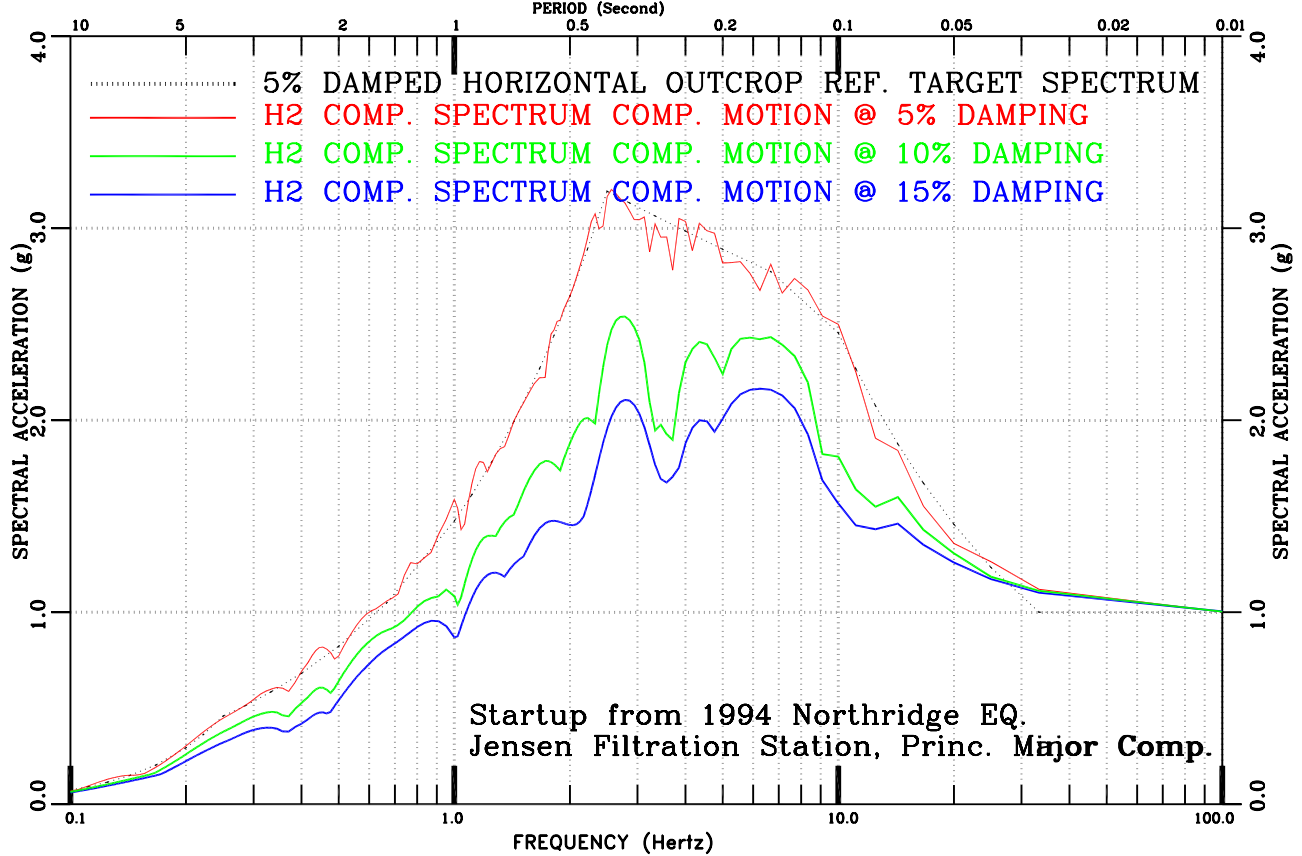
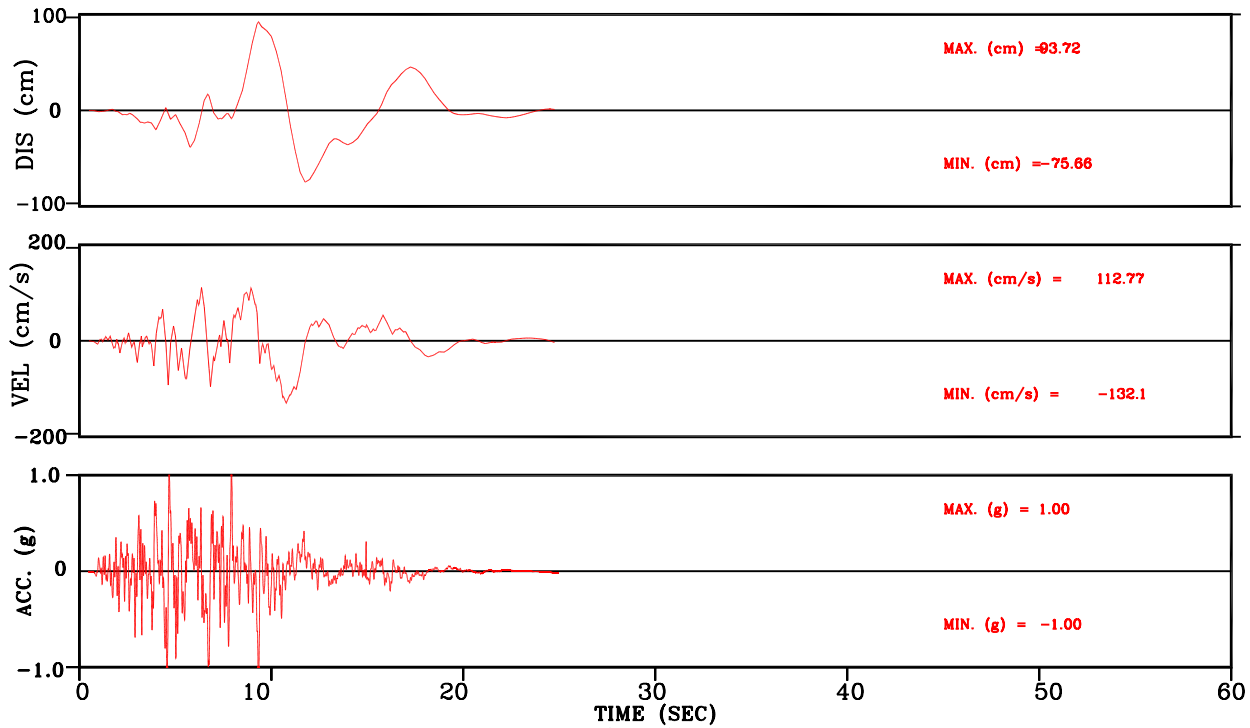


Figure III-98: Set-4 H2 Comp. Motion Conforming to Regulatory Guide 1.60 Spectral Shape

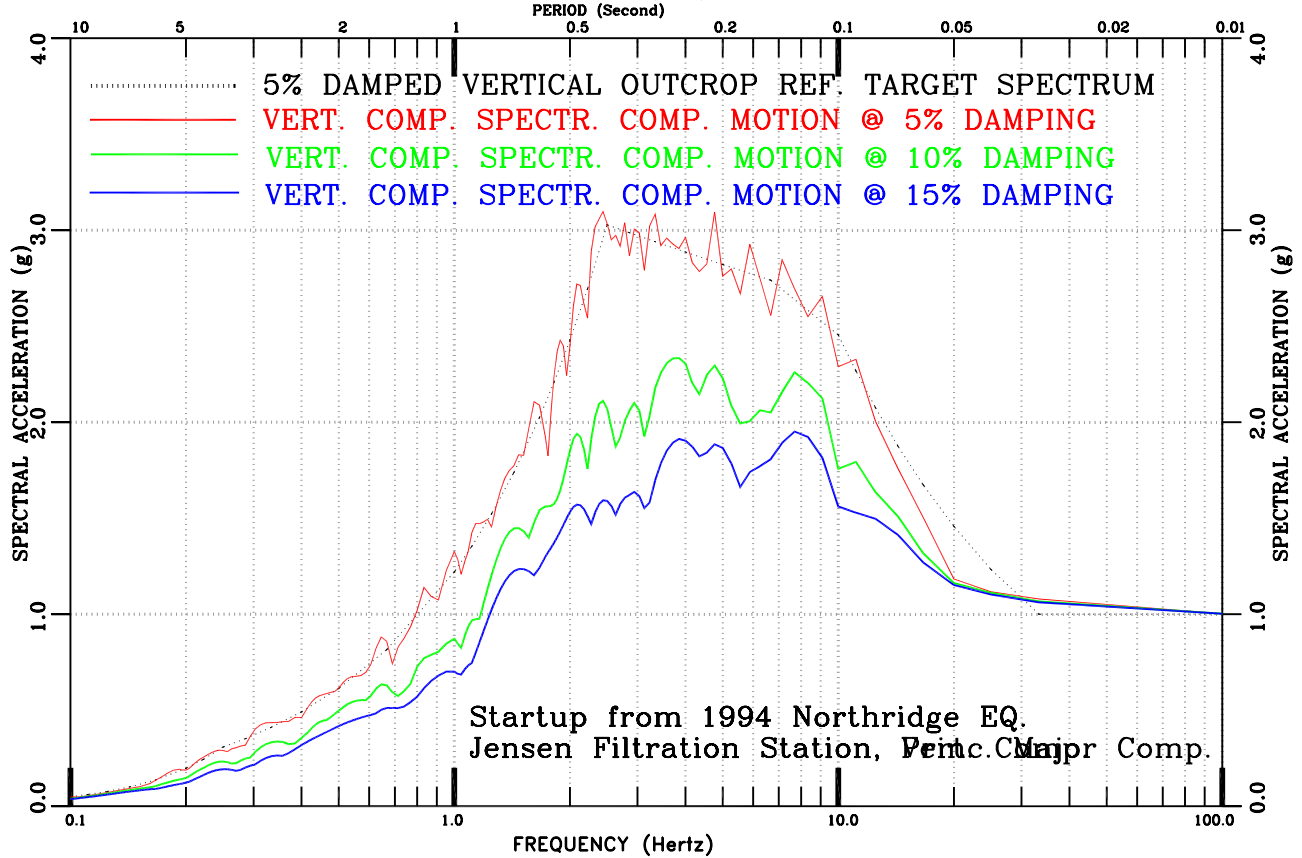
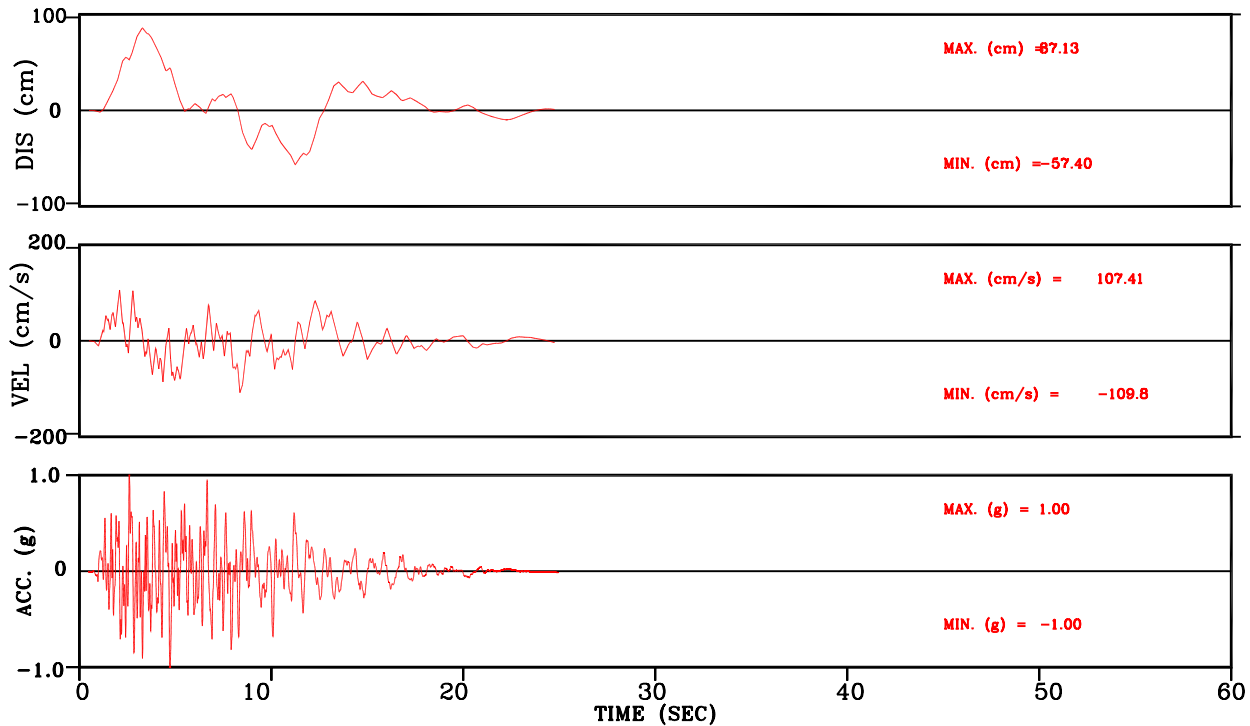


Figure III-99: Set-4 Vert. Comp. Motion Conforming to Regulatory Guide 1.60 Spectral Shape

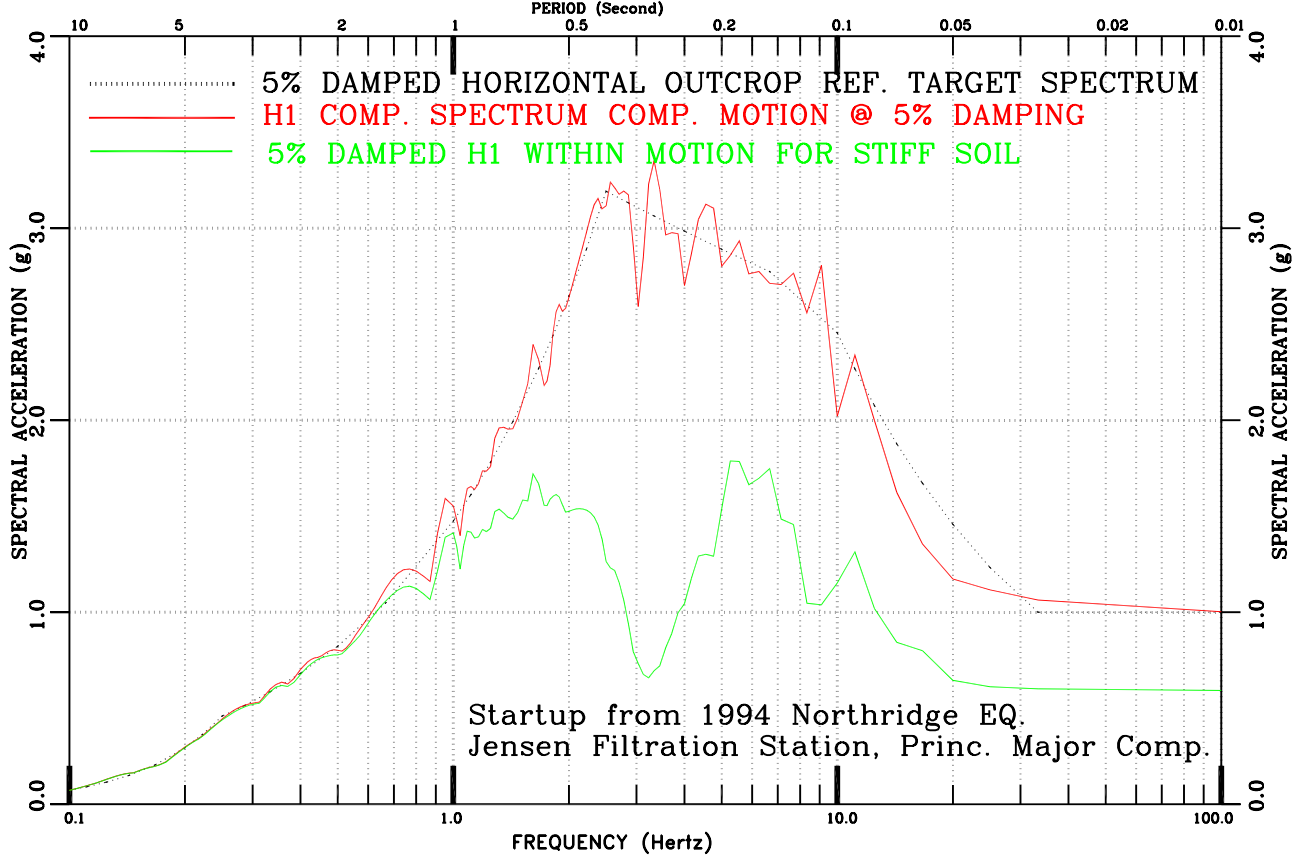
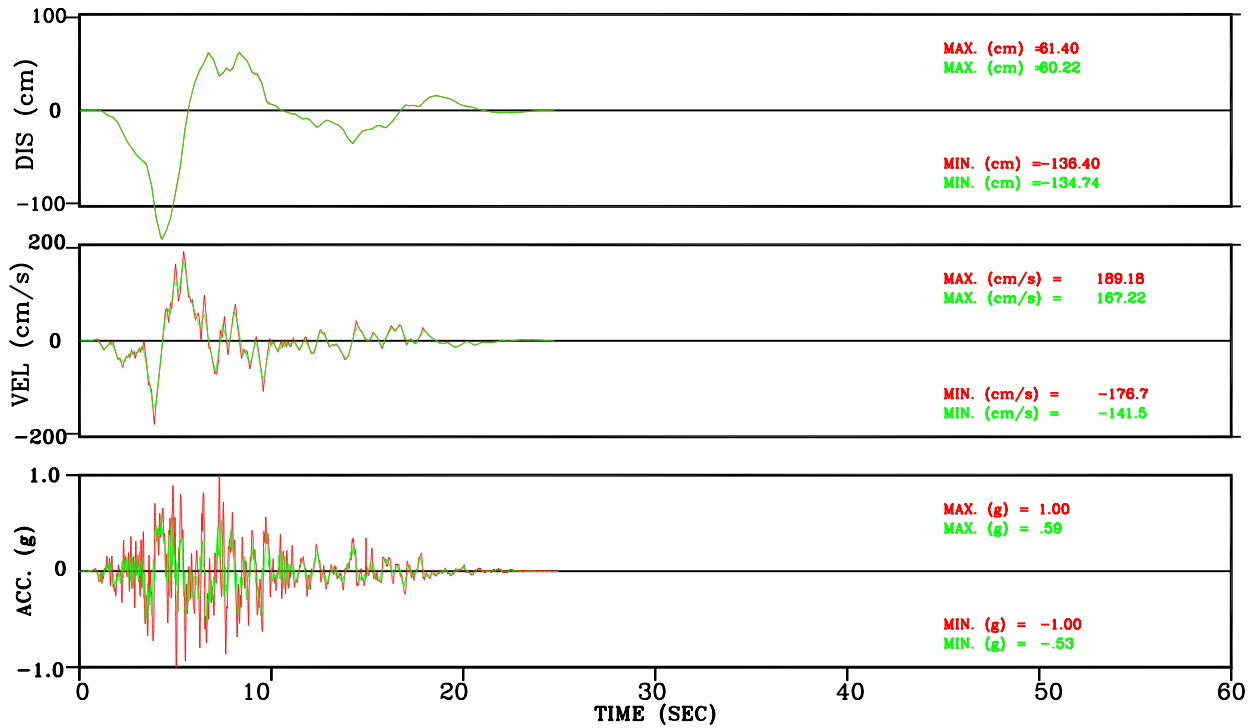


Figure III-100: Within vs. Surface Motion for Stiff Soil  
 Set-4 H1 Comp. Motion Conforming to Regulatory Guide 1.60 Spectral Shape

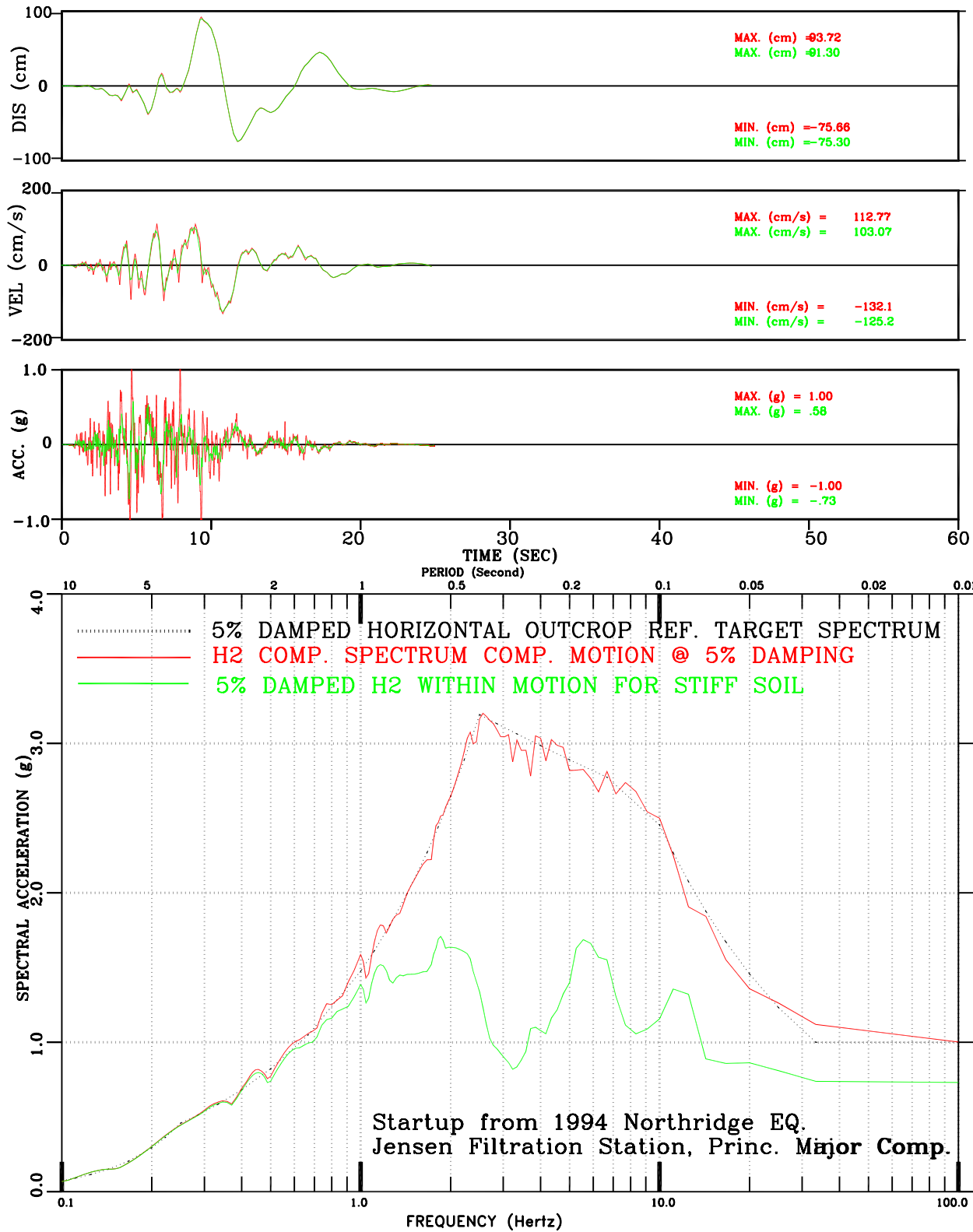


Figure III-101: Within vs. Surface Motion for Stiff Soil  
 Set-4 H2 Comp. Motion Conforming to Regulatory Guide 1.60 Spectral Shape

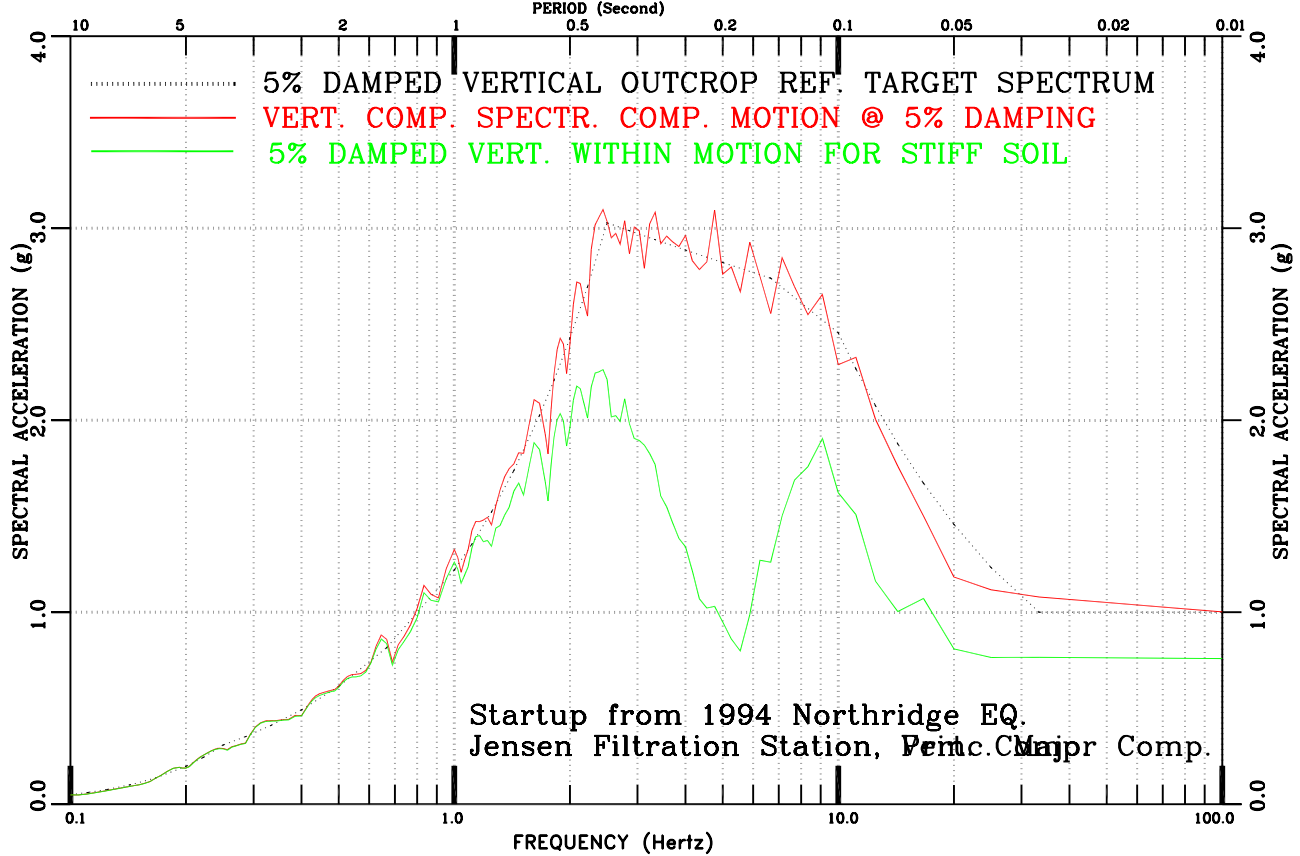
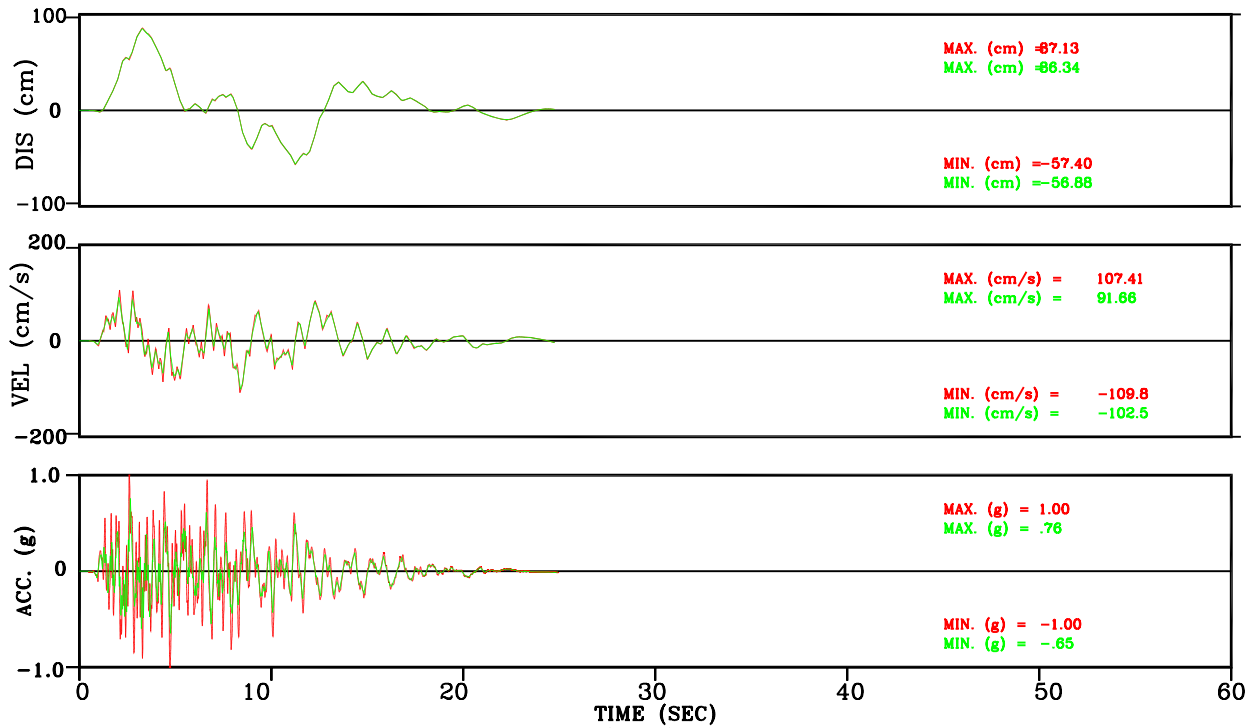


Figure III-102: Within vs. Surface Motion for Stiff Soil  
 Set-4 Vert. Comp. Motion Conforming to Regulatory Guide 1.60 Spectral Shape

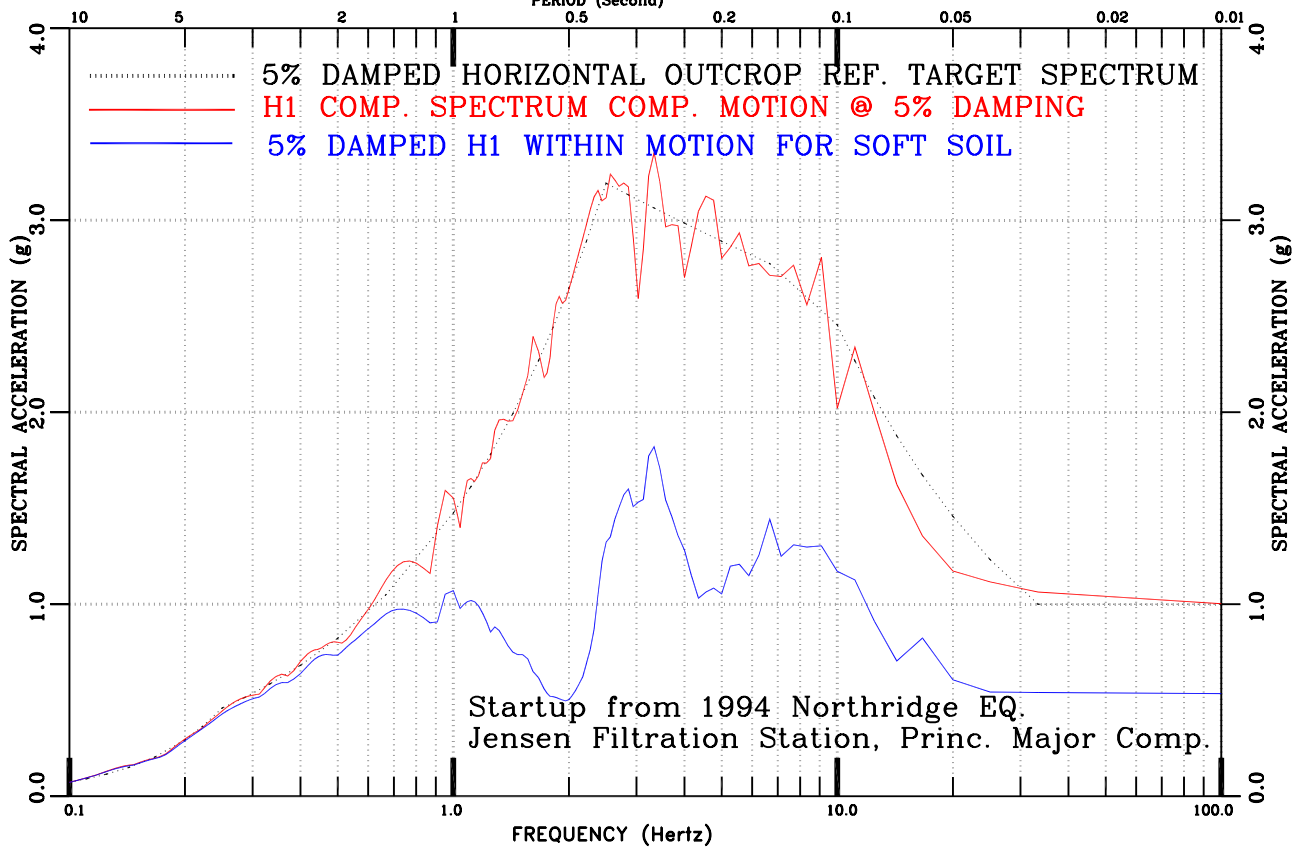
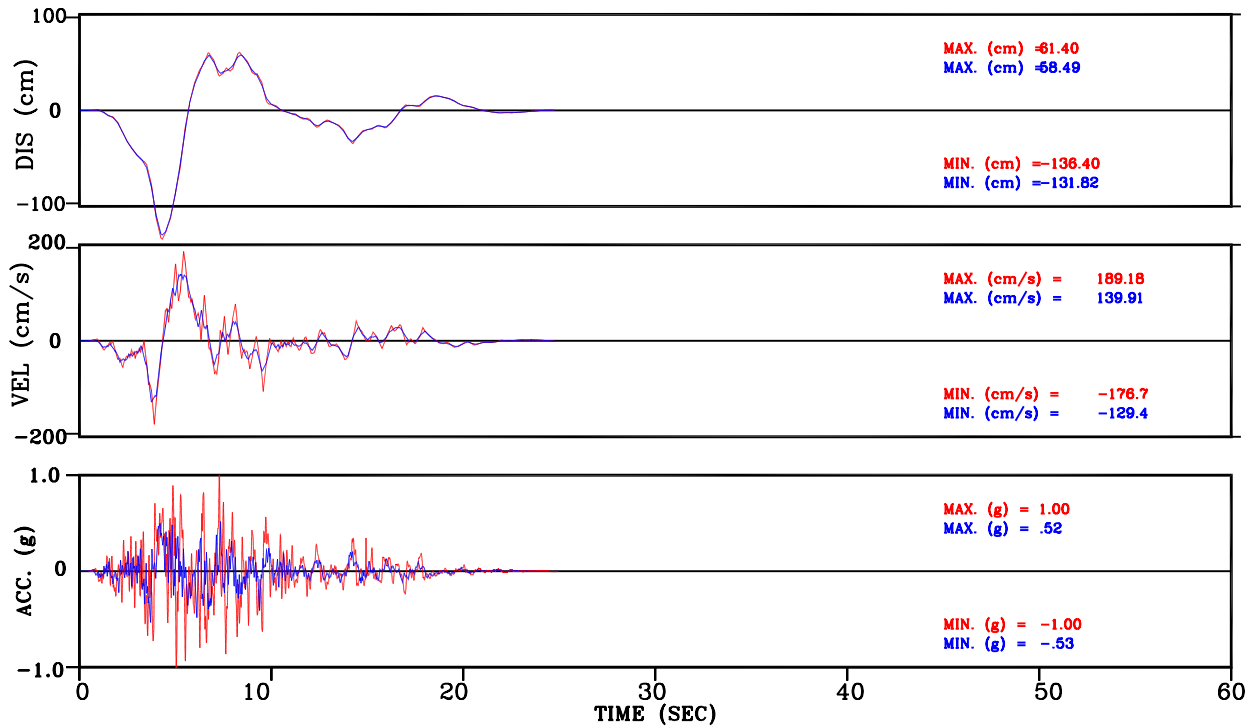


Figure III-103: Within vs. Surface Motion for Soft Soil  
 Set-4 H1 Comp. Motion Conforming to Regulatory Guide 1.60 Spectral Shape

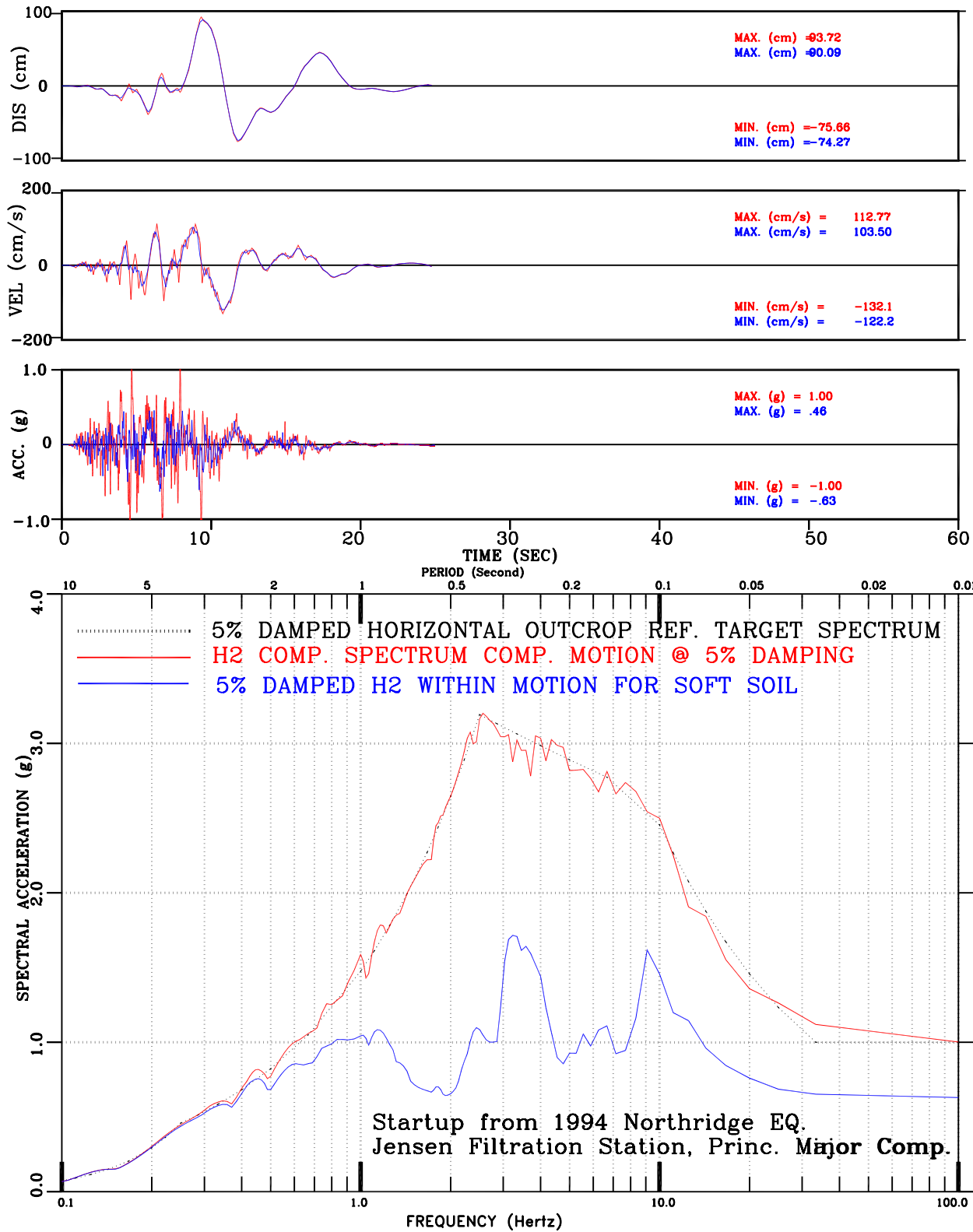


Figure III-104: Within vs. Surface Motion for Soft Soil  
Set-4 H2 Comp. Motion Conforming to Regulatory Guide 1.60 Spectral Shape

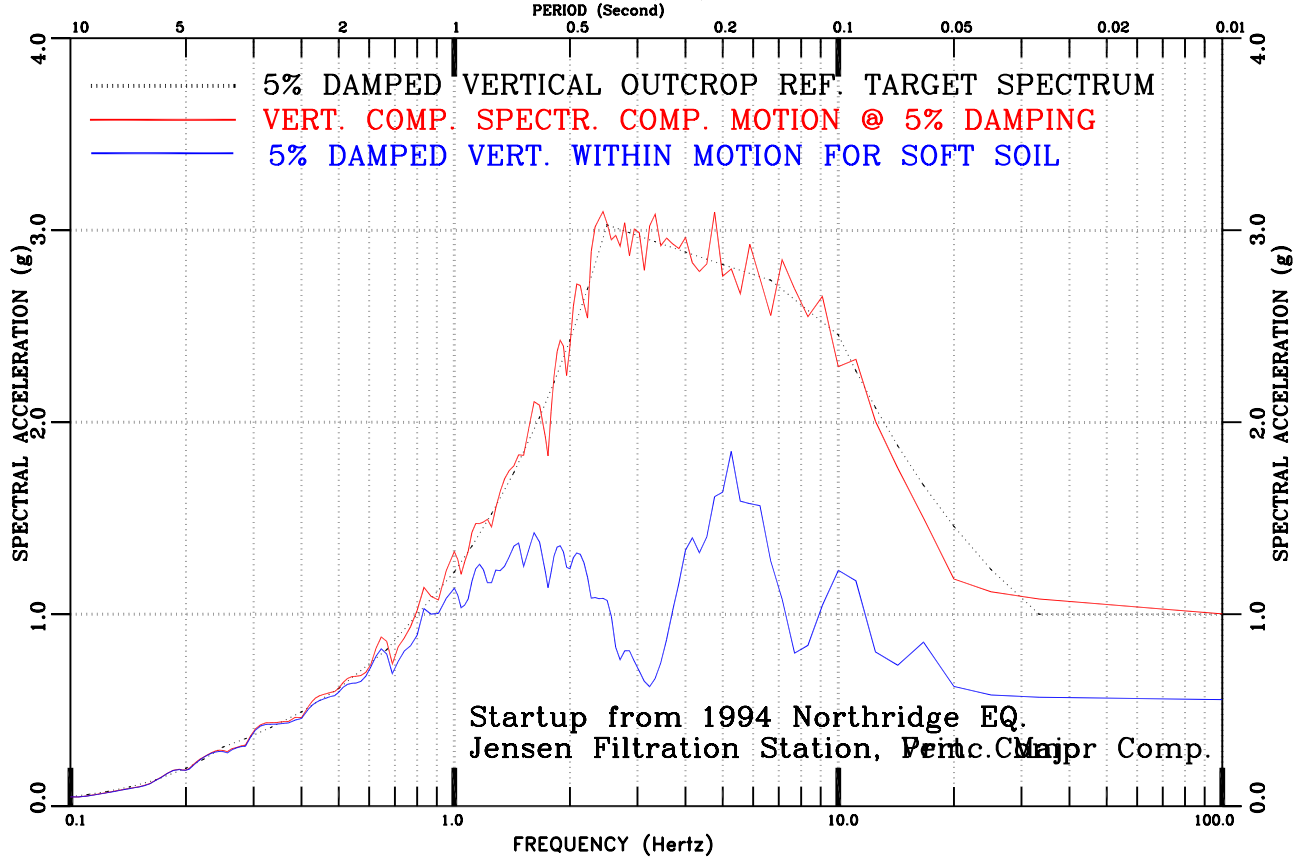
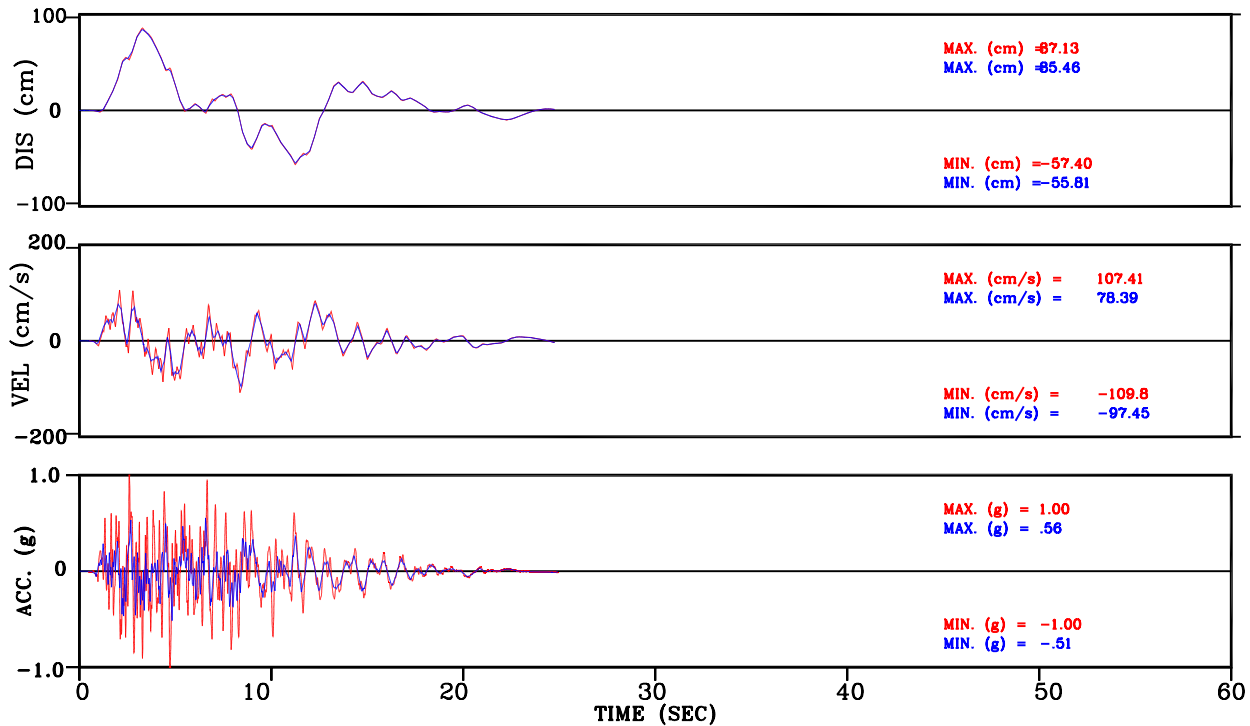


Figure III-105: Within vs. Surface Motion for Soft Soil  
Set-4 Vert. Comp. Motion Conforming to Regulatory Guide 1.60 Spectral Shape

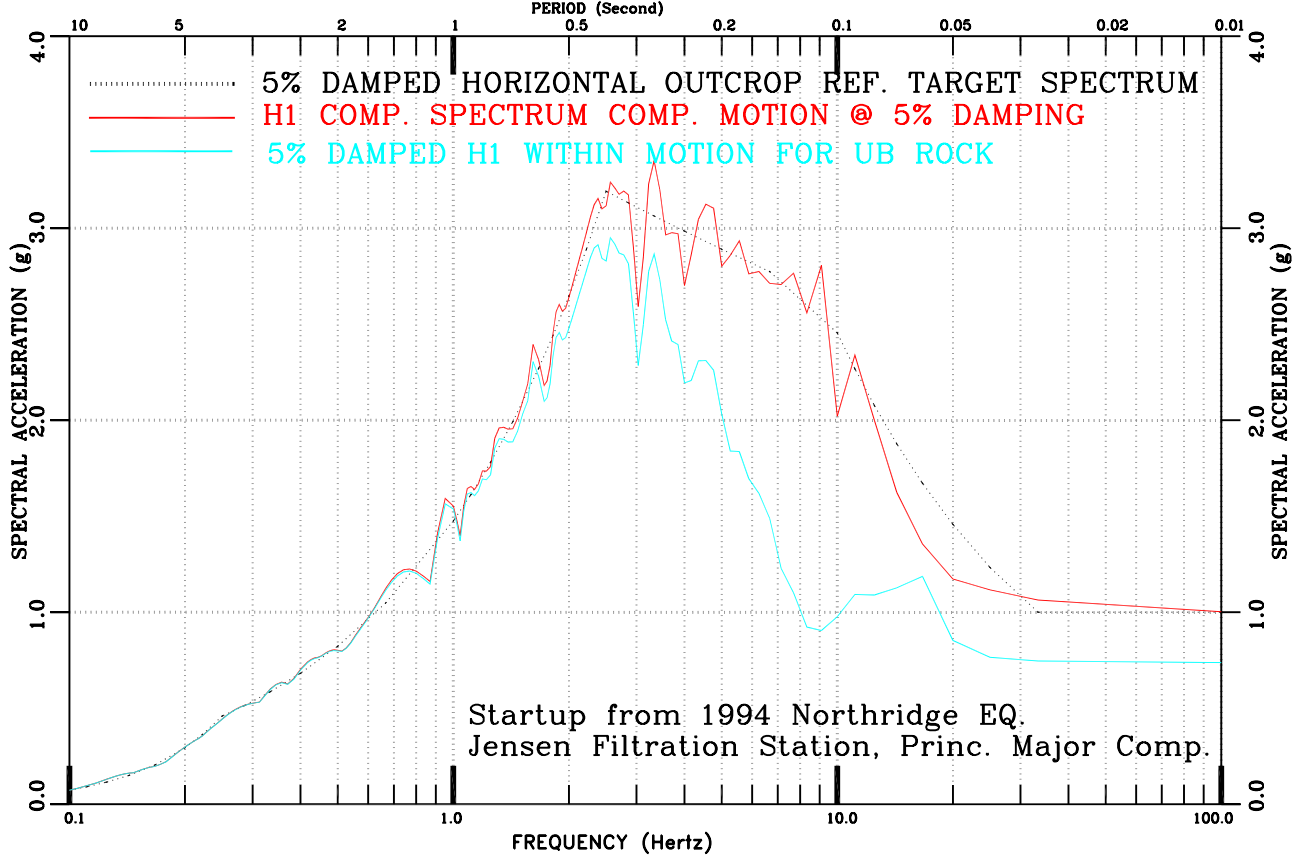
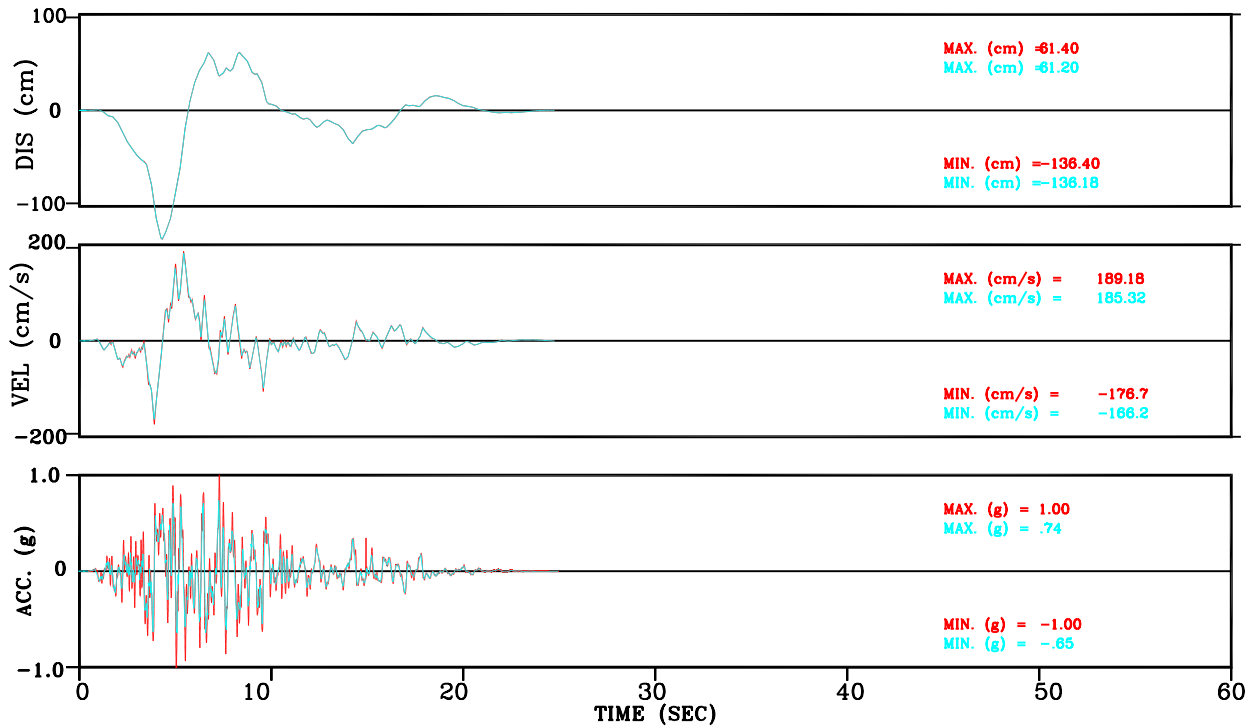


Figure III-106: Within vs. Surface Motion for UB Rock  
Set-4 H1 Comp. Motion Conforming to Regulatory Guide 1.60 Spectral Shape

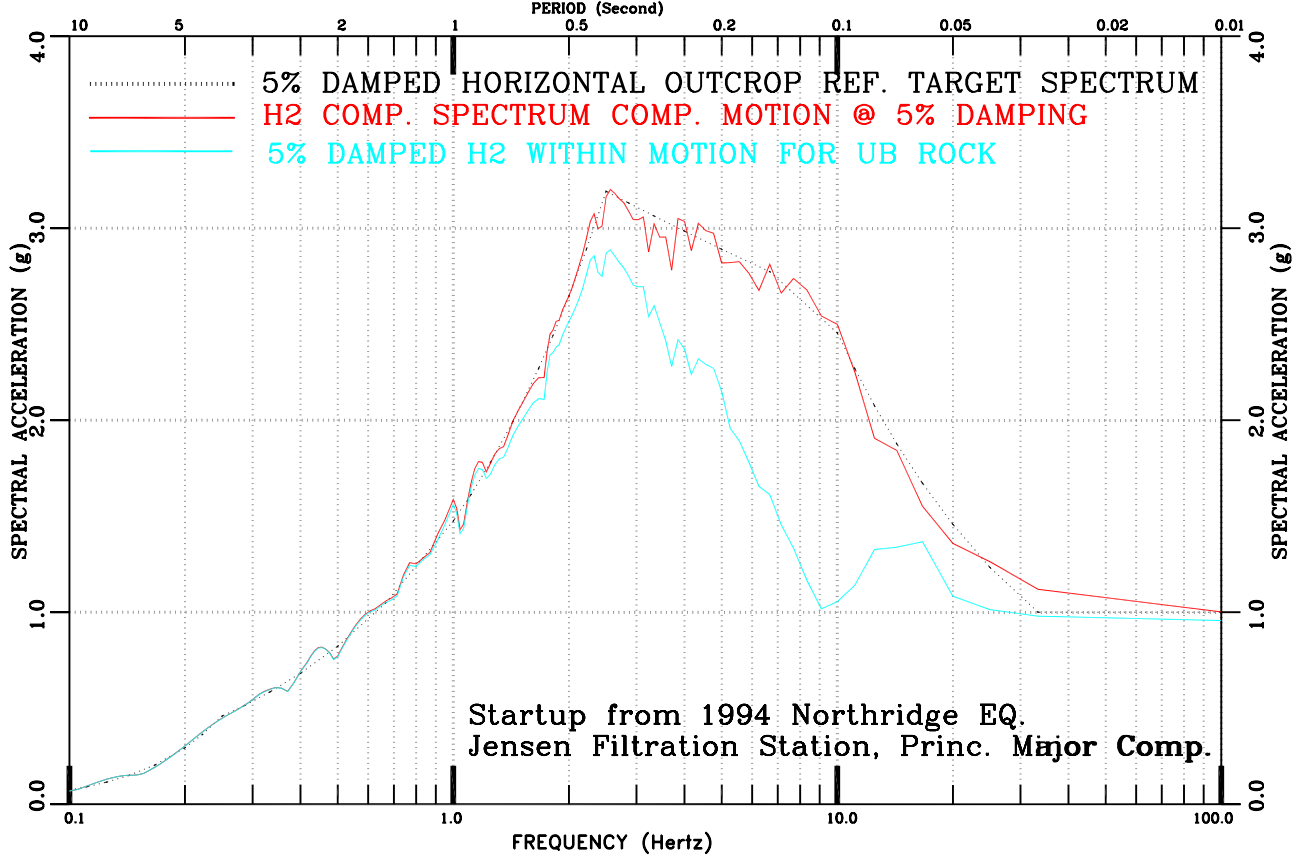
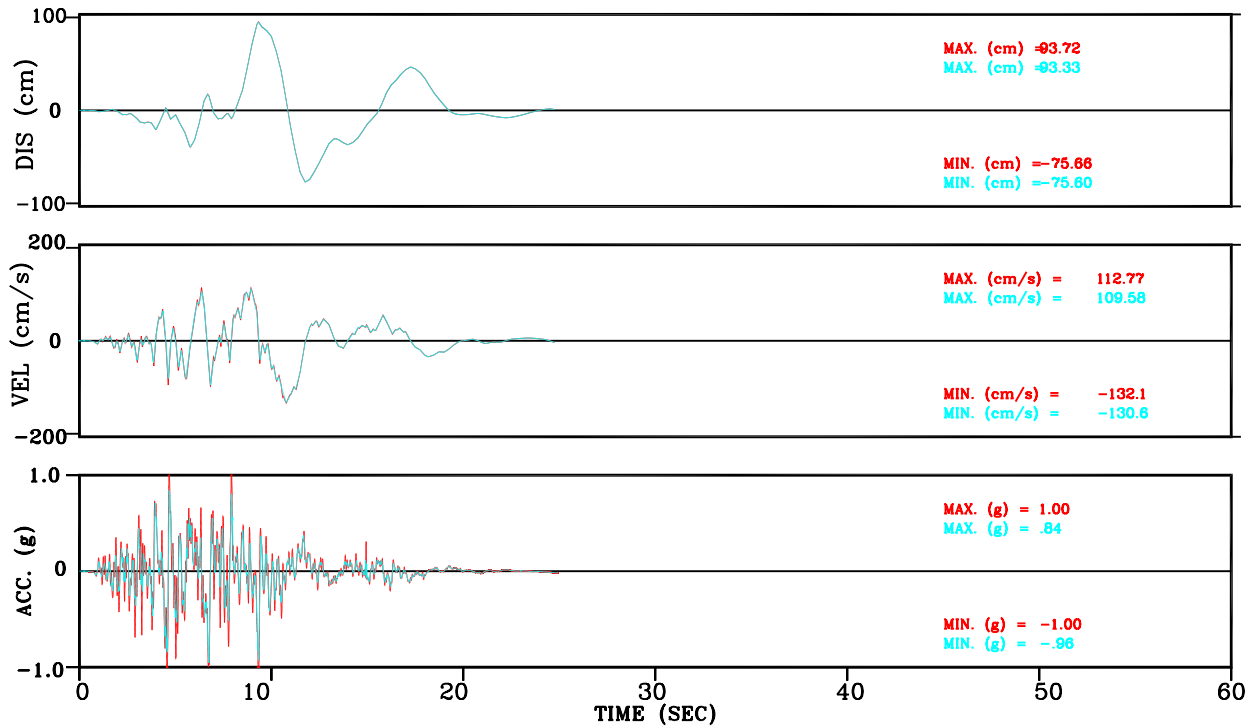


Figure III-107: Within vs. Surface Motion for UB Rock  
 Set-4 H2 Comp. Motion Conforming to Regulatory Guide 1.60 Spectral Shape

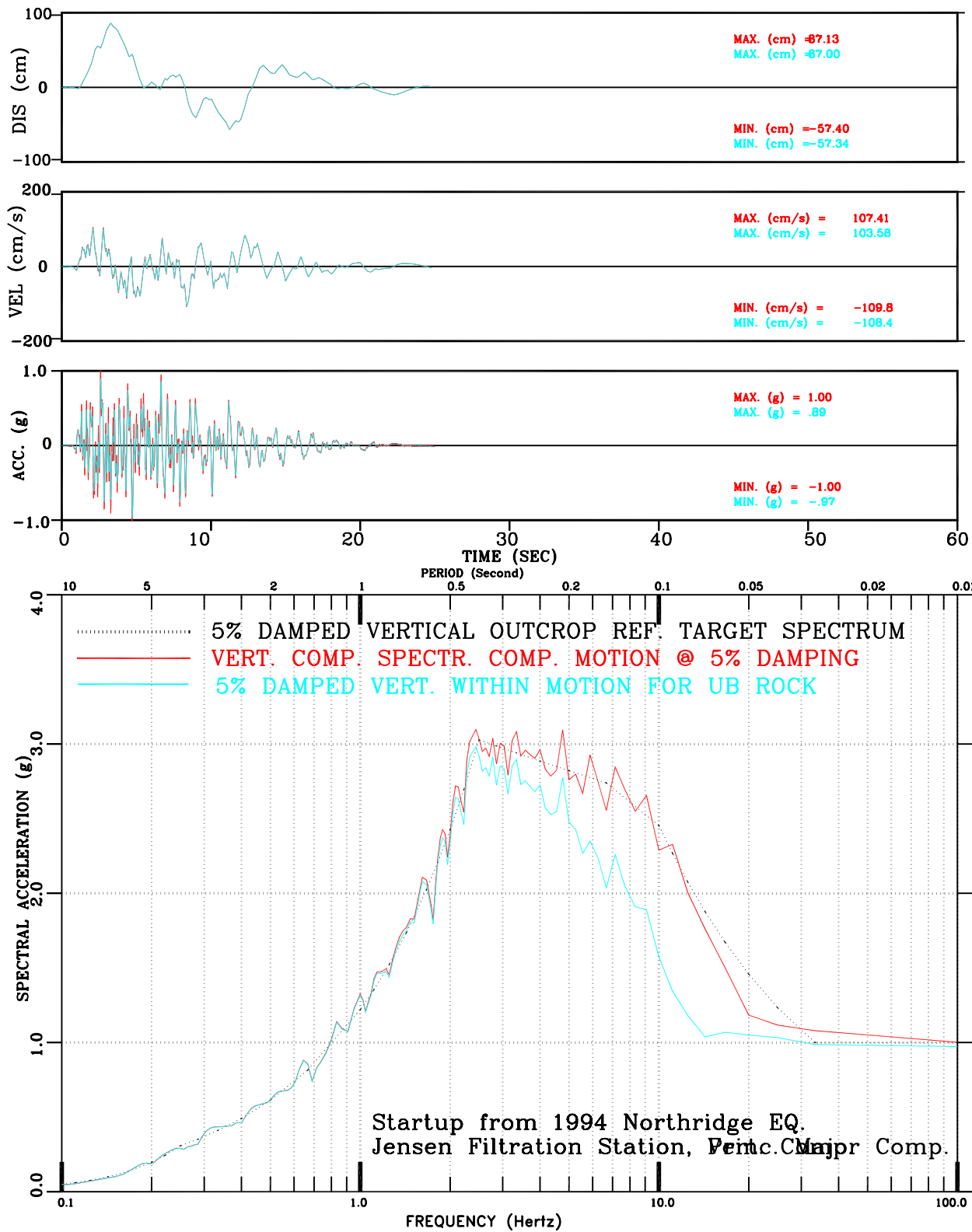


Figure III-108: Within vs. Surface Motion for UB Rock  
 Set-4 Vert. Comp. Motion Conforming to Regulatory Guide 1.60 Spectral Shape

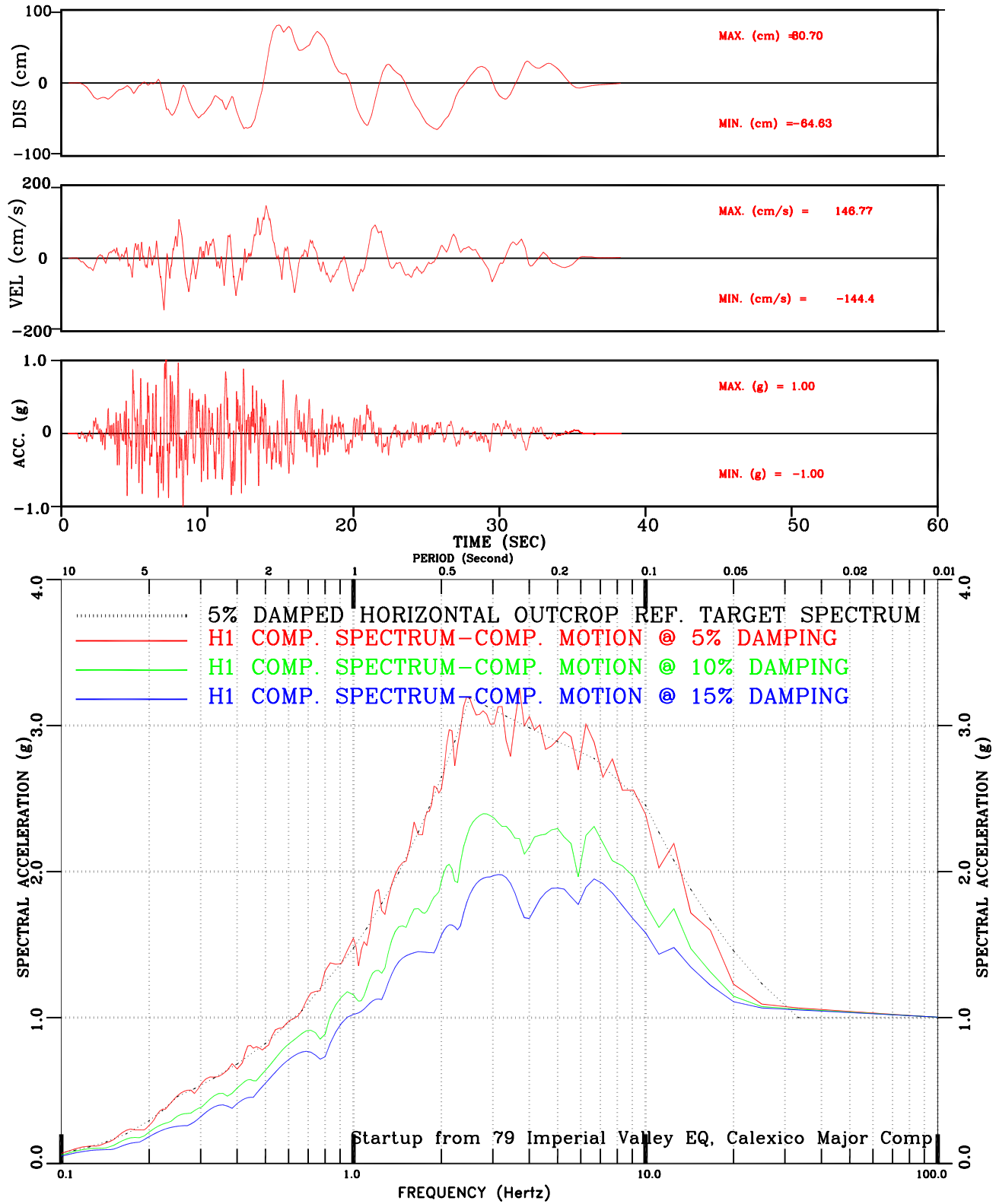


Figure III-109: Set-5 H1 Comp. Motion Conforming to REGULATORY GUIDE 1.60 Spectral Shape

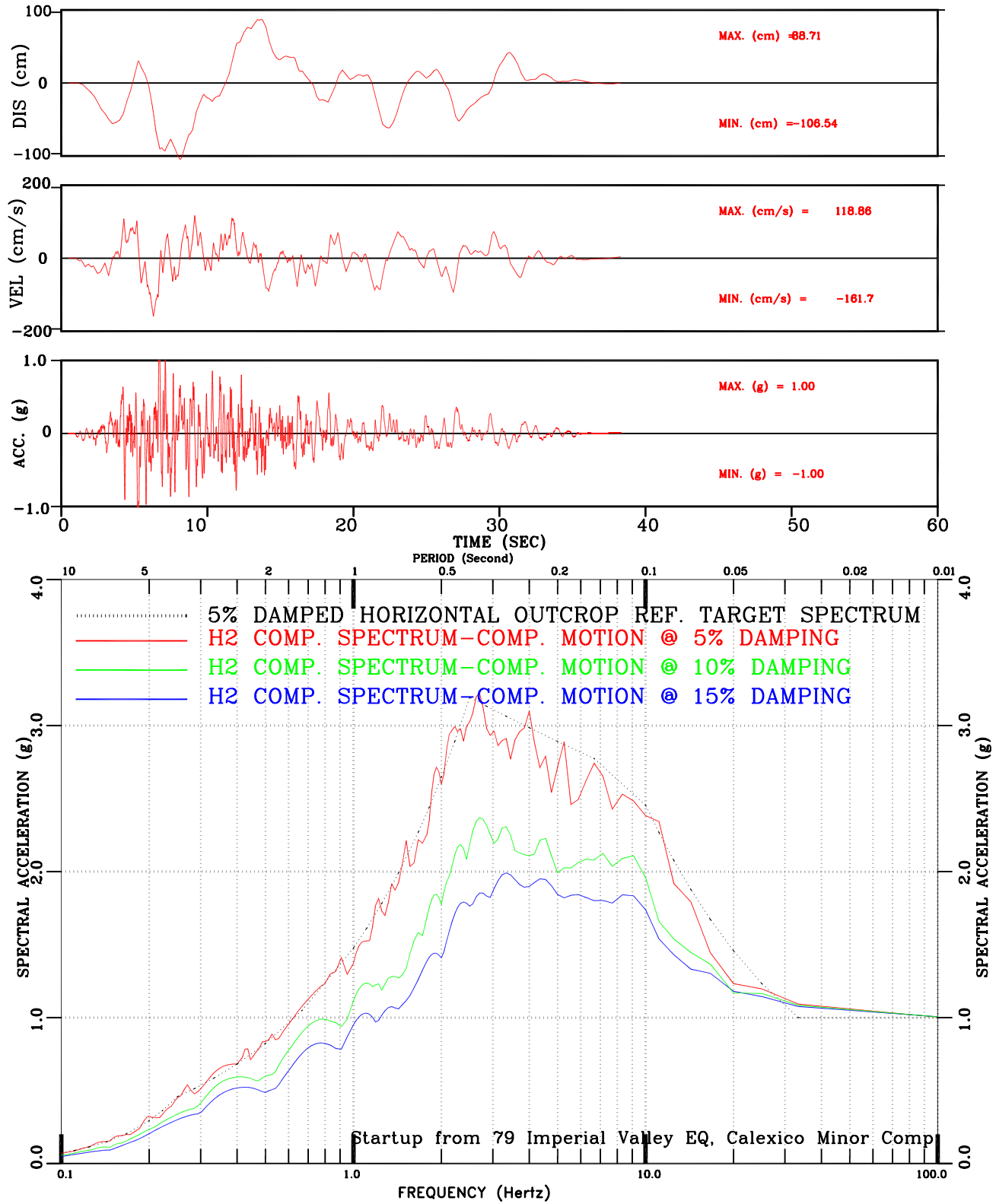


Figure III-110: Set-5 H2 Comp. Motion Conforming to REGULATORY GUIDE 1.60 Spectral Shape

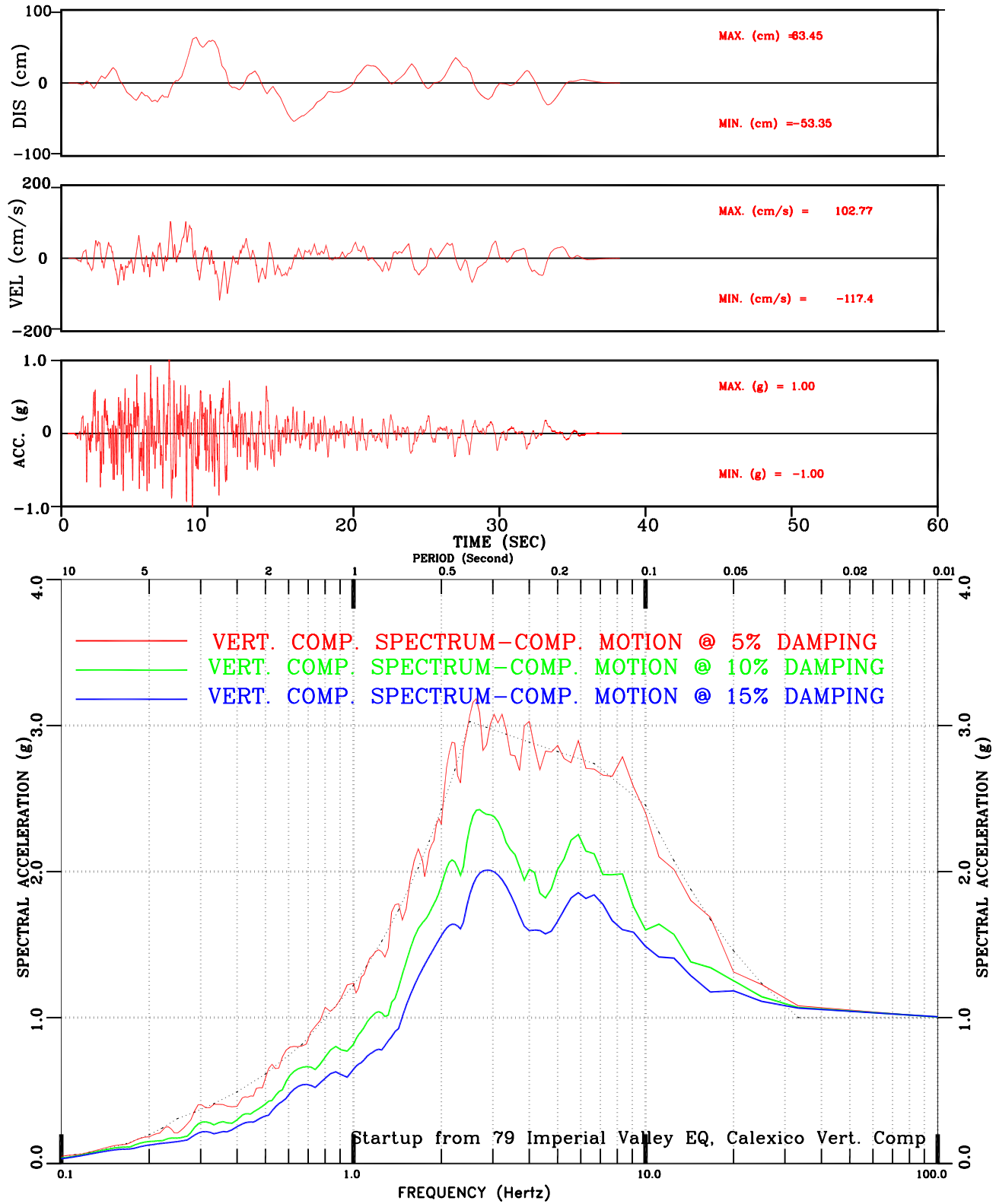


Figure III-111: Set-5 Vert Comp. Motion Conforming to REGULATORY GUIDE 1.60 Spectral Shape

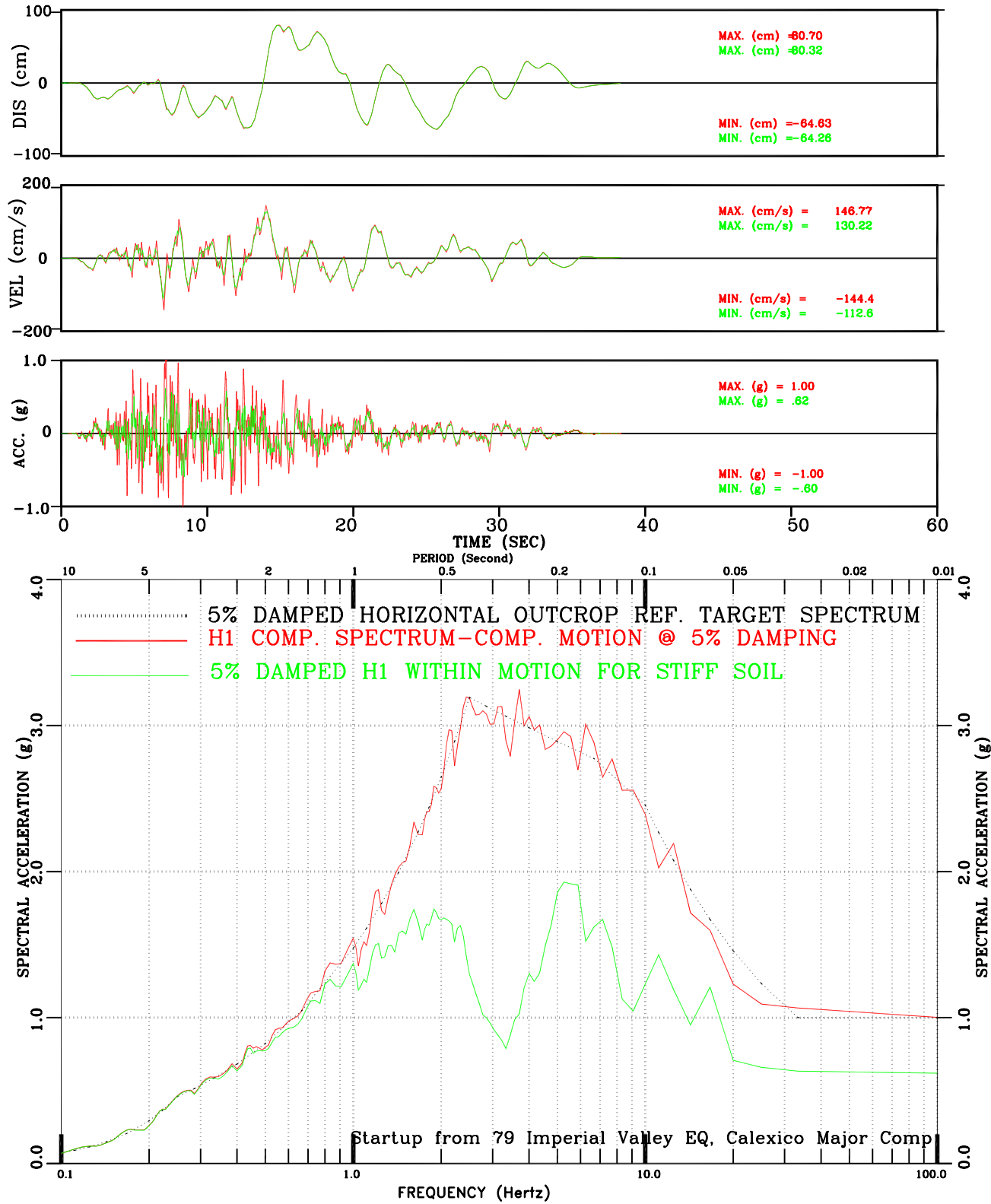


Figure III-112: Within vs. Surface Motion for Stiff Soil  
 Set-5 H1 Comp. Motion Conforming to Regulatory Guide 1.60 Spectral Shape

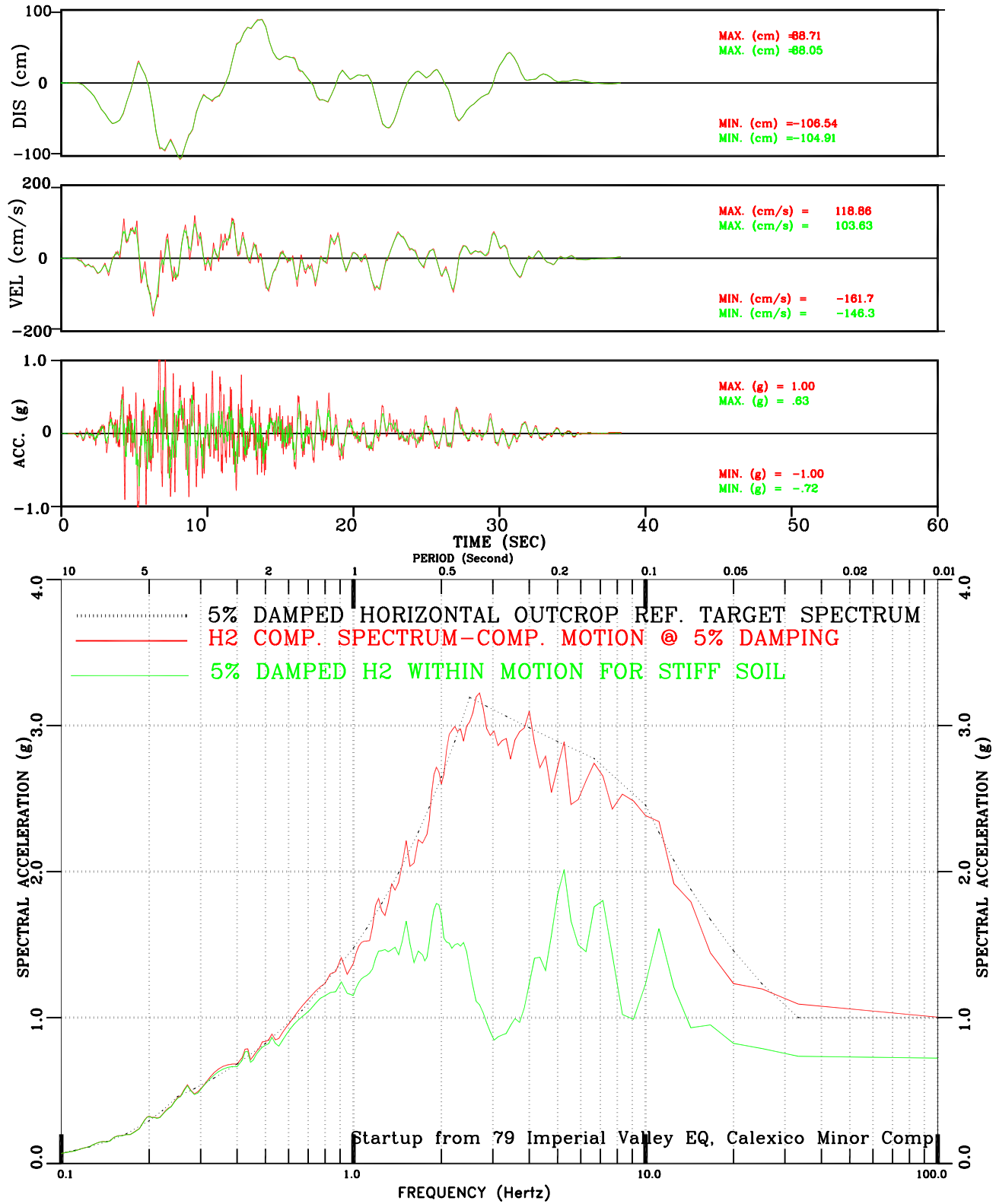


Figure III-113: Within vs. Surface Motion for Stiff Soil  
 Set-5 H2 Comp. Motion Conforming to Regulatory Guide 1.60 Spectral Shape

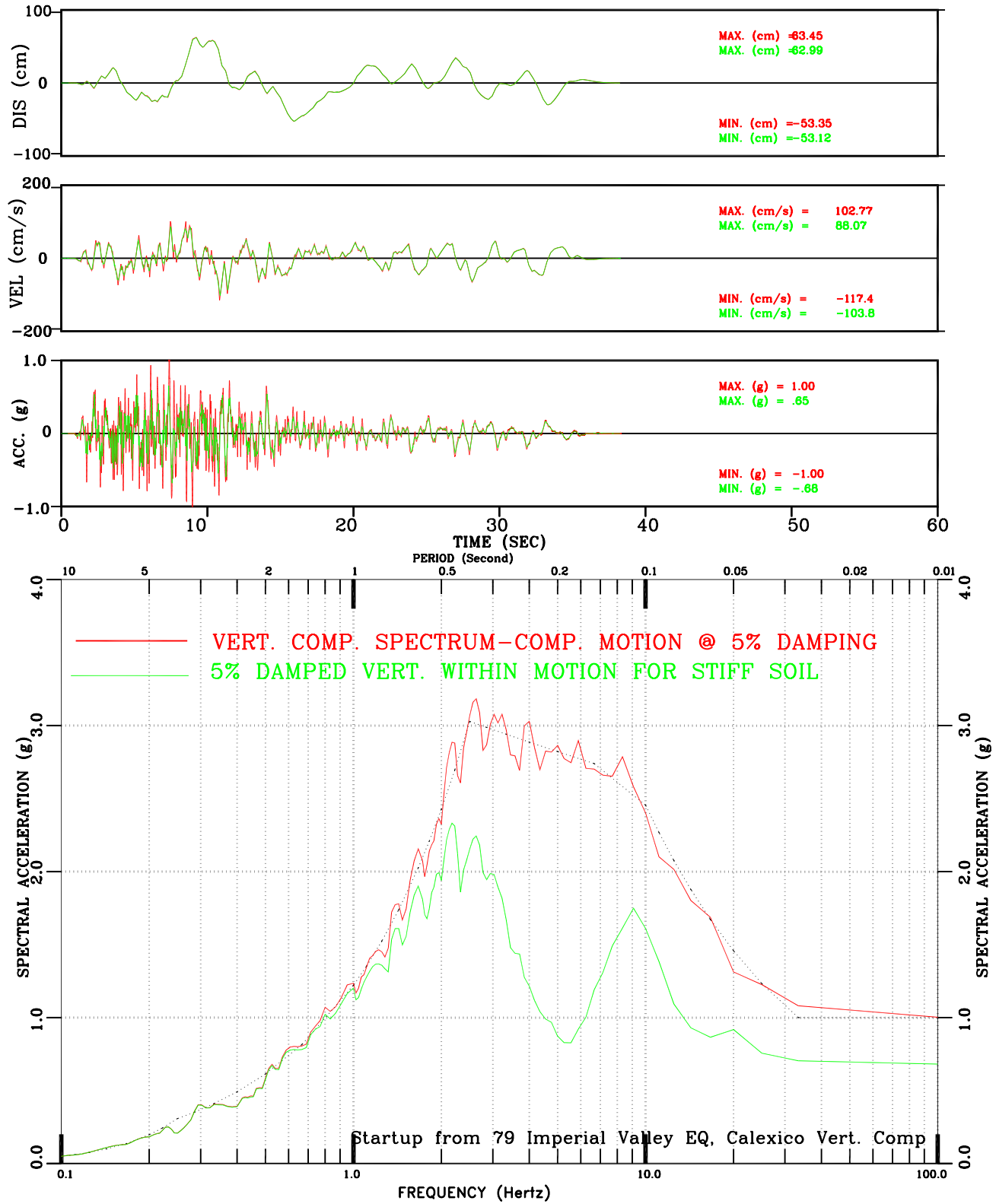


Figure III-114: Within vs. Surface Motion for Stiff Soil  
 Set-5 Vert. Comp. Motion Conforming to Regulatory Guide 1.60 Spectral Shape

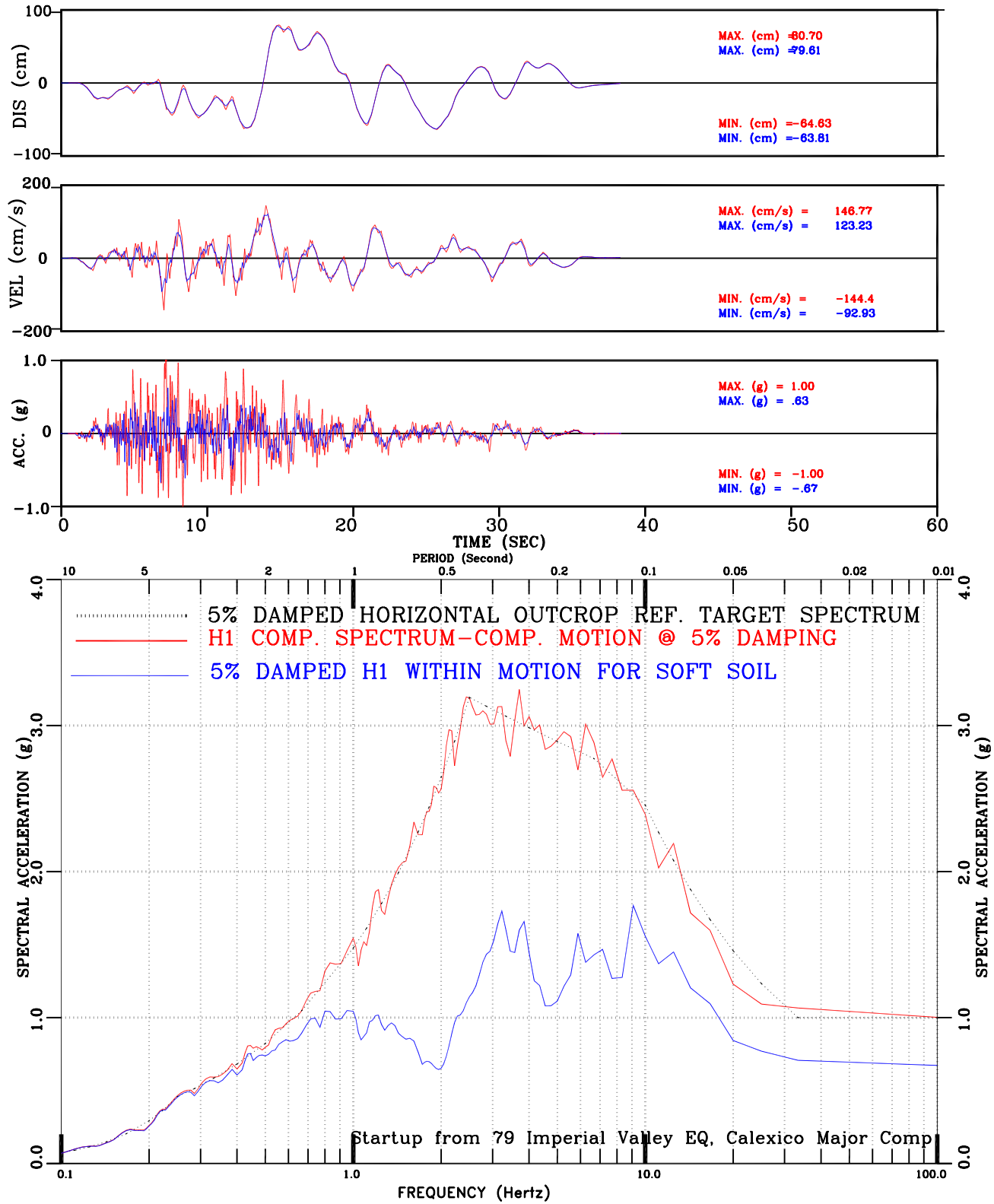


Figure III-115: Within vs. Surface Motion for Soft Soil  
 Set-5 H1 Comp. Motion Conforming to Regulatory Guide 1.60 Spectral Shape

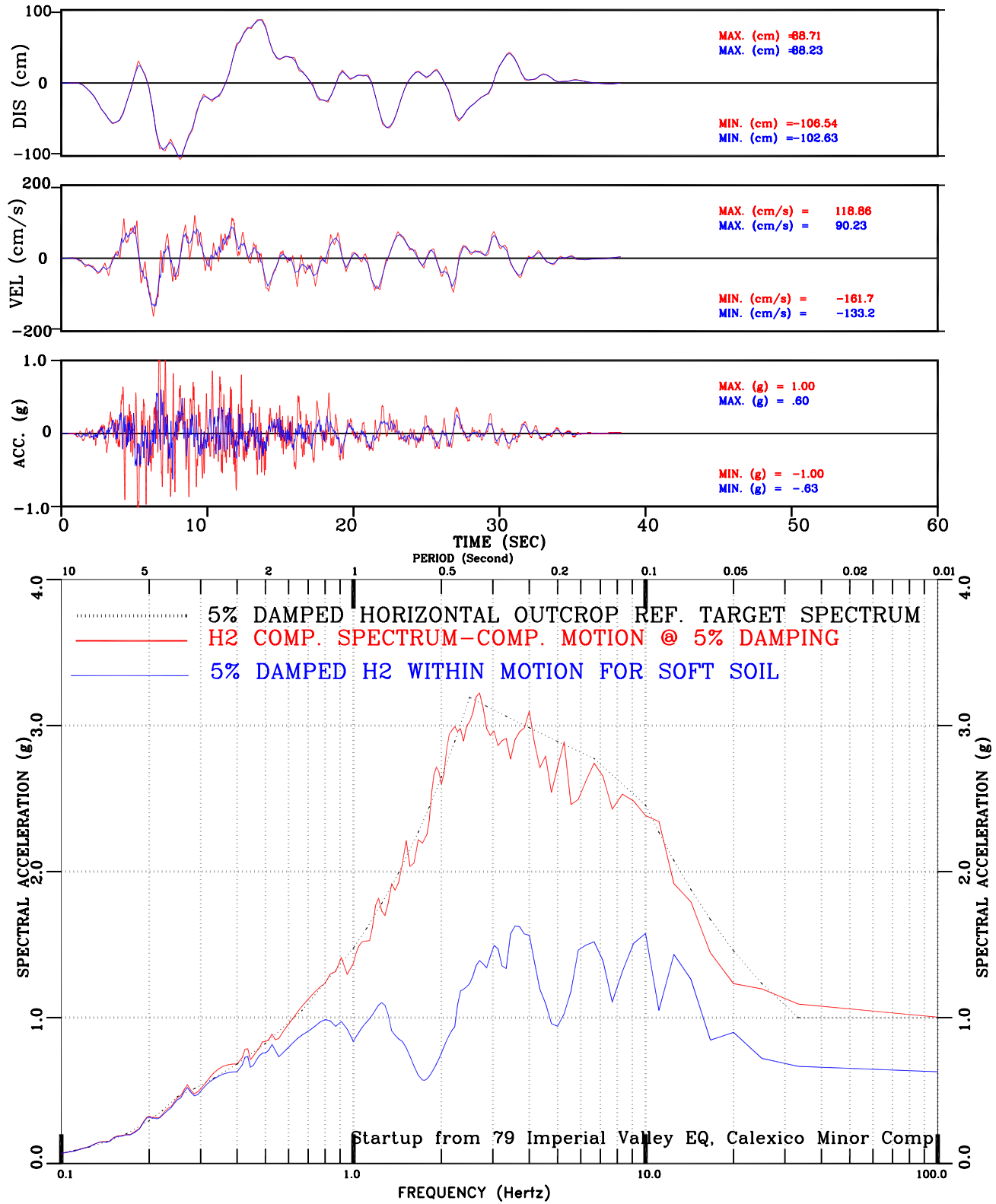


Figure III-116: Within vs. Surface Motion for Soft Soil  
 Set-5 H2 Comp. Motion Conforming to Regulatory Guide 1.60 Spectral Shape

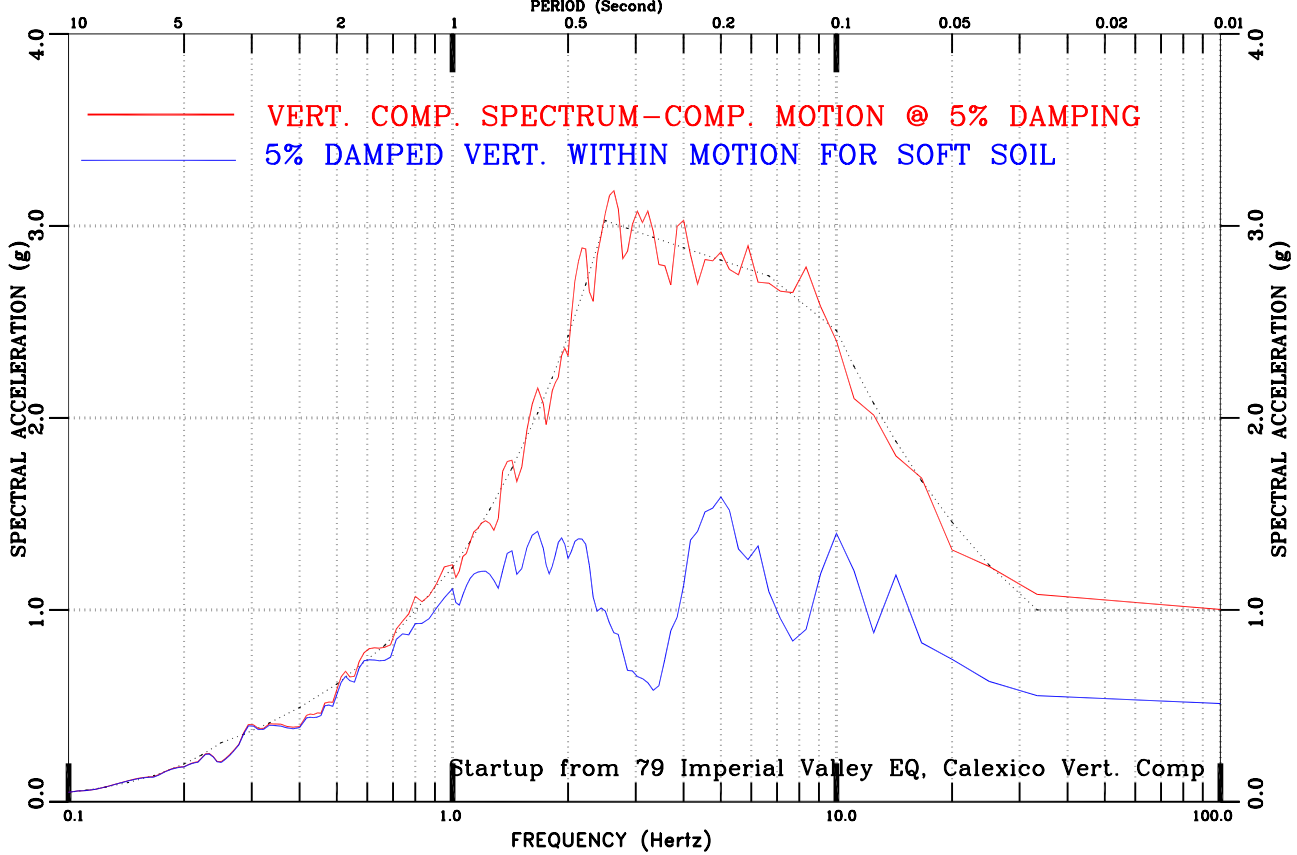
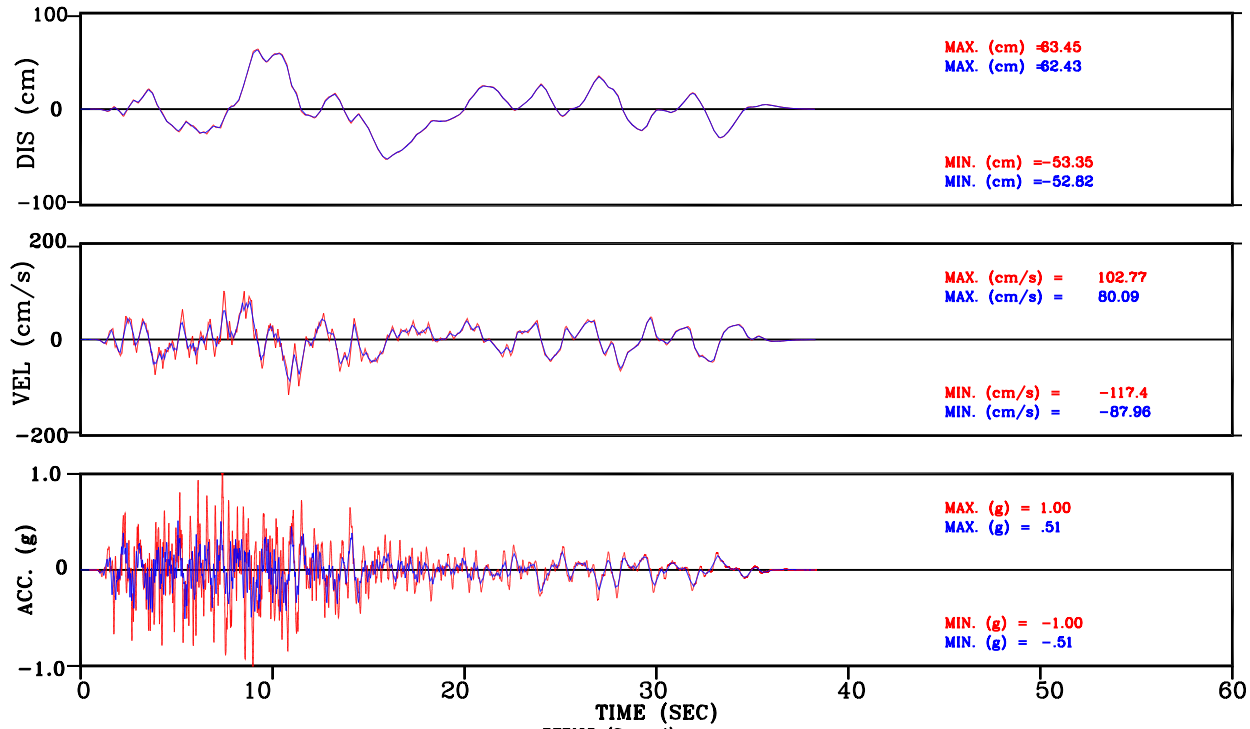


Figure III-117: Within vs. Surface Motion for Soft Soil  
 Set-5 Vert. Comp. Motion Conforming to Regulatory Guide 1.60 Spectral Shape

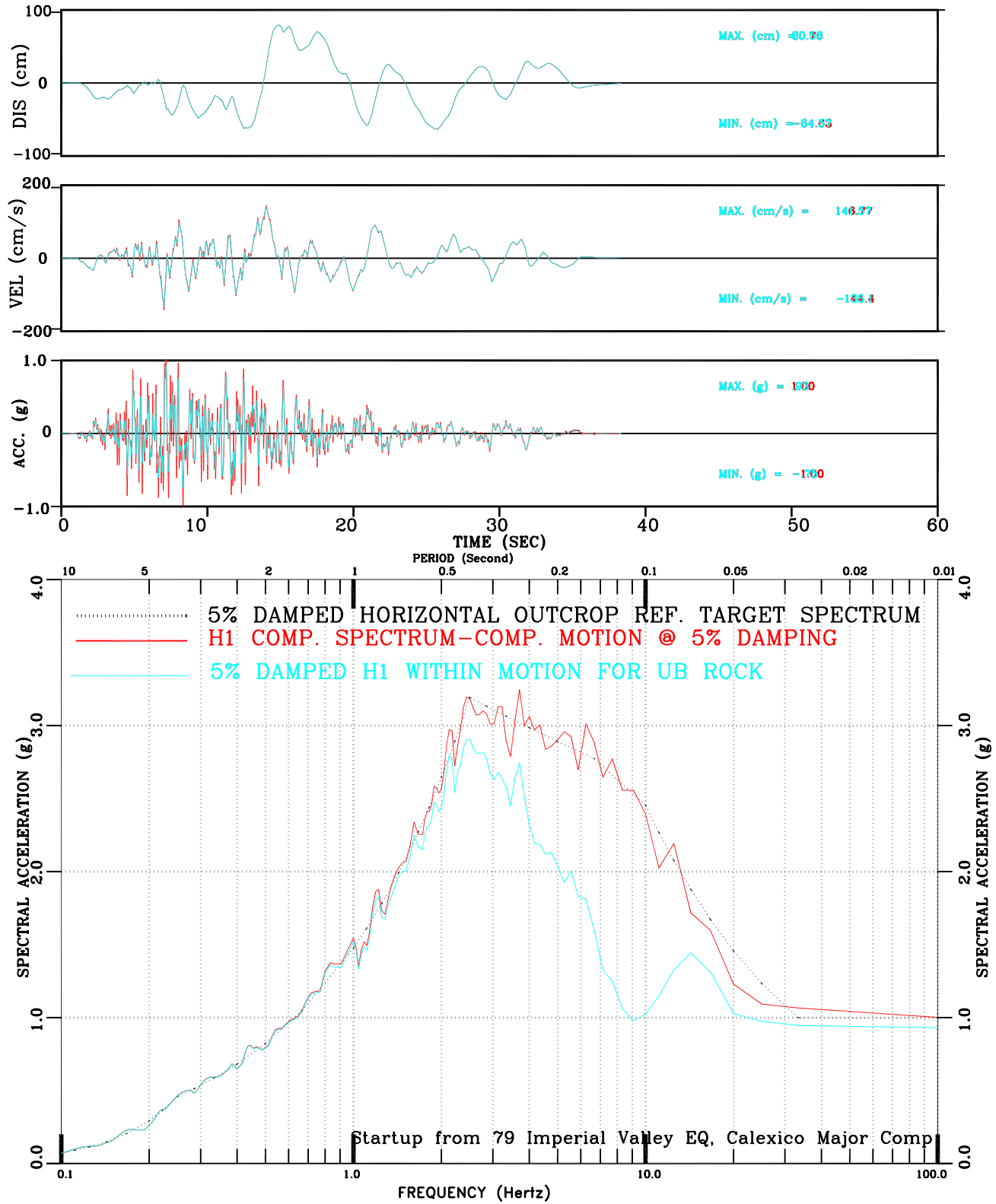


Figure III-118: Within vs. Surface Motion for UB Rock  
 Set-5 H1 Comp. Motion Conforming to Regulatory Guide 1.60 Spectral Shape

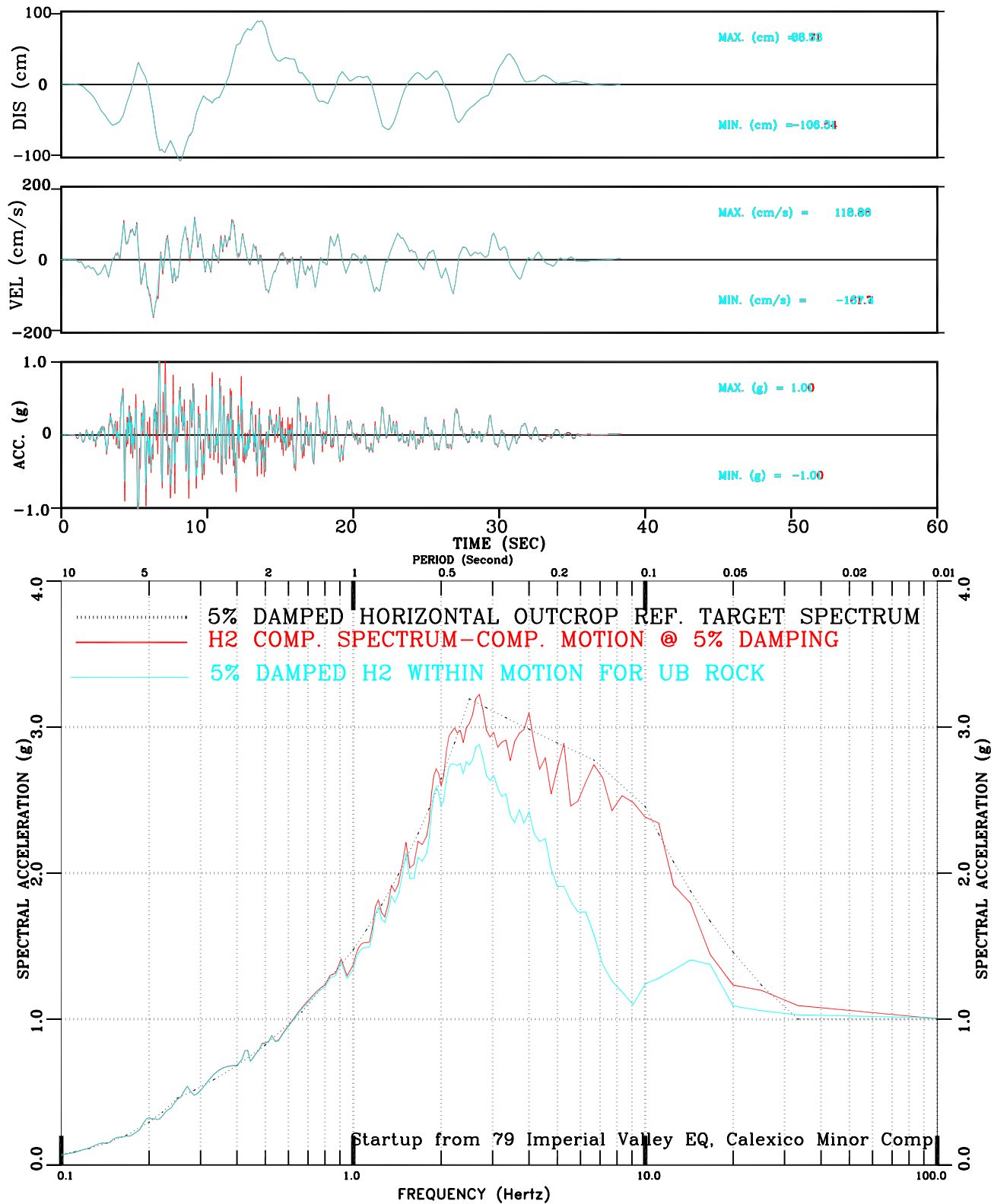


Figure III-119: Within vs. Surface Motion for UB Rock  
 Set-5 H2 Comp. Motion Conforming to Regulatory Guide 1.60 Spectral Shape

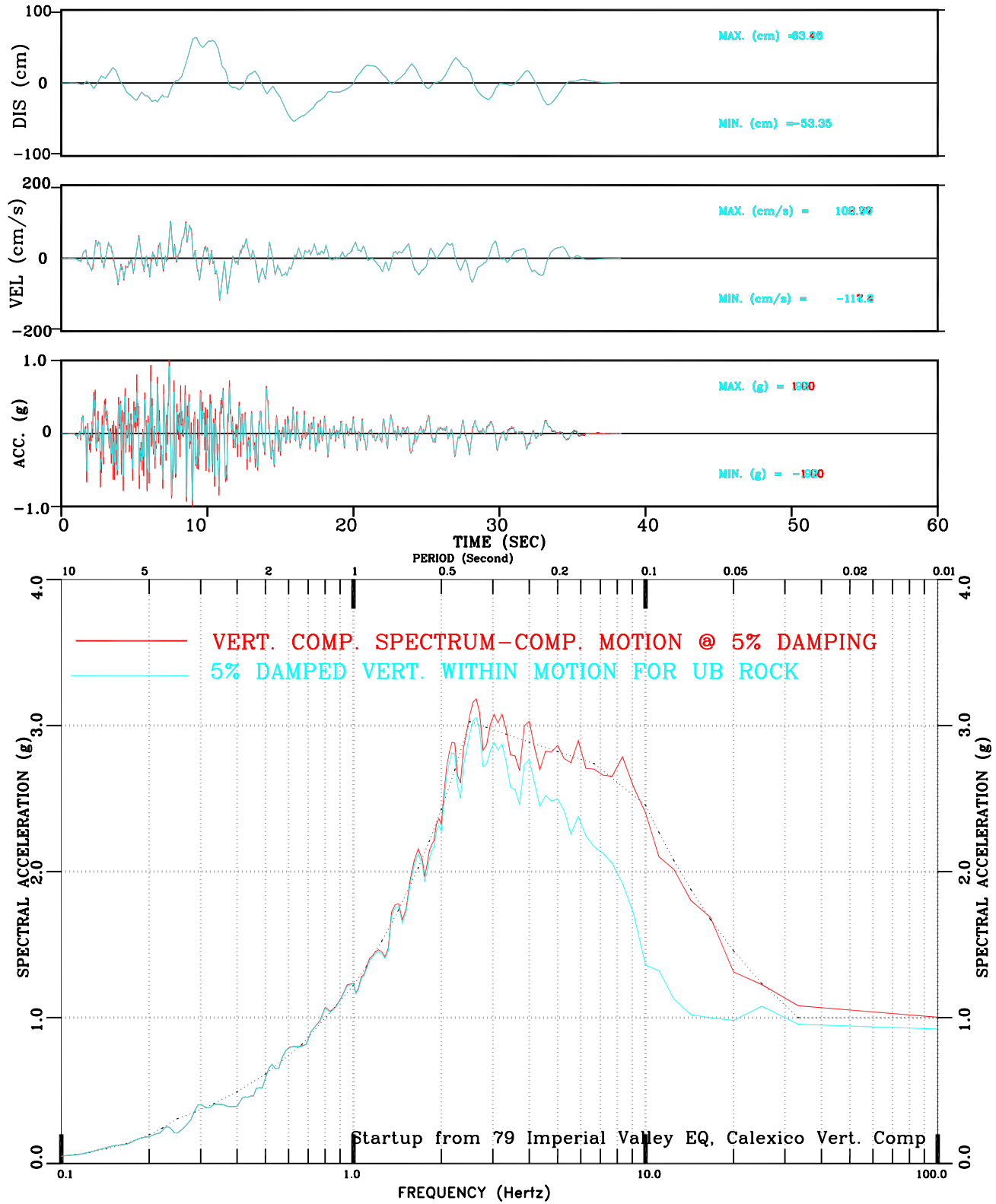


Figure III-120: Within vs. Surface Motion for UB Rock  
 Set-5 Vert. Comp. Motion Conforming to Regulatory Guide 1.60 Spectral Shape

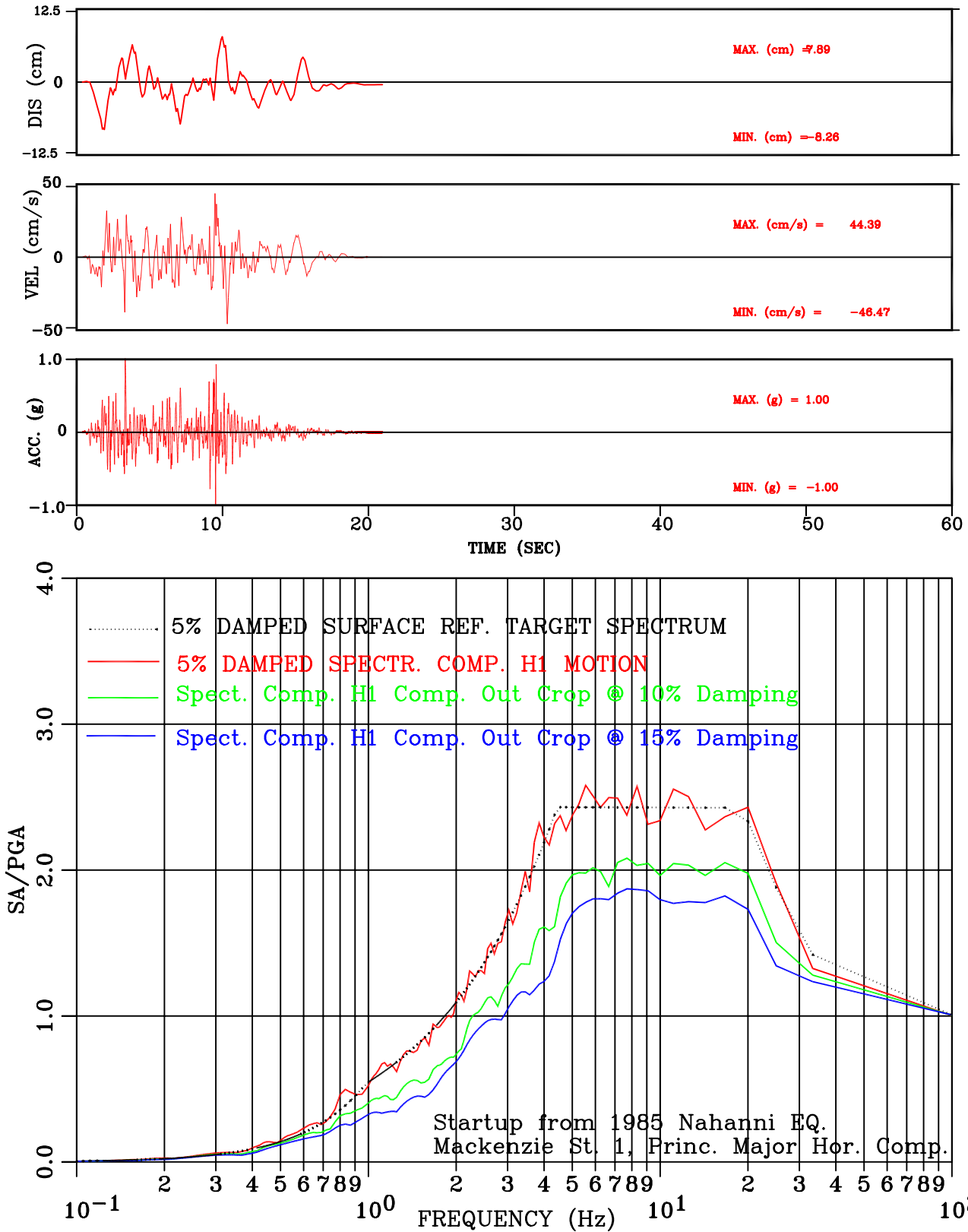


Figure III-121: Set-1 H1 Comp. Motion Conforming to NUREG/CR-6728 Spectral Shape

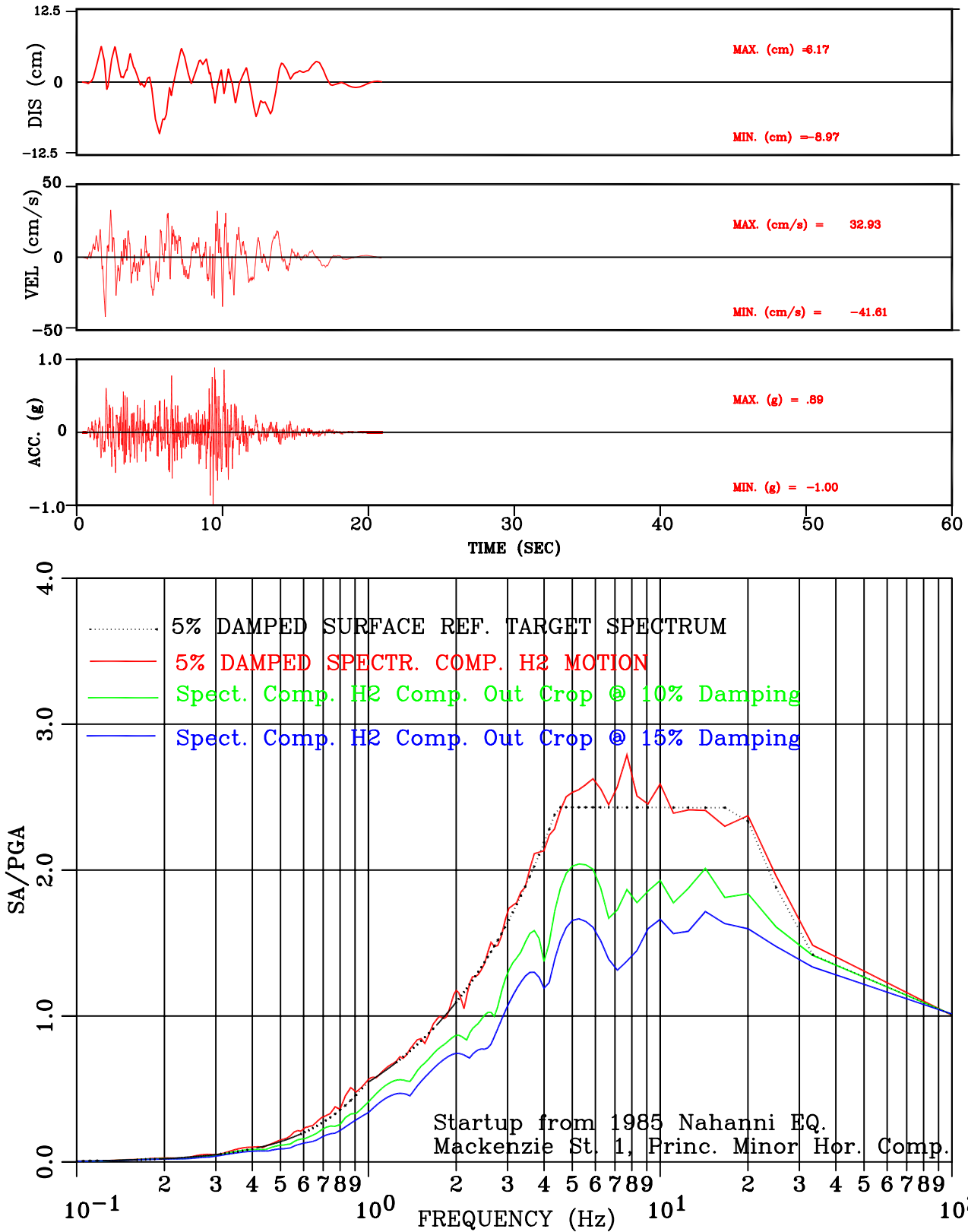


Figure III-122: Set-1 H2 Comp. Motion Conforming to NUREG/CR-6728 Spectral Shape

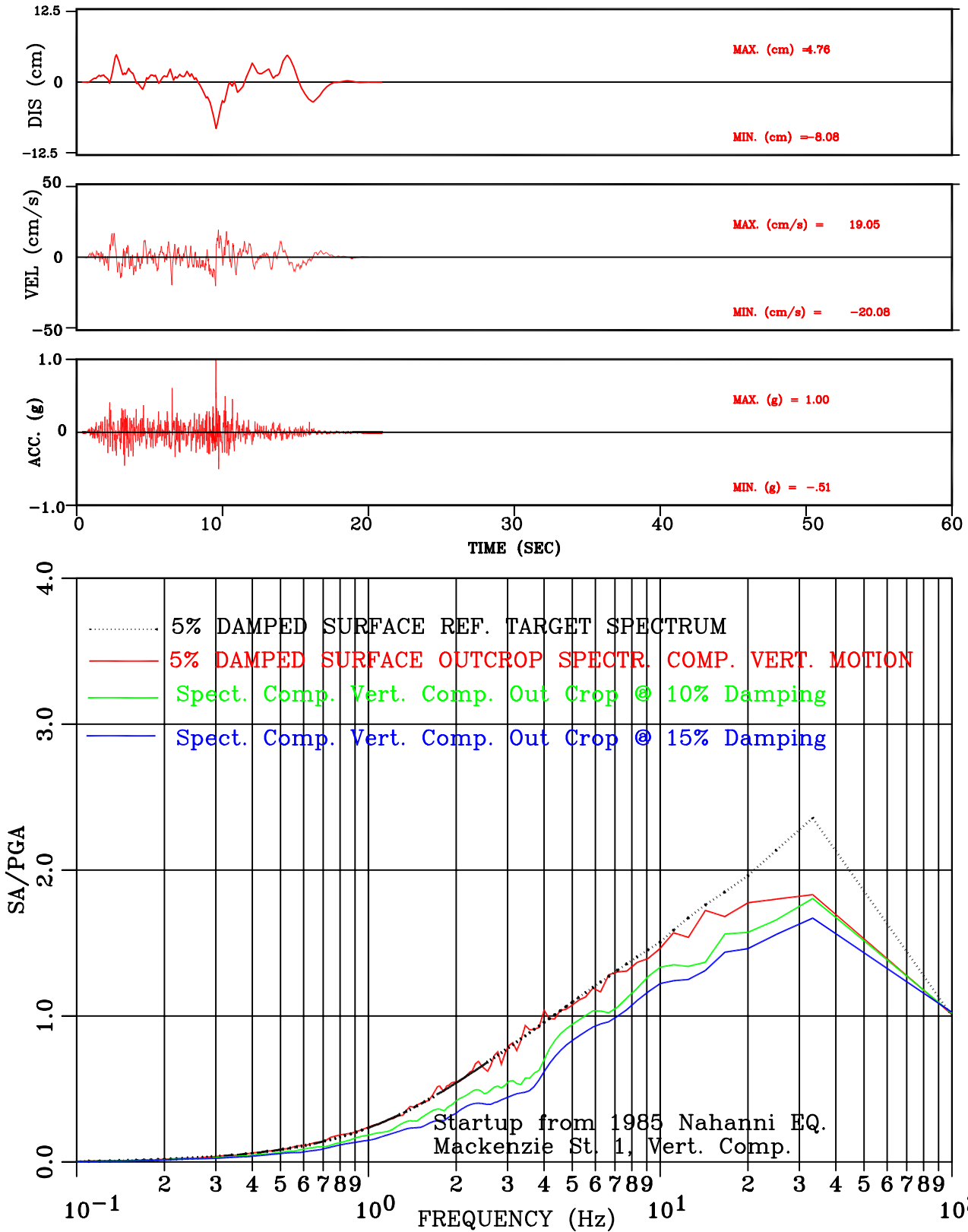


Figure III-123: Set-1 Vert. Comp. Motion Conforming to NUREG/CR-6728 Spectral Shape

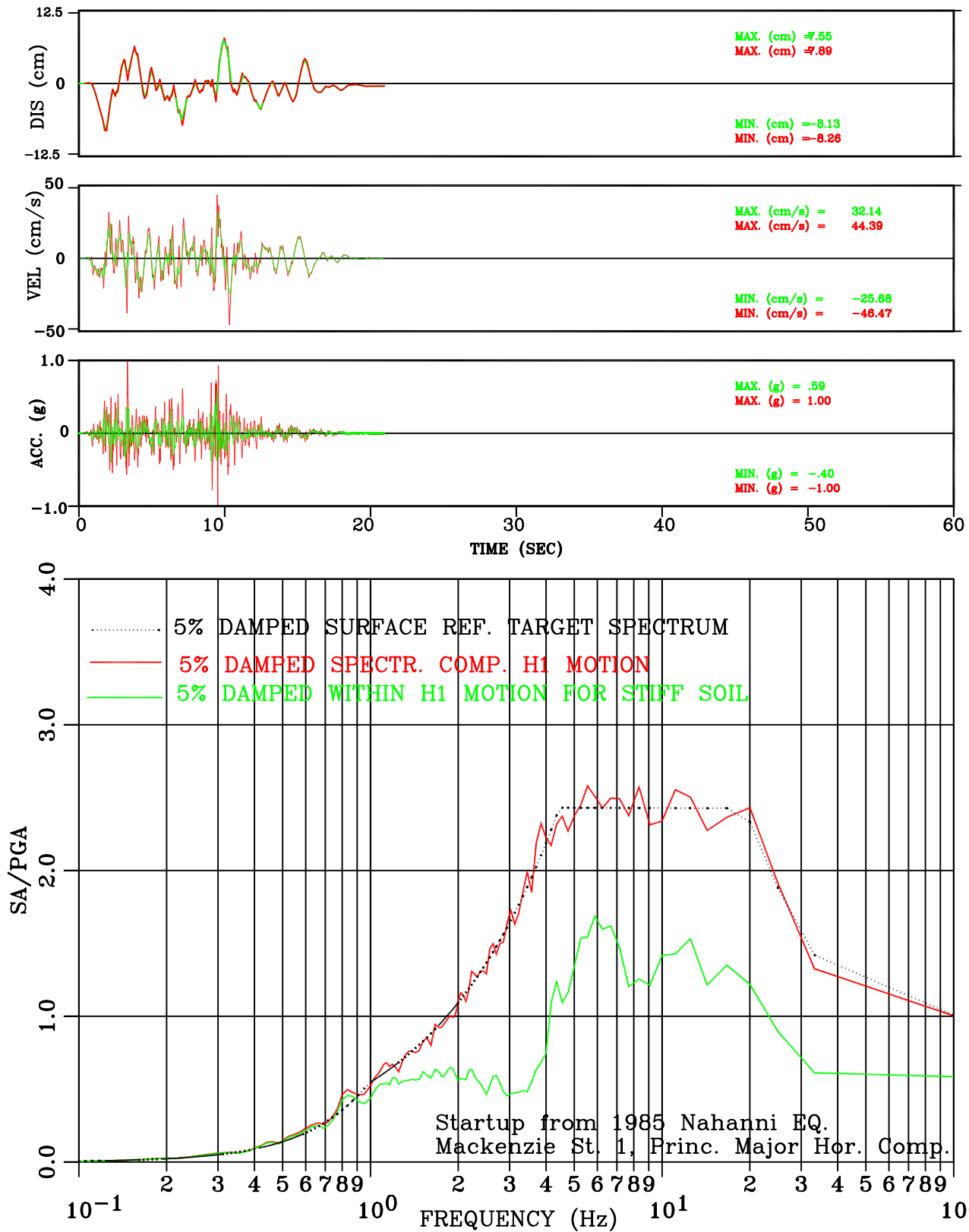


Figure III-124: Within vs. Surface Motion for Stiff Soil  
Set-1 H1 Comp. Motion Conforming to NUREG/CR-6728 Spectral Shape

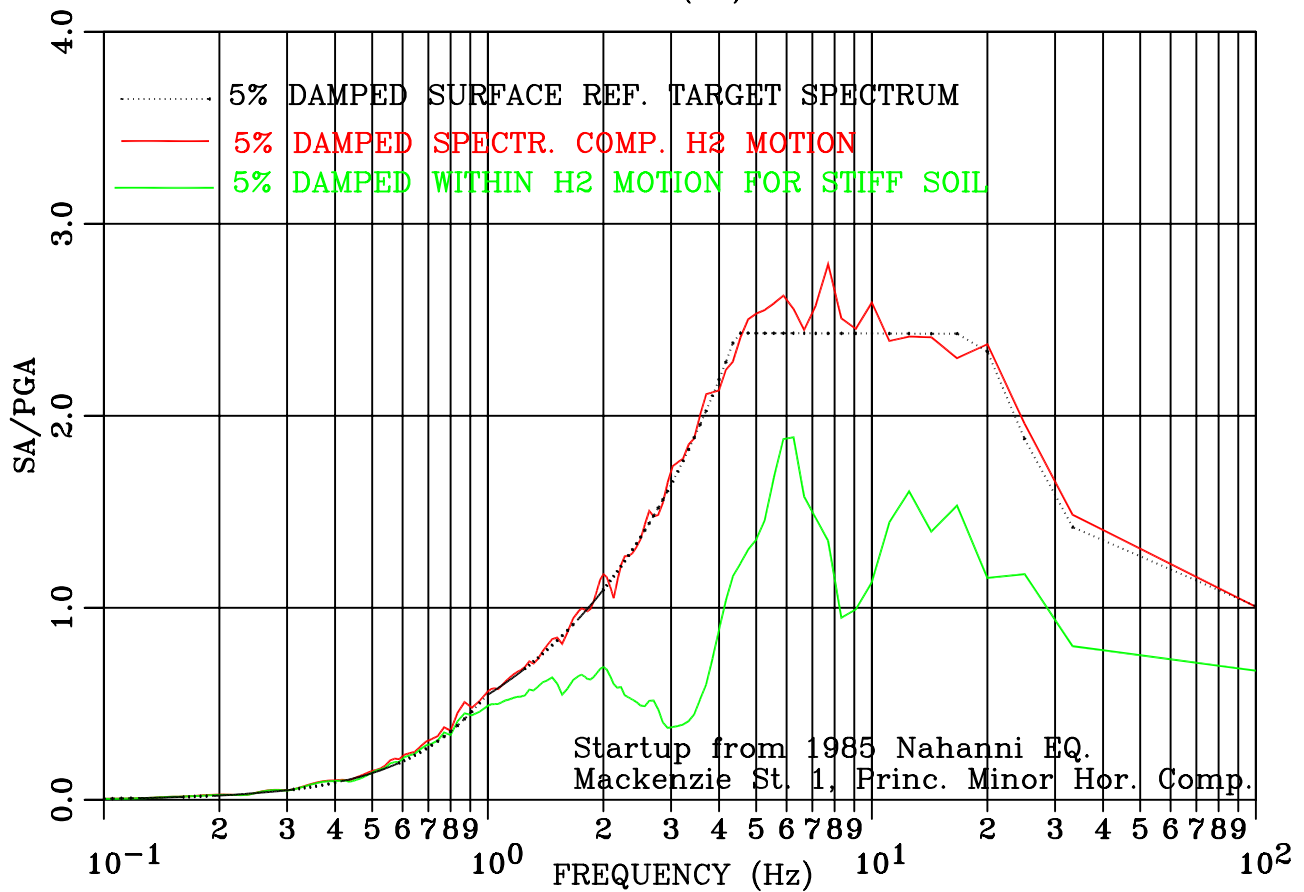
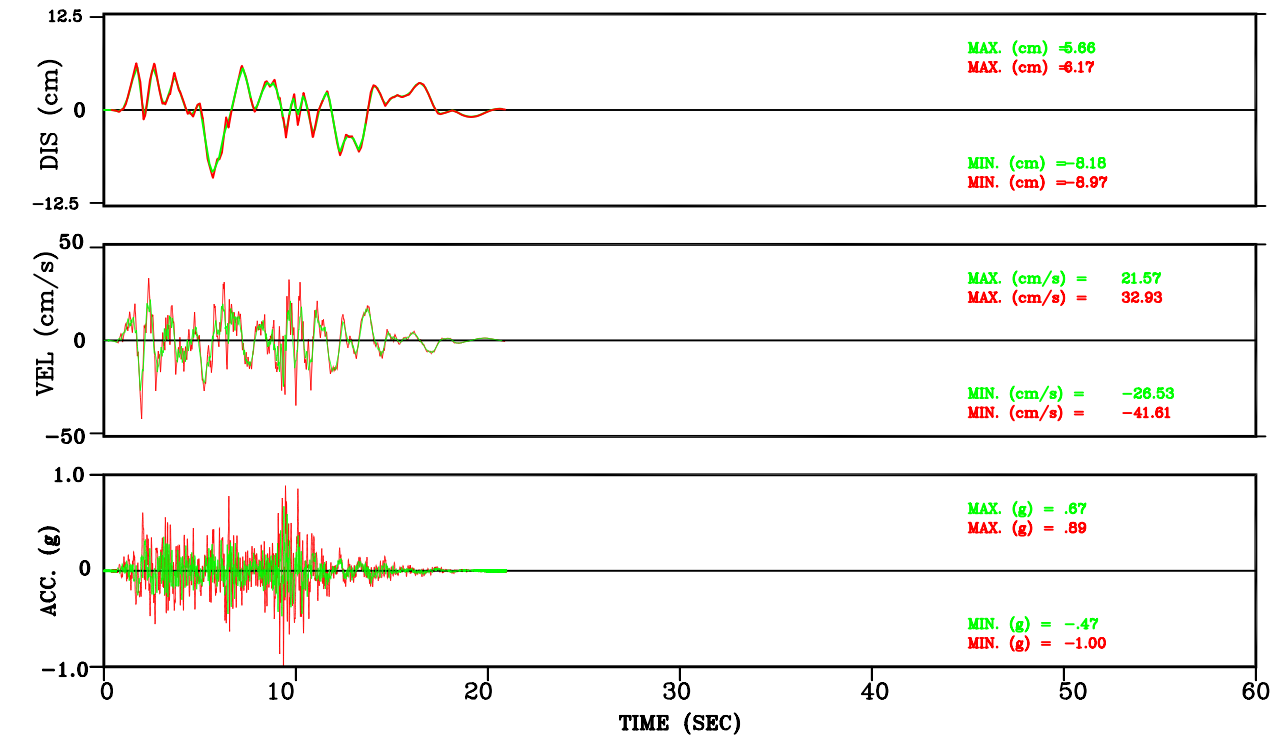


Figure III-125: Within vs. Surface Motion for Stiff Soil  
 Set-1 H2 Comp. Motion Conforming to NUREG/CR-6728 Spectral Shape

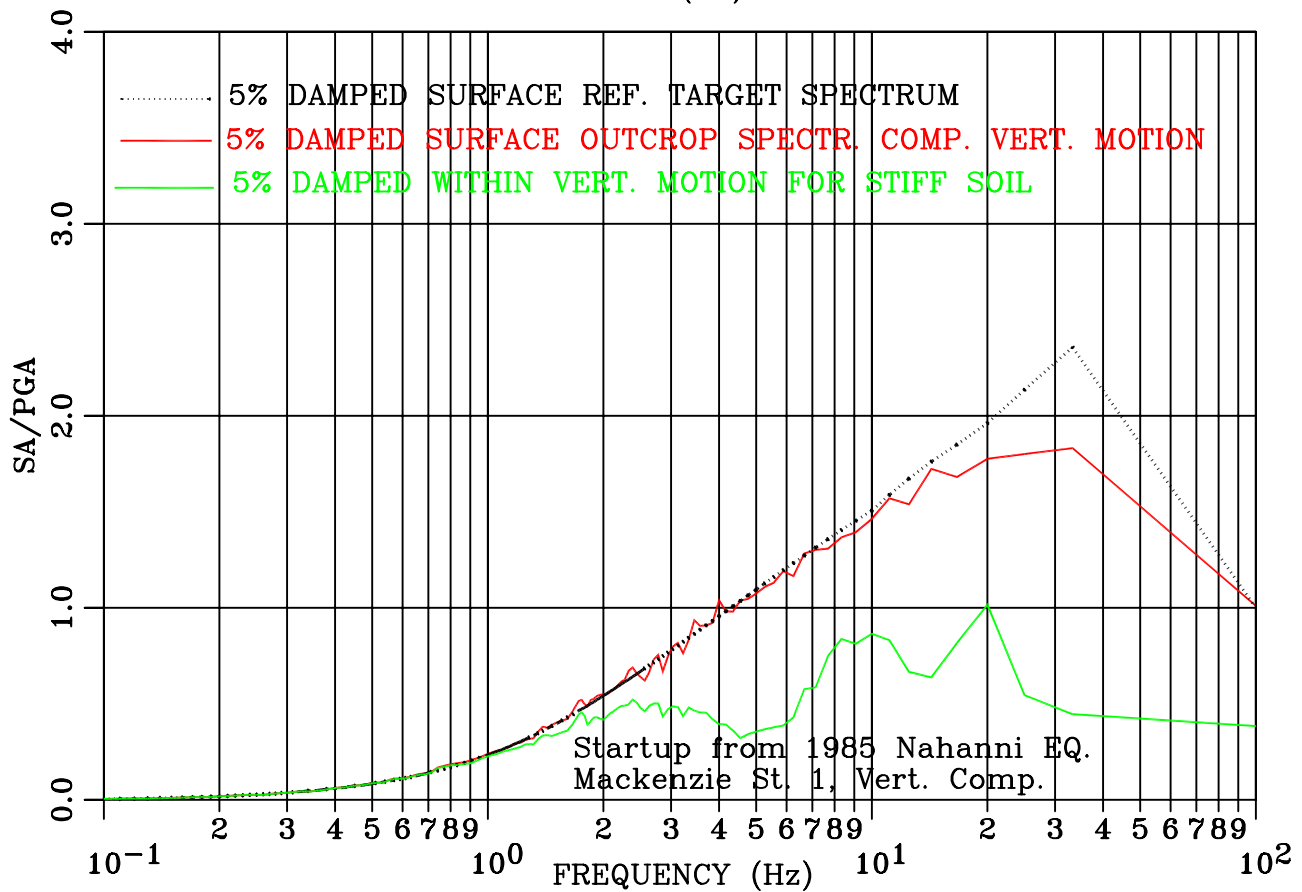
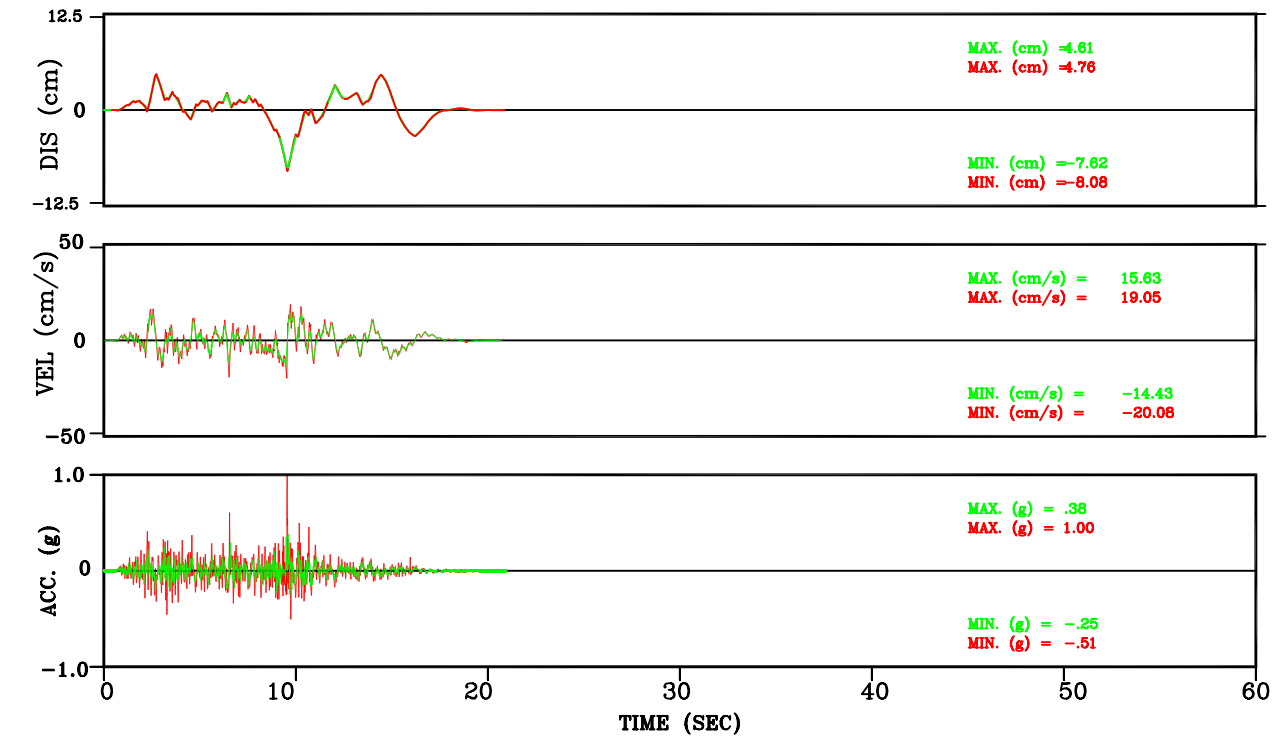


Figure III-126: Within vs. Surface Motion for Stiff Soil  
 Set-1 Vert. Comp. Motion Conforming to NUREG/CR-6728 Spectral Shape

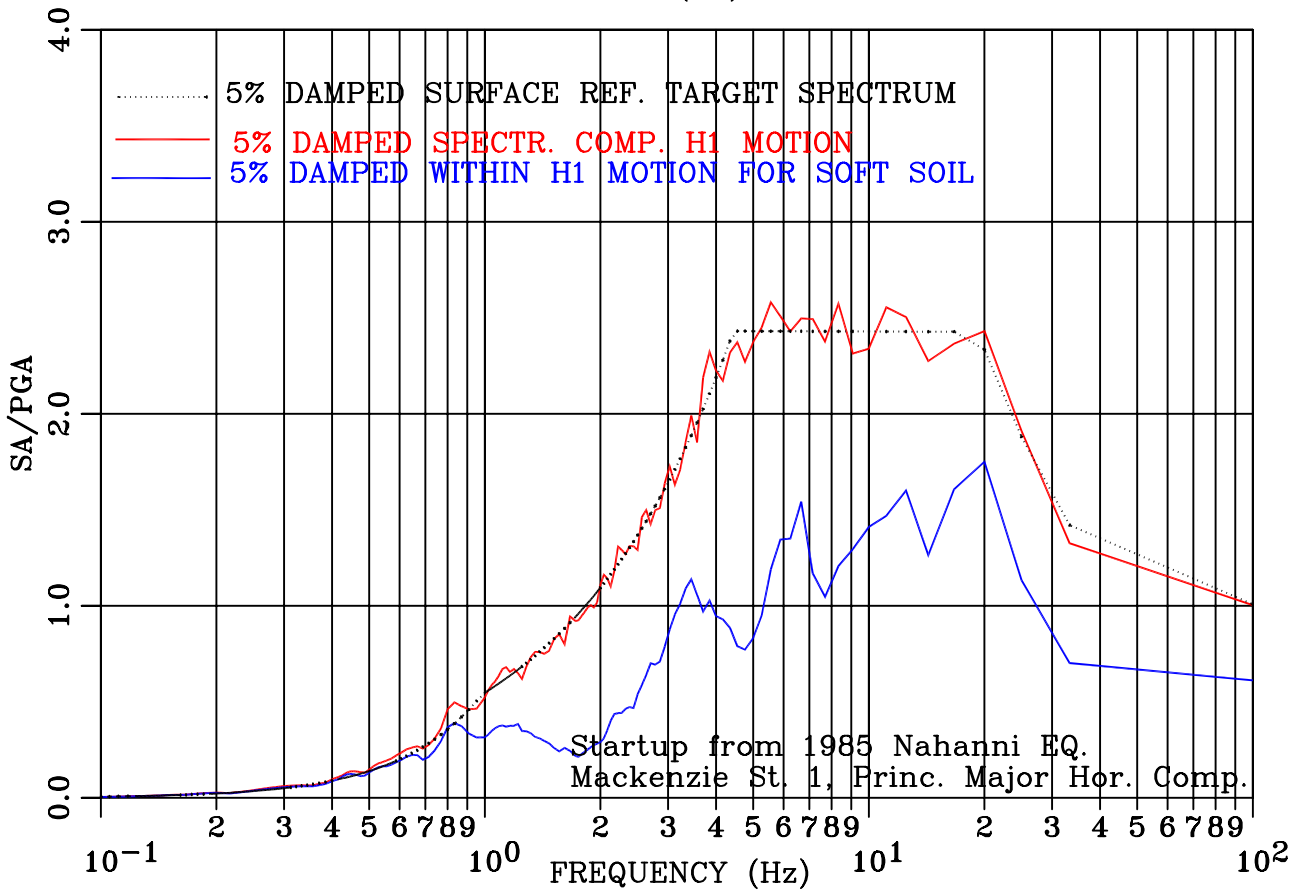
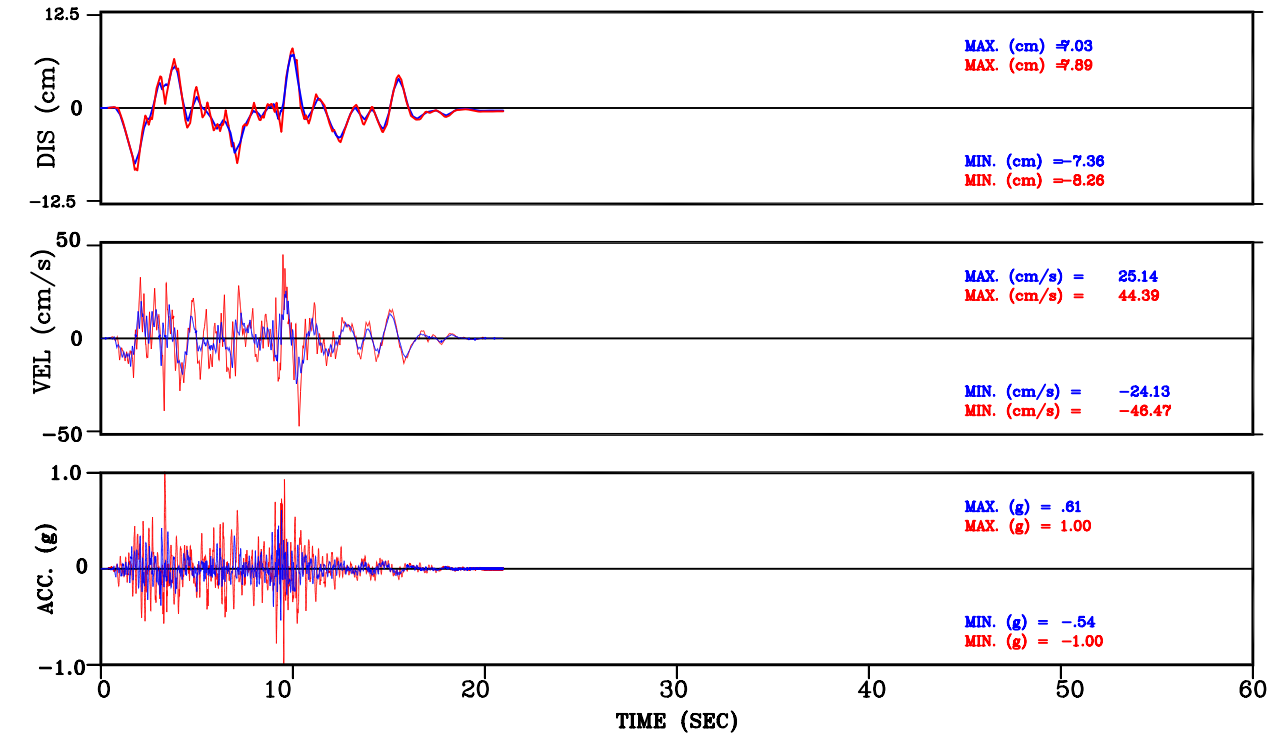


Figure III-127: Within vs. Surface Motion for Soft Soil  
Set-1 H1 Comp. Motion Conforming to NUREG/CR-6728 Spectral Shape

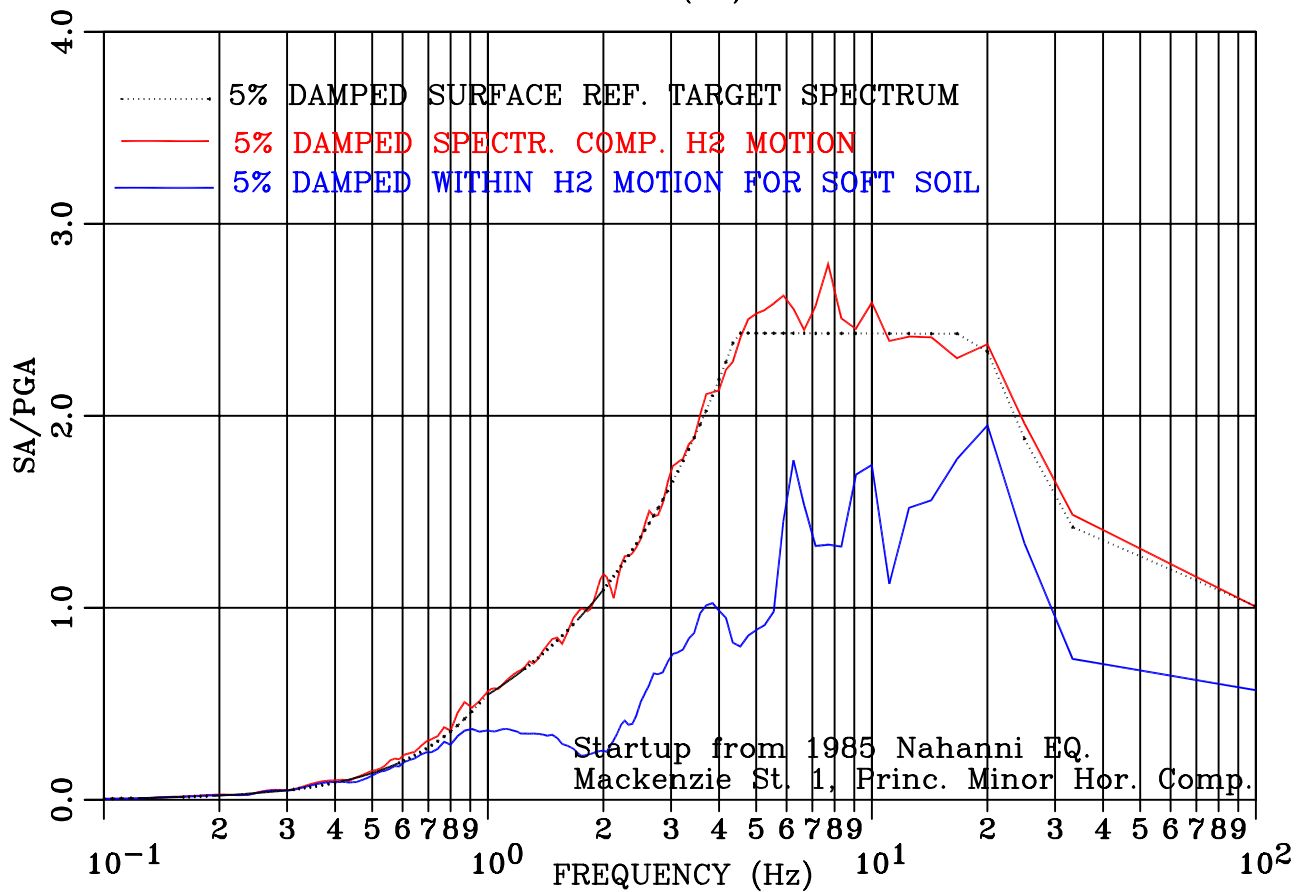
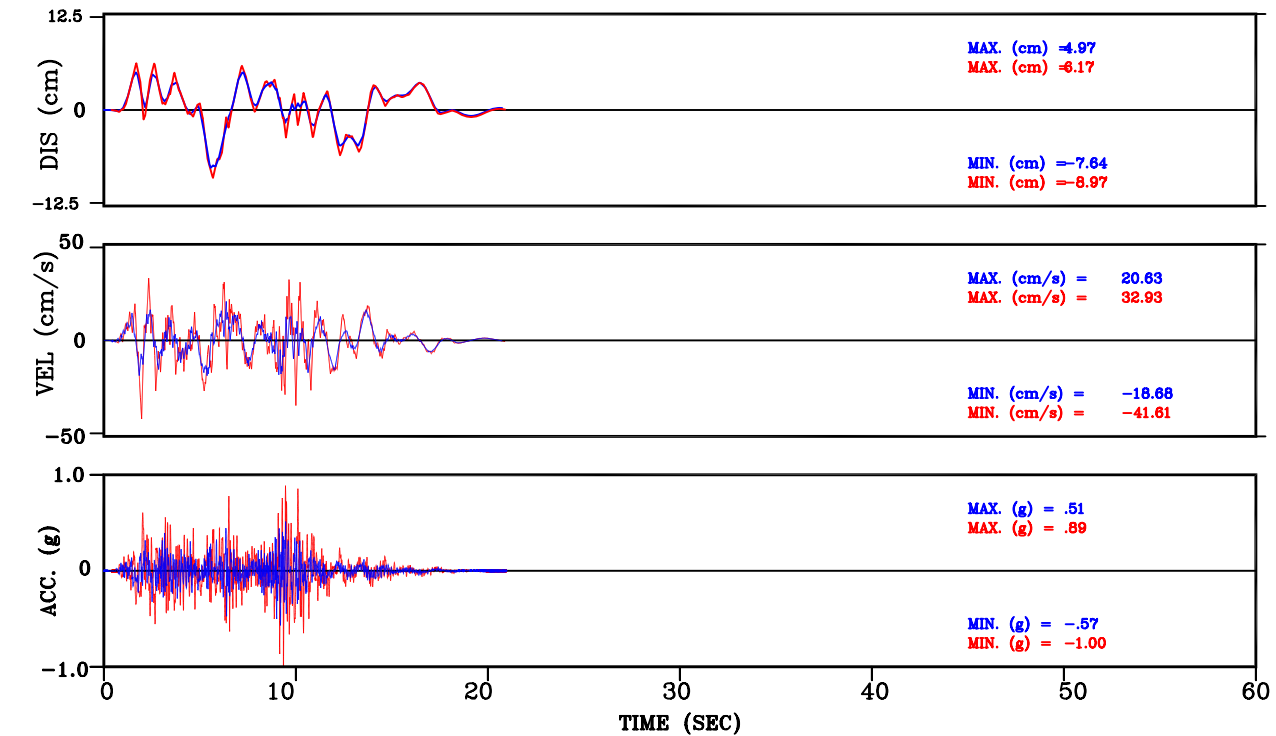


Figure III-128: Within vs. Surface Motion for Soft Soil  
Set-1 H2 Comp. Motion Conforming to NUREG/CR-6728 Spectral Shape

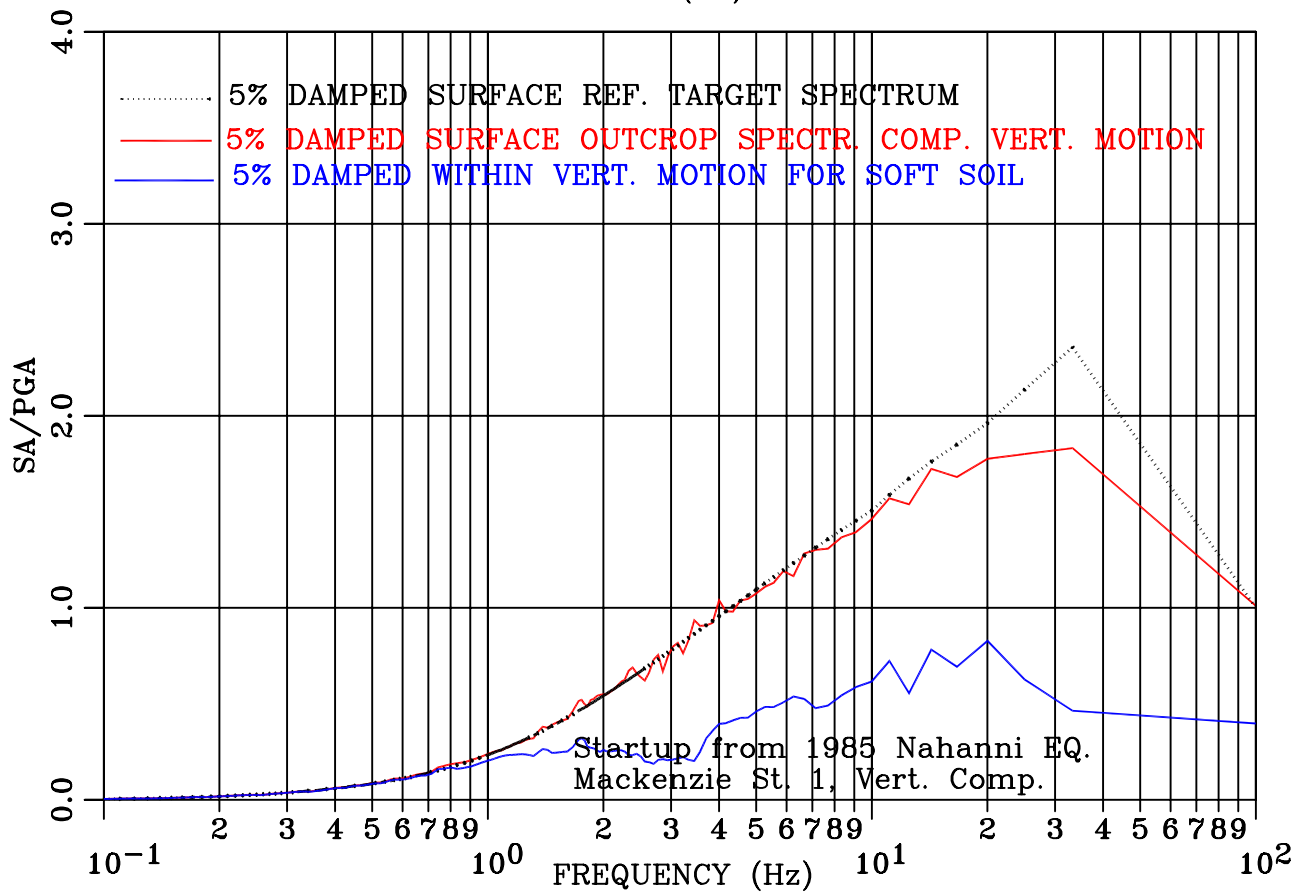
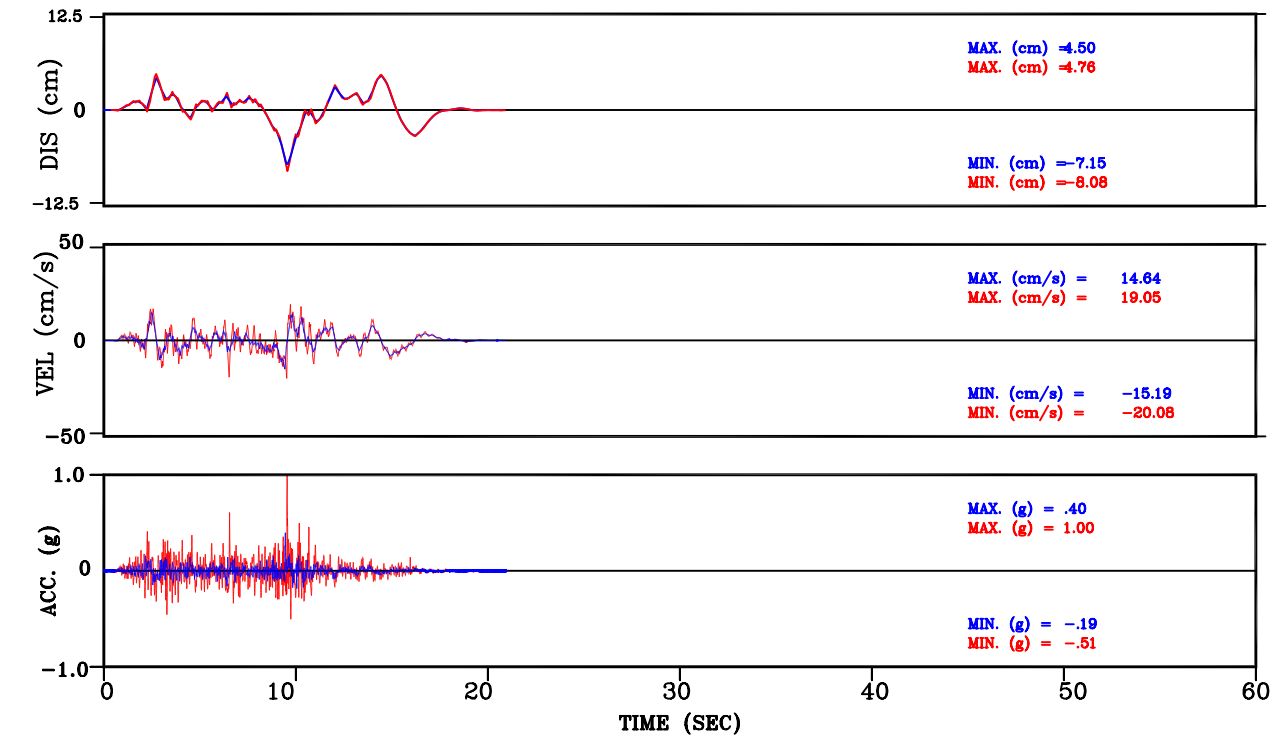


Figure III-129: Within vs. Surface Motion for Soft Soil  
 Set-1 Vert. Comp. Motion Conforming to NUREG/CR-6728 Spectral Shape

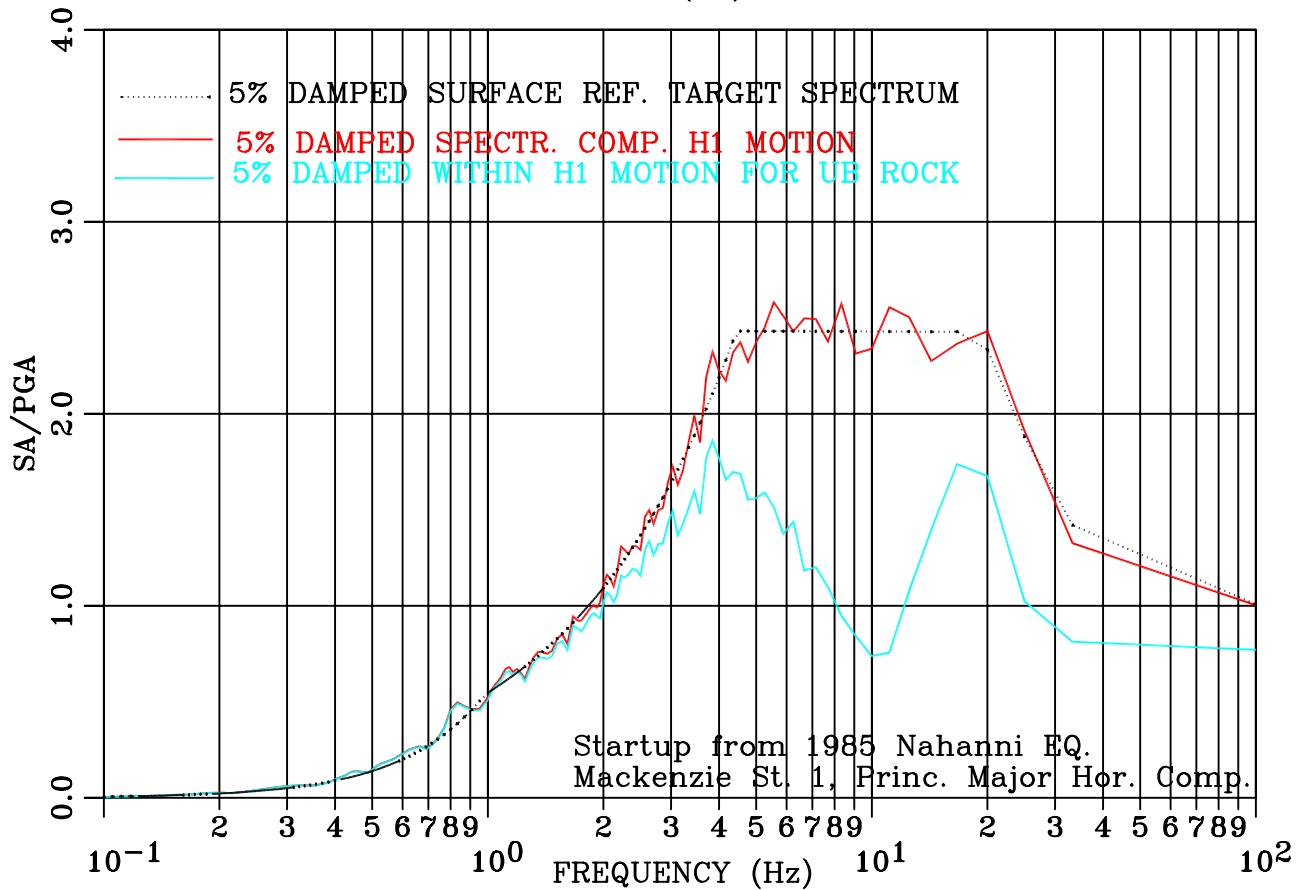
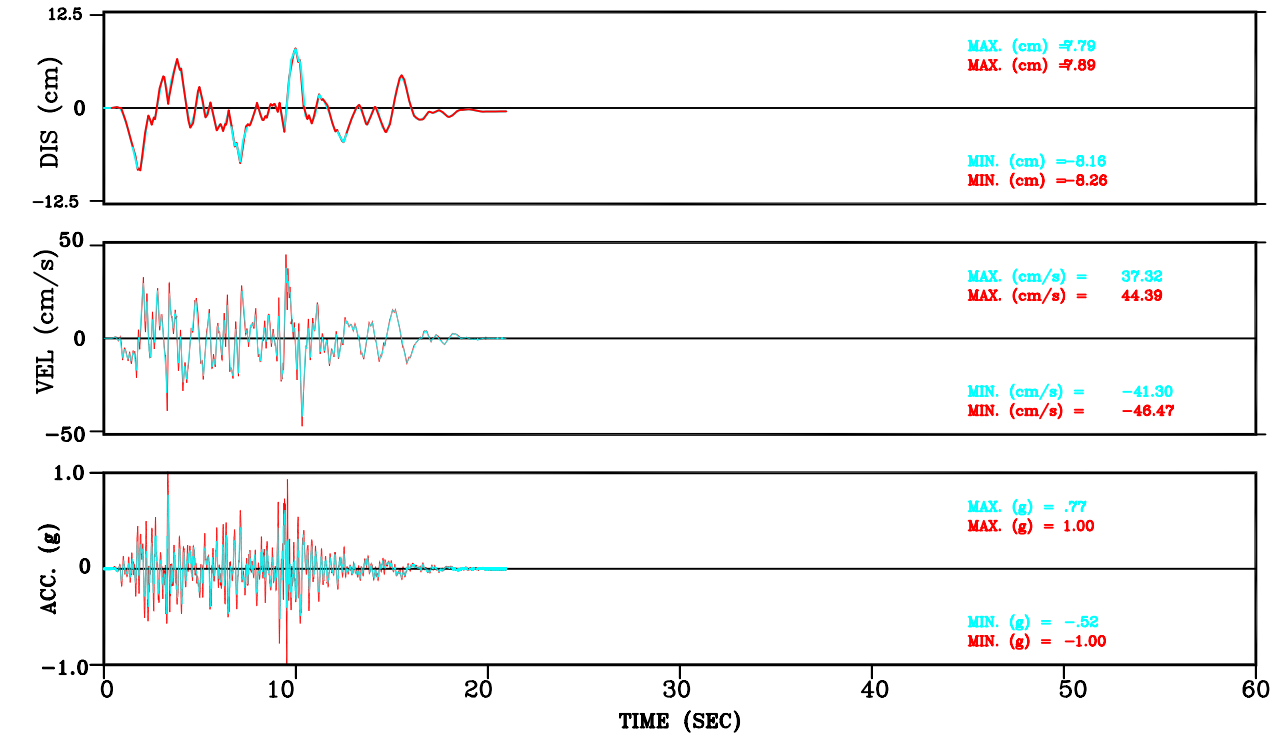


Figure III-130: Within vs. Surface Motion for UB Rock  
Set-1 H1 Comp. Motion Conforming to NUREG/CR-6728 Spectral Shape

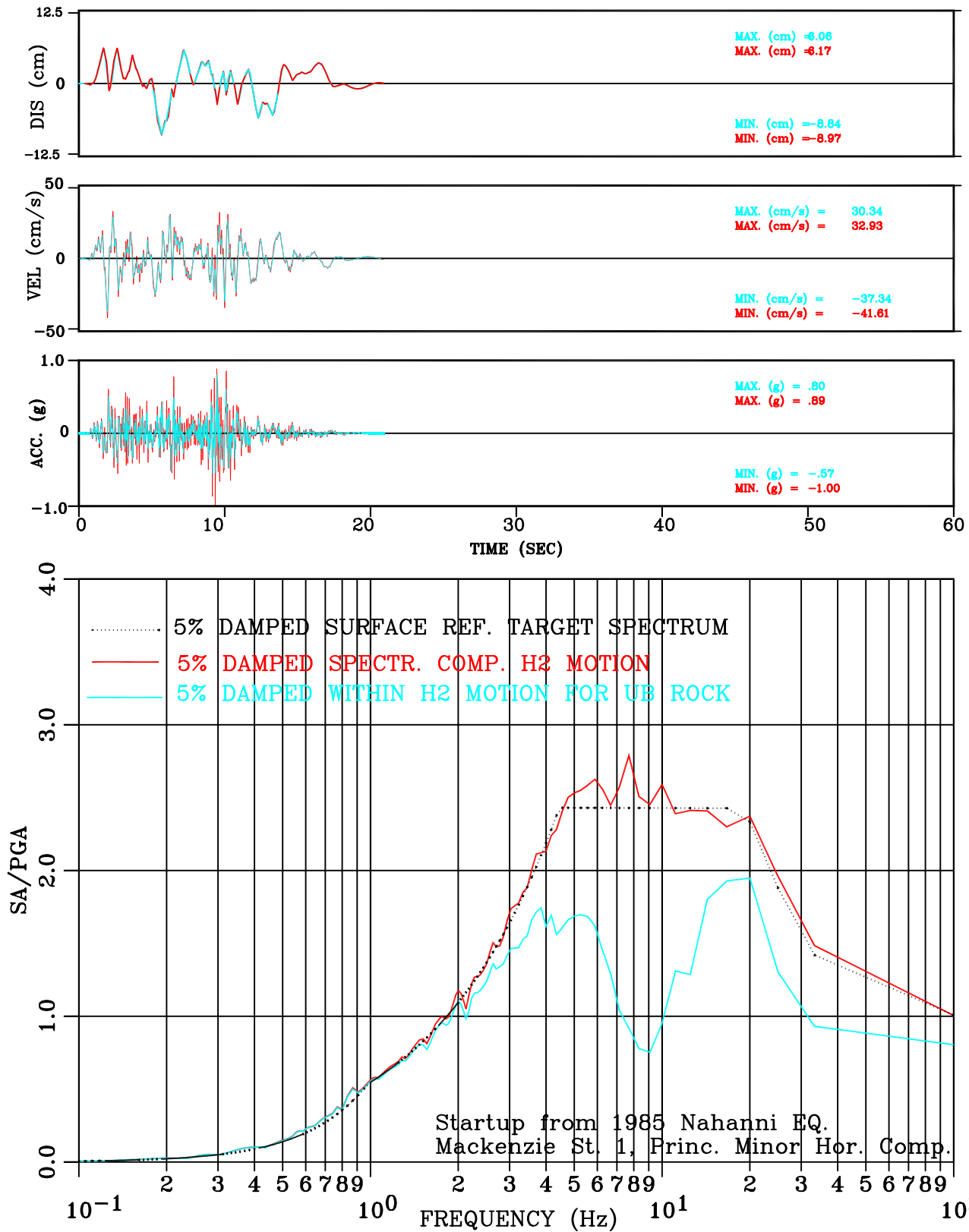


Figure III-131: Within vs. Surface Motion for UB Rock Set-1 H2 Comp. Motion Conforming to NUREG/CR-6728 Spectral Shape

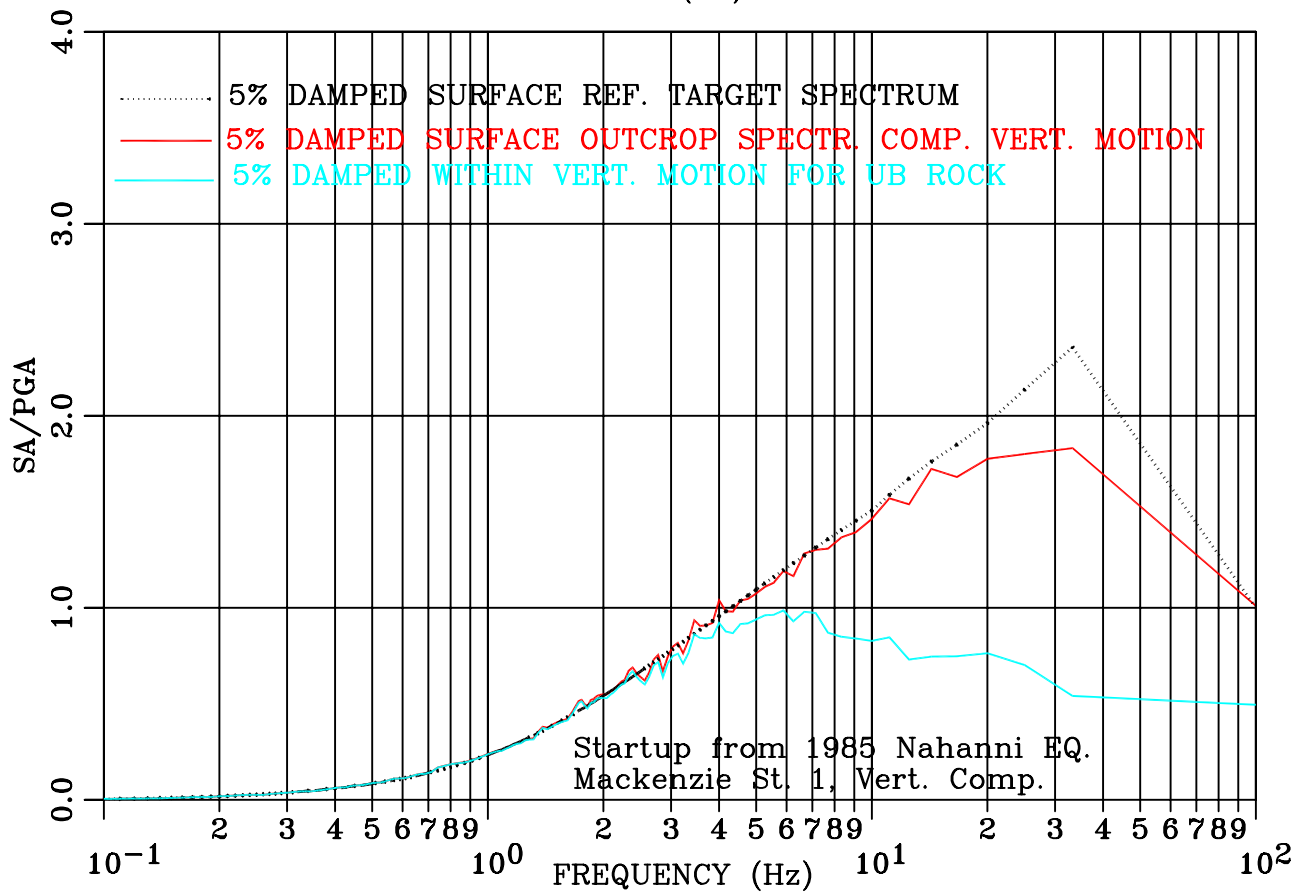
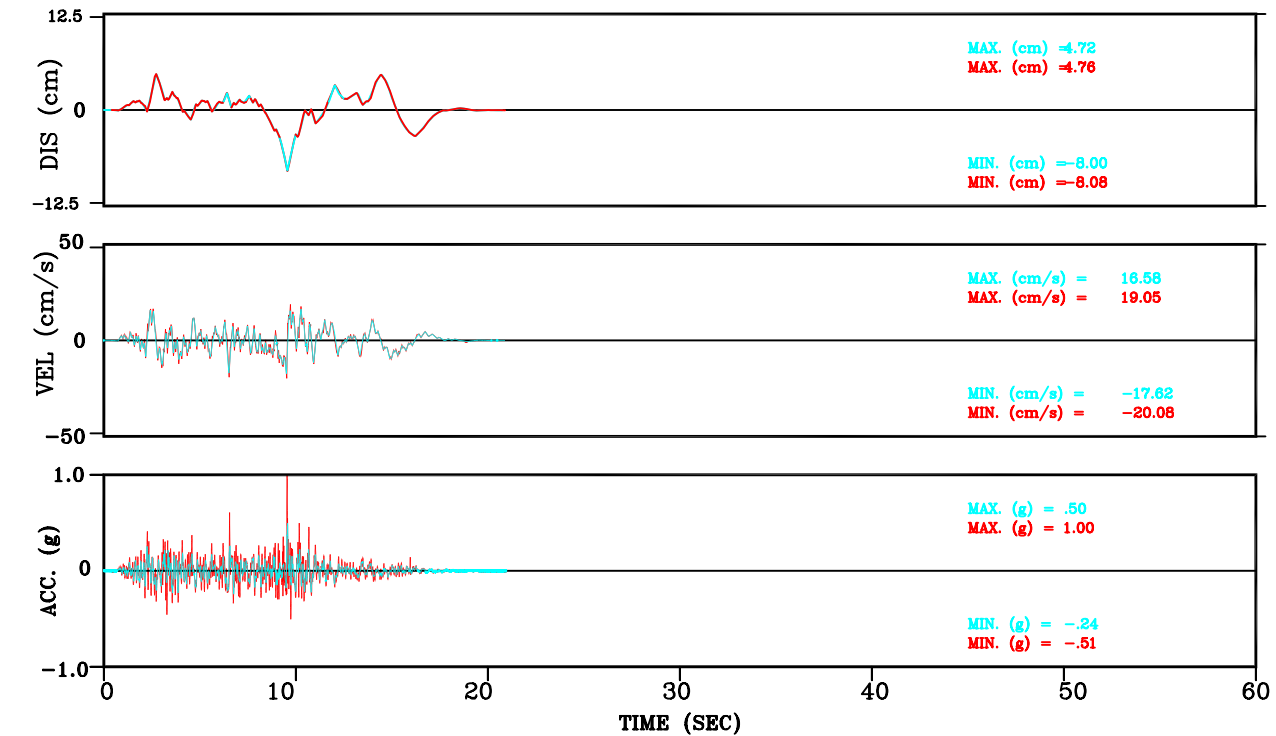


Figure III-132: Within vs. Surface Motion for UB Rock  
Set-1 Vert. Comp. Motion Conforming to NUREG/CR-6728 Spectral Shape

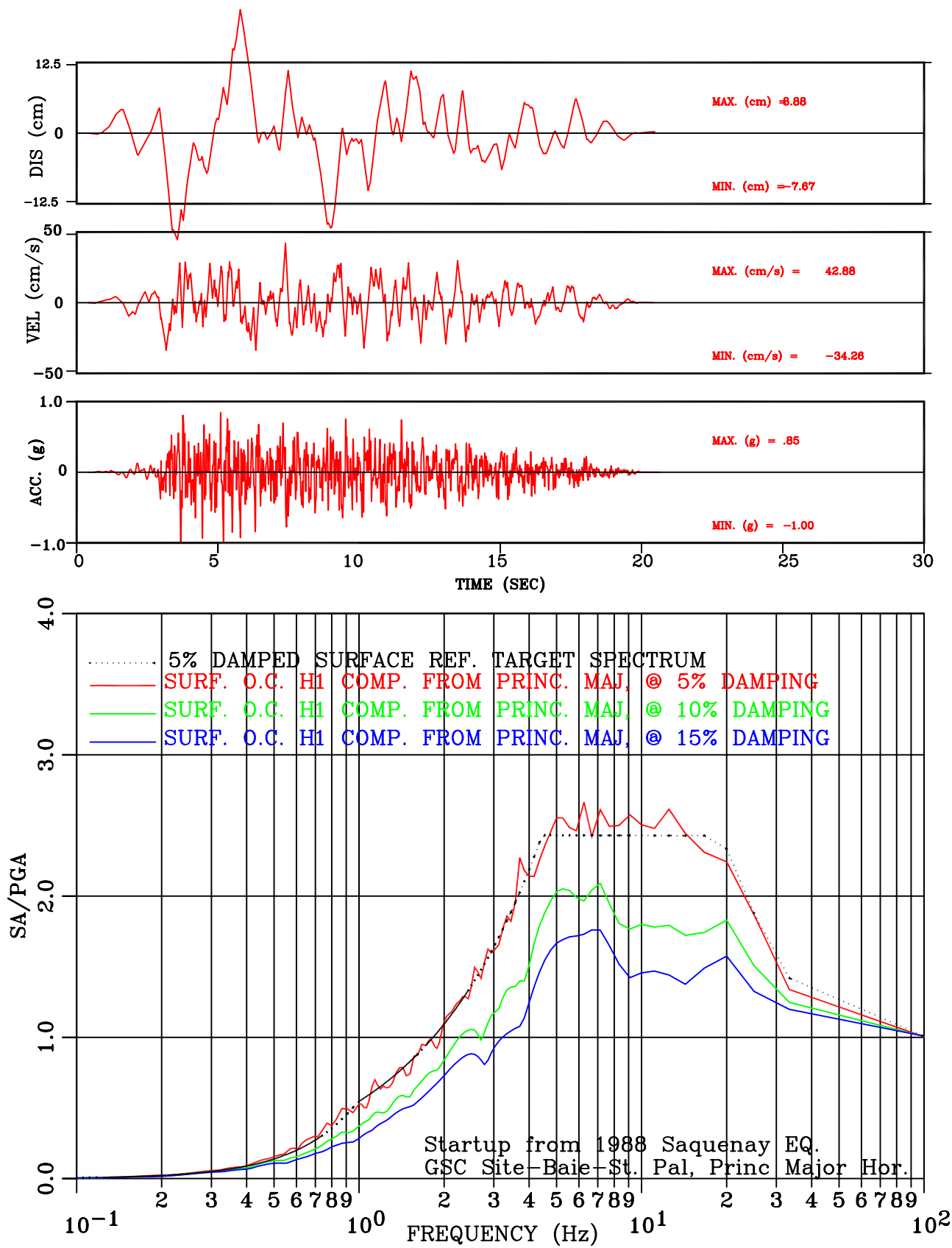


Figure III-133: Set-2 H1 Comp. Motion Conforming to NUREG/CR-6728 Spectral Shape

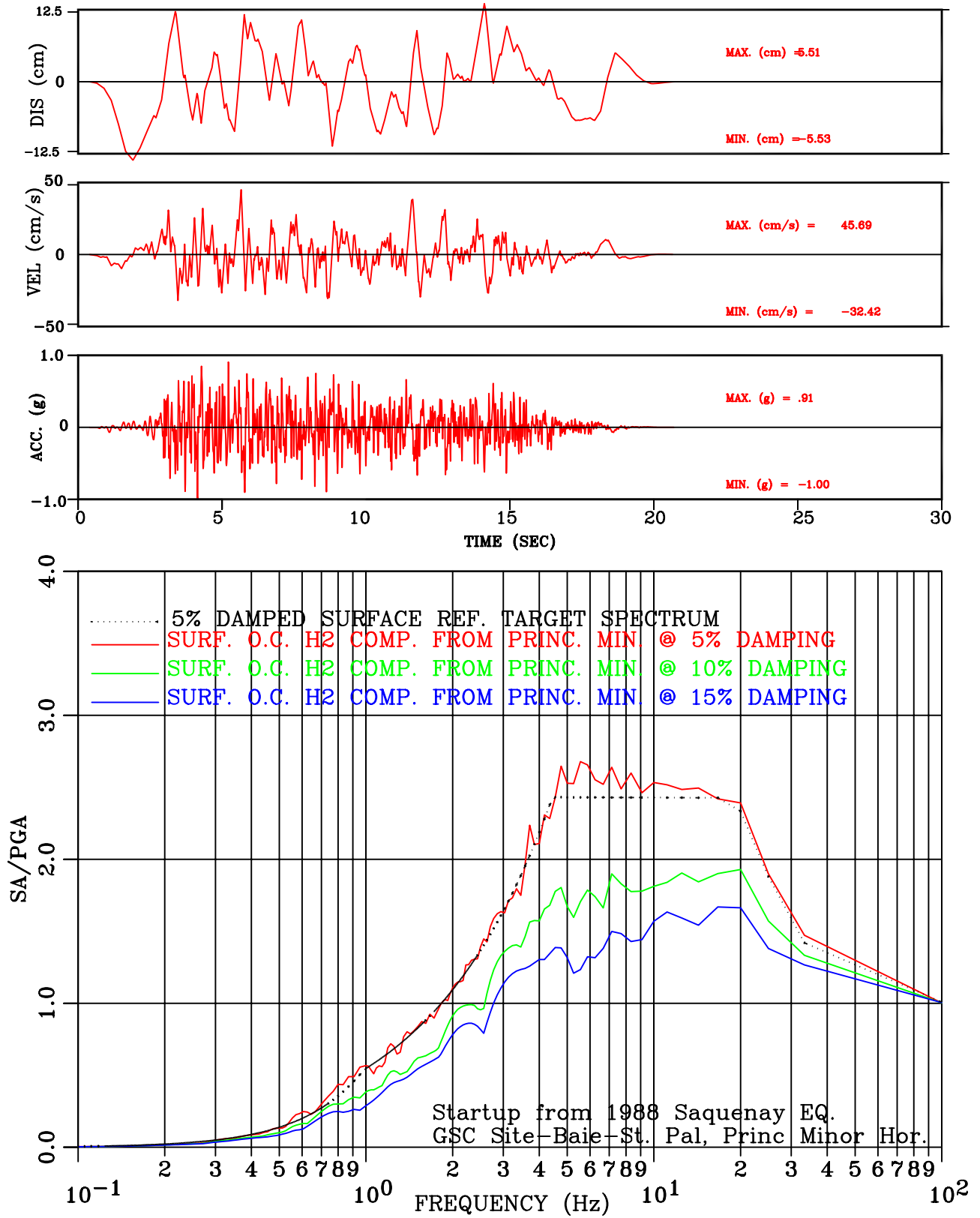


Figure III-134: Set-2 H2 Comp. Motion Conforming to NUREG/CR-6728 Spectral Shape

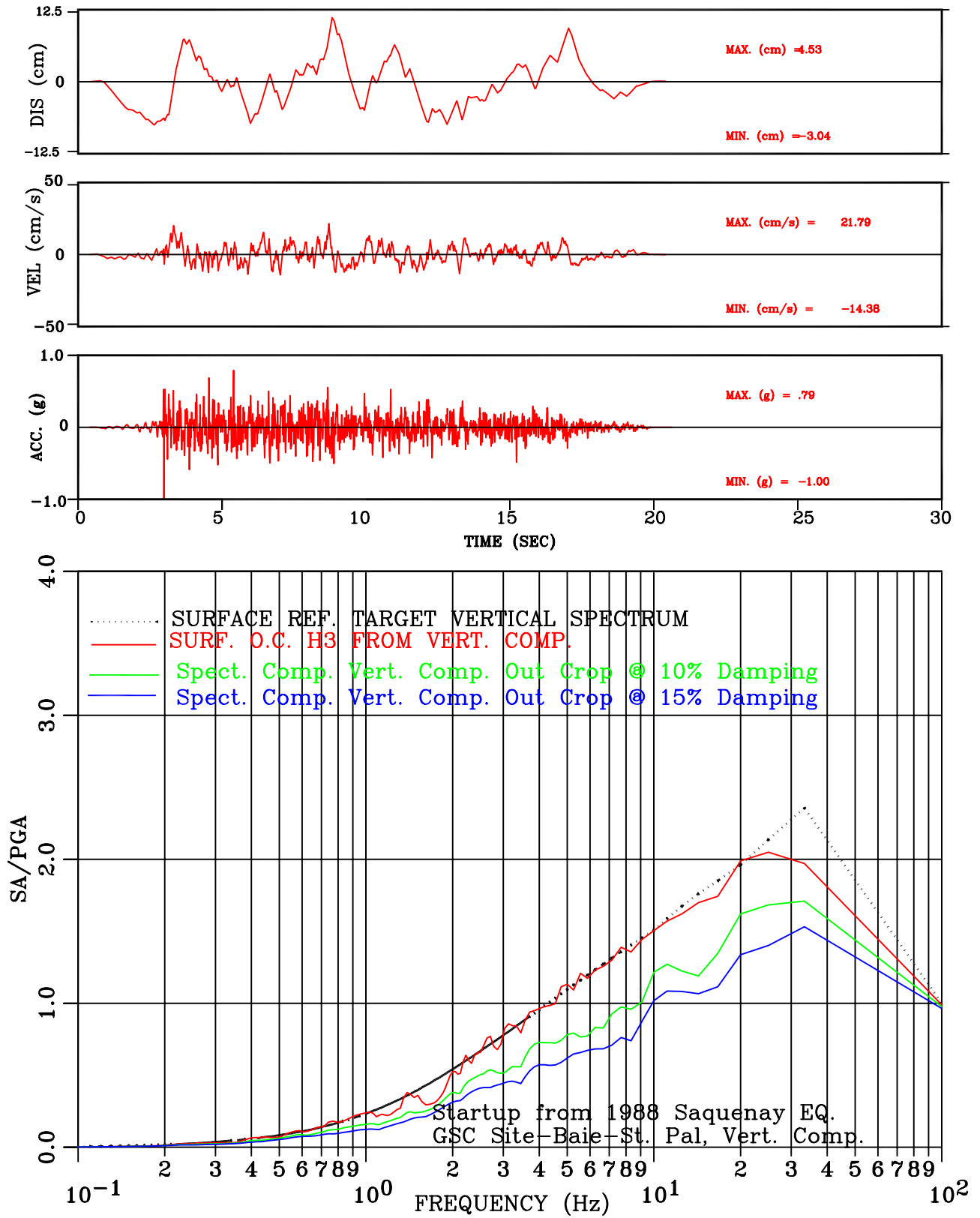


Figure III-135: Set-2 Vert. Comp. Motion Conforming to NUREG/CR-6728 Spectral Shape

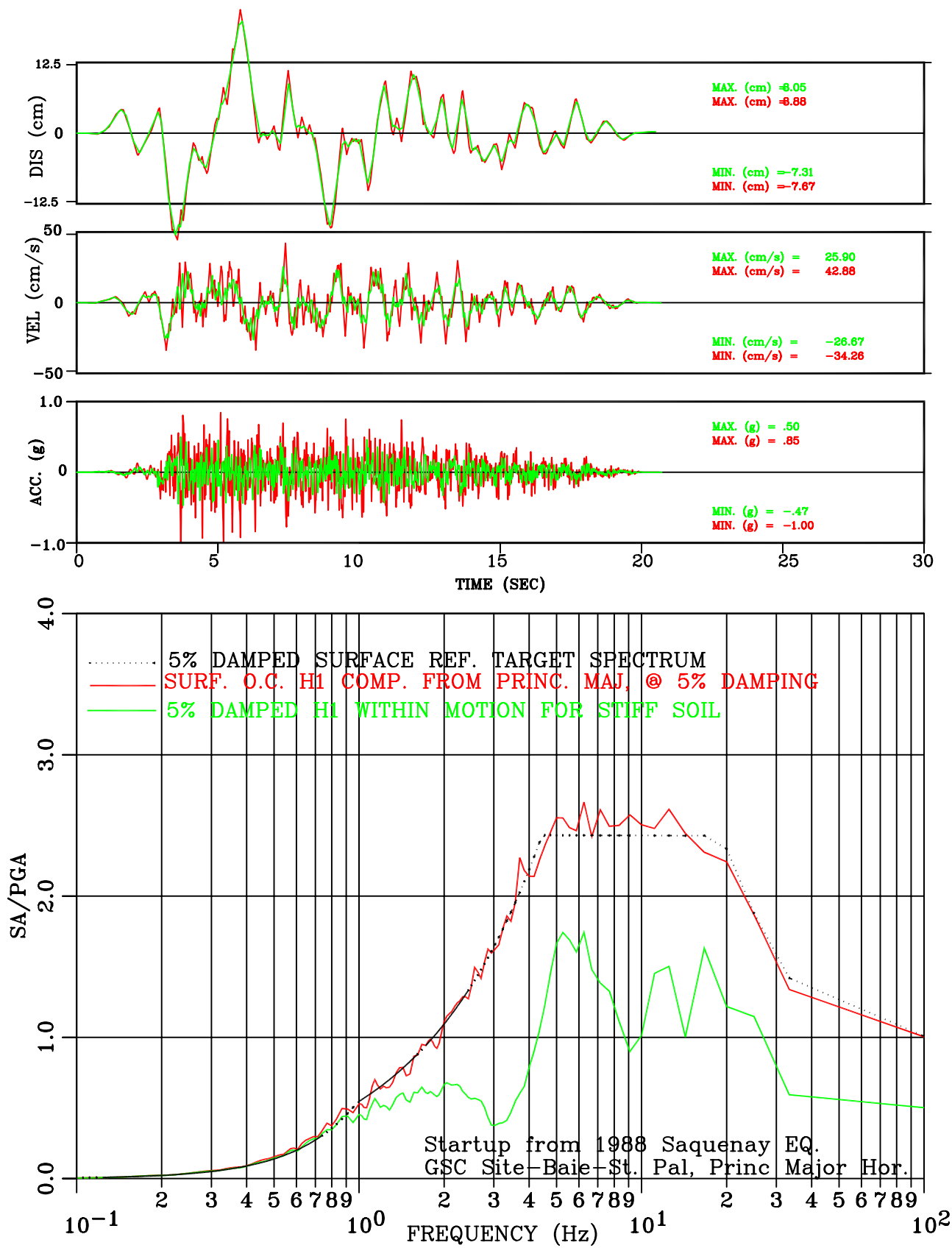


Figure III-136: Within vs. Surface Motion for Stiff Soil  
 Set-2 H1 Comp. Motion Conforming to NUREG/CR-6728 Spectral Shape

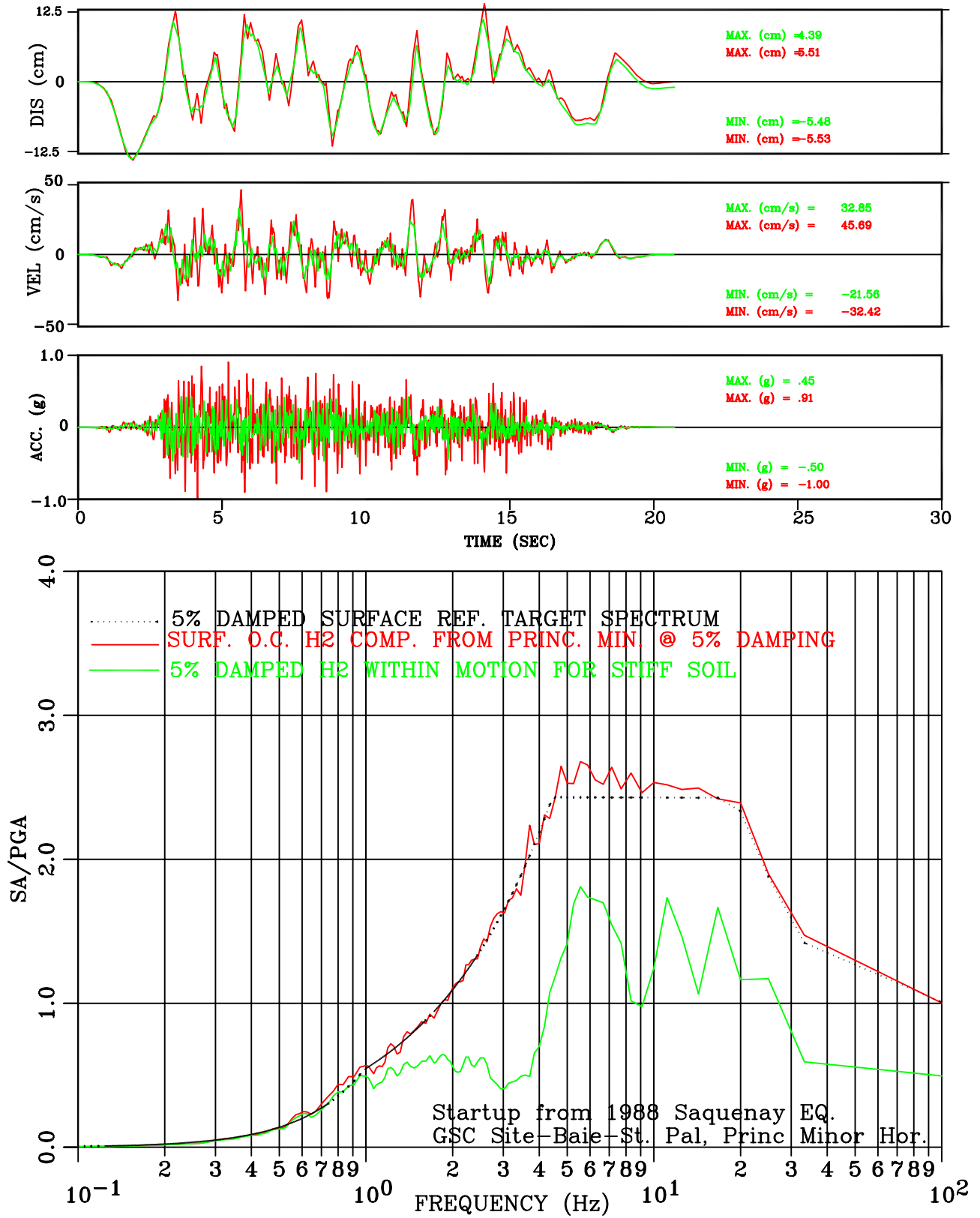


Figure III-137: Within vs. Surface Motion for Stiff Soil  
 Set-2 H2 Comp. Motion Conforming to NUREG/CR-6728 Spectral Shape

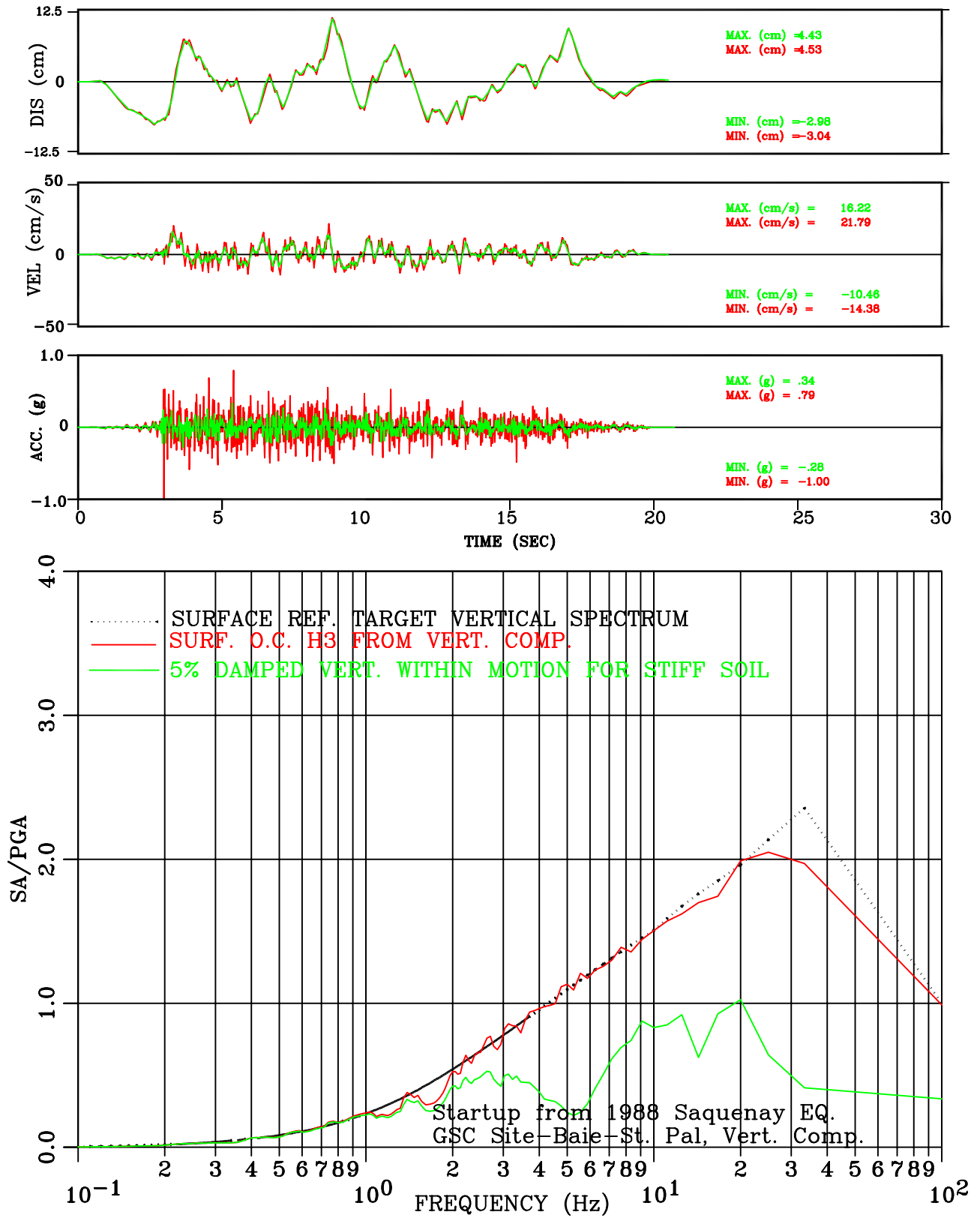


Figure III-138: Within vs. Surface Motion for Stiff Soil Set-2 Vert. Comp. Motion Conforming to NUREG/CR-6728 Spectral Shape

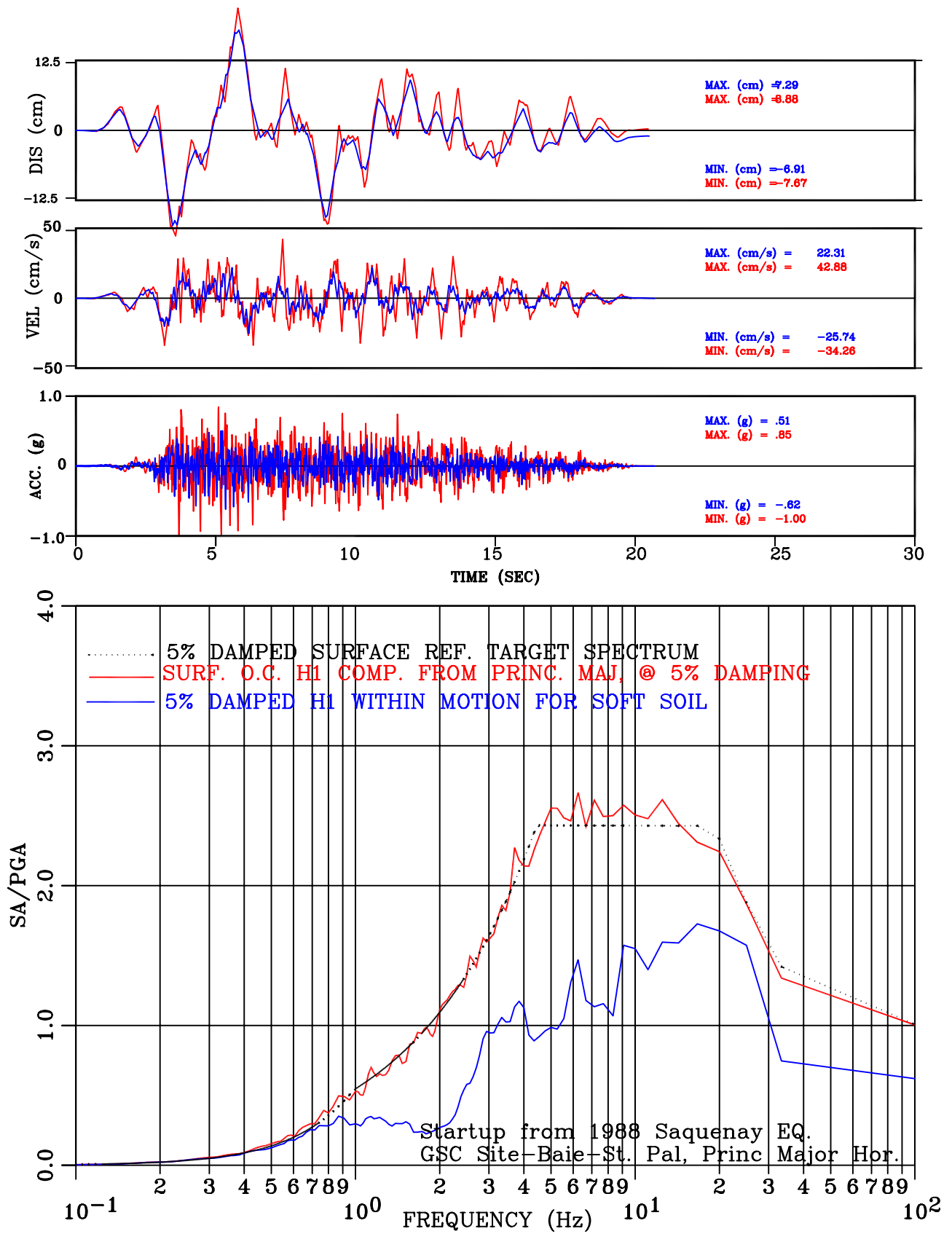


Figure III-139: Within vs. Surface Motion for Soft Soil  
 Set-2 H1 Comp. Motion Conforming to NUREG/CR-6728 Spectral Shape

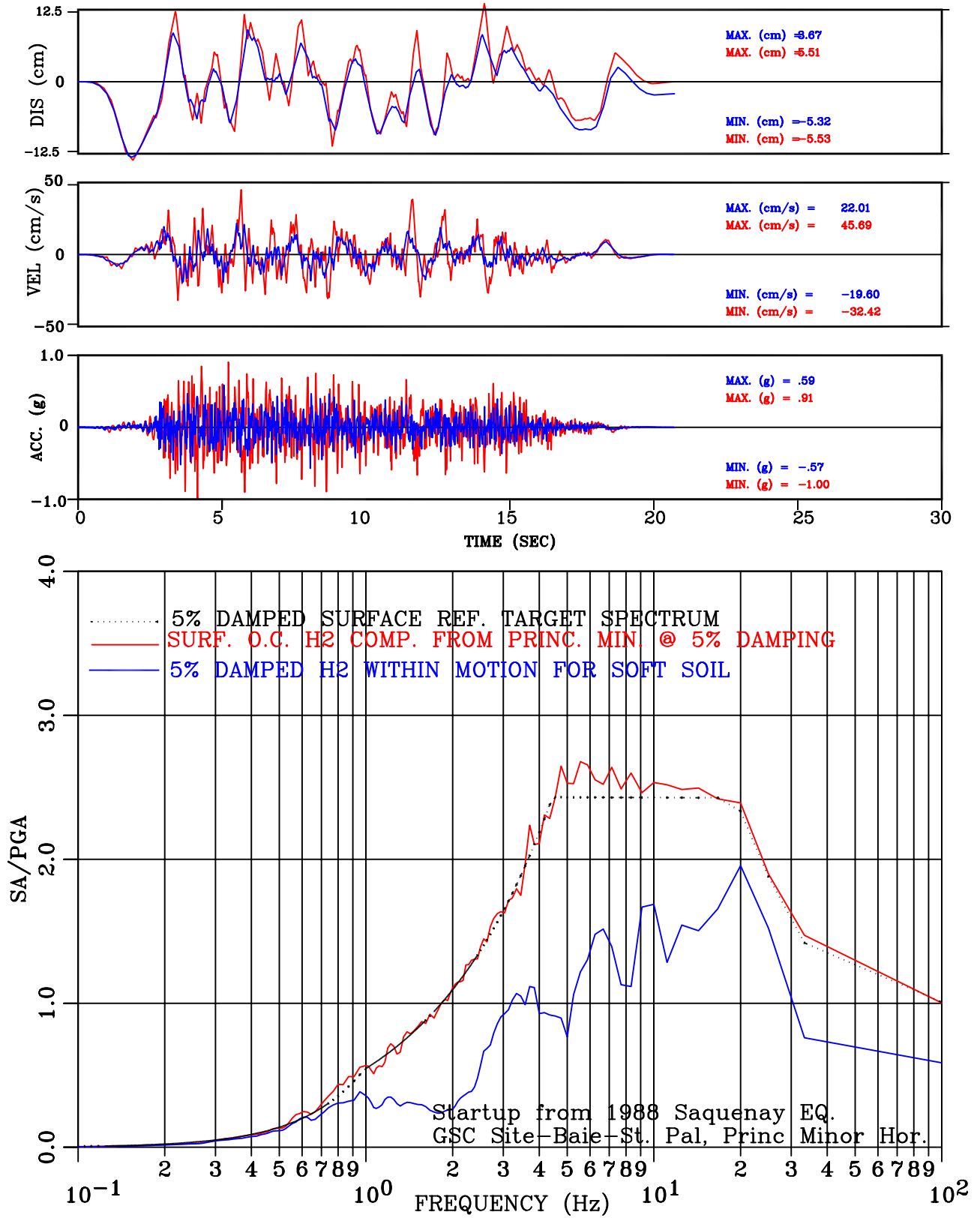


Figure III-140: Within vs. Surface Motion for Soft Soil  
Set-2 H2 Comp. Motion Conforming to NUREG/CR-6728 Spectral Shape

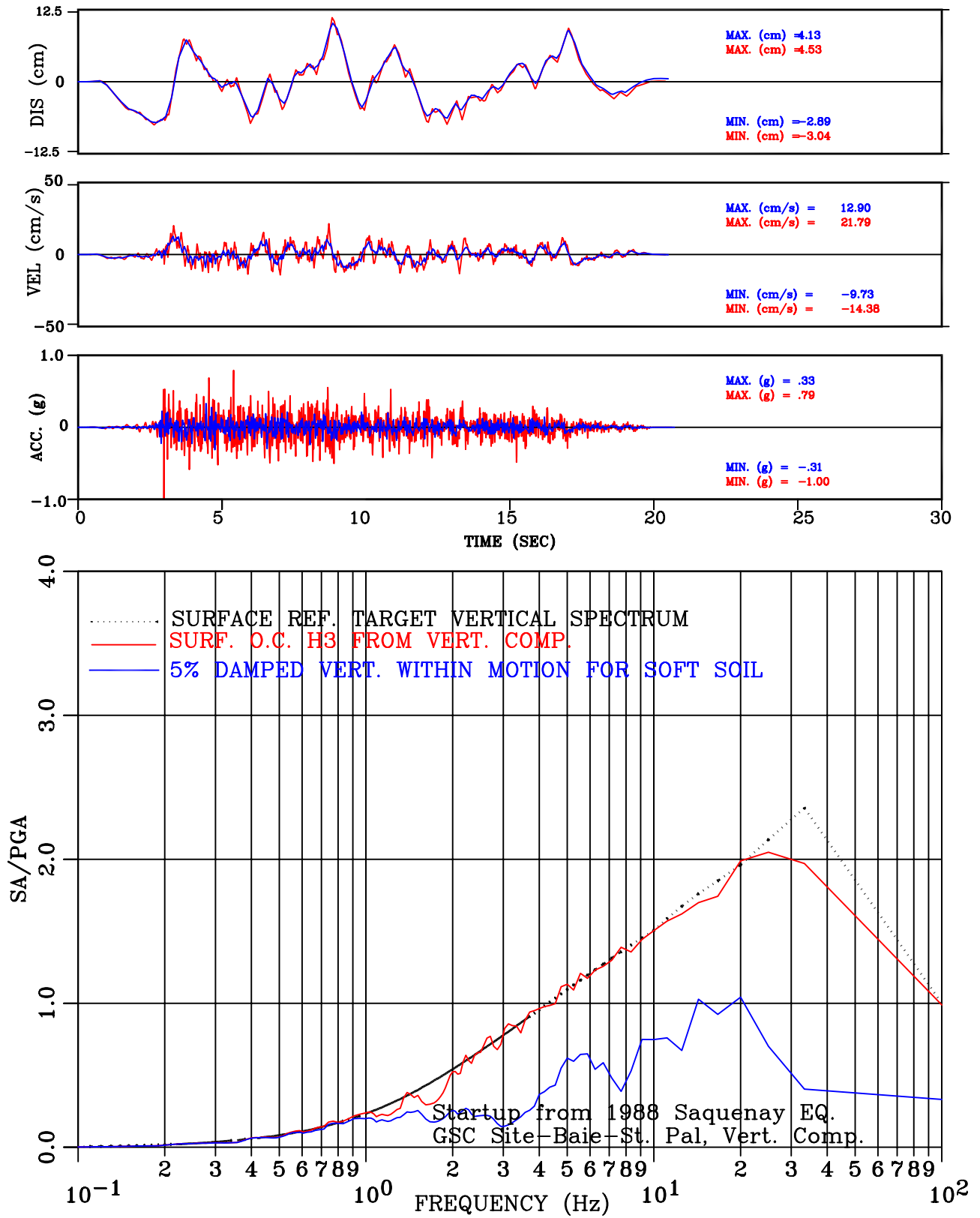


Figure III-141: Within vs. Surface Motion for Soft Soil  
Set-2 Vert. Comp. Motion Conforming to NUREG/CR-6728 Spectral Shape

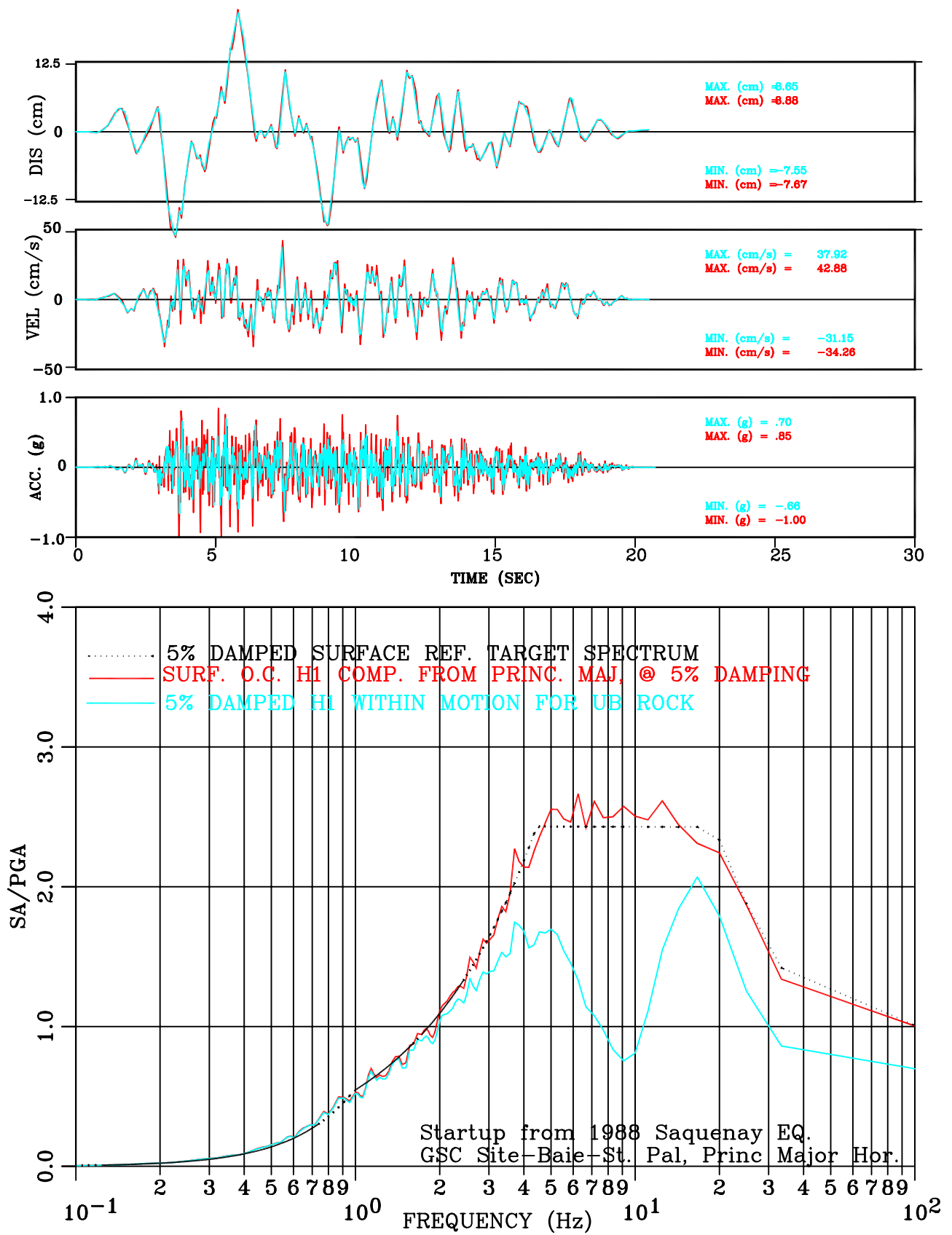


Figure III-142: Within vs. Surface Motion for UB Rock  
Set-2 H1 Comp. Motion Conforming to NUREG/CR-6728 Spectral Shape

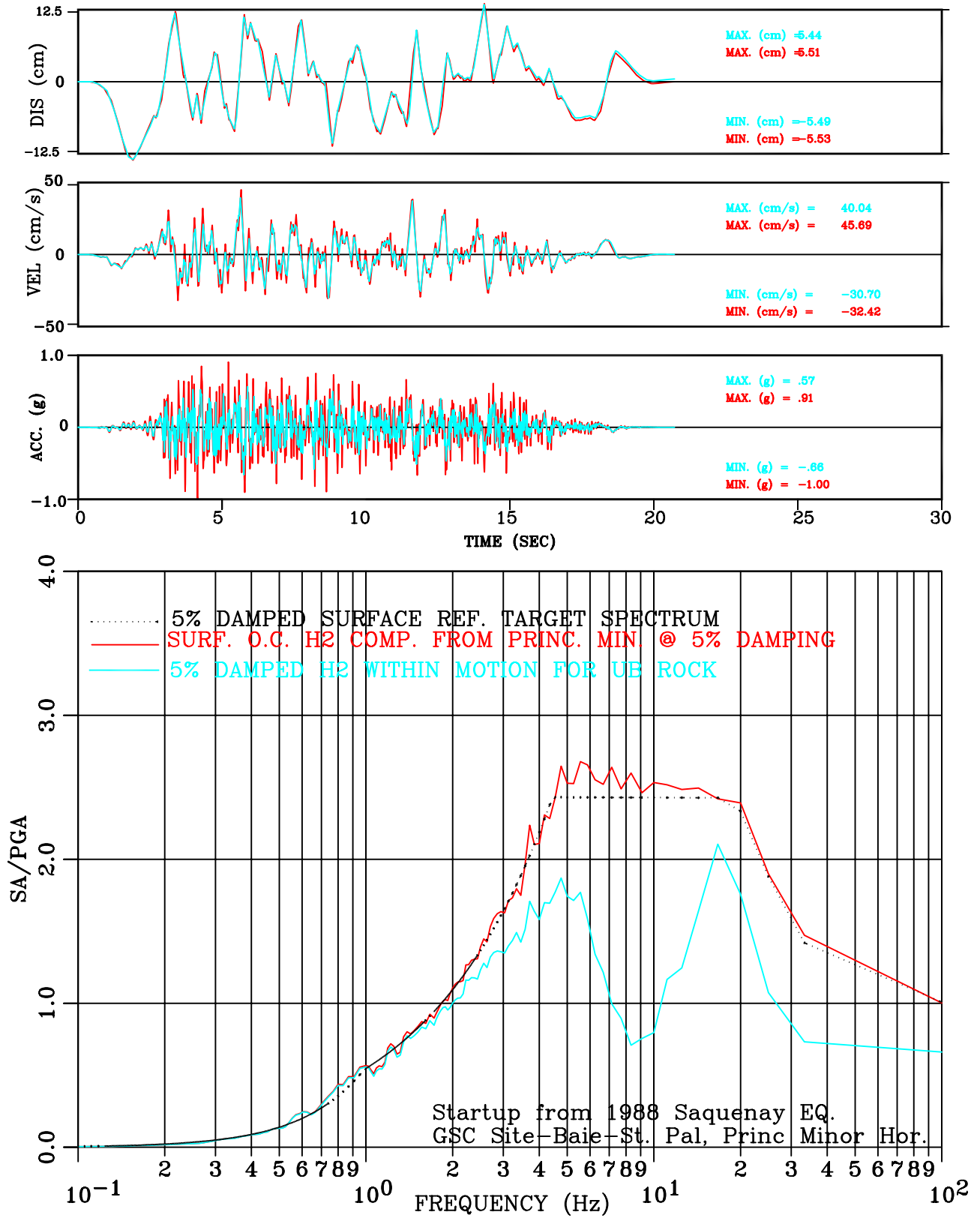


Figure III-143: Within vs. Surface Motion for UB Rock  
 Set-2 H2 Comp. Motion Conforming to NUREG/CR-6728 Spectral Shape

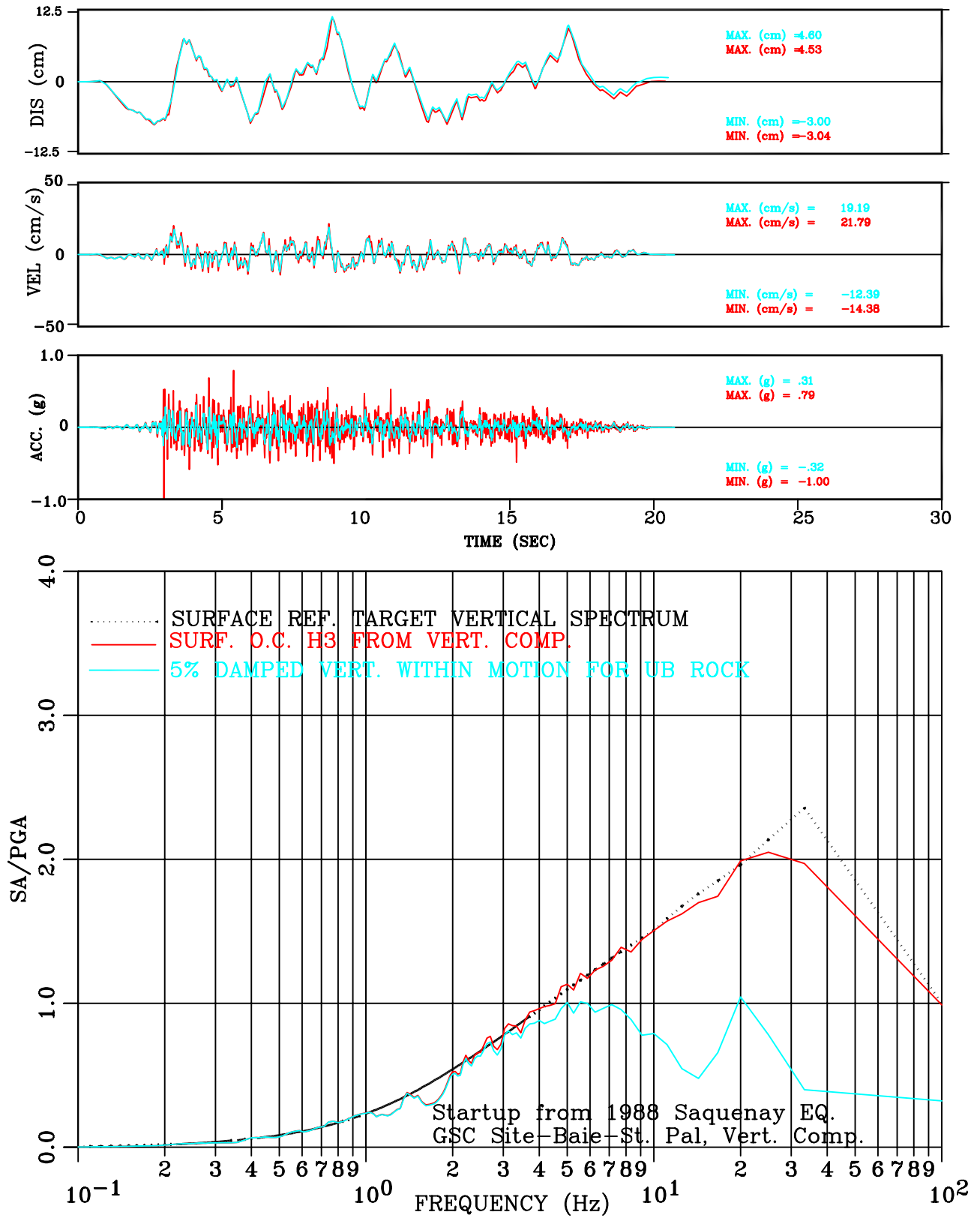


Figure III-144: Within vs. Surface Motion for UB Rock  
Set-2 Vert. Comp. Motion Conforming to NUREG/CR-6728 Spectral Shape

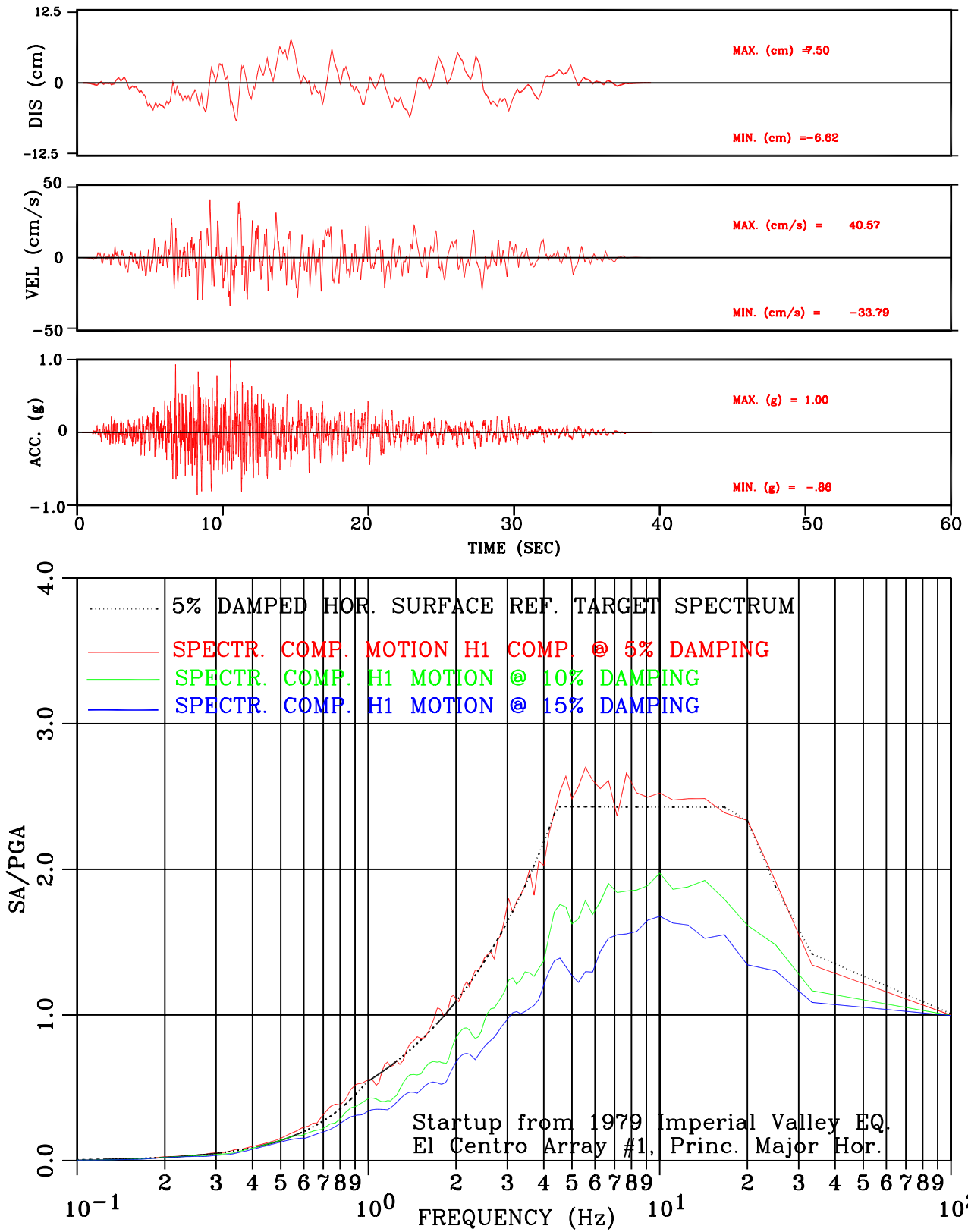


Figure III-145: Set-3 H1 Comp. Motion Conforming to NUREG/CR-6728 Spectral Shape

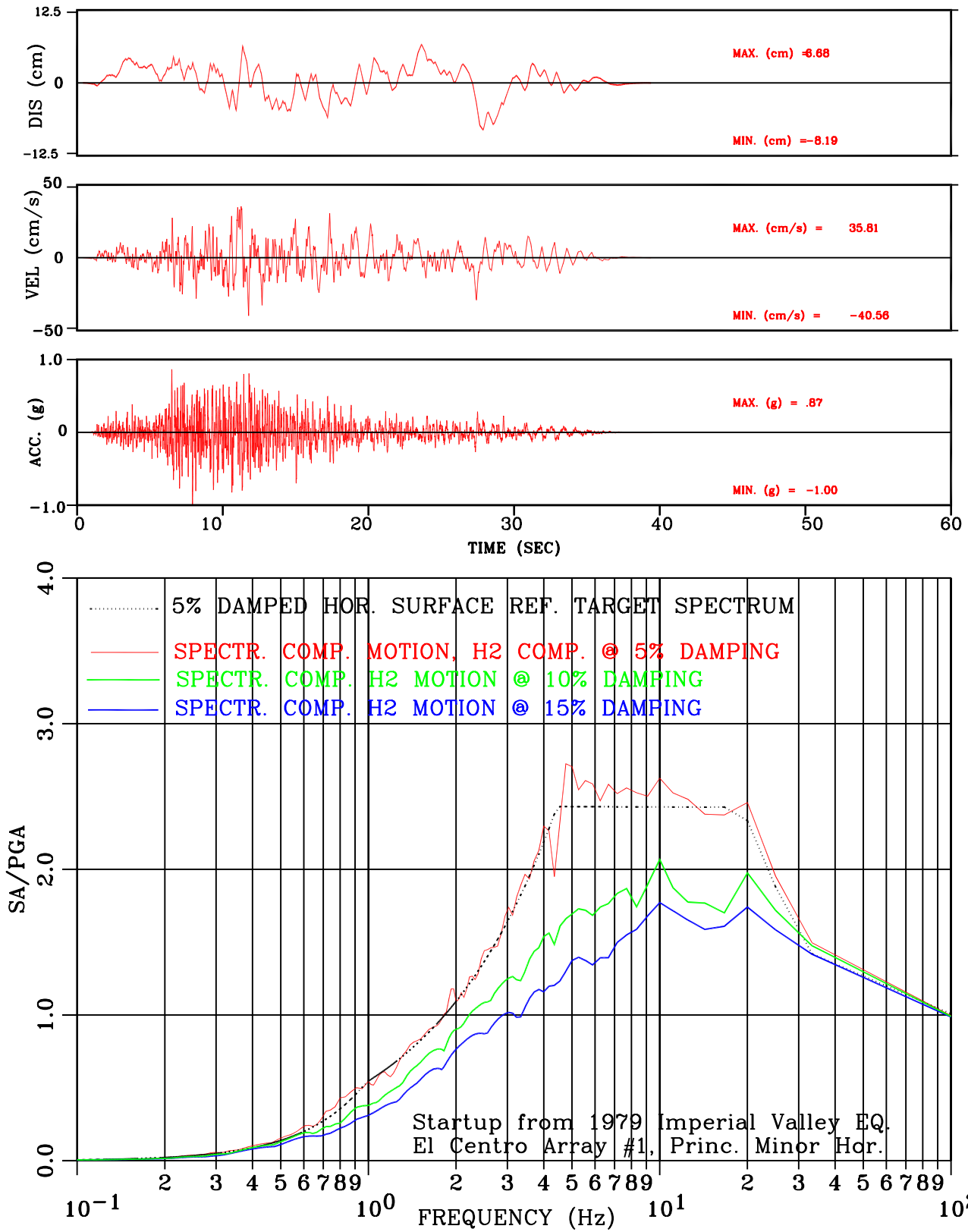


Figure III-146: Set-3 H2 Comp. Motion Conforming to NUREG/CR-6728 Spectral Shape

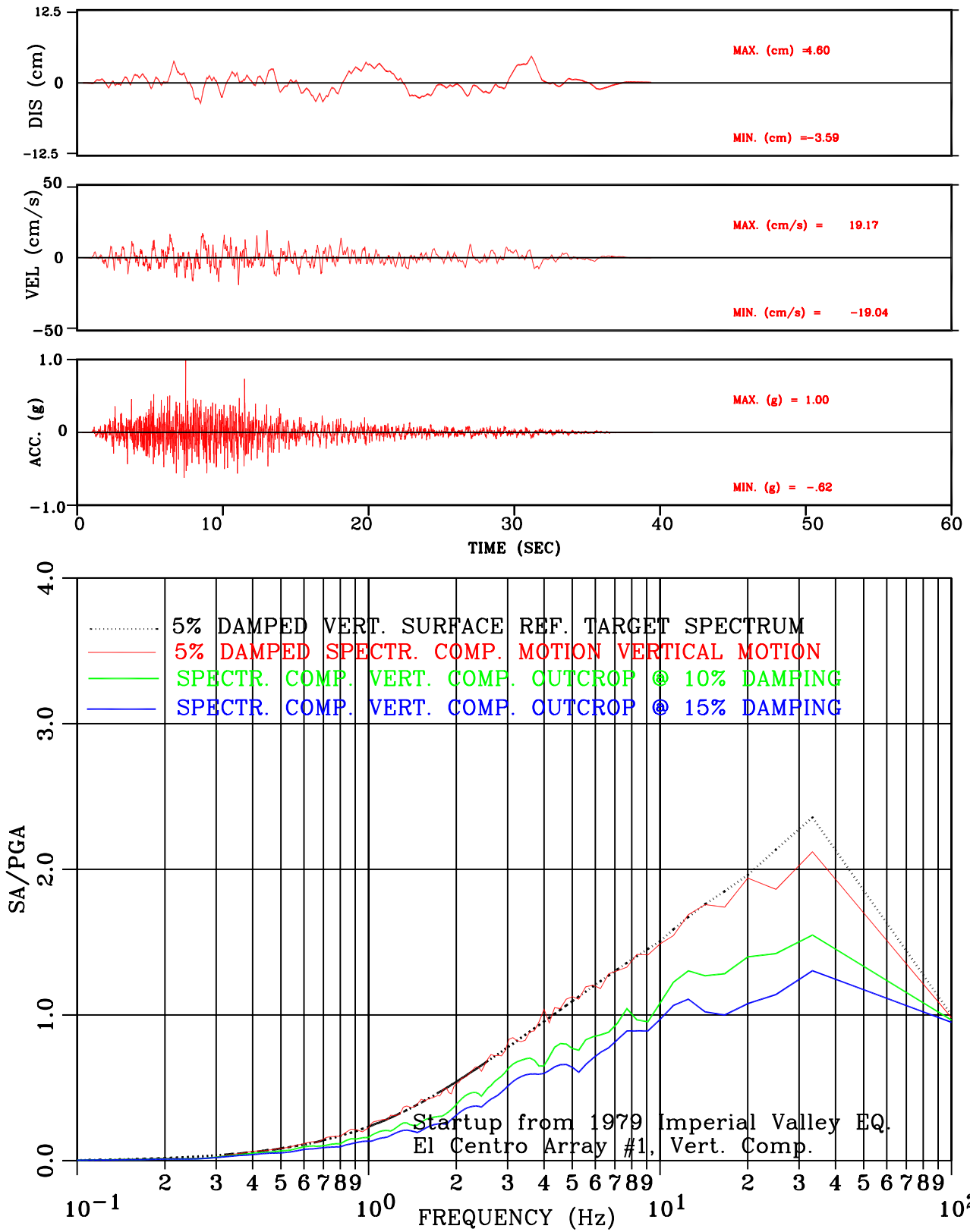


Figure III-147: Set-3 Vert. Comp. Motion Conforming to NUREG/CR-6728 Spectral Shape

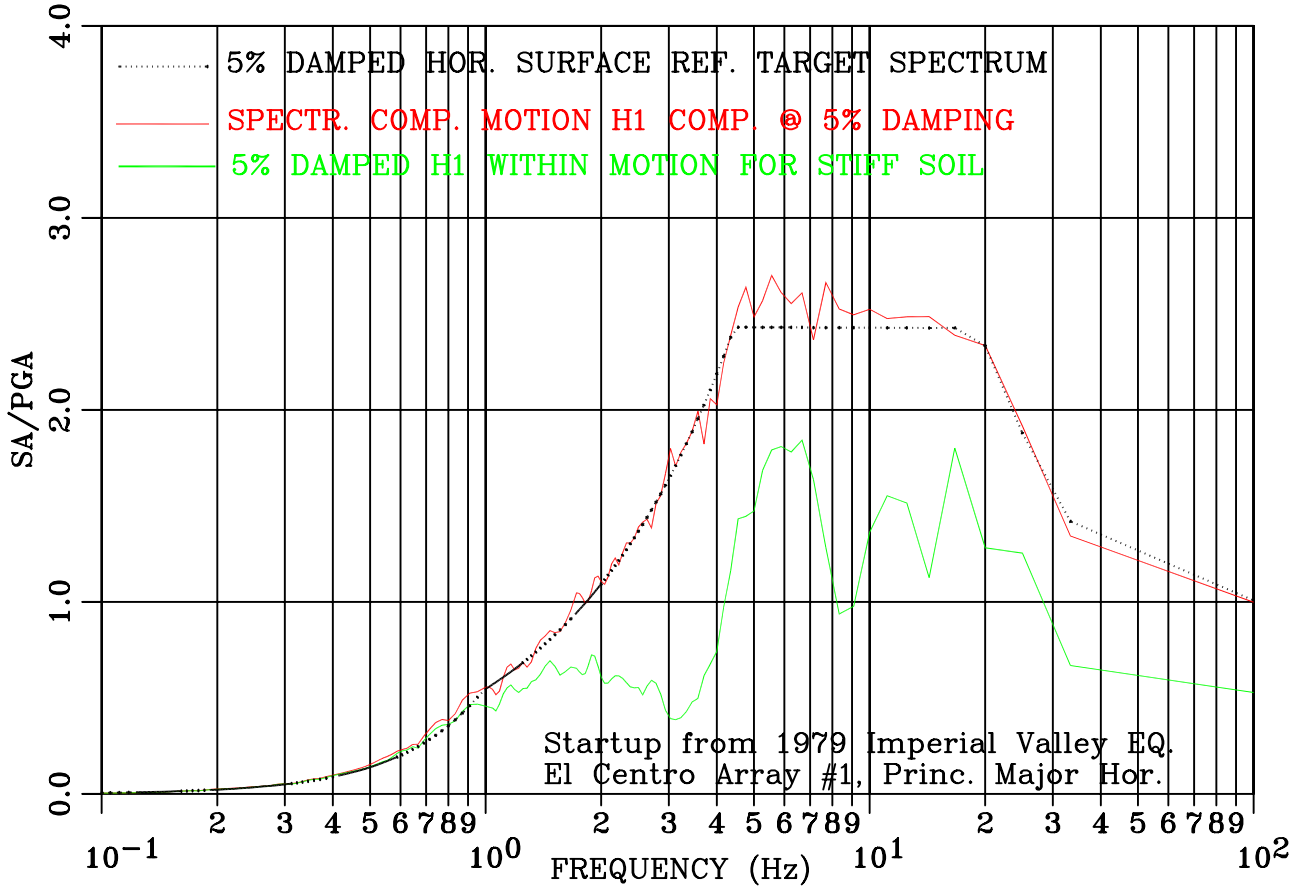
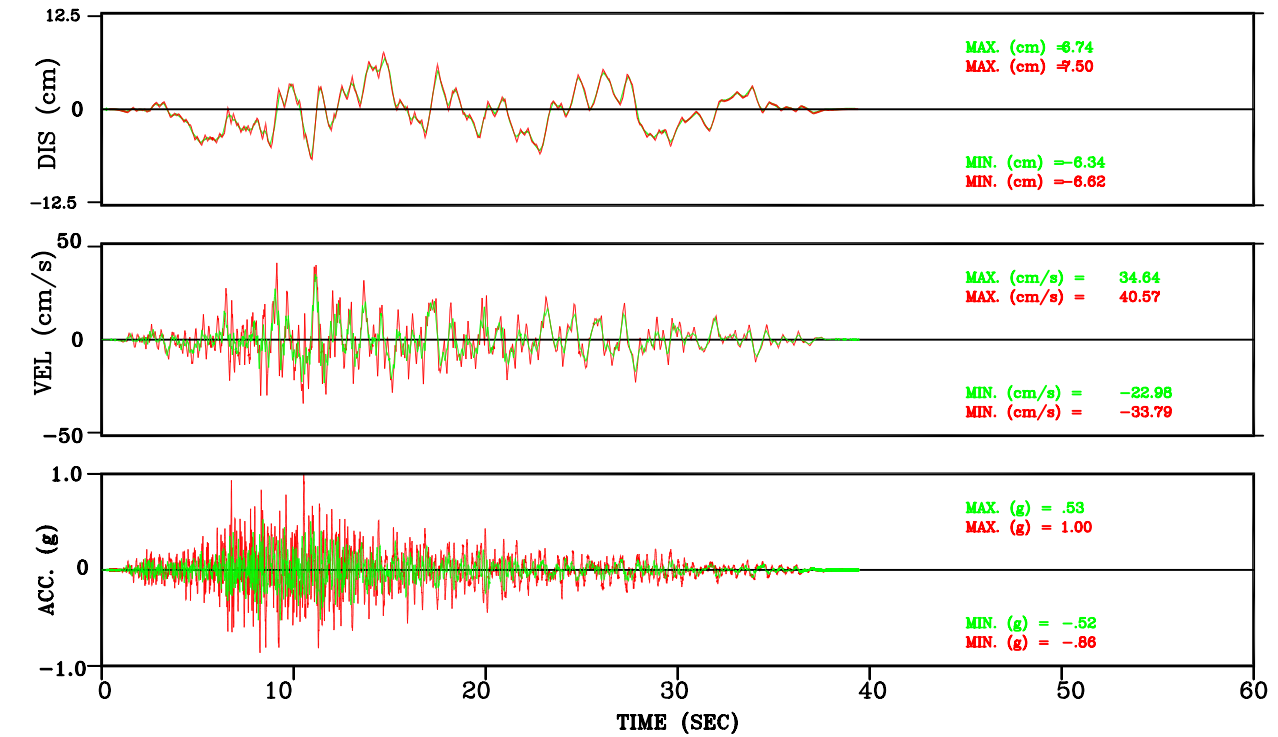


Figure III-148: Within vs. Surface Motion for Stiff Soil  
 Set-3 H1 Comp. Motion Conforming to NUREG/CR-6728 Spectral Shape

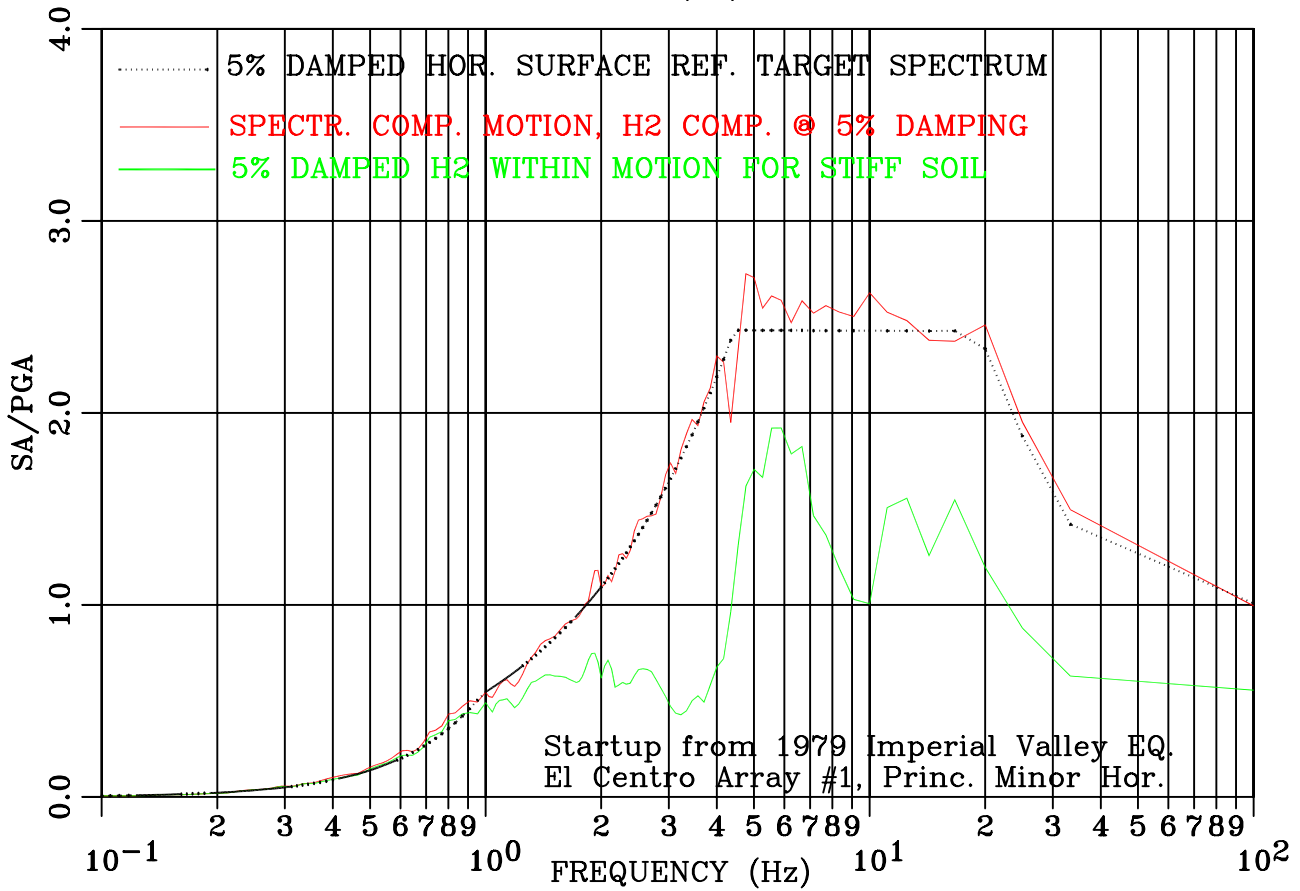
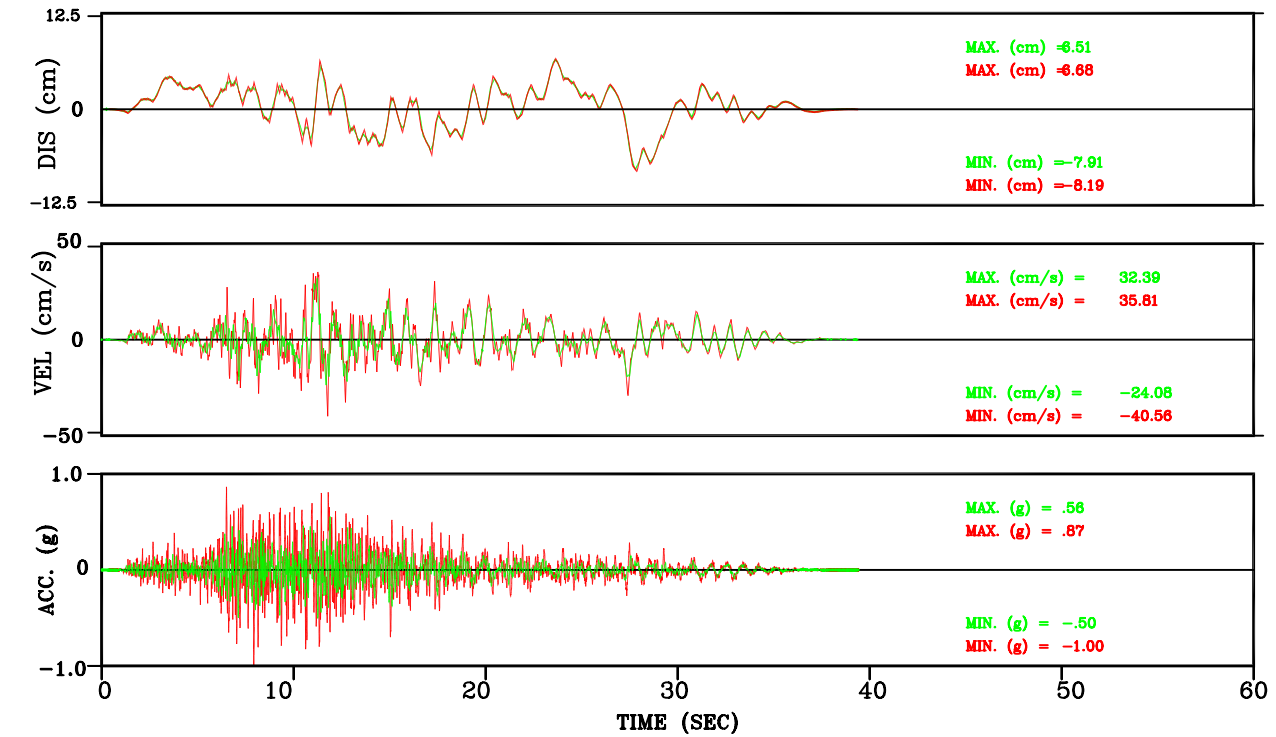


Figure III-149: Within vs. Surface Motion for Stiff Soil  
 Set-3 H2 Comp. Motion Conforming to NUREG/CR-6728 Spectral Shape

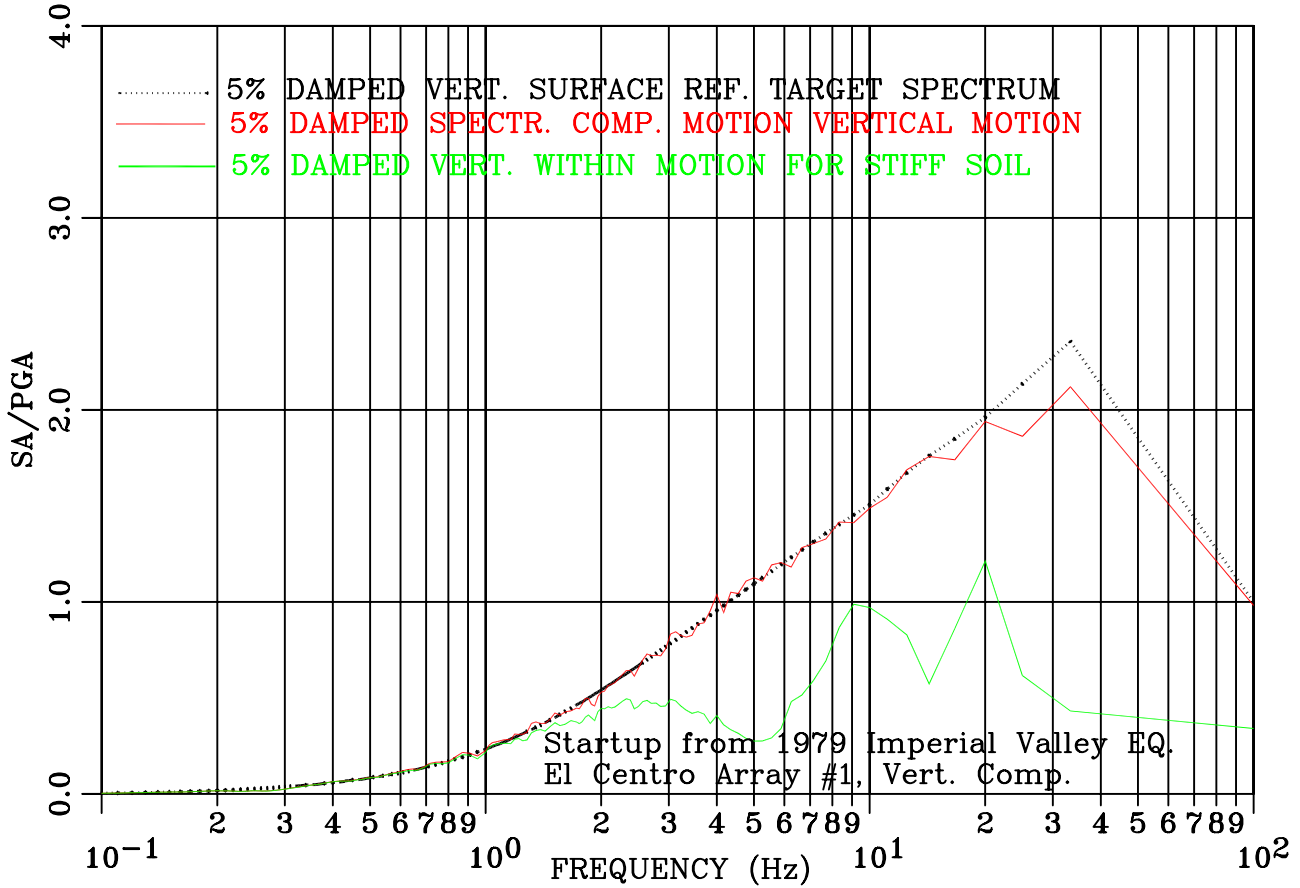
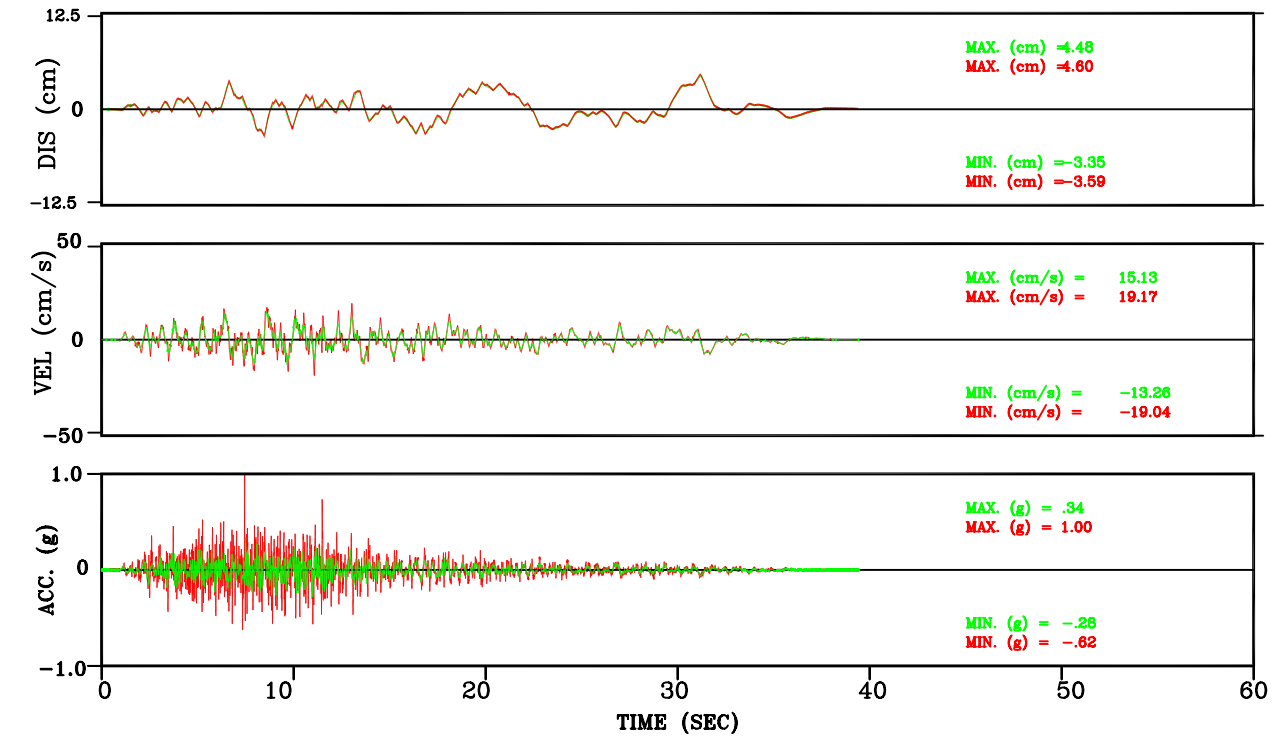


Figure III-150: Within vs. Surface Motion for Stiff Soil  
 Set-3 Vert. Comp. Motion Conforming to NUREG/CR-6728 Spectral Shape

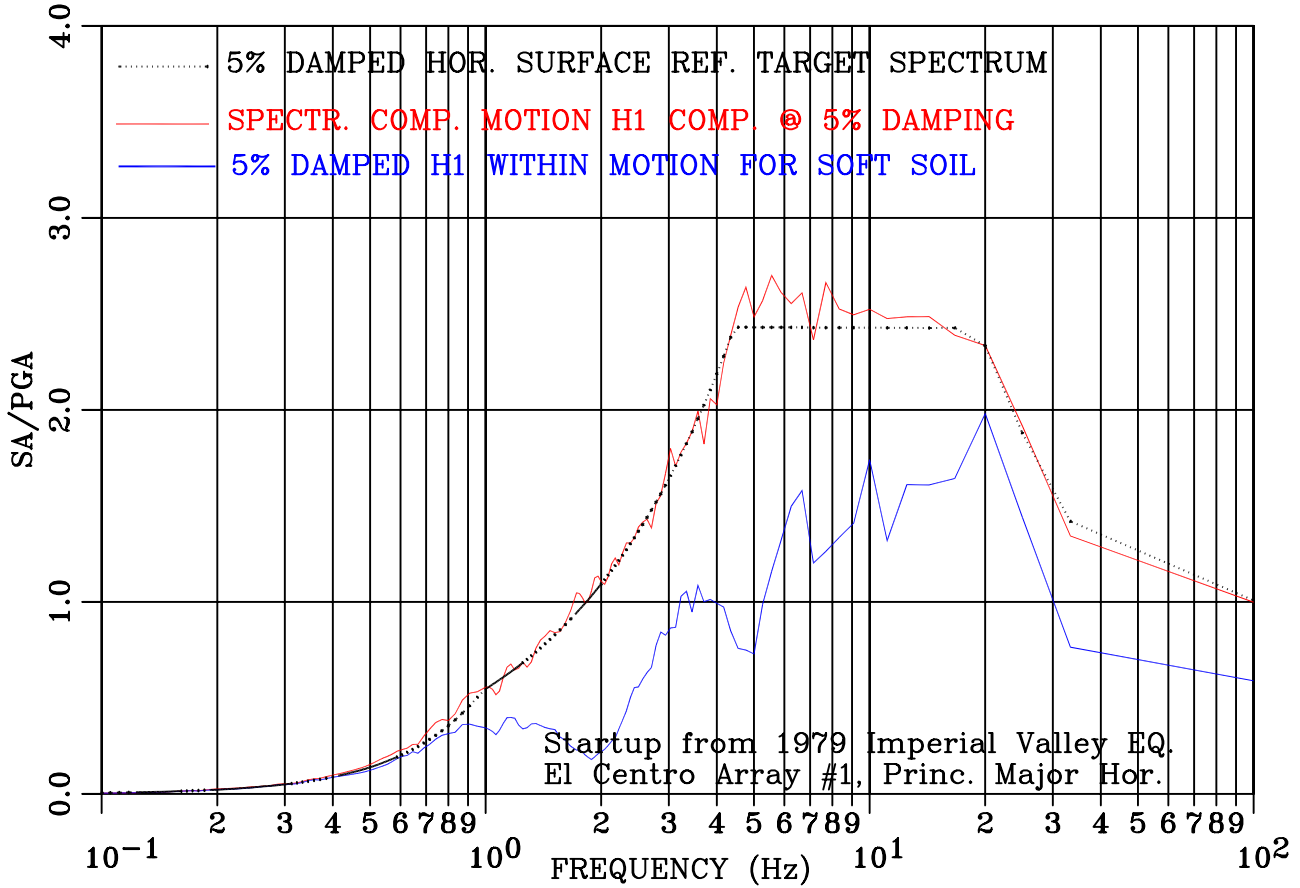
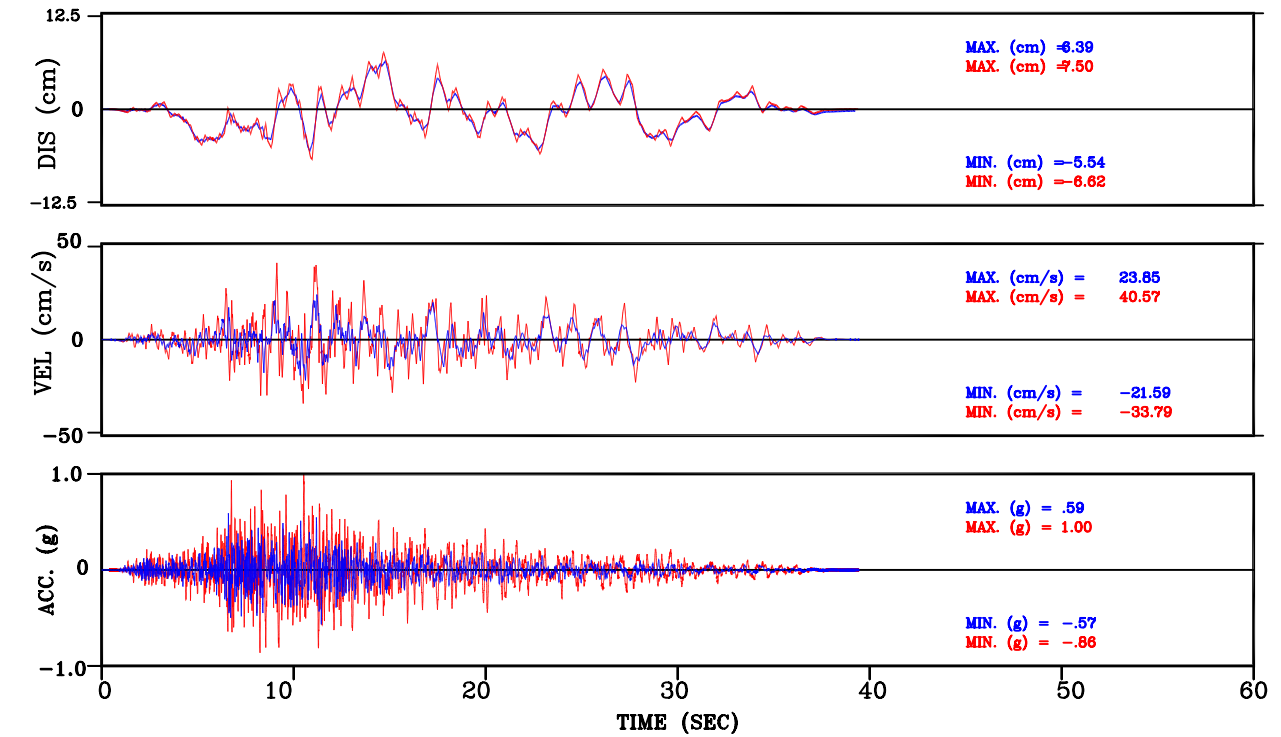


Figure III-151: Within vs. Surface Motion for Soft Soil  
 Set-3 H1 Comp. Motion Conforming to NUREG/CR-6728 Spectral Shape

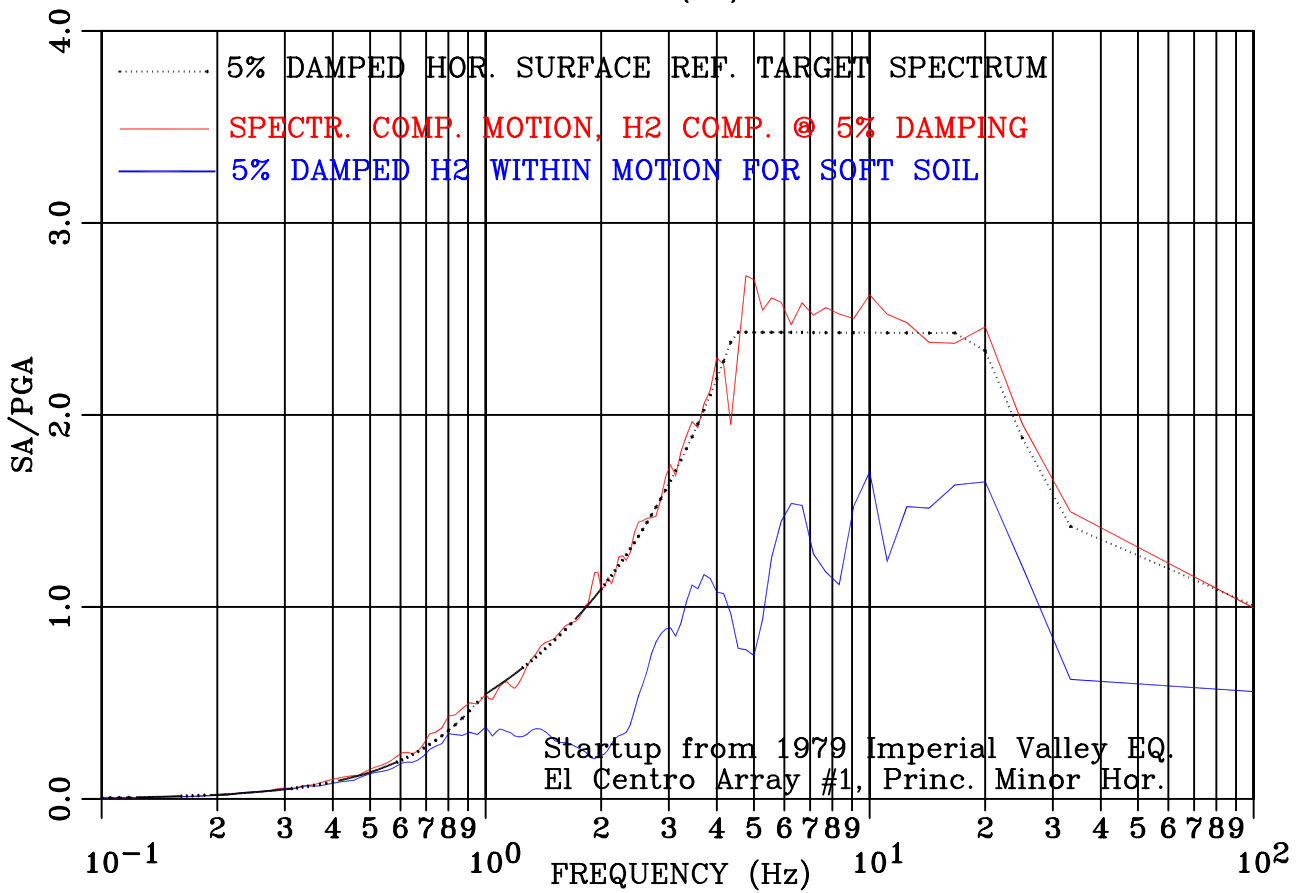
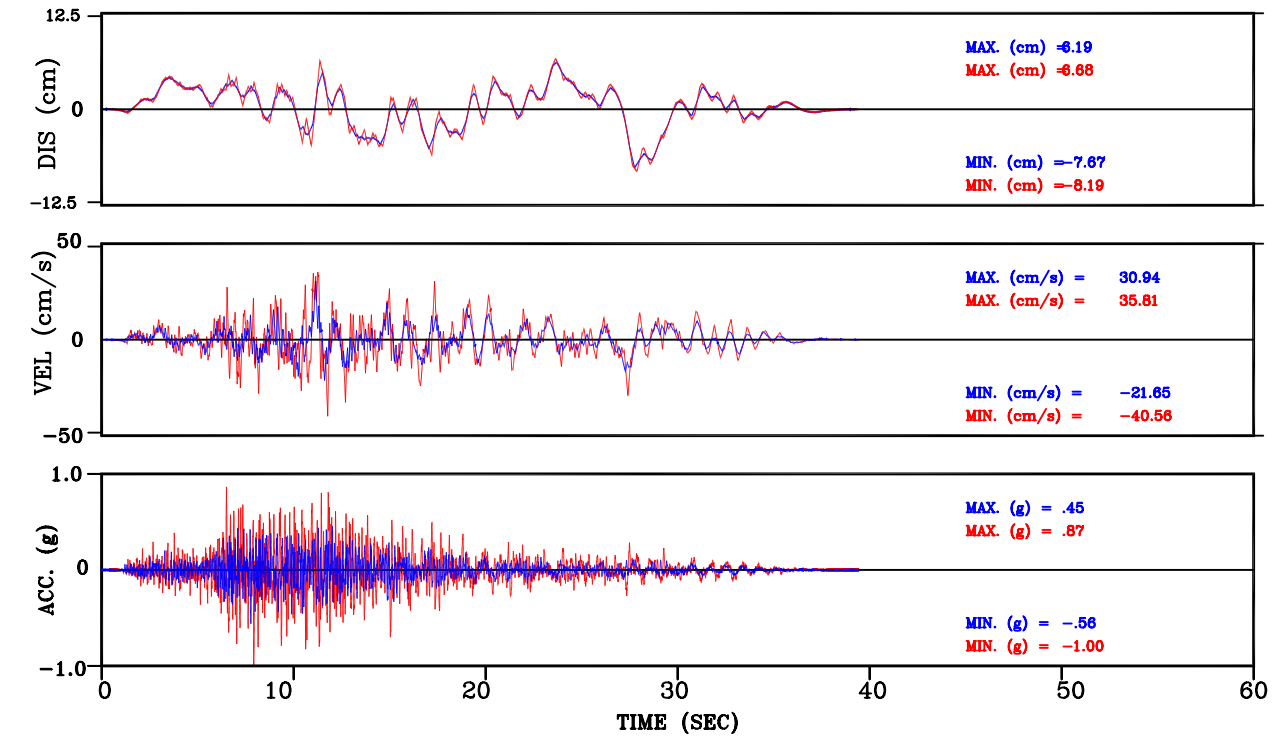


Figure III-152: Within vs. Surface Motion for Soft Soil  
 Set-3 H2 Comp. Motion Conforming to NUREG/CR-6728 Spectral Shape

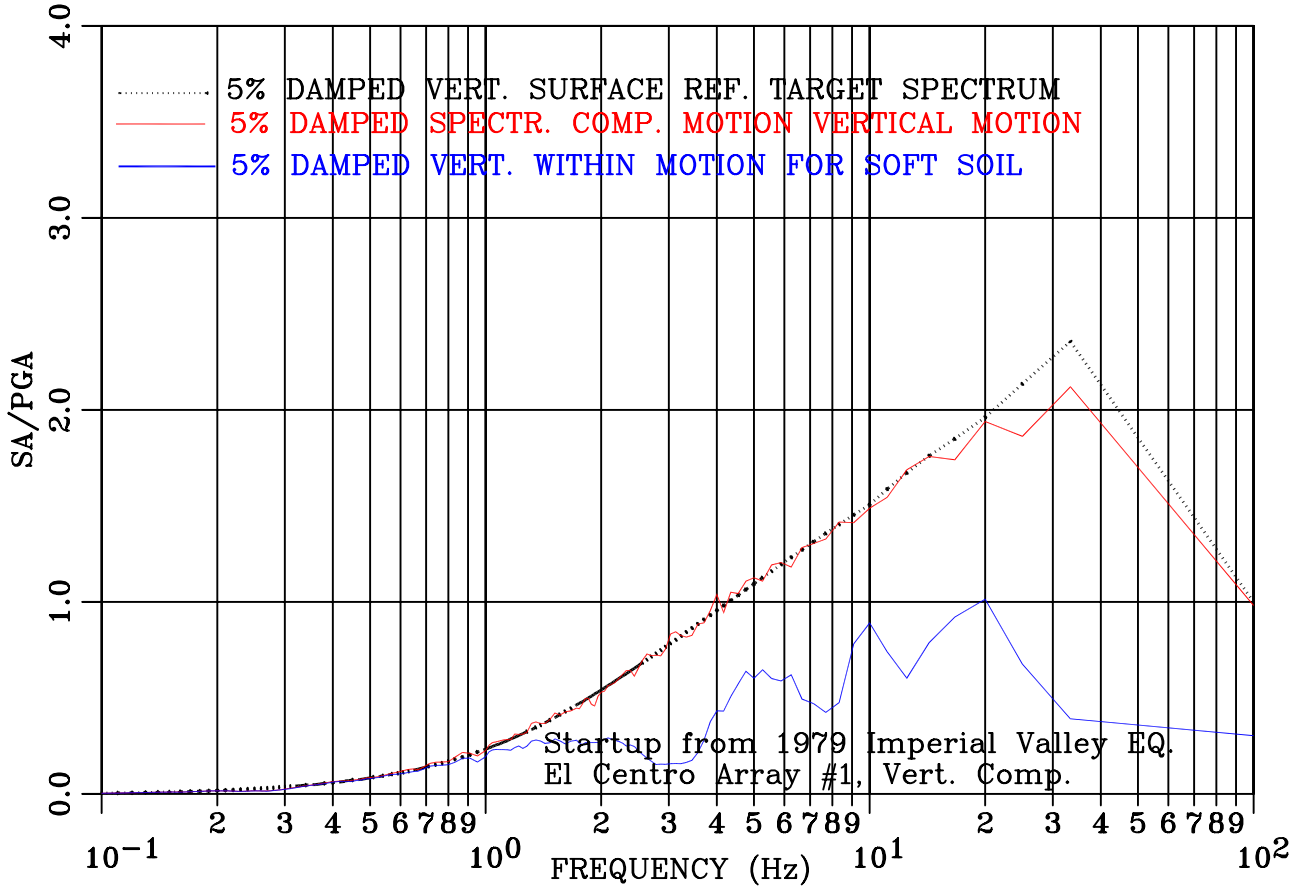
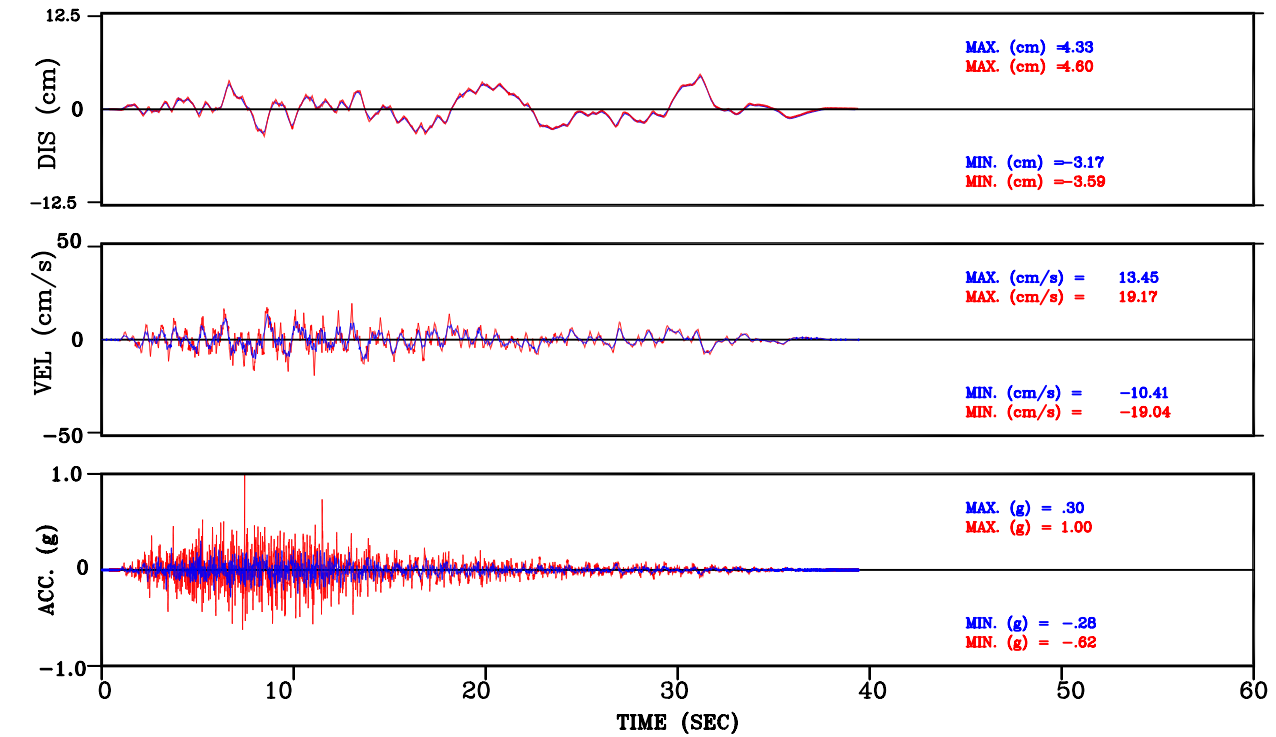


Figure III-153: Within vs. Surface Motion for Soft Soil  
 Set-3 Vert. Comp. Motion Conforming to NUREG/CR-6728 Spectral Shape

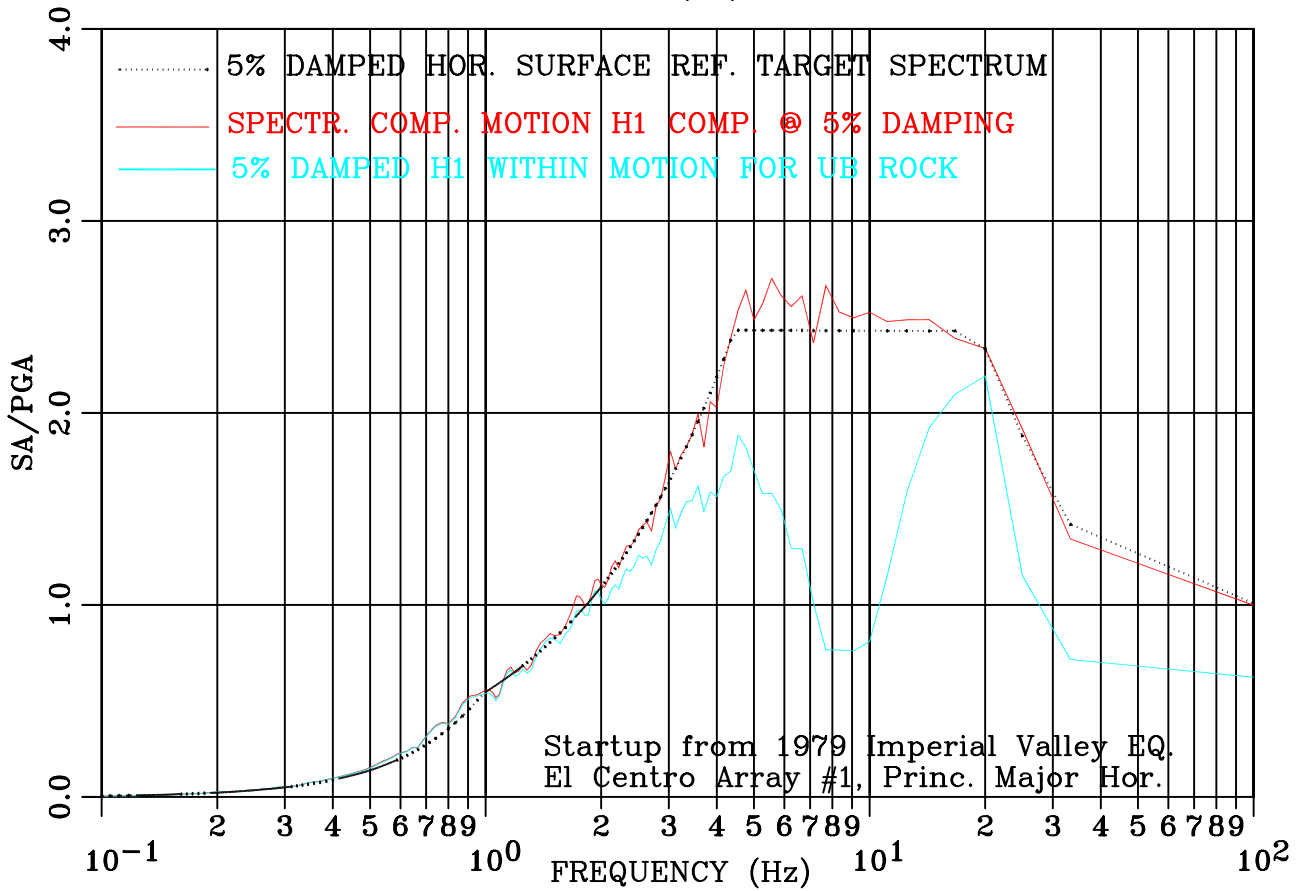
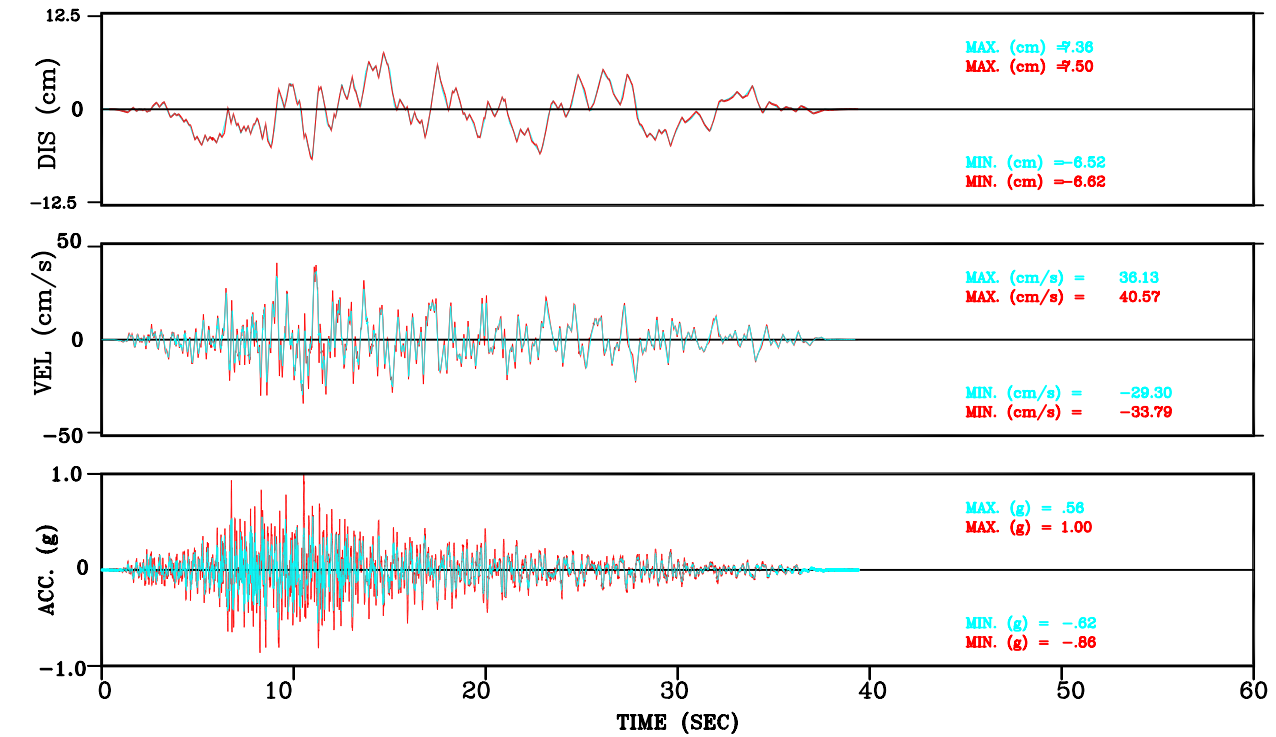


Figure III-154: Within vs. Surface Motion for UB Rock  
 Set-3 H1 Comp. Motion Conforming to NUREG/CR-6728 Spectral Shape

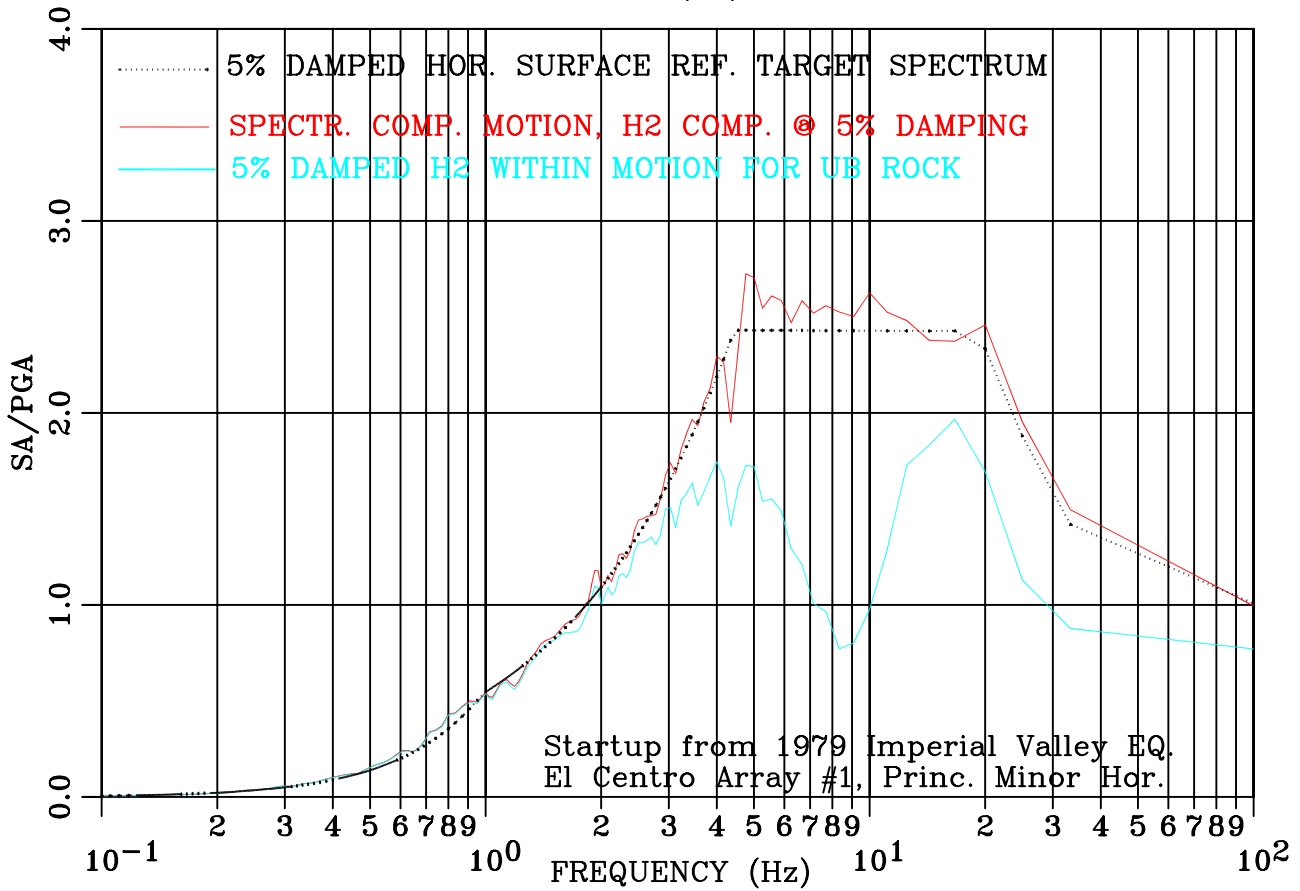
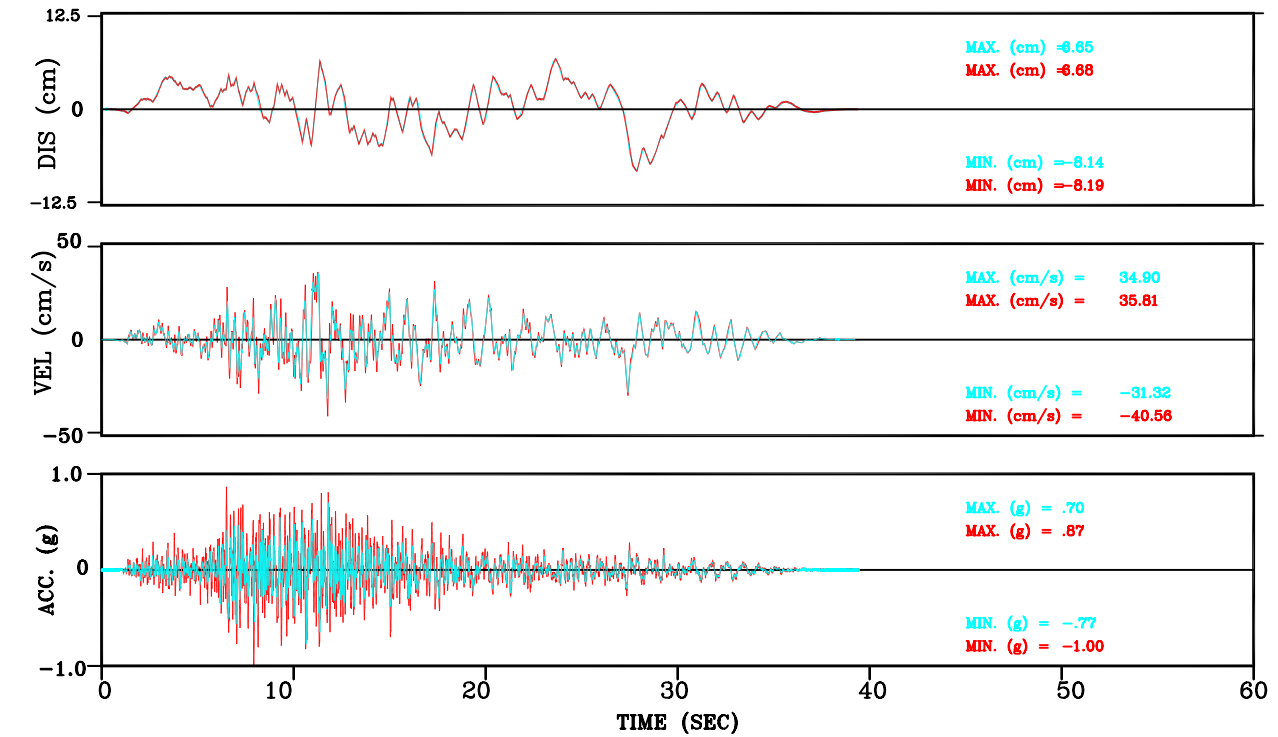


Figure III-155: Within vs. Surface Motion for UB Rock  
 Set-3 H2 Comp. Motion Conforming to NUREG/CR-6728 Spectral Shape

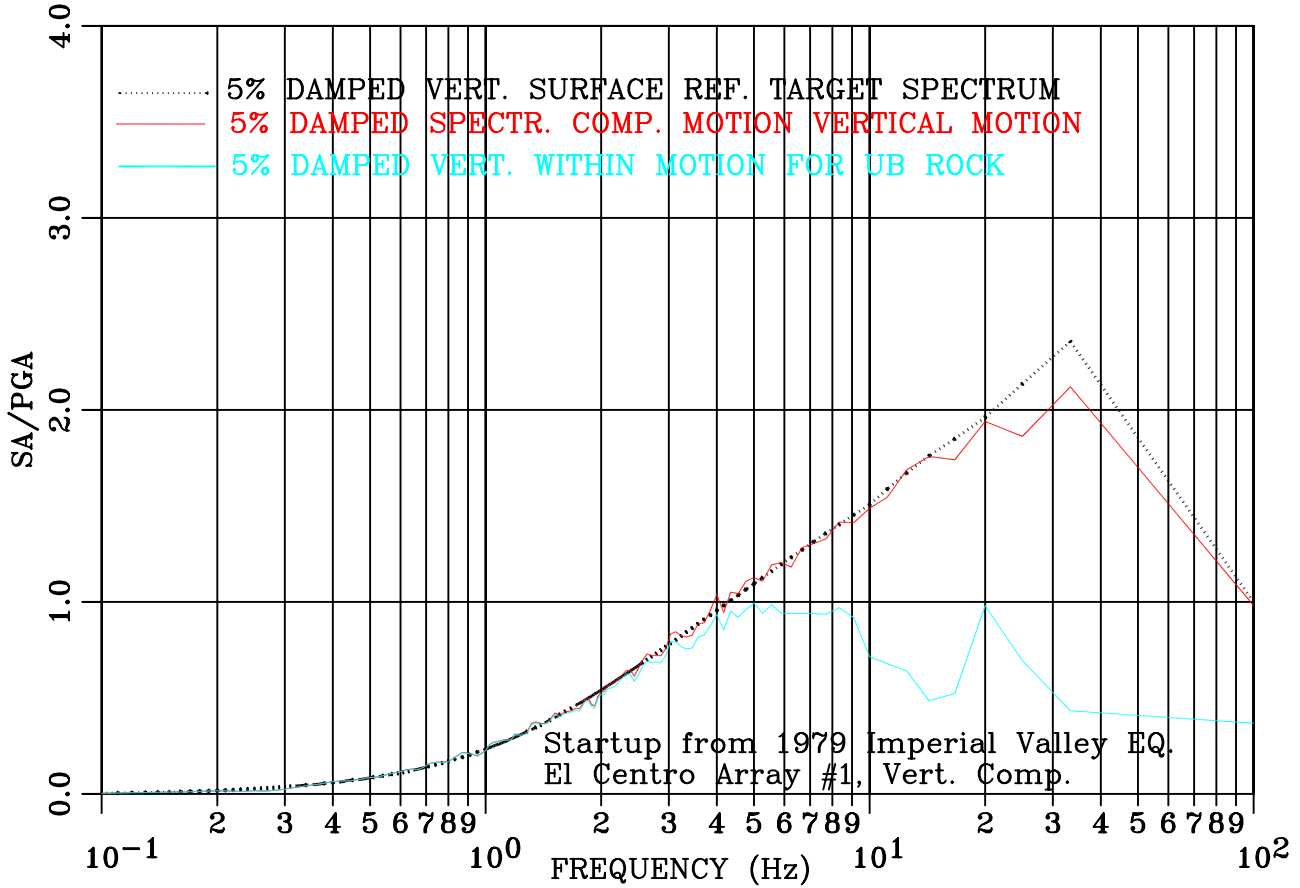
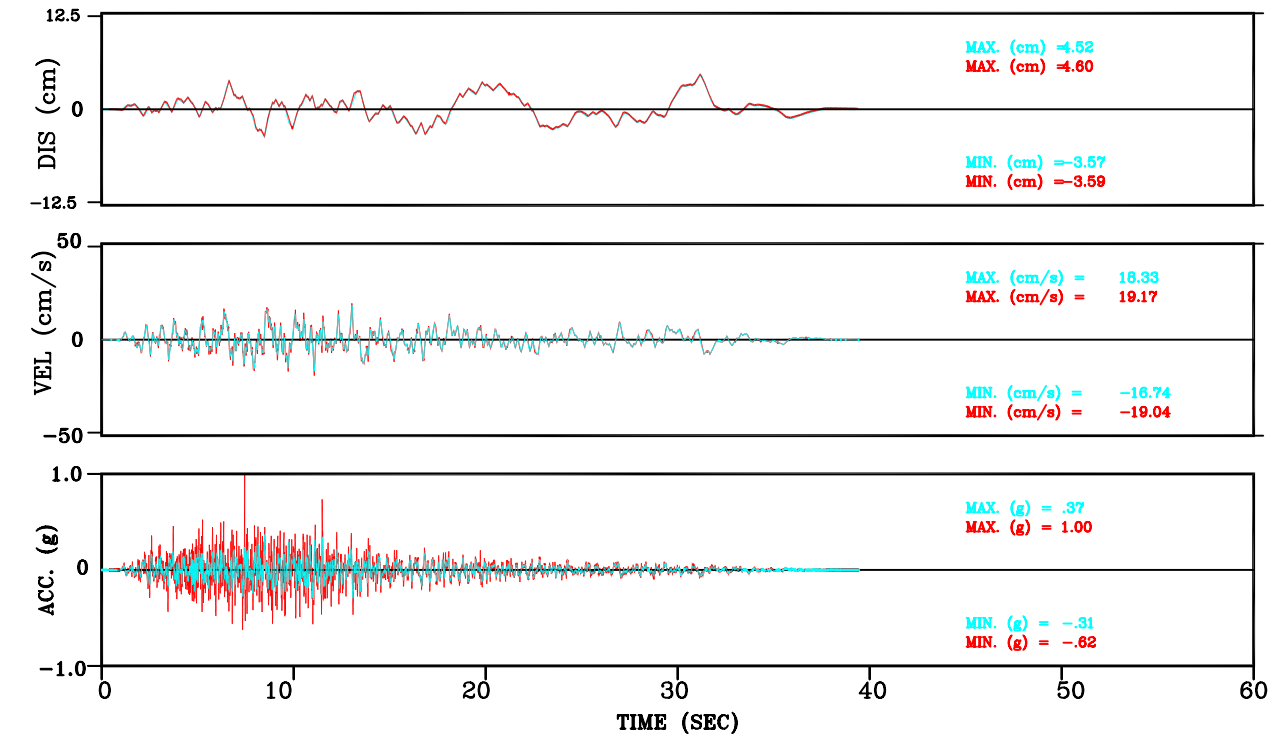


Figure III-156: Within vs. Surface Motion for UB Rock  
Set-3 Vert. Comp. Motion Conforming to NUREG/CR-6728 Spectral Shape

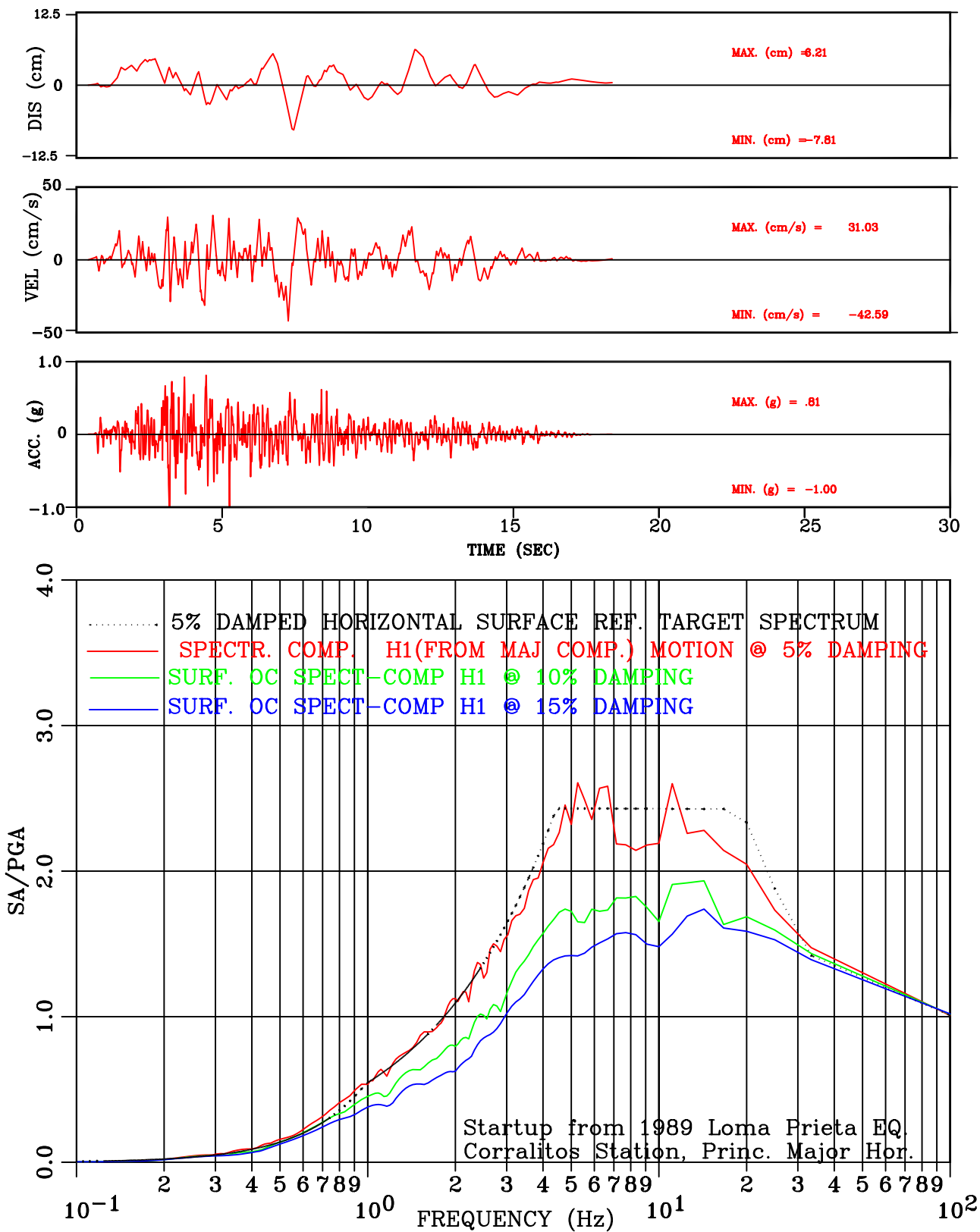


Figure III-157: Set-4 H1 Comp. Motion Conforming to NUREG/CR-6728 Spectral Shape

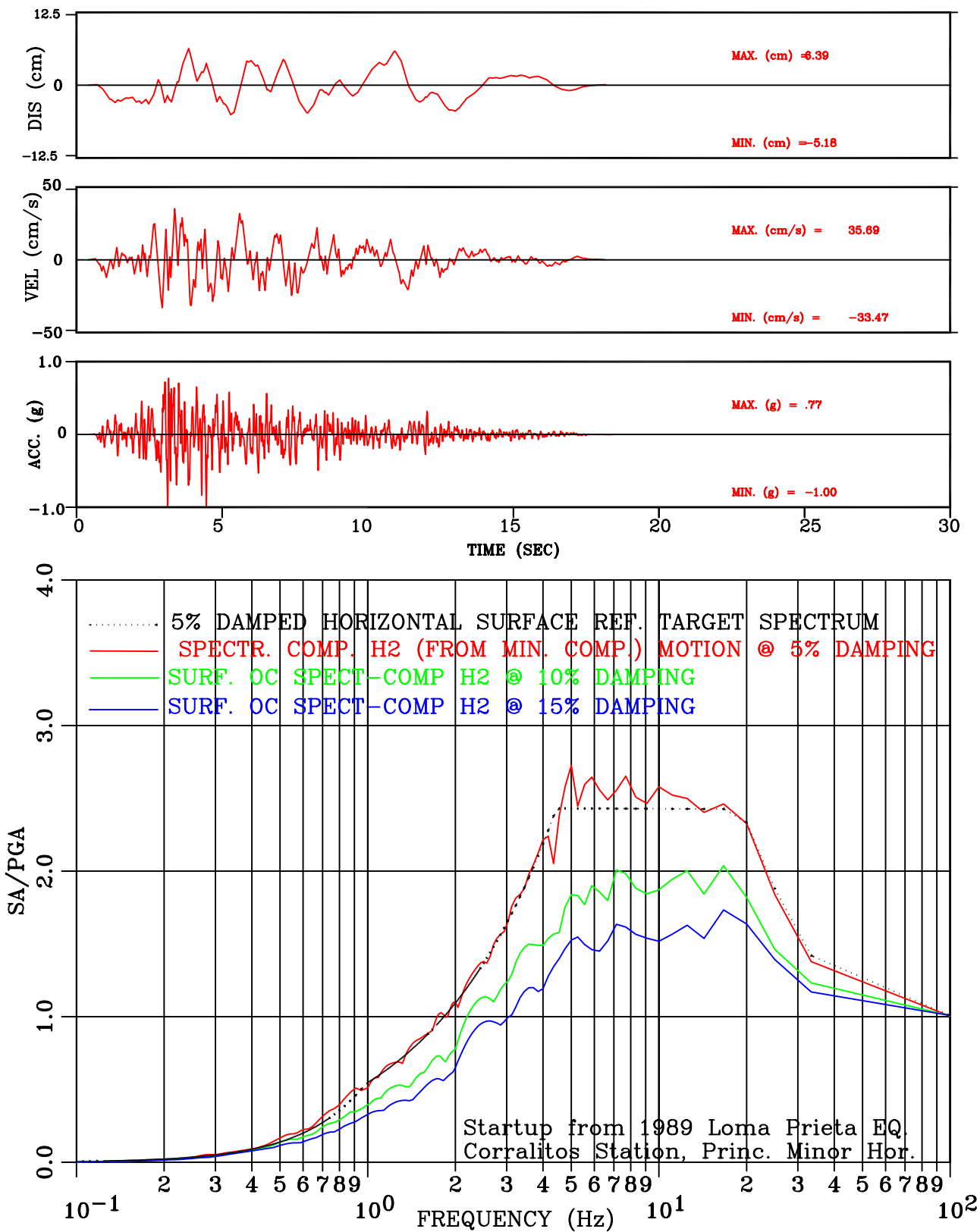


Figure III-158: Set-4 H2 Comp. Motion Conforming to NUREG/CR-6728 Spectral Shape

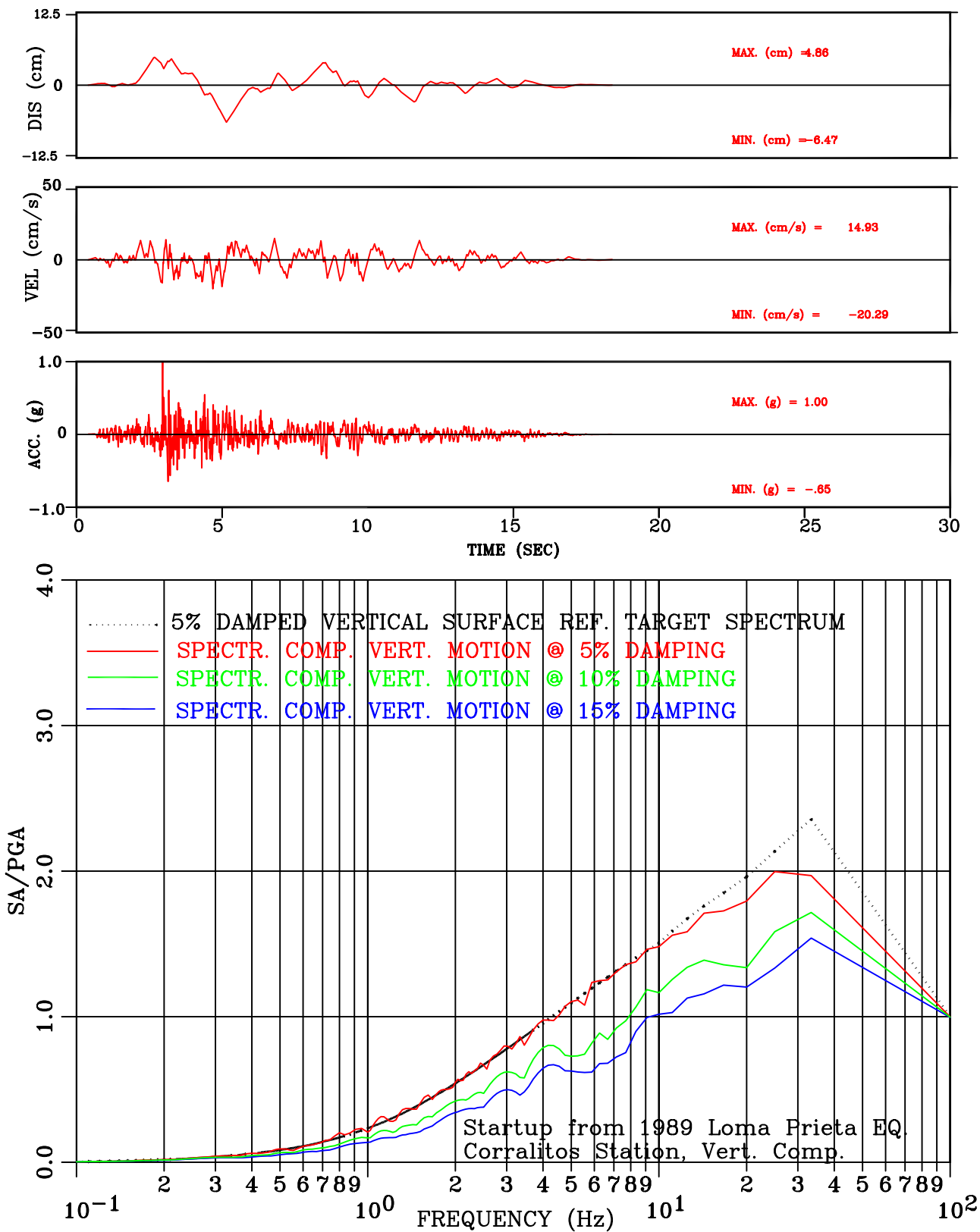


Figure III-159: Set-4 Vert. Comp. Motion Conforming to NUREG/CR-6728 Spectral Shape

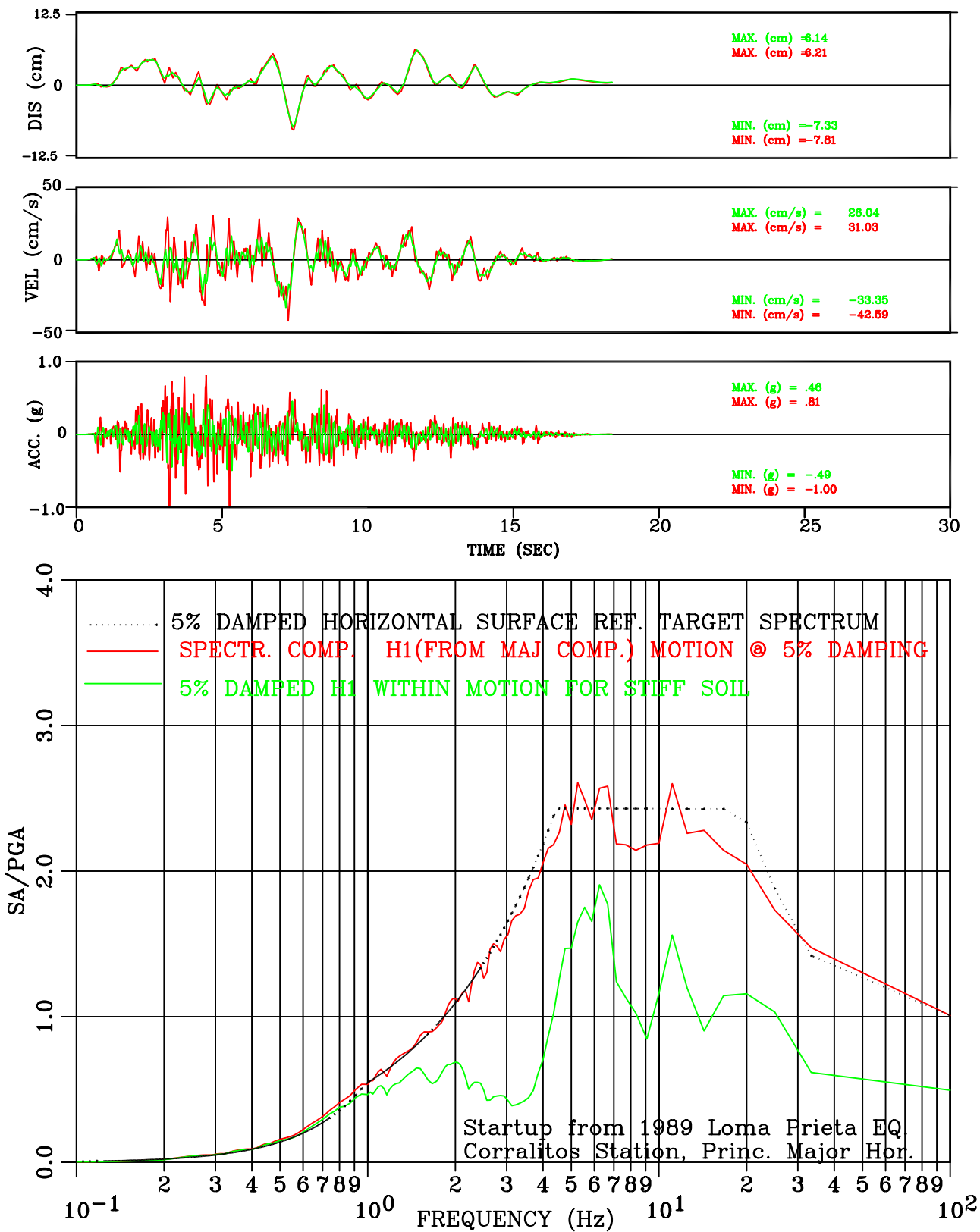


Figure III-160: Within vs. Surface Motion for Stiff Soil  
 Set-4 H1 Comp. Motion Conforming to NUREG/CR-6728 Spectral Shape

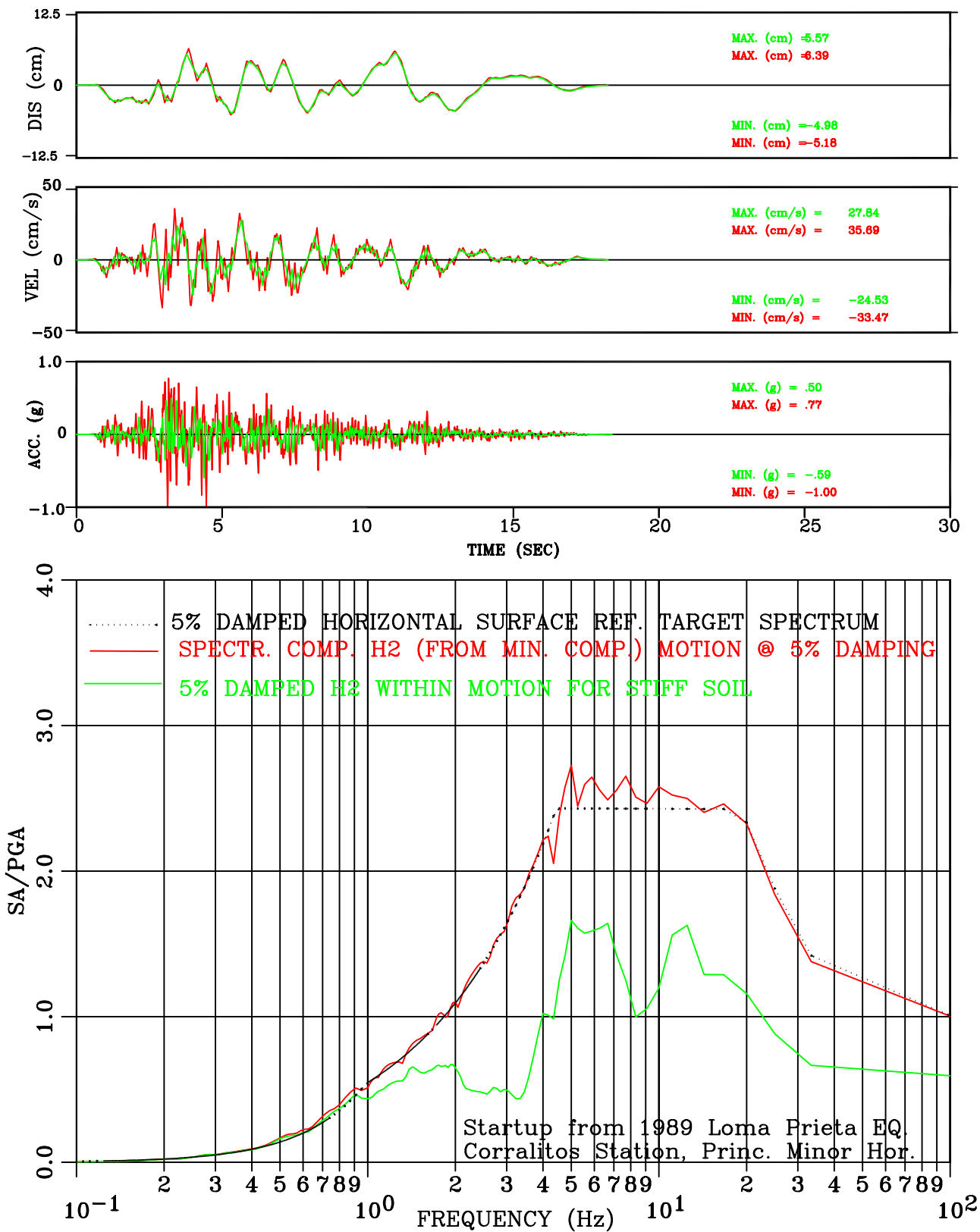


Figure III-161: Within vs. Surface Motion for Stiff Soil  
 Set-4 H2 Comp. Motion Conforming to NUREG/CR-6728 Spectral Shape

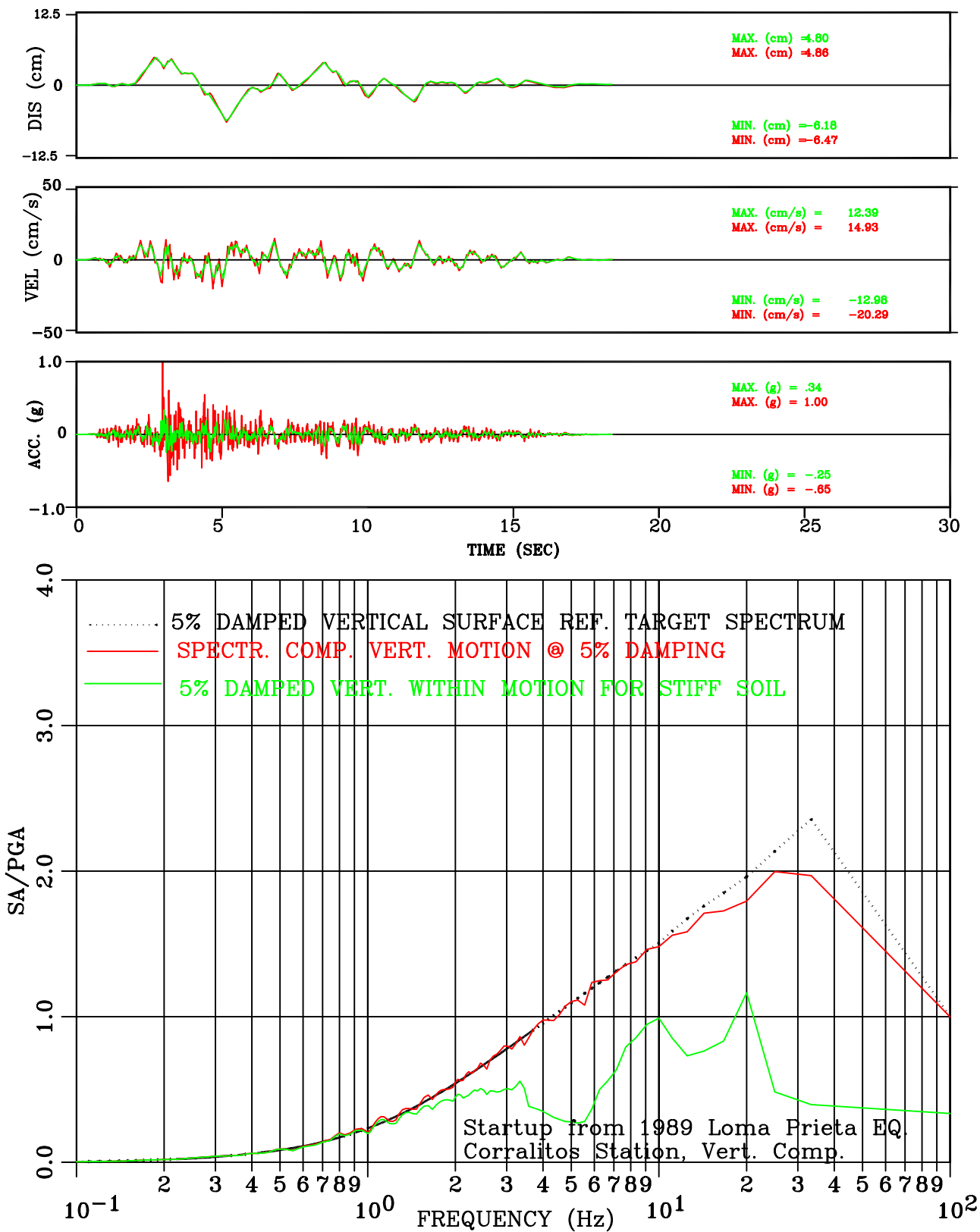


Figure III-162: Within vs. Surface Motion for Stiff Soil  
 Set-4 Vert. Comp. Motion Conforming to NUREG/CR-6728 Spectral Shape

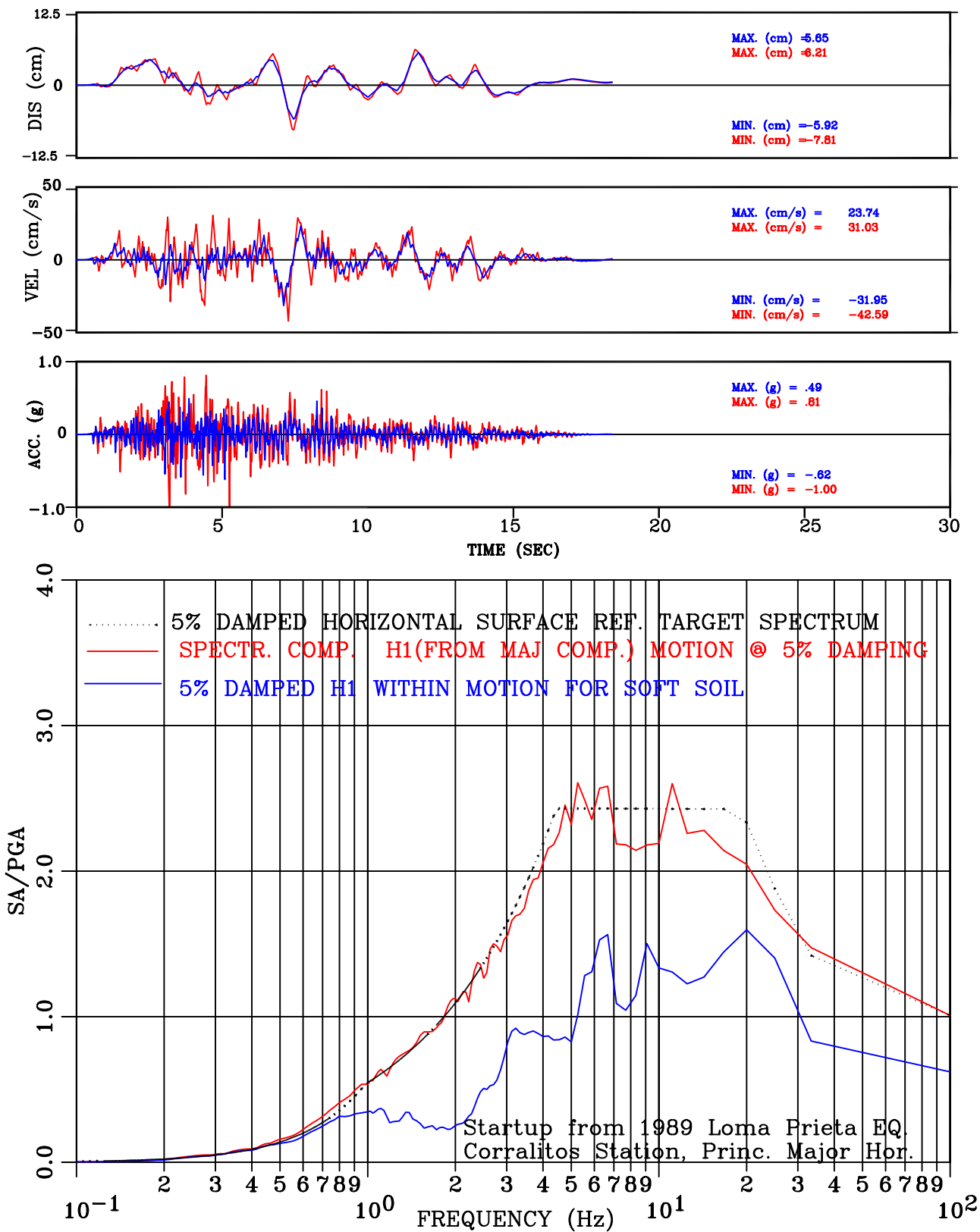


Figure III-163: Within vs. Surface Motion for Soft Soil  
Set-4 H1 Comp. Motion Conforming to NUREG/CR-6728 Spectral Shape

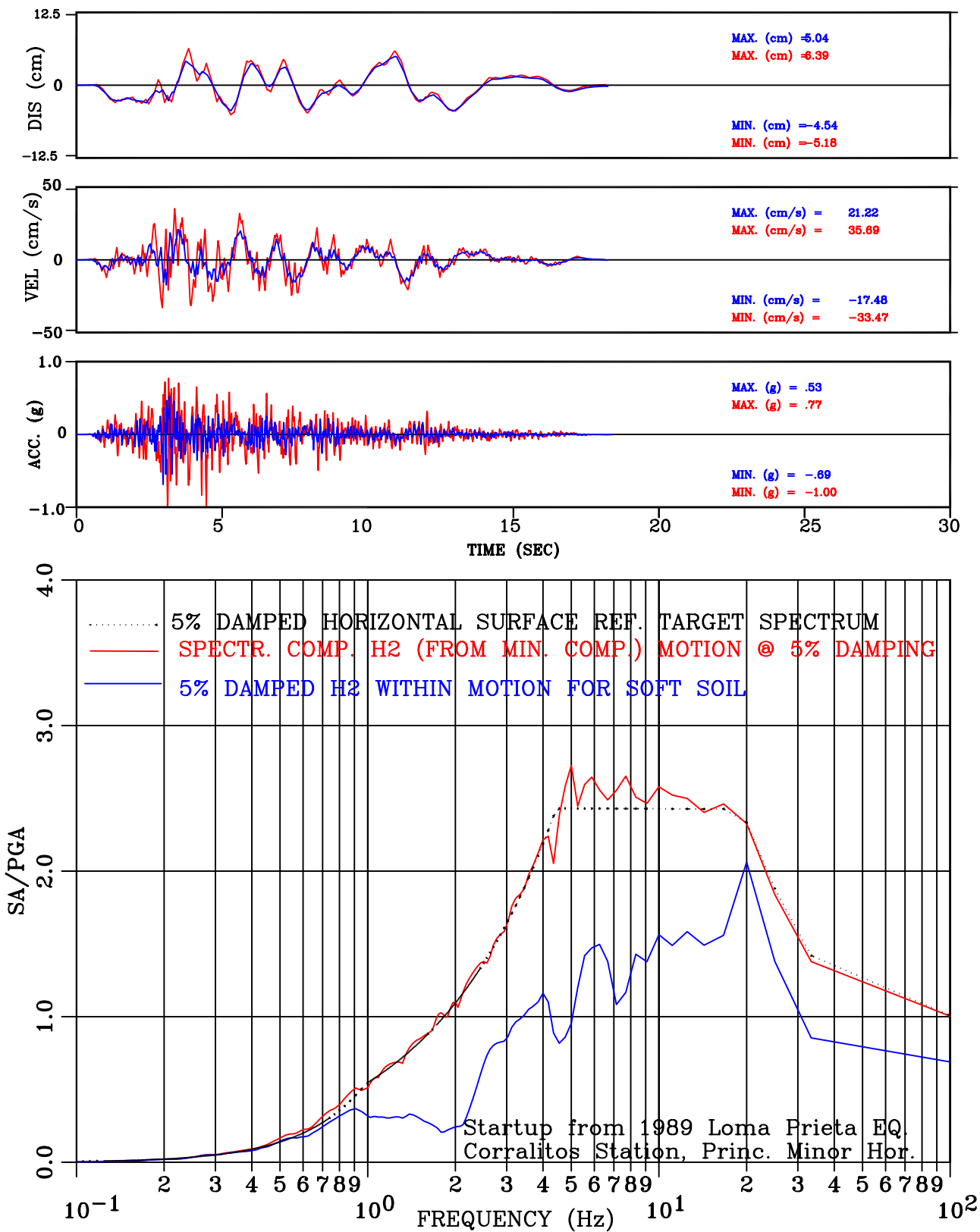


Figure III-164: Within vs. Surface Motion for Soft Soil  
 Set-4 H2 Comp. Motion Conforming to NUREG/CR-6728 Spectral Shape

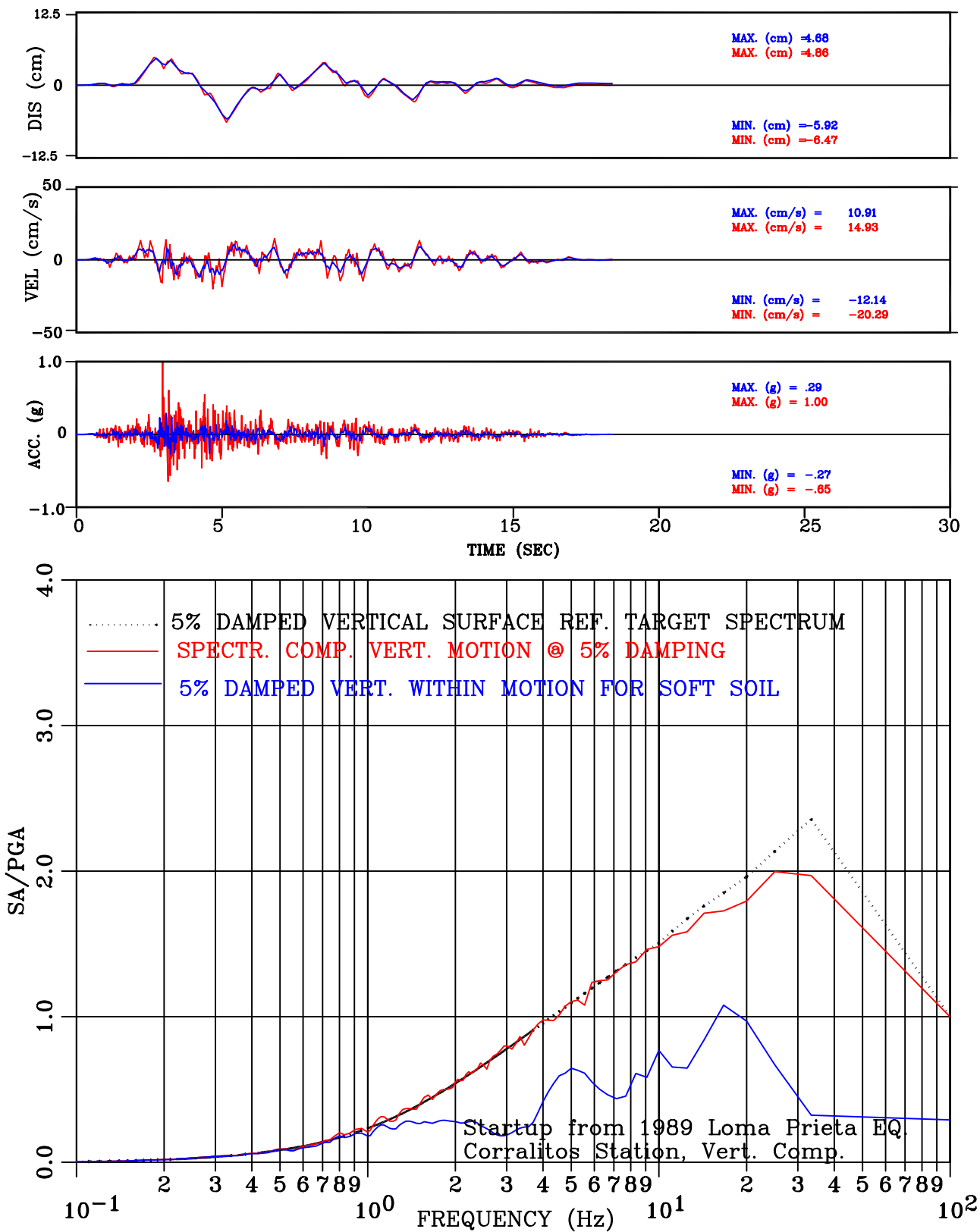


Figure III-165: Within vs. Surface Motion for Soft Soil  
Set-4 Vert. Comp. Motion Conforming to NUREG/CR-6728 Spectral Shape

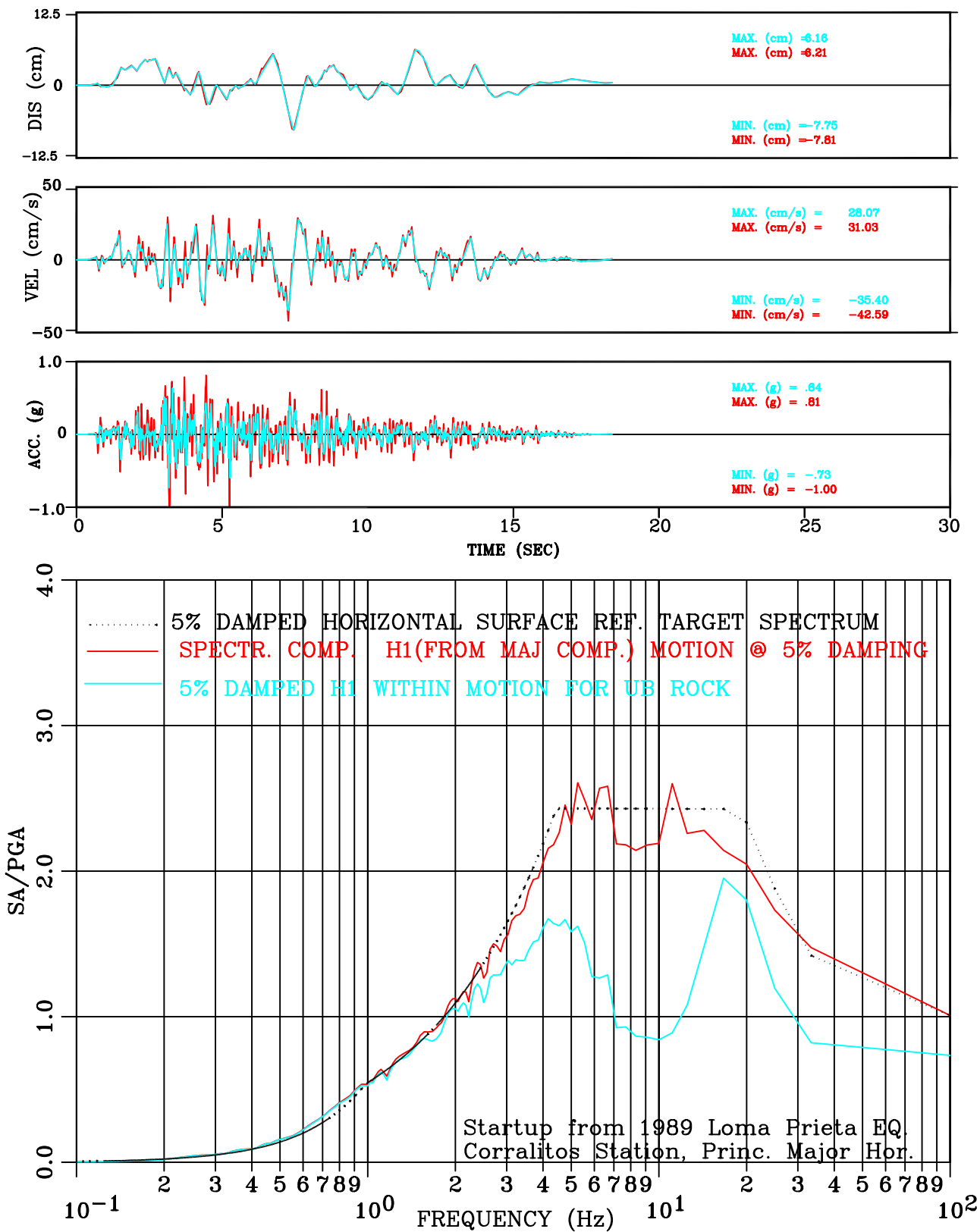


Figure III-166: Within vs. Surface Motion for UB Rock  
 Set-4 H1 Comp. Motion Conforming to NUREG/CR-6728 Spectral Shape

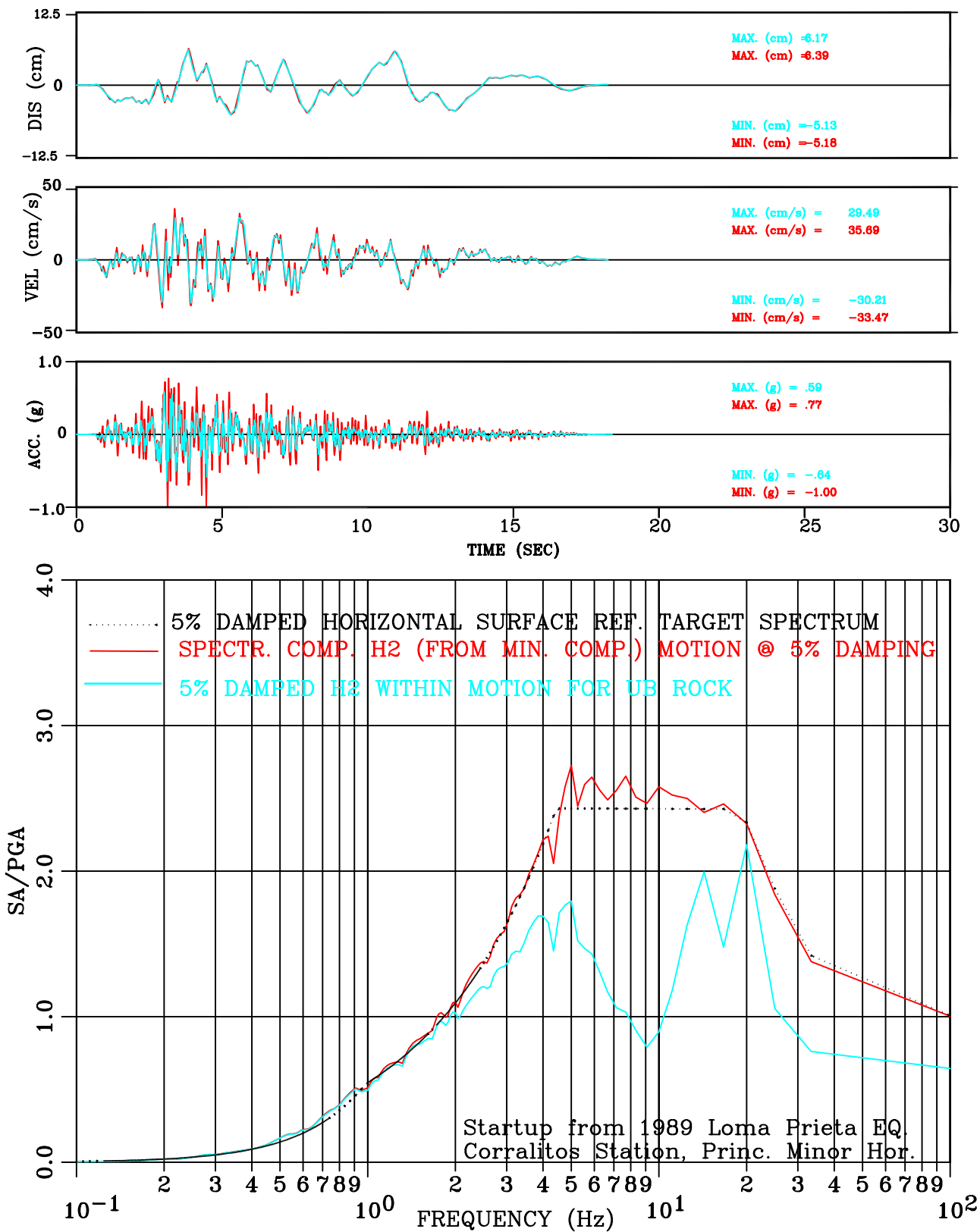


Figure III-167: Within vs. Surface Motion for UB Rock  
Set-4 H2 Comp. Motion Conforming to NUREG/CR-6728 Spectral Shape

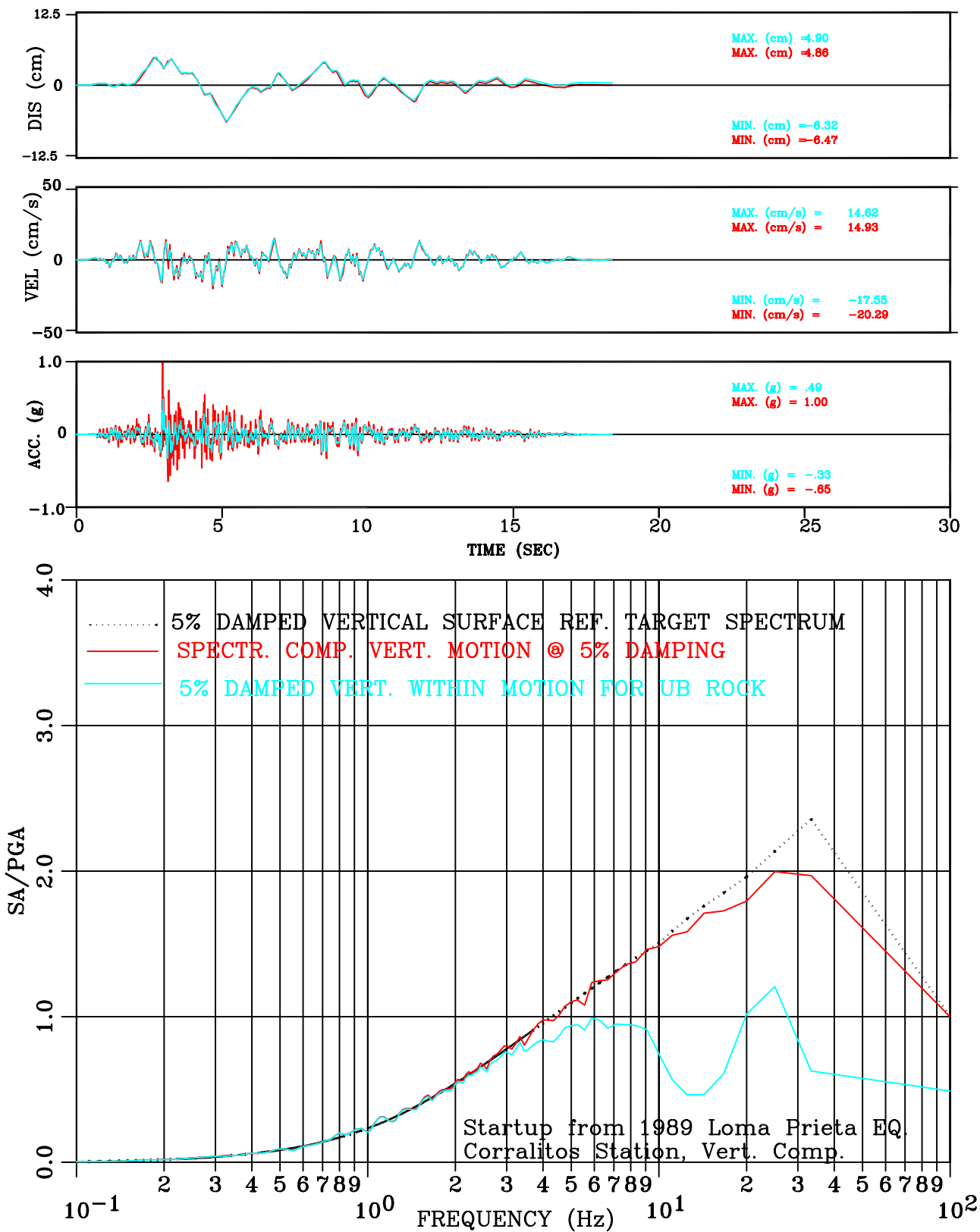


Figure III-168: Within vs. Surface Motion for UB Rock  
Set-4 Vert. Comp. Motion Conforming to NUREG/CR-6728 Spectral Shape

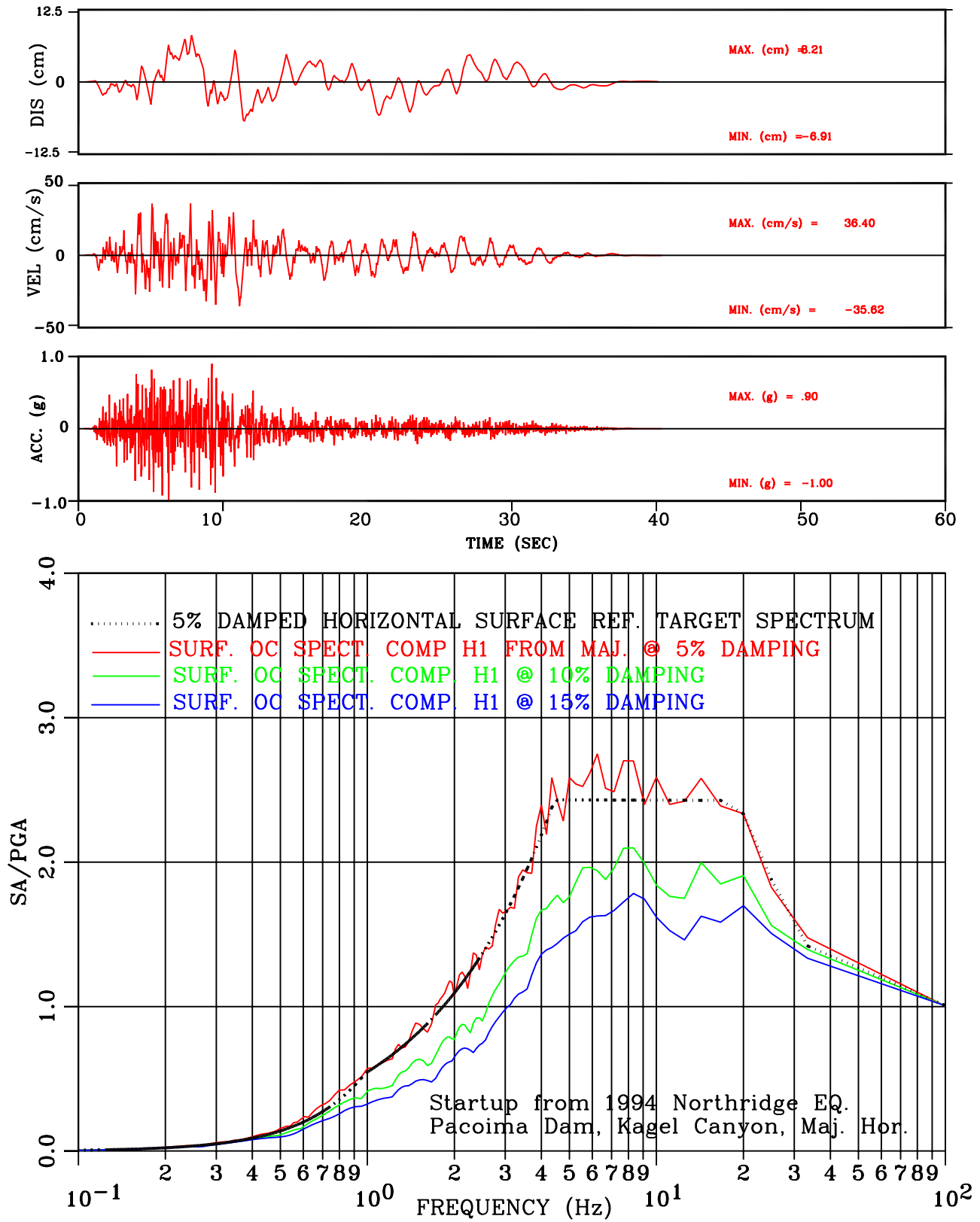


Figure III-169: Set-5 H1 Comp. Motion Conforming to NUREG/CR-6728 Spectral Shape

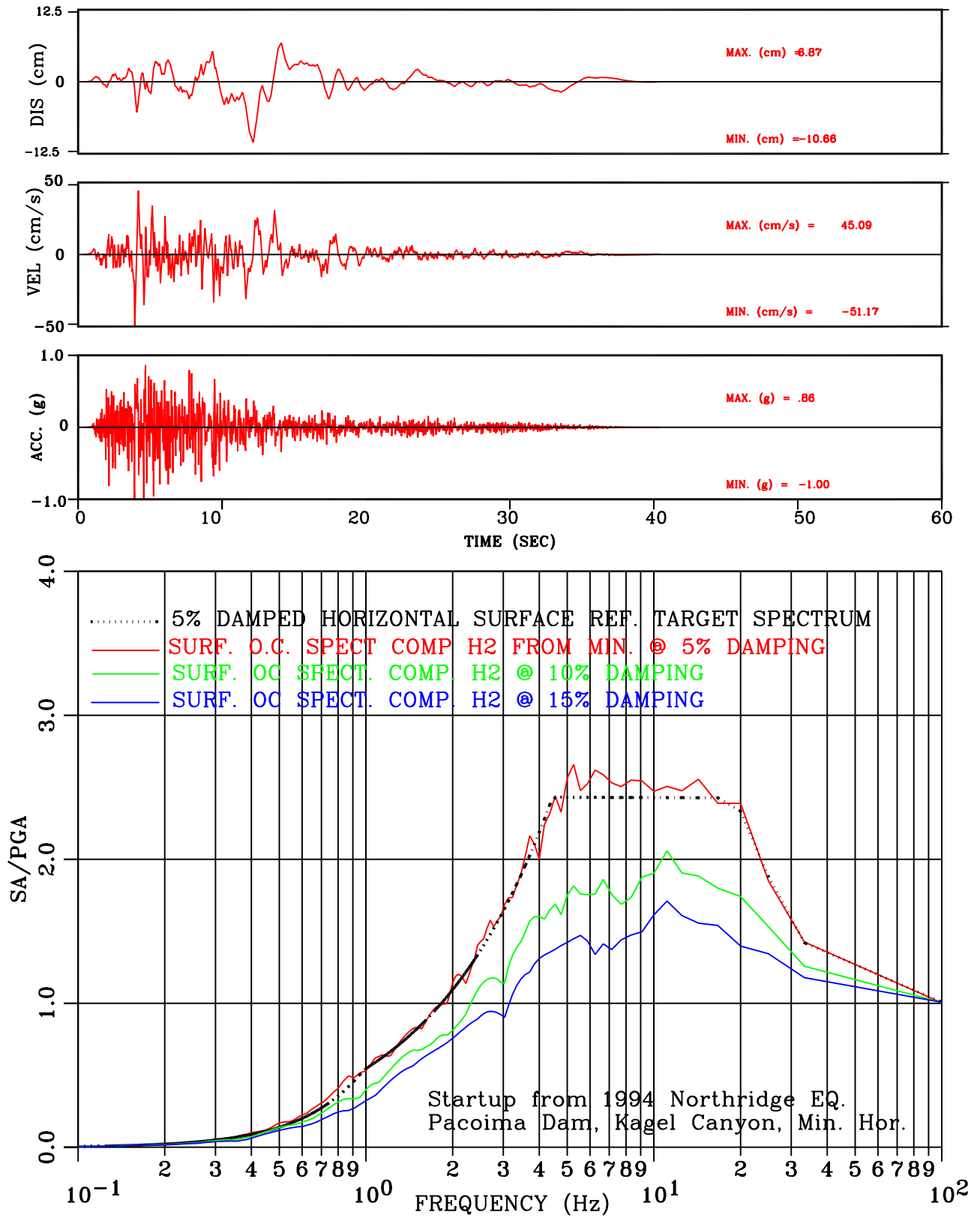


Figure III-170: Set-5 H2 Comp. Motion Conforming to NUREG/CR-6728 Spectral Shape

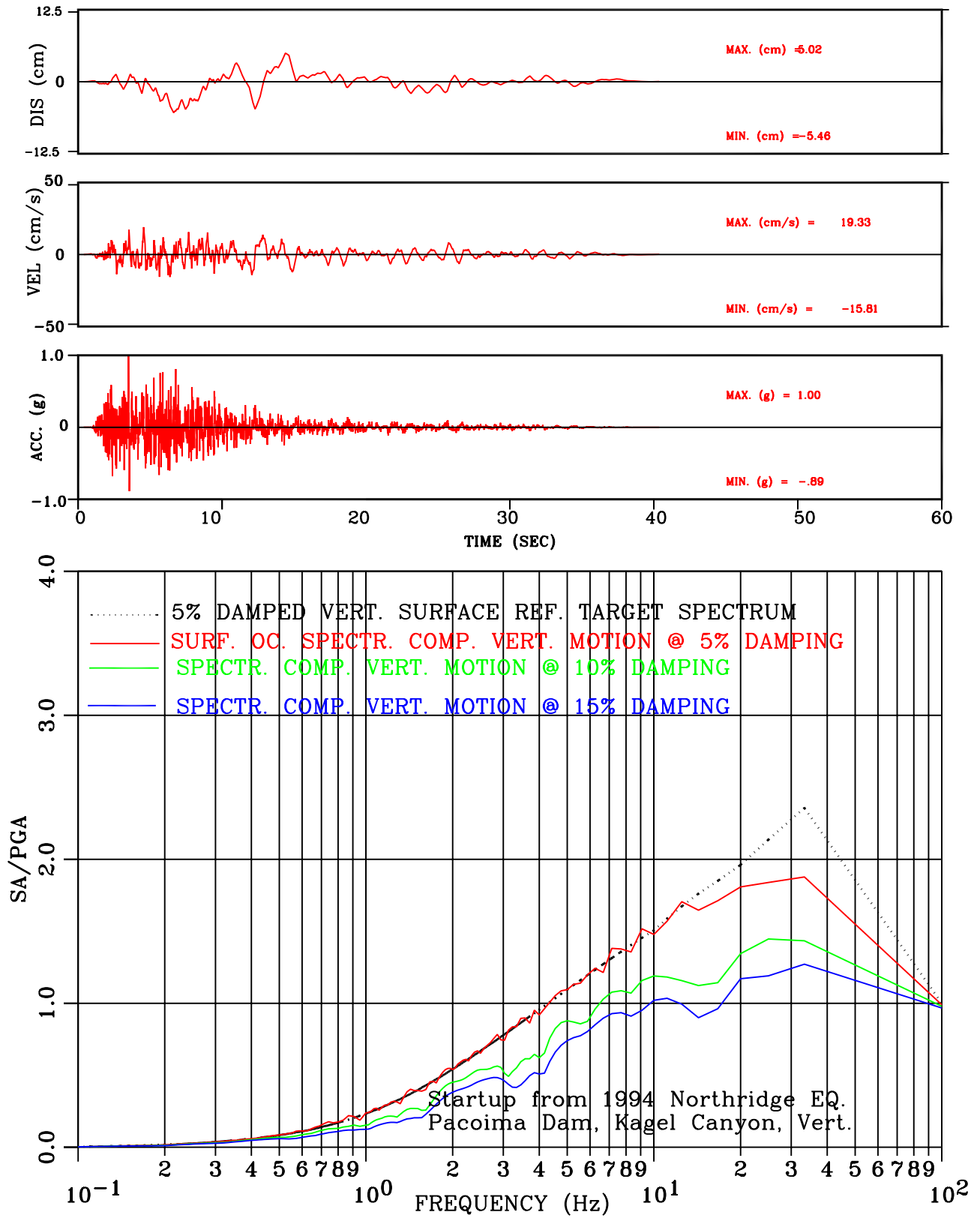


Figure III-171: Set-5 Vert. Comp. Motion Conforming to NUREG/CR-6728 Spectral Shape

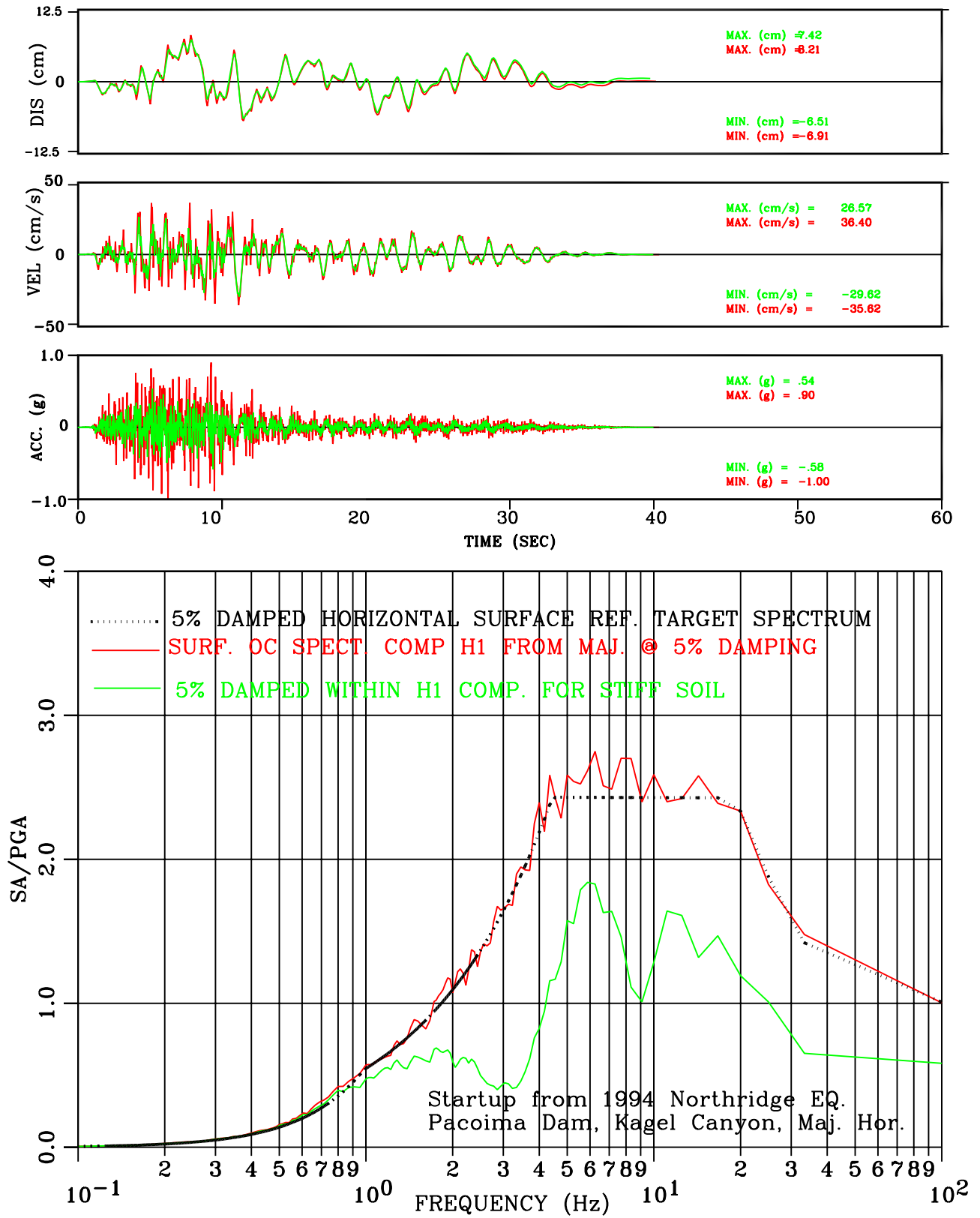


Figure III-172: With vs. Surface Motion for Stiff Soil  
 Set-5 H1 Comp. Motion Conforming to NUREG/CR-6728 Spectral Shape

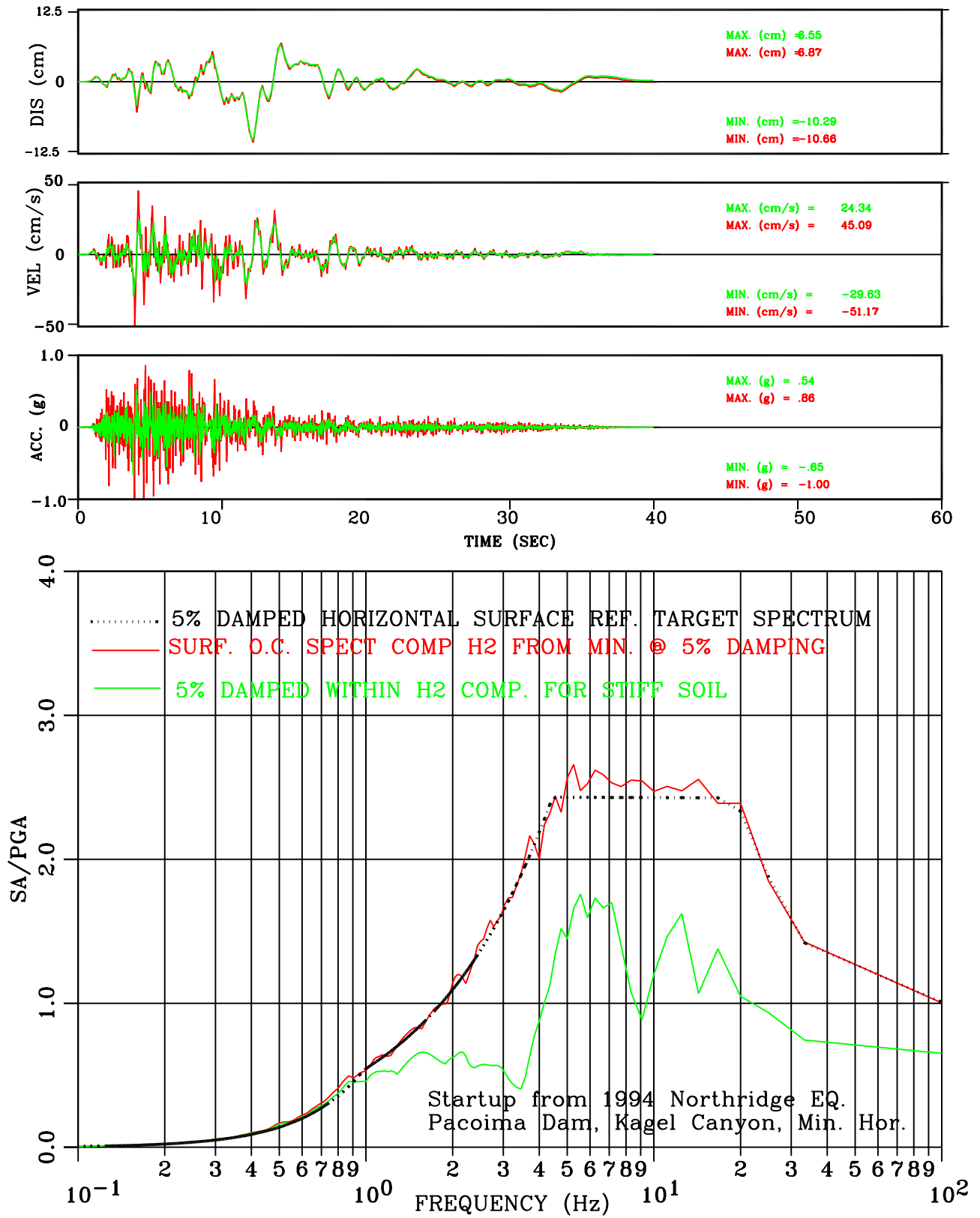


Figure III-173: With vs. Surface Motion for Stiff Soil  
Set-5 H2 Comp. Motion Conforming to NUREG/CR-6728 Spectral Shape

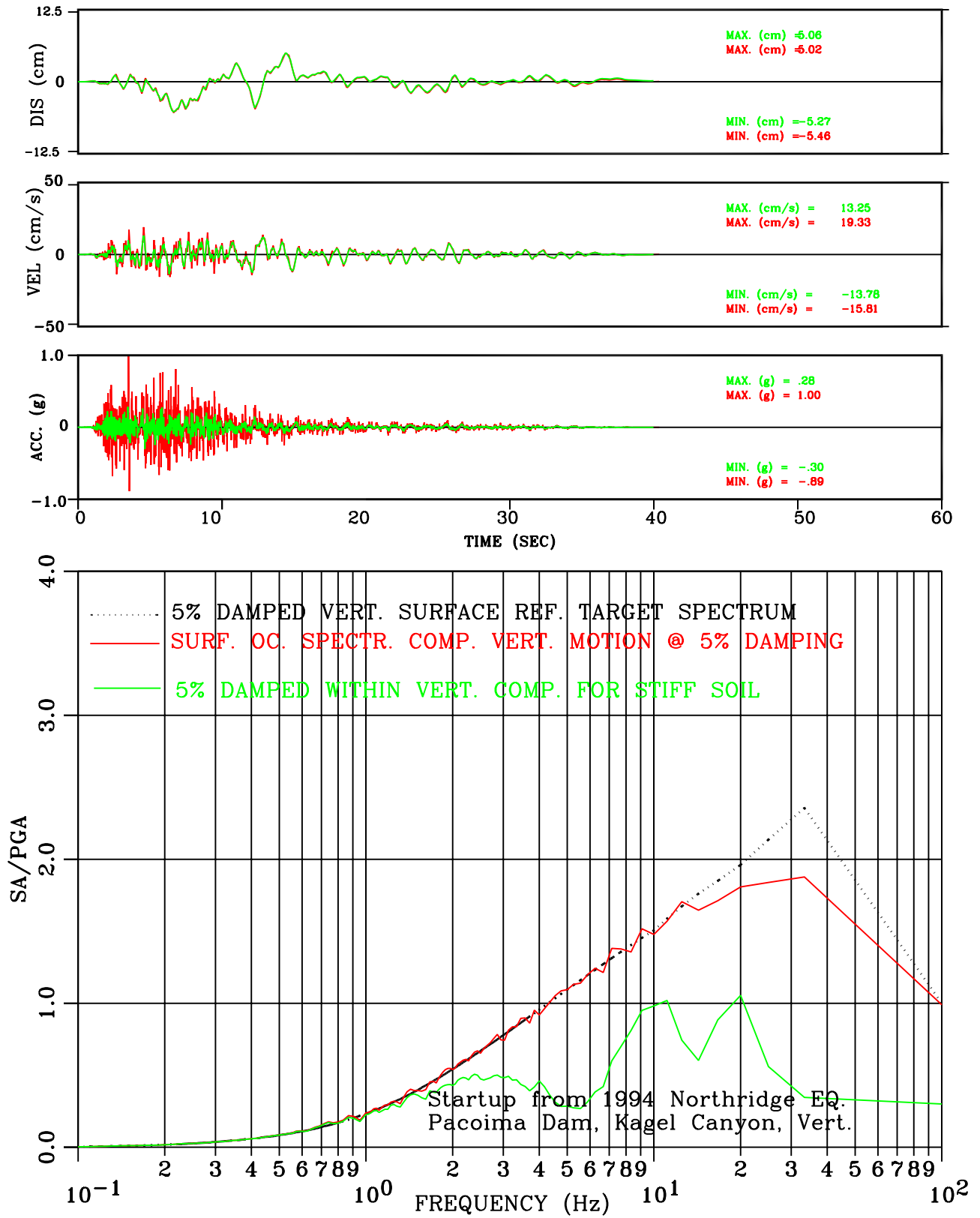


Figure III-174: With vs. Surface Motion for Stiff Soil  
Set-5 Vert. Comp. Motion Conforming to NUREG/CR-6728 Spectral Shape

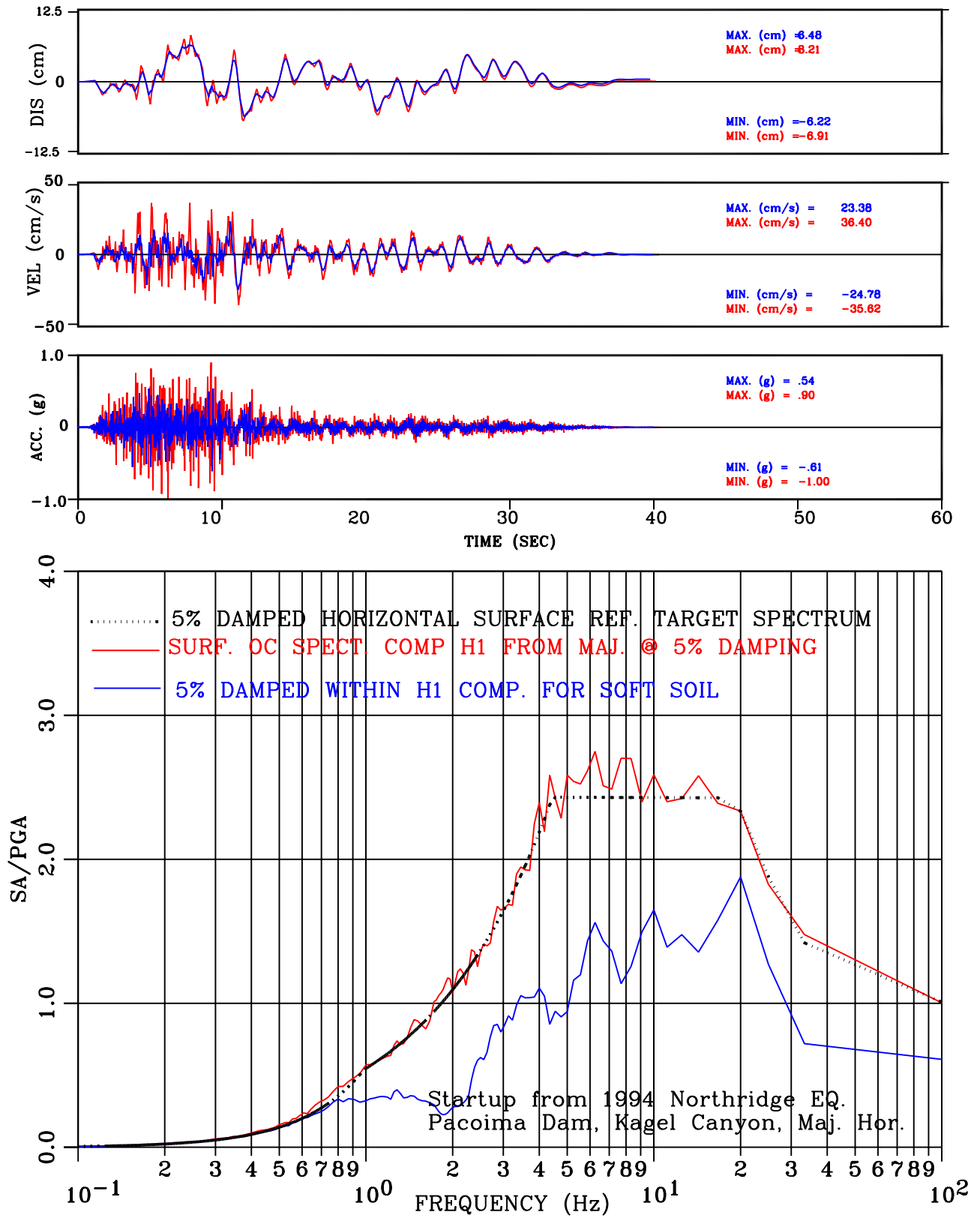


Figure III-175: With vs. Surface Motion for Soft Soil  
Set-5 H1 Comp. Motion Conforming to NUREG/CR-6728 Spectral Shape

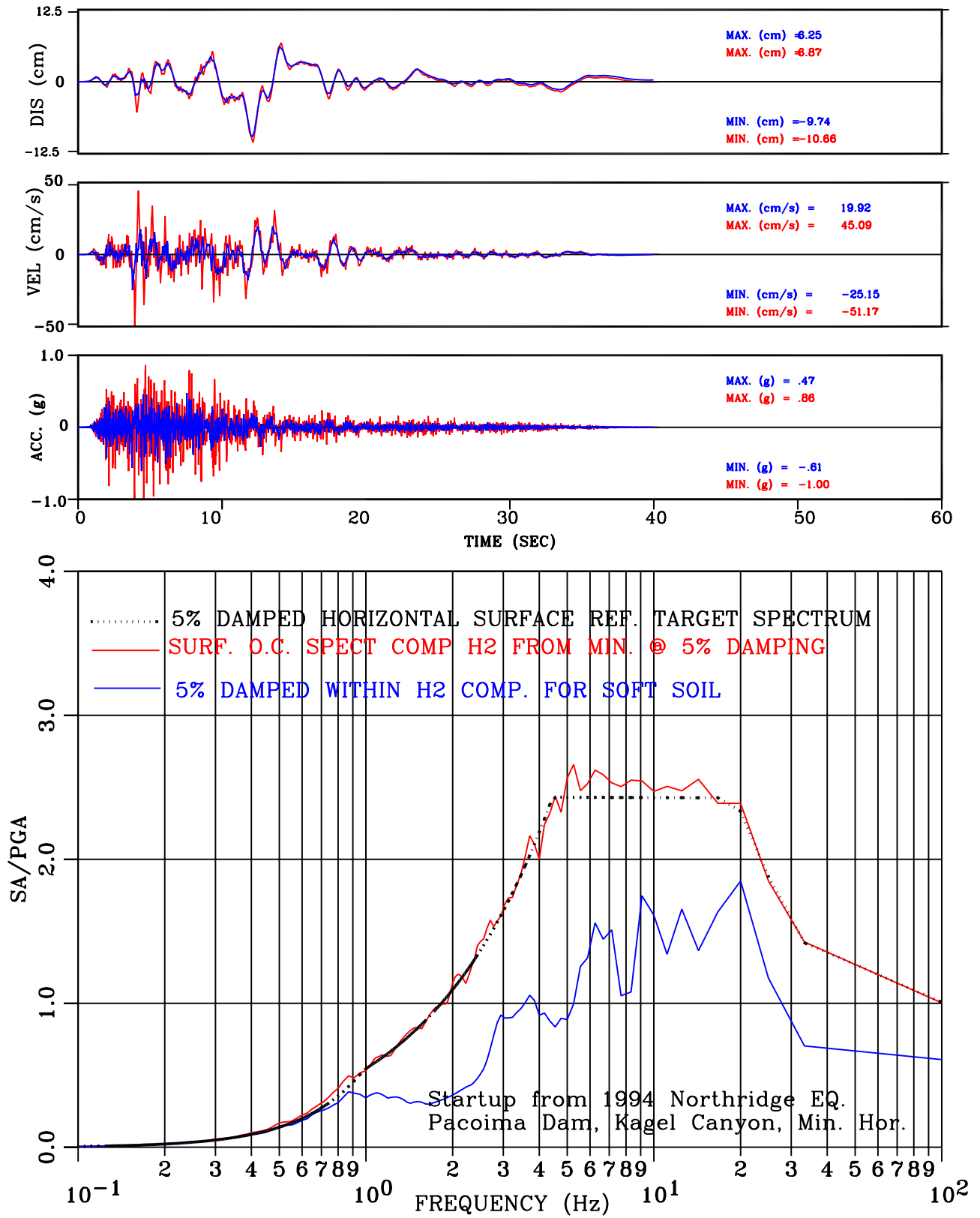


Figure III-176: With vs. Surface Motion for Soft Soil  
 Set-5 H2 Comp. Motion Conforming to NUREG/CR-6728 Spectral Shape

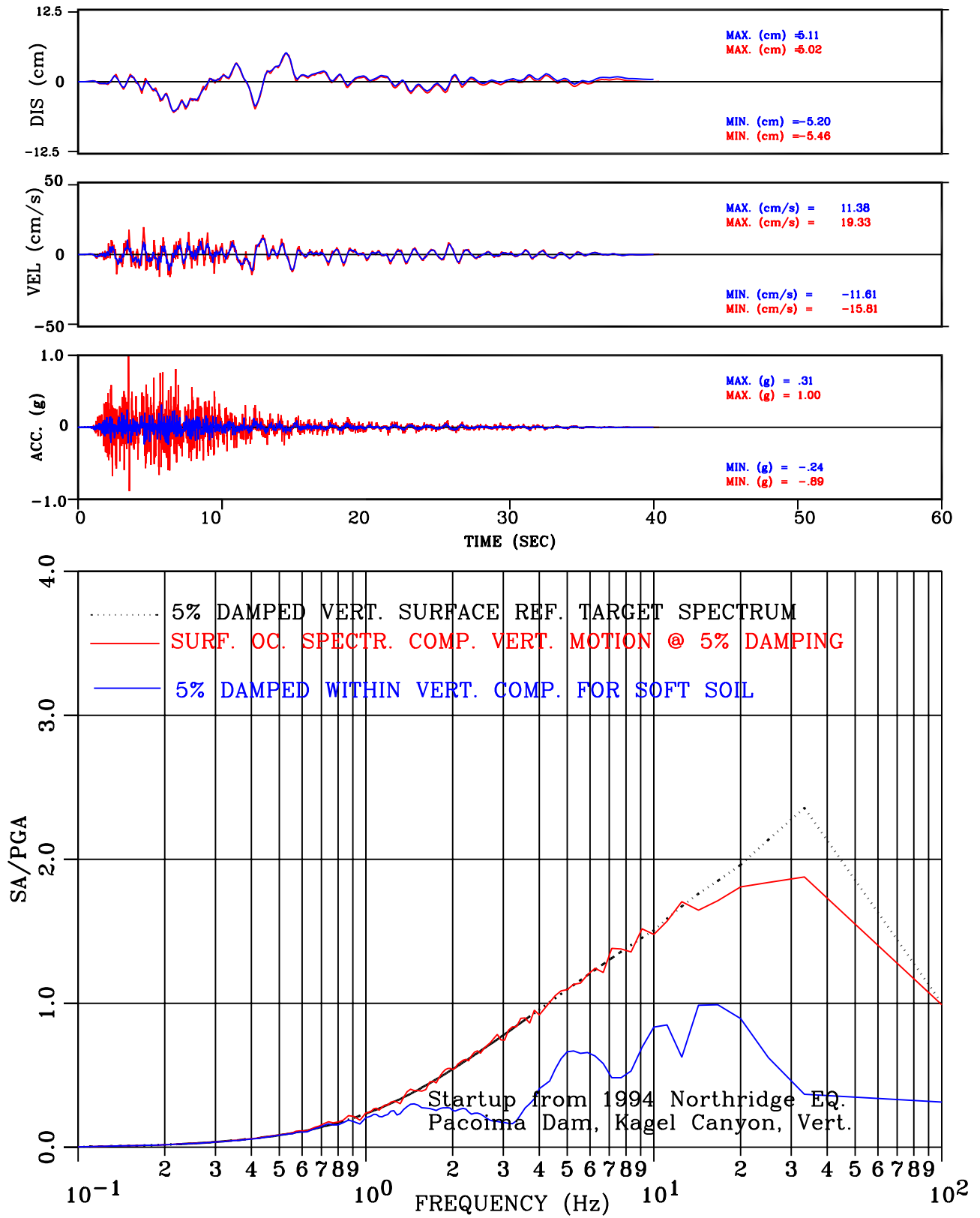


Figure III-177: With vs. Surface Motion for Soft Soil  
Set-5 Vert. Comp. Motion Conforming to NUREG/CR-6728 Spectral Shape

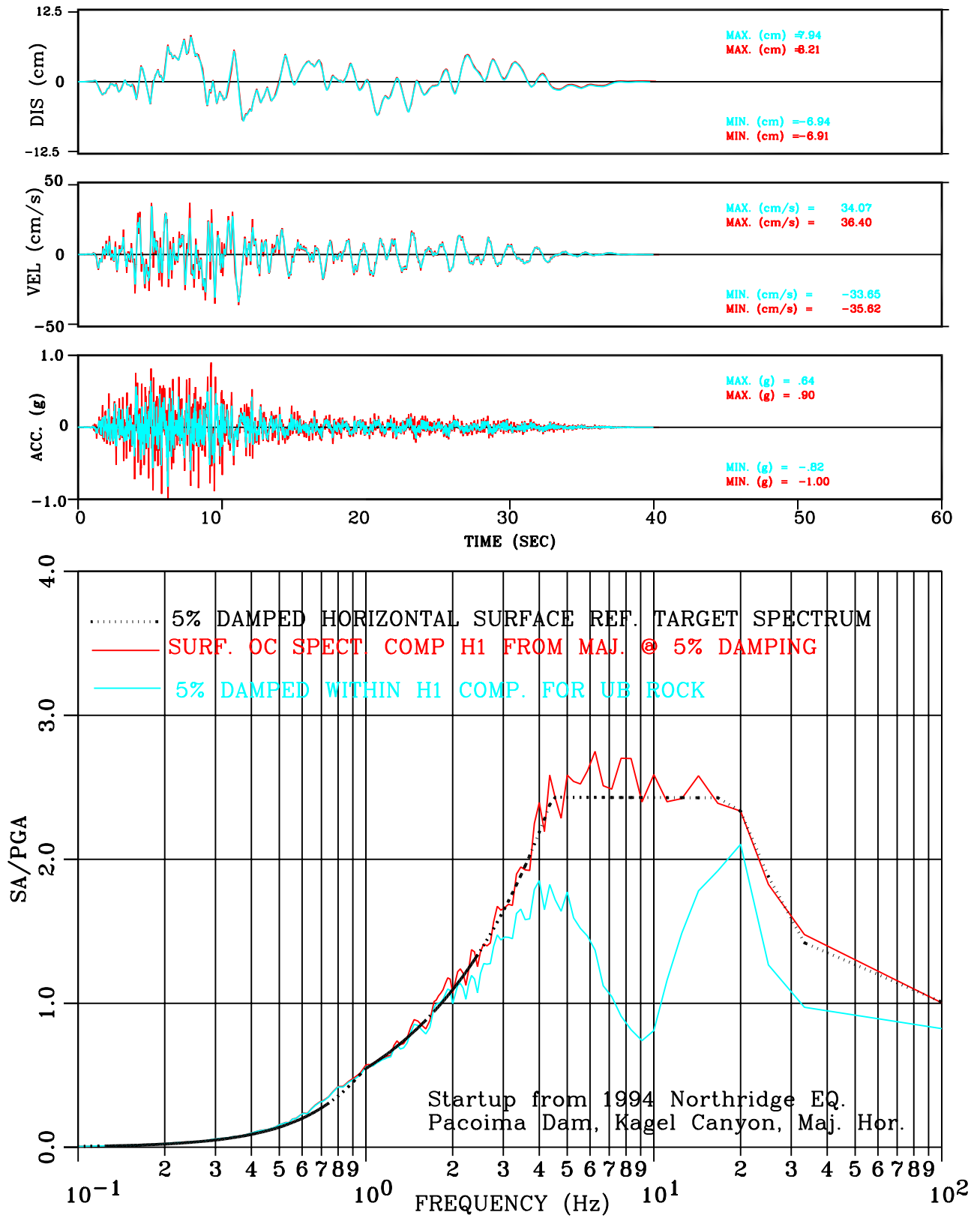


Figure III-178: With vs. Surface Motion for UB Rock  
 Set-5 H1 Comp. Motion Conforming to NUREG/CR-6728 Spectral Shape

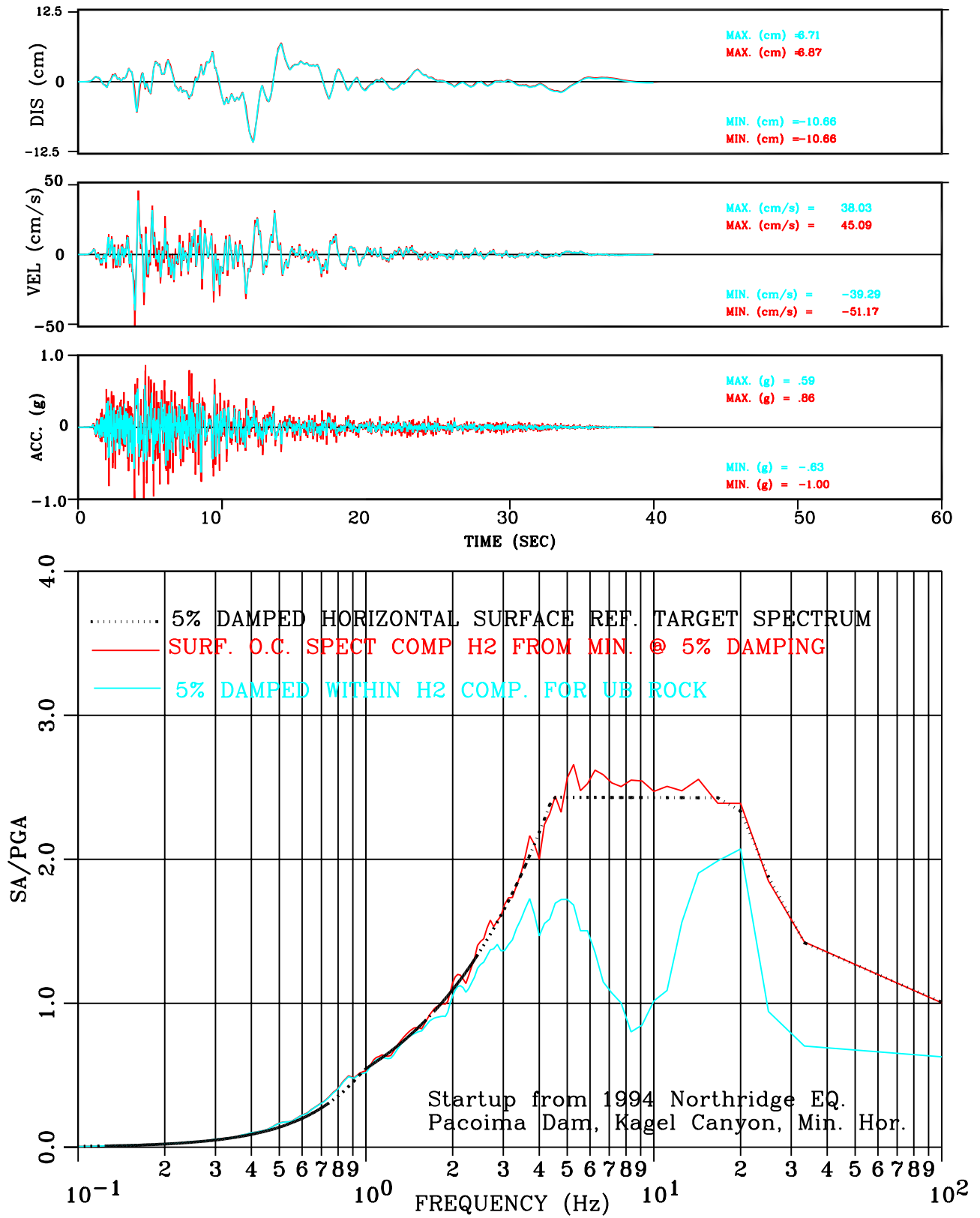


Figure III-179: With vs. Surface Motion for UB Rock  
 Set-5 H2 Comp. Motion Conforming to NUREG/CR-6728 Spectral Shape

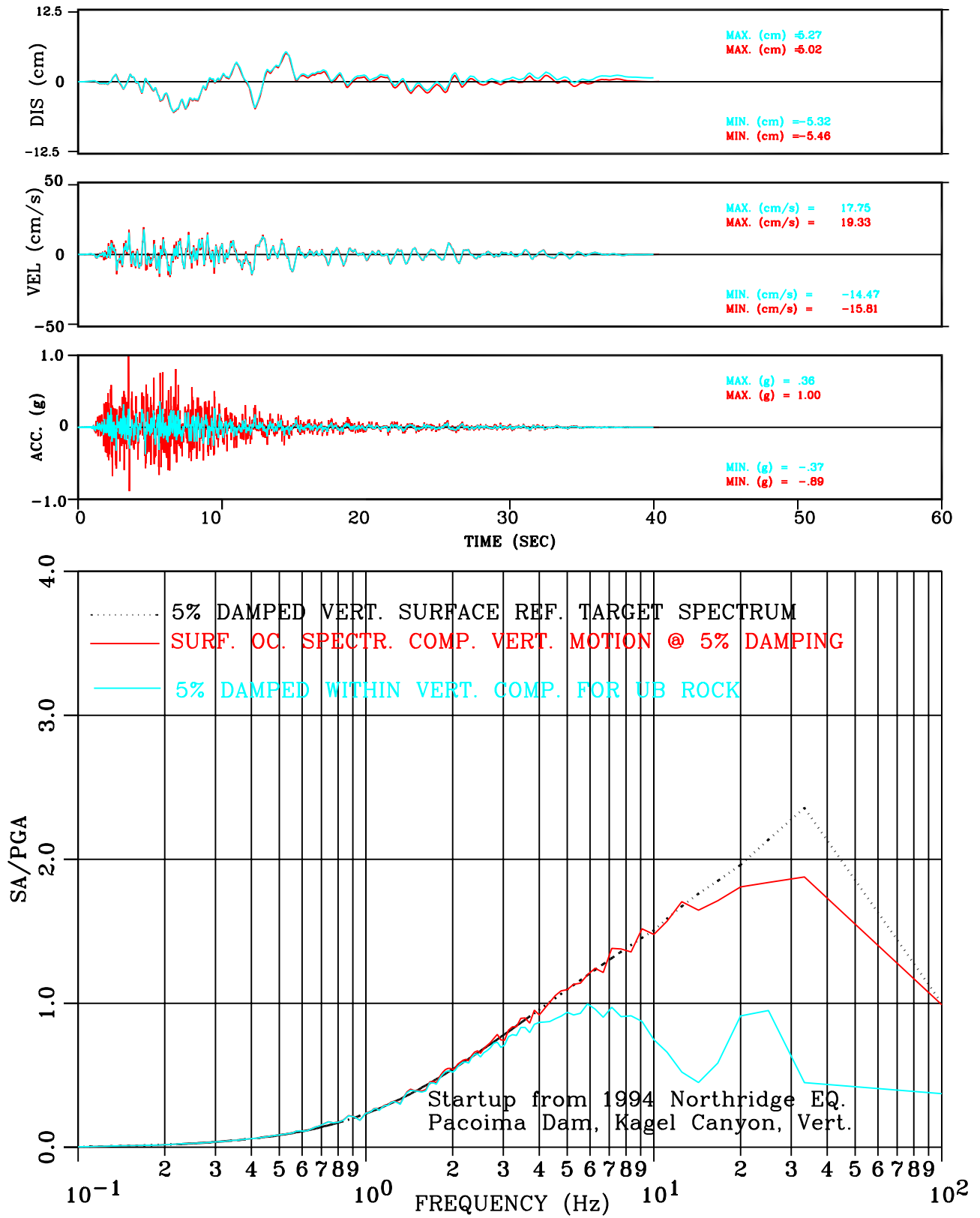


Figure III-180: With vs. Surface Motion for UB Rock  
Set-5 Vert. Comp. Motion Conforming to NUREG/CR-6728 Spectral Shape



## **Appendix IV: Plots of Analytical Soil Column Response**



## Appendix IV: Plots of Analytical Soil Column Response

The target surface ground motions are modified using a deconvolution procedure to produce acceleration histories to be applied to the base of the soil column. The deconvolution procedure is based on the assumption that the soil mass behaves as an idealized one-dimensional soil column. If the soil column used in the finite element models perfectly replicates those assumptions, the ground motion measured at the surface of the soil column without the presence of any structures should closely match the original surface motion.

To assess the ability of the model used in this work to replicate the original surface ground motion, the cask and pad have been removed from the soil column models, and each of the three soil columns (soft soil, stiff soil, and rock) has been subjected to the five deconvolved base ground motion records for each of the three spectral shapes used in this study. The boundary conditions on the soil column model ensure that the ground motion is nearly identical at any two nodes located on the same vertical layer of the column.

The plots provided in this appendix compare the spectral content of the original surface ground motion with the spectral content of the motion of a point at the center of the top surface of the analytical soil column model. Plots are provided for the 1<sup>st</sup> horizontal and vertical components of ground motion. These plots show the pseudo-spectral acceleration (PSA) with 5% damping, and are plotted in terms of the ratio of the PSA to the peak ground acceleration (PGA) in a given direction. Each plot shows the spectral shape of the original surface motion, as well as the analytical surface motion obtained using the soft soil, stiff soil, and rock profiles.

From these plots, it is evident that in all cases, the spectral shape of the analytical surface motion reasonably matches that of the original surface input motion at periods higher than approximately 0.3 s. The plots are cut off at 1.4 s, and at periods higher than this, there is very close agreement in all cases. At higher frequencies, the deviations between the analytical surface motion and the original surface motion are much larger. In general, the response at the surface of the stiffer soil column models is closer to the original surface motion than is that for the soft soil column model, especially at higher frequencies. Also, the horizontal components of the analytical surface motion are generally closer to the original ground motion.

It is believed that the major source of the discrepancies between the original surface motion and the analytical surface motion is the fact that the representation of damping in the finite element models is different from the damping used in the deconvolution procedure. In the deconvolution procedure, damping is frequency independent. In contrast, with the Rayleigh damping procedure used in the finite element analysis code, the amount of damping in a given mode is dependent on the frequency of that mode and on the values of the mass and stiffness proportional damping coefficients. In this work, only mass-proportional damping was used because of the excessively long run times that result from the use of stiffness-proportional damping with the explicit time integration method.

While there are clearly discrepancies between the original surface motions and the analytical surface motions in the high frequency range in some cases, these are not believed to have a significant effect on the cask response. Once uplift occurs, the cask response appears to be dominated by the seismic input in the range from about 0.5 Hz to 2 Hz, and in this range, the analytical spectral response closely matches the target spectral content.

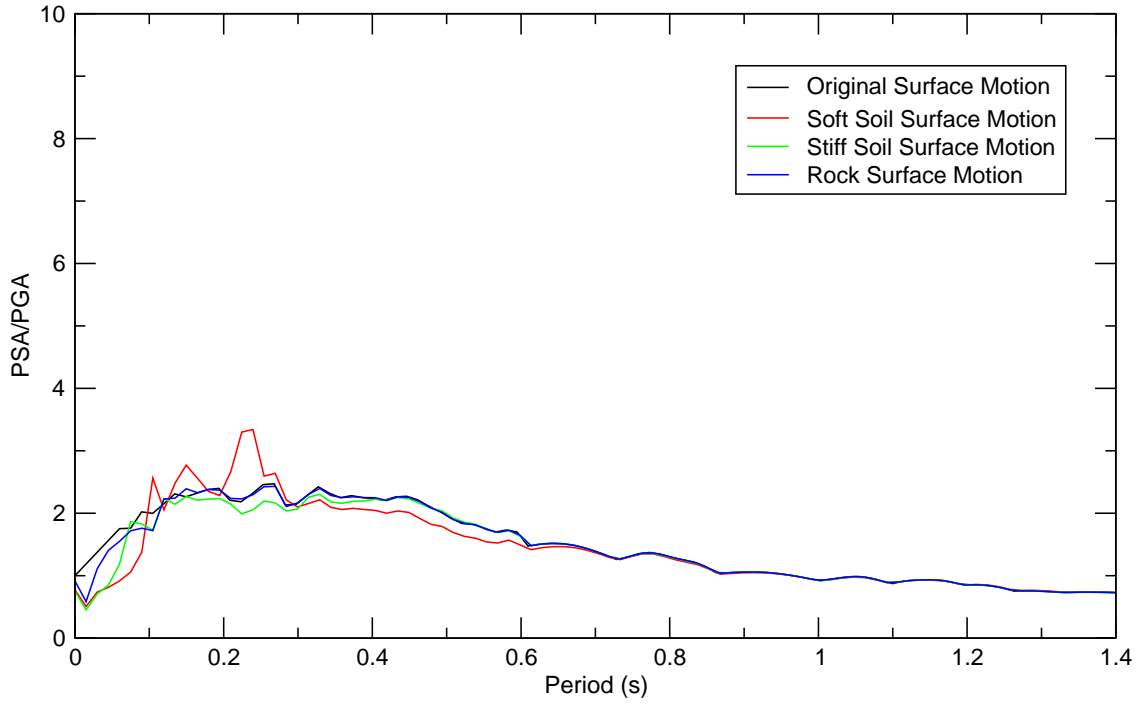


Figure IV.1: Comparison of Original Surface Motion and Motion at Top of Soil Column Model, NUREG/CR-0098 Spectral Shape, Case 1 Earthquake, 1<sup>st</sup> Horizontal Component

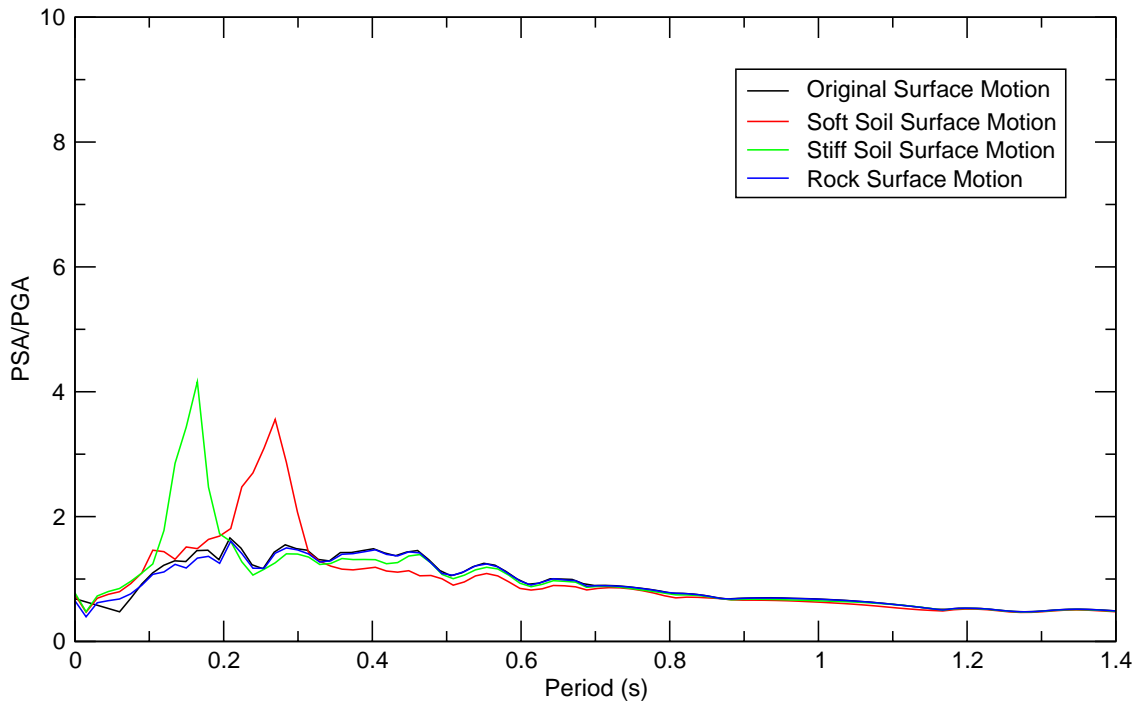


Figure IV.2: Comparison of Original Surface Motion and Motion at Top of Soil Column Model, NUREG/CR-0098 Spectral Shape, Case 1 Earthquake, Vertical Component

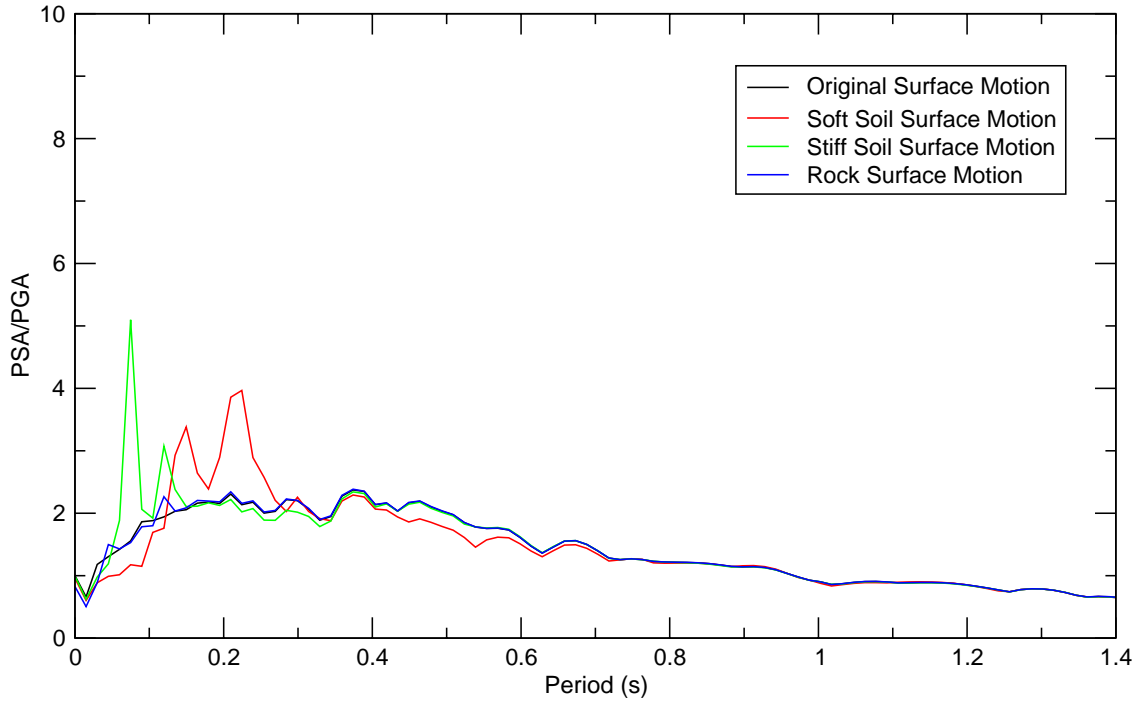


Figure IV.3: Comparison of Original Surface Motion and Motion at Top of Soil Column Model, NUREG/CR-0098 Spectral Shape, Case 2 Earthquake, 1<sup>st</sup> Horizontal Component

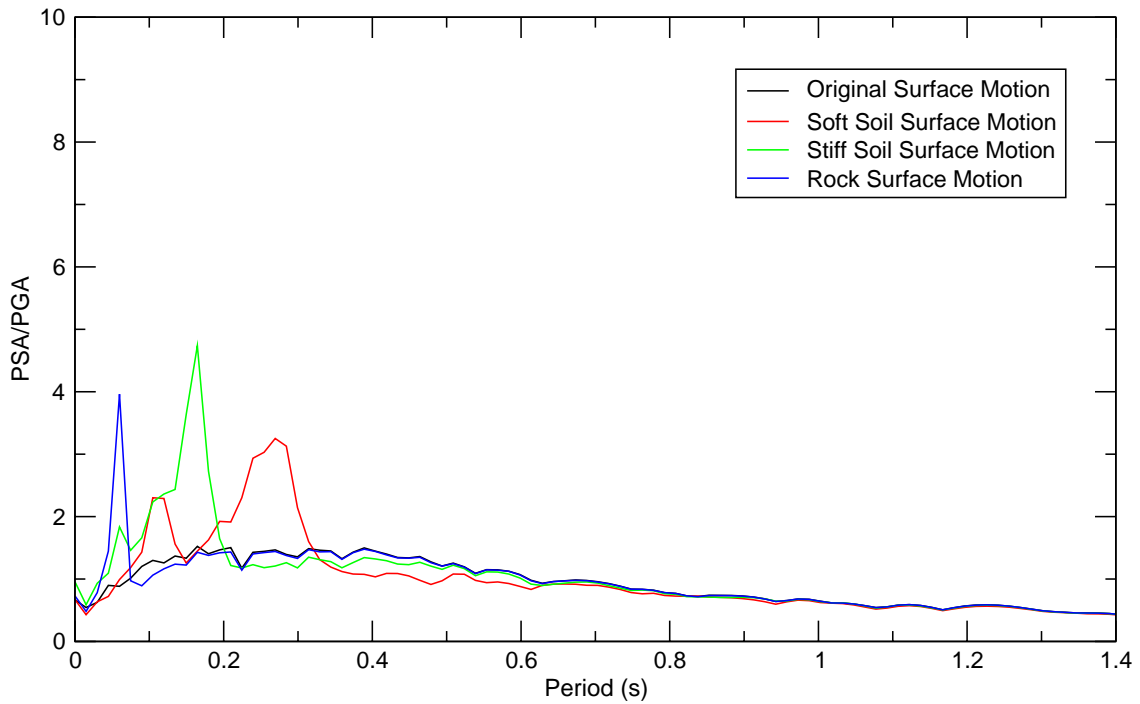


Figure IV.4: Comparison of Original Surface Motion and Motion at Top of Soil Column Model, NUREG/CR-0098 Spectral Shape, Case 2 Earthquake, Vertical Component

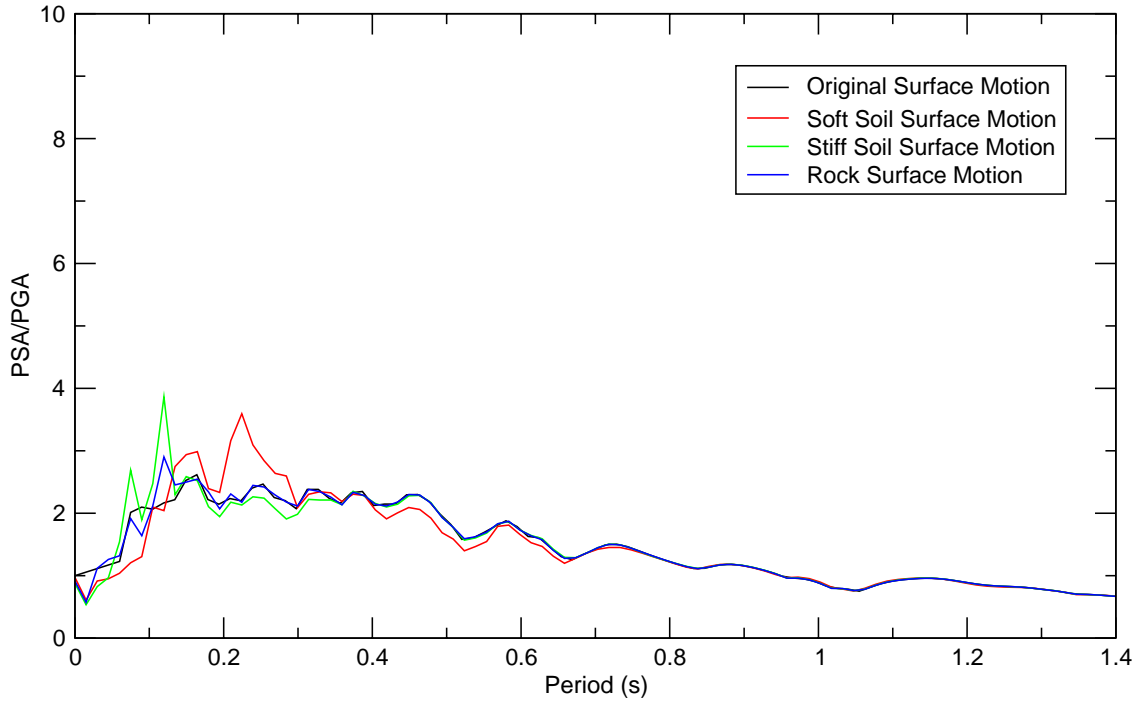


Figure IV.5: Comparison of Original Surface Motion and Motion at Top of Soil Column Model, NUREG/CR-0098 Spectral Shape, Case 3 Earthquake, 1<sup>st</sup> Horizontal Component

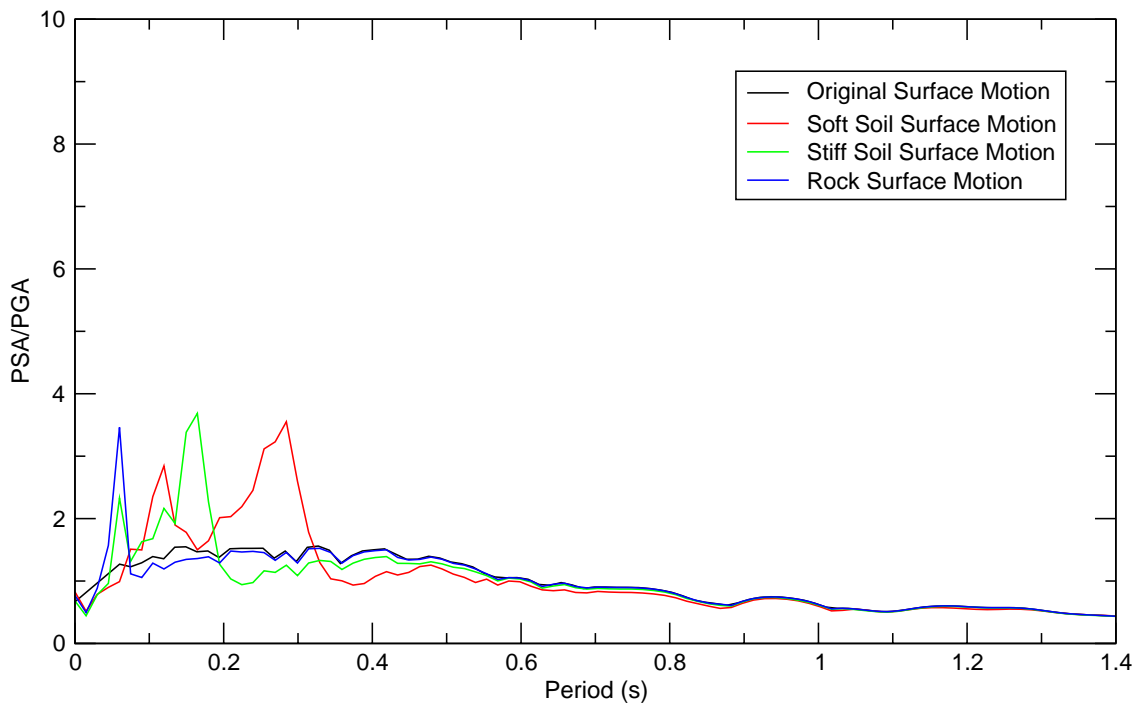


Figure IV.6: Comparison of Original Surface Motion and Motion at Top of Soil Column Model, NUREG/CR-0098 Spectral Shape, Case 3 Earthquake, Vertical Component

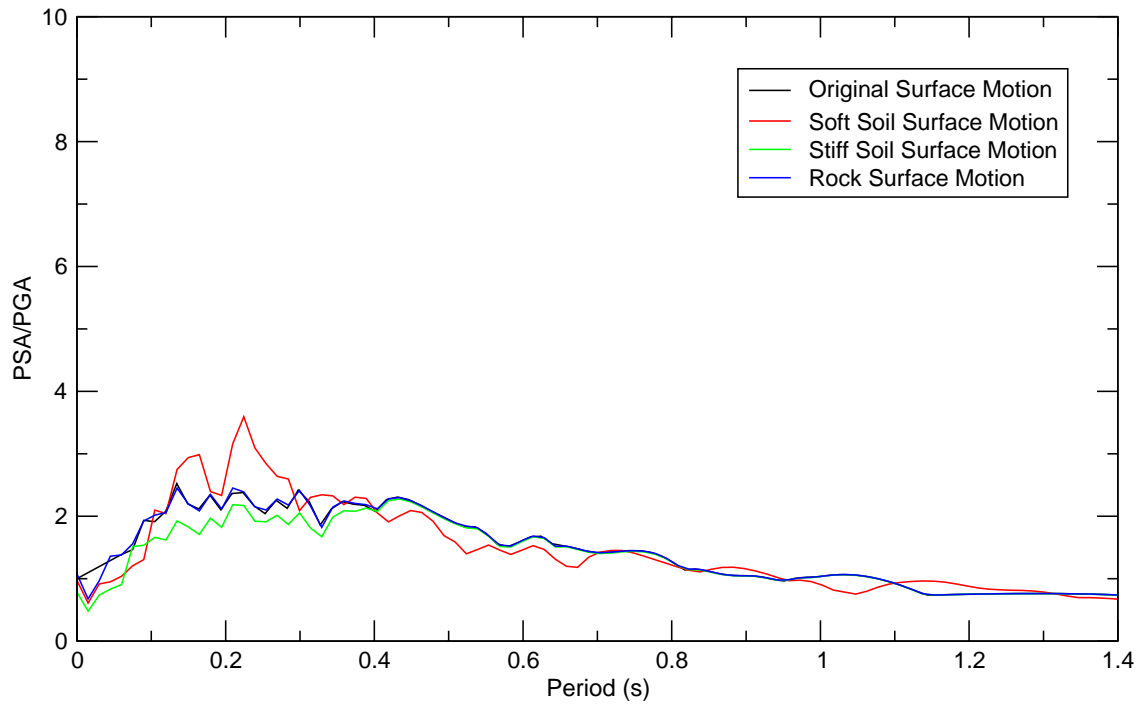


Figure IV.7: Comparison of Original Surface Motion and Motion at Top of Soil Column Model, NUREG/CR-0098 Spectral Shape, Case 4 Earthquake, 1<sup>st</sup> Horizontal Component

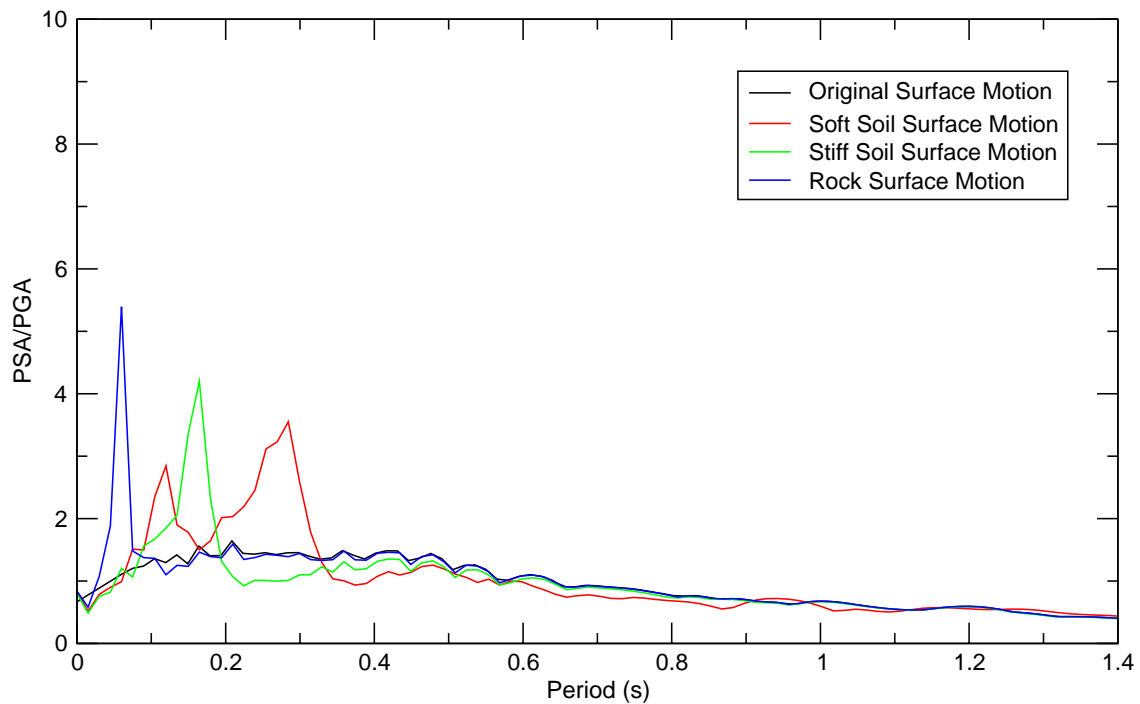


Figure IV.8: Comparison of Original Surface Motion and Motion at Top of Soil Column Model, NUREG/CR-0098 Spectral Shape, Case 4 Earthquake, Vertical Component

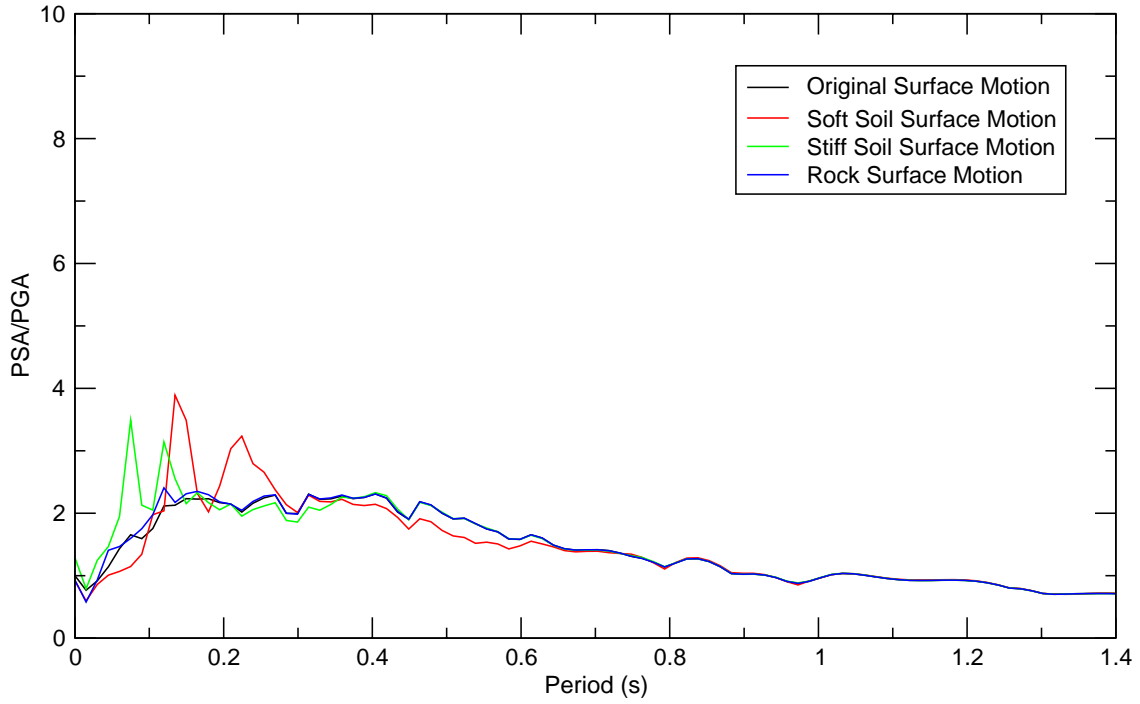


Figure IV.9: Comparison of Original Surface Motion and Motion at Top of Soil Column Model, NUREG/CR-0098 Spectral Shape, Case 5 Earthquake, 1<sup>st</sup> Horizontal Component

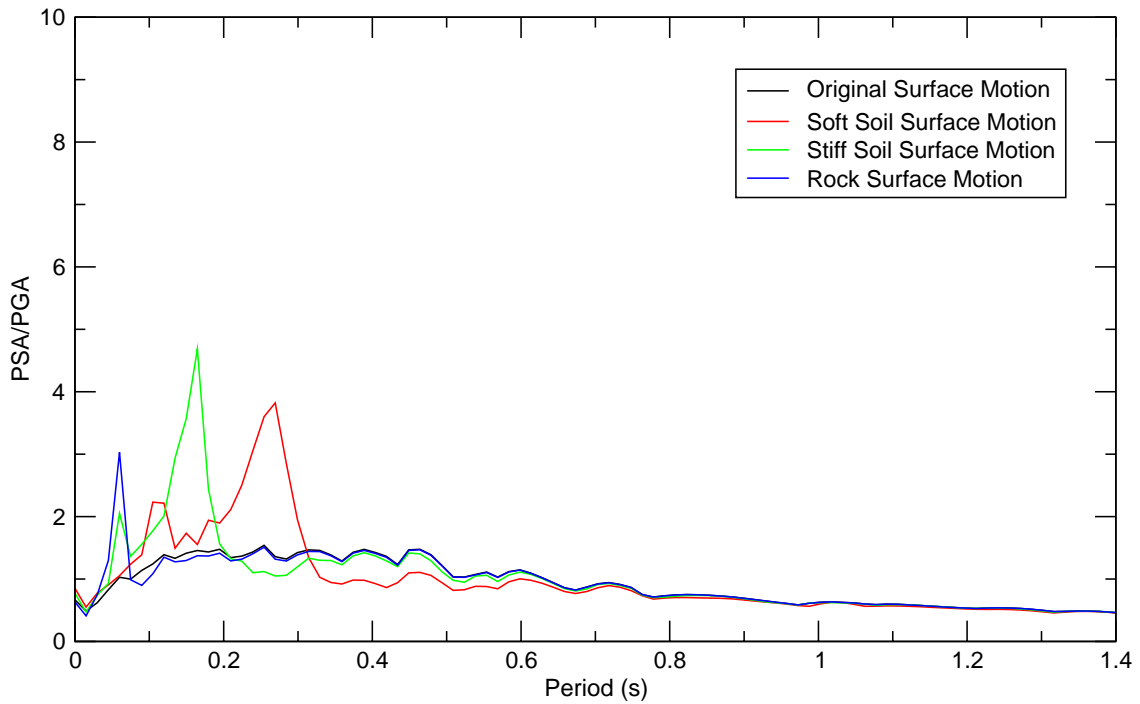


Figure IV.10: Comparison of Original Surface Motion and Motion at Top of Soil Column Model, NUREG/CR-0098 Spectral Shape, Case 5 Earthquake, Vertical Component

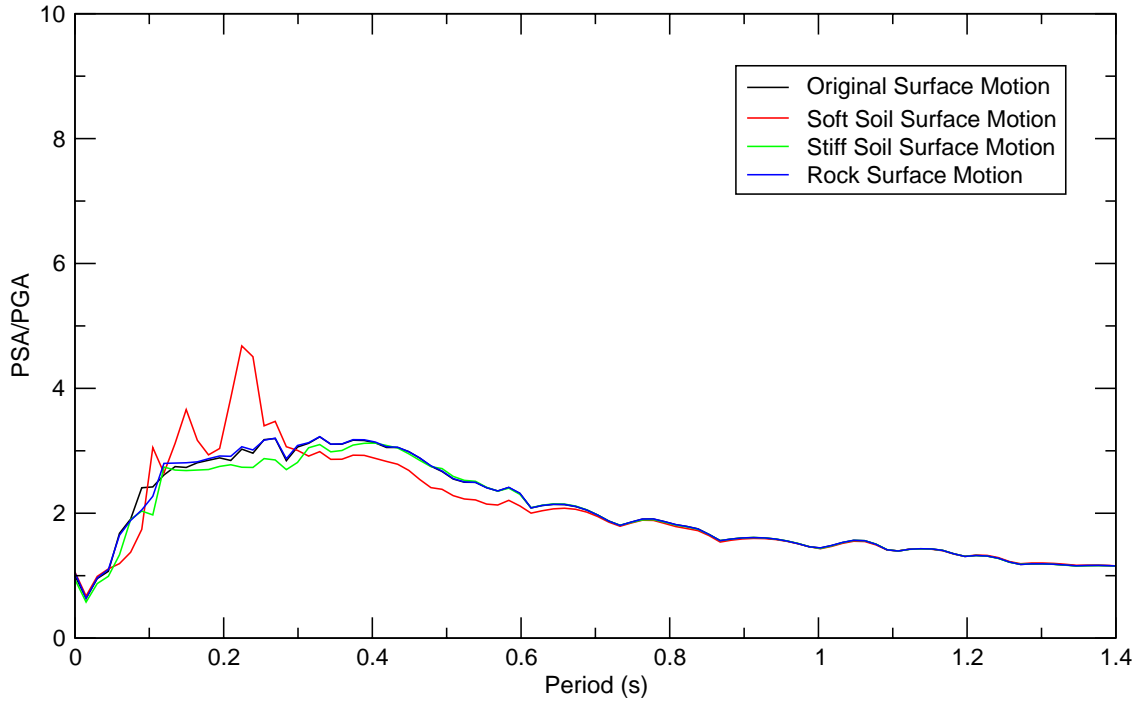


Figure IV.11: Comparison of Original Surface Motion and Motion at Top of Soil Column Model, Regulatory Guide 1.60 Spectral Shape, Case 1 Earthquake, 1<sup>st</sup> Horizontal Component

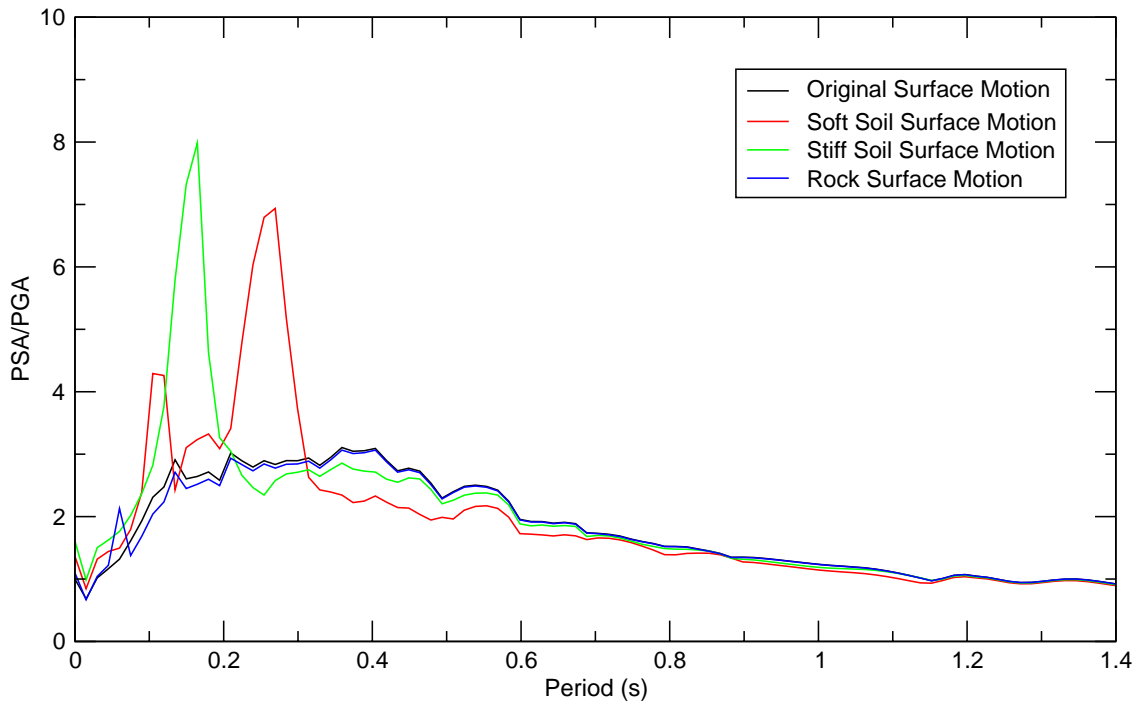


Figure IV.12: Comparison of Original Surface Motion and Motion at Top of Soil Column Model, Regulatory Guide 1.60 Spectral Shape, Case 1 Earthquake, Vertical Component

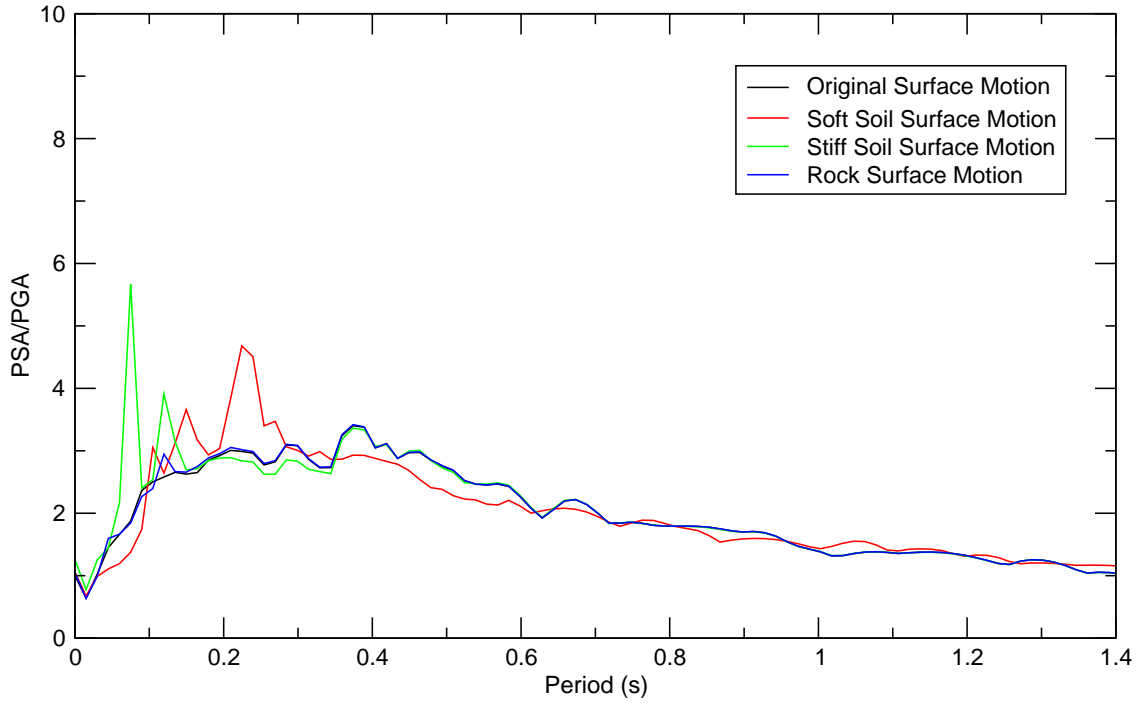


Figure IV.13: Comparison of Original Surface Motion and Motion at Top of Soil Column Model, Regulatory Guide 1.60 Spectral Shape, Case 2 Earthquake, 1<sup>st</sup> Horizontal Component

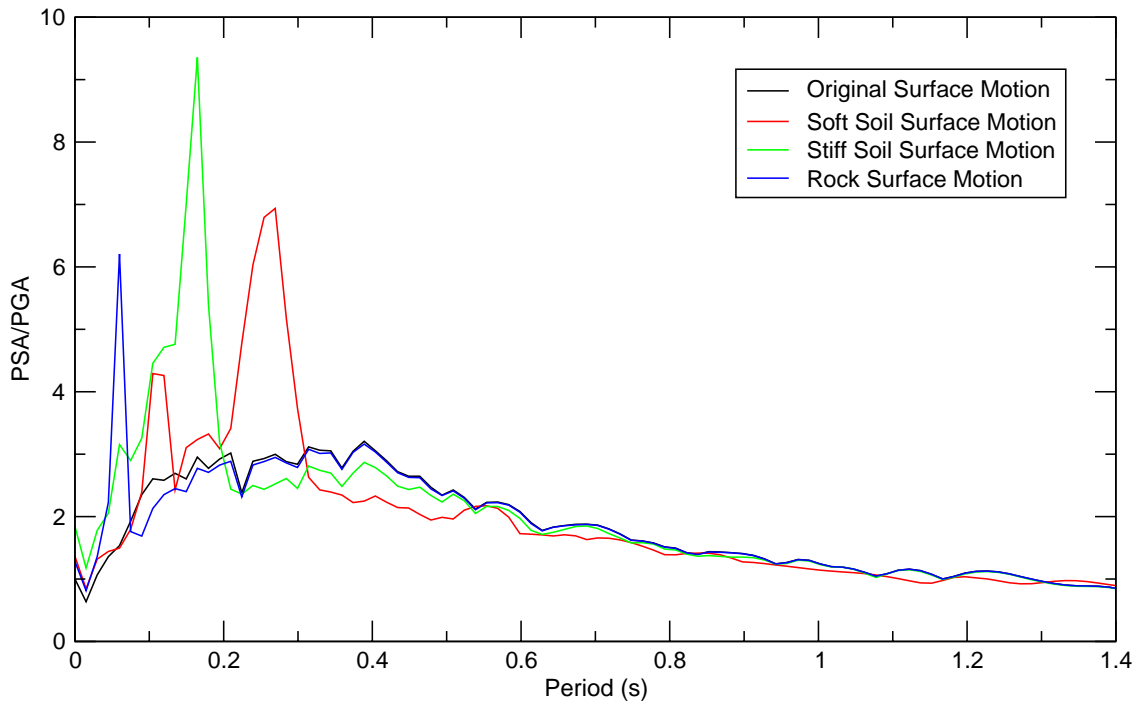


Figure IV.14: Comparison of Original Surface Motion and Motion at Top of Soil Column Model, Regulatory Guide 1.60 Spectral Shape, Case 2 Earthquake, Vertical Component

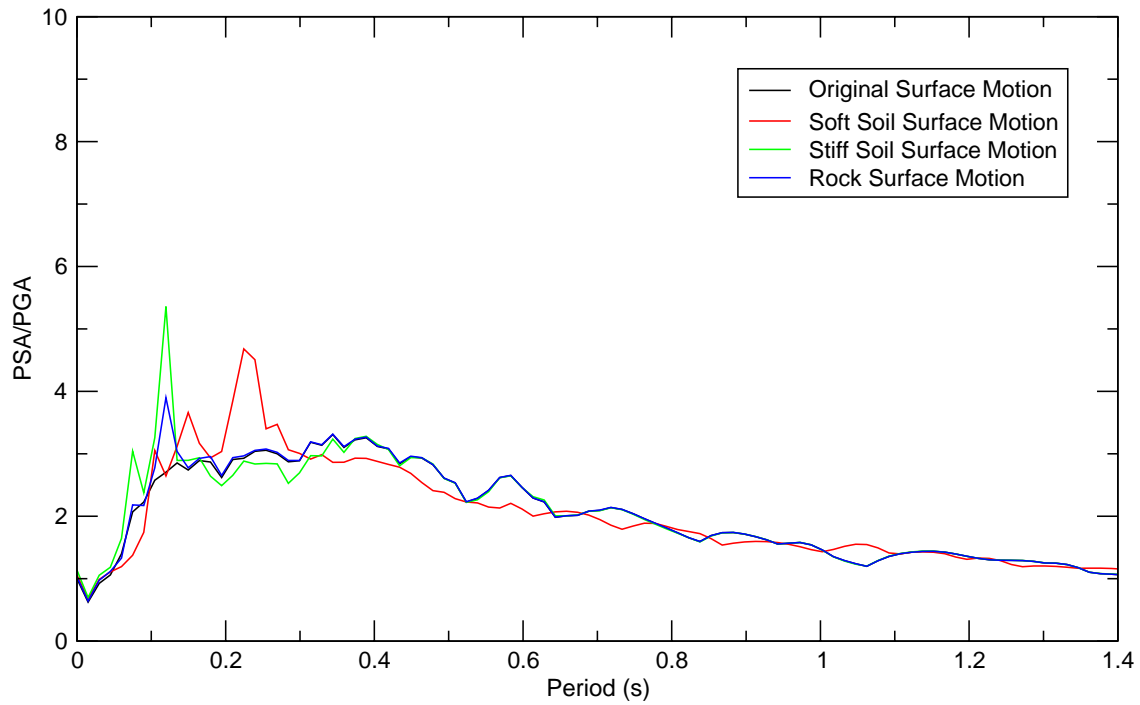


Figure IV.15: Comparison of Original Surface Motion and Motion at Top of Soil Column Model, Regulatory Guide 1.60 Spectral Shape, Case 3 Earthquake, 1<sup>st</sup> Horizontal Component

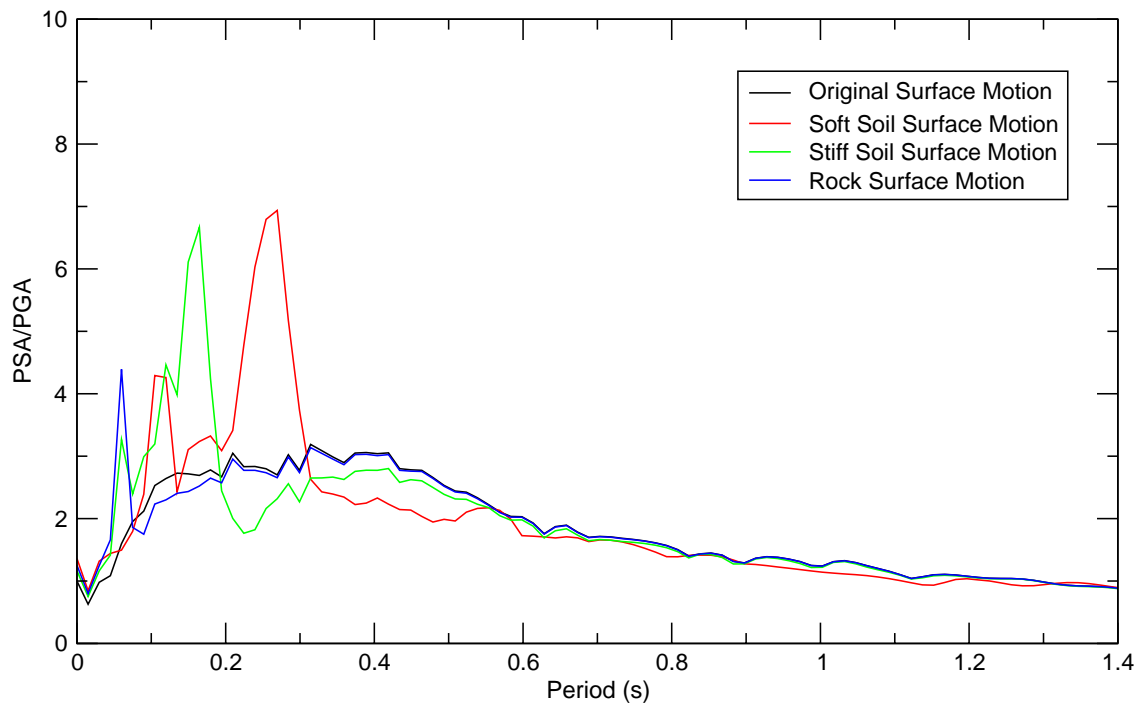


Figure IV.16: Comparison of Original Surface Motion and Motion at Top of Soil Column Model, Regulatory Guide 1.60 Spectral Shape, Case 3 Earthquake, Vertical Component

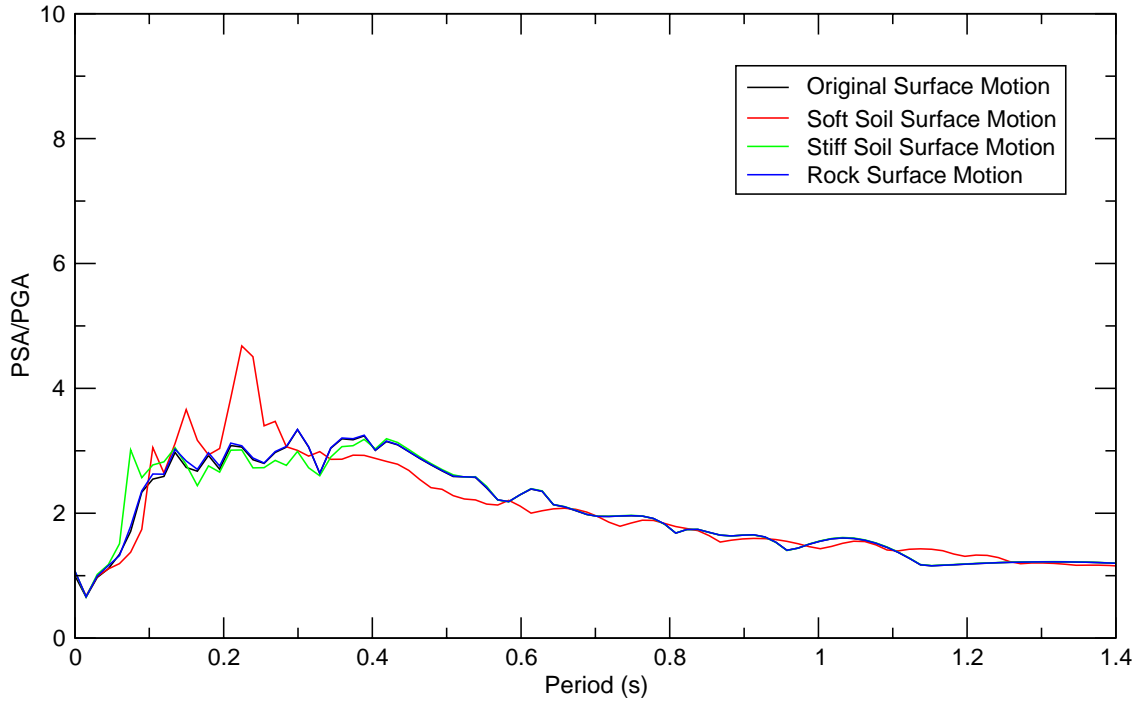


Figure IV.17: Comparison of Original Surface Motion and Motion at Top of Soil Column Model, Regulatory Guide 1.60 Spectral Shape, Case 4 Earthquake, 1<sup>st</sup> Horizontal Component

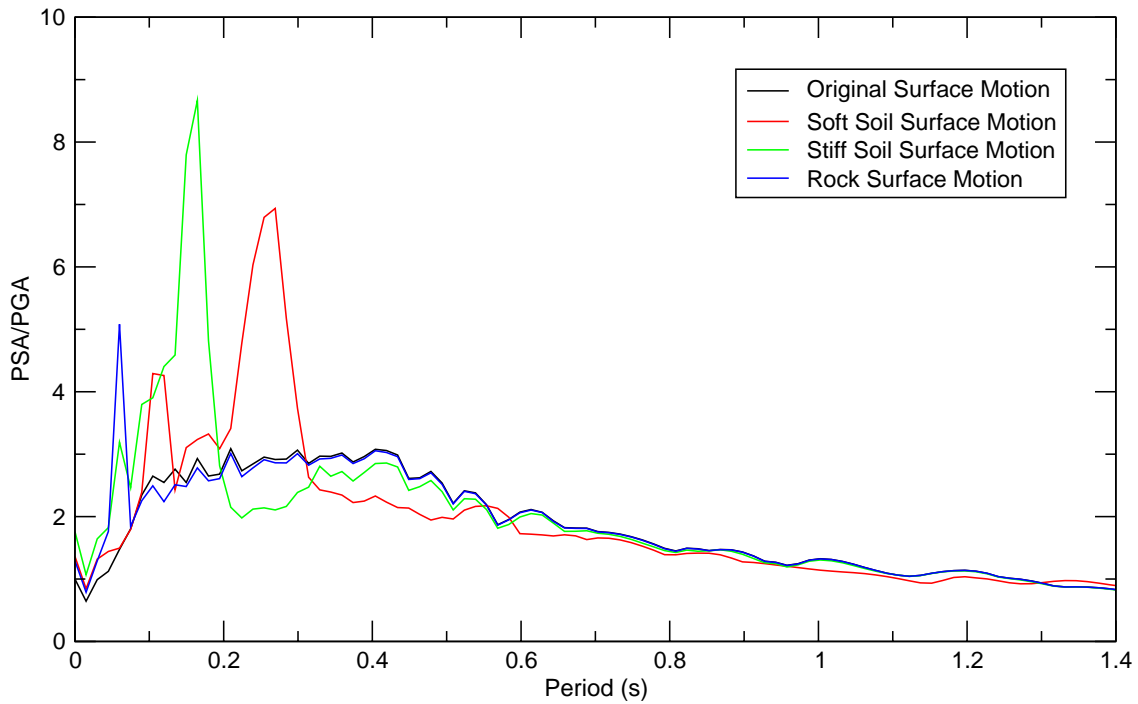


Figure IV.18: Comparison of Original Surface Motion and Motion at Top of Soil Column Model, Regulatory Guide 1.60 Spectral Shape, Case 4 Earthquake, Vertical Component

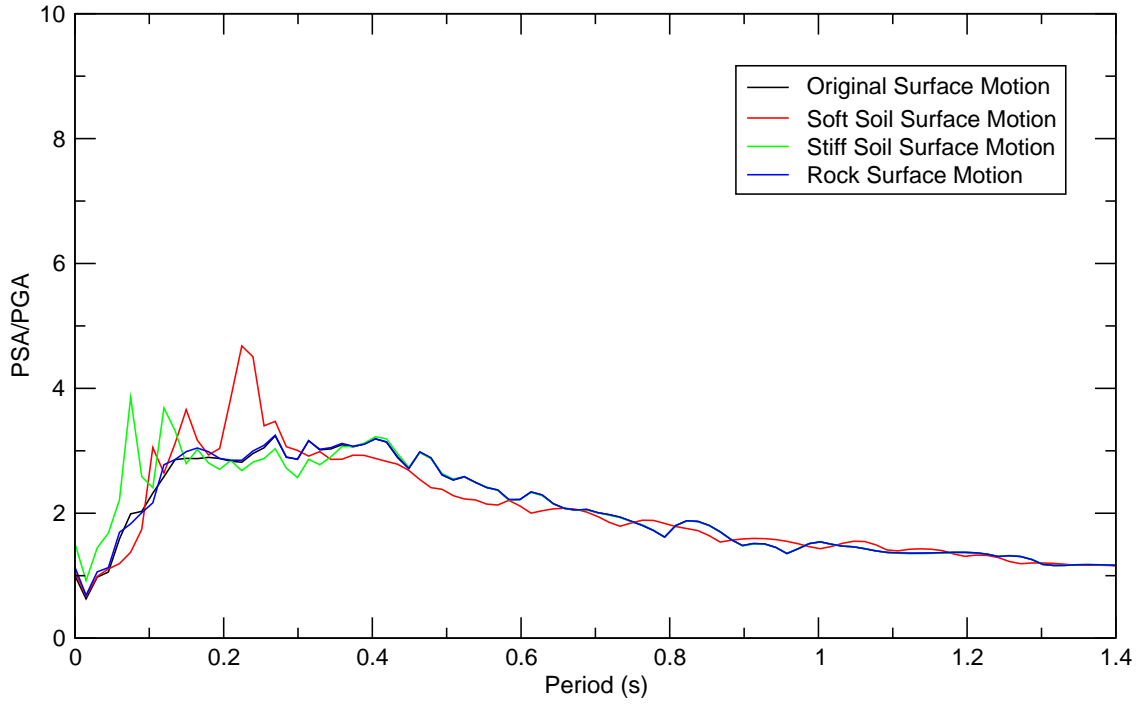


Figure IV.19: Comparison of Original Surface Motion and Motion at Top of Soil Column Model, Regulatory Guide 1.60 Spectral Shape, Case 5 Earthquake, 1<sup>st</sup> Horizontal Component

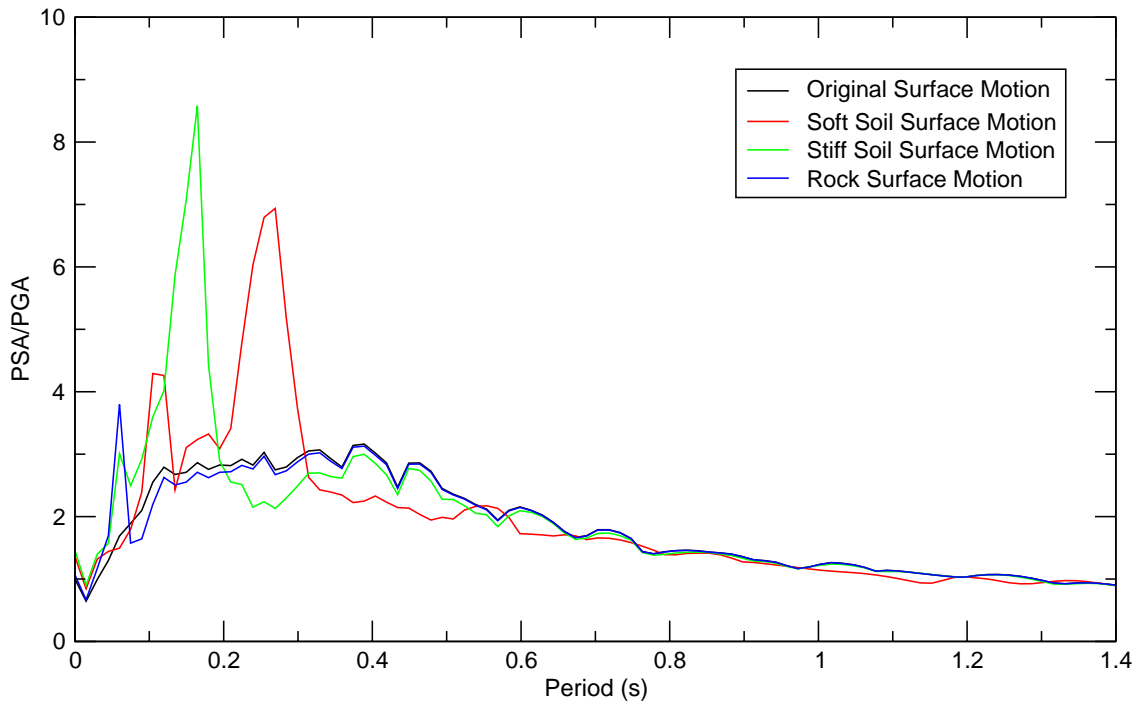


Figure IV.20: Comparison of Original Surface Motion and Motion at Top of Soil Column Model, Regulatory Guide 1.60 Spectral Shape, Case 5 Earthquake, Vertical Component

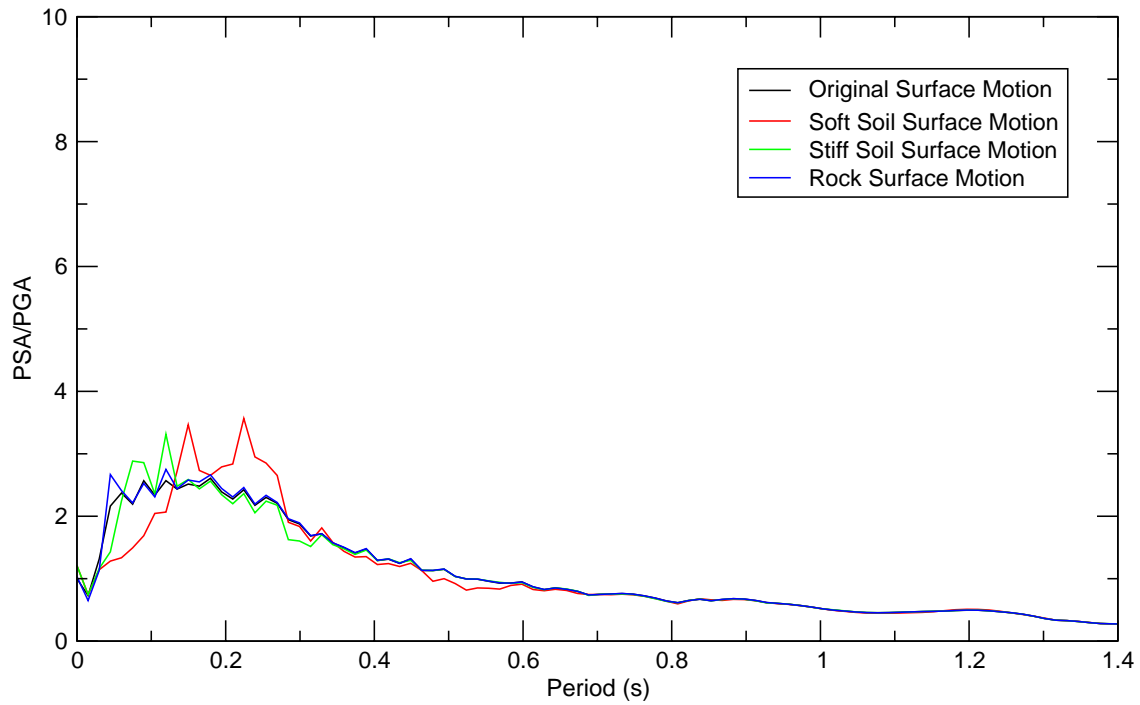


Figure IV.21: Comparison of Original Surface Motion and Motion at Top of Soil Column Model, NUREG/CR-6728 Spectral Shape, Case A Earthquake, 1<sup>st</sup> Horizontal Component

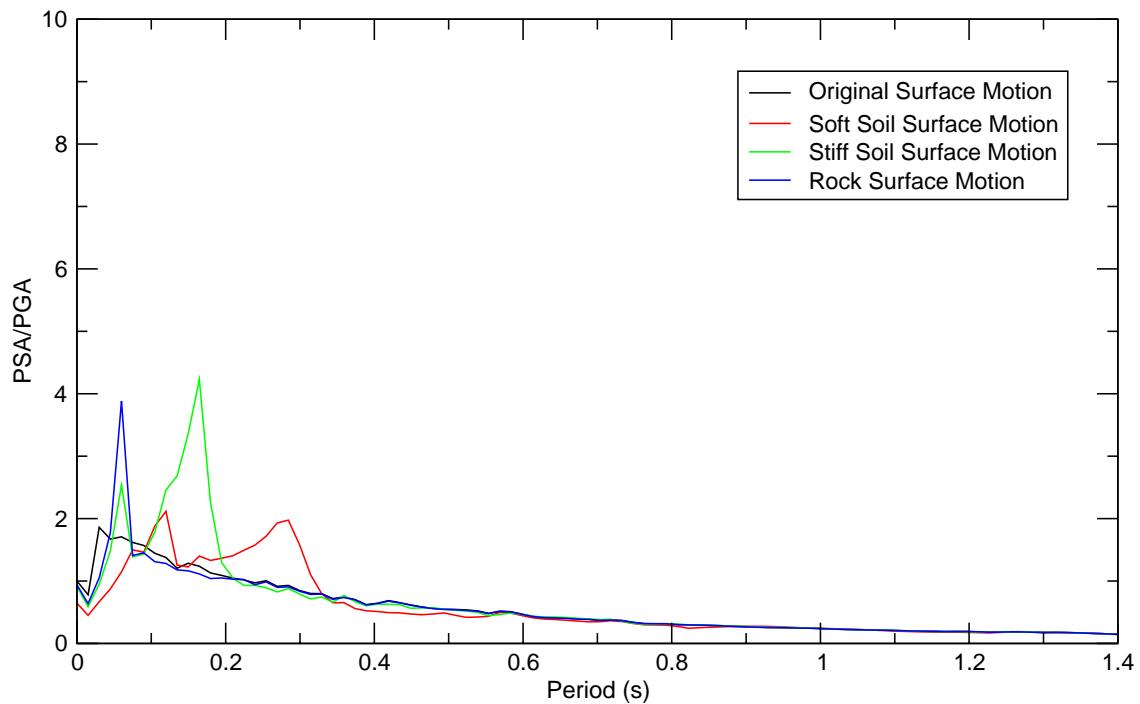


Figure IV.22: Comparison of Original Surface Motion and Motion at Top of Soil Column Model, NUREG/CR-6728 Spectral Shape, Case A Earthquake, Vertical Component

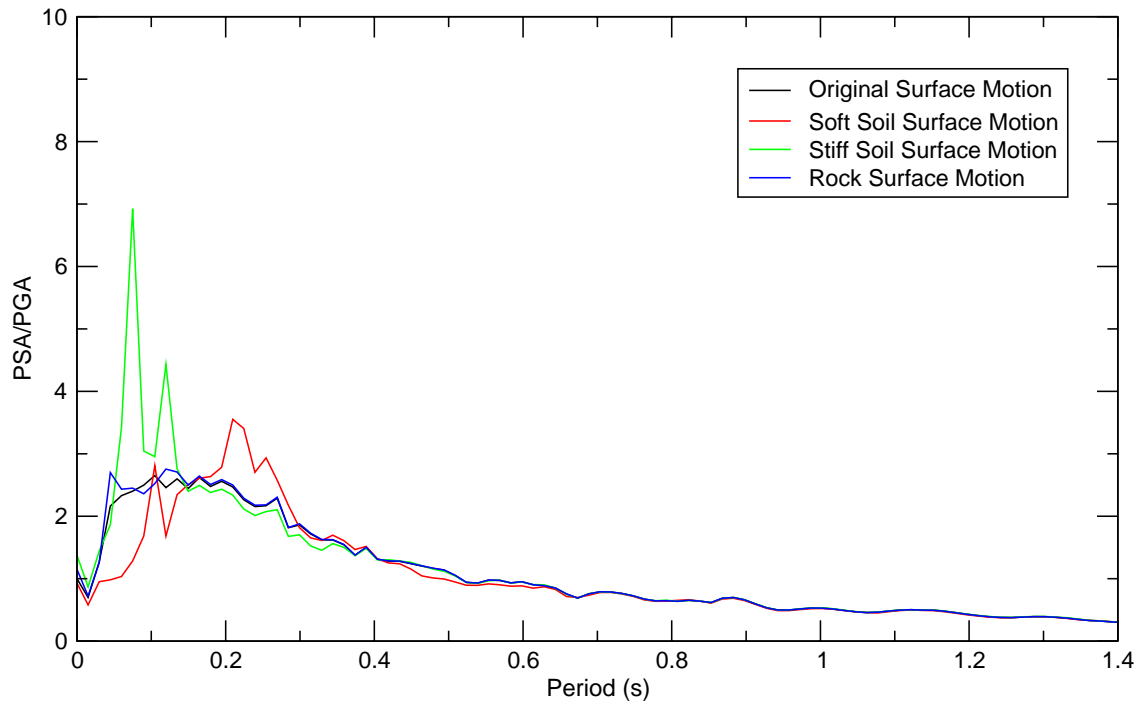


Figure IV.23: Comparison of Original Surface Motion and Motion at Top of Soil Column Model, NUREG/CR-6728 Spectral Shape, Case B Earthquake, 1<sup>st</sup> Horizontal Component

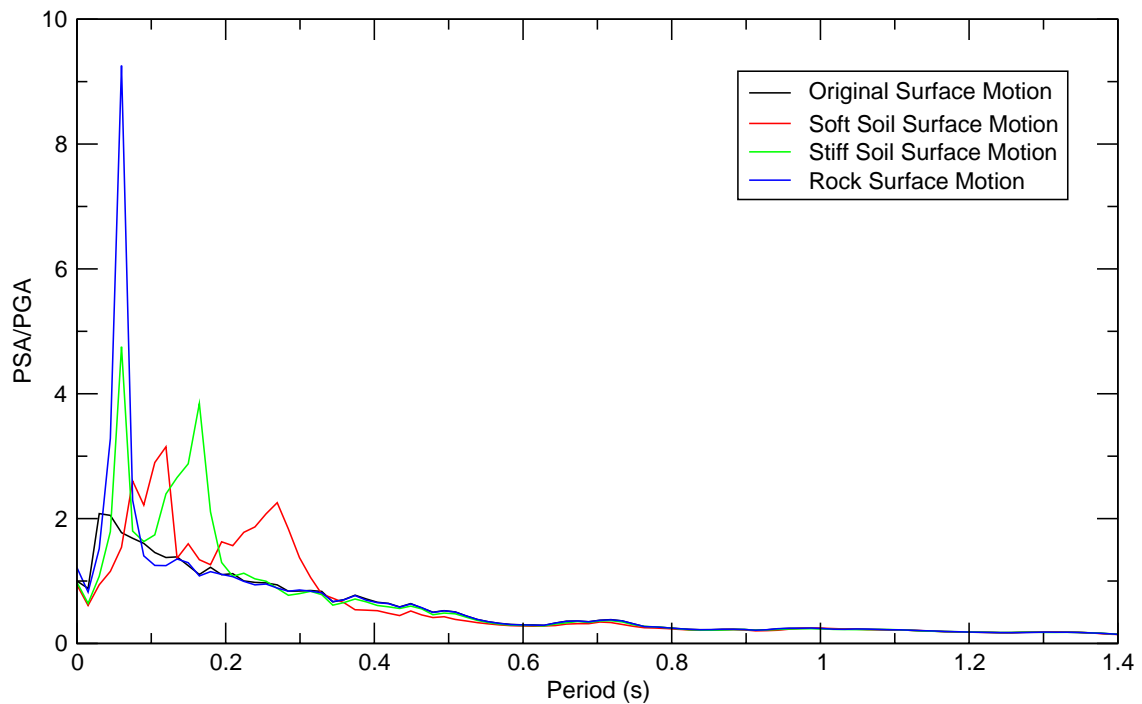


Figure IV.24: Comparison of Original Surface Motion and Motion at Top of Soil Column Model, NUREG/CR-6728 Spectral Shape, Case B Earthquake, Vertical Component

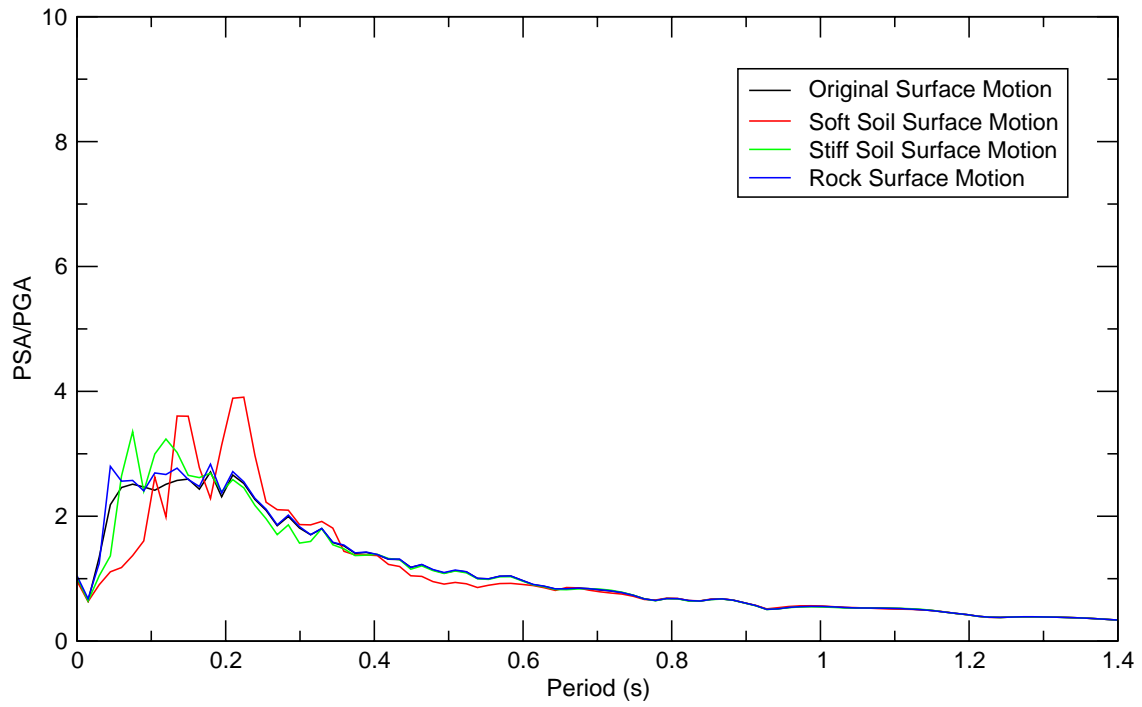


Figure IV.25: Comparison of Original Surface Motion and Motion at Top of Soil Column Model, NUREG/CR-6728 Spectral Shape, Case C Earthquake, 1<sup>st</sup> Horizontal Component

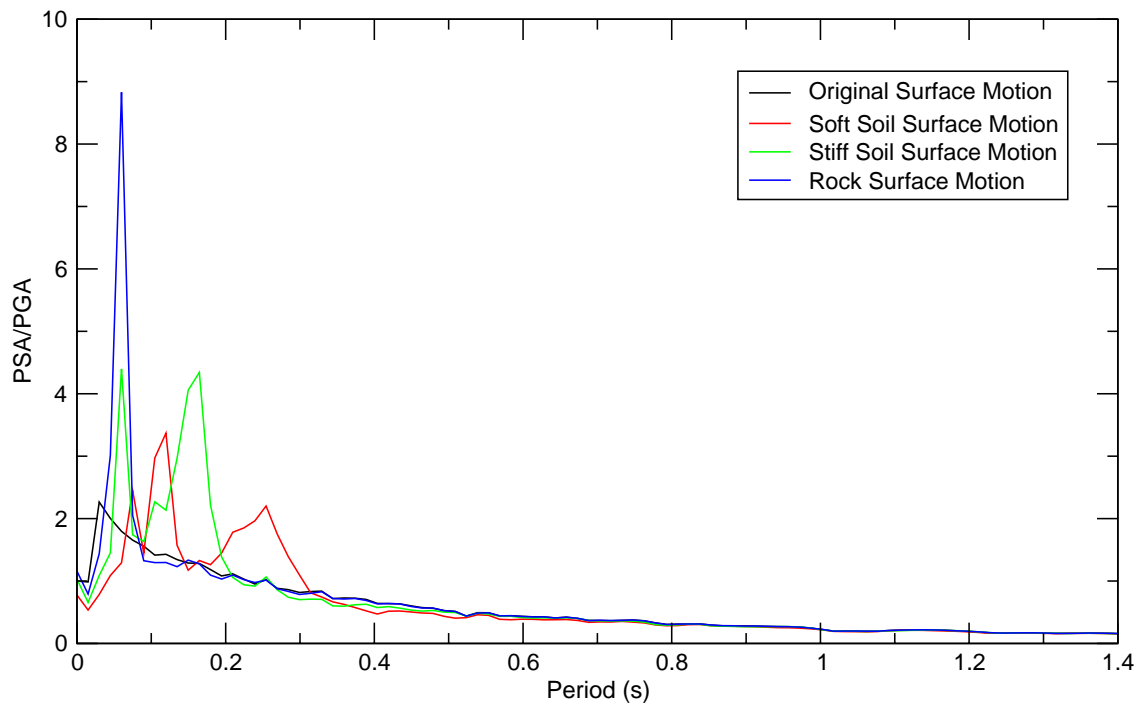


Figure IV.26: Comparison of Original Surface Motion and Motion at Top of Soil Column Model, NUREG/CR-6728 Spectral Shape, Case C Earthquake, Vertical Component

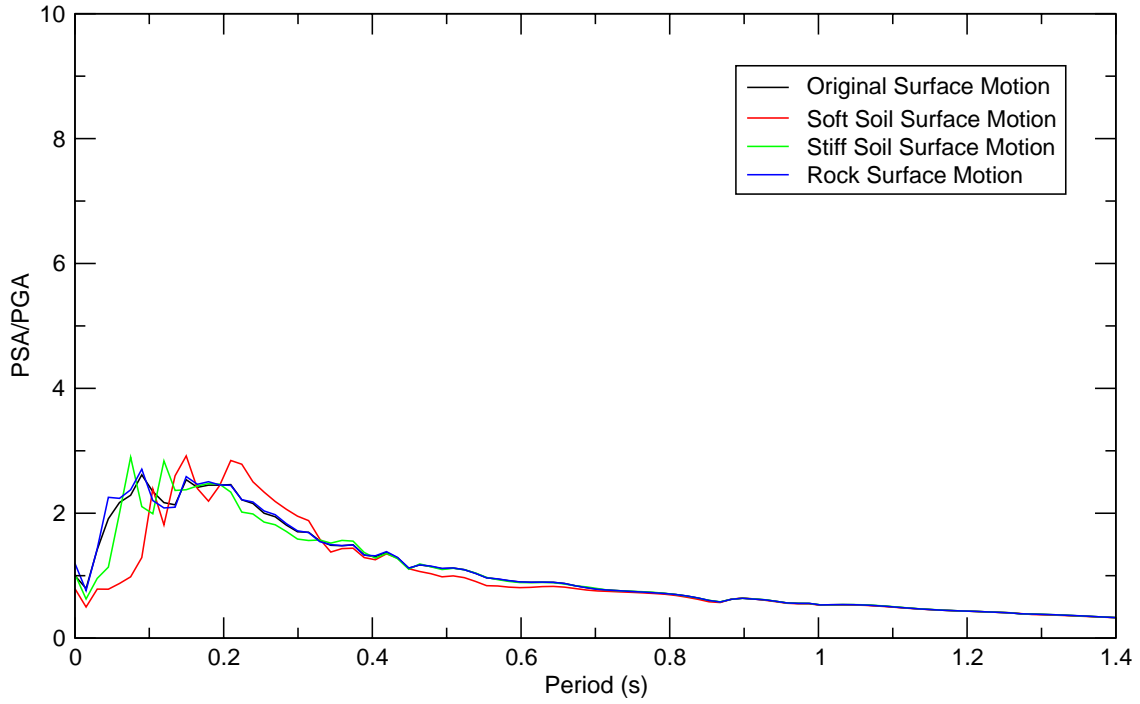


Figure IV.27: Comparison of Original Surface Motion and Motion at Top of Soil Column Model, NUREG/CR-6728 Spectral Shape, Case D Earthquake, 1<sup>st</sup> Horizontal Component

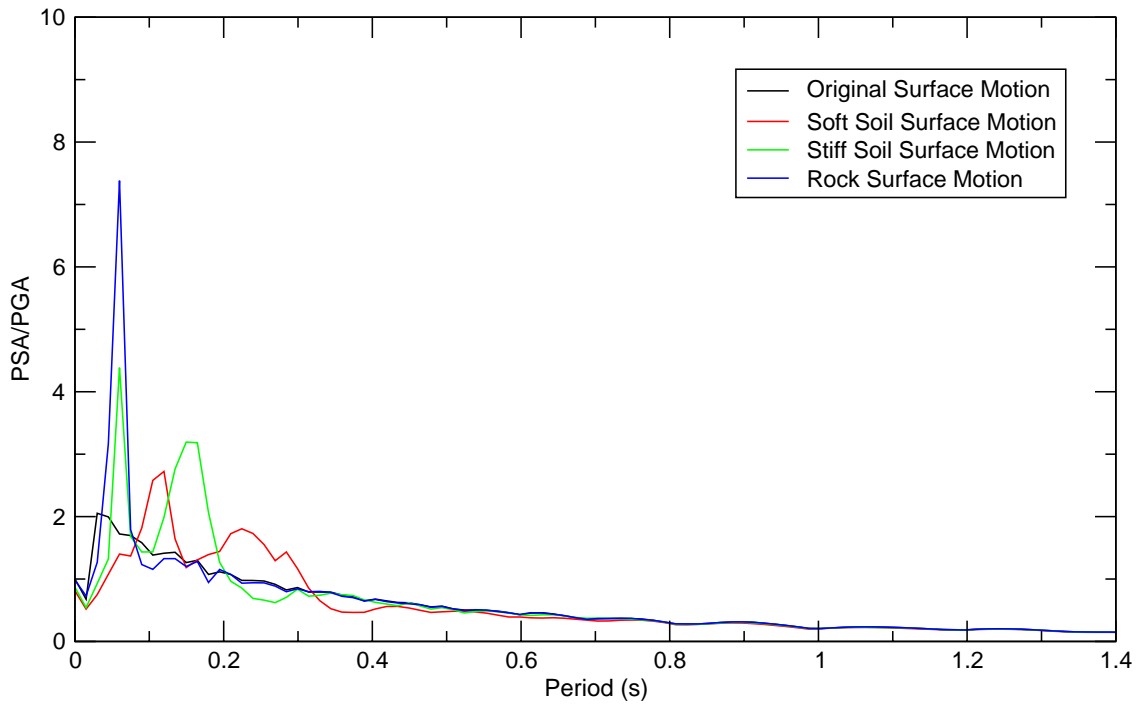


Figure IV.28: Comparison of Original Surface Motion and Motion at Top of Soil Column Model, NUREG/CR-6728 Spectral Shape, Case D Earthquake, Vertical Component

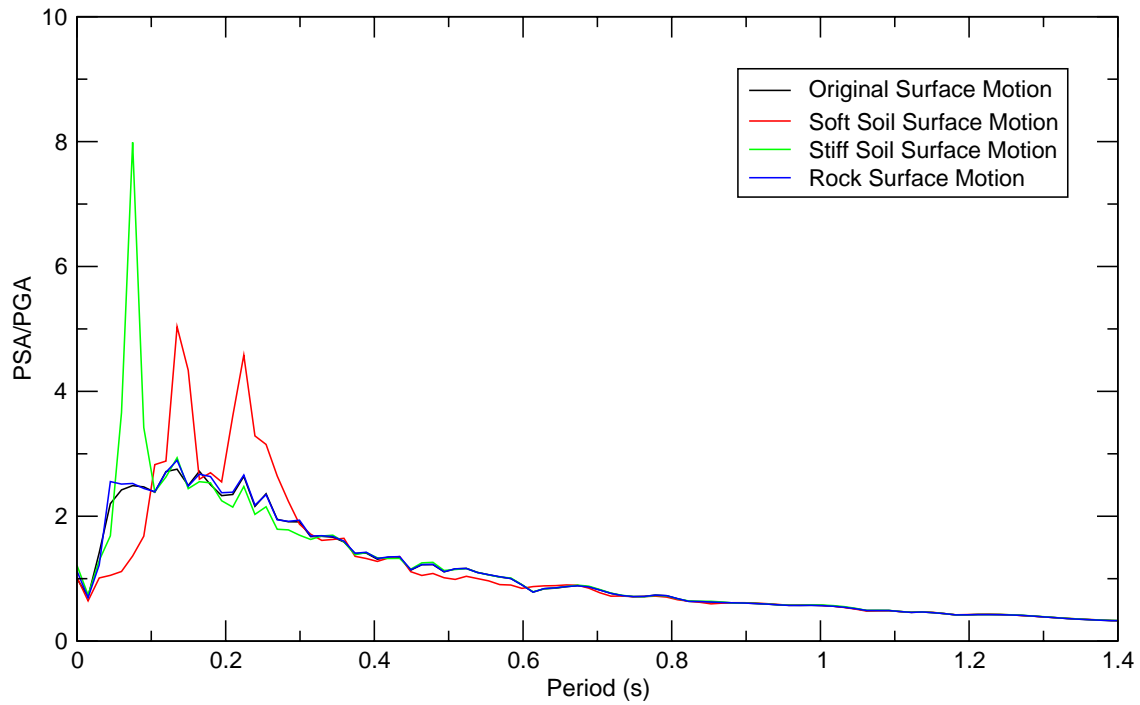


Figure IV.29: Comparison of Original Surface Motion and Motion at Top of Soil Column Model, NUREG/CR-6728 Spectral Shape, Case E Earthquake, 1<sup>st</sup> Horizontal Component

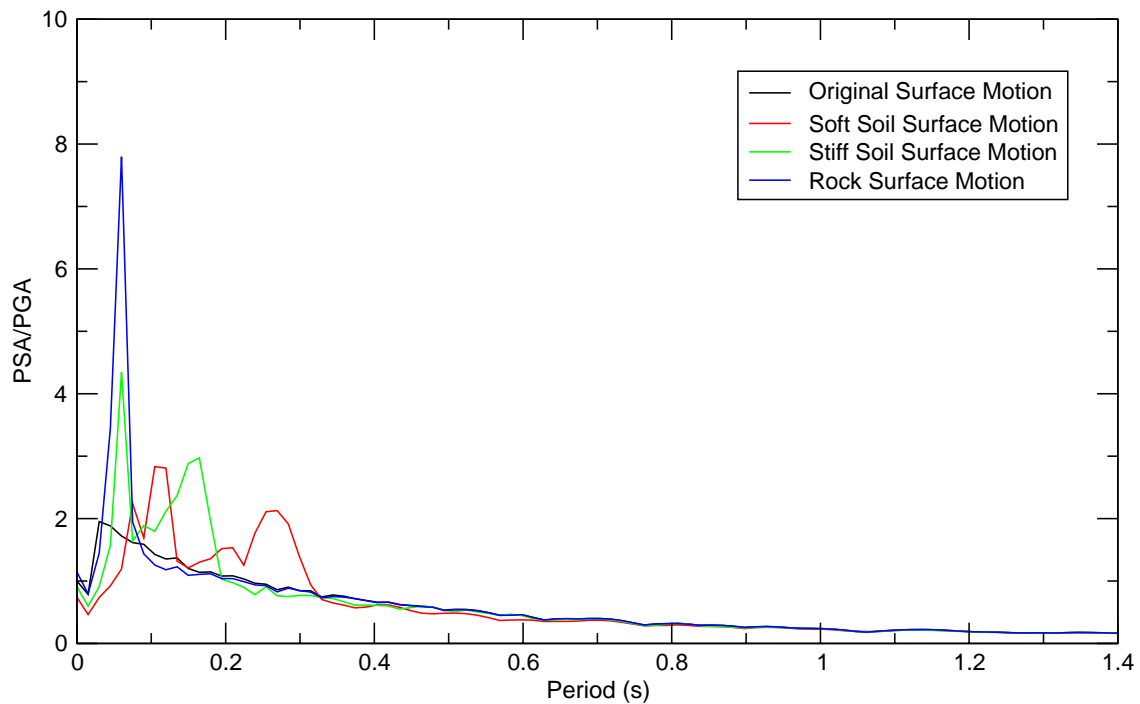


Figure IV.30: Comparison of Original Surface Motion and Motion at Top of Soil Column Model, NUREG/CR-6728 Spectral Shape, Case E Earthquake, Vertical Component

## **Appendix V: Complete Parametric Cask Analysis Results**



## Appendix V: Complete Parametric Cask Analysis Results

A complete summary of the parametric cask analysis results is provided in this appendix. This presentation is split in two parts. In Section V.1, the response of the cylindrical cask and rectangular module under all of the conditions considered in this study is presented in tabular form. A subset of this data is plotted graphically in Section V.2.

### V.1 Tabular Presentation of Results

Separate tables are provided in this section to show the cask response in terms of three key parameters: peak horizontal cask top displacement relative to the pad, peak cask rotation, and peak horizontal cask bottom displacement relative to the pad. Initially, all cask analyses were run at a number of pre-determined levels of peak ground acceleration (PGA). In cases where the cask tipped over, additional analyses were performed at more refined increments of PGA to better define the point at which the cask first tips over. This was done only for selected analysis cases, so in the tables there are a number of combinations of parameters for which analyses were not run. These cases are denoted in the tables with “---”. In the cases when the cask overturns, the peak cask displacements and rotations are no longer meaningful. Thus, these cases are denoted as “Tips”, and the cells are black to highlight these cases.

Because of the nonlinear nature of the cask behavior, the peak cask response does not always increase monotonically with increasing ground motion. In a few cases, the cask overturned at a given level of ground motion, but did not overturn at a higher level of ground motion. The results for these cases are reported, but there is an asterisk “\*” to the right of the result in the tables to denote these special cases.

Table V.1: Peak Cask Top Displacements (m), Cylindrical Cask, NUREG/CR-0098 Earthquakes

		Soft Soil			Stiff Soil			Rock		
		$\mu=0.2$	$\mu=0.55$	$\mu=0.8$	$\mu=0.2$	$\mu=0.55$	$\mu=0.8$	$\mu=0.2$	$\mu=0.55$	$\mu=0.8$
Case 1	0.25g	0.008	0.003	0.003	0.003	0.002	0.002	0.005	0.002	0.002
	0.60g	0.106	0.399	0.377	0.091	0.291	1.087	0.103	1.627	0.193
	1.00g	0.288	2.312	2.451	0.357	1.901	2.281	0.363	1.250	1.347
	1.10g	---	2.269	---	---	---	---	---	---	1.400
	1.25g	0.460	Tips	2.459	0.515	1.257	1.079	0.530	2.577	Tips
Case 2	0.25g	0.008	0.004	0.004	0.004	0.002	0.002	0.005	0.003	0.004
	0.60g	0.085	0.104	0.091	0.101	0.120	0.137	0.101	0.301	0.721
	0.80g	---	---	1.431	---	---	1.327	---	---	---
	0.90g	---	---	1.175	---	---	0.367	---	---	---
	1.00g	0.175	0.439	Tips	0.289	0.689	Tips	0.313	1.603	1.162
	1.10g	---	---	Tips	---	---	1.290*	---	---	1.852
	1.25g	0.267	2.718	Tips	0.415	0.642	2.458*	0.512	1.381	Tips
Case 3	0.25g	0.012	0.004	0.004	0.004	0.002	0.002	0.005	0.005	0.006
	0.60g	0.085	0.286	0.126	0.037	0.241	0.431	0.057	0.343	0.459
	1.00g	0.162	0.492	0.445	0.165	0.565	1.006	0.160	0.901	1.071
	1.10g	---	---	2.523	---	---	---	---	---	---
	1.25g	0.273	3.204	Tips	0.299	2.279	1.752	0.273	2.803	2.276
Case 4	0.25g	0.009	0.003	0.003	0.002	0.001	0.001	0.003	0.002	0.002
	0.60g	0.073	0.079	0.074	0.048	0.025	0.250	0.054	0.154	0.191
	1.00g	0.228	1.084	0.881	0.204	0.304	0.849	0.196	0.945	0.577
	1.25g	0.304	1.227	0.908	0.300	0.672	0.986	0.316	2.029	0.818
Case 5	0.25g	0.013	0.004	0.004	0.005	0.002	0.002	0.005	0.003	0.003
	0.60g	0.065	0.165	0.298	0.064	0.113	0.335	0.101	0.972	0.528
	1.00g	0.178	0.734	0.332	0.162	0.562	2.591	0.162	2.712	0.442
	1.10g	---	---	---	---	---	Tips	---	---	---
	1.25g	0.291	0.726	2.730	0.237	2.530	Tips	0.241	0.704	3.260

Table V.2: Peak Cask Top Displacements (m), Cylindrical Cask, Regulatory Guide 1.60 Earthquakes

		Soft Soil			Stiff Soil			Rock		
		$\mu=0.2$	$\mu=0.55$	$\mu=0.8$	$\mu=0.2$	$\mu=0.55$	$\mu=0.8$	$\mu=0.2$	$\mu=0.55$	$\mu=0.8$
Case 1	0.25g	0.034	0.007	0.006	0.009	0.001	0.001	0.012	0.003	0.008
	0.40g	0.116	0.351	0.426	0.100	0.206	0.345	0.109	0.456	1.116
	0.50g	0.211	1.134	1.114	0.225	1.362	1.217	0.239	0.856	2.417
	0.55g	---	---	2.082	---	---	2.221	---	---	---
	0.60g	0.356	2.464	Tips	0.397	1.905	Tips	0.409	2.099	2.433
	0.80g	---	Tips	2.425*	---	1.052	2.069*	---	1.591	2.057
	1.00g	1.105	Tips	Tips	1.162	Tips	Tips	1.150	Tips	Tips
Case 2	0.25g	0.040	0.026	0.029	0.026	0.003	0.003	0.027	0.008	0.021
	0.40g	0.103	0.077	0.304	0.112	0.096	0.355	0.113	0.084	0.076
	0.50g	0.120	0.356	0.145	0.187	0.615	0.194	0.199	0.234	0.262
	0.60g	0.162	0.331	2.009	0.269	0.777	1.374	0.264	1.396	1.736
	0.80g	---	Tips	0.946	---	1.933	Tips	---	Tips	---
	1.00g	0.406	Tips	Tips	0.488	Tips	Tips	0.568	Tips	2.758
Case 3	0.25g	0.041	0.010	0.009	0.012	0.002	0.002	0.012	0.008	0.008
	0.40g	0.092	0.065	0.067	0.031	0.338	0.393	0.059	0.125	0.672
	0.50g	0.129	0.837	0.732	0.065	1.422	0.716	0.114	0.180	0.667
	0.60g	0.166	0.873	3.097	0.144	1.560	1.007	0.185	0.897	1.918
	0.80g	---	1.410	Tips	---	1.526	1.437	---	Tips	2.882
	1.00g	0.757	Tips	Tips	0.712	Tips	Tips	0.728	Tips	Tips
Case 4	0.25g	0.118	0.259	0.299	0.013	0.002	0.002	0.016	0.006	0.008
	0.40g	0.264	0.497	0.889	0.076	0.141	0.473	0.092	0.036	0.858
	0.50g	0.349	0.542	0.671	0.164	0.386	0.178	0.186	0.405	0.651
	0.60g	0.427	0.587	1.062	0.291	0.270	0.809	0.319	0.415	0.850
	0.80g	---	---	3.484	---	1.405	Tips	---	---	0.818
	1.00g	1.169	2.081	Tips	0.716	Tips	Tips	0.802	1.114	Tips
Case 5	0.25g	0.031	0.006	0.006	0.018	0.002	0.002	0.019	0.004	0.004
	0.40g	0.085	0.397	0.479	0.073	0.473	0.432	0.100	0.510	0.444
	0.50g	0.138	0.610	0.194	0.119	0.681	1.377	0.138	0.446	0.484
	0.60g	0.198	0.582	0.395	0.177	0.686	0.506	0.190	0.461	1.200
	0.80g	---	Tips	Tips	---	Tips	Tips	---	1.861	Tips
	1.00g	0.765	Tips	Tips	0.558	Tips	Tips	0.588	Tips	Tips

Table V.3: Peak Cask Top Displacements (m), Cylindrical Cask, NUREG/CR-6728 Earthquakes

		Soft Soil			Stiff Soil			Rock		
		$\mu=0.2$	$\mu=0.55$	$\mu=0.8$	$\mu=0.2$	$\mu=0.55$	$\mu=0.8$	$\mu=0.2$	$\mu=0.55$	$\mu=0.8$
Case A	0.25g	0.018	0.006	0.006	0.005	0.003	0.003	0.006	0.008	0.008
	0.60g	0.037	0.052	0.055	0.038	0.074	0.060	0.036	0.097	0.222
	1.00g	0.111	0.310	0.229	0.122	0.598	0.568	0.124	0.323	0.303
	1.25g	0.189	0.223	0.239	0.177	0.254	0.333	0.182	0.279	0.316
Case B	0.25g	0.008	0.006	0.006	0.004	0.004	0.004	0.004	0.009	0.006
	0.60g	0.049	0.082	0.157	0.029	0.050	0.348	0.027	0.069	0.053
	1.00g	0.095	0.314	0.546	0.072	0.358	0.381	0.075	0.142	0.352
	1.25g	0.141	0.210	0.473	0.096	0.348	0.530	0.097	0.310	0.279
Case C	0.25g	0.013	0.005	0.005	0.005	0.004	0.004	0.007	0.007	0.016
	0.60g	0.073	0.130	0.037	0.026	0.088	0.051	0.025	0.084	0.128
	1.00g	0.114	0.360	0.342	0.087	0.518	0.227	0.078	0.383	0.649
	1.25g	0.144	0.216	0.555	0.127	0.830	0.759	0.113	0.739	0.510
Case D	0.25g	0.012	0.004	0.004	0.004	0.002	0.002	0.003	0.005	0.005
	0.60g	0.027	0.040	0.046	0.034	0.045	0.073	0.025	0.050	0.061
	1.00g	0.072	0.134	0.107	0.095	0.221	0.622	0.049	0.216	0.175
	1.25g	0.101	0.117	0.139	0.156	0.258	0.307	0.066	0.228	0.320
Case E	0.25g	0.016	0.006	0.006	0.005	0.003	0.003	0.005	0.008	0.009
	0.60g	0.061	0.073	0.081	0.032	0.207	0.076	0.034	0.107	0.212
	1.00g	0.141	0.122	0.140	0.088	0.174	0.200	0.101	0.531	0.098
	1.25g	0.174	0.149	0.096	0.148	0.421	0.545	0.151	0.192	0.801

Table V.4: Peak Cask Top Displacements (m), Rectangular Module, NUREG/CR-0098 Earthquakes

		Soft Soil			Stiff Soil			Rock		
		$\mu=0.2$	$\mu=0.55$	$\mu=0.8$	$\mu=0.2$	$\mu=0.55$	$\mu=0.8$	$\mu=0.2$	$\mu=0.55$	$\mu=0.8$
Case 1	0.25g	0.004	0.001	0.001	0.001	0.000	0.000	0.001	0.001	0.001
	0.60g	0.113	0.011	0.004	0.094	0.001	0.001	0.108	0.004	0.002
	1.00g	0.299	0.086	0.084	0.362	0.034	0.037	0.355	0.079	0.027
	1.25g	0.474	0.166	0.128	0.513	0.116	0.135	0.524	0.169	0.096
Case 2	0.25g	0.008	0.001	0.001	0.002	0.000	0.000	0.002	0.000	0.000
	0.60g	0.086	0.015	0.005	0.103	0.007	0.005	0.102	0.006	0.002
	1.00g	0.187	0.133	0.086	0.274	0.094	0.078	0.300	0.073	0.042
	1.25g	0.295	0.218	0.136	0.414	0.186	0.111	0.467	0.136	0.139
Case 3	0.25g	0.004	0.001	0.001	0.002	0.000	0.000	0.003	0.000	0.000
	0.60g	0.092	0.011	0.015	0.031	0.003	0.002	0.061	0.007	0.002
	1.00g	0.176	0.130	0.067	0.146	0.025	0.033	0.178	0.042	0.056
	1.25g	0.251	0.217	0.109	0.278	0.057	0.101	0.281	0.089	0.095
Case 4	0.25g	0.004	0.000	0.000	0.001	0.000	0.000	0.001	0.000	0.000
	0.60g	0.067	0.009	0.002	0.046	0.001	0.001	0.056	0.006	0.001
	1.00g	0.236	0.083	0.065	0.211	0.045	0.054	0.215	0.069	0.057
	1.25g	0.319	0.117	0.096	0.314	0.109	0.102	0.314	0.154	0.104
Case 5	0.25g	0.007	0.001	0.001	0.003	0.000	0.000	0.004	0.000	0.000
	0.60g	0.060	0.017	0.005	0.062	0.006	0.003	0.095	0.006	0.003
	1.00g	0.163	0.085	0.091	0.160	0.080	0.041	0.164	0.078	0.043
	1.25g	0.270	0.113	0.236	0.234	0.142	0.123	0.243	0.177	0.082

Table V.5: Peak Cask Top Displacements (m), Rectangular Module, Regulatory Guide 1.60 Earthquakes

		Soft Soil			Stiff Soil			Rock		
		$\mu=0.2$	$\mu=0.55$	$\mu=0.8$	$\mu=0.2$	$\mu=0.55$	$\mu=0.8$	$\mu=0.2$	$\mu=0.55$	$\mu=0.8$
Case 1	0.25g	0.032	0.001	0.001	0.006	0.000	0.000	0.009	0.000	0.000
	0.60g	0.359	0.074	0.070	0.393	0.031	0.010	0.411	0.048	0.010
	1.00g	1.124	0.225	0.211	1.114	0.226	0.130	1.134	0.202	0.147
	1.25g	1.706	0.425	0.189	1.696	0.457	0.345	1.679	0.389	0.384
Case 2	0.25g	0.038	0.001	0.001	0.023	0.000	0.000	0.020	0.000	0.000
	0.60g	0.167	0.093	0.041	0.249	0.052	0.031	0.261	0.043	0.029
	1.00g	0.470	0.293	0.151	0.541	0.307	0.258	0.523	0.245	0.112
	1.25g	0.712	0.362	0.273	0.615	0.441	0.211	0.576	0.404	0.299
Case 3	0.25g	0.021	0.001	0.001	0.006	0.000	0.000	0.009	0.000	0.000
	0.60g	0.169	0.081	0.023	0.141	0.013	0.040	0.194	0.019	0.007
	1.00g	0.702	0.243	0.145	0.749	0.125	0.162	0.816	0.160	0.128
	1.25g	1.105	0.373	0.361	1.091	0.287	0.250	1.169	0.319	0.226
Case 4	0.25g	0.130	0.070	0.119	0.009	0.000	0.000	0.011	0.000	0.000
	0.60g	0.411	0.290	0.383	0.291	0.038	0.016	0.312	0.050	0.018
	1.00g	0.978	0.572	0.627	0.767	0.295	0.231	0.832	0.230	0.123
	1.25g	1.462	0.703	0.830	0.835	0.416	0.452	1.142	0.566	0.323
Case 5	0.25g	0.024	0.001	0.001	0.016	0.000	0.000	0.014	0.000	0.000
	0.60g	0.182	0.060	0.084	0.170	0.048	0.022	0.184	0.040	0.012
	1.00g	0.729	0.187	0.289	0.554	0.171	0.317	0.595	0.259	0.185
	1.25g	1.245	0.310	0.641	1.428	0.302	0.473	1.093	0.322	0.307

Table V.6: Peak Cask Top Displacements (m), Rectangular Module, NUREG/CR-6728 Earthquakes

		Soft Soil			Stiff Soil			Rock		
		$\mu=0.2$	$\mu=0.55$	$\mu=0.8$	$\mu=0.2$	$\mu=0.55$	$\mu=0.8$	$\mu=0.2$	$\mu=0.55$	$\mu=0.8$
Case A	0.25g	0.006	0.001	0.001	0.002	0.000	0.000	0.004	0.001	0.001
	0.60g	0.030	0.014	0.009	0.039	0.004	0.004	0.046	0.010	0.009
	1.00g	0.099	0.072	0.051	0.120	0.033	0.021	0.138	0.039	0.033
	1.25g	0.175	0.106	0.070	0.177	0.055	0.053	0.201	0.062	0.041
Case B	0.25g	0.003	0.001	0.001	0.004	0.000	0.000	0.007	0.001	0.001
	0.60g	0.036	0.006	0.006	0.023	0.012	0.007	0.027	0.016	0.017
	1.00g	0.102	0.027	0.044	0.072	0.045	0.035	0.070	0.048	0.039
	1.25g	0.133	0.067	0.056	0.099	0.049	0.058	0.091	0.039	0.043
Case C	0.25g	0.004	0.001	0.001	0.004	0.000	0.000	0.004	0.001	0.001
	0.60g	0.066	0.009	0.008	0.024	0.008	0.008	0.031	0.016	0.010
	1.00g	0.130	0.054	0.034	0.069	0.048	0.020	0.089	0.026	0.027
	1.25g	0.151	0.087	0.045	0.111	0.057	0.046	0.101	0.070	0.061
Case D	0.25g	0.005	0.001	0.001	0.002	0.000	0.000	0.002	0.001	0.001
	0.60g	0.038	0.009	0.005	0.025	0.005	0.004	0.022	0.004	0.004
	1.00g	0.093	0.055	0.027	0.087	0.035	0.029	0.080	0.020	0.025
	1.25g	0.114	0.057	0.041	0.149	0.061	0.047	0.257	0.065	0.038
Case E	0.25g	0.009	0.001	0.001	0.003	0.000	0.000	0.003	0.002	0.001
	0.60g	0.051	0.021	0.022	0.033	0.011	0.007	0.042	0.013	0.010
	1.00g	0.135	0.067	0.043	0.089	0.032	0.028	0.078	0.020	0.033
	1.25g	0.186	0.107	0.050	0.143	0.060	0.052	0.154	0.056	0.063

Table V.7: Peak Cask Rotations (deg), Cylindrical Cask, NUREG/CR-0098 Earthquakes

		Soft Soil			Stiff Soil			Rock		
		$\mu=0.2$	$\mu=0.55$	$\mu=0.8$	$\mu=0.2$	$\mu=0.55$	$\mu=0.8$	$\mu=0.2$	$\mu=0.55$	$\mu=0.8$
Case 1	0.25g	0.034	0.007	0.006	0.009	0.001	0.001	0.012	0.003	0.008
	0.40g	0.116	0.351	0.426	0.100	0.206	0.345	0.109	0.456	1.116
	0.50g	0.211	1.134	1.114	0.225	1.362	1.217	0.239	0.856	2.417
	0.55g	---	---	2.082	---	---	2.221	---	---	---
	0.60g	0.356	2.464	Tips	0.397	1.905	Tips	0.409	2.099	2.433
	0.80g	---	Tips	2.425*	---	1.052	2.069*	---	1.591	2.057
	1.00g	1.105	Tips	Tips	1.162	Tips	Tips	1.150	Tips	Tips
Case 2	0.25g	0.040	0.026	0.029	0.026	0.003	0.003	0.027	0.008	0.021
	0.40g	0.103	0.077	0.304	0.112	0.096	0.355	0.113	0.084	0.076
	0.50g	0.120	0.356	0.145	0.187	0.615	0.194	0.199	0.234	0.262
	0.60g	0.162	0.331	2.009	0.269	0.777	1.374	0.264	1.396	1.736
	0.80g	---	Tips	0.946	---	1.933	Tips	---	Tips	---
	1.00g	0.406	Tips	Tips	0.488	Tips	Tips	0.568	Tips	2.758
	Case 3	0.25g	0.041	0.010	0.009	0.012	0.002	0.002	0.012	0.008
0.40g		0.092	0.065	0.067	0.031	0.338	0.393	0.059	0.125	0.672
0.50g		0.129	0.837	0.732	0.065	1.422	0.716	0.114	0.180	0.667
0.60g		0.166	0.873	3.097	0.144	1.560	1.007	0.185	0.897	1.918
0.80g		---	1.410	Tips	---	1.526	1.437	---	Tips	2.882
1.00g		0.757	Tips	Tips	0.712	Tips	Tips	0.728	Tips	Tips
Case 4	0.25g	0.118	0.259	0.299	0.013	0.002	0.002	0.016	0.006	0.008
	0.40g	0.264	0.497	0.889	0.076	0.141	0.473	0.092	0.036	0.858
	0.50g	0.349	0.542	0.671	0.164	0.386	0.178	0.186	0.405	0.651
	0.60g	0.427	0.587	1.062	0.291	0.270	0.809	0.319	0.415	0.850
	0.80g	---	---	3.484	---	1.405	Tips	---	---	0.818
	1.00g	1.169	2.081	Tips	0.716	Tips	Tips	0.802	1.114	Tips
Case 5	0.25g	0.031	0.006	0.006	0.018	0.002	0.002	0.019	0.004	0.004
	0.40g	0.085	0.397	0.479	0.073	0.473	0.432	0.100	0.510	0.444
	0.50g	0.138	0.610	0.194	0.119	0.681	1.377	0.138	0.446	0.484
	0.60g	0.198	0.582	0.395	0.177	0.686	0.506	0.190	0.461	1.200
	0.80g	---	Tips	Tips	---	Tips	Tips	---	1.861	Tips
	1.00g	0.765	Tips	Tips	0.558	Tips	Tips	0.588	Tips	Tips

Table V.8: Peak Cask Rotations (deg), Cylindrical Cask, Regulatory Guide 1.60 Earthquakes

		Soft Soil			Stiff Soil			Rock		
		$\mu=0.2$	$\mu=0.55$	$\mu=0.8$	$\mu=0.2$	$\mu=0.55$	$\mu=0.8$	$\mu=0.2$	$\mu=0.55$	$\mu=0.8$
Case 1	0.25g	0.02	0.05	0.05	0.01	0.01	0.01	0.01	0.03	0.06
	0.40g	0.02	1.87	3.87	0.01	1.92	2.91	0.01	3.08	9.20
	0.50g	0.03	6.40	6.79	0.01	7.37	7.79	0.01	7.29	18.02
	0.55g	---	---	15.65	---	---	16.78	---	---	---
	0.60g	0.03	16.24	Tips	0.01	13.92	Tips	0.01	12.68	16.67
	0.80g	---	Tips	21.77*	---	9.35	21.42*	---	14.70	19.02
	1.00g	0.22	Tips	Tips	0.77	Tips	Tips	0.02	Tips	Tips
Case 2	0.25g	0.02	0.20	0.23	0.01	0.03	0.03	0.01	0.05	0.18
	0.40g	0.03	0.55	2.44	0.01	0.82	2.53	0.01	0.65	0.79
	0.50g	0.03	1.83	1.02	0.01	4.93	1.41	0.02	1.26	2.17
	0.60g	0.03	2.28	16.11	0.02	7.73	9.21	0.02	11.92	17.24
	0.80g	---	Tips	7.55	---	14.52	Tips	---	Tips	---
	1.00g	0.10	Tips	Tips	0.40	Tips	Tips	0.19	Tips	21.68
	Case 3	0.25g	0.02	0.09	0.09	0.01	0.02	0.02	0.01	0.08
0.40g		0.03	0.59	0.44	0.01	2.70	3.67	0.01	0.97	4.41
0.50g		0.03	6.61	5.37	0.01	12.74	5.29	0.01	1.45	4.70
0.60g		0.04	5.84	19.77	0.01	9.00	8.60	0.02	4.75	20.13
0.80g		---	12.17	Tips	---	11.69	12.27	---	Tips	23.55
1.00g		0.12	Tips	Tips	0.02	Tips	Tips	0.23	Tips	Tips
Case 4		0.25g	0.03	1.40	2.10	0.01	0.02	0.02	0.01	0.05
	0.40g	0.03	2.06	8.08	0.01	1.17	4.09	0.02	0.29	7.04
	0.50g	0.03	4.11	5.56	0.01	2.95	1.54	0.01	3.00	5.17
	0.60g	0.03	4.66	7.98	0.02	2.12	5.33	0.02	4.08	6.33
	0.80g	---	---	24.70	---	8.22	Tips	---	---	4.63
	1.00g	0.12	17.24	Tips	0.08	Tips	Tips	0.29	8.16	Tips
	Case 5	0.25g	0.02	0.06	0.06	0.01	0.02	0.02	0.01	0.03
0.40g		0.02	3.40	4.20	0.01	3.46	3.99	0.01	4.22	4.53
0.50g		0.03	3.80	1.60	0.01	4.87	12.50	0.01	3.49	4.00
0.60g		0.03	3.71	3.39	0.01	3.40	3.03	0.02	3.69	10.64
0.80g		---	Tips	Tips	---	Tips	Tips	---	15.14	Tips
1.00g		0.22	Tips	Tips	0.09	Tips	Tips	0.05	Tips	Tips

Table V.9: Peak Cask Rotations (deg), Cylindrical Cask, NUREG/CR-6728 Earthquakes

		Soft Soil			Stiff Soil			Rock		
		$\mu=0.2$	$\mu=0.55$	$\mu=0.8$	$\mu=0.2$	$\mu=0.55$	$\mu=0.8$	$\mu=0.2$	$\mu=0.55$	$\mu=0.8$
Case A	0.25g	0.02	0.05	0.05	0.01	0.03	0.03	0.01	0.07	0.07
	0.60g	0.03	0.32	0.38	0.01	0.66	0.59	0.02	0.53	1.67
	1.00g	0.04	2.14	2.01	0.01	4.74	4.45	0.11	1.69	2.18
	1.25g	0.05	1.81	2.48	0.01	2.00	3.02	0.11	2.09	2.84
Case B	0.25g	0.02	0.06	0.05	0.01	0.04	0.04	0.01	0.06	0.05
	0.60g	0.03	0.60	1.39	0.01	0.48	2.97	0.08	0.54	0.29
	1.00g	0.04	2.79	4.19	0.02	1.85	3.25	0.23	0.79	2.84
	1.25g	0.04	1.66	3.24	0.04	2.96	4.17	0.26	2.81	2.15
Case C	0.25g	0.02	0.05	0.04	0.01	0.03	0.03	0.01	0.05	0.13
	0.60g	0.03	1.19	0.32	0.01	0.67	0.55	0.02	0.80	0.94
	1.00g	0.03	3.16	3.50	0.02	3.84	1.78	0.13	3.55	5.80
	1.25g	0.06	1.10	4.01	0.04	7.07	5.11	0.30	4.67	4.34
Case D	0.25g	0.02	0.04	0.04	0.01	0.02	0.02	0.01	0.04	0.04
	0.60g	0.02	0.37	0.44	0.01	0.36	0.67	0.02	0.44	0.45
	1.00g	0.03	0.51	0.66	0.02	2.01	5.43	0.16	1.81	1.45
	1.25g	0.04	0.95	1.38	0.03	2.02	2.66	0.25	1.91	2.30
Case E	0.25g	0.02	0.05	0.05	0.01	0.02	0.02	0.01	0.07	0.08
	0.60g	0.03	0.55	0.70	0.01	1.78	0.57	0.01	0.84	1.71
	1.00g	0.03	0.62	1.37	0.03	1.63	1.83	0.14	4.35	0.93
	1.25g	0.04	1.05	1.07	0.05	3.42	4.60	0.23	1.32	6.14

Table V.10: Peak Cask Rotations (deg), Rectangular Module, NUREG/CR-0098 Earthquakes

		Soft Soil			Stiff Soil			Rock		
		$\mu=0.2$	$\mu=0.55$	$\mu=0.8$	$\mu=0.2$	$\mu=0.55$	$\mu=0.8$	$\mu=0.2$	$\mu=0.55$	$\mu=0.8$
Case 1	0.25g	0.00	0.00	0.01	0.00	0.00	0.00	0.00	0.01	0.01
	0.60g	0.01	0.02	0.04	0.00	0.00	0.01	0.00	0.01	0.01
	1.00g	0.01	0.03	0.71	0.00	0.01	0.30	0.00	0.06	0.26
	1.25g	0.01	0.12	1.17	0.00	0.01	1.23	0.00	0.06	0.69
Case 2	0.25g	0.00	0.01	0.01	0.00	0.00	0.00	0.00	0.00	0.00
	0.60g	0.01	0.02	0.04	0.00	0.01	0.04	0.00	0.01	0.02
	1.00g	0.01	0.03	0.55	0.00	0.03	0.72	0.00	0.03	0.32
	1.25g	0.01	0.07	1.18	0.00	0.05	0.87	0.00	0.02	1.15
Case 3	0.25g	0.00	0.01	0.01	0.00	0.00	0.00	0.00	0.00	0.00
	0.60g	0.01	0.04	0.12	0.00	0.01	0.02	0.00	0.01	0.02
	1.00g	0.01	0.18	0.55	0.00	0.02	0.35	0.00	0.02	0.50
	1.25g	0.01	0.21	0.86	0.00	0.03	0.79	0.00	0.03	0.68
Case 4	0.25g	0.00	0.00	0.00	0.00	0.00	0.00	0.00	0.00	0.00
	0.60g	0.01	0.01	0.02	0.00	0.00	0.01	0.00	0.01	0.01
	1.00g	0.01	0.02	0.55	0.00	0.01	0.30	0.00	0.02	0.28
	1.25g	0.01	0.03	0.81	0.00	0.01	0.95	0.01	0.29	0.80
Case 5	0.25g	0.00	0.01	0.01	0.00	0.00	0.00	0.00	0.00	0.00
	0.60g	0.01	0.02	0.04	0.00	0.01	0.02	0.00	0.01	0.03
	1.00g	0.01	0.09	0.71	0.00	0.02	0.26	0.00	0.02	0.32
	1.25g	0.01	0.17	1.85	0.00	0.05	1.37	0.00	0.10	0.79

Table V.11: Peak Cask Rotations (deg), Rectangular Module, Regulatory Guide 1.60 Earthquakes

		Soft Soil			Stiff Soil			Rock		
		$\mu=0.2$	$\mu=0.55$	$\mu=0.8$	$\mu=0.2$	$\mu=0.55$	$\mu=0.8$	$\mu=0.2$	$\mu=0.55$	$\mu=0.8$
Case 1	0.25g	0.01	0.01	0.01	0.00	0.00	0.00	0.00	0.00	0.00
	0.60g	0.01	0.02	0.68	0.00	0.01	0.04	0.00	0.01	0.06
	1.00g	0.04	0.17	1.86	0.10	0.16	1.06	0.00	0.06	1.16
	1.25g	0.52	1.37	1.49	1.12	0.34	2.23	0.05	0.65	1.83
Case 2	0.25g	0.00	0.01	0.01	0.00	0.00	0.00	0.00	0.00	0.00
	0.60g	0.01	0.02	0.23	0.00	0.01	0.30	0.00	0.03	0.27
	1.00g	0.05	0.08	1.48	0.08	0.07	2.45	0.01	0.06	0.96
	1.25g	0.09	0.24	2.59	0.15	0.10	1.78	0.07	0.15	2.39
Case 3	0.25g	0.00	0.01	0.01	0.00	0.00	0.00	0.00	0.00	0.00
	0.60g	0.01	0.12	0.18	0.00	0.01	0.40	0.00	0.01	0.05
	1.00g	0.09	0.24	1.18	0.01	0.03	1.24	0.02	0.11	1.04
	1.25g	0.25	0.98	3.17	0.04	0.07	1.88	0.05	0.27	2.00
Case 4	0.25g	0.01	0.24	1.13	0.00	0.00	0.00	0.00	0.00	0.00
	0.60g	0.01	1.90	3.65	0.00	0.01	0.05	0.00	0.01	0.04
	1.00g	0.02	3.54	5.63	0.02	0.06	1.91	0.02	0.13	0.67
	1.25g	0.13	5.18	6.96	0.38	0.48	4.68	0.14	0.66	2.20
Case 5	0.25g	0.00	0.01	0.01	0.00	0.00	0.00	0.00	0.00	0.00
	0.60g	0.01	0.07	0.65	0.00	0.01	0.14	0.00	0.02	0.11
	1.00g	0.07	0.28	2.70	0.03	0.07	3.43	0.01	0.11	2.08
	1.25g	0.46	0.53	5.34	0.39	1.09	4.21	0.09	0.23	3.04

Table V.12: Peak Cask Rotations (deg), Rectangular Module, NUREG/CR-6728 Earthquakes

		Soft Soil			Stiff Soil			Rock		
		$\mu=0.2$	$\mu=0.55$	$\mu=0.8$	$\mu=0.2$	$\mu=0.55$	$\mu=0.8$	$\mu=0.2$	$\mu=0.55$	$\mu=0.8$
Case A	0.25g	0.00	0.01	0.01	0.00	0.00	0.00	0.00	0.01	0.01
	0.60g	0.01	0.02	0.09	0.00	0.02	0.03	0.00	0.03	0.08
	1.00g	0.01	0.03	0.33	0.00	0.04	0.19	0.00	0.05	0.29
	1.25g	0.01	0.05	0.69	0.00	0.09	0.48	0.01	0.10	0.36
Case B	0.25g	0.01	0.01	0.01	0.00	0.00	0.00	0.00	0.01	0.01
	0.60g	0.01	0.02	0.06	0.00	0.04	0.06	0.00	0.02	0.11
	1.00g	0.01	0.07	0.41	0.00	0.08	0.26	0.09	0.10	0.41
	1.25g	0.01	0.17	0.56	0.00	0.12	0.31	0.11	0.18	0.37
Case C	0.25g	0.00	0.01	0.01	0.00	0.00	0.00	0.00	0.01	0.01
	0.60g	0.01	0.03	0.08	0.00	0.01	0.06	0.00	0.02	0.07
	1.00g	0.01	0.15	0.34	0.00	0.04	0.20	0.04	0.12	0.12
	1.25g	0.01	0.18	0.38	0.01	0.05	0.29	0.17	0.16	0.32
Case D	0.25g	0.00	0.01	0.01	0.00	0.00	0.00	0.00	0.01	0.01
	0.60g	0.01	0.02	0.04	0.00	0.01	0.03	0.00	0.01	0.03
	1.00g	0.01	0.07	0.26	0.00	0.03	0.14	0.01	0.08	0.15
	1.25g	0.01	0.09	0.32	0.00	0.04	0.21	0.15	0.21	0.32
Case E	0.25g	0.01	0.01	0.01	0.00	0.00	0.00	0.00	0.01	0.01
	0.60g	0.01	0.07	0.19	0.00	0.04	0.07	0.00	0.02	0.07
	1.00g	0.01	0.16	0.34	0.00	0.08	0.22	0.03	0.09	0.21
	1.25g	0.01	0.29	0.39	0.00	0.09	0.45	0.06	0.14	0.59

Table V.13: Peak Cask Bottom Displacements (m), Cylindrical Cask, NUREG/CR-0098 Earthquakes

		Soft Soil			Stiff Soil			Rock		
		$\mu=0.2$	$\mu=0.55$	$\mu=0.8$	$\mu=0.2$	$\mu=0.55$	$\mu=0.8$	$\mu=0.2$	$\mu=0.55$	$\mu=0.8$
Case 1	0.25g	0.007	0.001	0.001	0.003	0.000	0.001	0.004	0.001	0.001
	0.60g	0.105	0.231	0.179	0.090	0.162	0.219	0.103	1.137	0.101
	1.00g	0.288	1.337	1.325	0.357	0.706	1.556	0.363	0.701	0.286
	1.10g	---	1.092	---	---	---	---	---	---	0.326
	1.25g	0.460	Tips	1.577	0.515	0.596	0.540	0.530	0.908	Tips
Case 2	0.25g	0.007	0.001	0.001	0.004	0.000	0.001	0.005	0.001	0.002
	0.60g	0.085	0.049	0.051	0.101	0.063	0.061	0.101	0.129	0.234
	0.80g	---	---	0.271	---	---	0.412	---	---	---
	0.90g	---	---	0.429	---	---	0.100	---	---	---
	1.00g	0.174	0.364	Tips	0.289	0.253	Tips	0.313	0.473	0.400
	1.10g	---	---	Tips	---	---	0.68*	---	---	1.126
	1.25g	0.266	1.272	Tips	0.415	0.454	1.072*	0.512	0.880	Tips
Case 3	0.25g	0.011	0.001	0.001	0.003	0.000	0.001	0.005	0.001	0.002
	0.60g	0.084	0.141	0.035	0.037	0.121	0.118	0.057	0.119	0.162
	1.00g	0.162	0.316	0.211	0.164	0.236	0.524	0.160	0.755	0.479
	1.10g	---	---	1.491	---	---	---	---	---	---
	1.25g	0.272	1.241	Tips	0.299	0.590	0.560	0.273	1.307	1.029
Case 4	0.25g	0.007	0.000	0.000	0.002	0.000	0.000	0.002	0.001	0.001
	0.60g	0.073	0.027	0.029	0.047	0.008	0.051	0.054	0.082	0.064
	1.00g	0.228	0.687	0.519	0.204	0.130	0.550	0.193	0.364	0.333
	1.25g	0.304	0.727	0.552	0.300	0.337	0.471	0.320	0.731	0.350
Case 5	0.25g	0.012	0.000	0.001	0.005	0.001	0.001	0.005	0.001	0.002
	0.60g	0.064	0.058	0.151	0.063	0.048	0.185	0.101	0.338	0.226
	1.00g	0.178	0.379	0.123	0.162	0.385	1.053	0.162	1.192	0.119
	1.10g	---	---	---	---	---	Tips	---	---	---
	1.25g	0.291	0.406	1.009	0.237	0.984	Tips	0.241	0.535	1.290

Table V.14: Peak Cask Bottom Displacements (m), Cylindrical Cask, Regulatory Guide 1.60 Earthquakes

		Soft Soil			Stiff Soil			Rock		
		$\mu=0.2$	$\mu=0.55$	$\mu=0.8$	$\mu=0.2$	$\mu=0.55$	$\mu=0.8$	$\mu=0.2$	$\mu=0.55$	$\mu=0.8$
Case 1	0.25g	0.033	0.003	0.002	0.009	0.000	0.000	0.011	0.001	0.003
	0.40g	0.115	0.194	0.151	0.100	0.084	0.172	0.108	0.247	0.263
	0.50g	0.210	0.710	0.657	0.225	0.903	0.729	0.239	0.309	0.933
	0.55g	---	---	1.007	---	---	1.046	---	---	---
	0.60g	0.356	1.581	Tips	0.397	0.982	Tips	0.409	1.531	1.064
	0.80g	---	Tips	1.08*	---	0.292	0.610*	---	0.653	1.004
	1.00g	1.108	Tips	Tips	1.161	Tips	Tips	1.150	Tips	Tips
Case 2	0.25g	0.039	0.014	0.007	0.026	0.001	0.001	0.026	0.004	0.003
	0.40g	0.103	0.039	0.073	0.112	0.039	0.151	0.113	0.039	0.025
	0.50g	0.120	0.232	0.050	0.187	0.229	0.114	0.199	0.126	0.102
	0.60g	0.161	0.189	0.931	0.269	0.241	0.805	0.264	0.317	0.346
	0.80g	---	Tips	0.392	---	1.462	Tips	---	Tips	---
	1.00g	0.406	Tips	Tips	0.488	Tips	Tips	0.567	Tips	0.845
	Case 3	0.25g	0.040	0.004	0.003	0.012	0.001	0.001	0.011	0.003
0.40g		0.092	0.033	0.026	0.031	0.117	0.162	0.059	0.050	0.281
0.50g		0.128	0.441	0.373	0.065	0.404	0.261	0.114	0.097	0.375
0.60g		0.165	0.444	1.315	0.144	1.088	0.645	0.185	0.574	0.842
0.80g		---	0.717	Tips	---	0.816	0.589	---	Tips	1.307
1.00g		0.757	Tips	Tips	0.712	Tips	Tips	0.728	Tips	Tips
Case 4		0.25g	0.118	0.138	0.148	0.013	0.000	0.001	0.016	0.003
	0.40g	0.264	0.342	0.335	0.076	0.054	0.152	0.091	0.017	0.340
	0.50g	0.348	0.285	0.513	0.163	0.171	0.085	0.186	0.199	0.191
	0.60g	0.427	0.394	0.719	0.291	0.096	0.389	0.319	0.172	0.411
	0.80g	---	---	2.285	---	0.870	Tips	---	---	0.378
	1.00g	1.166	0.961	Tips	0.716	Tips	Tips	0.802	0.640	Tips
	Case 5	0.25g	0.031	0.002	0.002	0.018	0.001	0.001	0.019	0.002
0.40g		0.084	0.139	0.113	0.073	0.234	0.117	0.100	0.242	0.187
0.50g		0.138	0.298	0.096	0.119	0.408	0.388	0.138	0.197	0.219
0.60g		0.198	0.352	0.161	0.177	0.455	0.228	0.190	0.230	0.717
0.80g		---	Tips	Tips	---	Tips	Tips	---	0.638	Tips
1.00g		0.764	Tips	Tips	0.558	Tips	Tips	0.587	Tips	Tips

Table V.15: Peak Cask Bottom Displacements (m), Cylindrical Cask, NUREG/CR-6728 Earthquakes

		Soft Soil			Stiff Soil			Rock		
		$\mu=0.2$	$\mu=0.55$	$\mu=0.8$	$\mu=0.2$	$\mu=0.55$	$\mu=0.8$	$\mu=0.2$	$\mu=0.55$	$\mu=0.8$
Case A	0.25g	0.018	0.001	0.001	0.005	0.001	0.001	0.006	0.004	0.002
	0.60g	0.037	0.031	0.032	0.038	0.029	0.018	0.036	0.043	0.071
	1.00g	0.111	0.152	0.082	0.122	0.246	0.205	0.124	0.203	0.095
	1.25g	0.189	0.180	0.112	0.177	0.149	0.129	0.185	0.160	0.136
Case B	0.25g	0.008	0.001	0.001	0.004	0.001	0.001	0.004	0.006	0.003
	0.60g	0.049	0.054	0.067	0.029	0.018	0.079	0.026	0.019	0.037
	1.00g	0.095	0.151	0.201	0.072	0.219	0.146	0.072	0.100	0.161
	1.25g	0.140	0.110	0.263	0.096	0.181	0.183	0.096	0.145	0.156
Case C	0.25g	0.013	0.001	0.001	0.005	0.001	0.001	0.007	0.003	0.006
	0.60g	0.072	0.068	0.025	0.026	0.039	0.015	0.025	0.016	0.044
	1.00g	0.113	0.154	0.133	0.087	0.243	0.098	0.077	0.067	0.128
	1.25g	0.142	0.131	0.206	0.127	0.208	0.332	0.114	0.351	0.164
Case D	0.25g	0.011	0.001	0.001	0.004	0.000	0.000	0.003	0.001	0.001
	0.60g	0.026	0.019	0.018	0.034	0.017	0.023	0.024	0.015	0.023
	1.00g	0.071	0.122	0.094	0.095	0.047	0.161	0.047	0.079	0.069
	1.25g	0.099	0.106	0.127	0.156	0.085	0.178	0.073	0.110	0.168
Case E	0.25g	0.016	0.001	0.001	0.004	0.002	0.002	0.004	0.003	0.003
	0.60g	0.061	0.030	0.030	0.031	0.051	0.022	0.034	0.056	0.060
	1.00g	0.140	0.081	0.048	0.088	0.100	0.056	0.100	0.143	0.043
	1.25g	0.173	0.124	0.060	0.147	0.229	0.159	0.149	0.103	0.223

Table V.16: Peak Cask Bottom Displacements (m), Rectangular Module, NUREG/CR-0098 Earthquakes

		Soft Soil			Stiff Soil			Rock		
		$\mu=0.2$	$\mu=0.55$	$\mu=0.8$	$\mu=0.2$	$\mu=0.55$	$\mu=0.8$	$\mu=0.2$	$\mu=0.55$	$\mu=0.8$
Case 1	0.25g	0.004	0.000	0.000	0.001	0.000	0.000	0.001	0.000	0.000
	0.60g	0.113	0.010	0.001	0.094	0.001	0.000	0.108	0.004	0.001
	1.00g	0.299	0.085	0.019	0.362	0.034	0.019	0.355	0.079	0.015
	1.25g	0.474	0.165	0.057	0.513	0.116	0.031	0.524	0.169	0.041
Case 2	0.25g	0.008	0.000	0.000	0.002	0.000	0.000	0.001	0.000	0.000
	0.60g	0.086	0.014	0.000	0.103	0.007	0.003	0.102	0.006	0.001
	1.00g	0.187	0.133	0.037	0.274	0.093	0.026	0.300	0.071	0.024
	1.25g	0.295	0.217	0.046	0.414	0.186	0.031	0.467	0.135	0.041
Case 3	0.25g	0.004	0.000	0.000	0.002	0.000	0.000	0.003	0.000	0.000
	0.60g	0.091	0.010	0.002	0.031	0.003	0.000	0.061	0.007	0.001
	1.00g	0.176	0.129	0.038	0.146	0.024	0.008	0.178	0.042	0.018
	1.25g	0.251	0.215	0.034	0.278	0.057	0.025	0.281	0.088	0.037
Case 4	0.25g	0.004	0.000	0.000	0.001	0.000	0.000	0.001	0.000	0.000
	0.60g	0.066	0.008	0.000	0.046	0.001	0.000	0.056	0.005	0.001
	1.00g	0.236	0.083	0.033	0.211	0.044	0.037	0.215	0.068	0.057
	1.25g	0.319	0.116	0.026	0.314	0.109	0.071	0.314	0.154	0.060
Case 5	0.25g	0.007	0.000	0.000	0.003	0.000	0.000	0.003	0.000	0.000
	0.60g	0.060	0.016	0.002	0.062	0.006	0.001	0.095	0.005	0.002
	1.00g	0.163	0.085	0.047	0.160	0.080	0.018	0.164	0.077	0.024
	1.25g	0.270	0.113	0.087	0.234	0.141	0.042	0.243	0.177	0.042

Table V.17: Peak Cask Bottom Displacements (m), Rectangular Module, Regulatory Guide 1.60 Earthquakes

		Soft Soil			Stiff Soil			Rock		
		$\mu=0.2$	$\mu=0.55$	$\mu=0.8$	$\mu=0.2$	$\mu=0.55$	$\mu=0.8$	$\mu=0.2$	$\mu=0.55$	$\mu=0.8$
Case 1	0.25g	0.032	0.000	0.000	0.006	0.000	0.000	0.009	0.000	0.000
	0.60g	0.359	0.074	0.045	0.393	0.030	0.007	0.411	0.048	0.007
	1.00g	1.123	0.223	0.073	1.114	0.226	0.097	1.134	0.202	0.069
	1.25g	1.705	0.410	0.188	1.696	0.456	0.280	1.679	0.388	0.256
Case 2	0.25g	0.038	0.000	0.000	0.023	0.000	0.000	0.020	0.000	0.000
	0.60g	0.167	0.092	0.024	0.249	0.052	0.018	0.261	0.042	0.015
	1.00g	0.470	0.292	0.096	0.541	0.306	0.063	0.523	0.245	0.089
	1.25g	0.712	0.361	0.181	0.615	0.441	0.174	0.576	0.404	0.173
Case 3	0.25g	0.021	0.000	0.000	0.006	0.000	0.000	0.009	0.000	0.000
	0.60g	0.169	0.080	0.015	0.141	0.013	0.008	0.194	0.019	0.003
	1.00g	0.702	0.243	0.073	0.749	0.125	0.063	0.816	0.159	0.075
	1.25g	1.105	0.308	0.192	1.091	0.287	0.135	1.169	0.319	0.144
Case 4	0.25g	0.130	0.067	0.008	0.009	0.000	0.000	0.011	0.000	0.000
	0.60g	0.411	0.252	0.124	0.291	0.037	0.016	0.312	0.049	0.017
	1.00g	0.978	0.407	0.091	0.767	0.295	0.144	0.832	0.228	0.076
	1.25g	1.462	0.589	0.195	0.835	0.416	0.090	1.142	0.566	0.301
Case 5	0.25g	0.024	0.000	0.000	0.016	0.000	0.000	0.014	0.000	0.000
	0.60g	0.182	0.060	0.036	0.170	0.048	0.007	0.184	0.040	0.003
	1.00g	0.728	0.184	0.142	0.554	0.171	0.147	0.595	0.259	0.107
	1.25g	1.245	0.309	0.219	1.428	0.255	0.202	1.092	0.322	0.151

Table V.18: Peak Cask Bottom Displacements (m), Rectangular Module, NUREG/CR-6728 Earthquakes

		Soft Soil			Stiff Soil			Rock		
		$\mu=0.2$	$\mu=0.55$	$\mu=0.8$	$\mu=0.2$	$\mu=0.55$	$\mu=0.8$	$\mu=0.2$	$\mu=0.55$	$\mu=0.8$
Case A	0.25g	0.006	0.000	0.000	0.002	0.000	0.000	0.004	0.000	0.000
	0.60g	0.030	0.013	0.001	0.039	0.004	0.001	0.046	0.008	0.002
	1.00g	0.100	0.072	0.038	0.120	0.030	0.009	0.138	0.038	0.025
	1.25g	0.175	0.106	0.034	0.177	0.051	0.015	0.201	0.061	0.021
Case B	0.25g	0.003	0.000	0.000	0.004	0.000	0.000	0.006	0.001	0.000
	0.60g	0.036	0.006	0.001	0.023	0.012	0.003	0.027	0.014	0.007
	1.00g	0.101	0.026	0.026	0.072	0.045	0.016	0.070	0.047	0.018
	1.25g	0.133	0.066	0.038	0.100	0.049	0.049	0.092	0.035	0.030
Case C	0.25g	0.004	0.000	0.000	0.003	0.000	0.000	0.004	0.001	0.000
	0.60g	0.065	0.008	0.001	0.024	0.007	0.002	0.031	0.015	0.006
	1.00g	0.129	0.053	0.015	0.069	0.047	0.014	0.088	0.025	0.025
	1.25g	0.151	0.087	0.033	0.110	0.056	0.019	0.101	0.069	0.043
Case D	0.25g	0.004	0.000	0.000	0.002	0.000	0.000	0.002	0.001	0.000
	0.60g	0.038	0.008	0.002	0.025	0.005	0.004	0.022	0.004	0.003
	1.00g	0.092	0.055	0.012	0.087	0.035	0.025	0.080	0.017	0.017
	1.25g	0.114	0.057	0.031	0.149	0.060	0.043	0.257	0.062	0.035
Case E	0.25g	0.009	0.000	0.000	0.003	0.000	0.000	0.003	0.001	0.000
	0.60g	0.051	0.016	0.005	0.033	0.010	0.002	0.042	0.012	0.008
	1.00g	0.135	0.061	0.026	0.089	0.032	0.017	0.078	0.018	0.018
	1.25g	0.186	0.106	0.033	0.143	0.056	0.039	0.154	0.056	0.014

## V.2 Graphical Presentation of Results

Graphical plots of a subset of the data presented in Section V.1 are provided in this section to aid in understanding the results. Plots are provided for the peak cask top displacement and peak cask rotation. These two parameters are the most important for evaluating cask designs. A number of sets are grouped into each of the figures shown here. Each plot shows either the peak top displacement or rotation of a given cask design subjected to all of the earthquakes conforming to a given spectral shape. A separate line is shown for a set of results where everything is kept equal except for the magnitude of the ground motion. In each figure, there are 15 lines to represent the analysis results for the five ground motion records and three friction coefficients.

For the cylindrical cask, which tips over in some cases, there is a dilemma of how to plot the results for the cases that overturn. There is no meaningful value for the peak rotation or top displacement in these cases, so the approach taken here is to assign very high values for these cases, so that if a cask tips over in a series of analyses, the line representing that series extends vertically from the highest point before tipping over occurs. This provides a visual representation of these results, which is important because omitting them could be potentially misleading. In a few cases, the cask overturns at one level of PGA but then does not overturn with a higher PGA. In these cases, the vertical line comes back down to the data point at the higher ground motion level.

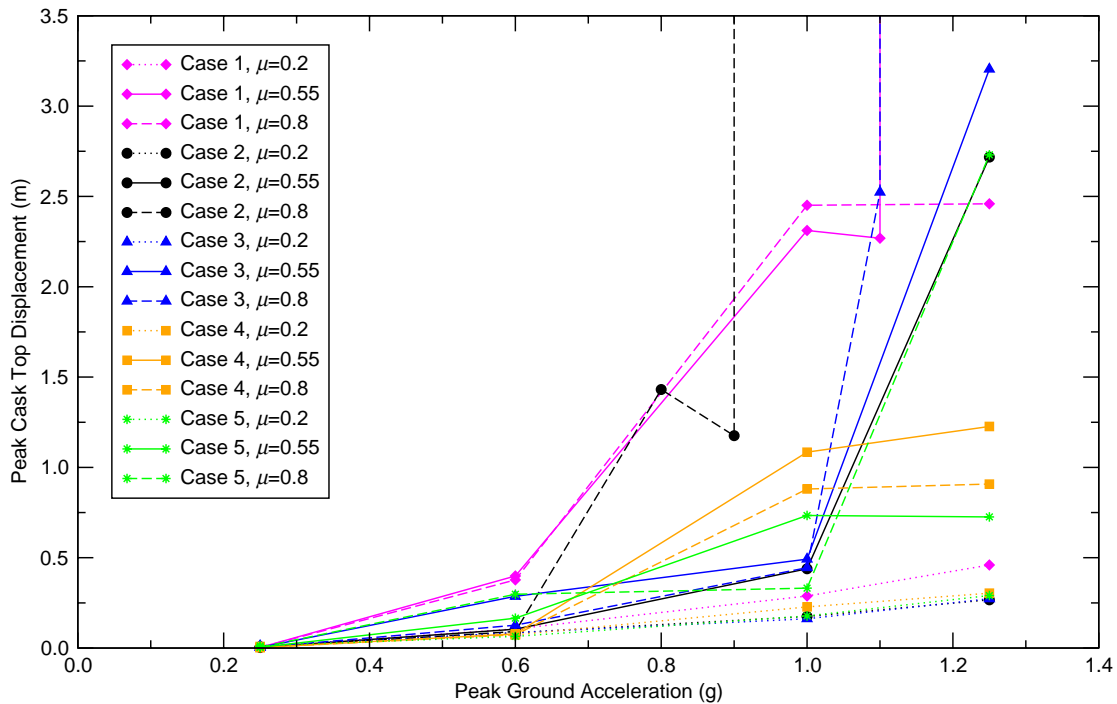


Figure V.1: Peak Cask Top Displacements, Cylindrical Cask, Soft Soil, NUREG/CR-0098 Earthquakes

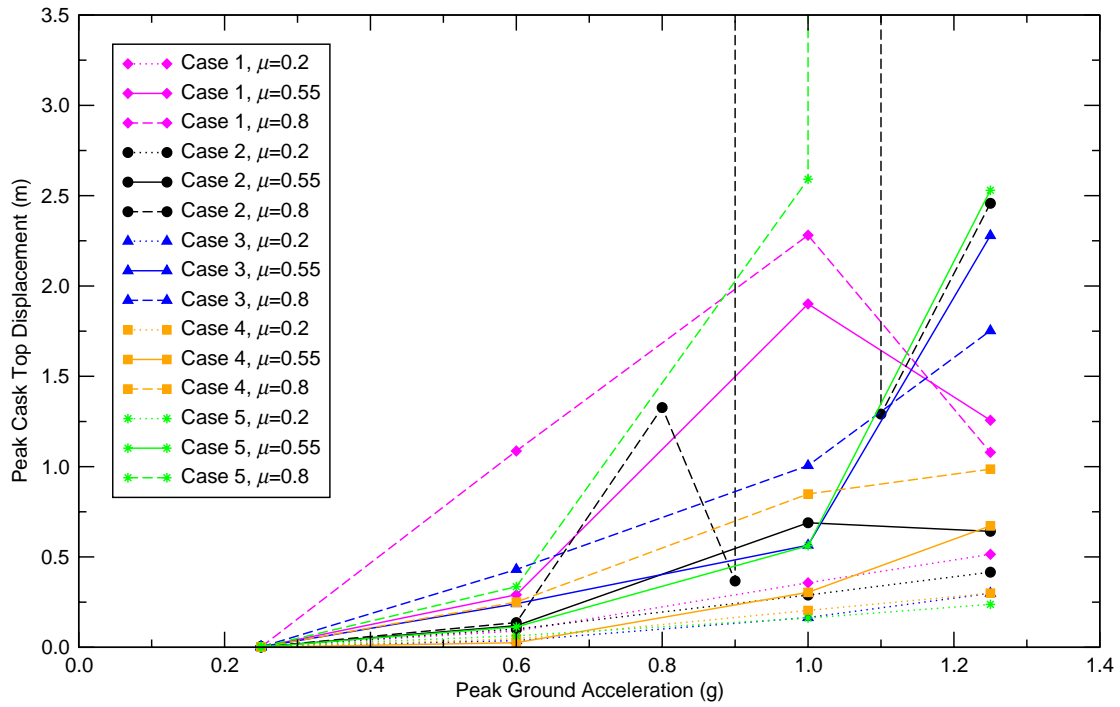


Figure V.2: Peak Cask Top Displacements, Cylindrical Cask, Stiff Soil, NUREG/CR-0098 Earthquakes

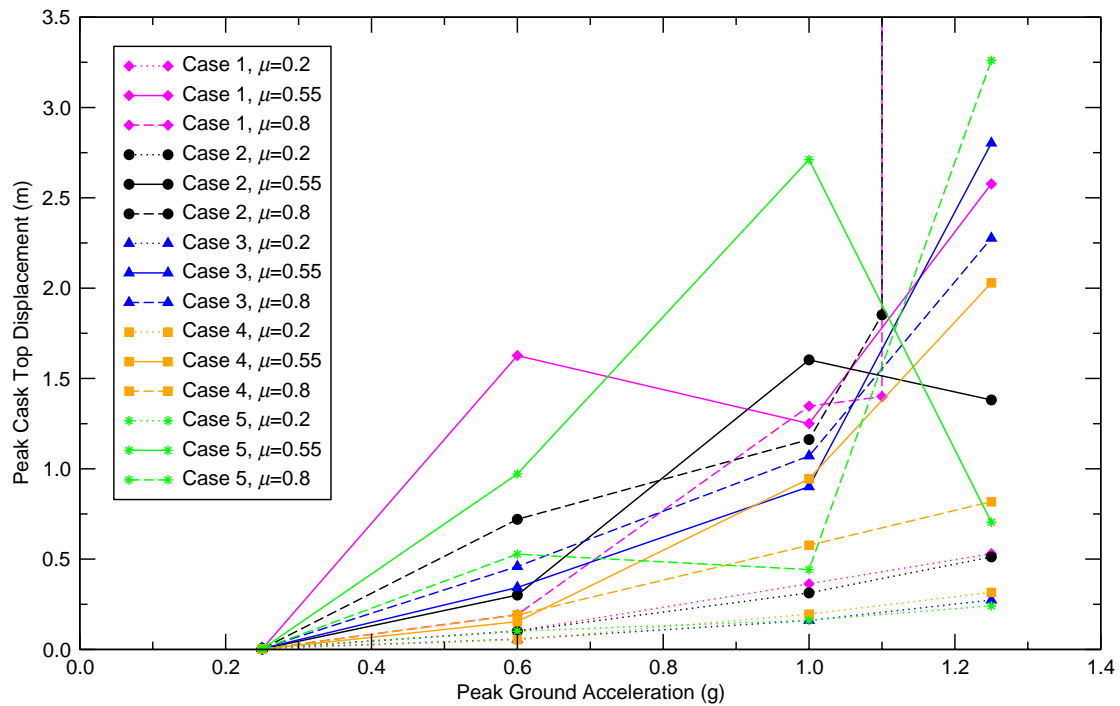


Figure V.3: Peak Cask Top Displacements, Cylindrical Cask, Rock, NUREG/CR-0098 Earthquakes

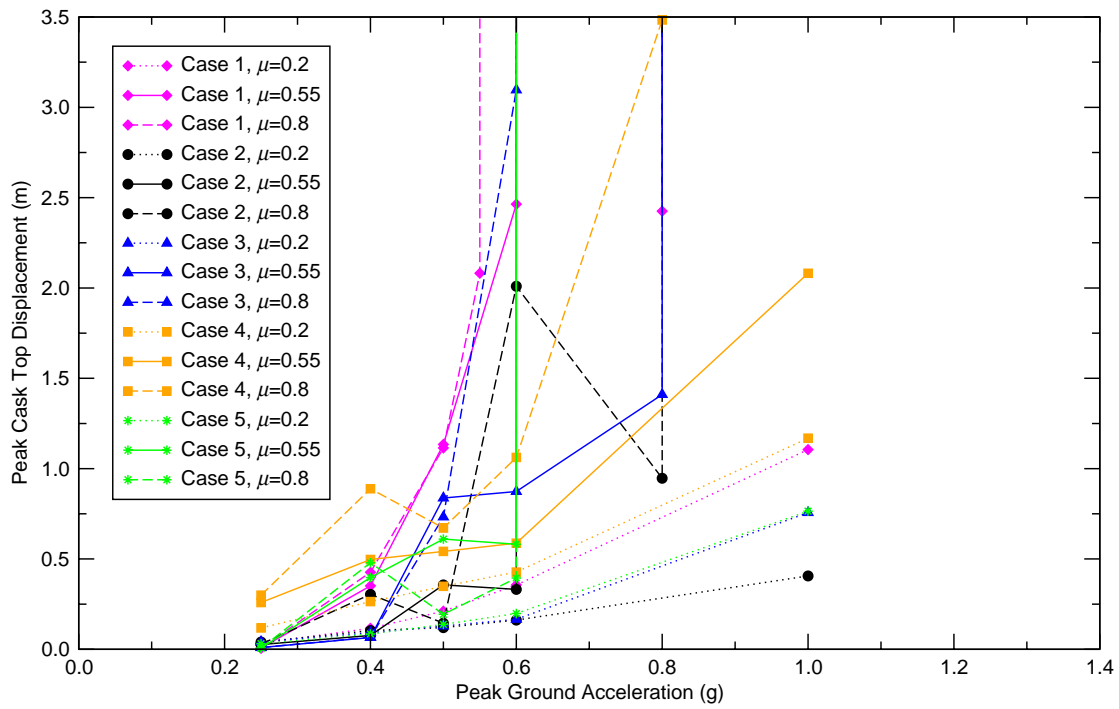


Figure V.4: Peak Cask Top Displacements, Cylindrical Cask, Soft Soil, Regulatory Guide 1.60 Earthquakes

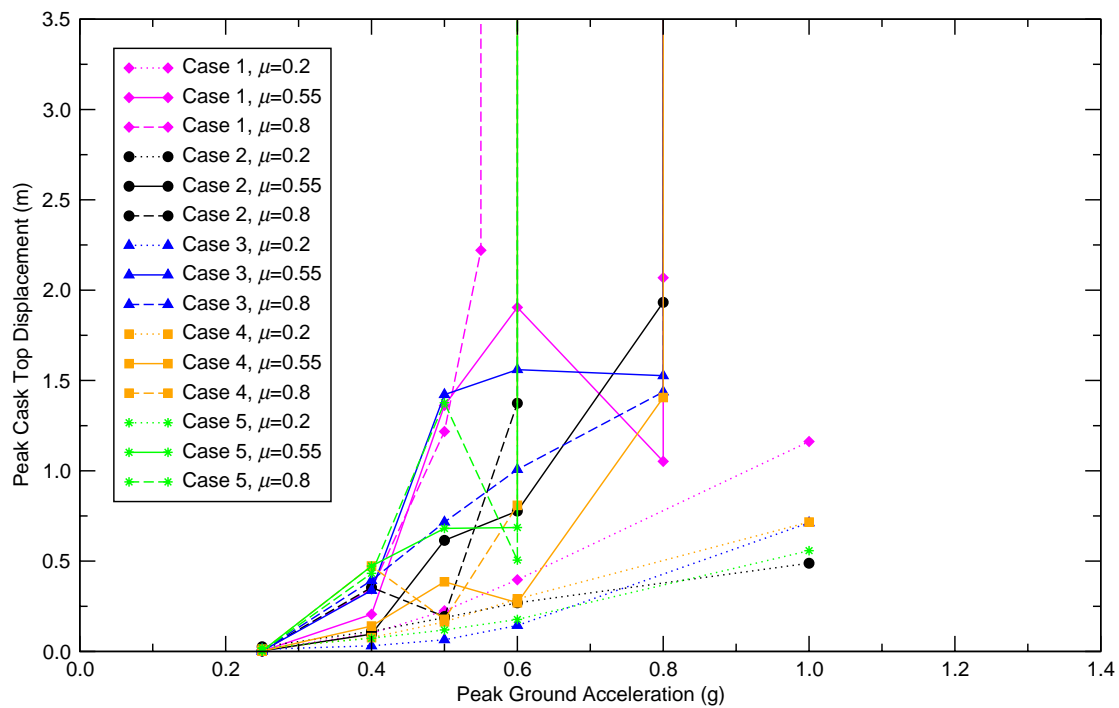


Figure V.5: Peak Cask Top Displacements, Cylindrical Cask, Stiff Soil, Regulatory Guide 1.60 Earthquakes

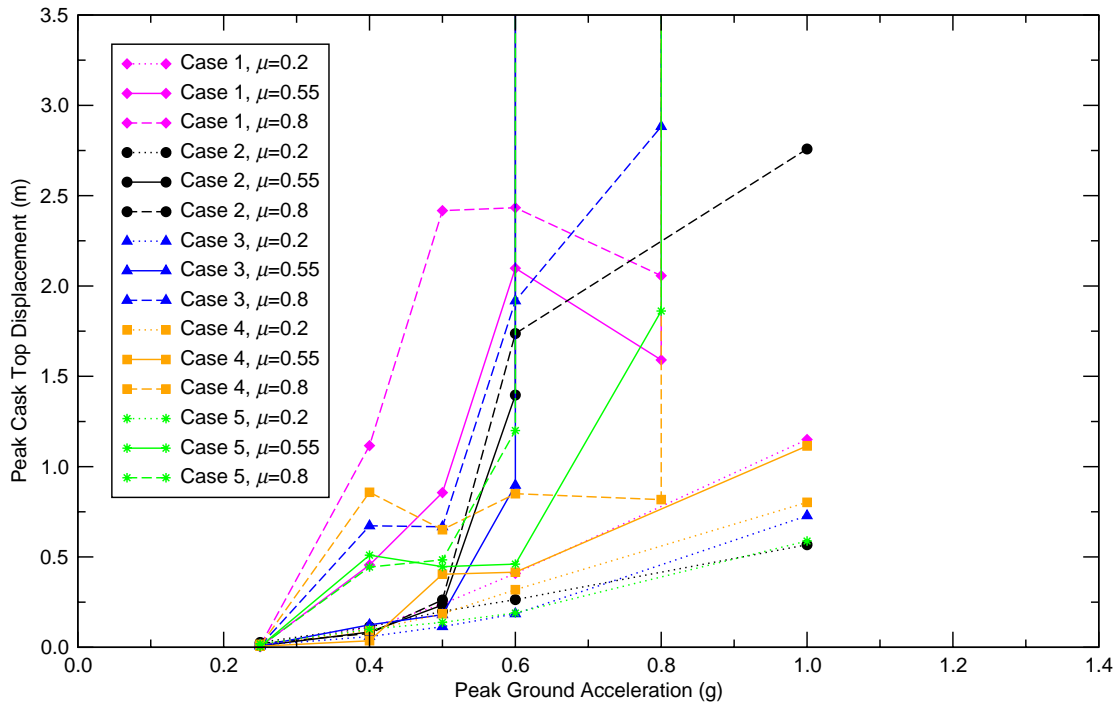


Figure V.6: Peak Cask Top Displacements, Cylindrical Cask, Rock, Regulatory Guide 1.60 Earthquakes

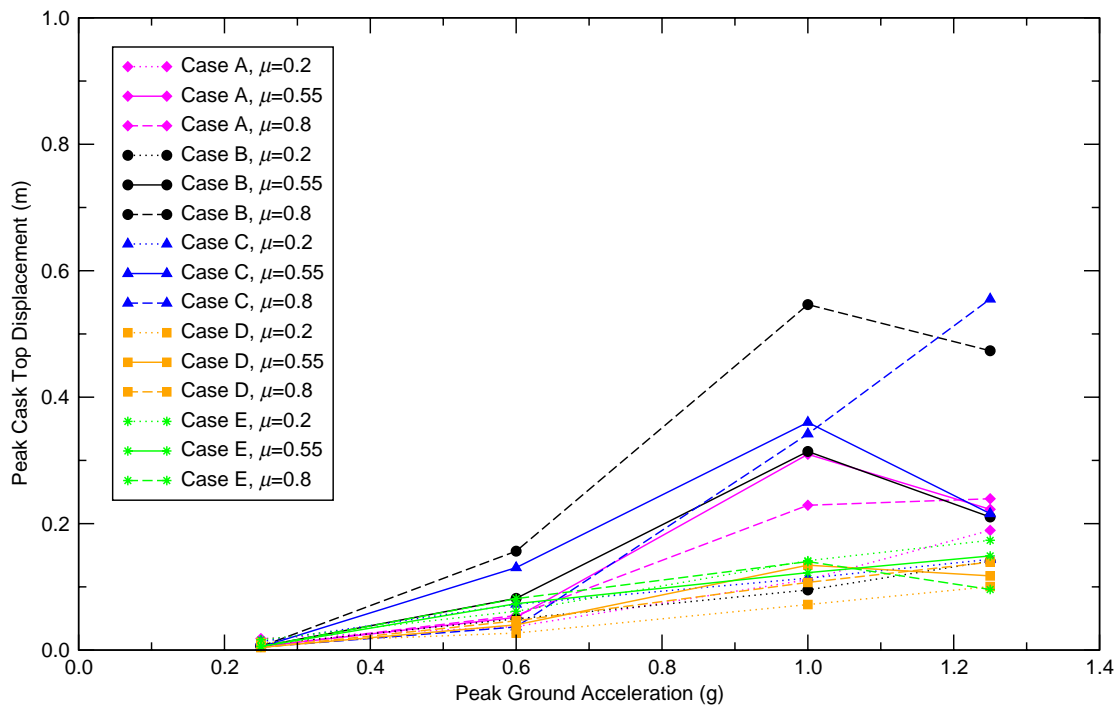


Figure V.7: Peak Cask Top Displacements, Cylindrical Cask, Soft Soil, NUREG/CR-6728 Earthquakes

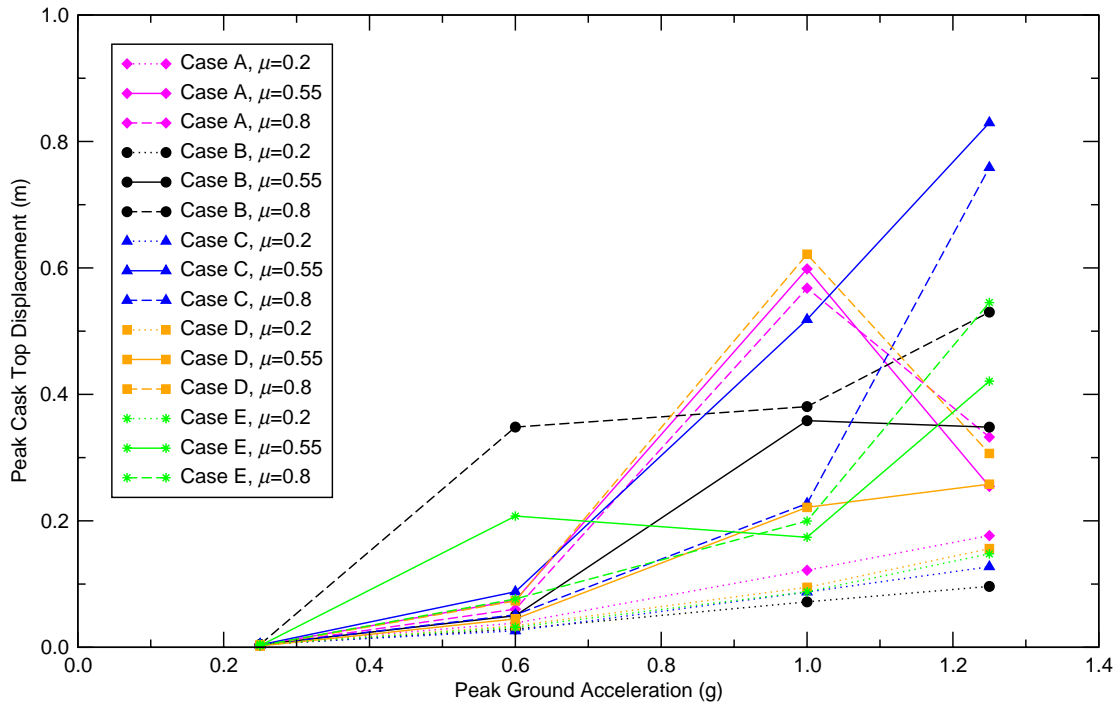


Figure V.8: Peak Cask Top Displacements, Cylindrical Cask, Stiff Soil, NUREG/CR-6728 Earthquakes

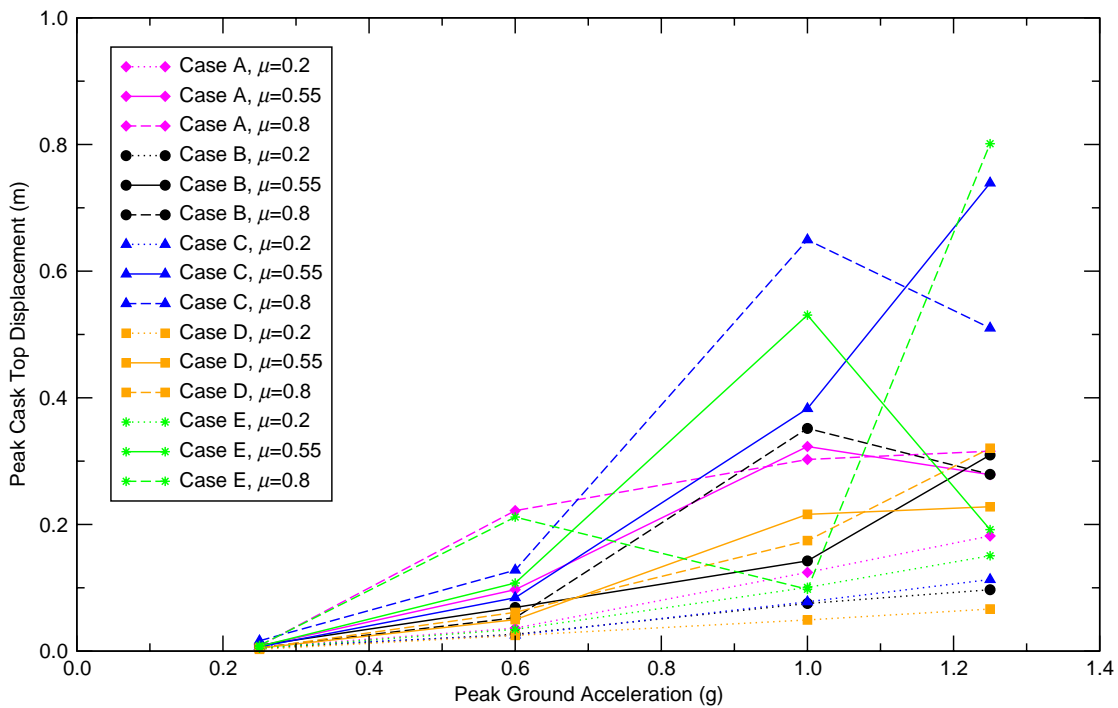


Figure V.9: Peak Cask Top Displacements, Cylindrical Cask, Rock, NUREG/CR-6728 Earthquakes

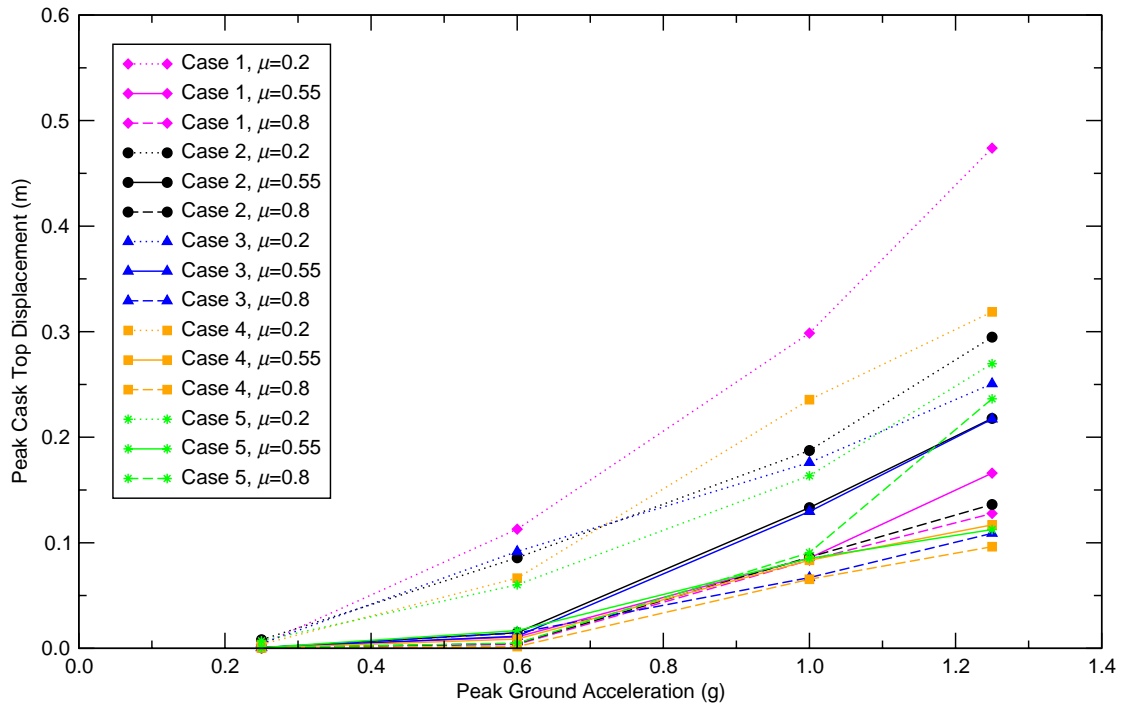


Figure V.10: Peak Cask Top Displacements, Rectangular Module, Soft Soil, NUREG/CR-0098 Earthquakes

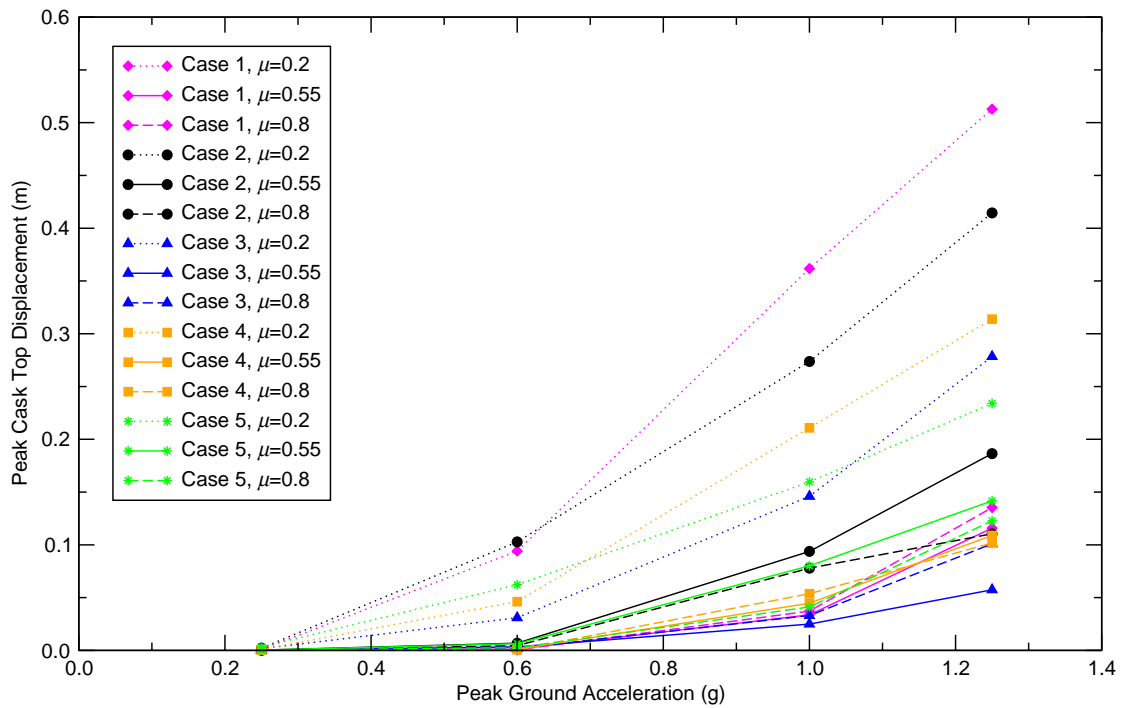


Figure V.11: Peak Cask Top Displacements, Rectangular Module, Stiff Soil, NUREG/CR-0098 Earthquakes

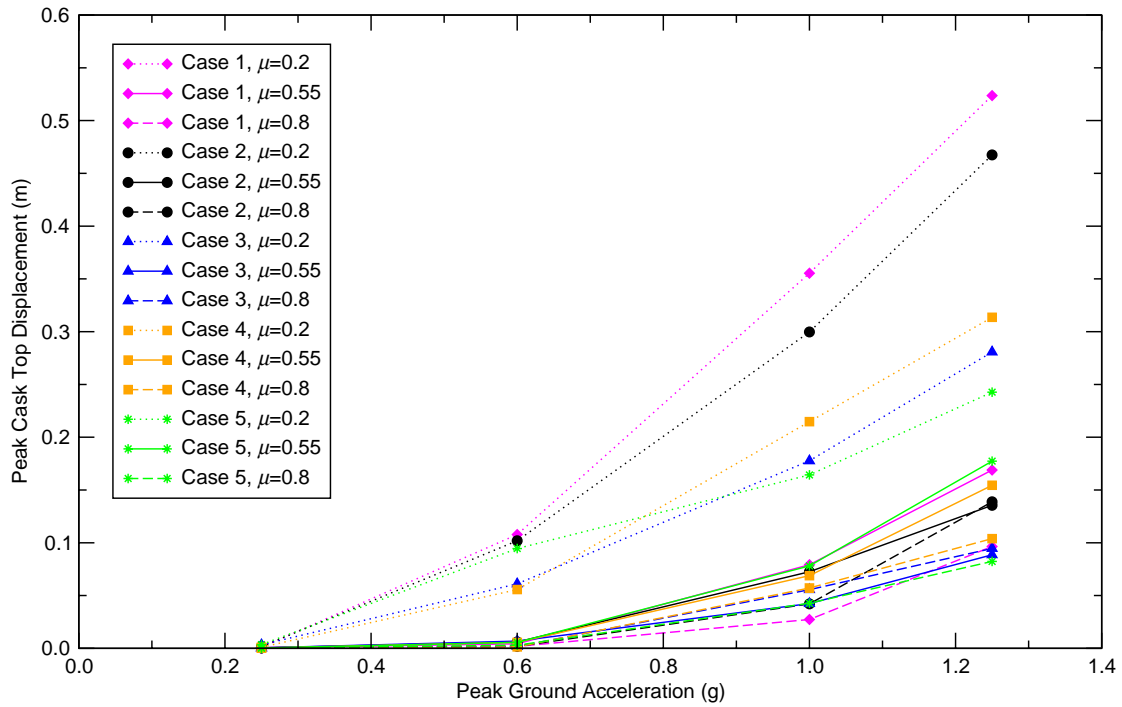


Figure V.12: Peak Cask Top Displacements, Rectangular Module, Rock, NUREG/CR-0098 Earthquakes

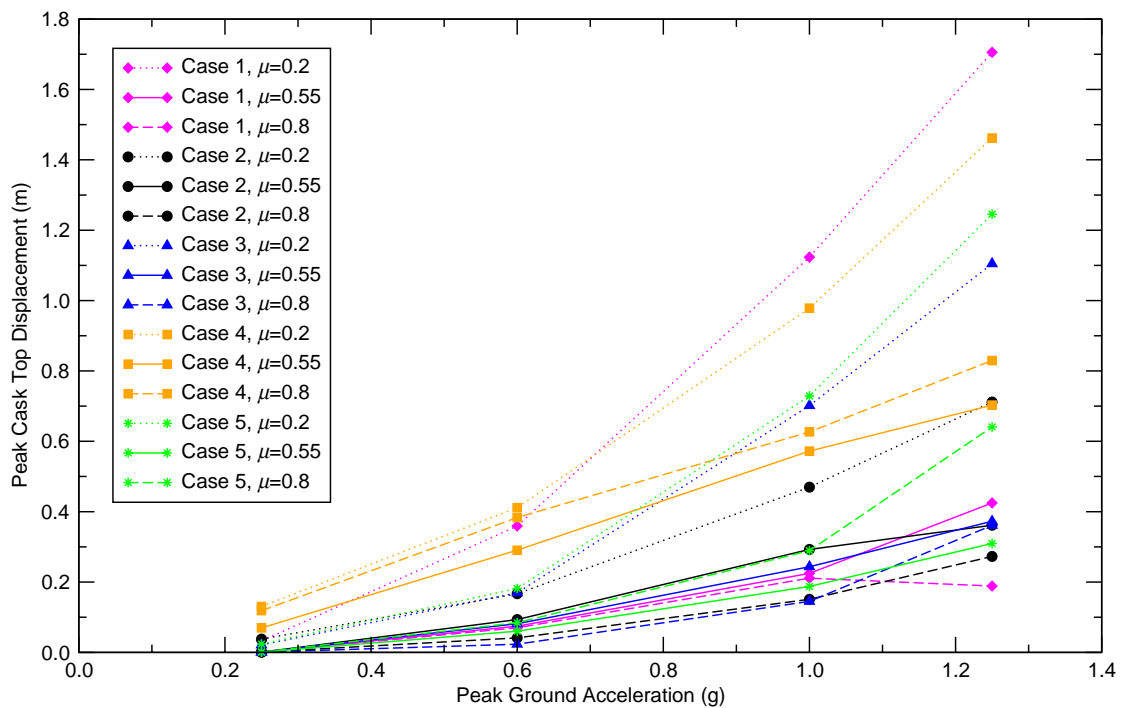


Figure V.13: Peak Cask Top Displacements, Rectangular Module, Soft Soil, Regulatory Guide 1.60 Earthquakes

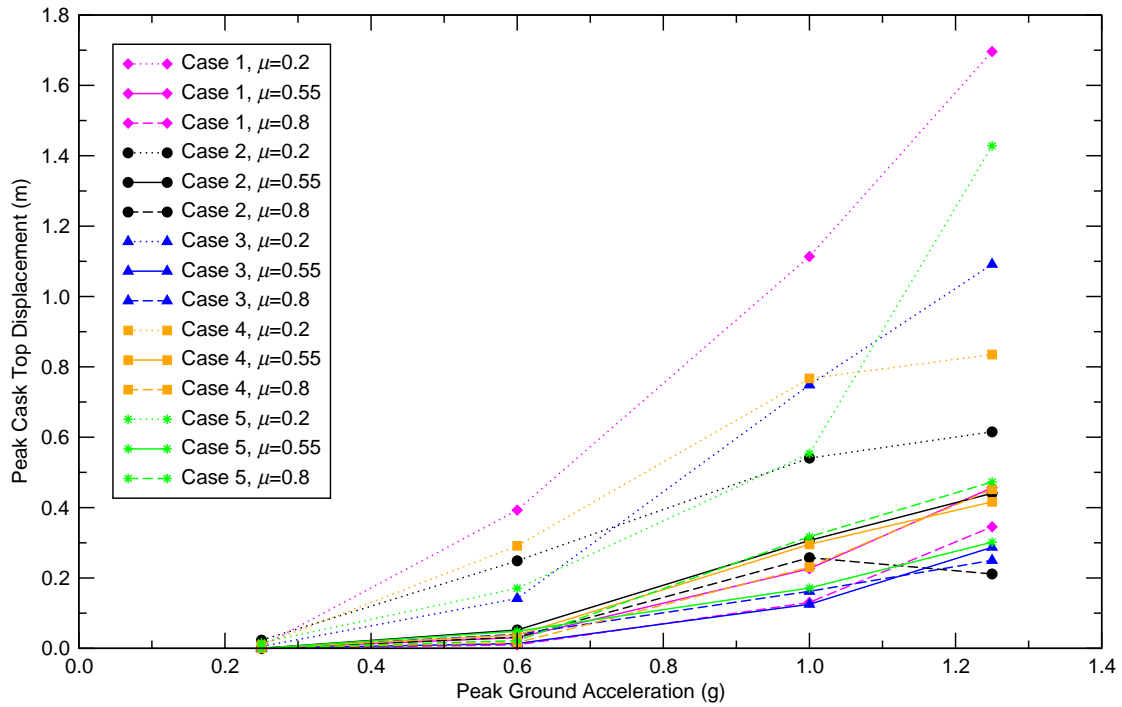


Figure V.14: Peak Cask Top Displacements, Rectangular Module, Stiff Soil, Regulatory Guide 1.60 Earthquakes

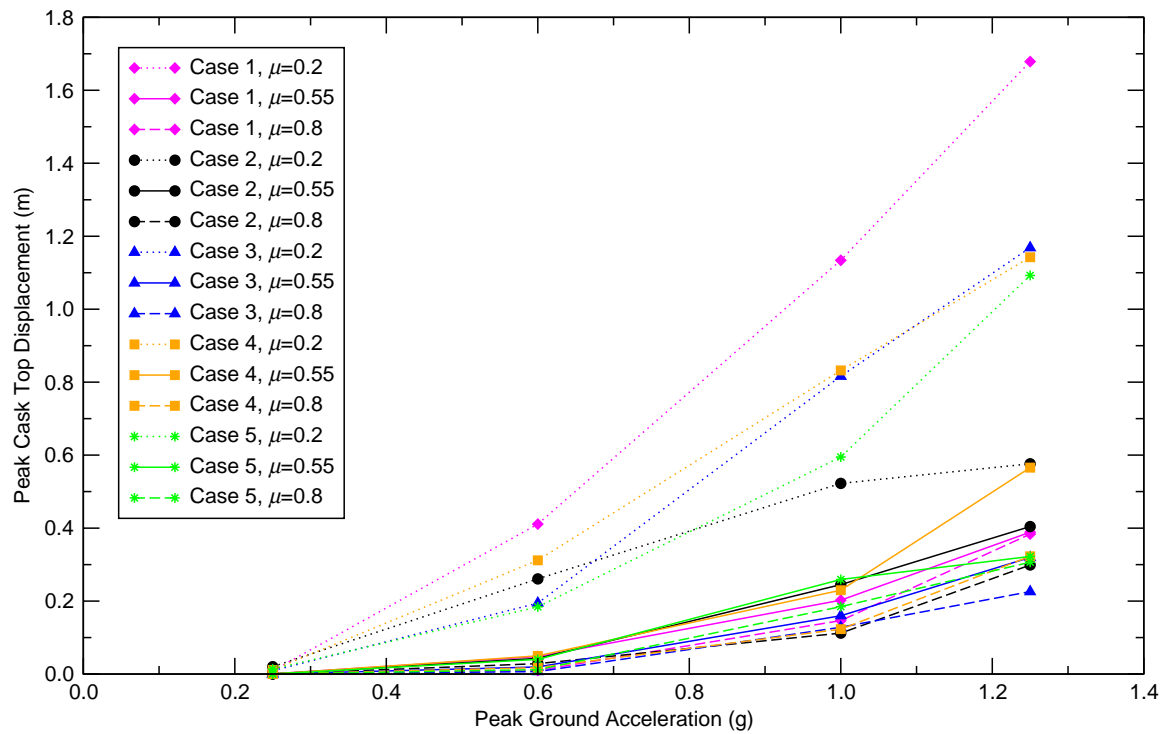


Figure V.15: Peak Cask Top Displacements, Rectangular Module, Rock, Regulatory Guide 1.60 Earthquakes

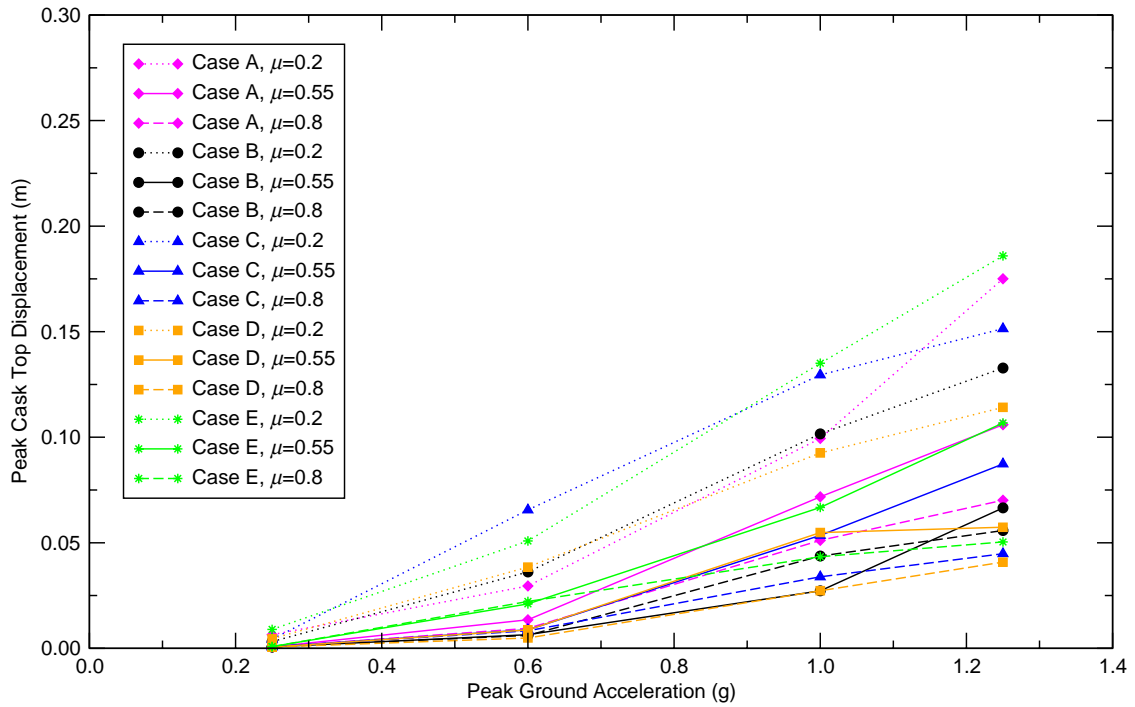


Figure V.16: Peak Cask Top Displacements, Rectangular Module, Soft Soil, NUREG/CR-6728 Earthquakes

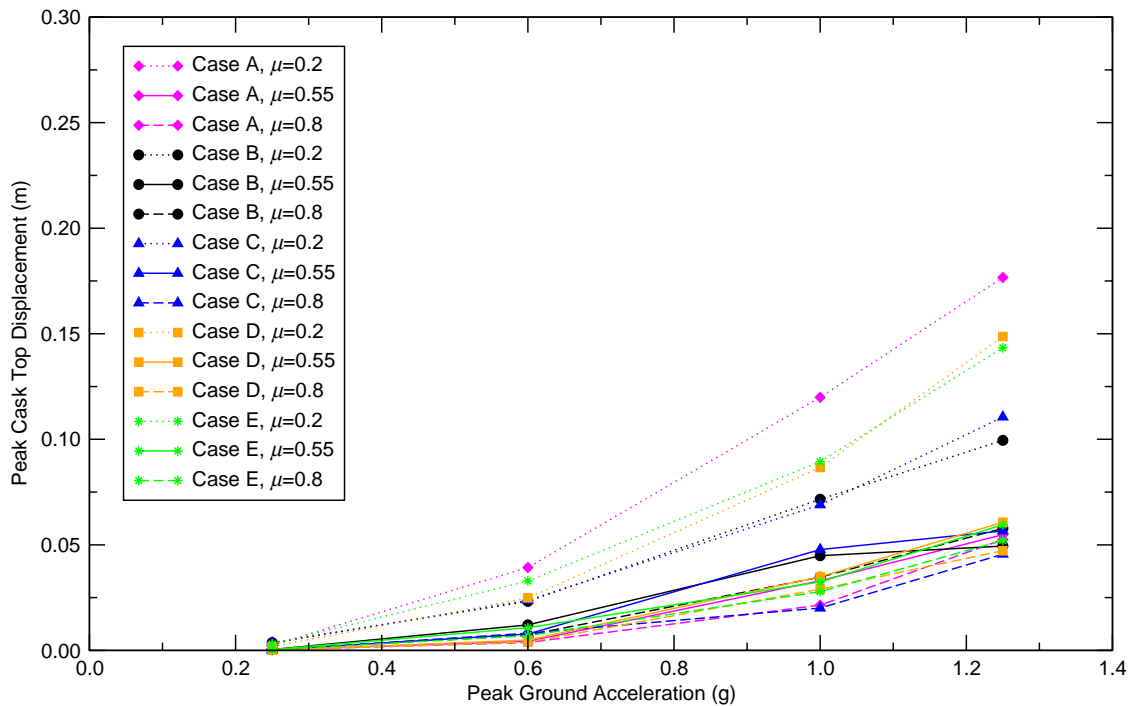


Figure V.17: Peak Cask Top Displacements, Rectangular Module, Stiff Soil, NUREG/CR-6728 Earthquakes

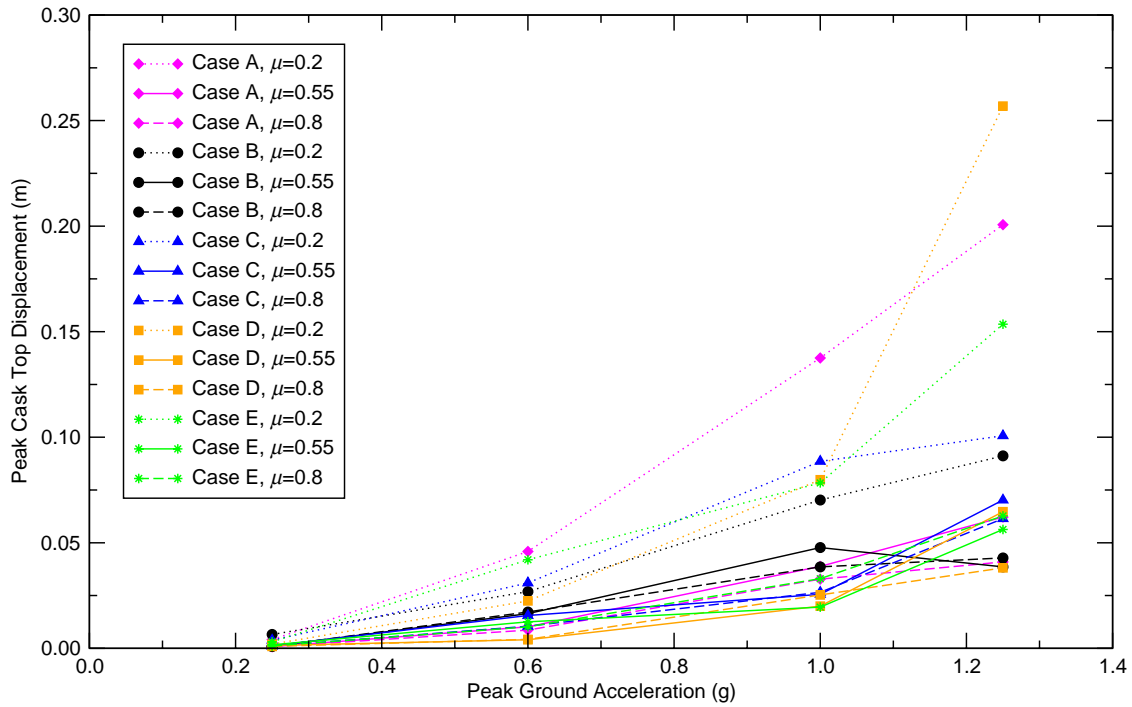


Figure V.18: Peak Cask Top Displacements, Rectangular Module, Rock, NUREG/CR-6728 Earthquakes

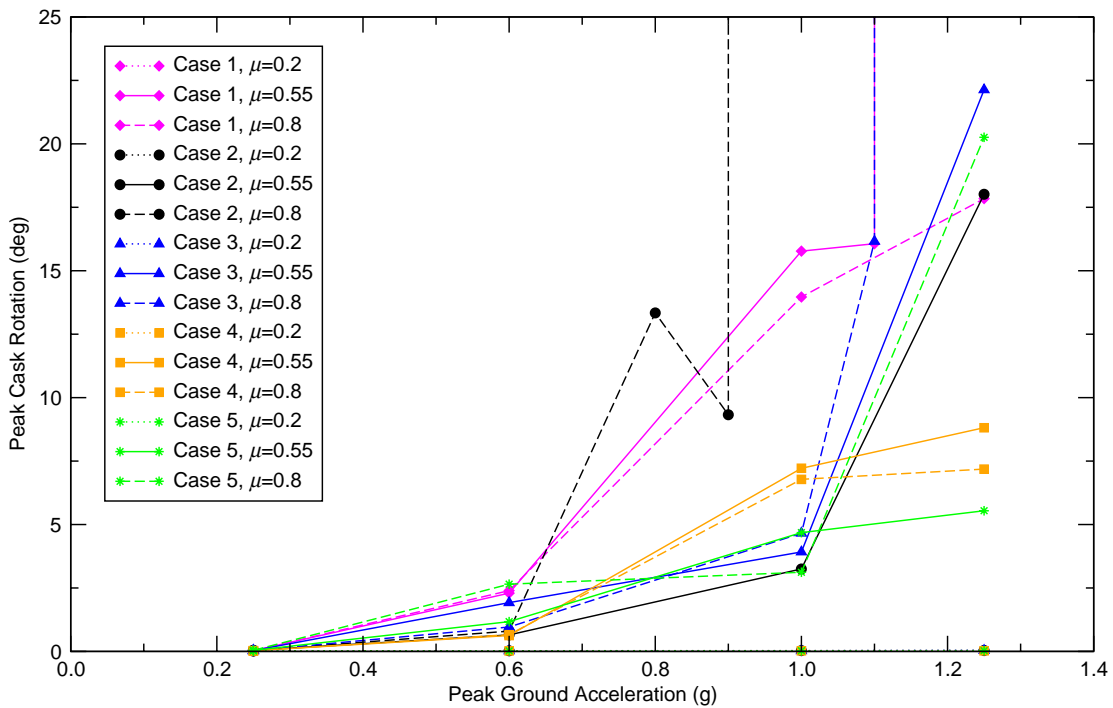


Figure V.19: Peak Cask Rotations, Cylindrical Cask, Soft Soil, NUREG/CR-0098 Earthquakes

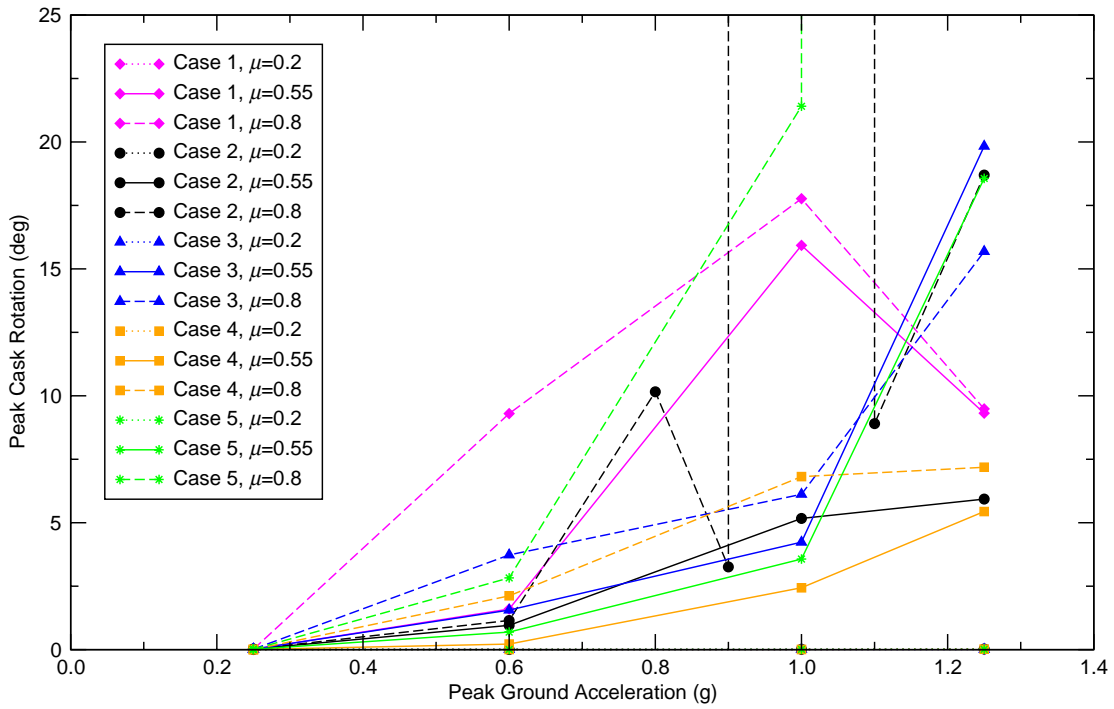


Figure V.20: Peak Cask Rotations, Cylindrical Cask, Stiff Soil, NUREG/CR-0098 Earthquakes

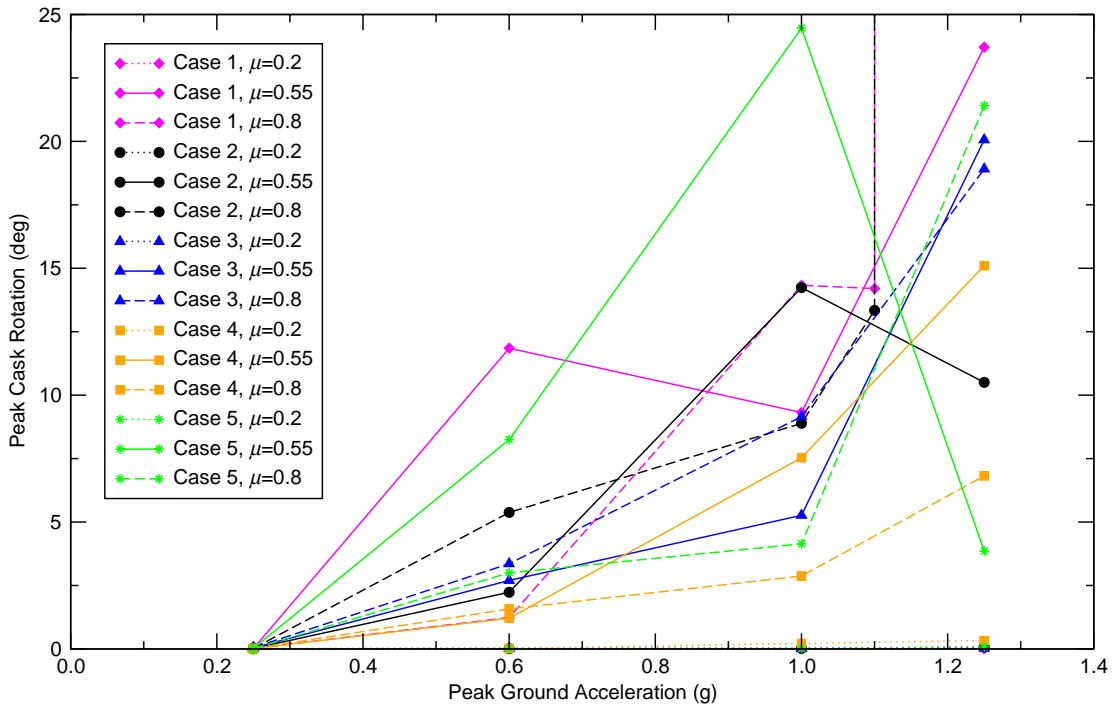


Figure V.21: Peak Cask Rotations, Cylindrical Cask, Rock, NUREG/CR-0098 Earthquakes

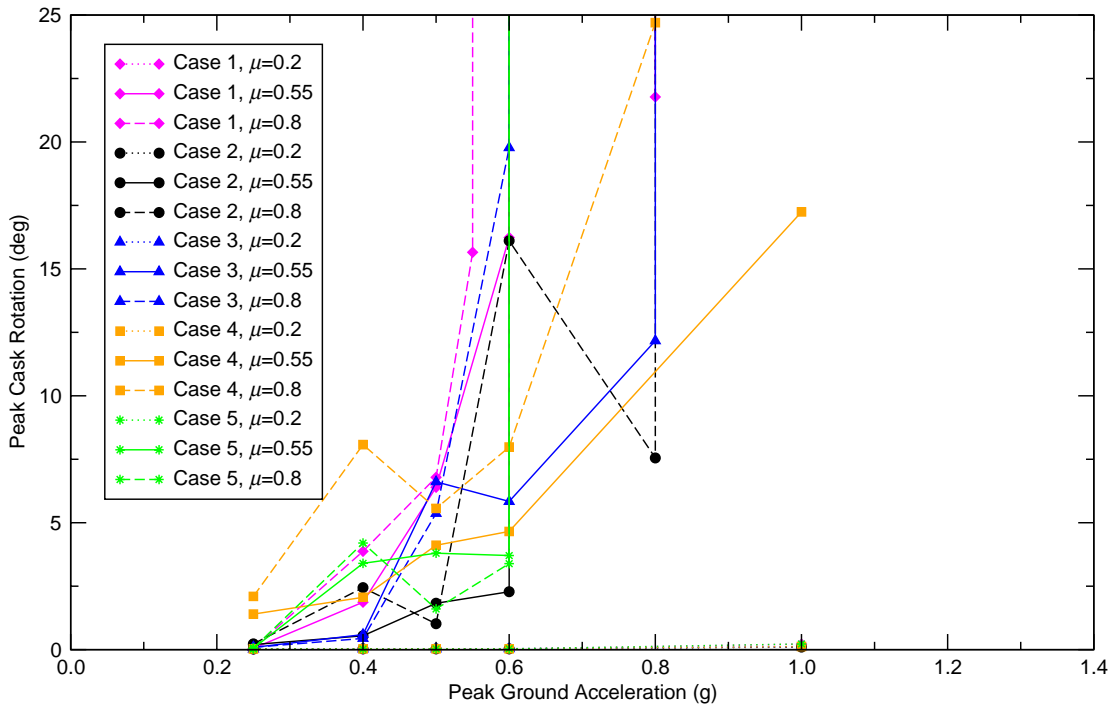


Figure V.22: Peak Cask Rotations, Cylindrical Cask, Soft Soil, Regulatory Guide 1.60 Earthquakes

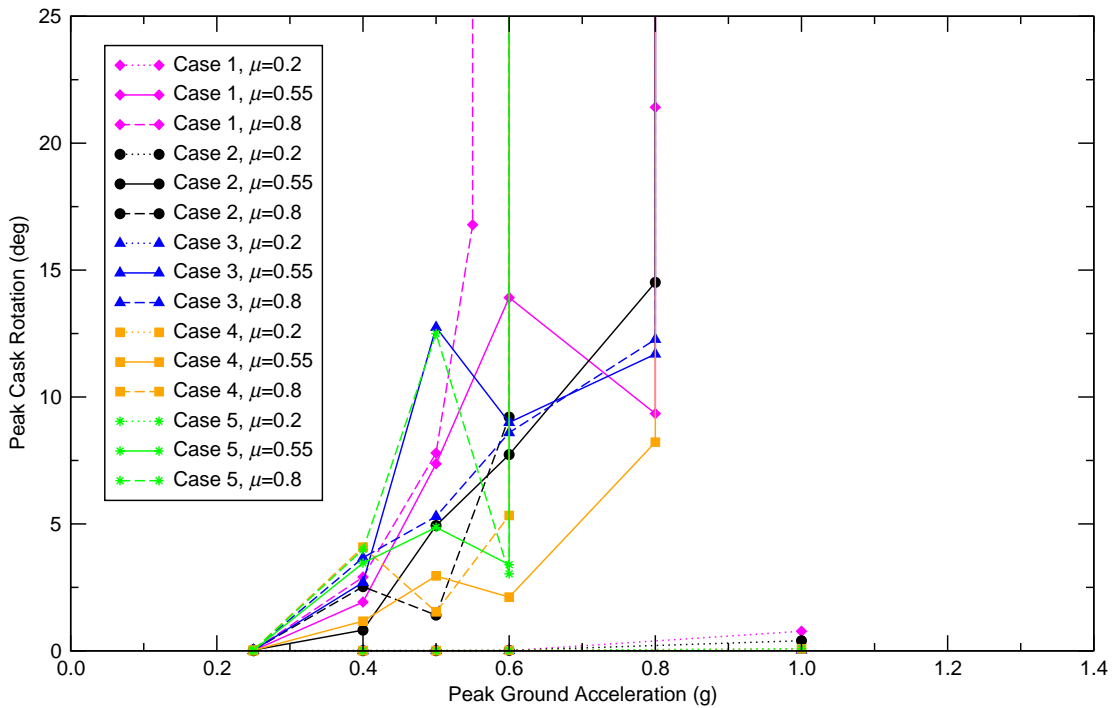


Figure V.23: Peak Cask Rotations, Cylindrical Cask, Stiff Soil, Regulatory Guide 1.60 Earthquakes

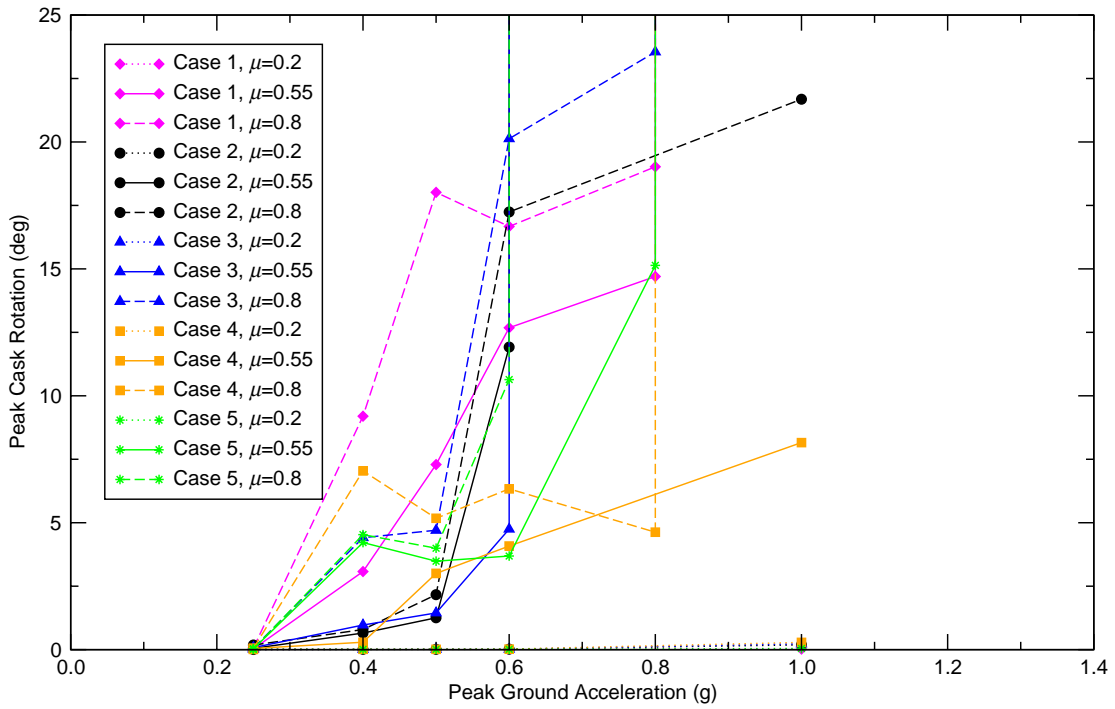


Figure V.24: Peak Cask Rotations, Cylindrical Cask, Rock, Regulatory Guide 1.60 Earthquakes

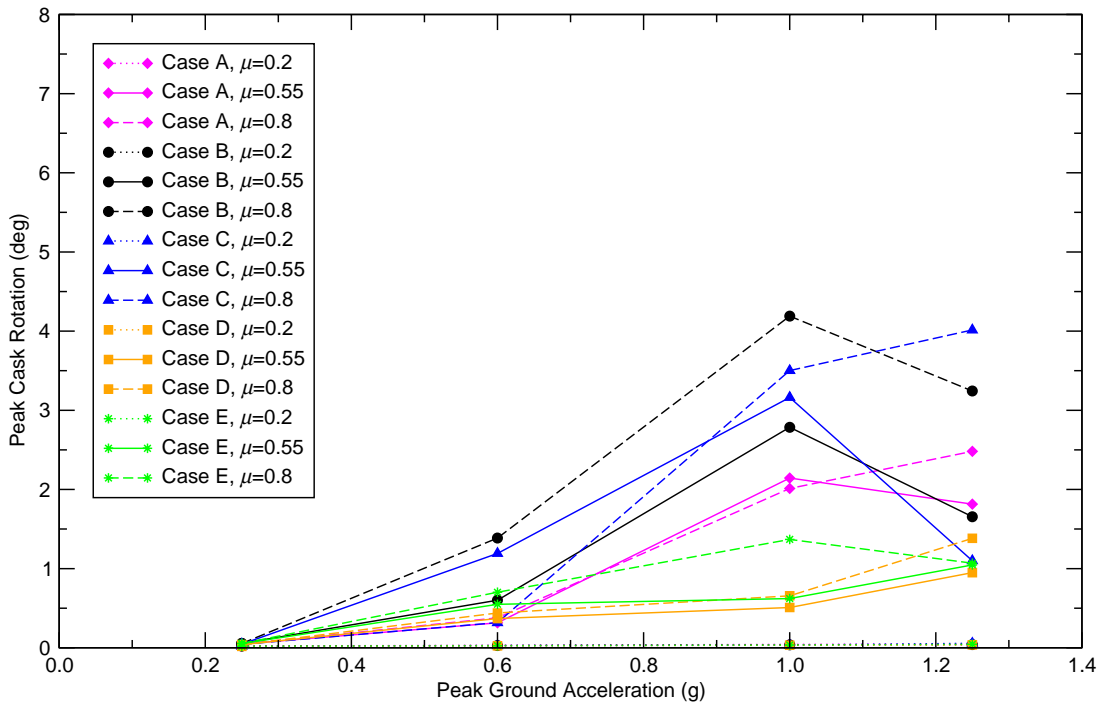


Figure V.25: Peak Cask Rotations, Cylindrical Cask, Soft Soil, NUREG/CR-6728 Earthquakes

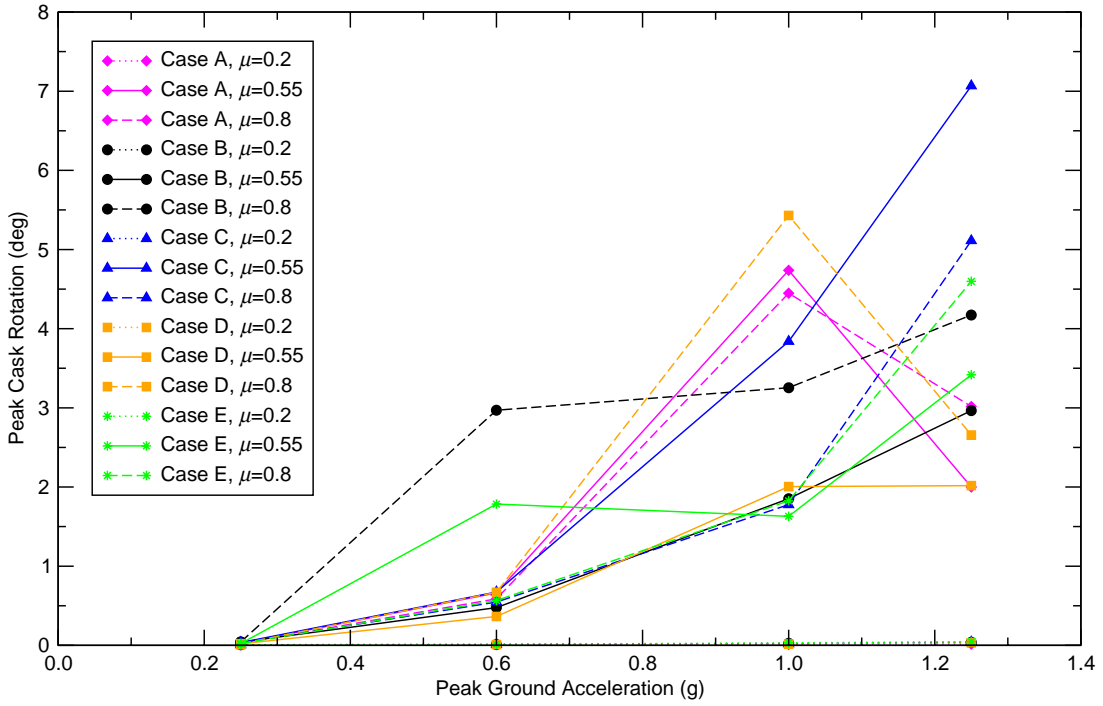


Figure V.26: Peak Cask Rotations, Cylindrical Cask, Stiff Soil, NUREG/CR-6728 Earthquakes

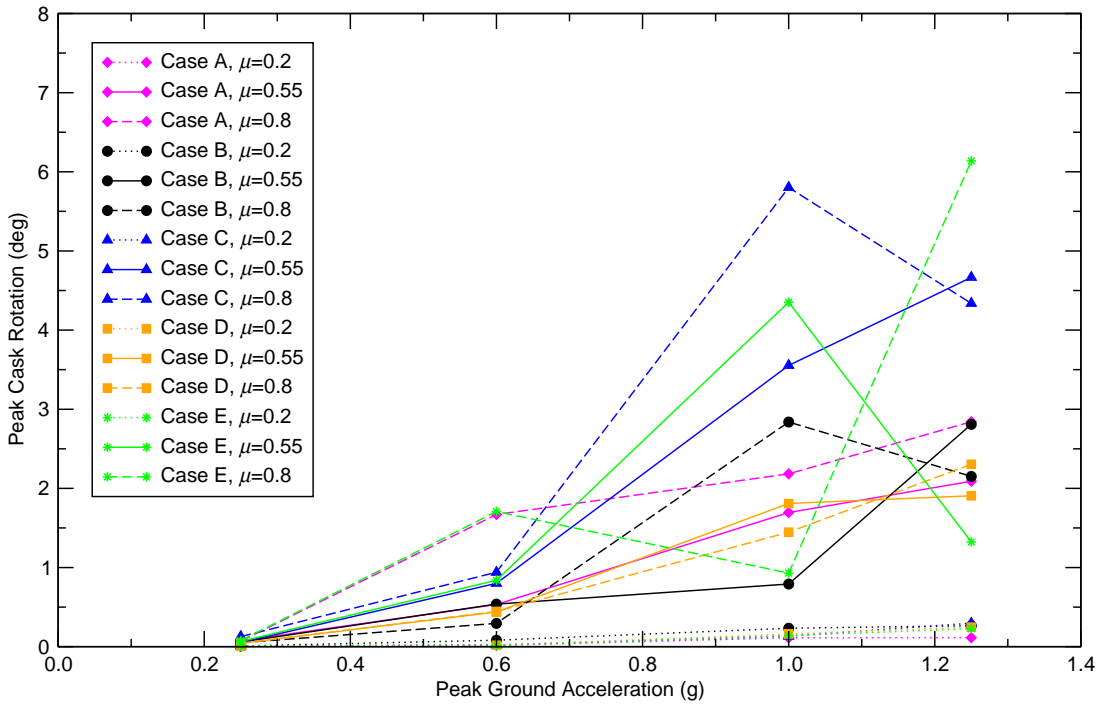


Figure V.27: Peak Cask Rotations, Cylindrical Cask, Rock, NUREG/CR-6728 Earthquakes

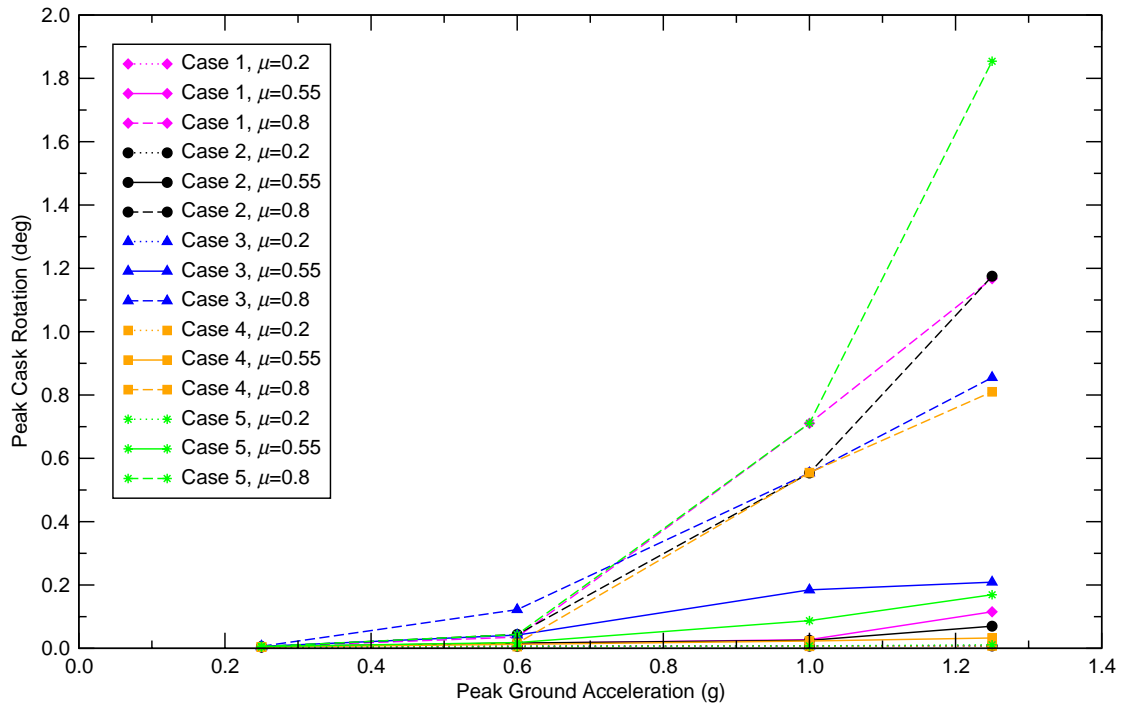


Figure V.28: Peak Cask Rotations, Rectangular Module, Soft Soil, NUREG/CR-0098 Earthquakes

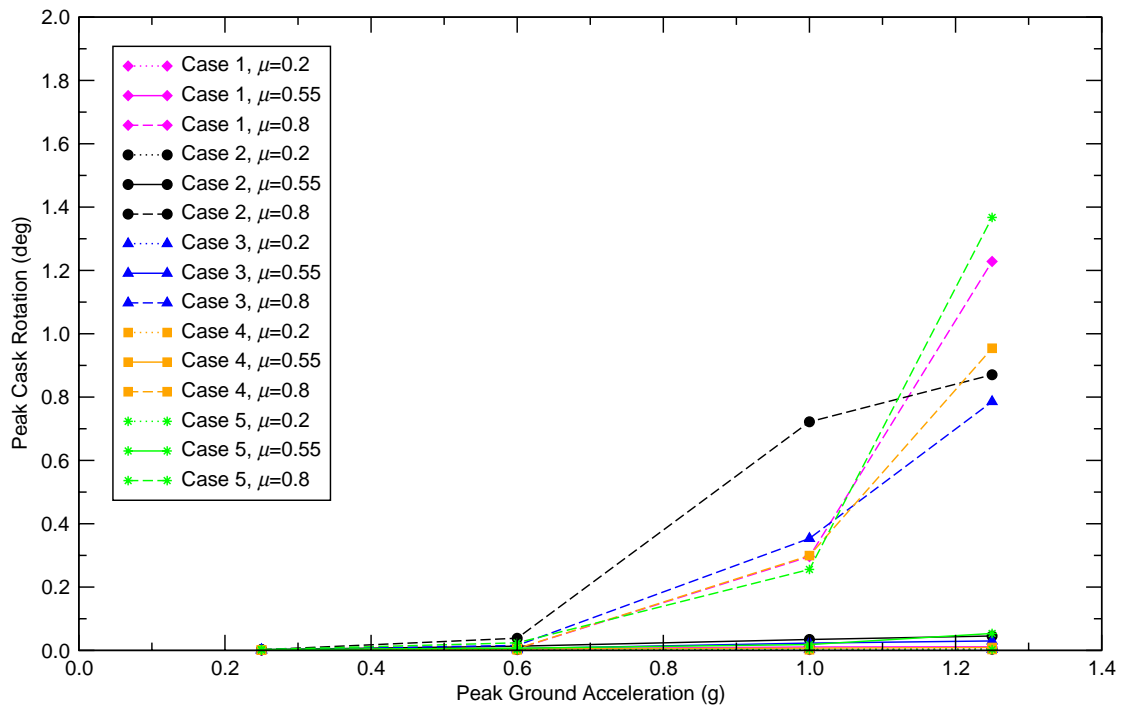


Figure V.29: Peak Cask Rotations, Rectangular Module, Stiff Soil, NUREG/CR-0098 Earthquakes

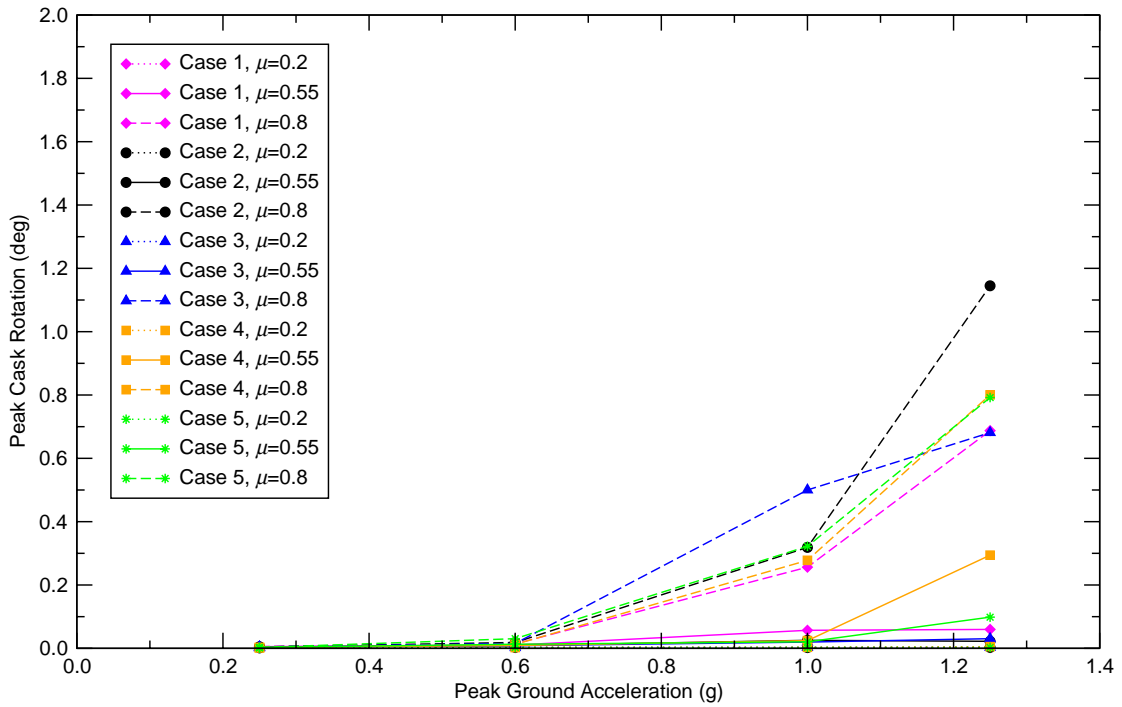


Figure V.30: Peak Cask Rotations, Rectangular Module, Rock, NUREG/CR-0098 Earthquakes

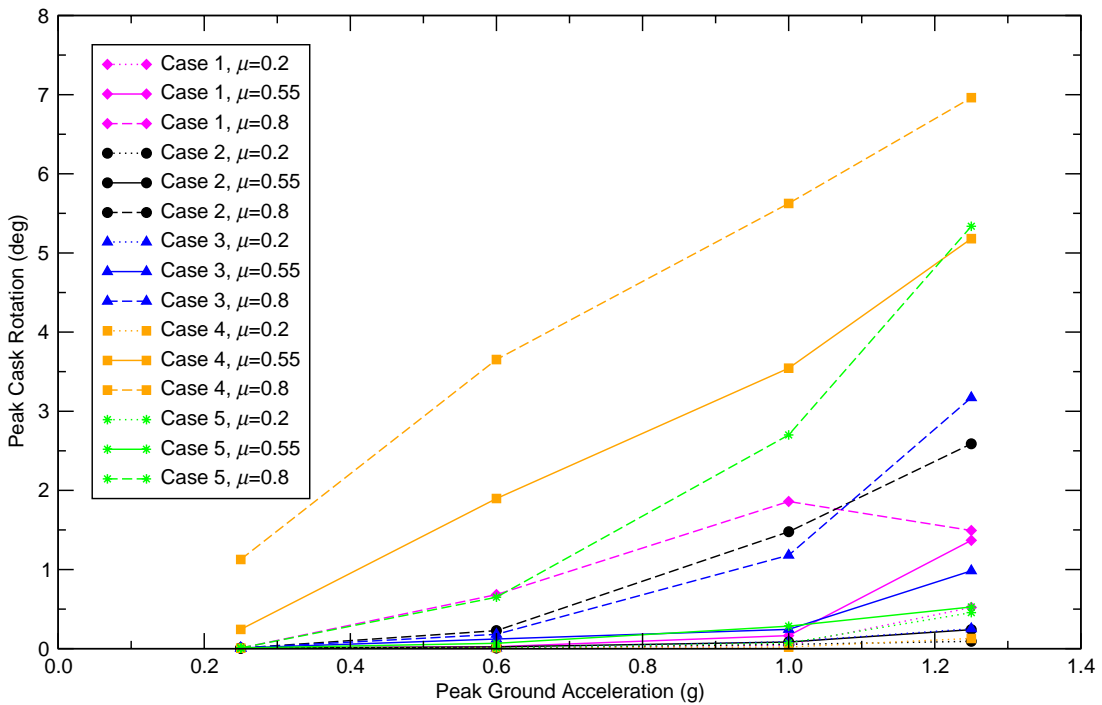


Figure V.31: Peak Cask Rotations, Rectangular Module, Soft Soil, Regulatory Guide 1.60 Earthquakes

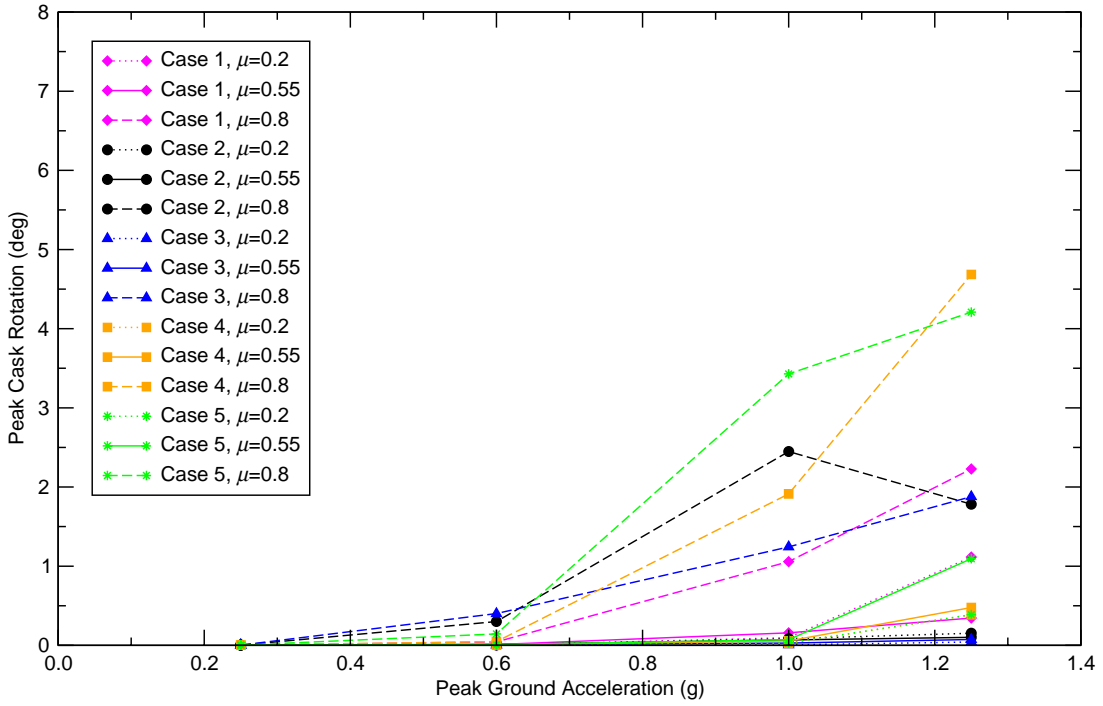


Figure V.32: Peak Cask Rotations, Rectangular Module, Stiff Soil, Regulatory Guide 1.60 Earthquakes

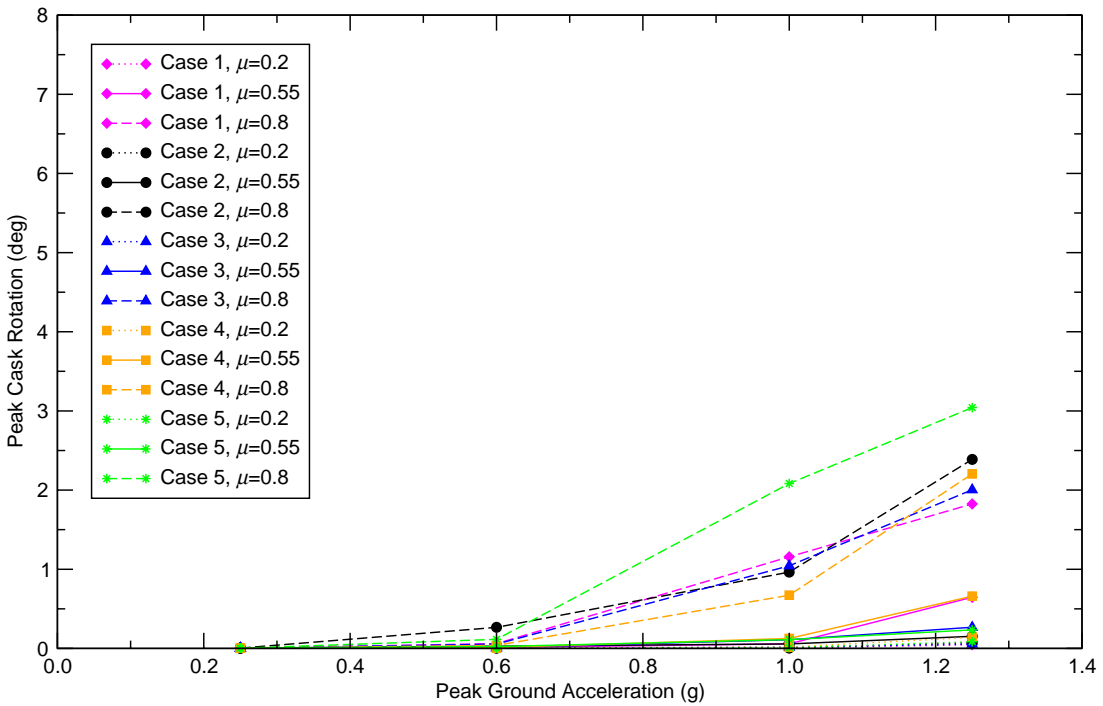


Figure V.33: Peak Cask Rotations, Rectangular Module, Rock, Regulatory Guide 1.60 Earthquakes

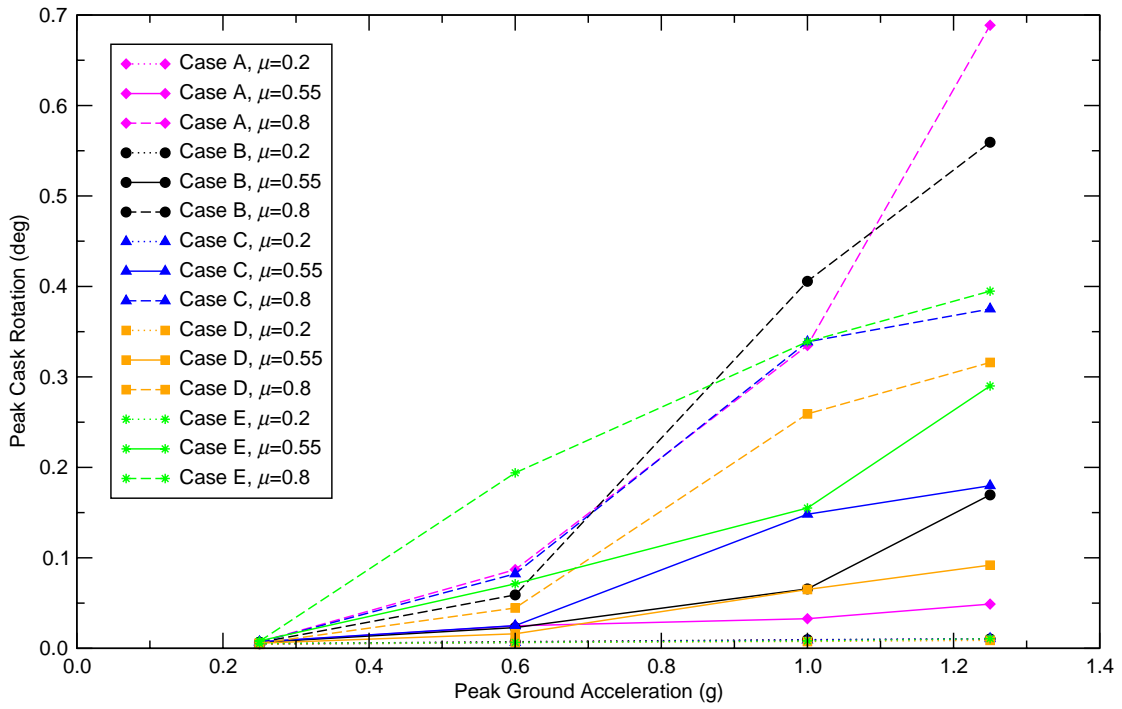


Figure V.34: Peak Cask Rotations, Rectangular Module, Soft Soil, NUREG/CR-6728 Earthquakes

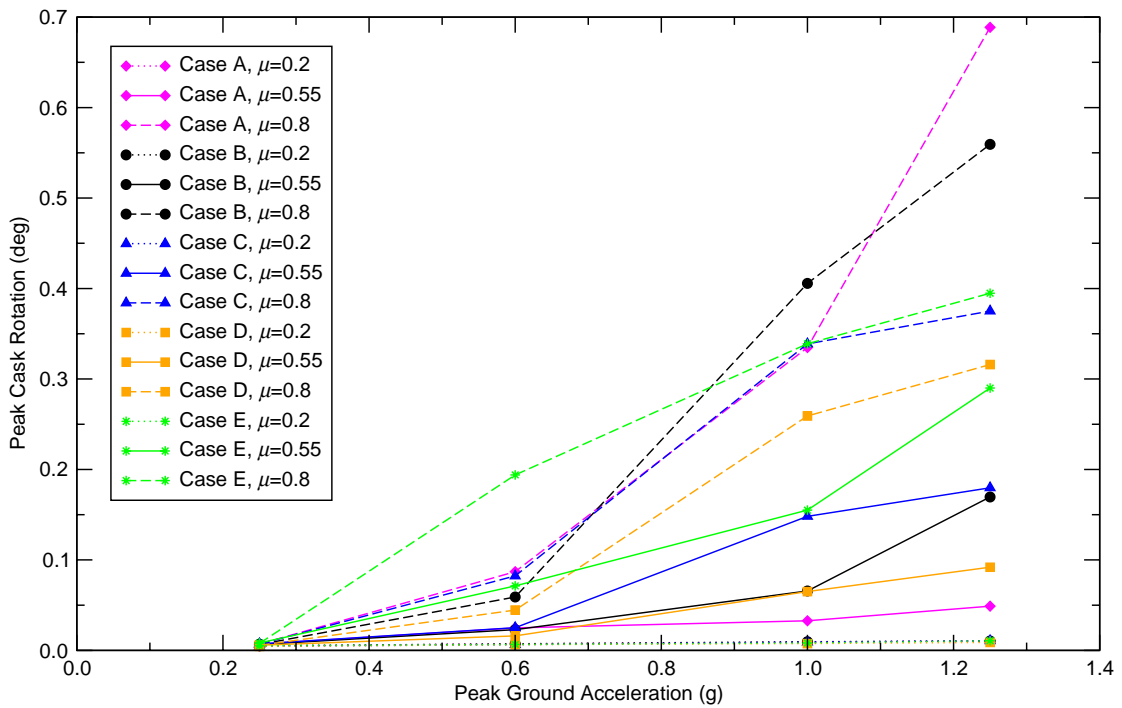


Figure V.35: Peak Cask Rotations, Rectangular Module, Stiff Soil, NUREG/CR-6728 Earthquakes

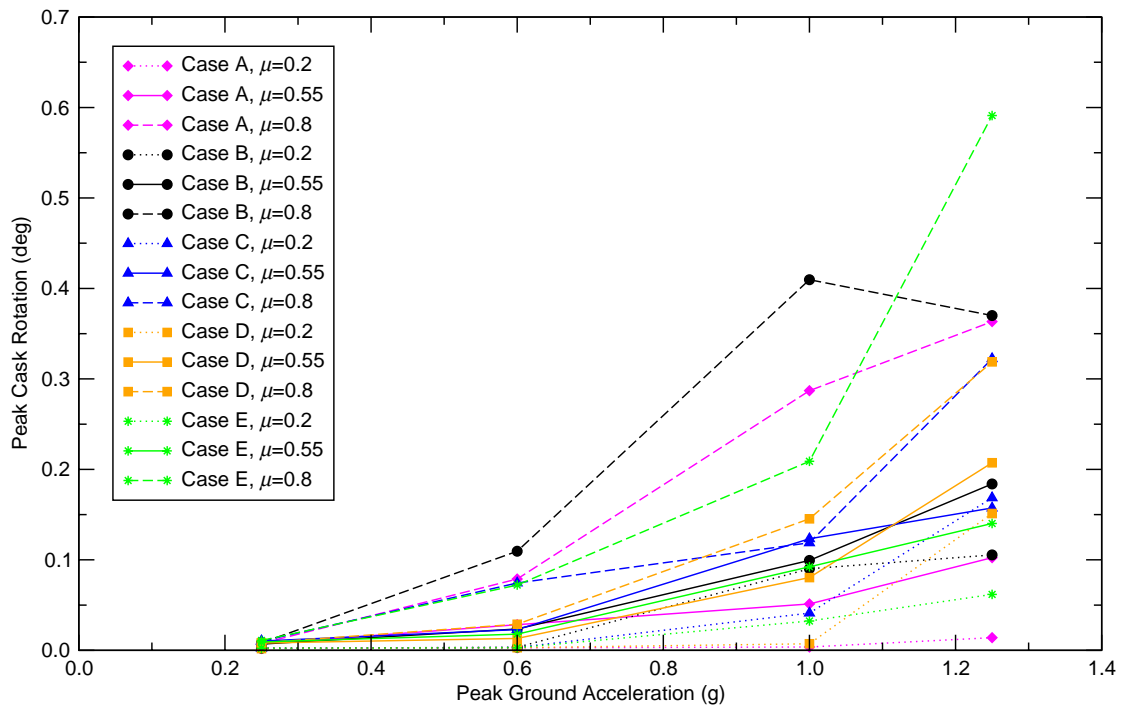


Figure V.36: Peak Cask Rotations, Rectangular Module, Rock, NUREG/CR-6728 Earthquakes

## **Appendix VI: Nomograms of Cask Responses**



## **Appendix VI: Nomograms of Cask Responses**

This appendix provides regression fits of the cask response results in terms of the peak horizontal cask top displacement relative to the pad and the peak cask rotation. The response of the cask as a function of the ground motion is fit reasonably by an exponential equation, which appears as a linear plot if logarithmic scales are used for the two axes. Two types of plots are provided. In Section VI.1, curve fits are provided for sets of analysis results coming from the same spectral shape. In Section VI.2, the results from all three spectral shapes are grouped together, and these are plotted in terms of the 5% damped 1 Hz pseudo-spectral acceleration (PSA) rather than the peak ground acceleration (PGA).

In all of these plots, if an analysis result in a series indicated that the cask tipped over, that result, as well as any results from analyses with higher levels of ground motion, was omitted from the data set used for curve fitting and is not plotted. A heavy vertical line and annotation are used to indicate the ground motion level at which the first cask overturning is observed. In all of the regression plots shown here, curves and equations are provided for the median least squares fit as well as the 84% and 16% confidence bands (median plus and minus one standard deviation). These plots can be used as nomograms for determining the cask response at a given level of confidence under a given level of ground motion.

### **VI.1 Nomograms for Individual Spectral Shapes with Combined Soil Types**

The cask response is not very sensitive to the soil type, so the results from all three soil types used in this study have been grouped together to provide larger data sets for regression analysis. The cask response is much more sensitive to the coefficient of friction between the cask and pad, and the cask design. In this section, analysis results from a given cask design, spectral shape, and cask/pad friction coefficient are grouped together. These plots are shown on logarithmic scales. The individual analysis results obtained using the soft soil, stiff soil, and rock profiles are color-coded separately and shown on these plots. Regression fits are provided for the peak cask top displacement and peak cask rotation as a function of PGA.

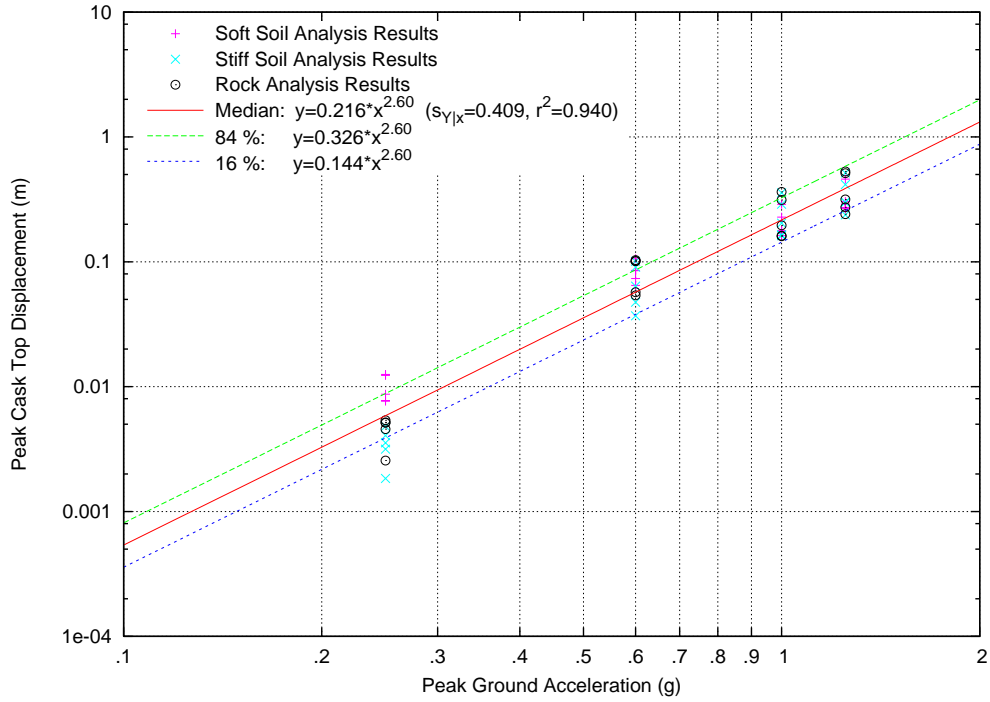


Figure VI.1: Peak Top Displacement Regression Fit, Cylindrical Cask, NUREG/CR-0098 Earthquakes, Cask/Pad  $\mu=0.2$ , All Soil Profiles

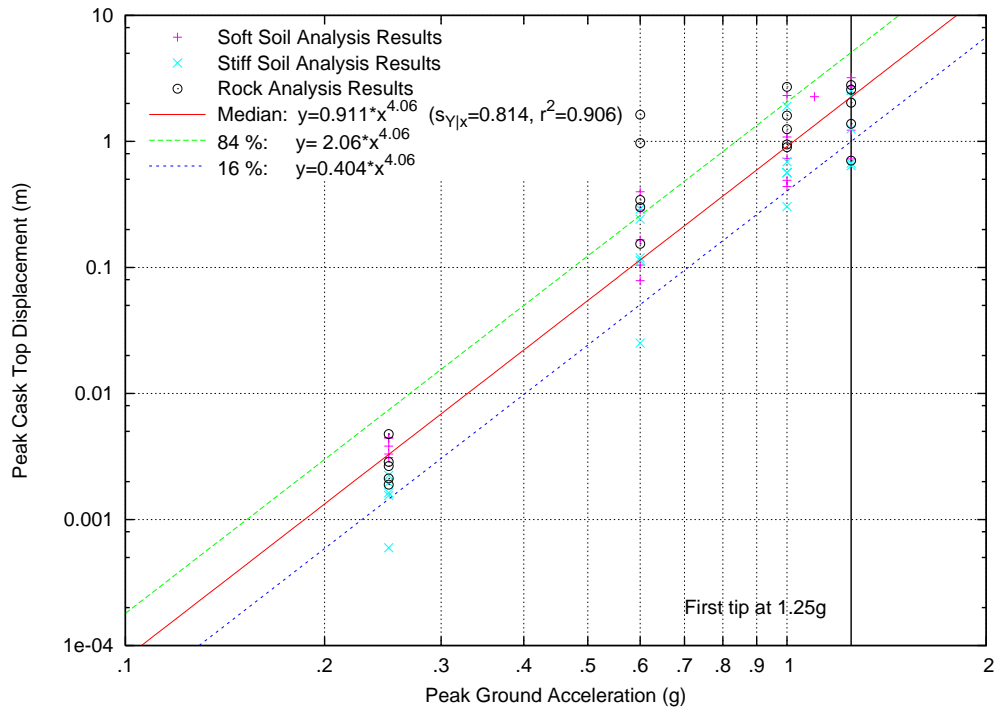


Figure VI.2: Peak Top Displacement Regression Fit, Cylindrical Cask, NUREG/CR-0098 Earthquakes, Cask/Pad  $\mu=0.55$ , All Soil Profiles

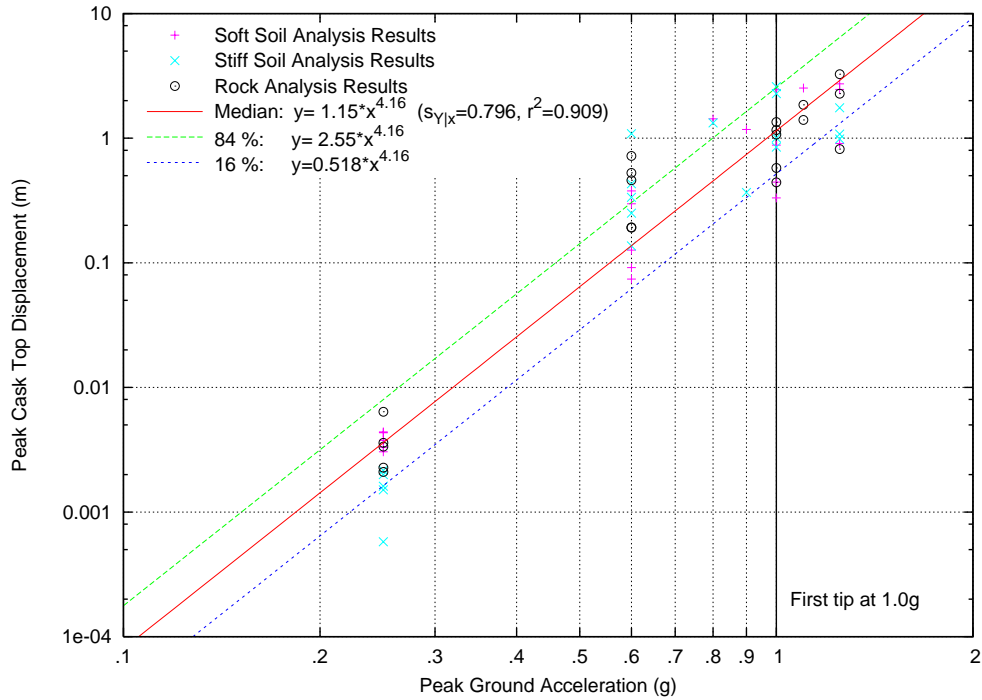


Figure VI.3: Peak Top Displacement Regression Fit, Cylindrical Cask, NUREG/CR-0098 Earthquakes, Cask/Pad  $\mu=0.8$ , All Soil Profiles

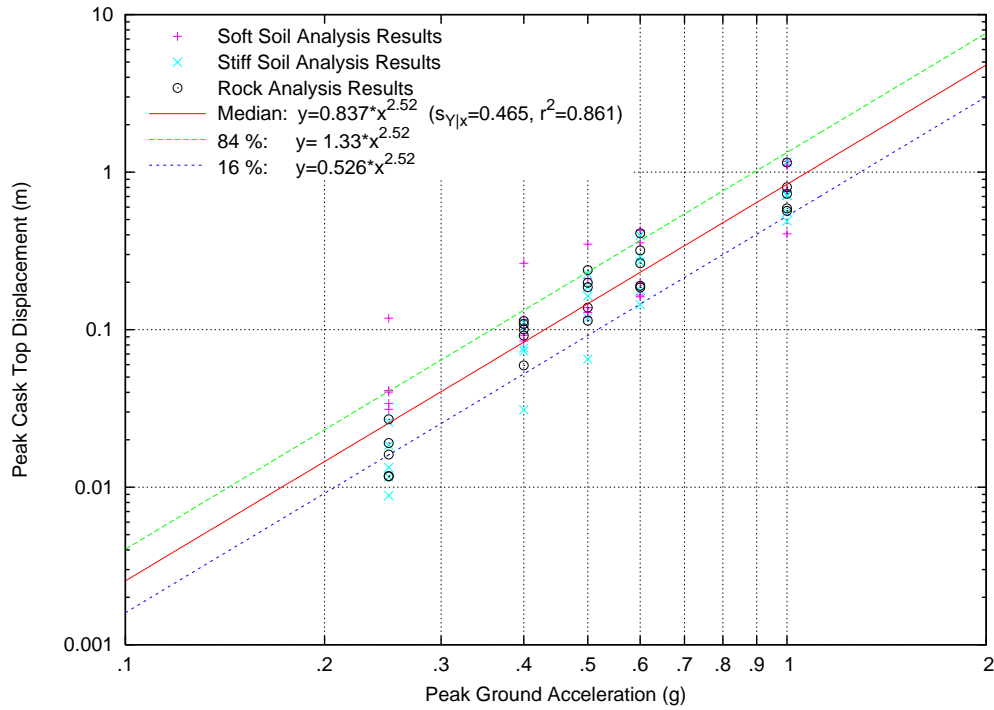


Figure VI.4: Peak Top Displacement Regression Fit, Cylindrical Cask, Regulatory Guide 1.60 Earthquakes, Cask/Pad  $\mu=0.2$ , All Soil Profiles

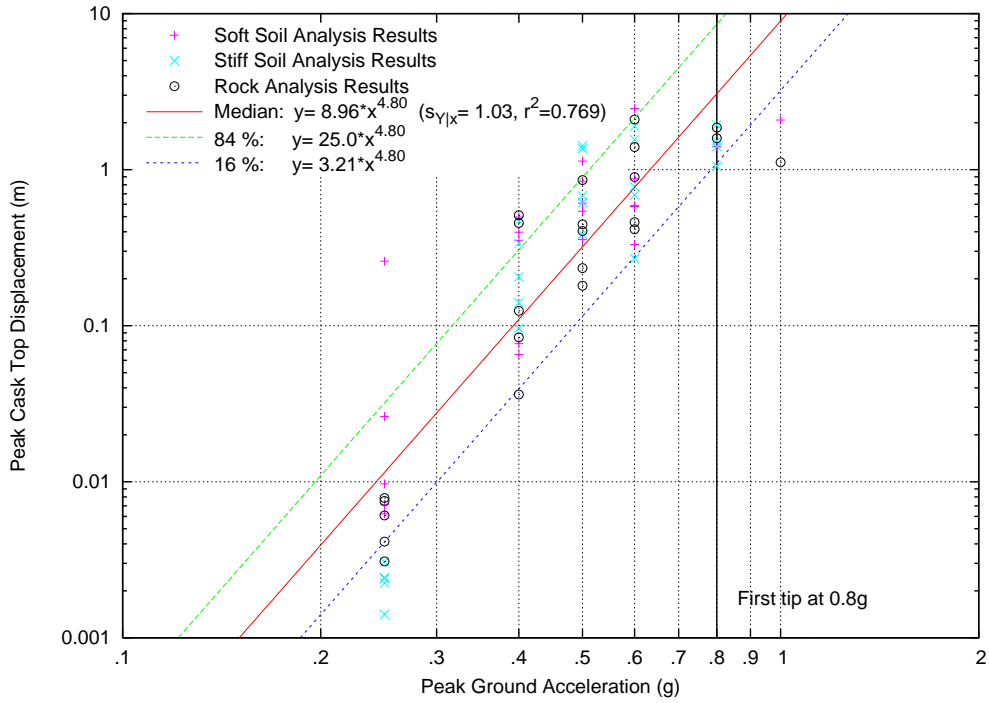


Figure VI.5: Peak Top Displacement Regression Fit, Cylindrical Cask, Regulatory Guide 1.60 Earthquakes, Cask/Pad  $\mu=0.55$ , All Soil Profiles

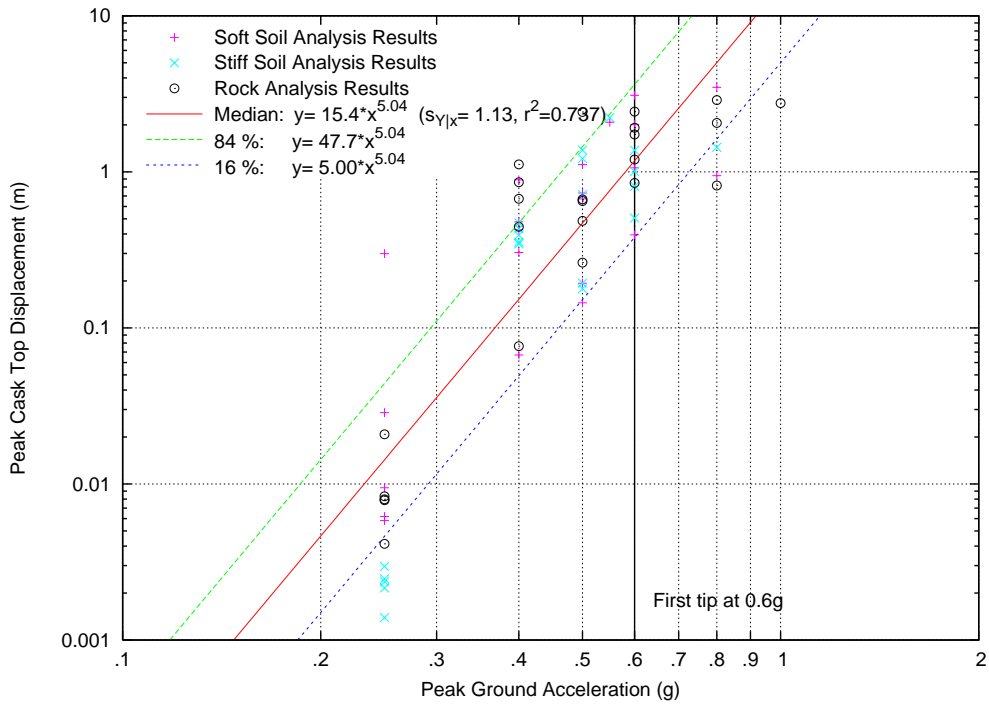


Figure VI.6: Peak Top Displacement Regression Fit, Cylindrical Cask, Regulatory Guide 1.60 Earthquakes, Cask/Pad  $\mu=0.8$ , All Soil Profiles

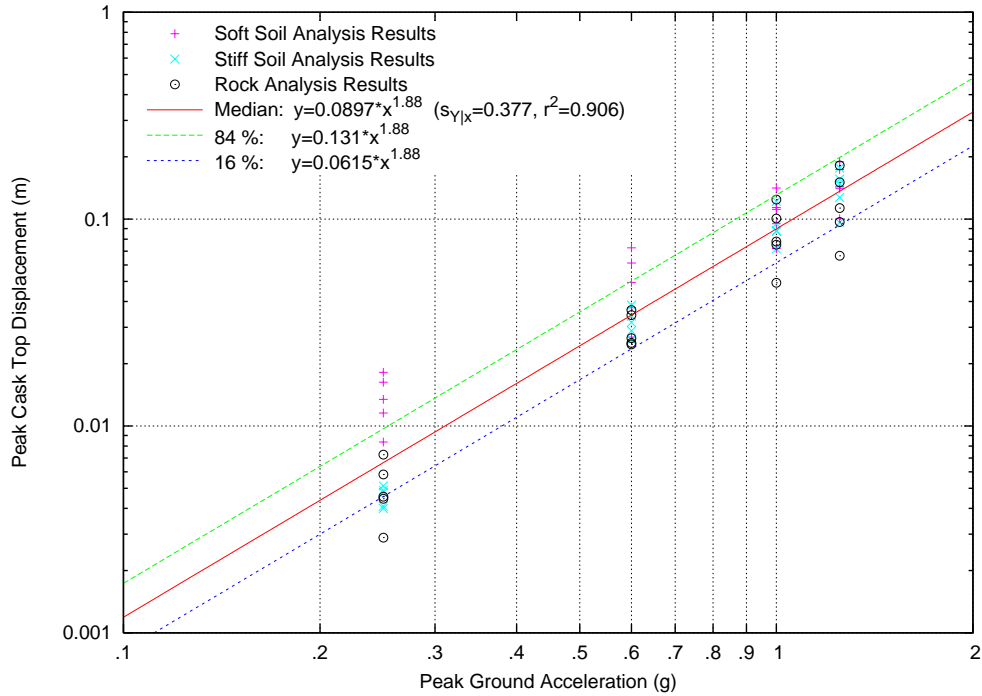


Figure VI.7: Peak Top Displacement Regression Fit, Cylindrical Cask, NUREG/CR-6728 Earthquakes, Cask/Pad  $\mu=0.2$ , All Soil Profiles

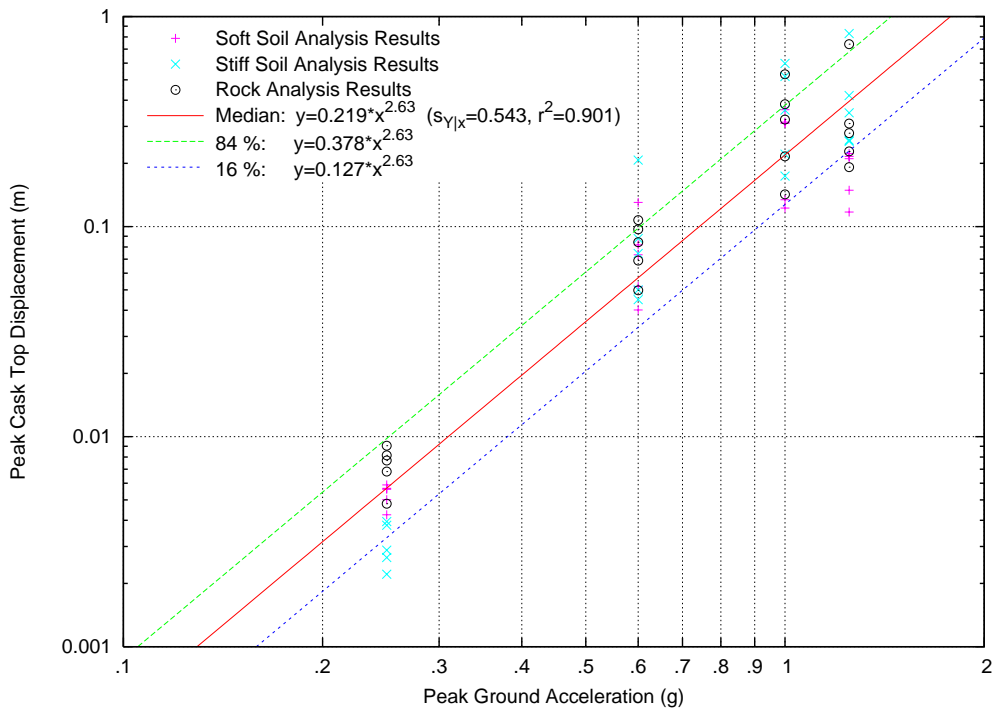


Figure VI.8: Peak Top Displacement Regression Fit, Cylindrical Cask, NUREG/CR-6728 Earthquakes, Cask/Pad  $\mu=0.55$ , All Soil Profiles

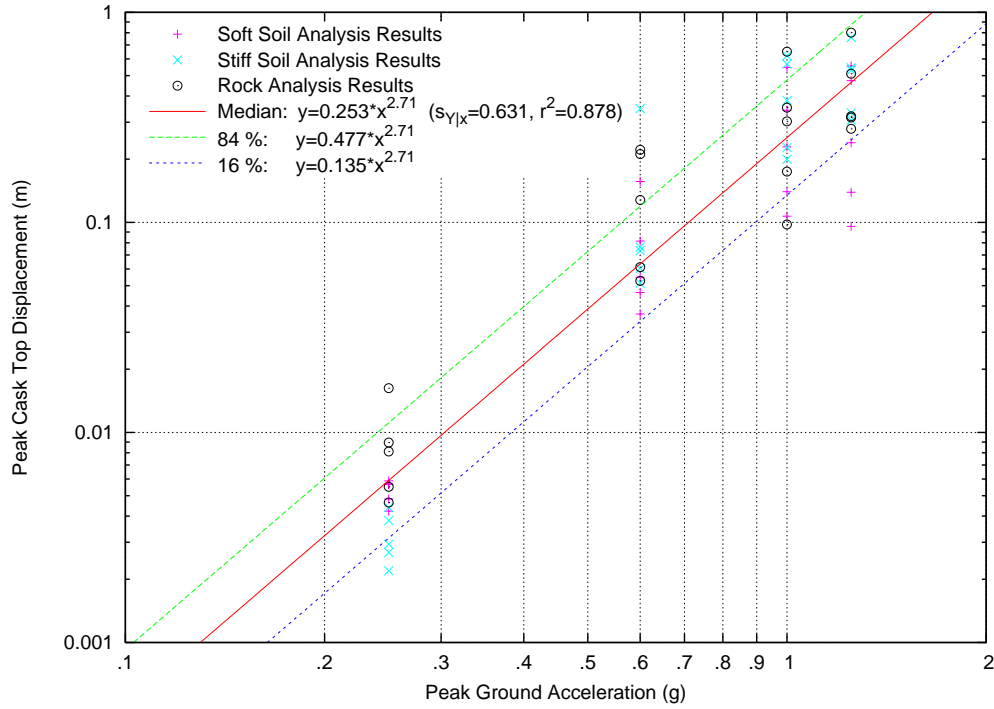


Figure VI.9: Peak Top Displacement Regression Fit, Cylindrical Cask, NUREG/CR-6728 Earthquakes, Cask/Pad  $\mu=0.8$ , All Soil Profiles

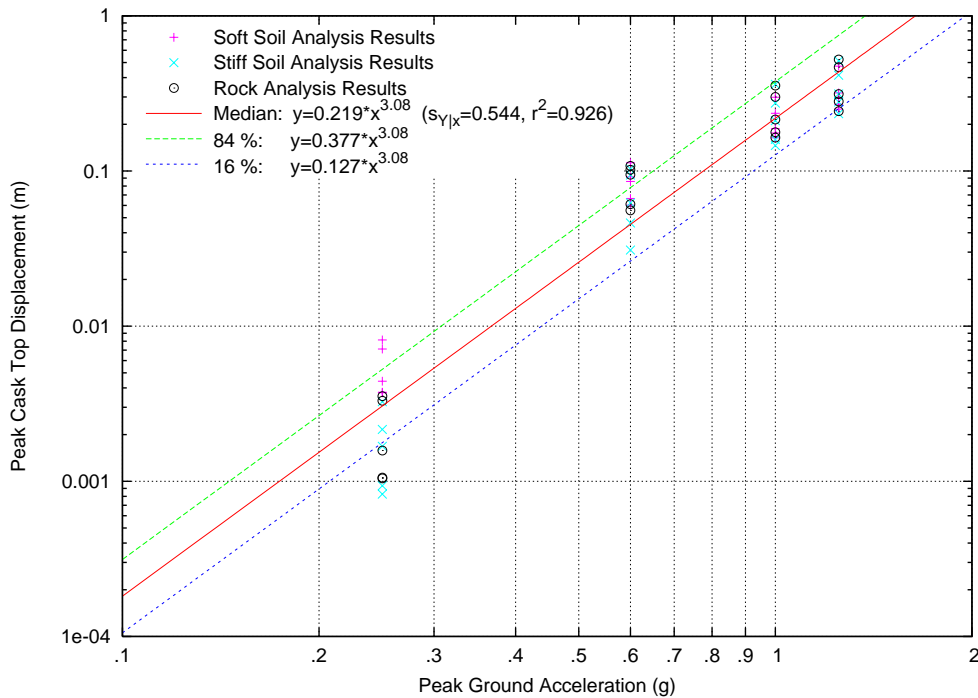


Figure VI.10: Peak Top Displacement Regression Fit, Rectangular Module, NUREG/CR-0098 Earthquakes, Cask/Pad  $\mu=0.2$ , All Soil Profiles

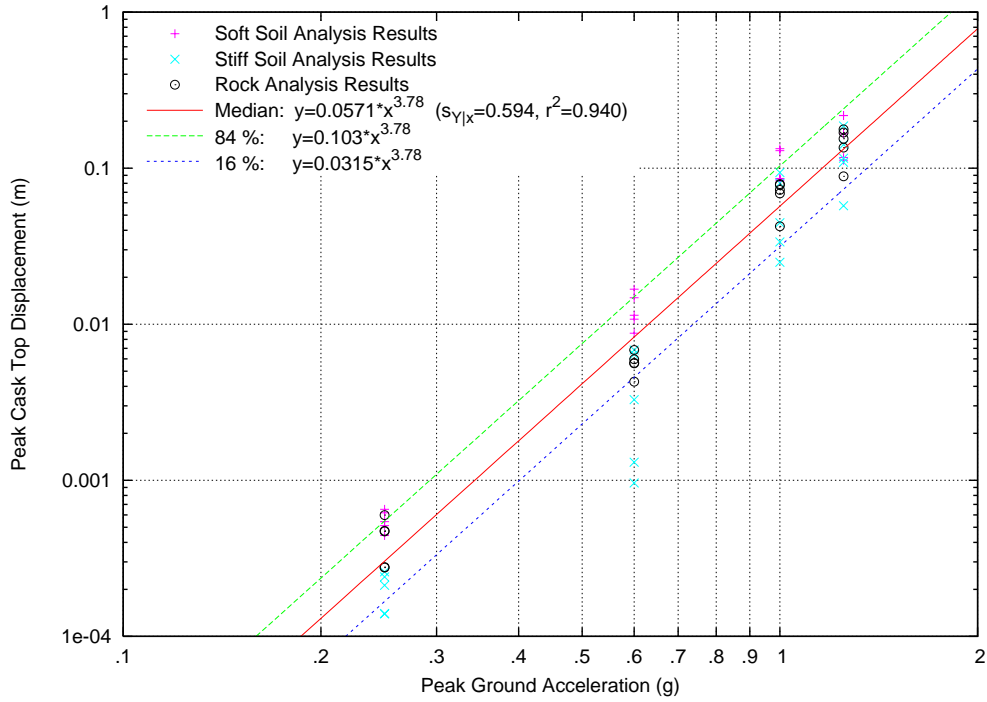


Figure VI.11: Peak Top Displacement Regression Fit, Rectangular Module, NUREG/CR-0098 Earthquakes, Cask/Pad  $\mu=0.55$ , All Soil Profiles

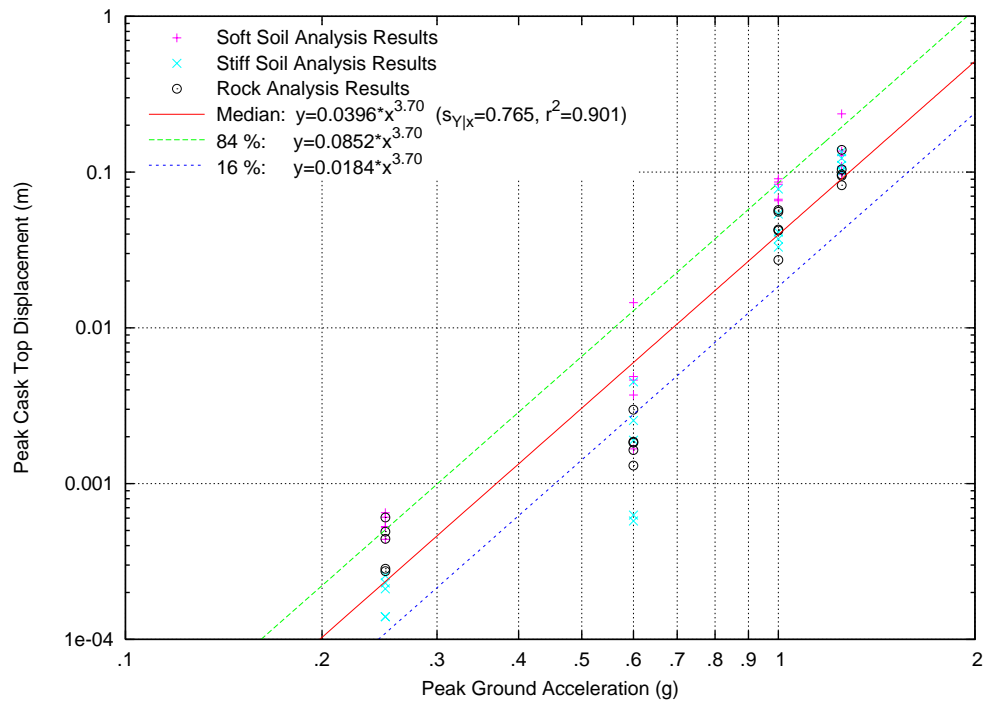


Figure VI.12: Peak Top Displacement Regression Fit, Rectangular Module, NUREG/CR-0098 Earthquakes, Cask/Pad  $\mu=0.8$ , All Soil Profiles

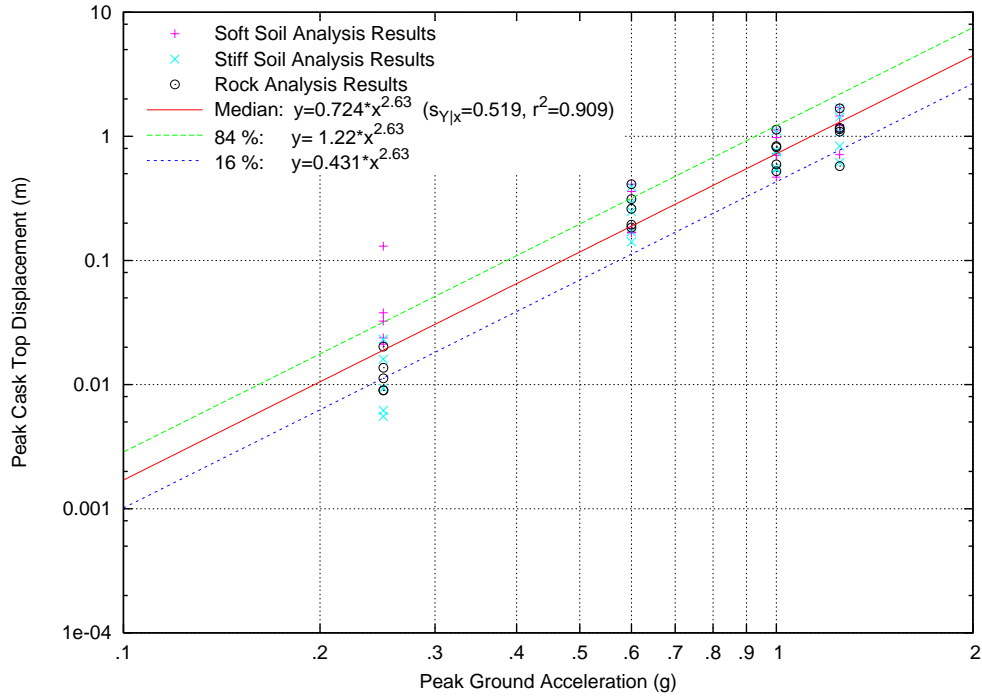


Figure VI.13: Peak Top Displacement Regression Fit, Rectangular Module, Regulatory Guide 1.60 Earthquakes, Cask/Pad  $\mu=0.2$ , All Soil Profiles

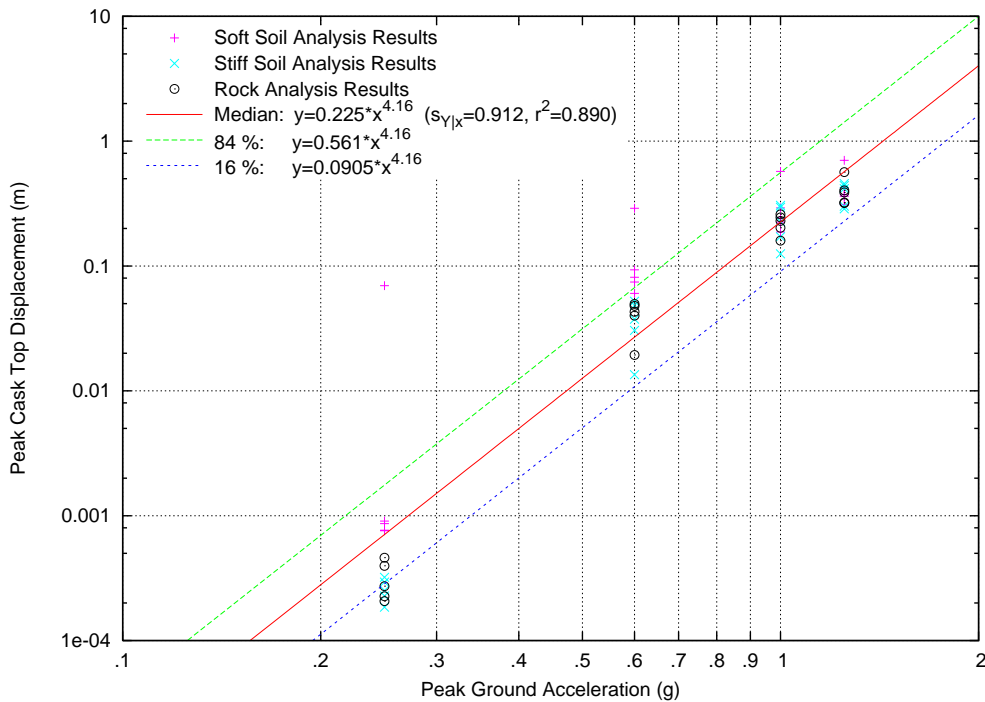


Figure VI.14: Peak Top Displacement Regression Fit, Rectangular Module, Regulatory Guide 1.60 Earthquakes, Cask/Pad  $\mu=0.55$ , All Soil Profiles

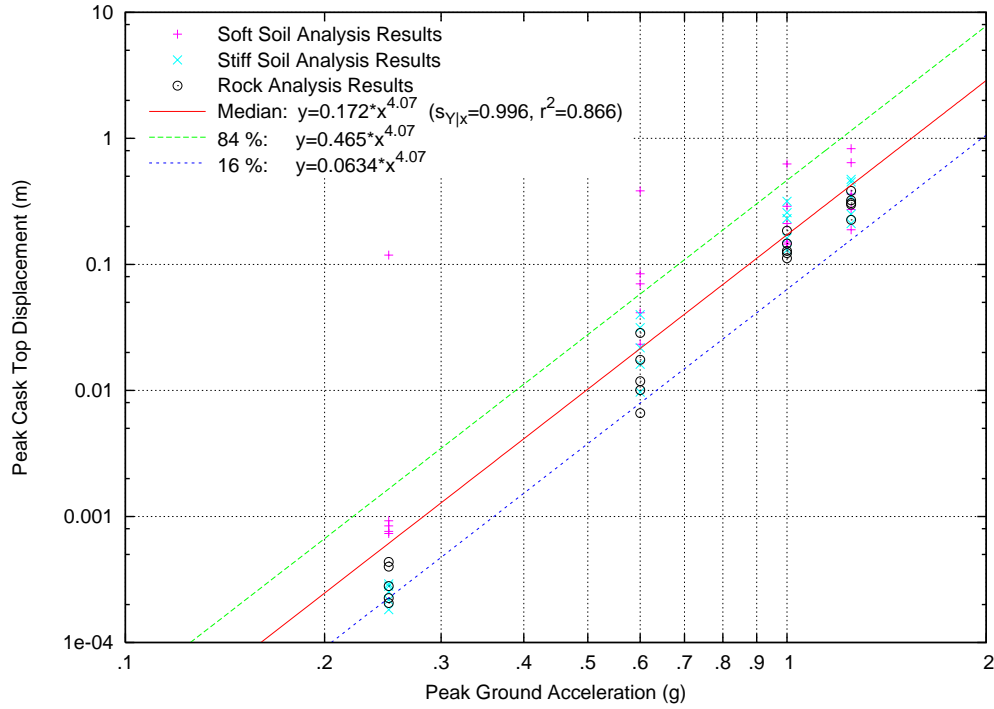


Figure VI.15: Peak Top Displacement Regression Fit, Rectangular Module, Regulatory Guide 1.60 Earthquakes, Cask/Pad  $\mu=0.8$ , All Soil Profiles

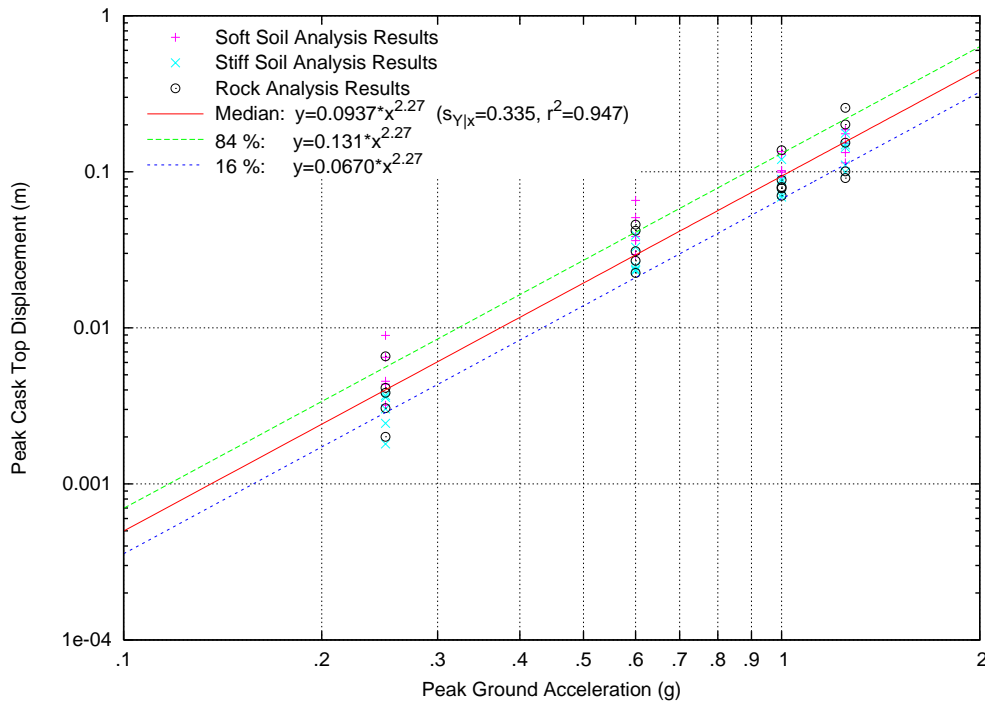


Figure VI.16: Peak Top Displacement Regression Fit, Rectangular Module, NUREG/CR-6728 Earthquakes, Cask/Pad  $\mu=0.2$ , All Soil Profiles

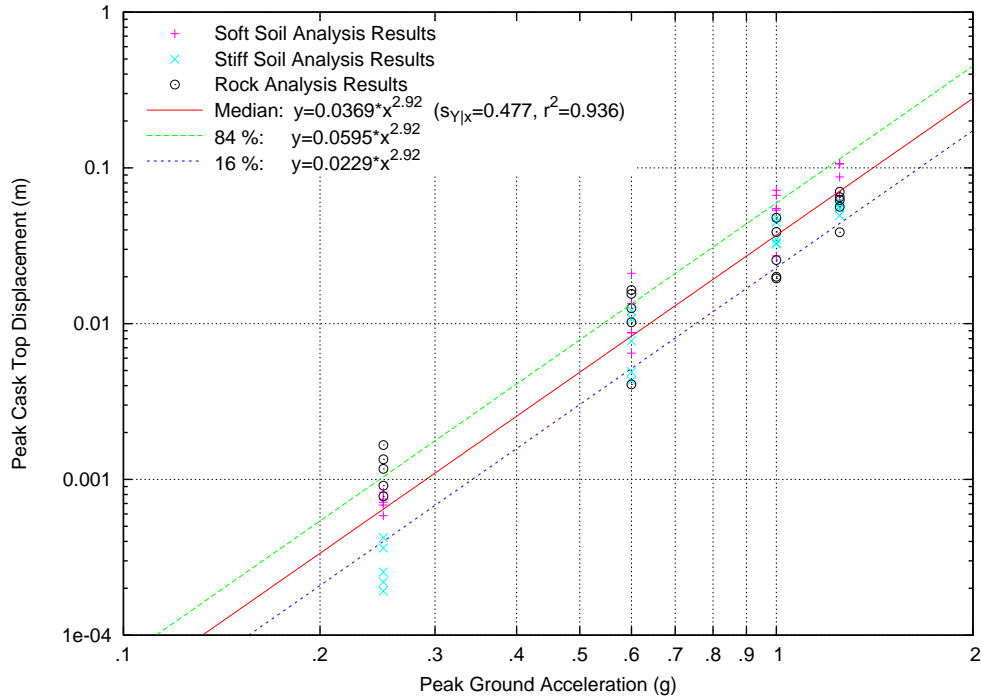


Figure VI.17: Peak Top Displacement Regression Fit, Rectangular Module, NUREG/CR-6728 Earthquakes, Cask/Pad  $\mu=0.55$ , All Soil Profiles

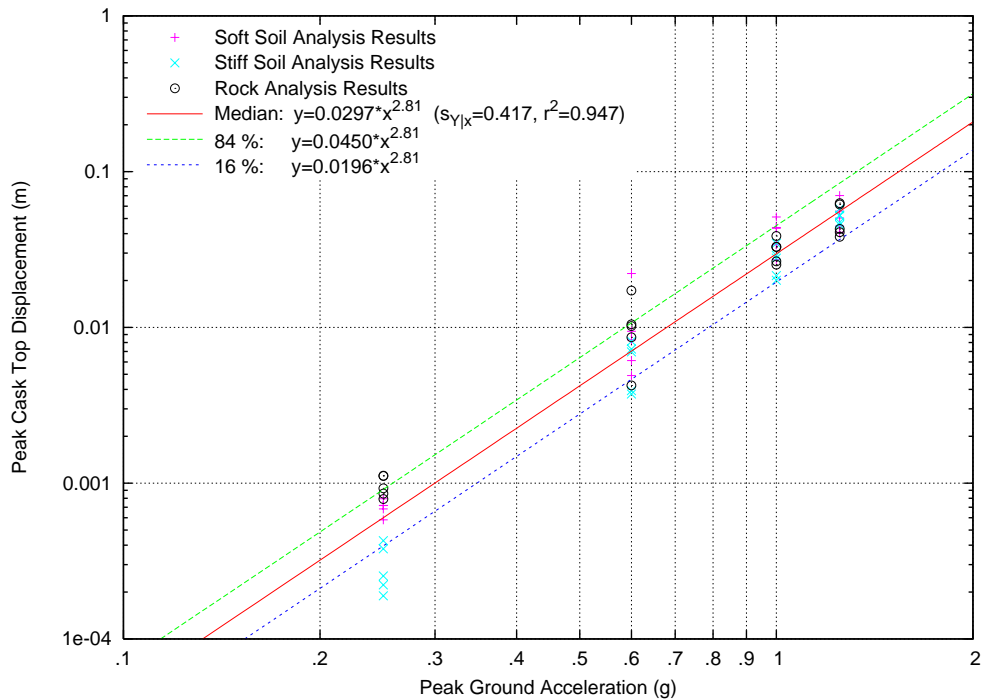


Figure VI.18: Peak Top Displacement Regression Fit, Rectangular Module, NUREG/CR-6728 Earthquakes, Cask/Pad  $\mu=0.8$ , All Soil Profiles

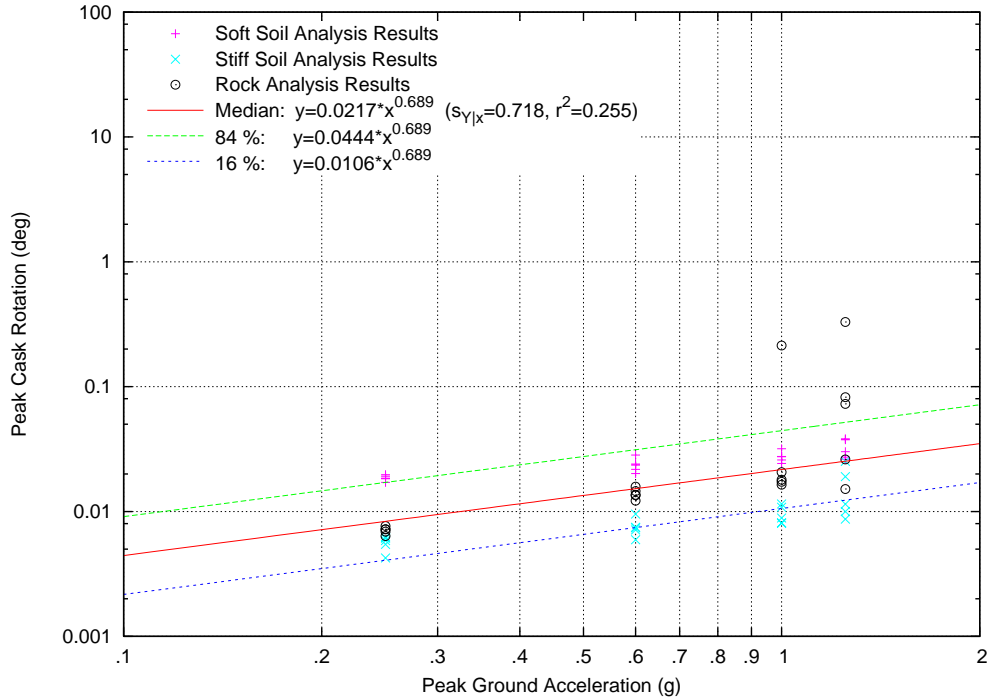


Figure VI.19: Peak Rotation Regression Fit, Cylindrical Cask, NUREG/CR-0098 Earthquakes, Cask/Pad  $\mu=0.2$ , All Soil Profiles

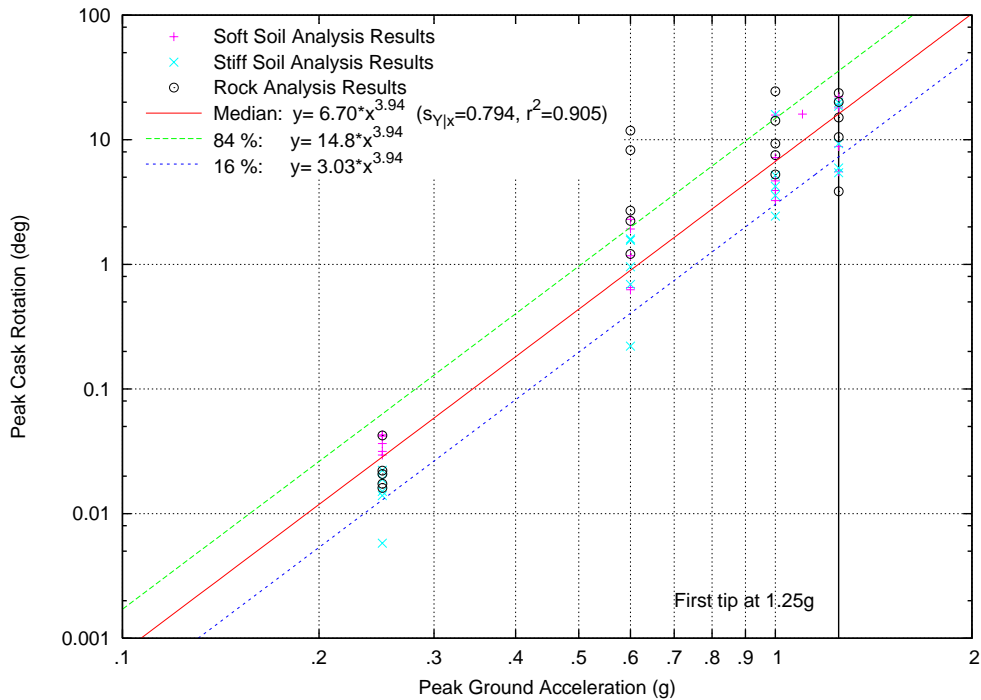


Figure VI.20: Peak Rotation Regression Fit, Cylindrical Cask, NUREG/CR-0098 Earthquakes, Cask/Pad  $\mu=0.55$ , All Soil Profiles

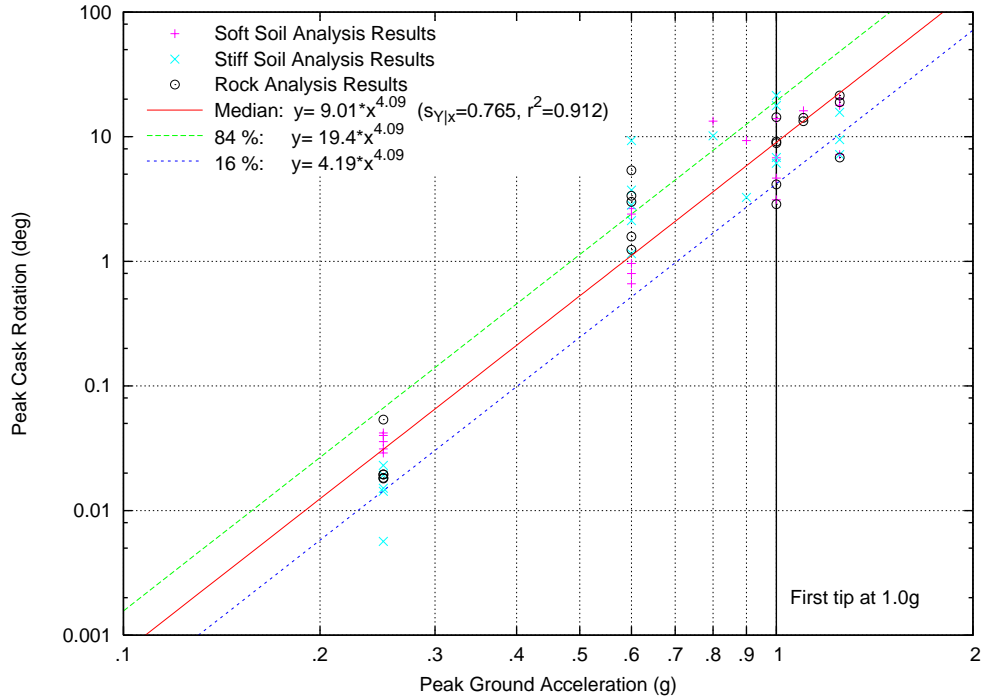


Figure VI.21: Peak Rotation Regression Fit, Cylindrical Cask, NUREG/CR-0098 Earthquakes, Cask/Pad  $\mu=0.8$ , All Soil Profiles

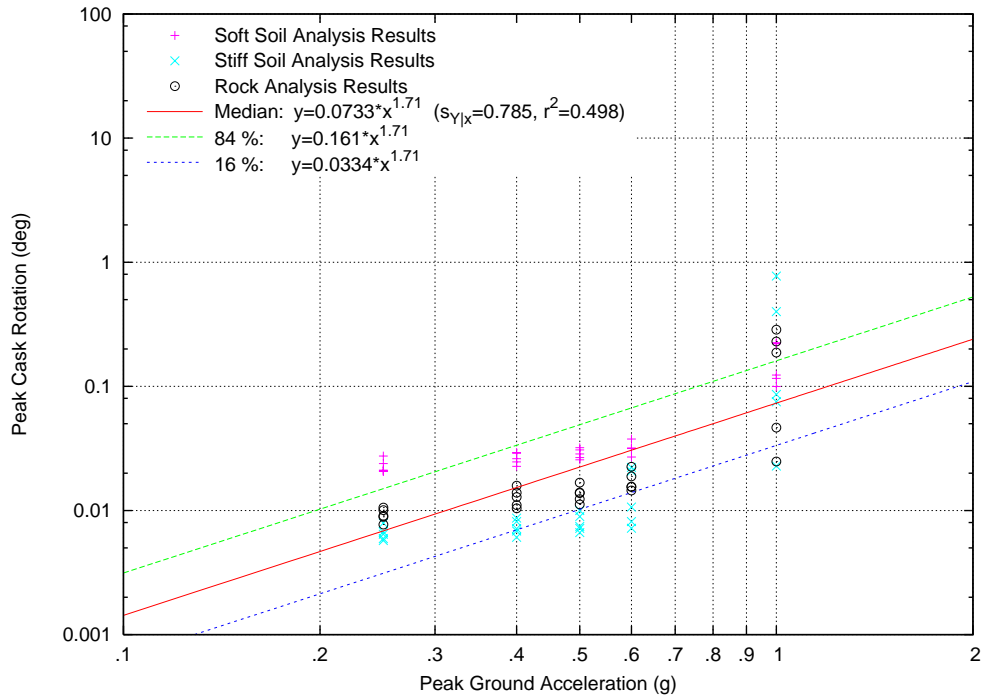


Figure VI.22: Peak Rotation Regression Fit, Cylindrical Cask, Regulatory Guide 1.60 Earthquakes, Cask/Pad  $\mu=0.2$ , All Soil Profiles

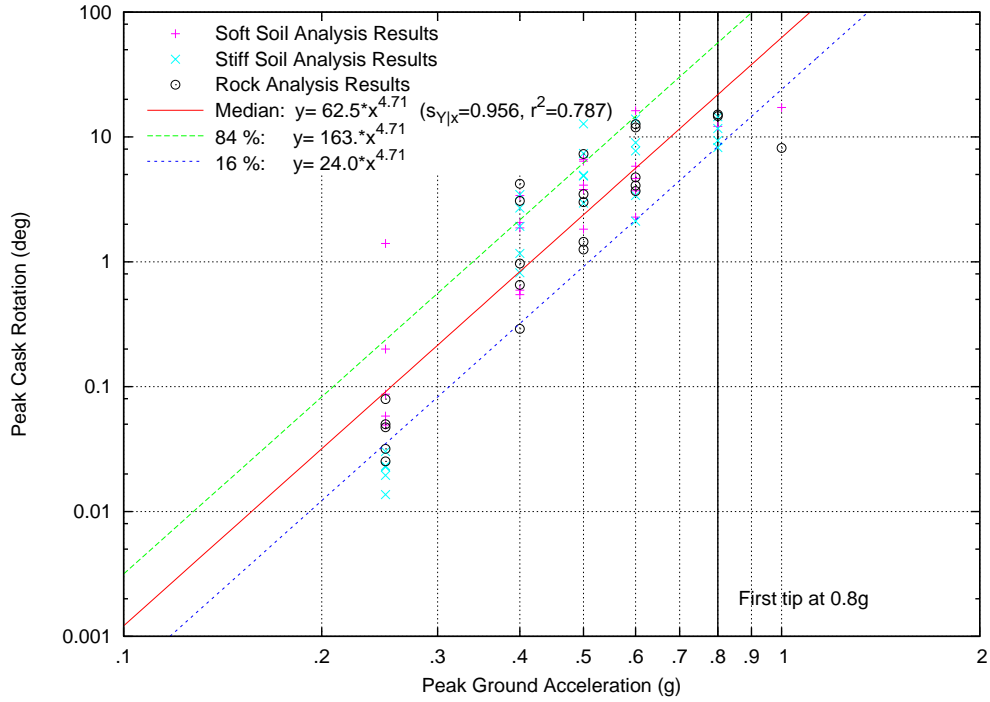


Figure VI.23: Peak Rotation Regression Fit, Cylindrical Cask, Regulatory Guide 1.60 Earthquakes, Cask/Pad  $\mu=0.55$ , All Soil Profiles

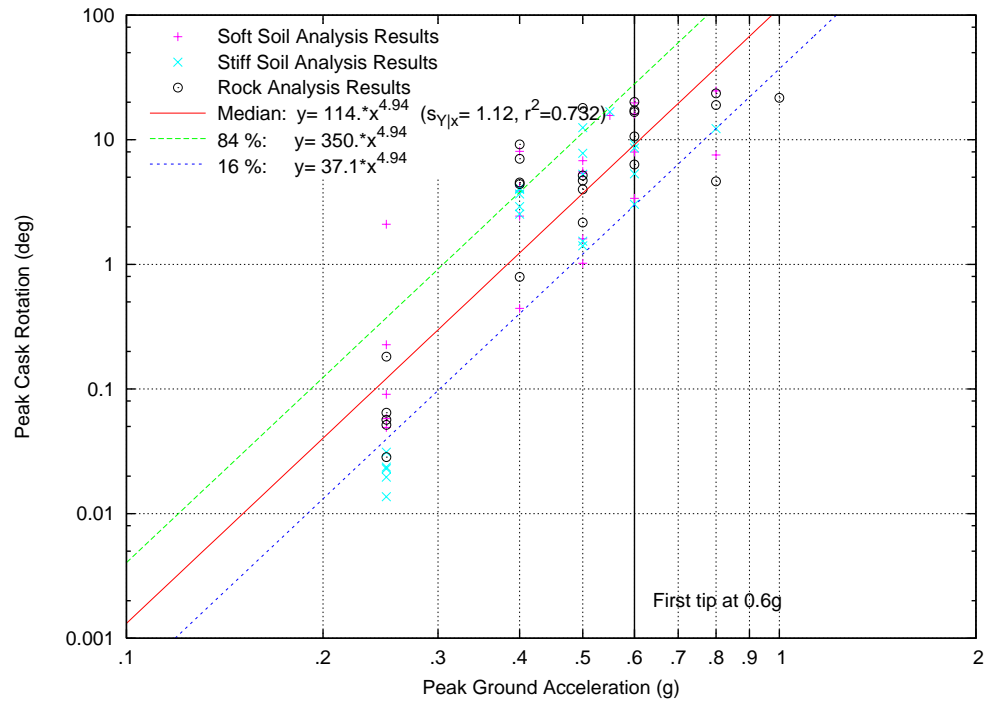


Figure VI.24: Peak Rotation Regression Fit, Cylindrical Cask, Regulatory Guide 1.60 Earthquakes, Cask/Pad  $\mu=0.8$ , All Soil Profiles

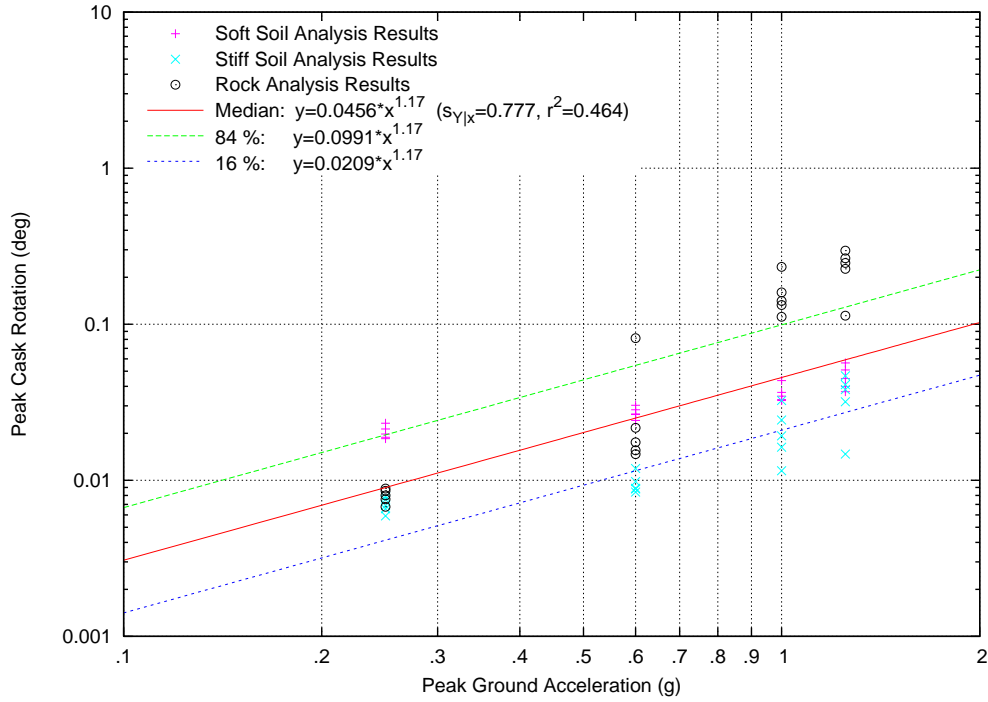


Figure VI.25: Peak Rotation Regression Fit, Cylindrical Cask, NUREG/CR-6728 Earthquakes, Cask/Pad  $\mu=0.2$ , All Soil Profiles

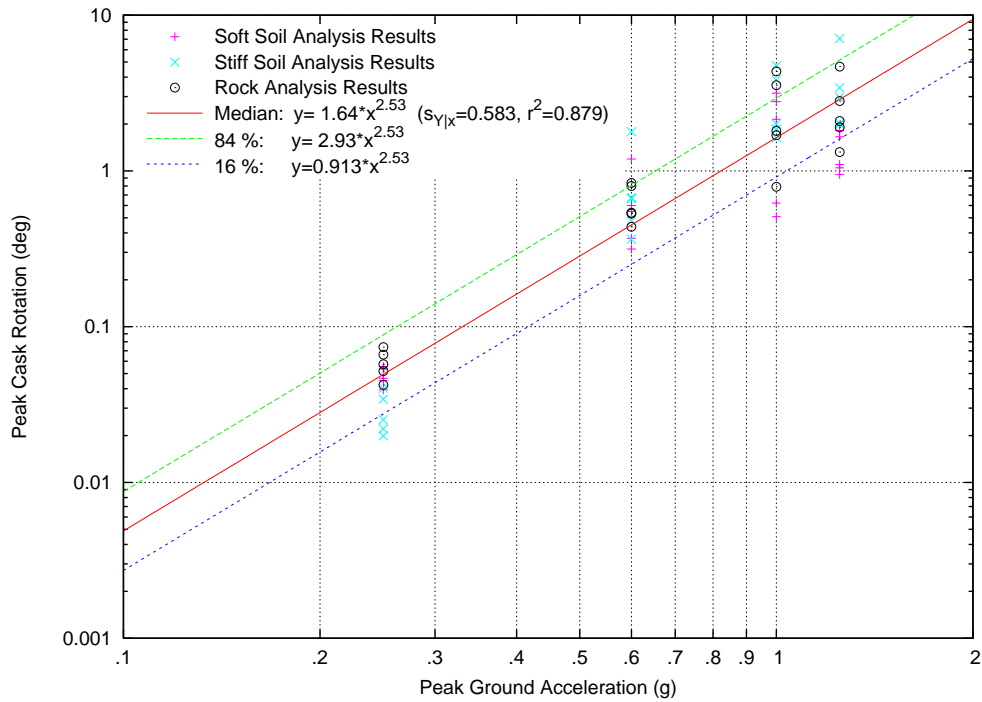


Figure VI.26: Peak Rotation Regression Fit, Cylindrical Cask, NUREG/CR-6728 Earthquakes, Cask/Pad  $\mu=0.55$ , All Soil Profiles

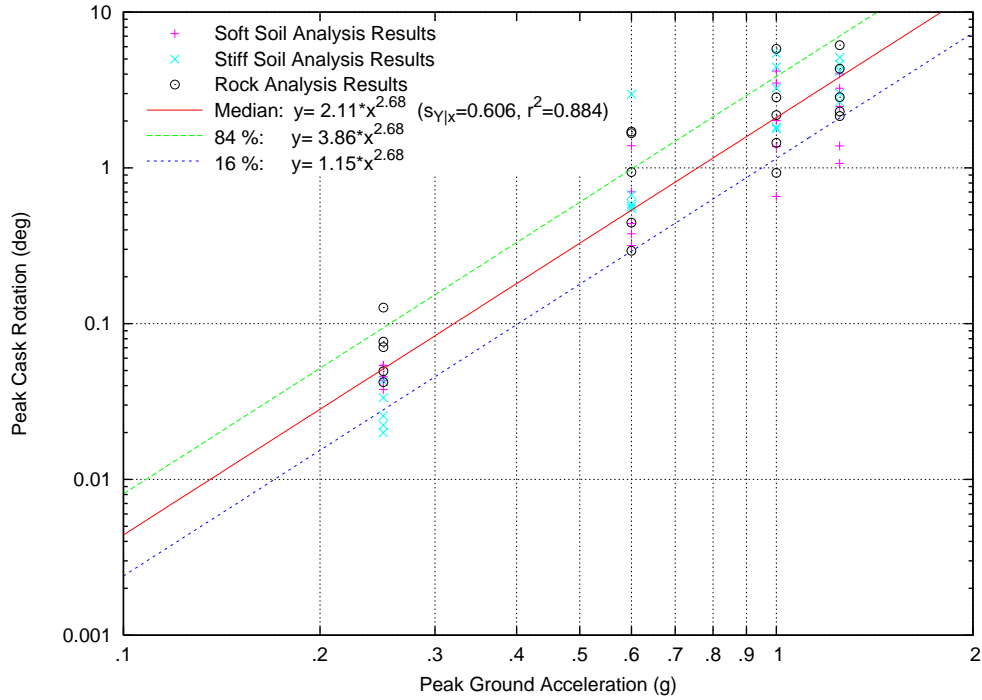


Figure VI.27: Peak Rotation Regression Fit, Cylindrical Cask, NUREG/CR-6728 Earthquakes, Cask/Pad  $\mu=0.8$ , All Soil Profiles

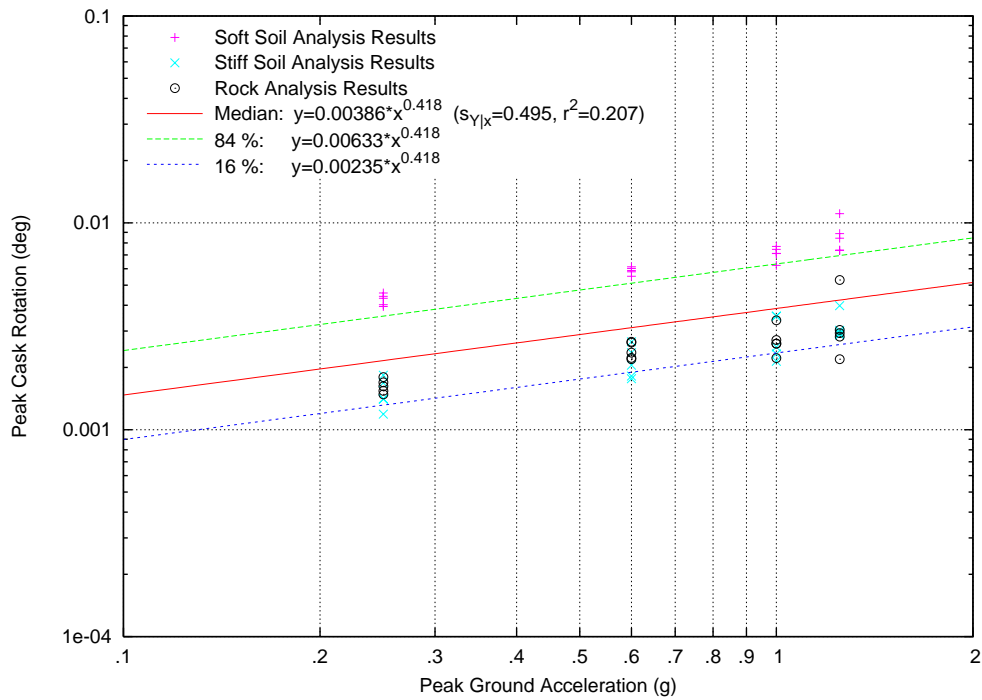


Figure VI.28: Peak Rotation Regression Fit, Rectangular Module, NUREG/CR-0098 Earthquakes, Cask/Pad  $\mu=0.2$ , All Soil Profiles

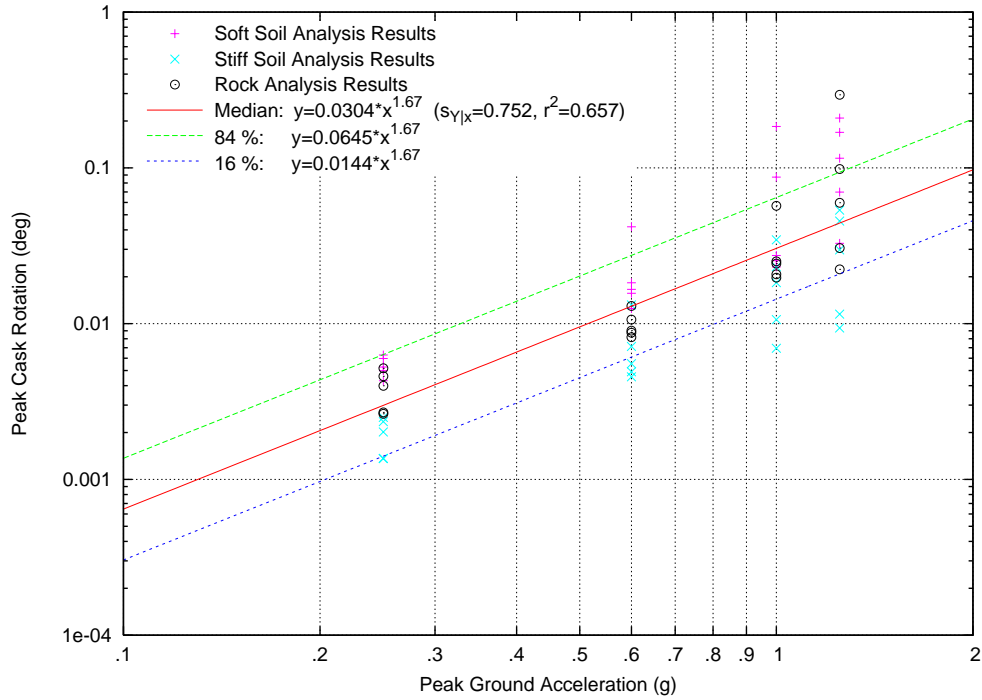


Figure VI.29: Peak Rotation Regression Fit, Rectangular Module, NUREG/CR-0098 Earthquakes, Cask/Pad  $\mu=0.55$ , All Soil Profiles

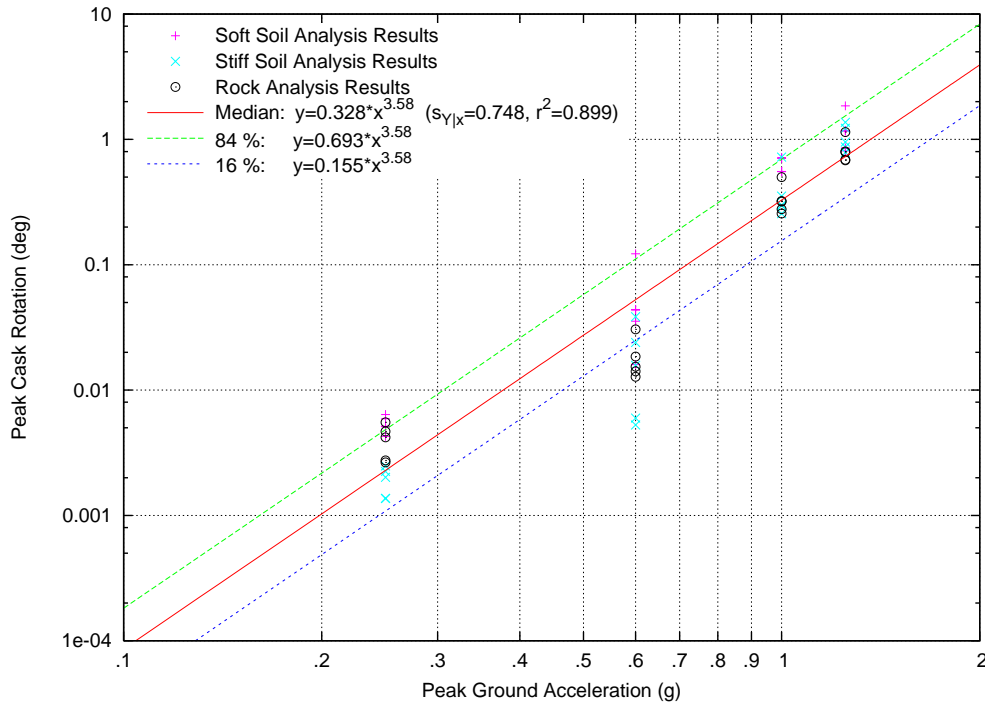


Figure VI.30: Peak Rotation Regression Fit, Rectangular Module, NUREG/CR-0098 Earthquakes, Cask/Pad  $\mu=0.8$ , All Soil Profiles

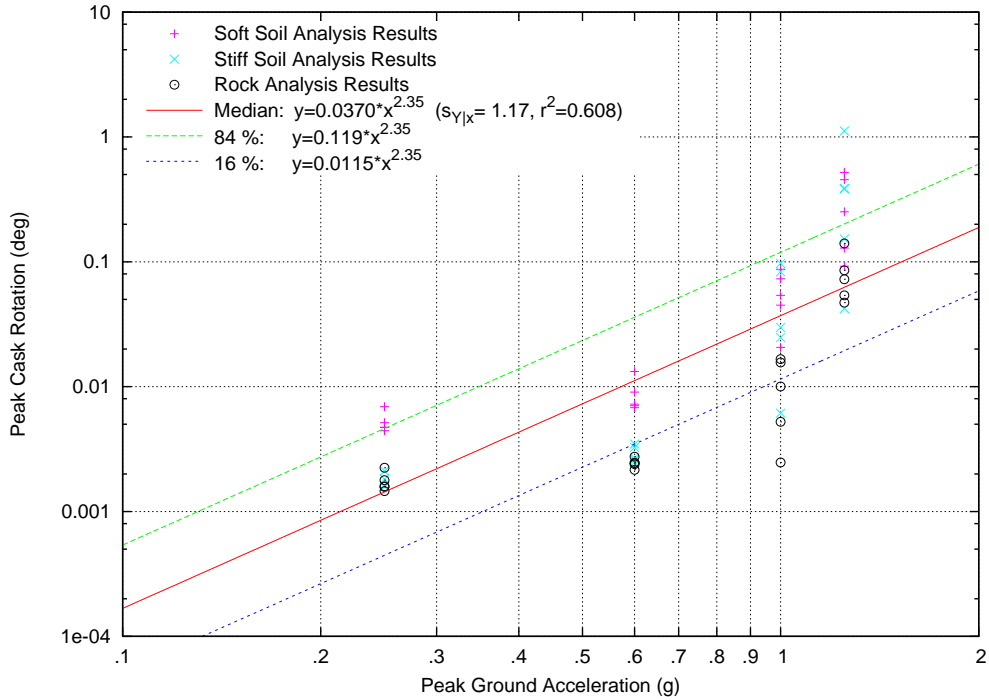


Figure VI.31: Peak Rotation Regression Fit, Rectangular Module, Regulatory Guide 1.60 Earthquakes, Cask/Pad  $\mu=0.2$ , All Soil Profiles

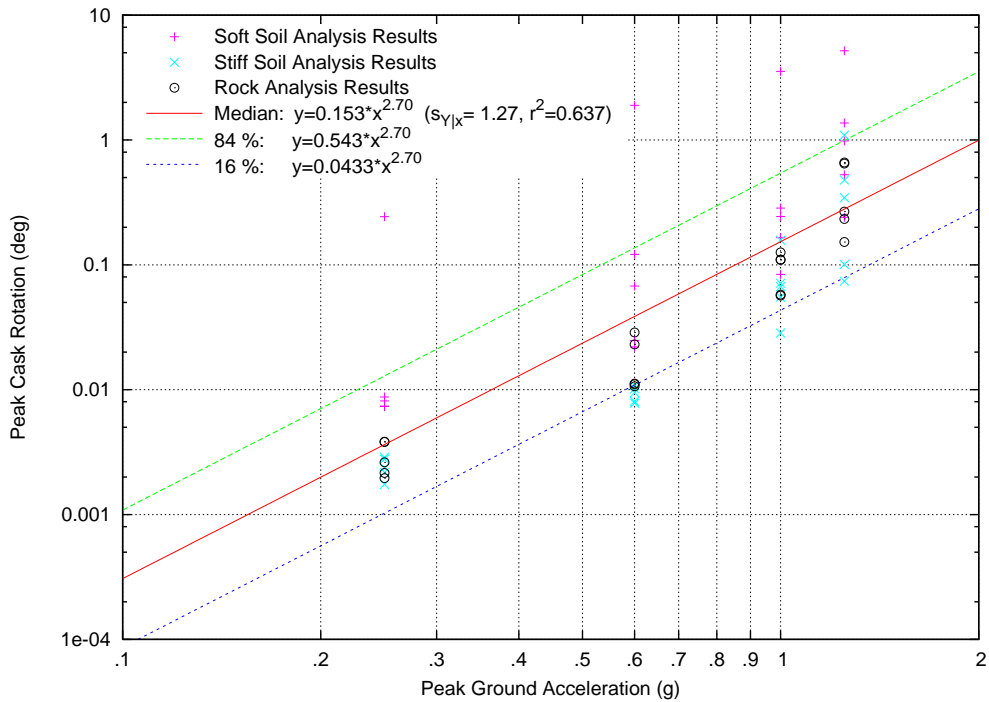


Figure VI.32: Peak Rotation Regression Fit, Rectangular Module, Regulatory Guide 1.60 Earthquakes, Cask/Pad  $\mu=0.55$ , All Soil Profiles

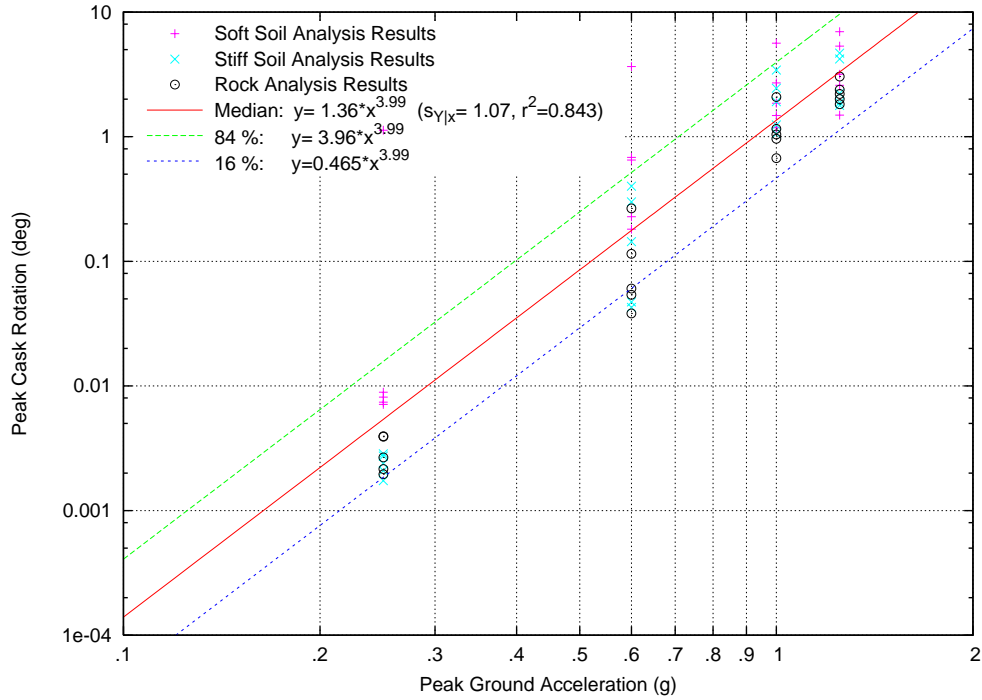


Figure VI.33: Peak Rotation Regression Fit, Rectangular Module, Regulatory Guide 1.60 Earthquakes, Cask/Pad  $\mu=0.8$ , All Soil Profiles

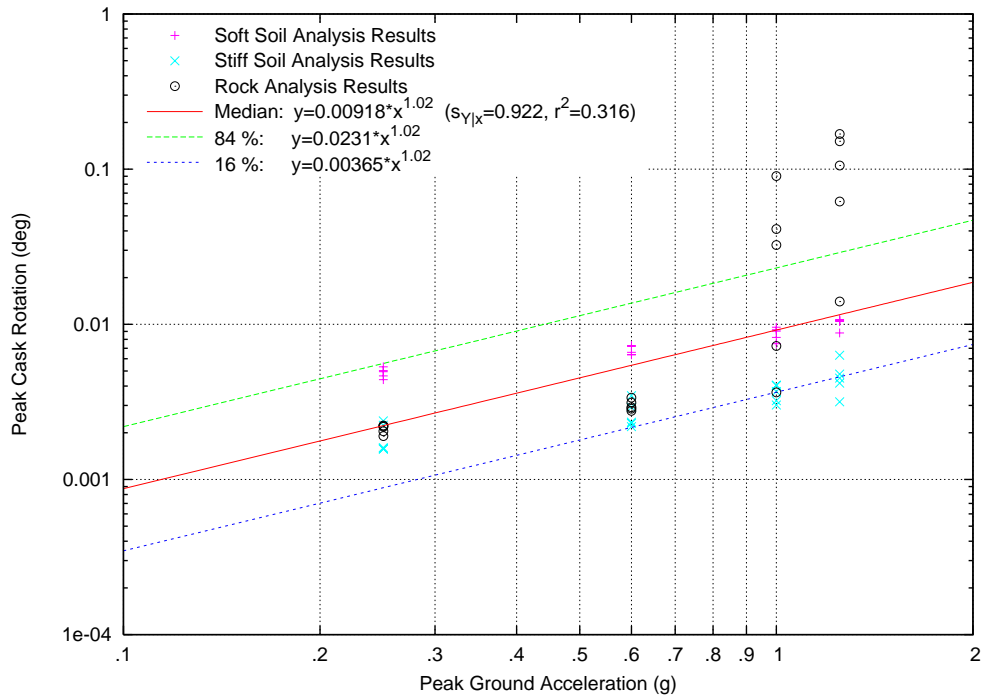


Figure VI.34: Peak Rotation Regression Fit, Rectangular Module, NUREG/CR-6728 Earthquakes, Cask/Pad  $\mu=0.2$ , All Soil Profiles

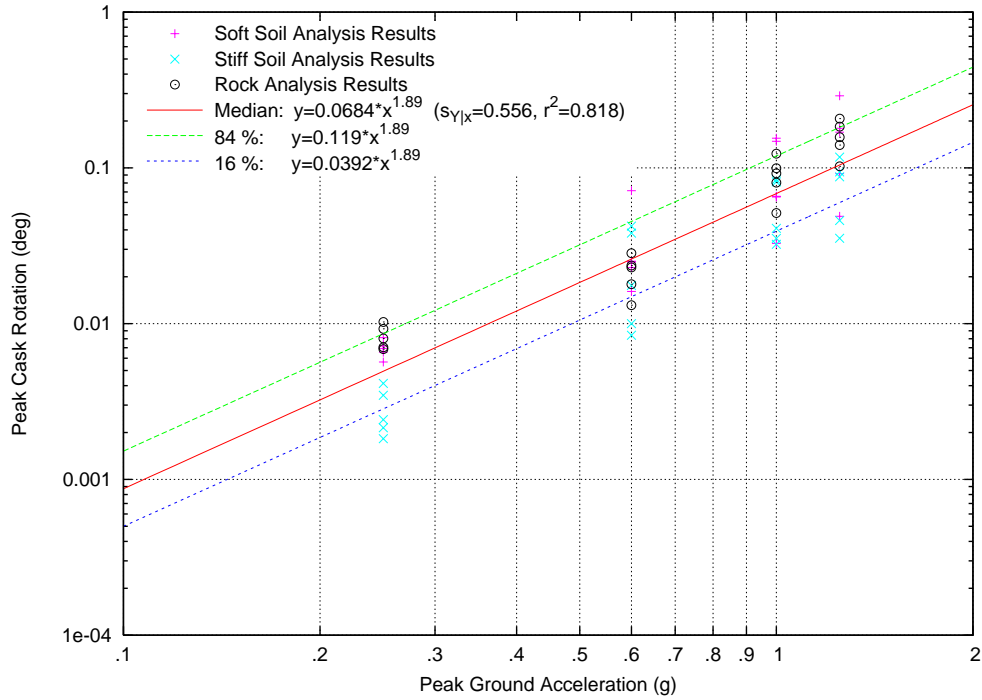


Figure VI.35: Peak Rotation Regression Fit, Rectangular Module, NUREG/CR-6728 Earthquakes, Cask/Pad  $\mu=0.55$ , All Soil Profiles

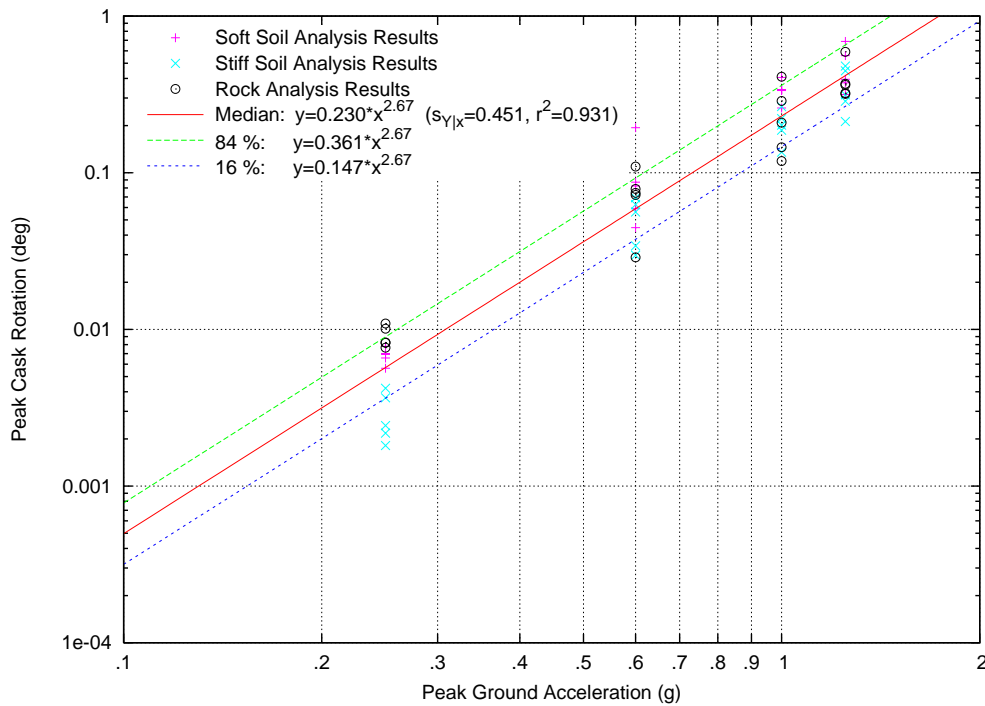


Figure VI.36: Peak Rotation Regression Fit, Rectangular Module, NUREG/CR-6728 Earthquakes, Cask/Pad  $\mu=0.8$ , All Soil Profiles

## **VI.2 Nomograms for Combined Spectral Shapes in Terms of 1 Hz PSA**

An additional grouping has been performed on the data sets used to generate the regression plots shown in the previous section. The results obtained for all three spectral shapes are grouped together, but instead of using PGA as the ground motion parameter, the PSA at 5% damped 1Hertz (Hz) is used. This parameter is a better indicator of the cask response than the PGA and allows the analysis results from the three spectral shapes to be grouped together. Regression plots are provided for each combination of the two cask designs and three cask/pad friction coefficients. As was done in the previous section, the results for the three soil profiles are grouped together into the same data set. Plots of the peak cask top displacement and peak rotation are provided on both logarithmic and linear scales.

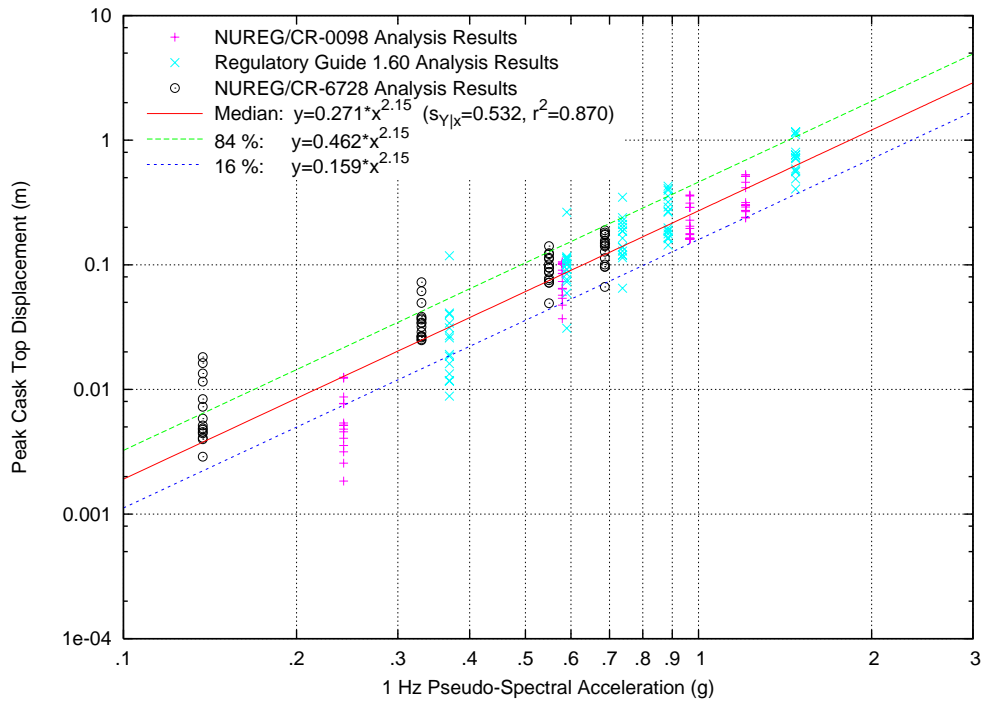


Figure VI.37: Peak Top Displacement Regression Fit in Terms of 1 Hz PSA, Logarithmic Scale, Cylindrical Cask, All Earthquakes, Cask/Pad  $\mu=0.2$ , All Soil Profiles

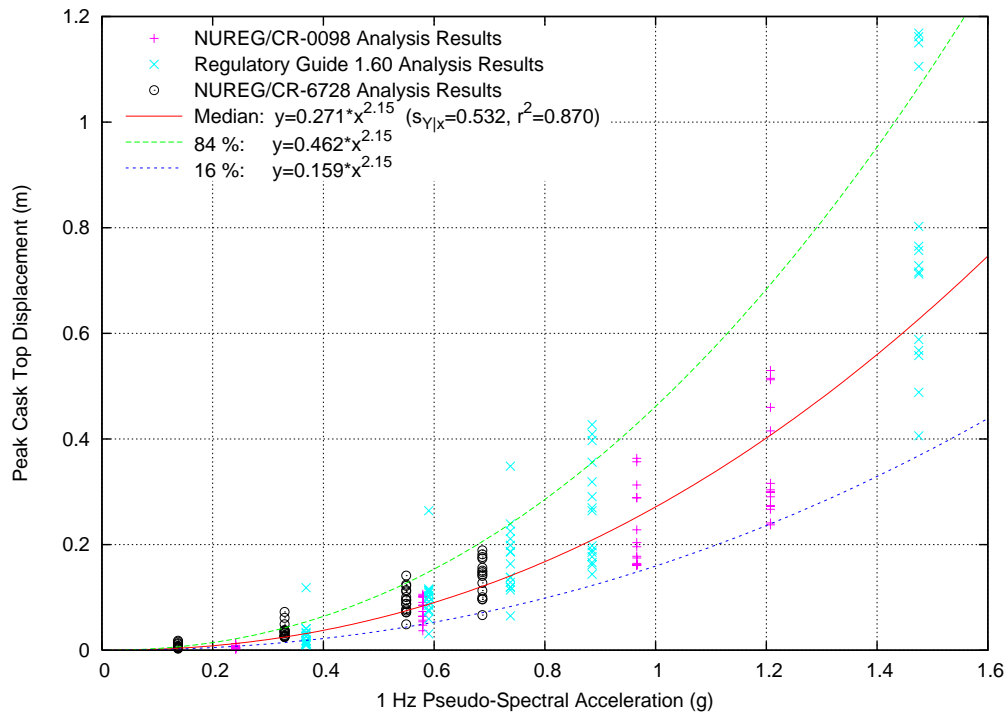


Figure VI.38: Peak Top Displacement Regression Fit in Terms of 1 Hz PSA, Linear Scale, Cylindrical Cask, All Earthquakes, Cask/Pad  $\mu=0.2$ , All Soil Profiles

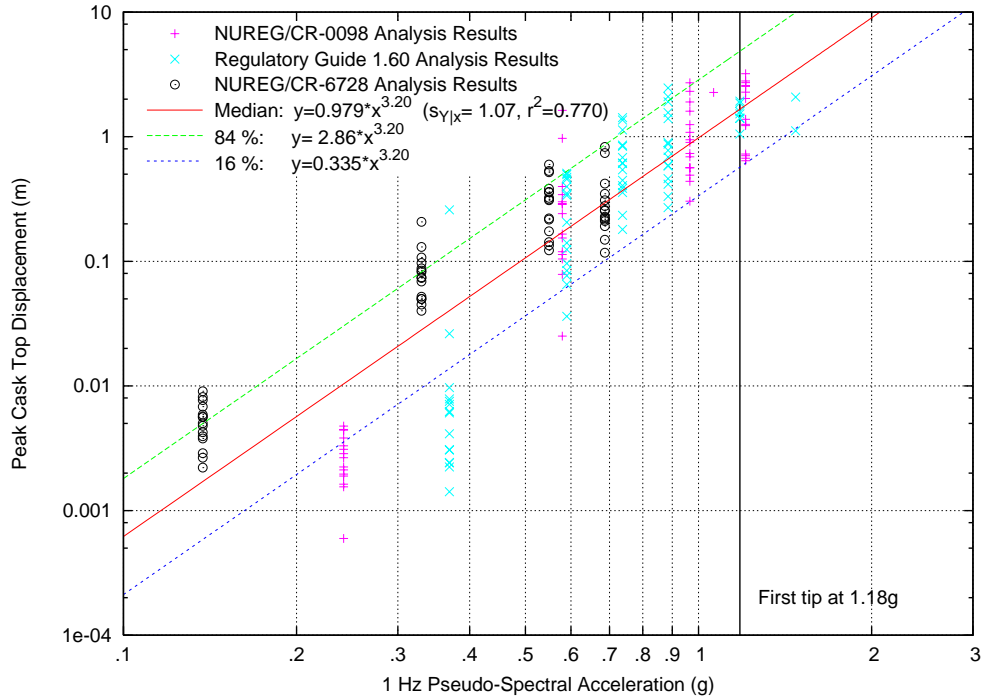


Figure VI.39: Peak Top Displacement Regression Fit in Terms of 1 Hz PSA, Logarithmic Scale, Cylindrical Cask, All Earthquakes, Cask/Pad  $\mu=0.55$ , All Soil Profiles

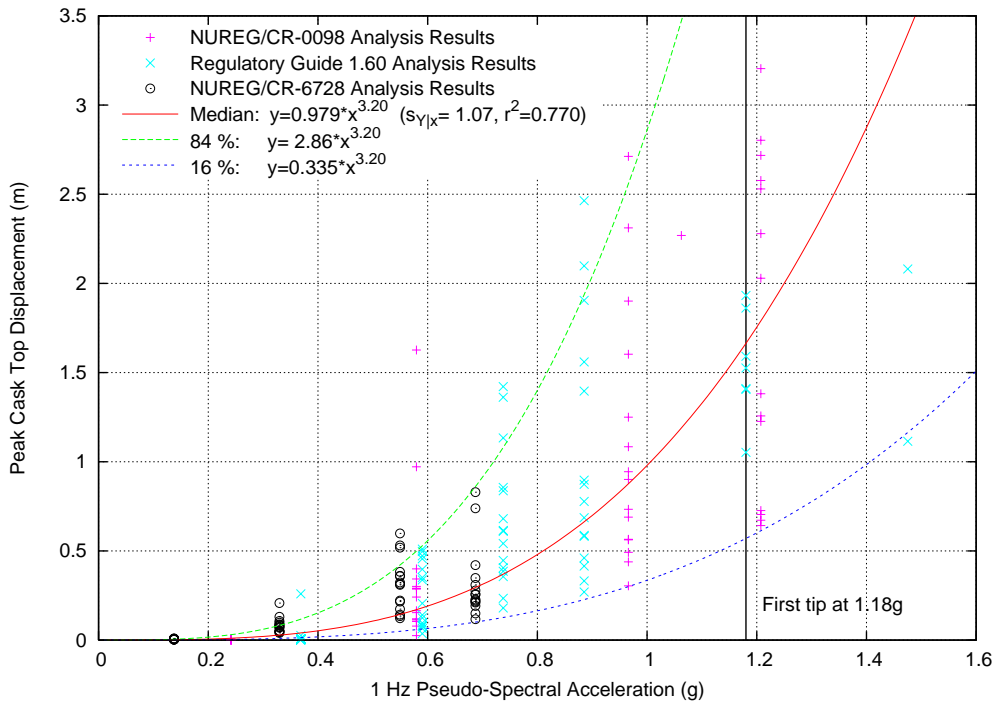


Figure VI.40: Peak Top Displacement Regression Fit in Terms of 1 Hz PSA, Linear Scale, Cylindrical Cask, All Earthquakes, Cask/Pad  $\mu=0.55$ , All Soil Profiles

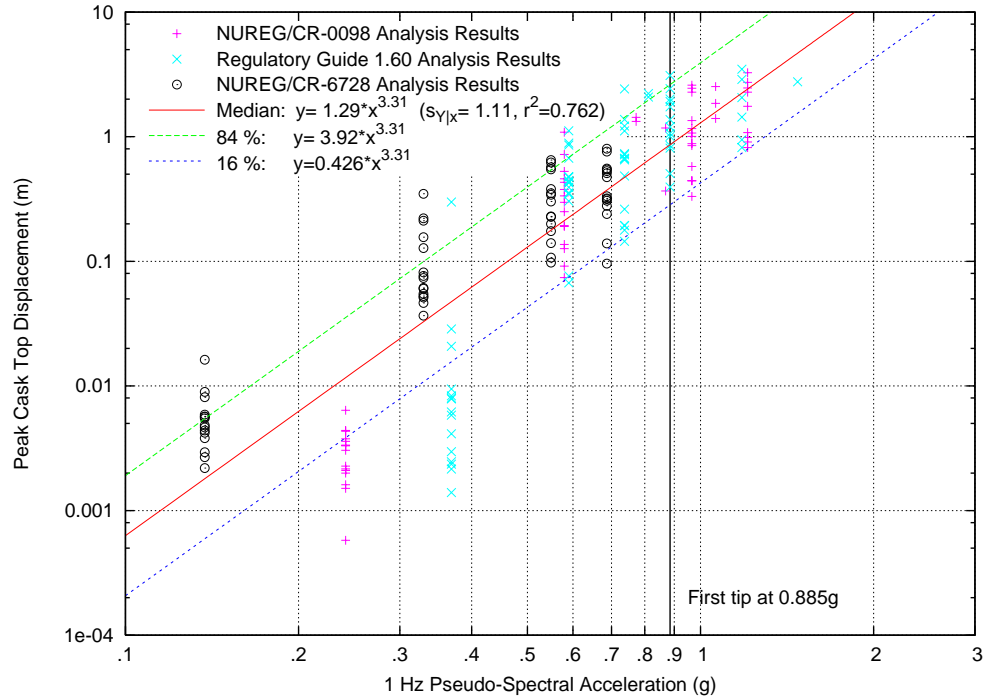


Figure VI.41: Peak Top Displacement Regression Fit in Terms of 1 Hz PSA, Logarithmic Scale, Cylindrical Cask, All Earthquakes, Cask/Pad  $\mu=0.8$ , All Soil Profiles

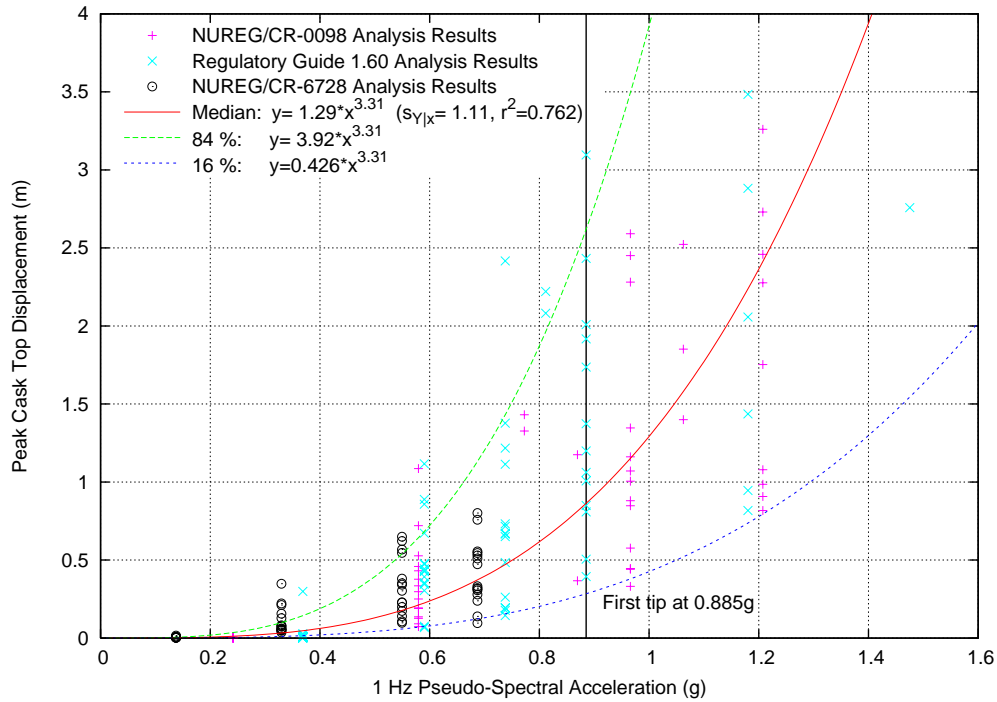


Figure VI.42: Peak Top Displacement Regression Fit in Terms of 1 Hz PSA, Linear Scale, Cylindrical Cask, All Earthquakes, Cask/Pad  $\mu=0.8$ , All Soil Profiles

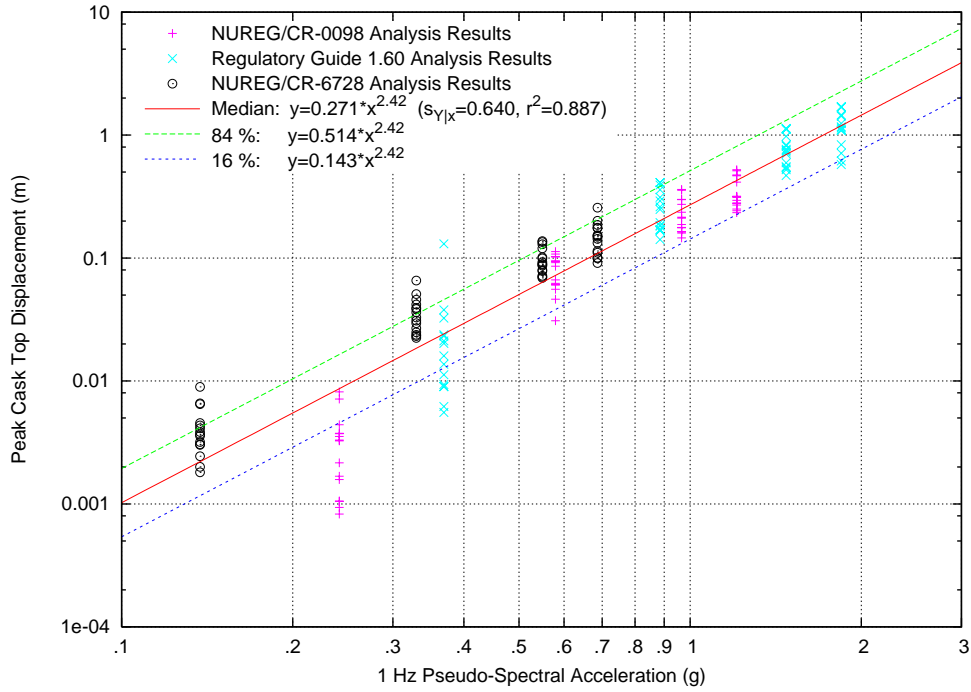


Figure VI.43: Peak Top Displacement Regression Fit in Terms of 1 Hz PSA, Logarithmic Scale, Rectangular Module, All Earthquakes, Cask/Pad  $\mu=0.2$ , All Soil Profiles

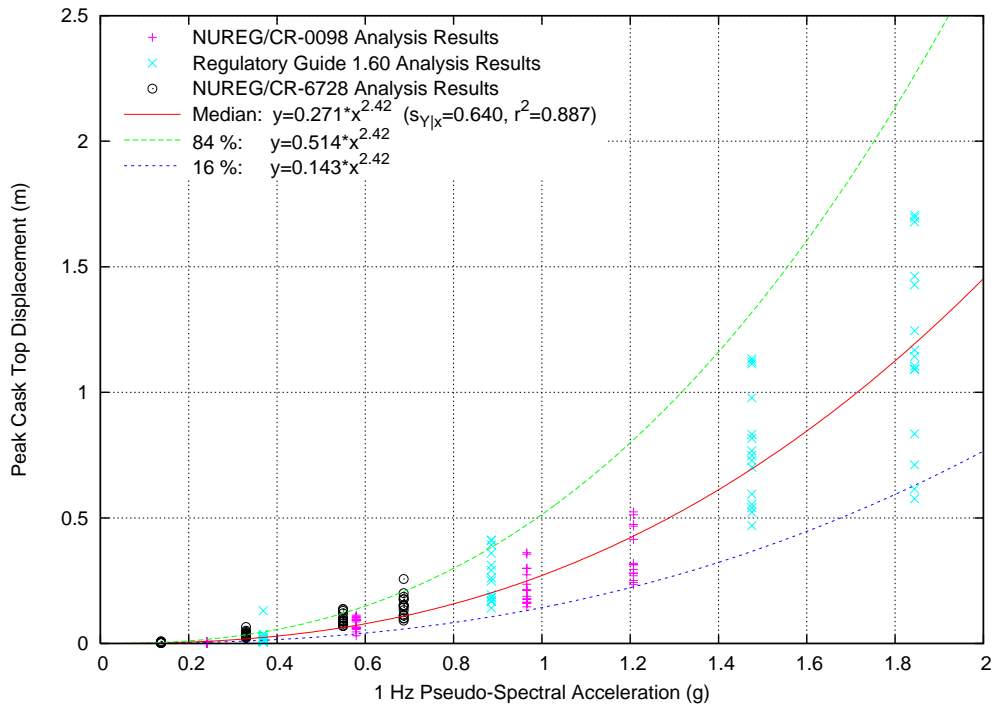


Figure VI.44: Peak Top Displacement Regression Fit in Terms of 1 Hz PSA, Linear Scale, Rectangular Module, All Earthquakes, Cask/Pad  $\mu=0.2$ , All Soil Profiles

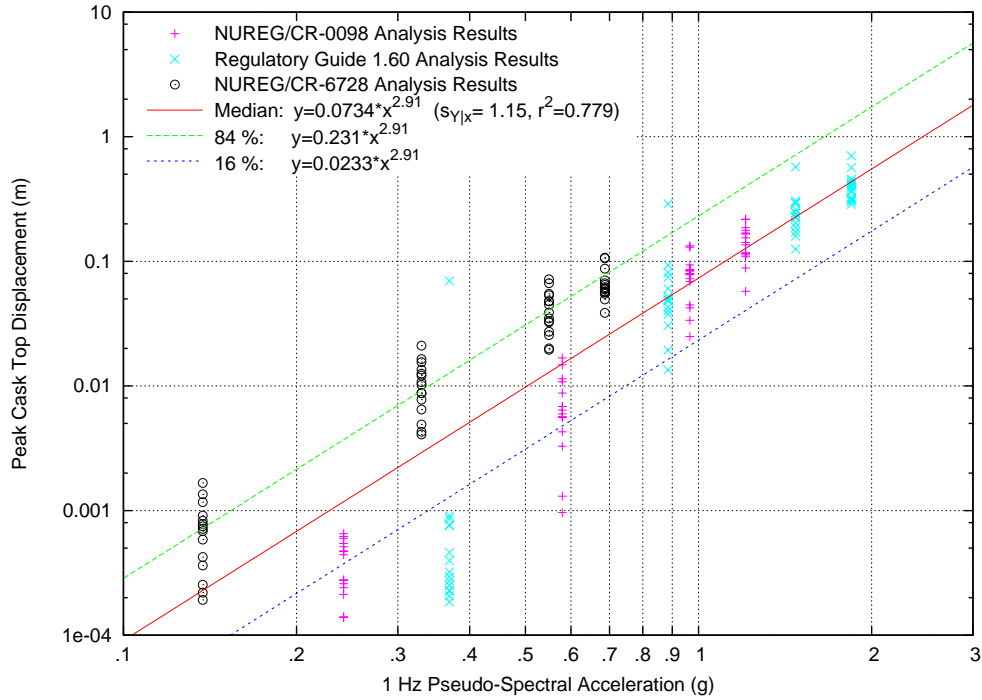


Figure VI.45: Peak Top Displacement Regression Fit in Terms of 1 Hz PSA, Logarithmic Scale, Rectangular Module, All Earthquakes, Cask/Pad  $\mu=0.55$ , All Soil Profiles

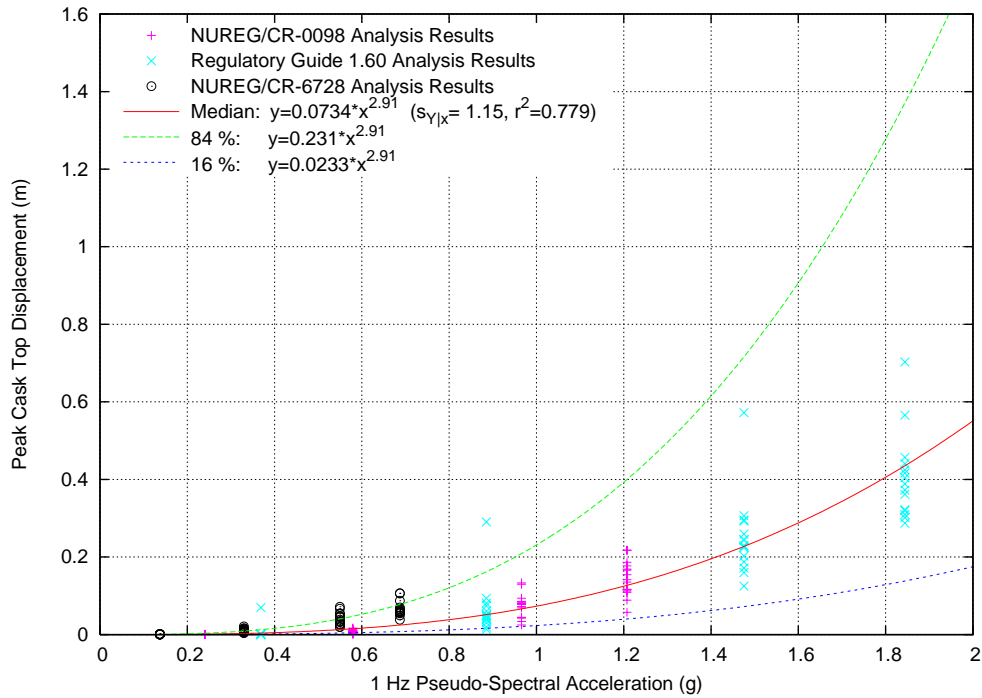


Figure VI.46: Peak Top Displacement Regression Fit in Terms of 1 Hz PSA, Linear Scale, Rectangular Module, All Earthquakes, Cask/Pad  $\mu=0.55$ , All Soil Profiles

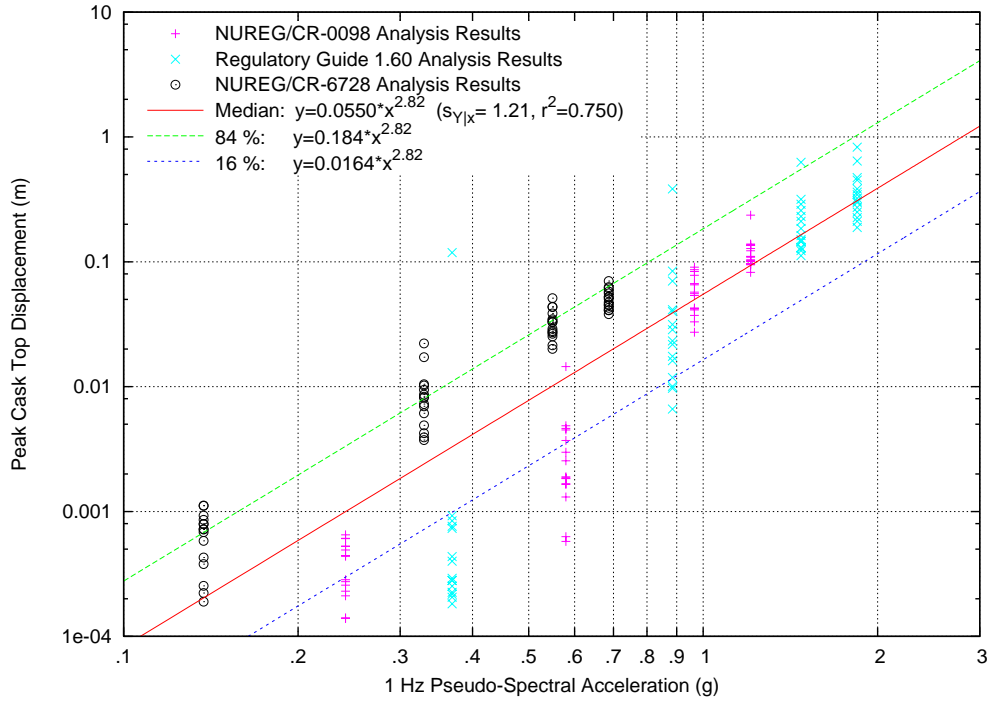


Figure VI.47: Peak Top Displacement Regression Fit in Terms of 1 Hz PSA, Logarithmic Scale, Rectangular Module, All Earthquakes, Cask/Pad  $\mu=0.8$ , All Soil Profiles

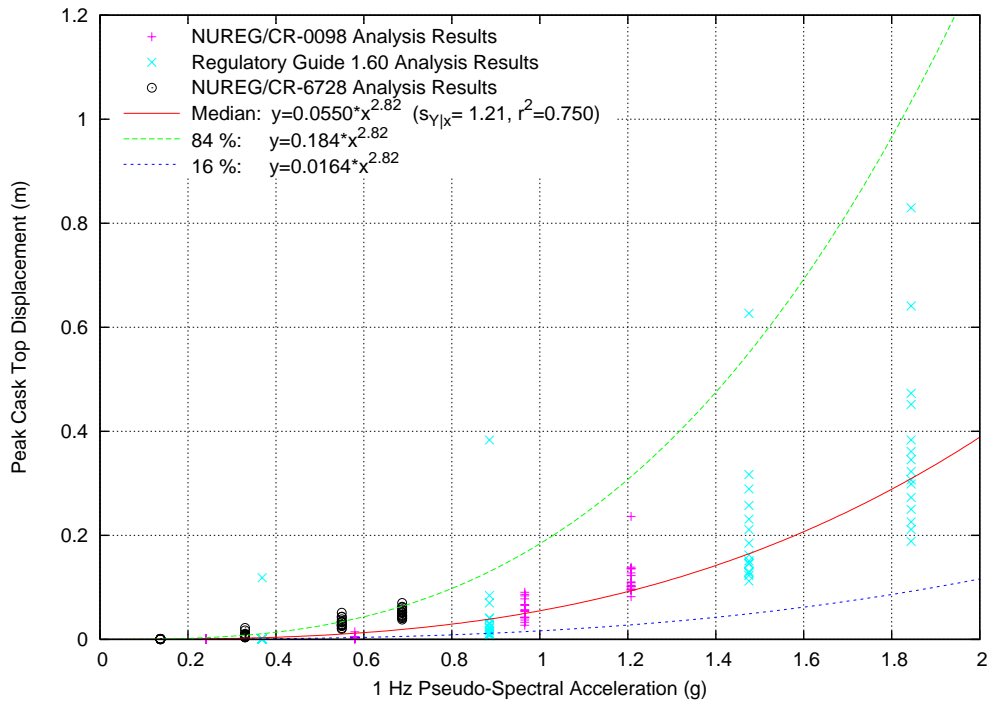


Figure VI.48: Peak Top Displacement Regression Fit in Terms of 1 Hz PSA, Linear Scale, Rectangular Module, All Earthquakes, Cask/Pad  $\mu=0.8$ , All Soil Profiles

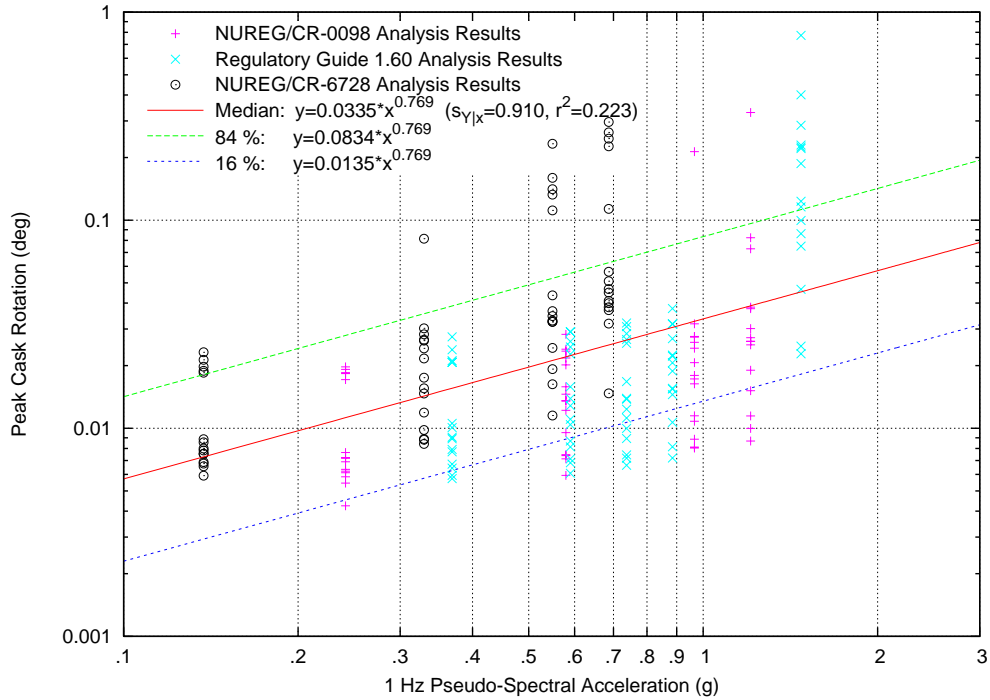


Figure VI.49: Peak Rotation Regression Fit in Terms of 1 Hz PSA, Logarithmic Scale, Cylindrical Cask, All Earthquakes, Cask/Pad  $\mu=0.2$ , All Soil Profiles

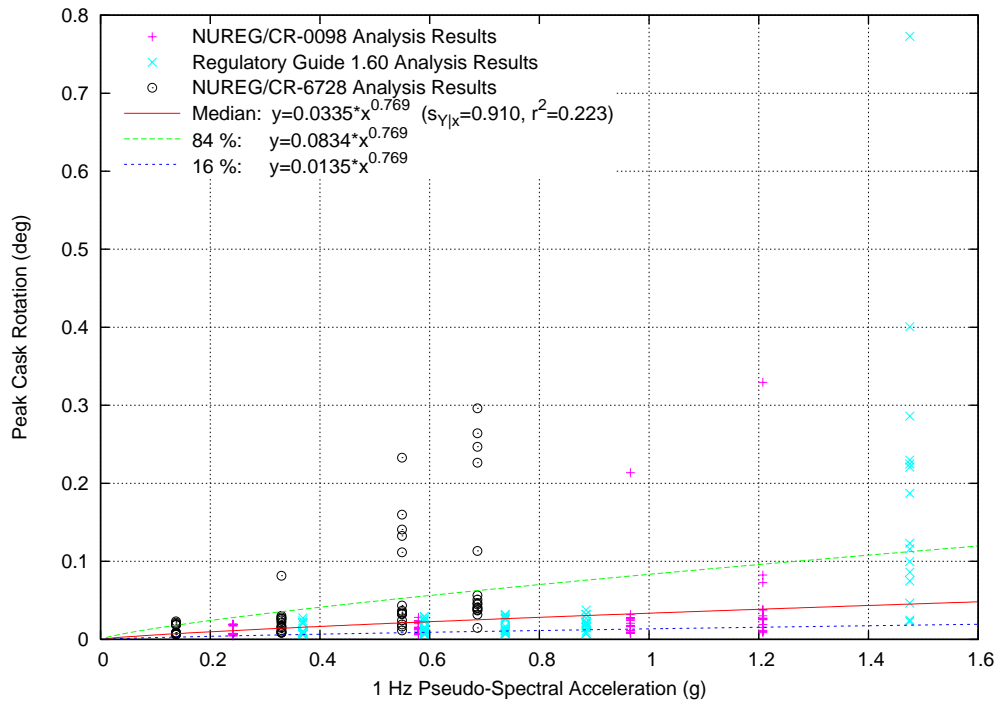


Figure VI.50: Peak Rotation Regression Fit in Terms of 1 Hz PSA, Linear Scale, Cylindrical Cask, All Earthquakes, Cask/Pad  $\mu=0.2$ , All Soil Profiles

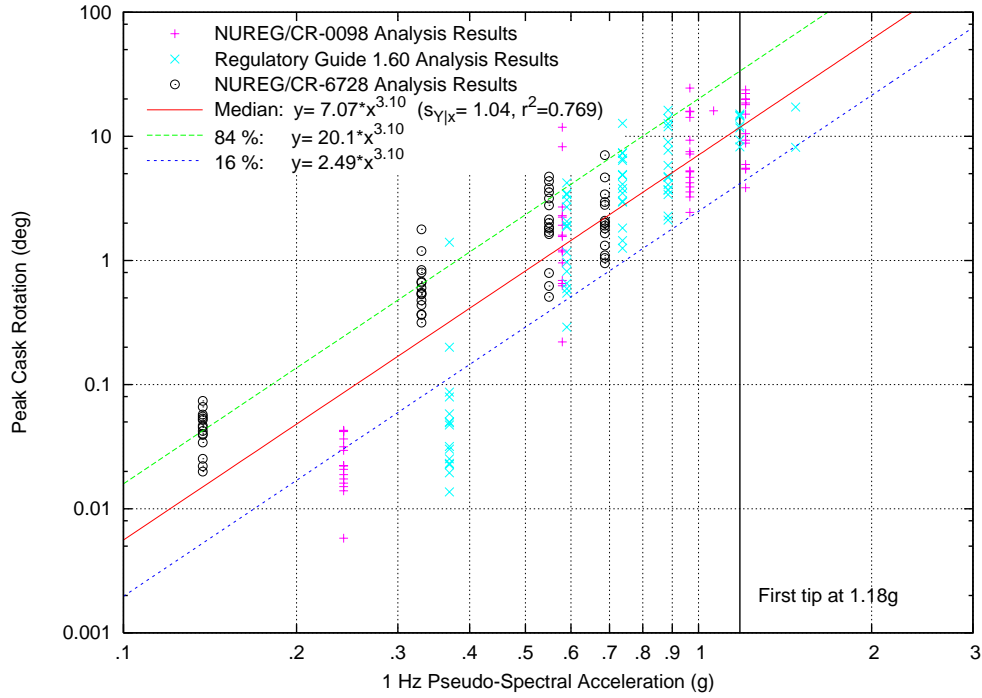


Figure VI.51: Peak Rotation Regression Fit in Terms of 1 Hz PSA, Logarithmic Scale, Cylindrical Cask, All Earthquakes, Cask/Pad  $\mu=0.55$ , All Soil Profiles

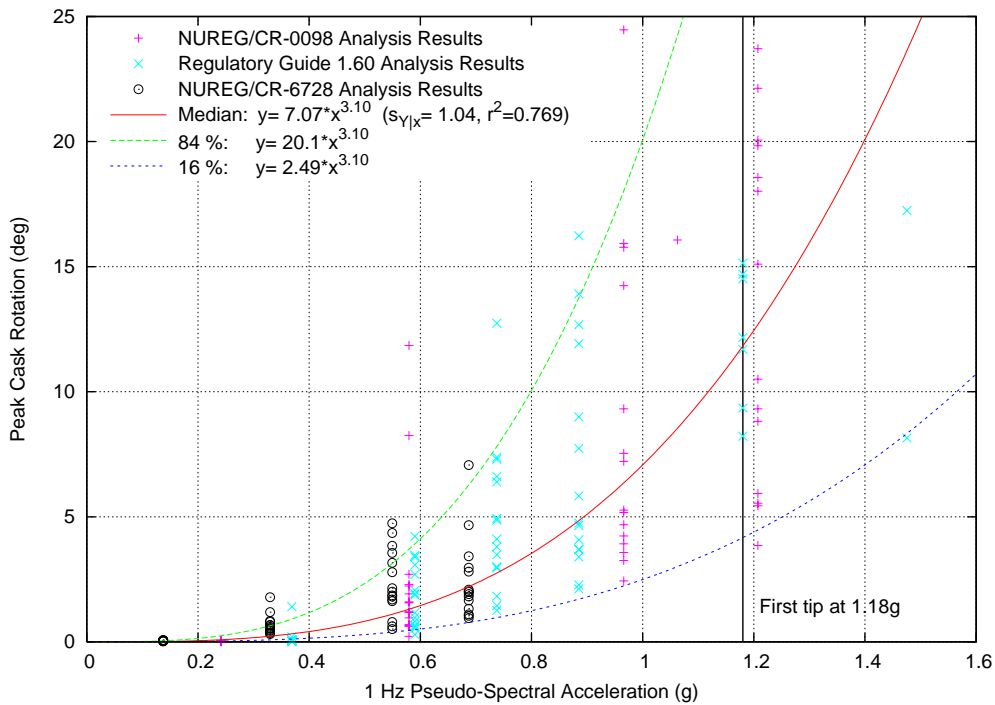


Figure VI.52: Peak Rotation Regression Fit in Terms of 1 Hz PSA, Linear Scale, Cylindrical Cask, All Earthquakes, Cask/Pad  $\mu=0.55$ , All Soil Profiles

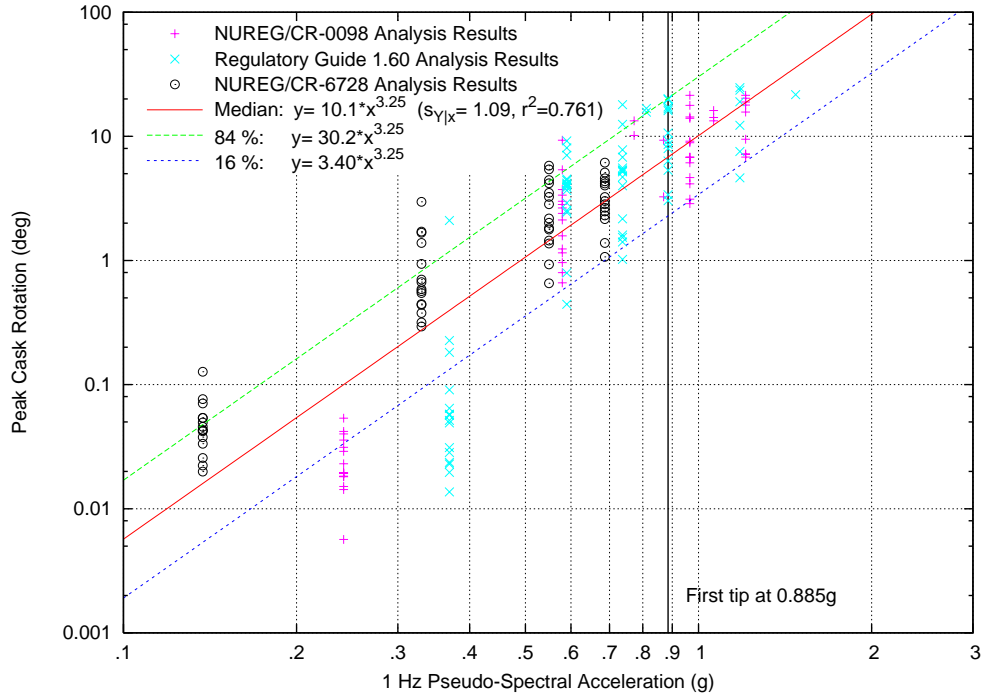


Figure VI.53: Peak Rotation Regression Fit in Terms of 1 Hz PSA, Logarithmic Scale, Cylindrical Cask, All Earthquakes, Cask/Pad  $\mu=0.8$ , All Soil Profiles

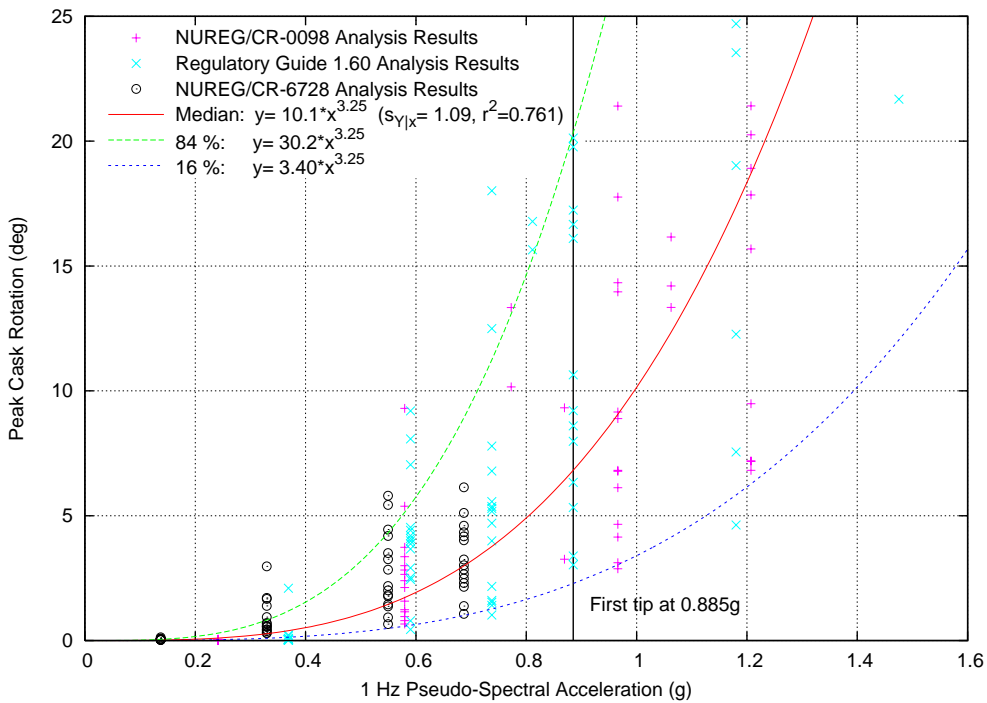


Figure VI.54: Peak Rotation Regression Fit in Terms of 1 Hz PSA, Linear Scale, Cylindrical Cask, All Earthquakes, Cask/Pad  $\mu=0.8$ , All Soil Profiles

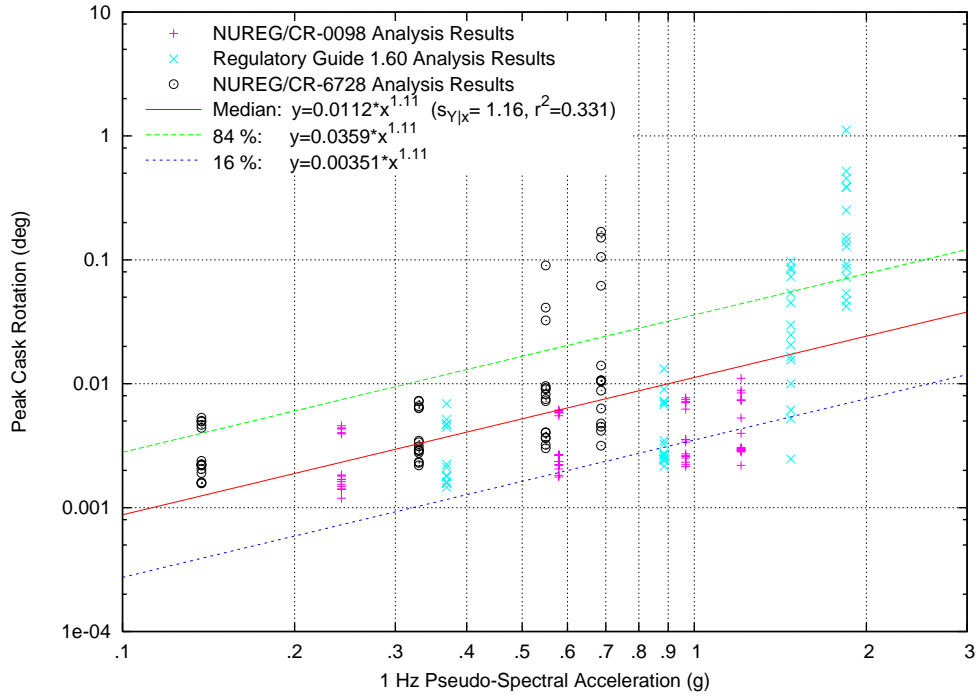


Figure VI.55: Peak Rotation Regression Fit in Terms of 1 Hz PSA, Logarithmic Scale, Rectangular Module, All Earthquakes, Cask/Pad  $\mu=0.2$ , All Soil Profiles

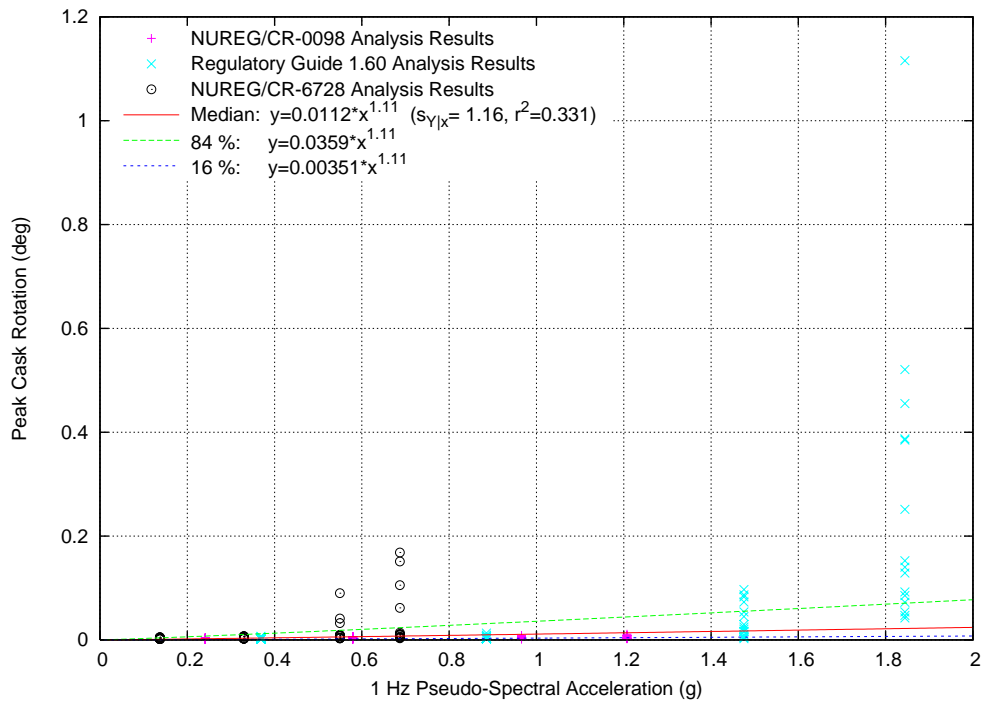


Figure VI.56: Peak Rotation Regression Fit in Terms of 1 Hz PSA, Linear Scale, Rectangular Module, All Earthquakes, Cask/Pad  $\mu=0.2$ , All Soil Profiles

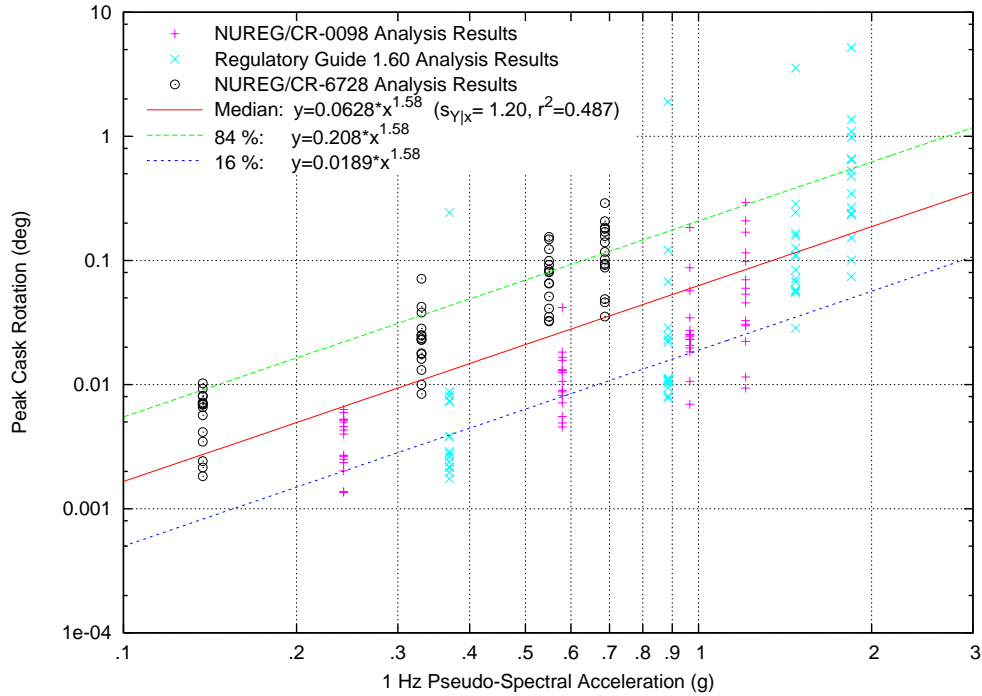


Figure VI.57: Peak Rotation Regression Fit in Terms of 1 Hz PSA, Logarithmic Scale, Rectangular Module, All Earthquakes, Cask/Pad  $\mu=0.55$ , All Soil Profiles

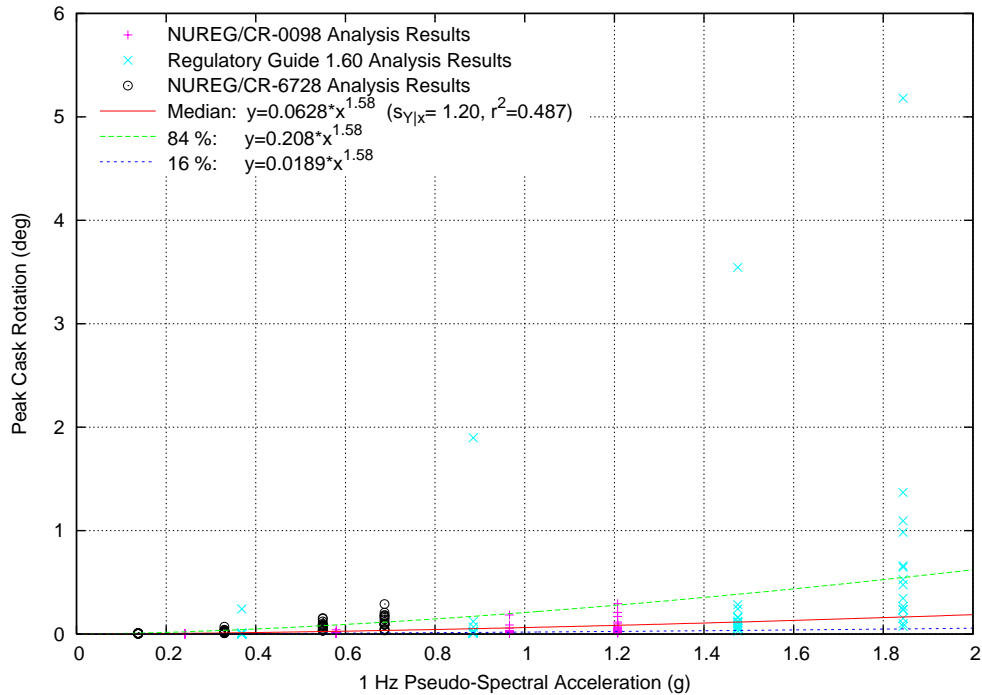


Figure VI.58: Peak Rotation Regression Fit in Terms of 1 Hz PSA, Linear Scale, Rectangular Module, All Earthquakes, Cask/Pad  $\mu=0.55$ , All Soil Profiles

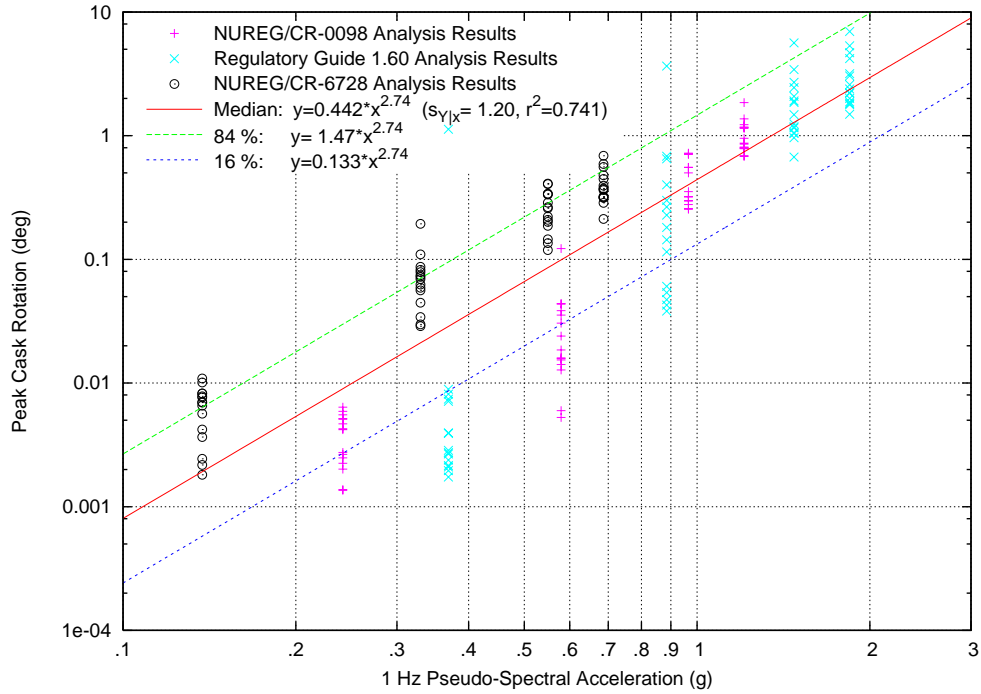


Figure VI.59: Peak Rotation Regression Fit in Terms of 1 Hz PSA, Logarithmic Scale, Rectangular Module, All Earthquakes, Cask/Pad  $\mu=0.8$ , All Soil Profiles

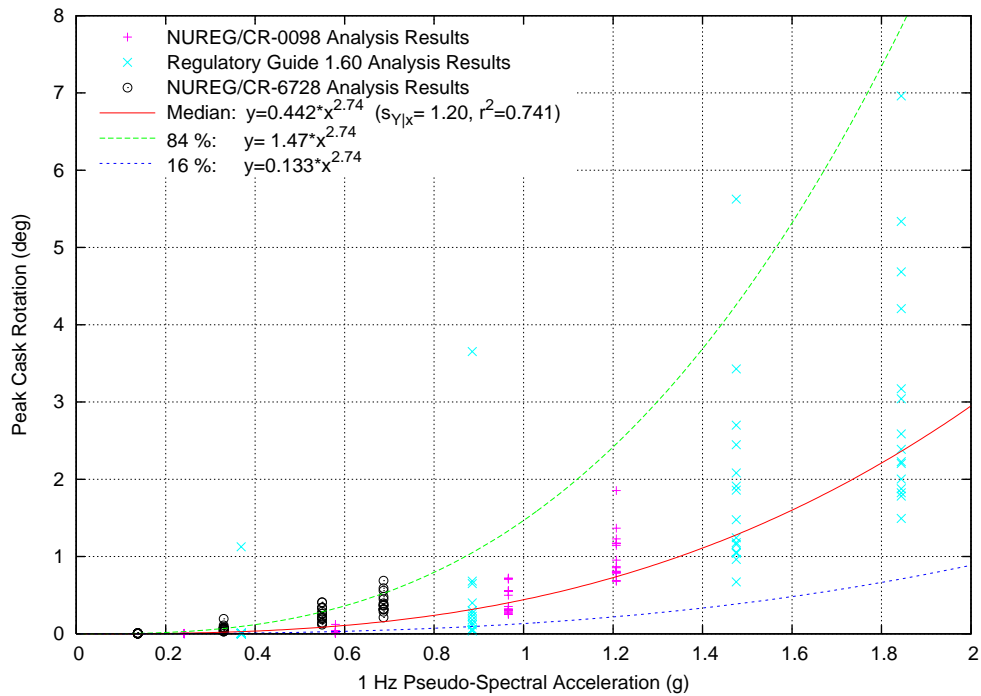


Figure VI.60: Peak Rotation Regression Fit in Terms of 1 Hz PSA, Linear Scale, Rectangular Module, All Earthquakes, Cask/Pad  $\mu=0.8$ , All Soil Profiles

## **Appendix VII: Tabulation of Curve Fitting Parameters and Example Calculations**



## Appendix VII: Tabulation of Curve Fitting Parameters and Example Calculations

The nomograms for the cask response shown in Appendix VI can be used to estimate the peak cask top displacement and peak cask rotation for specific applications. All of the nomograms were developed using the same power law equation from the procedure outlined in Section 5.5. The power law equation for the cask response  $y$  in terms of the ground motion parameter  $x$  at a confidence band  $m$  standard deviations above the median response was provided in Equation 5.12, and is re-iterated here:

$$y = A x^B \exp(m S_{Y|x}) \quad (\text{VII.1})$$

In this equation,  $A$  and  $B$  are the curve fitting coefficients and  $S_{Y|x}$  is the conditional standard deviation of the result data after undergoing a logarithmic transformation.

### VII.1 Tabulation of Curve Fitting Parameters

The values of  $A$ ,  $B$ , and  $S_{Y|x}$  have been provided in the legends of each of the plots in Appendix VI. To facilitate application of these results to site-specific cask response evaluations, these parameters are tabulated below in Tables VII.1 through VII.8. These tables show the parameters for the peak cask top displacement response and the peak cask rotation response. Columns denoted with “disp.” contain the parameters for the peak cask top displacement, and those denoted with “rot.” have the information for the rotation. Tables are provided for the results from the three individual spectral shapes, as well as for the combined results for all spectral shapes. There are separate tables for the cylindrical cask results and for the rectangular module results. The ground motion parameter,  $x$ , for the individual spectral shapes is peak ground acceleration (PGA), while the ground response parameter for the combined spectral shapes is the 5% damped 1 Hz Pseudo-Spectral Acceleration (PSA). When these parameters are used in conjunction with Equation VII.1, the response,  $y$ , is in meters for the top displacement and in degrees for the rotation angle.

Table VII.1: Curve Fitting Parameters for Cylindrical Cask, NUREG/CR-0098 Earthquakes, PGA

	<b>A (disp.)</b>	<b>B (disp.)</b>	<b>S<sub>Y x</sub> (disp.)</b>	<b>A (rot.)</b>	<b>B (rot.)</b>	<b>S<sub>Y x</sub> (rot.)</b>
$\mu=0.2$	0.216	2.60	0.409	0.0217	0.689	0.718
$\mu=0.55$	0.911	4.06	0.814	6.70	3.94	0.794
$\mu=0.8$	1.150	4.16	0.796	9.01	4.09	0.765

Table VII.2: Curve Fitting Parameters for Cylindrical Cask, Regulatory Guide 1.60 Earthquakes, PGA

	<b>A (disp.)</b>	<b>B (disp.)</b>	<b>S<sub>Y x</sub> (disp.)</b>	<b>A (rot.)</b>	<b>B (rot.)</b>	<b>S<sub>Y x</sub> (rot.)</b>
$\mu=0.2$	0.837	2.52	0.465	0.0733	1.71	0.785
$\mu=0.55$	8.96	4.80	1.03	62.5	4.71	0.956
$\mu=0.8$	15.4	5.04	1.13	114	4.94	1.12

Table VII.3: Curve Fitting Parameters for Cylindrical Cask, NUREG/CR-6728 Earthquakes, PGA

	<b>A (disp.)</b>	<b>B (disp.)</b>	$S_{y/x}$ (disp.)	<b>A (rot.)</b>	<b>B (rot.)</b>	$S_{y/x}$ (rot.)
$\mu=0.2$	0.0897	1.88	0.377	0.0456	1.17	0.777
$\mu=0.55$	0.219	2.63	0.543	1.64	2.53	0.583
$\mu=0.8$	0.253	2.71	0.631	2.11	2.68	0.606

Table VII.4: Curve Fitting Parameters for Rectangular Module, NUREG/CR-0098 Earthquakes, PGA

	<b>A (disp.)</b>	<b>B (disp.)</b>	$S_{y/x}$ (disp.)	<b>A (rot.)</b>	<b>B (rot.)</b>	$S_{y/x}$ (rot.)
$\mu=0.2$	0.219	3.08	0.544	0.00386	0.418	0.495
$\mu=0.55$	0.0571	3.78	0.594	0.0304	1.67	0.752
$\mu=0.8$	0.0396	3.70	0.765	0.328	3.58	0.748

Table VII.5: Curve Fitting Parameters for Rectangular Module, Regulatory Guide 1.60 Earthquakes, PGA

	<b>A (disp.)</b>	<b>B (disp.)</b>	$S_{y/x}$ (disp.)	<b>A (rot.)</b>	<b>B (rot.)</b>	$S_{y/x}$ (rot.)
$\mu=0.2$	0.724	2.63	0.519	0.037	2.35	1.17
$\mu=0.55$	0.225	4.16	0.912	0.153	2.70	1.27
$\mu=0.8$	0.172	4.07	0.996	1.36	3.99	1.07

Table VII.6: Curve Fitting Parameters for Rectangular Module, NUREG/CR-6728 Earthquakes, PGA

	<b>A (disp.)</b>	<b>B (disp.)</b>	$S_{y/x}$ (disp.)	<b>A (rot.)</b>	<b>B (rot.)</b>	$S_{y/x}$ (rot.)
$\mu=0.2$	0.0937	2.27	0.335	0.00918	1.02	0.922
$\mu=0.55$	0.0369	2.92	0.477	0.0684	1.89	0.556
$\mu=0.8$	0.0297	2.81	0.417	0.230	2.67	0.451

Table VII.7: Curve Fitting Parameters for Cylindrical Cask, All Spectral Shapes, 1 Hz PSA

	<b>A (disp.)</b>	<b>B (disp.)</b>	$S_{y/x}$ (disp.)	<b>A (rot.)</b>	<b>B (rot.)</b>	$S_{y/x}$ (rot.)
$\mu=0.2$	0.271	2.15	0.532	0.0335	0.769	0.91
$\mu=0.55$	0.979	3.20	1.07	7.07	3.10	1.04
$\mu=0.8$	1.29	3.31	1.11	10.1	3.25	1.09

Table VII.8: Curve Fitting Parameters for Rectangular Module, All Spectral Shapes, 1 Hz PSA

	<b>A (disp.)</b>	<b>B (disp.)</b>	$S_{y/x}$ (disp.)	<b>A (rot.)</b>	<b>B (rot.)</b>	$S_{y/x}$ (rot.)
$\mu=0.2$	0.271	2.42	0.640	0.0112	1.11	1.16
$\mu=0.55$	0.0734	2.91	1.15	0.0628	1.58	1.20
$\mu=0.8$	0.0550	2.82	1.21	0.442	2.74	1.20

## VII.2 Example Calculations

To illustrate the usage of the nomograms, example calculations for two site-specific applications are provided. The two example applications shown here are the Independent Spent Fuel Storage Installation at the Hatch Nuclear Power Station and the proposed Private Fuel Storage (PFS) Facility. Both of these sites use casks with the same characteristics as the cylindrical cask in the parametric study.

## VII.2.1 Hatch Example

Figure VII.1 shows a plot of the three horizontal spectral shapes used in this study to develop nomograms, along with the spectral shape of the Hatch site-specific design earthquake. These spectral shapes have all been normalized to the horizontal PGA. The horizontal PGA of the Hatch design earthquake is 0.15 g. From this plot, it can be seen that the Hatch design earthquake has a very similar shape to the NUREG/CR-0098 spectral shape in this study. Because of this close correspondence, it is reasonable to use the nomograms developed from that spectral shape for evaluating this site-specific case. To illustrate the procedure for using the nomograms derived from specific spectra, as well as that for the combined nomograms, both approaches will be illustrated here.

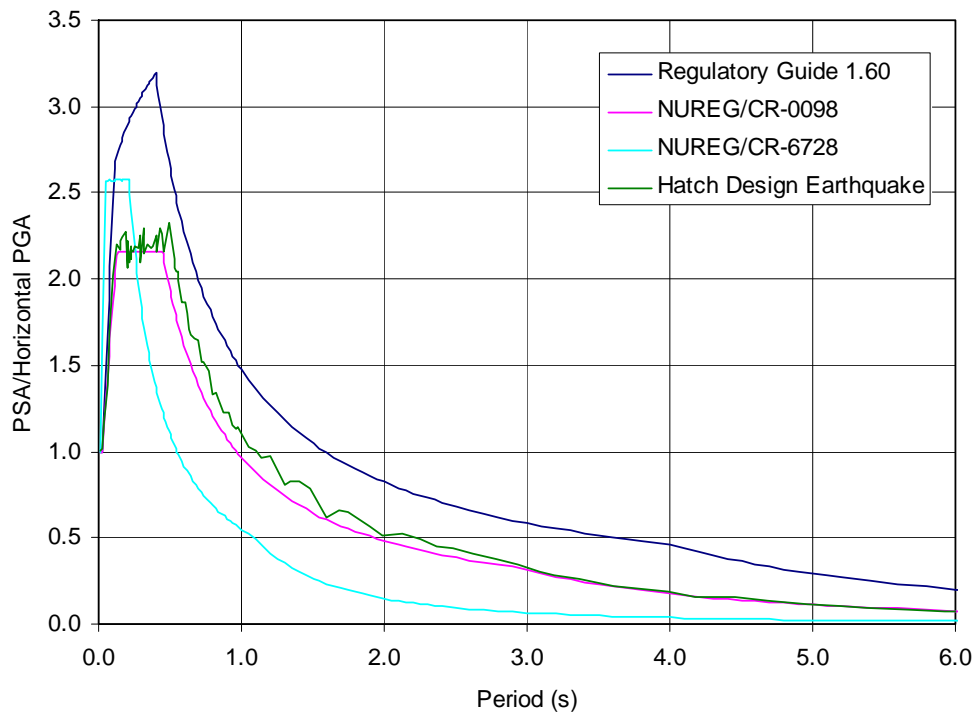


Figure VII.1: Comparison of Hatch Site-Specific Horizontal Spectral Shape with Spectral Shapes Used to Develop Nomograms in the Parametric Study

To apply the NUREG-CR/0098 spectral shape nomograms to this case, one would use the coefficients provided in Table VII.1, in conjunction with Equation VII.1. To compute the median response, one should set  $m=0$  in that equation. Because  $\exp(0)=1$ , the entire term related to the confidence band can simply be dropped out of the equation in that case. For the 84% confidence response, one should set  $m=1$ . Using the appropriate parameters from Table VII.1, the median cask top displacement with the lower bound  $\mu=0.2$  would be computed as:

$$\text{peak top displacement} = 0.216 \cdot 0.15^{2.6} = 0.0016\text{m} (0.061 \text{ in})$$

In a similar manner, the 84% cask response for that same case is calculated:

$$\text{peak top displacement} = 0.216 \cdot 0.15^{2.6} \cdot \exp(1.0 \cdot 0.409) = 0.0023\text{m} (0.092 \text{ in})$$

The same process is used to compute the peak rotation. The median rotation for that same case would be:

$$\text{peak rotation} = 0.0217 \cdot 0.15^{0.689} = 0.0059 \text{ deg}$$

The 84% rotation would be computed as:

$$\text{peak rotation} = 0.0217 \cdot 0.15^{0.689} \cdot \exp(1.0 \cdot 0.718) = 0.012 \text{ deg}$$

Similar calculations are performed using the appropriate parameters for the other coefficients of friction. A complete set of these computed cask top displacements and rotations using the nomograms for the NUREG/CR-0098 spectral shape is provided in Table VII.9.

Table VII.9: Cask Response Predicted by NUREG/CR-0098 Spectrum Nomograms for Hatch Example

	<b>Median Top Disp. m (in)</b>	<b>84% Top Disp. m (in)</b>	<b>Median Rotation (degrees)</b>	<b>84% Rotation (degrees)</b>
$\mu=0.2$	0.0016 (0.061)	0.0023 (0.092)	0.0059	0.012
$\mu=0.55$	0.00041 (0.016)	0.00093 (0.037)	0.0038	0.0084
$\mu=0.8$	0.00043 (0.017)	0.00095 (0.038)	0.0038	0.0083

The procedure to apply the combined nomograms is very similar to that illustrated above for a specific spectral shape. The major difference is that the 5% damped 1 Hz PSA is used instead of the PGA as the ground motion parameter. The parameters in Table VII.7 should be used to apply the combined nomogram for this application. The design earthquake at this site has a 5% damped 1 Hz PSA of 0.17 g. The median cask top displacement with the lower bound  $\mu=0.2$  is computed as:

$$\text{peak top displacement} = 0.271 \cdot 0.17^{2.15} = 0.0060 \text{ m (0.24 in)}$$

The corresponding 84% cask top displacement is:

$$\text{peak top displacement} = 0.271 \cdot 0.17^{2.15} \cdot \exp(1.0 \cdot 0.532) = 0.010 \text{ m (0.40 in)}$$

Rotations are computed in a similar manner. The median rotation is:

$$\text{peak rotation} = 0.0335 \cdot 0.17^{0.769} = 0.0086 \text{ deg}$$

Finally, the 84% rotation is computed as:

$$\text{peak rotation} = 0.0335 \cdot 0.17^{0.769} \cdot \exp(1.0 \cdot 0.910) = 0.021 \text{ deg}$$

A table of the complete set of cask top displacements and rotations computed using the combined nomograms is provided in Table VII.10. It can be seen that the combined nomograms indicate somewhat higher responses than the nomograms for the NUREG/CR-0098 spectral shape, but both sets of results are quite small in this case.

Table VII.10: Cask Response Predicted by Combined Nomograms for Hatch Example

	<b>Median Top Disp. m (in)</b>	<b>84% Top Disp. m (in)</b>	<b>Median Rotation (degrees)</b>	<b>84% Rotation (degrees)</b>
$\mu=0.2$	0.0060 (0.24)	0.010 (0.40)	0.0086	0.021
$\mu=0.55$	0.0034 (0.13)	0.0098 (0.39)	0.029	0.082
$\mu=0.8$	0.0037 (0.14)	0.011 (0.44)	0.032	0.095

## VII.2.2 Private Fuel Storage Example

Figure VII.2 shows the 5% damped pseudo-spectral acceleration spectrum of the horizontal ground motion records for the PFS design earthquake. As for the Hatch example, the spectra in this plot have all been normalized to the PGA to facilitate comparison of the spectral shapes. The PFS design earthquake has a PGA of 0.74 g, and a 5% damped, 1 Hz PSA of 0.53 g. It can be seen in this plot that the PFS design earthquake does not correspond as closely as the Hatch design earthquake did to any of the spectral shapes used in the parametric study. Because of this, calculations only are provided based on the combined nomograms for this case.

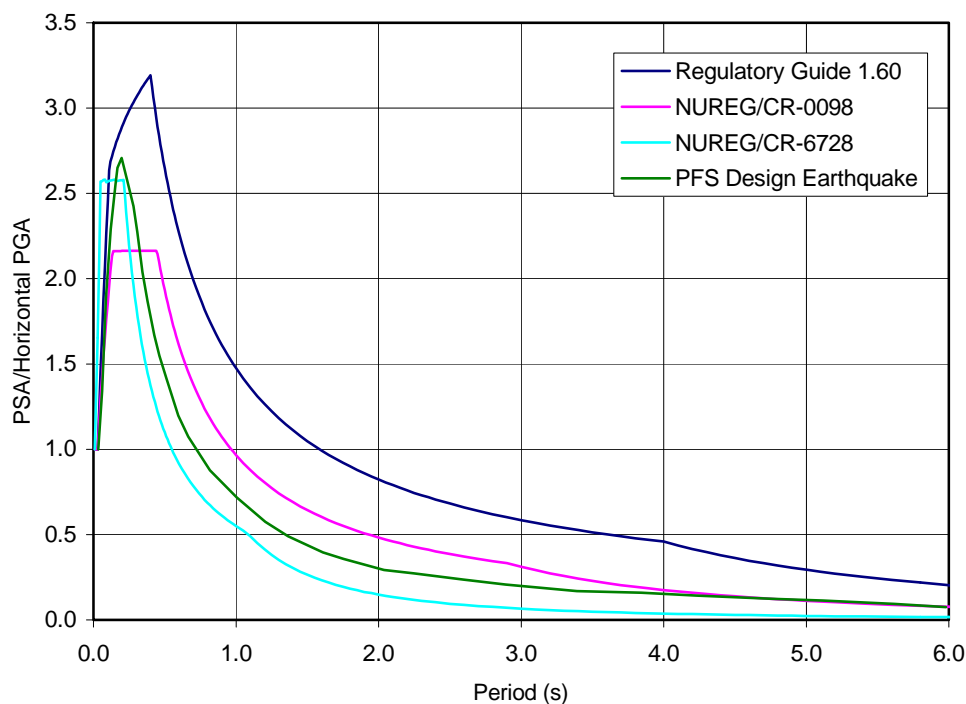


Figure VII.2: Comparison of PFS Site-Specific Horizontal Spectral Shape with Spectral Shapes Used to Develop Nomograms in the Parametric Study

Exactly the same procedure used for the Hatch example using the combined nomograms is used here to compute the cask response. The ground motion parameter used in these calculations is 0.53 g. This has been used in conjunction with the parameters in Table VII.7 and Equation VII.1 to produce the table of cask responses with varying values of  $\mu$  shown in Table VII.11.

Table VII.11: Cask Response Predicted by Combined Nomograms for PFS Example

	<b>Median Top Disp. m (in)</b>	<b>84% Top Disp. m (in)</b>	<b>Median Rotation (degrees)</b>	<b>84% Rotation (degrees)</b>
$\mu=0.2$	0.069 (2.7)	0.12 (4.6)	0.021	0.051
$\mu=0.55$	0.13 (5.1)	0.37 (15)	0.99	2.8
$\mu=0.8$	0.16 (6.2)	0.48 (19)	1.3	3.8



**BIBLIOGRAPHIC DATA SHEET**

*(See instructions on the reverse)*

1. REPORT NUMBER  
(Assigned by NRC, Add Vol., Supp., Rev.,  
and Addendum Numbers. if anv.)

2. TITLE AND SUBTITLE

3. DATE REPORT PUBLISHED

MONTH

YEAR

4. FIN OR GRANT NUMBER

5. AUTHOR(S)

6. TYPE OF REPORT

7. PERIOD COVERED *(Inclusive Dates)*

8. PERFORMING ORGANIZATION - NAME AND ADDRESS *(If NRC, provide Division, Office or Region, U.S. Nuclear Regulatory Commission, and mailing address; if contractor, provide name and mailing address.)*

9. SPONSORING ORGANIZATION - NAME AND ADDRESS *(If NRC, type "Same as above"; if contractor, provide NRC Division, Office or Region, U.S. Nuclear Regulatory Commission, and mailing address.)*

10. SUPPLEMENTARY NOTES

11. ABSTRACT *(200 words or less)*

12. KEY WORDS/DESCRIPTORS *(List words or phrases that will assist researchers in locating the report.)*

13. AVAILABILITY STATEMENT

unlimited

14. SECURITY CLASSIFICATION

*(This Page)*

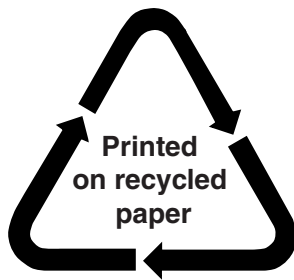
unclassified

*(This Report)*

unclassified

15. NUMBER OF PAGES

16. PRICE



**Federal Recycling Program**